Sample Project Reports

INDEX

“Design and Analysis of FinFET based SRAM cell.”

A thesis submitted in partial fulfillment of the requirements for the award of the degree of

Master of Technology

in

Electronics and Communication Engineering

By:

Vaishali Yadav
Roll No: 198135003

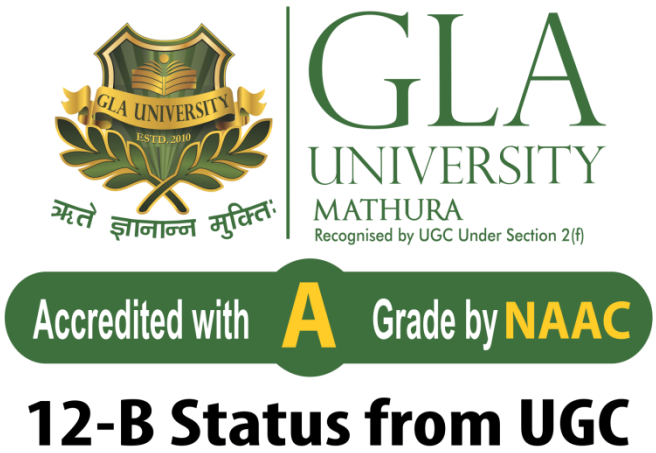

Department of Electronics & Communication Engineering

Institute of Engineering and Technology G.L.A University

Mathura -281406,INDIA

July,2020

CERTIFICATE

This is to certify that the report titled **"Design and Analysis of FinFET based SRAM Cell"** being submitted by ***Vaishali Yadav*** to the Institute of Engineering and Technology GLA University Mathura, for the award of the Master of Technology, is an original research work carried out by her under my supervision. In my opinion, this report has reached the standards fulfilling the requirements of the regulations relating to the degree. The results contained in this report have not been submitted in part or full to any other university or institute for the award of any degree/diploma.

Date: 5th July, 2021

Dr. Vinay Kumar Tomar
(Associate Professor)
Department of Electronics and Communication Engineering,
GLA University, Mathura

Head of Department
Electronics & Communication Engg.
GLA University, Mathura

Abstract

SRAM is high-speed memory, that's why it is widely use as cache memory presents inside the microprocessor. According to the Moore's law, transistor size is reduces, that will also scaled the supply voltage, results the value of static noise margin reduces which will affect the stability of SRAM cell. In this thesis, we design and compare the CMOS and FinFET based SRAM cells on the basis of stability, read delay and power dissipation of 6T,7T,8T,9T SRAM memory cell, Schmitt triggered based 10T SRAM cell and Proposed 10T SRAM cell. In CMOS based stability analysis has been performed with the variation in cell ratio and pull up ratio, temperature, process variation and supply voltage and FinFET based stability analysis has been performed with the variation in alpha and beta ratio which are depends on number of Fin. Butterfly curve methodology is used to calculate the stability parameters i.e RSNM. In this work a significant improvement is observed in RSNM, WSNM, Read power, Read delay and Write delay. All the peripherals of SRAM architecture like pre-charge, row/column decoder and write driver circuits are designed. Cadence Tools are used for simulation, at 45nm Technology for CMOS based SRAM cell with .5 power supply. FinFET based SRAM cell simulated at 18nm technology node in Cadence virtuoso tool with .3V to .6V.

Acknowledgement

I would like to express my gratitude to all of those who provided me with the resources and guidance to complete my thesis.

First, I am highly indebted to my guide **Dr. Vinay Kumar Tomar (Associate Professor)** for his guidance and constant supervision as well as for providing necessary information regarding the thesis and also for his support in completing the thesis.

I sincerely thank to the Chancellor and Vice-Chancellor of GLA University to provide a research oriented infrastructure.

I would like to thank the Head of Department **Dr. V. K. Deolia** and all the faculty members of the Department, their valuable suggestions and his valuable encouragement during the entire research work. They were really helpful especially during the stressed moments during all these years. My gratitude goes also to my colleagues and seniors at the Department of Electronic and Communications Engineering of GLA University.

I would like to express my gratitude towards my parents, my family members for their kind co-operation and encouragement which help me in completion of this thesis.

Vaishali Yadav

Department of Electronics and Communication Engineering

G.L.A University, Mathura (U.P.)

List of Figures

List of Tables

List of symbols and Abbreviation

VLSI	Very Large Scale Integration
CMOS	Complementary Metal Oxide Semiconductor
FinFET	Fin Field Effect Transistor
SOC	System on a Chip
SRAM	Static Random Access Memory
DRAM	Dynamic Random Access Memory
6T	Six Transistors
ST	Schmitt Triggered
VMSA	Voltage Mode Sense Amplifier
V_{dd}	Supply Voltage
WL	World Line
BL	Bit Line
BLB	Bit Line Bar
I/O Lines	Input/output Lines
ADE	Analog Design Environment
GPDK	Generic Process Design Kit
SINM	Static Current Noise Margin
SVNM	Static Voltage Noise Margin
SPNM	Static Power Noise Margin
WTI	Write Trip Current
WTV	Write Trip Voltage
WTP	Write Trip Power
Tp.	Temperature
SV	Supply Voltage

Contents

Chapter-1
Introduction

1.1 Overview:

These days, because of the increase in demand of portable devices and battery-operated devices as well as the increase in the demand of low power, less delay, high reliability [1] and high data transformation speed device become an important issue for memory design. Nowadays, due to the growing use of battery operated devices and the demand for extending the operation time of the systems with limited resources such as wireless sensor networks, medical instruments, and implantable devices, power consumption has turned to a major concern[2]. These memories facilitate a lot of advantage of digital over analog systems which makes digital systems so versatile and adaptable to many circumstances [3]. SRAM and DRAM are different types of cell design used as a semiconductor memory. SRAM facilitate storage of large data quantities for a long and short duration of time [4]. SRAMs are normally used for mobile applications as both off-chip and on-chip memories, because of their ease of use and low standby leakage [5]. Lots of effort has been carried out in the field of SRAM designs from 4T to 12T structures [6] [7].

SRAM is widely used in SOC in today's market demand and also requires a small size transistor to increase the integration density [8]. If we are switch from micron to sub-micron device technology then the cost of the device reduces and increases performance. In CMOS technology, by scale down device dimension, there are some effects occur such as SCE (short channel length effect) [9].Due to this performance of the device does not meet industry requirements, because of less drive current. In CMOS technology, scaling shows an important factor in the future due to the fundamental material and process technology. Gate oxide thickness is also another important factor, if we are cross the scaling limit then it will cause sudden changes in leakage current. To resolve this CMOS replaced by an ultra-thin body transistor. Ultra-thin body transistor leads to a decrease in subsurface leakage path but also high parasitic drain and source resistance [10]. But major issues in ultra-thin body transistors are having high series resistance. All issues found in ultra thin body transistor are overcome by FinFET technology.

To overcome SCE (Short channel length effect) in CMOS technology by using multi-gate devices FinFET has a non-planner, double-gate transistor built on SOI substrate. The main characteristics of FinFET is that conducting channel wrapped around by Si fin, it has a large surface area that helps to control the electric field, reduce leakage current in an 'off' state[11]. It has the advantage to eliminate the Short channel length effect and gate dielectric leakage current etc. Another advantage is that it requires a lower supply voltage to operate the transistor. FinFET has better-switching speed and current density. FinFET SRAM has less leakage current than CMOS SRAM [12].

Various approaches that are used to reduce power dissipation, like power supply scaling, dowry method, and power gating. Power supply scaling reduces dynamic power (in a quadratic way) as well as static power (in an exponential way). But the trade off occurs with write delay and write power through this method. Leakage power occupies the major part of the total power because the large part of SRAM cell array remains in hold mode for most of the time [13]. The leakage power is generally due to sub-threshold leakage current and gate leakage. When the $V_{gs}<V_{th}$ i.e. gate voltage to source voltage difference is less than the threshold voltage, in that case, the leakage power is less due to their structure , FinFET generate much lower leakage power and allow greater device density[14]. In the conventional 6T SRAM cell, it's a major challenge to obtain an optimal design in terms of Alpha ratio and beta due to the inverse relationship between read stability and write margin. The N-curve metric method is used which provides information about both read stability and write stability in one simulation process. In this work I have compare CMOS and FinFET based SRAM and analysis of the result then I have observed FinFET based SRAM has more stability, less power, large density of integration with low power supply voltage. I have implement and simulated 6T-10T FinFET based SRAM cell. I have proposed FinFET based 10T SRAM cell with improve stability and low power consumption. In this SRAM two techniques is used for read and write operation. This cell is single read and differential write due to this the RSNM and WSNM improved. Read decouple structure is used to read and loop cutting transistor technique for write. It also reduces the leakage power due to stacking of transistor. Therefore, authors have focused on to improve 10T cell stability parameters such as SVNM, SINM, WTV and WTI in 18nm technology with optimized alpha ratio and pull up ratio, which is responsible for the overall performance of SRAM cell. Several

combinations of alpha ratio and beta ratio were simulated for the different values of width and length to meet out the required values. To our literature survey, no one has reported in the literature such significant improvement in RSNM, WSNM, Read access time, Write access time ,Read power and write power cell with optimized alpha ratio and beta ratio. This same optimized cell and pull up ratio has implemented on Schmitt triggered based SRAM cell to get good stability and minimum delay and peak power. Because positive feedback mechanism of ST inverter, adjust the threshold value of inverter based on the input transition.

1.2 Literature Review

Kumar.Aswathy et.al presented [15] FinFET based 6T SRAM cell more stable as compared planner SRAM cell. It has less leakage power. **Ensan** et. al presented [16] low power 7T SRAM cell which has suitable read static noise margin by isolating read path and improved write static noise margin by disconnecting the feedback path of cross coupled inverter. **Kim.youngbok** et.al presented [17] FinFET based 8T SRAM cell reduce dynamic power consumption and increased static noise margin by using cut off the feedback connection between back to back inverters. **Pahuja** et. al presented[18] novel single ended 9T SRAM cell is proposed , it has improved read stability because it has single ended bit line scheme. Write stability is improved due to breaking down the feedback path. **Leila Bagheriye** et. al performed[19] of Highly stable, low power FinFET SRAM cells with exploiting dynamic back-gate biasing. By Using dynamic BG biasing scheme is used to reduce the leakage current. To improve the read current in the Pro-6T cell, a new WL driver is proposed to generate a negative voltage. This cell has a high RSNM/WSNM and consumes low static/dynamic power. By using FinFET It provides a high RSNM/WSNM and high read current. The Pro-8T cell has nearly the same area overhead as ST-2 cell while it has 2x and 1.33x lower read and write energy consumption than ST-2 cell.**R.B Almeida** et.al performed[20] the analysis of 6T SRAM cell in sub 45nm CMOS and FinFET technology. They observed the effects on delay, power, and noise margins, showing that process variability can introduce up to 100% of power deviation. Read Static Noise Margin (RSNM) presents about 20% of deviation under process variability and the cell noise robustness is reduced dramatically in worst cases. **M. Bansal et al. [21]** presented a novel 10T SRAM cell with reduced power consumption along with enhancement in stability**.** This cell has the penalty of an increase in area overhead. In addition to this, authors have also examined the effect of temperature and supply

voltage variation on various SRAM characteristics. Another FinFET based 8T SRAM cell has been reported by **Y. B. Kim et al. [22].** In this cell, higher static noise margin. **Liu. Zhiyu et al. [23]** reported a 9T SRAM operates in single ended read and differential write mode. In this cell, an increase in read static noise margin along with reduction in leakage power consumption was observed**. Ashish Sachdeva et al. [24]** presented a 10T SRAM cell with improved read/write stability and Ion to Ioff (bit-line leakage current) ratio (I_{on}/I_{off}). In this cell, half select issue was resolved and loop cutting methodology is used to reduce the power consumption**.**

1.3 Motivation

Nowadays the increasing demand of the application to strict power requirements with good performance such as wireless sensors, smart mobile devices. In medical field are required those applications which have low power dissipation and rapid performance. Static random access memory (SRAM) occupies most of the area of a modern VLSI chip. Accordingly, the performance and power consumption of a chip profoundly depends on SRAMs. Therefore, reducing the power consumption of SRAMs while meeting the desired requirements is very crucial.

1.4 Objectives

The objectives of the thesis are to Proposed 10T -SRAM bit-cell with improved stability and reduce power consumption and also compared this cell with 6T,7T,8T,9T,S10T SRAM cell. Proposed 10T SRAM cell has improved read/write stability, read access time and low power consumption at low power supply voltage. All SRAM cell have optimize with same alpha and beta ratio. I have also compare CMOS based SRAM with FinFET based SRAM.

1.5. Methodology

Cadence is a set of different design tools at different stages of the IC design process. Some of the design tools are used in this project like Virtuoso Schematic tool is used for schematic entry, Analog Design Environment (ADE) tool is used for the simulation process. This cadence tool uses Generic Process Design Kit (GPDK) provided by fabrication labs which contain all design-related information about the component.

1.6 Outline of Thesis

- **Chapter 2**- Gives the explanation FinFET and FinFET technology.
- **Chapter 3**- Describe of SRAM Architecture, with different blocks of architecture like conventional SRAM cell, pre-charge circuit, write driver circuit and sense amplifier circuit.
- **Chapter 3**-Explain the design metrics of SRAM cells, elaborates the techniques to find the stability of the SRAM cell .
- **Chapter 4** discusses about the proposed 10-T SRAM cells.
- **Chapter 5** present the simulation and comparison results of CMOS and FinFET based 6T SRAM cell.
- **Chapter 6** present the simulation results of optimized Proposed and Schmitt triggered based 10T SRAM cell , 9T,8T,7T and conventional 6T SRAM cell at 18nm technology and compare result shown with the help of graph.
- **Chapter 7** gives the conclusion.

Chapter 2
FinFET Technology

SRAM is one of the best memory cells which are used in the industry. In multimedia device process complex information in large capacity SRAM. A significant portion of today's digital system cover by the SRAM causing substantial total power is consumed by SRAM. SRAM is a semiconductor memory cell that store one-bit data in the form of binary. It is faster and consumes less power as compared to other memory cells. SRAM is widely used in SOC in today's market demand and also requires a small size transistor to increase the integration density [25]. If we are switch from micron to sub-micron device technology then the cost of the device reduces and increases performance. In CMOS technology, by scale down device dimension, there are some effects occur such as SCE (short channel length effect) [26].Due to this performance of the device does not meet industry requirements, because of less drive current. In CMOS technology, scaling shows an important factor in the future due to the fundamental material and process technology. Gate oxide thickness is also another important factor, if we are cross the scaling limit then it will cause sudden changes in leakage current. To resolve this CMOS replaced by an ultra-thin body transistor. Ultra-thin body transistor leads to a decrease in subsurface leakage path but also high parasitic drain and source resistance [27]. But major issues in ultra-thin body transistors are having high series resistance. All issues found in ultra thin body transistor are overcome by FinFET technology.

To overcome SCE (Short channel length effect) in CMOS technology by using multi-gate devices. FinFET has a non-planner, double-gate transistor built on SOI substrate. The main characteristics of FinFET is that conducting channel wrapped around by Si fin, it has a large surface area that helps to control the electric field, reduce leakage current in an ‘off’ state[28]. It has the advantage to eliminate the Short channel length effect and gate dielectric leakage current etc. Another advantage is that it requires a lower supply voltage to operate the transistor. FinFET has better-switching speed and current density. FinFET SRAM has less leakage current than CMOS SRAM [29].

2.1 FinFET

FinFET describe a nonplanner, double gate transistor built on an SOI substrate, based on the single gate transistor design. The important characteristics of FinFET is that conducting channel is wrapped around by a thin Si "fin" which forms the body of the device. The thickness of the fin determines the effective cannel length.

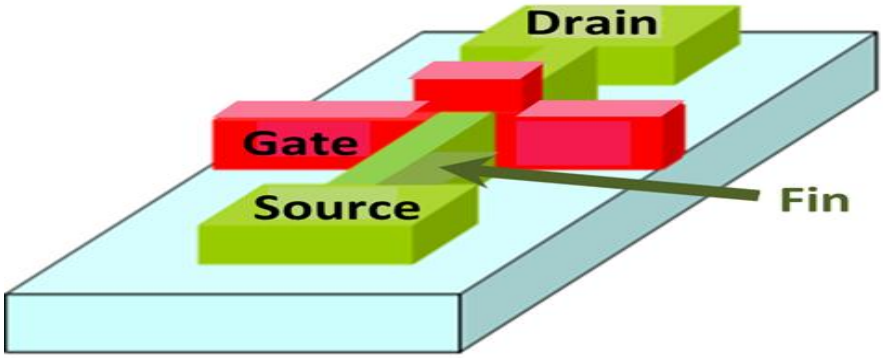

Fig.2.1 Basic structure of FinFET

2.1.1 Reason for Evolution of FinFET:

- For double gate SOI MOSFETs, the gates control the energy barrier between source and drain effectively.
- Therefore, Short Channel Effects(SCE) can be suppressed without increasing the channel impurity concentration.

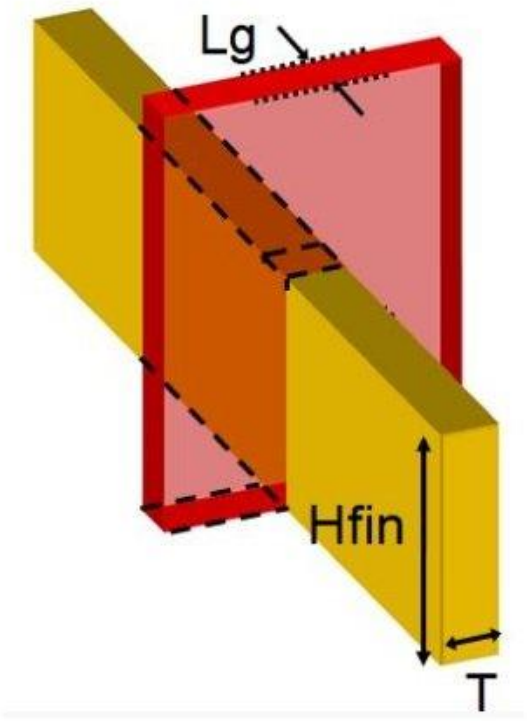

Fig.2.2 structure of FinFET

Fig shows the FinFET dimensions, where

- Lg: Gate length
- T: Fin thickness
- Hfin: Fin height
- W= transistor width (single fin)
- Weff= effective transistor width(multi fins)

2.1.2 FinFET advantages

- Better control over the channel
- Suppressed Short channel length effect
- Lower static leakage current
- Faster switching speed
- Higher drain current
- Lower switching voltage
- Low power consumption

2.1.3 FinFET Disadvantages

- Difficult to control dynamic vth
- Higher parasitic due to 3-D profile
- Very high capacitances
- High Fabrication cost
- Corner effect: electric field at the corner is always amplified compared to the electric field at the sidewall. This can be minimized using a nitrate layer in corners.

Chapter 3
SRAM

3.1 Introduction

SRAM is a volatile memory which operates as fast as the logic circuits, consuming a very low amount of power in the hold (standby) mode. An additional advantage of the SRAM cell is, it does not use extra fabrication cost because the fabrication process is the same as logic gates. These characteristics of SRAMs cannot be attained by the other memories such as Flash memories and DRAM. SRAMs are used as caches and used to interface between DRAMs and CPU. The SRAM array occupies one-fourth area of integrated circuit (IC) chip in today's time. Therefore, the characteristics of any (IC) chip such as supply voltage, power consumption and operating speed, and size is greatly defined by the characteristics of their SRAM memory. Consequently, to design an SRAM Architecture, a major requirement to get good performance, low cost, low power dissipation, and reliability.

3.2 History of SRAM cell

A concept introduced earlier was the high-R_L [30] cell which is a combination of four transistors SRAM and two high resistivity poly-silicon layer resistances which are used as a load of the inverter as shown in figure 2.1

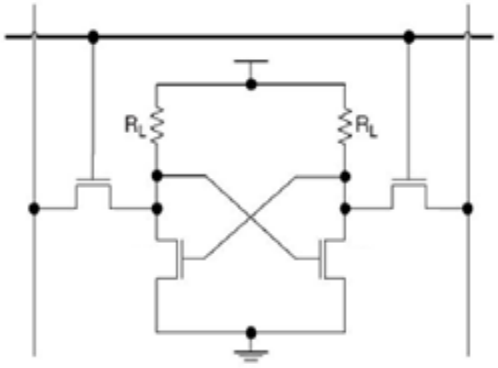

Fig.3.1 4T SRAM cell.

At lower supply voltages it is very difficult to operate with high R cell because poly-silicon layer load resistance consumes more power. After that 6T SRAM cell was introduced which is a

combination of four NMOS transistor and two PMOS transistor, Even though the 6T cell uses PMOS transistors as a load which increases the area of the cell, but it does not require further process to logic process. As well the load PMOS transistors in the SRAM bit-cell pull up the bit-cell nodes voltages fast, Because of that 6T SRAM bit-cell can operate at lesser power supply voltages than a high R SRAM bit-cell.

3.3. SRAM Architecture

A cache memory consists of SRAM cell array with peripheral circuitries such as pre-charge circuit, a sense amplifier, write driver ciruit and address (column/row) decoder, etc.

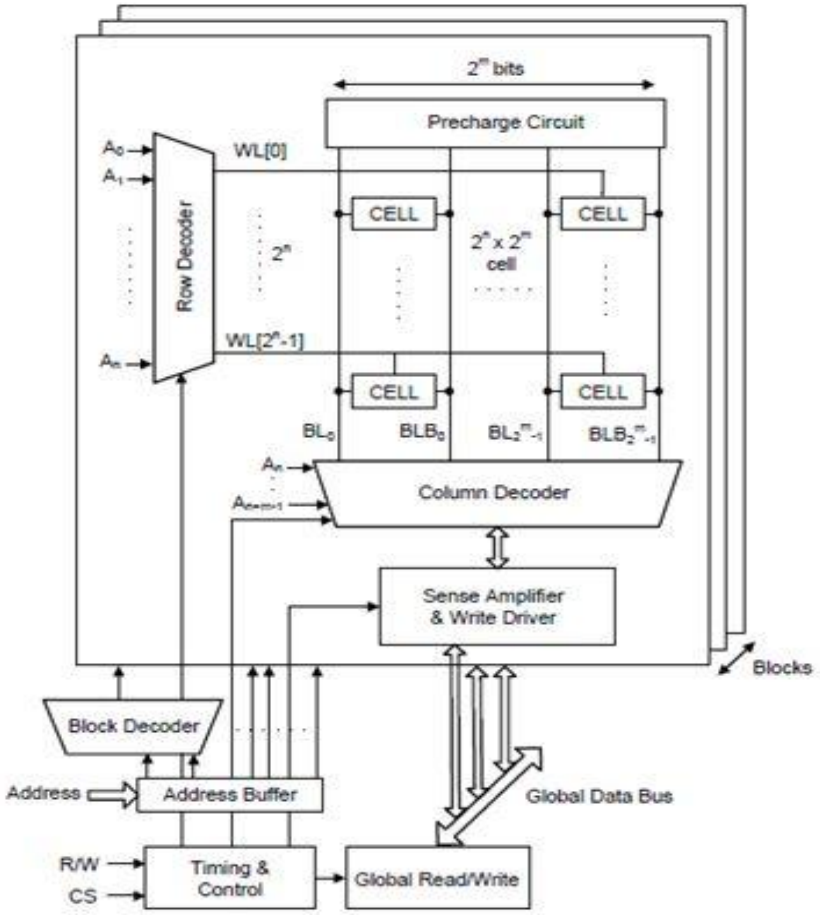

Fig3.2 Architecture of SRAM

These peripheral circuitries allow writing and reading into the array. SRAM cell array is two-dimensional arrangements of 2^n rows and 2^m columns. The single cell holds a single bit; each row is connected to the particular world line. And each world line is connected to the' number of bit-cell. Figure 2.2 shows the SRAM architecture with all the peripherals and control signals.

3.3.1 Function of SRAM Architecture

Figure 2.3 shows the block diagram of SRAM cell architecture. First, the process starts from the **Address latch**- It is a used transferring data as well as also used carrying address. When ALE is disable, it allow address bus to transfer data and when is enable it wll carrying address.It which receives the address.

- The higher order address bits are connected to the row decoder which selects a particular world line of the memory bit-cell array.
- The lower address bit goes to the column decoder which selects the particular bit-lines column.
- Read and write signal line select the particular read and write operation.
- For reading operation, the selected SRAM cell storage data in the array are amplified by the sense amplifier and transfer to the data out lines through data register.
- For a write operation, input data lines data transfer into the data register and data is written to the SRAM memory bit-cell through write driver circuit.
- Generally, data output and data input lines are same to form bidirectional data lines

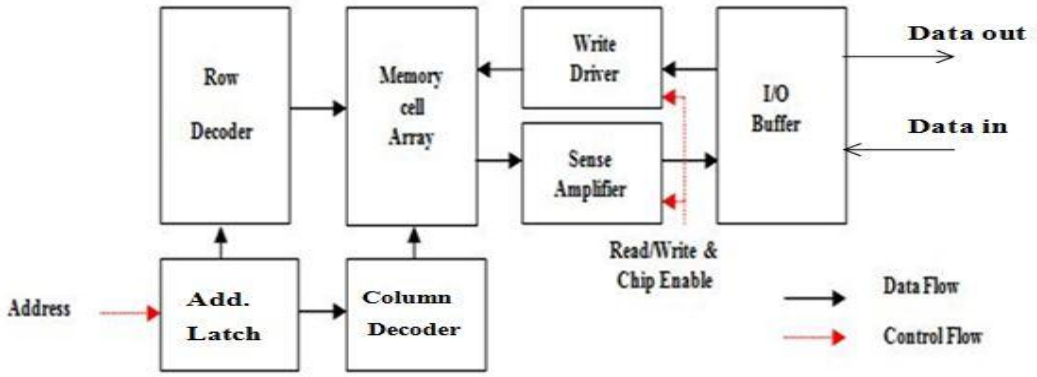

Fig.3.3 Functional Blocks Diagram of SRAM Architecture

3.3.2 SRAM Bit-cell

SRAM bit-cell is basically consist of two inverters which are connected back to back to each other as seen in Figure 3.4 (a) the output of the 2nd inverter (V_{out2}) is connected to the input of the 1st inverter (V_{in1}). If we consider the voltage transfer characteristics of the first inverter (V_{out1} vs V_{in1}) and for the 2nd inverter (V_{in2} vs. V_{out1}) as shown in Figure 3.4 (a) and (b) Respectively. From fig (c), point 'A' shows the output of the 2nd inverter is low and output of the 1st inverter is high, Point 'B' shows the output of the 2nd inverter is high and that the output of the 1st inverter is low. This shows that for any stable condition's outputs are a compliment to each other. This property is made use of to realize static random-access memory SRAM. Figure 3.4 (a)shows back to back inverter (b) shows transfer characteristics of a Meta-stable system, (c) shows the transfer characteristics of a stable system, (d) The curve also known as Butterfly curve. Point 'C' shows a meta-stable operating point, for this operating point when a small deviation is applying at the input of 1st inverter; it gets amplified by the gain of the 1st inverter and is applied to the input of the second inverter and again amplified by the gain of the second inverter. Because of this the value of the values of V_{out1} and V_{out2} increases and the bias point moves away from 'C' until it reaches either Point 'A' or Point 'B'.

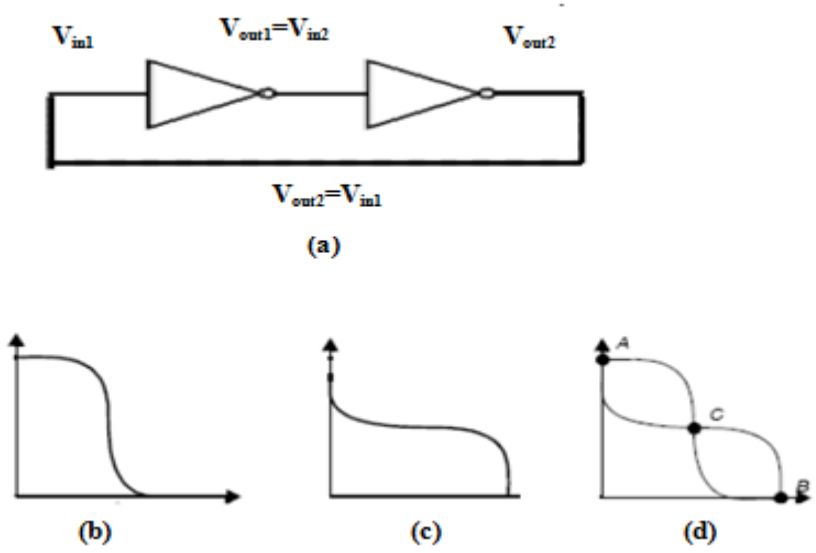

Fig.3.4 (a)shows back to back inverter (b) shows transfer characteristics of a Meta-stable system, (c) shows the transfer characteristics of a stable system, (d) The curve also known as Butterfly curve

3.3.3 SRAM operations:

A. Read Operation: Read operation initial conditions are both bit lines (bl & blb) must be pre-charged up to higher potential i.e. slightly less than V_{DD} and world line (WL) should be high.

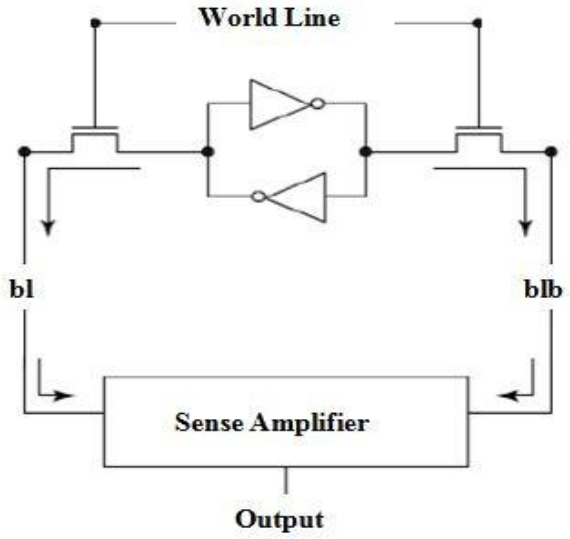

Fig.3.5 Block diagram of the Read operation

So, that access transistors can turned ON and provide path between bit-lines and storage nodes. Depending on the stored data value, any one of the bit line will start discharging through pull down transistor and that small voltage difference created across bit lines is sensed by the sense amplifier and it will give amplified data at output. Figure 3.5 shows the block diagram of read operation.

B. Write Operation: Write operation initial conditions are, both the bit-lines should be compliment to each other and WL should be high which will turn ON access transistors. So, we can write the data to the SRAM cell. Figure 3.6 shows the write operation block diagram. The data which we want to write in the memory is given to bit line. Figure 3.5 shows the read operation block diagram. And Figure 3.7 shows the cadence virtuoso schematic of 6T SRAM cell read circuitry.

C. Hold Condition: When WL is '0' both access transistors are OFF, this will not provide any connectivity between bit-lines and storage node this is the case of hold condition. In

this case memory cell stored the same data as the previous data, due to the presence of latching element present inside SRAM memory cell.

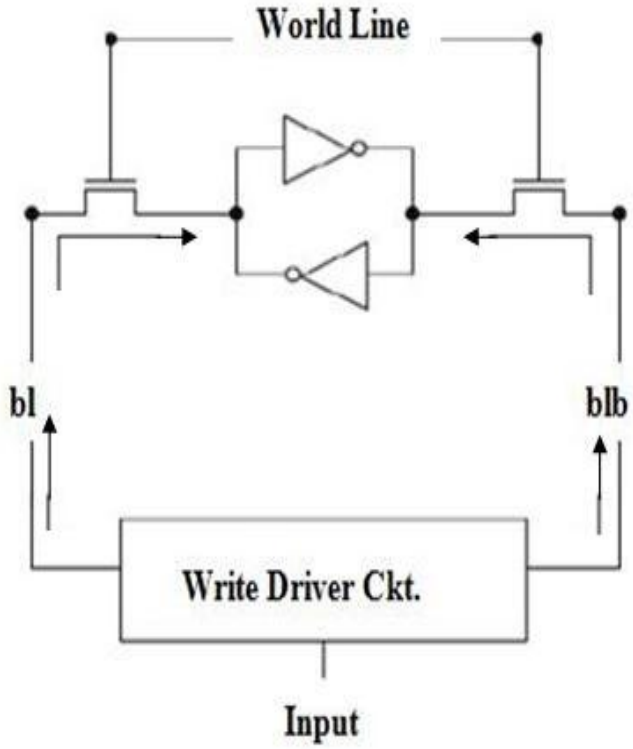

Fig.3.6 Block diagram of the Write operation

3.3.4 Transistor sizing:

Transistor sizing is one of the necessary requirements to improve the stability of SRAM cell. For conventional 6T SRAM cell, transistor sizing is done in two ways. First, for read stability ,the strength of pull down transistor should be more than the strength of the access transistor which is denote as Beta ratio. And for write stability, the strength of the load transistor must be less than the strength of access transistor, which is denoted as alpha ratio.

$$\textbf{Beta Ratio} = (N_{PD}/(N)_{AC}$$

$$\textbf{Alpha Ratio} = (N)_{PU}/(N)_{AC}$$

Where N is the number of fins in FinFET.

Large Beta ratio improve the read stability on the other hand small alpha ratio improve WSNM are preferred. Typically 1.5 to 2 value is required to maintain good RSNM and less than 1 alpha ratio is required to remove the write disturbance. In our work we find optimum value of alpha and beta ratio to reach a fine balance between WSNM and RSNM.

Pre-charge circuit is one of the important circuits for SRAM Architecture. Before each read and writes operation bit-line should be at the equal potential for meaningful operation. This pre-charged ckt. is used to pre-charge both bit lines voltages upto the higher potential. Figure 2.10 shows the pre-charge ckt. which consists of three PMOS transistors. In which two PMOS transistors used as pull-up and a PMOS which is used to equalize the voltage on both bit lines named as equalizer. This pre-charge circuit is controlled by Pre_C signal. Pre_C signal is an active low signal, it always keeps low voltage excluding write and read operation. The single pre-charged circuit is used for a single column of SRAM architecture. Single column bit-lines are generally connected with 32 to 128 SRAM bit-cells, Due to a large number of cells load capacitance will increase on bit lines. So, the size of the pre-charge transistor should be more, Hence it can provides a large driving current, to drive the bit lines column which are having large parasitic capacitances. A huge amount of power dissipation occurs due to the discharging and charging on bit lines during write and read operation. So, to improve the performance, pre charging of bit lines should be in an efficient way [31] [32].

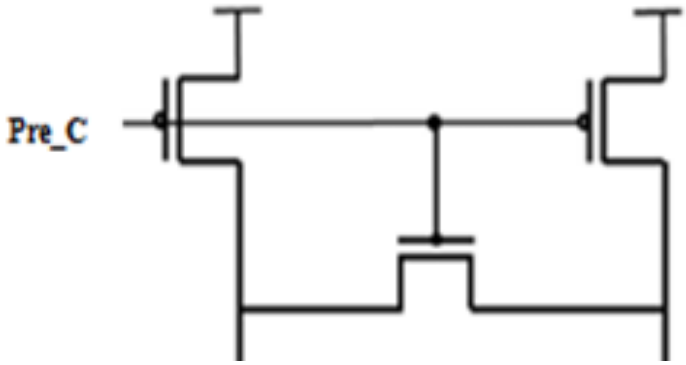

Fig.3.8 Pre-charged Circuit Diagram

3.3.5. Sense Amplifier:

Sense Amplifier is read circuitry which will help us to read the memory data from the SRAM cell. This circuit amplifies the small potential difference which develops across bit lines to the full swing output during read operation. This circuit is generally used to increase the speed of reading operation. Some of the other tasks such as power reduction, restoration of original data and reduction in delay are also performed by this circuit. The performance of memory is enhanced by dropping power consumption and the delay.

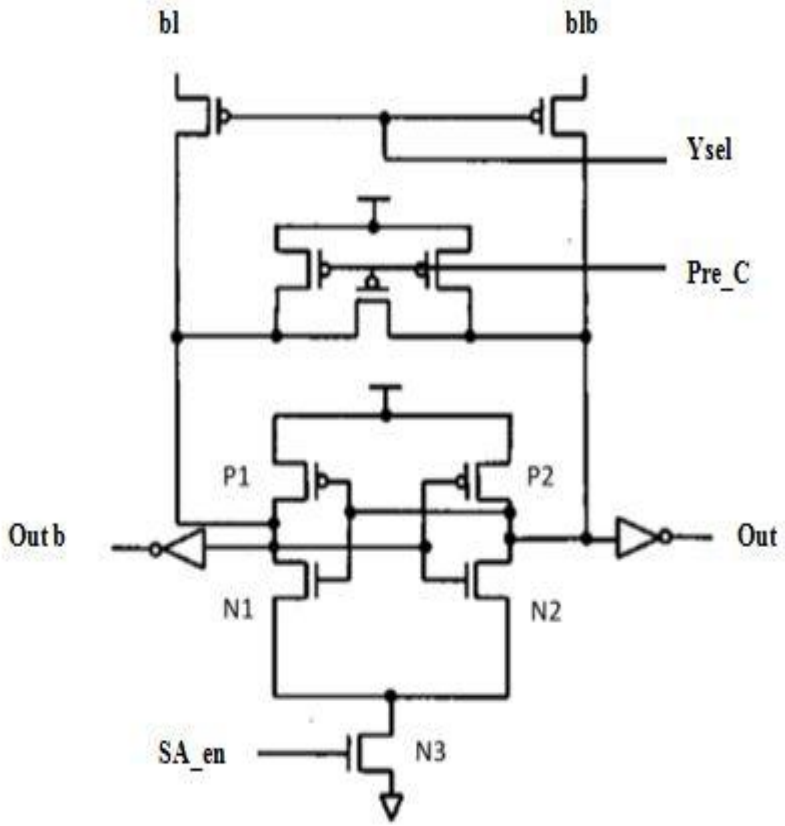

Fig.3.9 Diagram of Voltage-Mode Sense Amplifier

Figure 3.9 shows the differential voltage mode sense amplifier. The sense amplifier is enabled when signal SA_en is logic high and one of the bit line voltage is discharged up-to-the ground, through access transistor to the pull-down transistor. If the voltage of bl is less than the voltage of blb bit-line then this circuit gives active low full swing output i.e. logic '0'. Similarly, If the

voltage of blb is less than the voltage of bl then this circuit give active high full swing output i.e. logic '1'. Figure 4.10 shows the block diagram and timing diagram for three different read '0' cycle for t_1, t_2 and t_3.

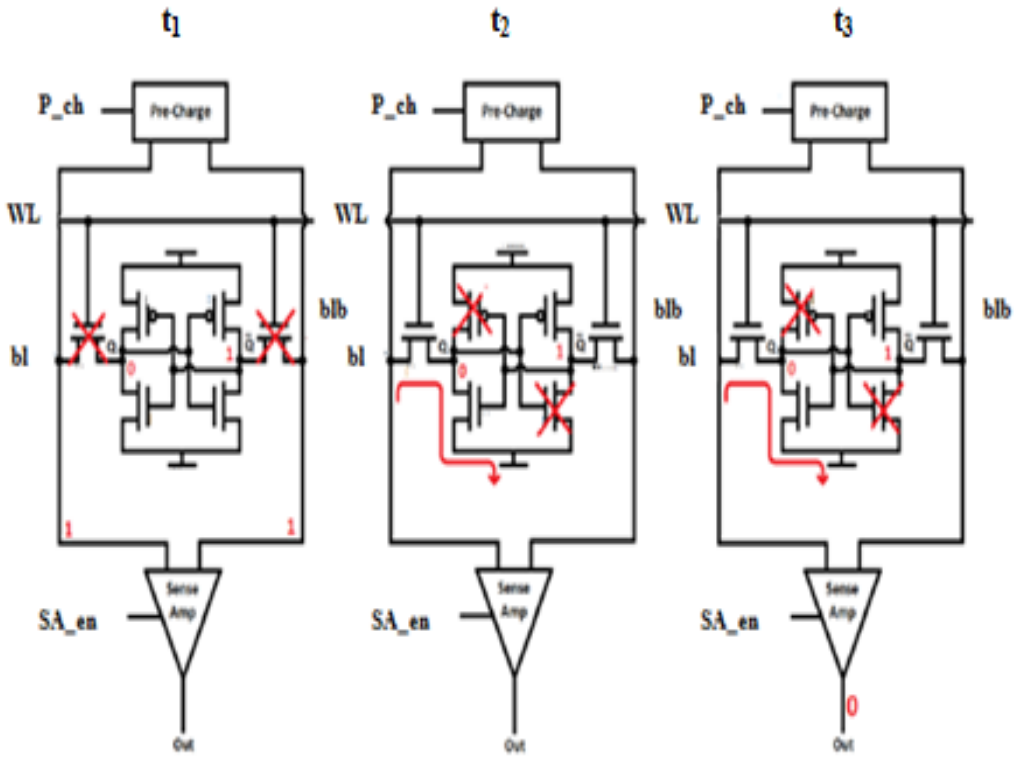

Fig.3.10 Block diagram and timing diagram for three different read '0' cycle for t_1, t_2 and t_3.

3.3.6. Write Driver:

Through this write, driver circuit data is written to the memory cell. Before each writes operation, both bit lines should be precharged. The write operation is performed by enabling the WE signal. N1, N2, N3, and N4 are the stack NMOS transistor used as the pass transistor as shown in figure 4.11. The source of N2 and N4 NMOS transistors are grounded. 'Data in' is the input data signal. To write logic '1', bl should charge up-to-the higher potential, simultaneously blb should discharge up-to-the lower potential. To write logic '0', bl should discharge up-to-the lower potential and blb should charge up-to-the higher potential. The single Write driver circuit

is used for a single column of SRAM architecture. So, that write driver circuit transistor sizing is quite large to provide large driving current .

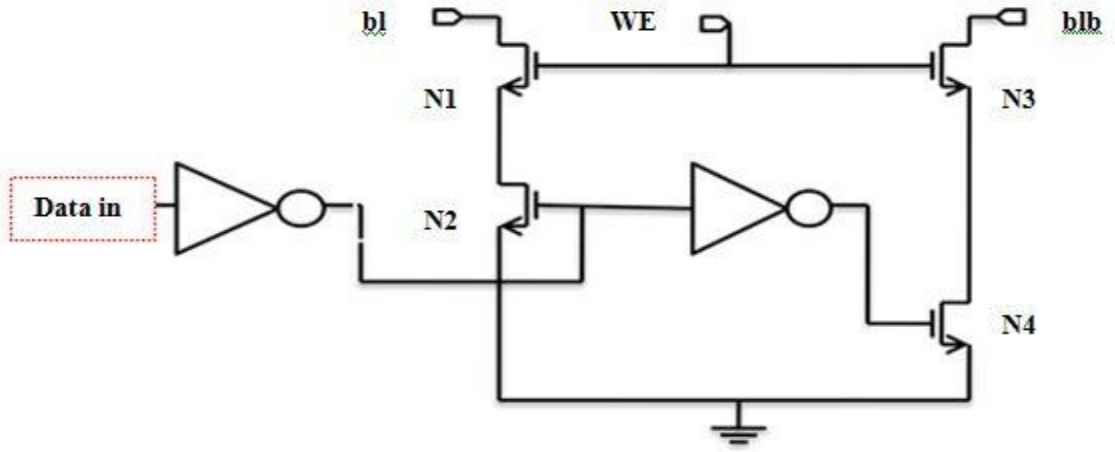

Fig.3.11 Write Driver Circuit Diagram

3.3.7. Address Decoder:

Address Decoder is a circuit which used to select particular world line or particular row of SRAM array at a time depending upon the decoder inputs. Having every address assigned to only one pin is waste of space. So, most of the memories use a decoder to reduce the number of pins [29][30]. Address decoder uses the combinations of logic 1's and logic 0's according to the unique input address. In some of the cases, pre-decoder is used to reduce a further number of pins. Figure 4.12 is the simple and gate based 4X16 decoder, which has 4 inputs i.e. A0, A1, A2,

A3 and 16 outputs namely WL(0) to WL(15). To explain one of the considerations If A3= '0', A2= '0', A1= '0' and A0= '1'then the WL (1) word line is selected.

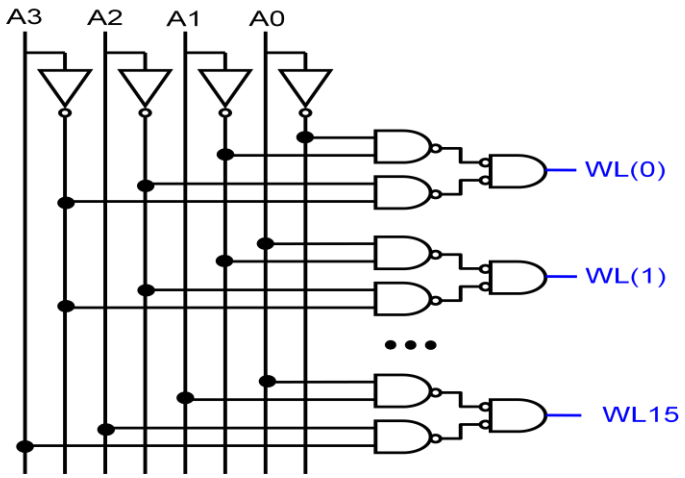

Fig.3.12 Address Decoder Circuit Diagram

3.3.8. Data Input and Output Lines:

Data input and output lines or buses are requiring bringing the input and output information of memory cell. Memory IC does can either have the same input and output data line or they have different input lines and output lines. Same data input and output line reduce the number of buses which save the space of IC. Same I/O data lines needed tri-state buffers at the output so that data only saw at during read operation as shown in figure 4.13.

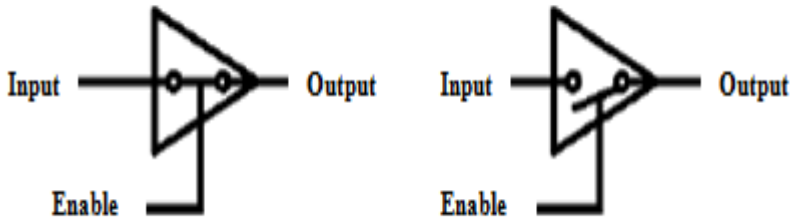

Fig.3.13. Tri State Buffer

The six different parameter that affect the timing performance of SRAM chip are shown through figure 3.13 timing diagram. The input from the external source are usually known as clock input represented by the first line of timing diagram. This clock speed is directly correlated to all the timing information of SRAM chip. The time period of clock cycle is represented by T_{cycle}. This T_{cycle} is minimum amount of time necessary to execute successive read/write operation of memory. It is not mandatory the same minimum amount of time require for read/write operation.

in spite of this, a system will generally use the same division of time to execute read/write operation in order to make simpler design .The maximum amount of clock frequency that can be tolerated by the SRAM chip is represented by 'f'. And this 'f' is inversely proportional to the clock time period as shown in equation ….(2.1)

$$f = 1/T_{cycle} \qquad \ldots\ldots(2.1)$$

The time required to set up the system before execution of read/write operation called setup time denoted by $T_{setup.}$ The set up time is taken into the consideration when precharging the bitline and when cell is ready to write the data.

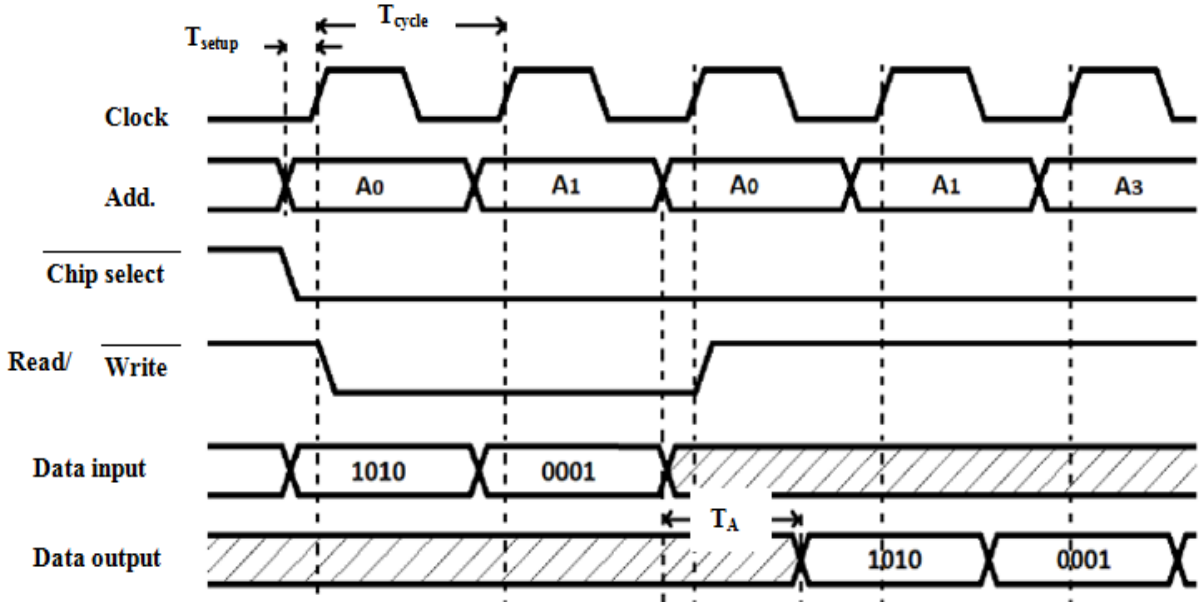

Fig 3.14 Timing Diagram of SRAM chip

The particular location of memory is denoted by the particular address as shown in the second row of the timing diagram. Read delay or read access time are measured w.r.t. the time when an address first appears. To operate a particular chip one enable signal is there i.e. chip select bar. The bar is used because the chip select signal is active low signal mean chip operate when the signal voltage is low otherwise it will go into the standby mode. The read and write control on-

chip is represented through the fourth line of the timing diagram. When this signal is low write operation will perform because the write operation is an active low signal, and whatever the data stored on that corresponding address location is transfer to the date in line which is represented by the fifth line of a timing diagram. If forth line signal is active high then read operation will perform and whatever the data stored on that corresponding address location is copied to the data output line. T_{AC} is read access time represented on the sixth row of the timing diagram. The time requires to perform read operation after the clock signal known as read access time. If $T_{AC} > T_{cycle}$, false data would be seen at the output and the SRAM chip would not be able to perform correct read/write operation for further cycles. The read access time is usually between 20% to 80% of the cycle time [31].

Chapter 4
Stability and performance Analysis of SRAM cell

If the bit-cell of SRAM are not working in ideal conditions, it will fail to retain the cell stored value. Weak SRAM cells are the cause of stability fault. There are different degrees of stability faults. Some SRAM cells may become unstable under some conditions and, others unstable for all conditions. Temperature, supply voltages, process variations and noise [32] are some other parameters that affect the stability of SRAM cells. So, to design a new SRAM cell, stability is one of the primary concerns. Stability stands the immunity of SRAM cell against the noise to retain the stored data. It quantified the maximum amount of the noise voltage SRAM can withstand without flipping the data at the storage node. Butterfly curve is one of the most common approaches to calculating the stability of the SRAM bit-cell. The disadvantage of this approach is, it only calculates the stability in term of voltages. The mathematical calculation is still needed to find stability in term of current. To calculate the SRAM bit-cell stability in both terms current and voltage through single simulation process, N-curve is used.

4.1 Stability Metrics of Memory

Conventionally cell stability has been calculated through noise margin for each read, write and hold operation. Noise margin represents the presence of bearable noise in terms of current and voltage. Here the stability noise margin is derived through two ways on the basis of internal and external nodes of SRAM memory cell. For both cases, noise margin represented in terms of voltage and current. Stability metrics define on the internal cell node is further calculated through two ways. First one is the butterfly curve method which is widely used previously, but through this method, many simulation processes have been done for different operation and it gives stability in terms of voltage only. And the second one is N-curve method, through this method all the stability parameters can be calculated in

a single simulation process. This method gives stability in terms of current and voltage. So, we used N-curve method in our thesis to calculate stability.

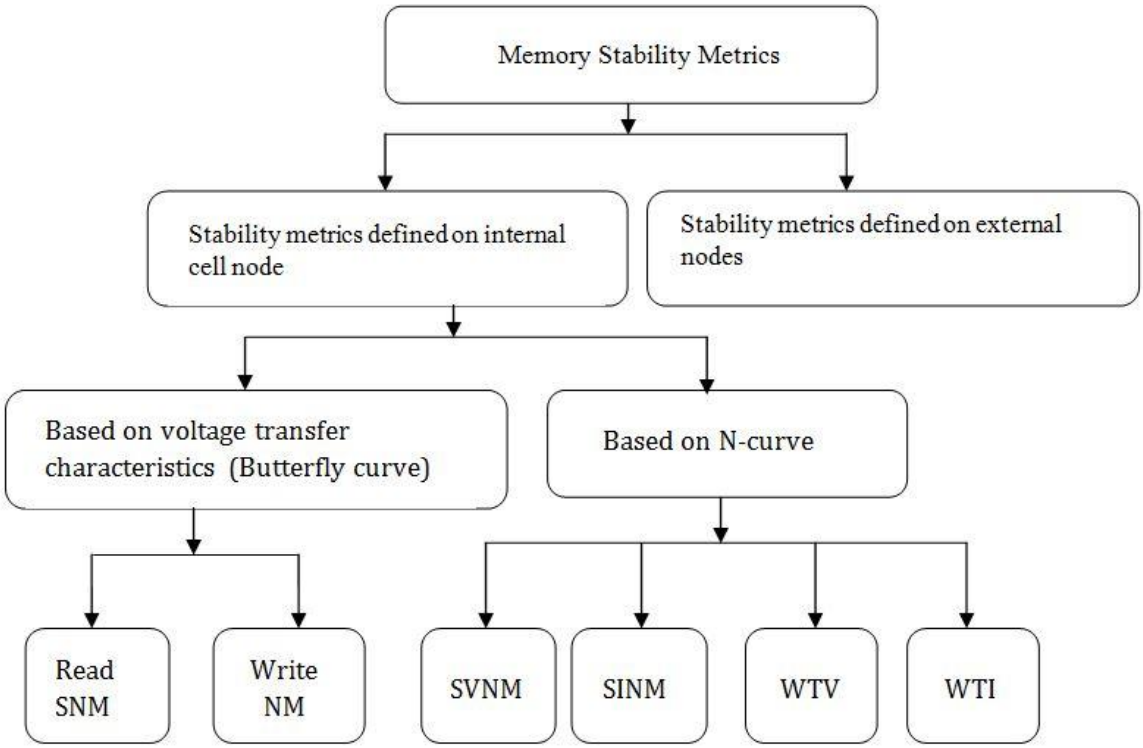

Fig. 4.1 Hierarchy of Memory Stability Metrics

4.2. SRAM cell Design Metrics

A. Read and hold stability:

Static current noise margins (SINM) and Static voltage noise margin (SVNM) are two parameters which are used to find out read and hold stability. SINM and SVNM are geometrically evaluated using N curve metric method. Before the content change, an extreme amount of DC current flow through the SRAM cell called SINM. It indicates the peak value of current between points 'A' and 'B' of N-Curve as shown in figure 4.2 (b). Before stored data change, the maximum bearable DC noise voltage at the storage node defined as SVNM. It indicates voltage variation between points 'A' and 'B' of N-curve as shown in figure 4.2 (b).

B. Write-ability:

The writeability of the SRAM cell is determined by the write trip current (WTI) and write trip voltage (WTV). When V_{DD} is fixed at the bit lines i.e. bl and blb, the maximum value of the

current flow mandatory to write the cell data defined as WTI. It indicates the peak value of negative current between points 'B' & 'C' node of N-curve as shown in figure 4.2 (b). When V_{DD} is fixed to both of the bit-lines, the necessary voltage drops to change the storage node data of a cell called WTV. It indicates the voltage variation between points 'B' & 'C' node of N-curve as shown in figure 4.2 (b).

C. Active or read/write power dissipation:

Active power composed of switching power which is consumed during the charging and discharging of a load on SRAM cell. Active power can be calculated by write trip power (WTP) and static power noise margin (SPNM) where WTP is the multiplication of WTI and WTV, and SPNM is the multiplication of SINM and SVNM.

D. Read Current:

Read current is the current travelling from the pre-charged bit-line to the conducting pull-down transistor through access transistor during read operation [33] as shown in figure 4.2. For good cell Read current should be as high as possible.

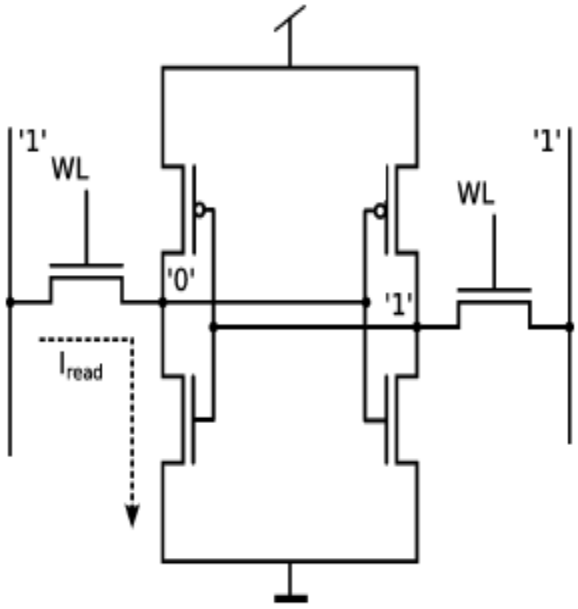

Fig.4.2 Read current of 6T SRAM cell

N-curve based Stability Analysis Metrics

N-curve is a curve which holds the detail about write and read stability that allows the complete functional analysis in terms of reliability. There are four parameters i.e. SVNM, SINM, WTI and WTV which are identified by using N curve. The first step in drawing the N-curve is to pre-

charge the pair of bit lines i.e. BL' and BLB up to V_{dd} and simultaneously word line is triggered to 'V_{dd}' as shown in figure 4.3 (a). In the second step, variable voltage source Vin is attached to the storage node VR that variate the voltage from 0 to V_{dd}.

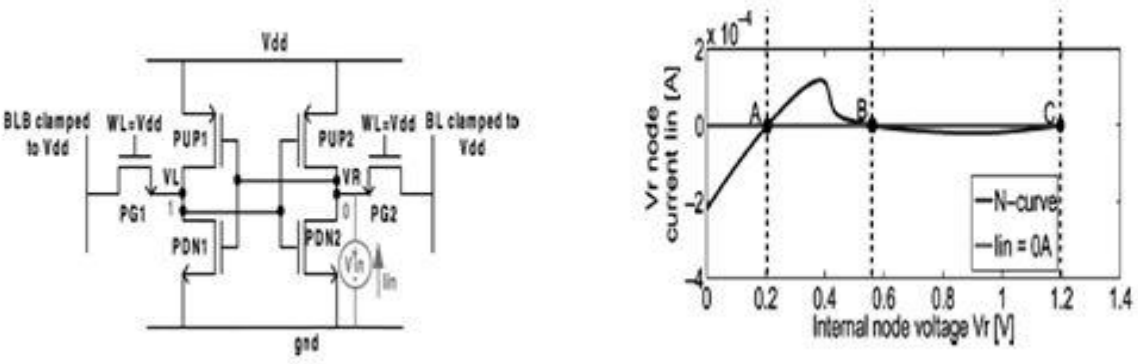

Fig.4.3 (a) 6T SRAM cell Schematic for N curve analysis and (b) 6 T SRAM cell N curve

The simulated result of N curve shows the relationship between Vin and Iin. Iin is the measured current when Vin voltage is varied from 0 to Vdd. Figure 4.3(b) of N curve shows Iin on Y-axis and Vin on X-axis. Basically, N-curve has 3 points i.e. 'A', 'B' and 'C' that crossing zero voltage line. The voltage variation between points 'A' and point 'B' shows SVNM. The highest value of current between points 'A' and 'B' shows SINM. In a similar way voltage dissimilarity between points 'B' and 'C' shows WTV. The maximum negative current among 'B' and 'C' shows WTI as shown in Figure 4.3(b).

4.4. Dependency of Average Power on various Parameters

4.4.1. Dependence on the supply voltage

Table 4.1 shows the effect of supply voltage on average power. As we can see from Table 4.1 These both are directly proportional to each other i.e. on increment of supply voltage average power is also increased. Below V_{dd} /2 bit-cell performance will be degraded that's why we vary the voltage from V_{dd}/2 to V_{dd} i.e. from 300mV to 600mV. At 300mV, we get minimum average power i.e. .0436µW , And at 600mV, we get maximum average power value i.e .688µW.

TABLE 4.1 Average Power For Different Supply Voltages

Supply Voltage (V)	Average Power (μW)
300m	.0436
400m	.149
500m	.359
600m	.688

4.5. Dependence of Read and Write delay on various Parameters

4.5.1. The dependency of supply voltages

Table 4.3 shows the dependency if supply voltage on Read and write delay for both data '0' and '1' operation. From the table, we can see that with an increase in supply voltage there is not any effect on read and write delay for the reason that of single SRAM cell has been taken under consideration. At 600mV supply voltage, the minimum delay can see in write '0' operation i.e. -66.61 nsec. for the reason that, in read operation, more swing occurs in charging and discharging of bit-lines.

TABLE 4.2 Read/Write Delay for Different Supply Voltages

Supply Voltage(V)	Read/Write delay for different supply voltages	
	Read '1'	*Write '1'*
300m	54.44	157.4
400m	45.37	103.4
500m	40	78.92
600m	35.93	66.61

4.5 Dependence of Stability on various Parameters

4.5.1 Dependency of the Alpha ratio :

Stability is basically depends on alpha and beta ratio. Write stability is depends on alpha ratio. For better write stability, width of access transistor or pass transistors is always greater than pull up transistors.

4.5.2 Dependency of Beta Ratio :

This is the other ratio which is related to stability. Read Stability of cell is depends on the beta ratio. For better read stability the strength of pull down transistors is greater than the strength of access transistors.

Chapter 5.
Proposed 10T SRAM Cell

In proposed FinFET based 10T SRAM consist of two core circuitry latch which are consist of PN1, NM1, PN2, and NM2 transistors. NM5 and NM6 are access transistors or pass transistor which is used to charge or discharge path during a read operation and transfer the data during a write operation. NM3 and NM4 transistor called dynamic loop cutting transistor which helps to improved write static noise margin. NM7 and NM8 transistors are consisting a read decouple structure which is improved the read static noise margin and resolve the access transistors conflict sizing. Due to read decouple structure facilitates the change in dimension of NM3 and NM4, it helps to improved write margin of SRAM cell. In this cell vary the transistors size just because of read decouple mechanism. This cell is also called a single ended read.

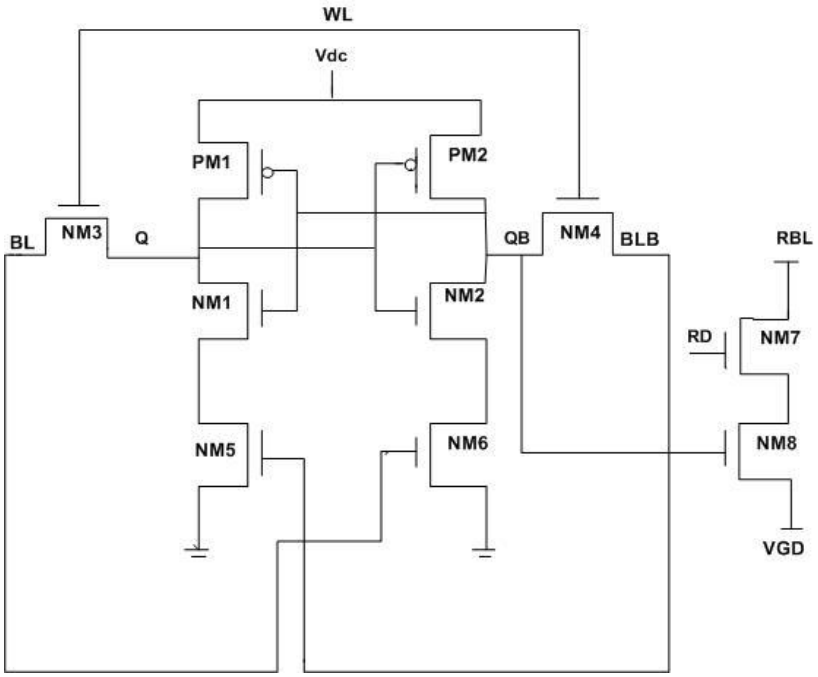

Fig.5.1 10T SRAM Cell

In this cell, RSNM and WSNM increase by reading decouple structure and dynamic loop cutting transistor respectively. Read power is reduced by using the stacking of transistors. A virtual ground terminal is used to minimize the leakage current.

In this cell, two technique are used

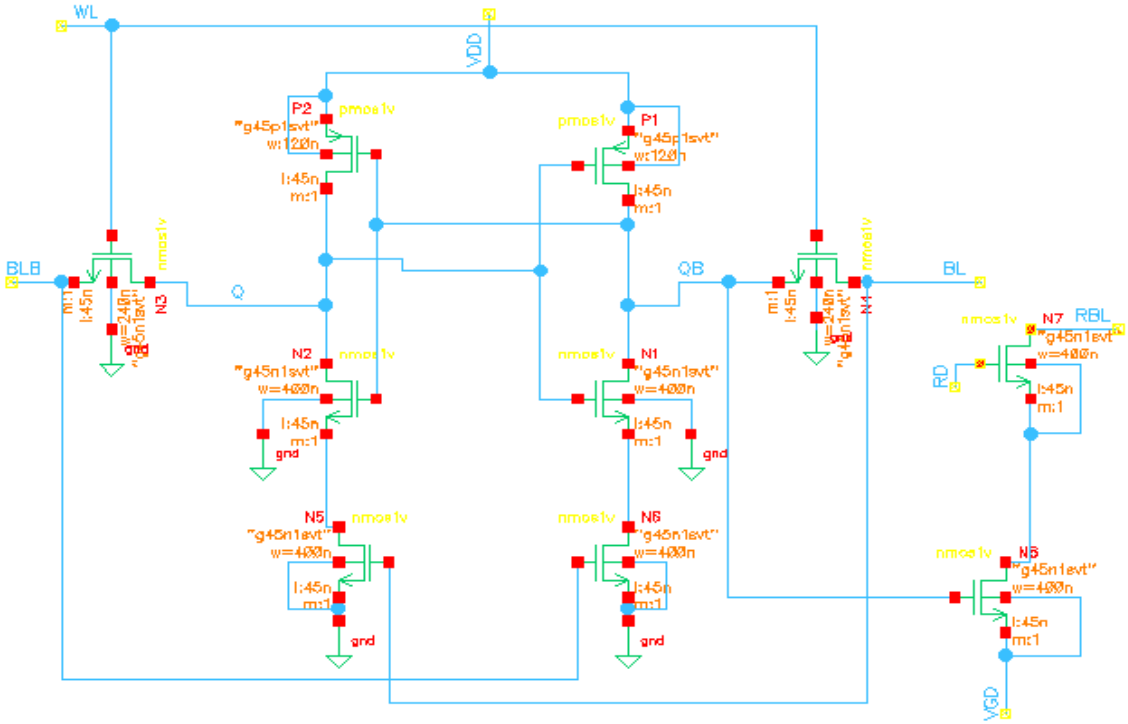

Fig.5.2 Schematic diagram of Proposed 10T SRAM Cell

5.1. Single END Decoupled SRAM

In a read operation, bit line are connects to pre charge with vdd while VGD connect with GND. RD Is remains at VDD to turn on transistor N6. Word line remains at logic low to separate node Q/QB from BL/BLB. The result available at RBL which depends on storage data node at Q or QB. Let us assume, during read operation Q=0, N1, P2,N3 and N4 transistors are turn off. N6 turn on due to RD connect with Vdd.

5.2 Write Technique With differential loop cutting

In write operation begin with VGD and WL connected with vdd , RD remains at logic low. Bit lines are connected GND/Vdd or Vdd/GND depending on written data on storage node Q and QB .For example write “0” at storage node Q by replacing “1” then BL connect with GND, BLB at logic high , loop cutting transistor N5 activate and N6 deactivated. Due to this left side core

latch of inverter disconnect from GND. It reduces pull down power of left inverter while increase pulls up power.

Table 5.1.Shows the different modes of 10T SRAM cells which are given below.

Signals	**Read**	**Write '0'**	**Write '1'**	**Hold**
RD	'1'	'0'	'0'	'0'
WL	'0'	'1'	'1'	'0'
VGD	'0'	'1'	'1'	'1'
BL	'1'	'1'	'0'	'1'
BLB	'1'	'0'	'1'	'1'
RBL	'1'	'0'	'0'	'0'

Chapter 6
Result and Discussion

Read operation: For read operation, read data available on RD and taken out from RBL. BL and BLB connected through precharge. RD and RBL connected through Vdd. WL and VGD connected with GND. Let us assume RD connected with logic '0', transistor NR2 is turn on to create logic '1'. The node voltage QBAR activate transistor NM6 and it discharge through NM5 and NM6 transistor. Read data through RBL depending on the bit stored at storage node. Fig 6.1 shows the read operation of Proposed 10T SRAM cell.

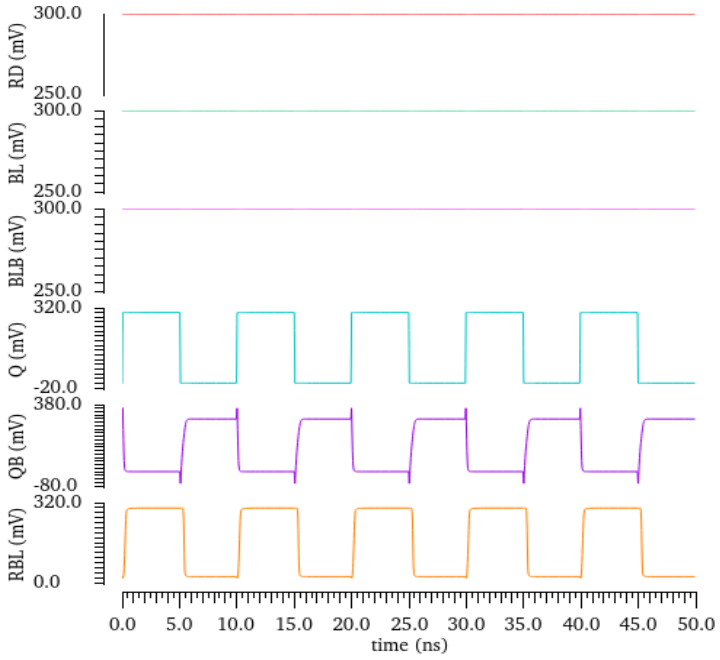

Fig.6.1 Transient waveform during read operation of 10T SRAM cell.

Write Operation : In write operation BL and BLB connected through logic '0/1' and logic '1/0' respectively depends on whether is written '0/1'or '1/0'. Let us assume write '0' or write '1' then BL is connected through '0' or '1' and BLB is connected with '1' or '0'. WL and VGD connected with Vdd. RD and RBL connected through GND. Fig. 6.2 shows the transient waveform during write operation o 10T SRAM .

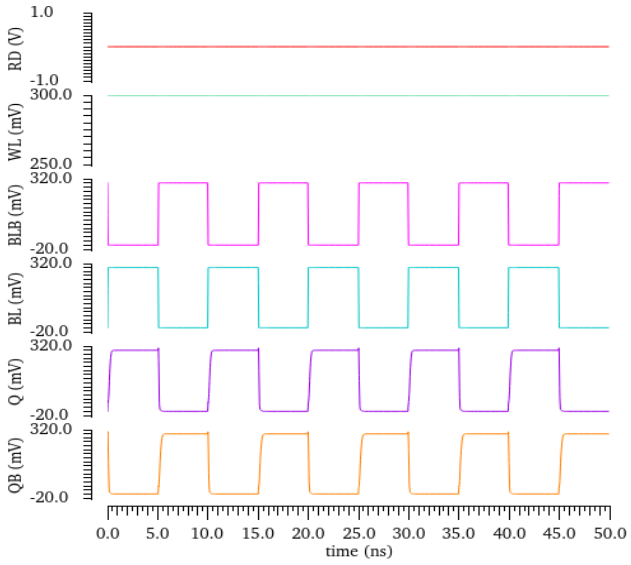

Fig6.2. Transient waveform during write operation of 10T SRAM

6.1. Stability

Stability is the important factor in SRAM which measure by the N curve or butterfly curve in terms of SNM. SNM define the maximum value of DC voltage that can be tolerated by SRAM cell without changing the store bit. There are two types of stability

6.1.1 RSNM (Read Static Noise margin)

For better read operation, RSNM should be high. To get better read stability the strength of pull down transistor is greater than strength of pass transistor. In Proposed 10T SRAM has high read stability because here is used read decouple structure technique. RSNM has been measured by inserting a square fitting box in obtained butterfly lobes. I have observed stability at 300mV to 600mV which are shown in table 6.1. Fig.6.3 shows the graph of stability of cells.

Table.6.1 Shows the read stability at different supply voltage

	RSNM(mV)					
Voltage(mV)	P10T	S10T	9T	8T	7T	6T
300	138	90	140	90	75	72
400	190	130	190	112	130	90
500	225	170	215	140	145	110
600	295	195	230	165	160	145

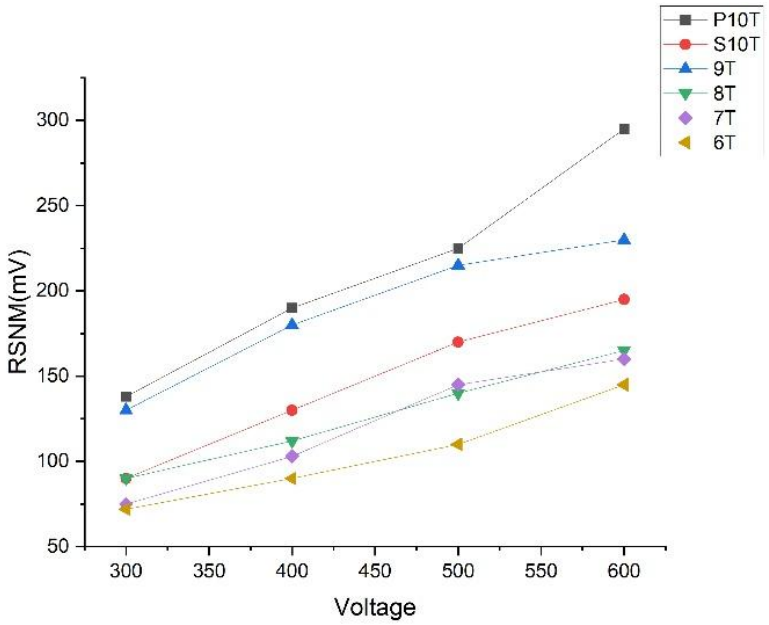

Fig.6.3 Read stability at different supply

6.1.2 WSNM(Write Static Noise Margin)

For better write stability, the strength of access transistor is greater than strength of pull up transistor. Proposed 10T SRAM cell has been higher stability. I have observed WSNM at 300mV to 600mV which are shown in table 6.2. Fig .6.4 shows the graph of write static noise margin.

Table.6.2 shows the different value of WSNM at different supply voltage

	WSNM(mV) at different supply voltages					
Voltage(mV)	P10T	S10T	9T	8T	7T	6T
300	207	153	152	159	99	147
400	253	192	175	200	147	181
500	306	237	224	236	186	223
600	367	285	261	284	223	259

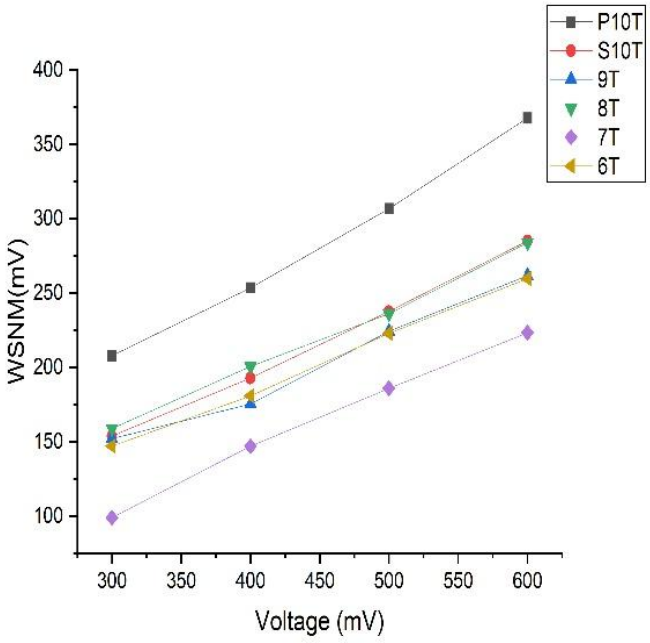

Fig.6.4 Write stability at different supply

6.2 Power dissipation:

In digital circuit, power plays the important factor. SRAM consume 70% of power of silicon chip on device. SRAM is widely used in portable device so it has low power consumption. There are two types of power consumption static and dynamic power. Dynamic power is consume at the time of read/write operation in SRAM. Static power is consuming at the time of hold state. Proposed 10T SRAM cell consume less power in comparison with other cell but write power less except S10T and 7T.

6.2.1 Read Power

In proposed 10T SRAM cell has lowest power at read operation. It consumes less power compared with other cell. I have observed read power at different supply voltage, range of supply voltage is 300mV to 600mV. Table6.3 shows the observation of read power and fig 6.5 shows the graph of read power.

Table.6.3 shows the read power of proposed 10T SRAM cell.

	Read power(µW) at different supply voltages					
Voltage(mV)	P10T	S10T	9T	8T	7T	6T
300	.042	.095	.046	.84	.064	.0436
400	.14	.35	.153	.136	.232	.149
500	.335	.861	.365	.319	.567	.359
600	.64	1.667	.7	.607	.80	.688

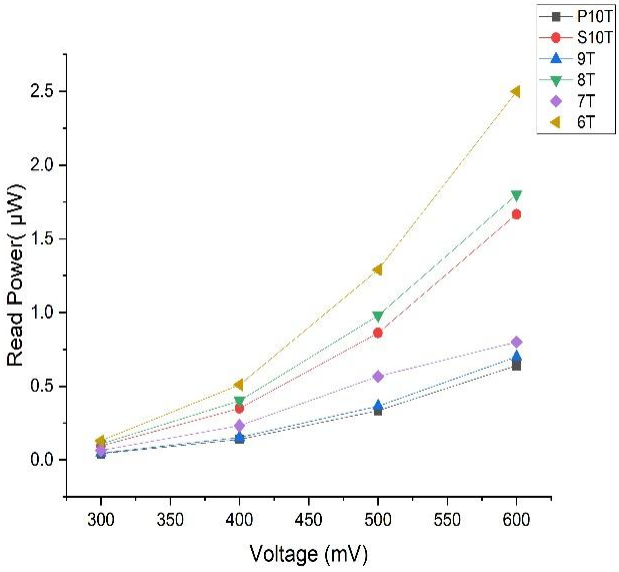

Fig.6.5 Write power at different supply

6.2.2Write power

In proposed 10T SRAM cell write power is not good compared with some cell. Propsed 10T SRAM cell write power less than 9T,8T and 6T bt higher than S10T and 7T. I have observed write power at different supply voltage, which are shows in table 6.4. Fig 6.5 shows the graph of write power.

Table.6.4 shows the write power at different supply voltages

	Write power(µW) at different supply voltages					
Voltages(mV)	P10T	S10T	9T	8T	7T	6T
300	.37	.363	.473	1.136	.166	.616
400	1.282	1.27	1.685	3.612	.542	1.951
500	3.035	2.894	4.2	8.346	1.259	4.496
600	5.783	5.537	8.45	15.91	2.379	8.853

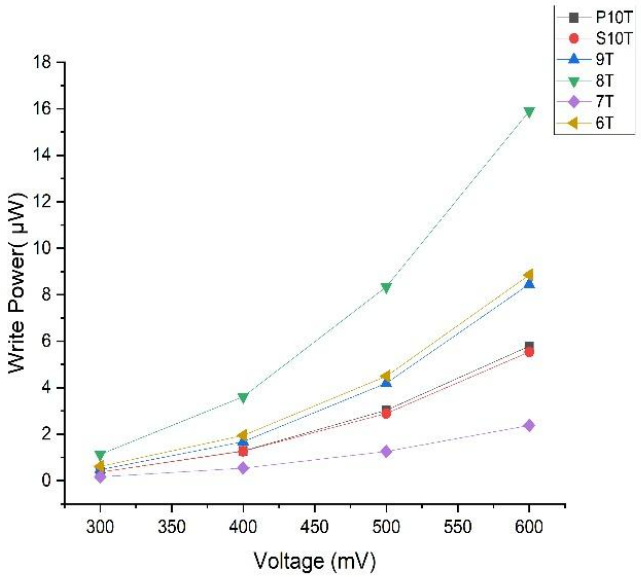

Fig.6.6 Write power at different supply

6.3 Delay/Access Time

In this SRAM cell has less read access time compared to other SRAM cells. In this cell observed the minimum value of read access time. Read delay is improved with other cell but write delay improved in comparison with 7T and 9T**.**

6.3.1 Read access time

During the read operation, the time taken by bit lines to discharge by about 10% of the peak value i.e. called read access time. Delay defines the speed of the cell. Proposed 10T SRAM cell has lowest read delay compared with other cell. Table 6.5 shows the observation of read delay at different supply. Fig. 6.7shows the graph of read access time.

Table.6.5 shows the read access time at different supply voltages

Read access time(pS) at different supply voltage						
Voltage(mV)	P10T	S10T	9T	8T	7T	6T
300	44.81	59.81	63.4	50.66	92.37	54.44
400	32.84	51.28	51.19	41.6	88.84	45.37
500	26.33	46.74	44.65	36.23	88.72	40
600	23.89	43.28	40.22	32.32	85.3	35.93

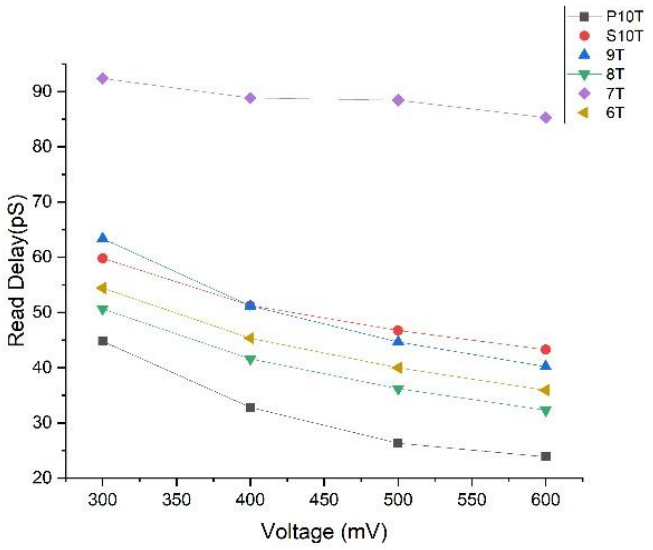

Fig.6.7 Read delay of different supply

6.3.3 Write access time

The time taken between 50% of WL activation to other flip the cell i.e. called write access time. Table 6.6 shows the write access time of all cell. Fig 6.8 shows the graph of write delay of SRAM cell.

Table 6.6 shows the write access time of 10T SRAM cell

Write delay(pS) at different supply voltage						
voltage	P10T	S10T	9T	8T	7T	6T
300	183.2	107	170.7	204.1	209.12	157.4
400	118.9	72.36	110.2	127.8	113.2	102.4
500	91.35	57.27	84.25	95.43	69.7	78.92
600	77.03	48.9	70.69	78.38	47.4	66.61

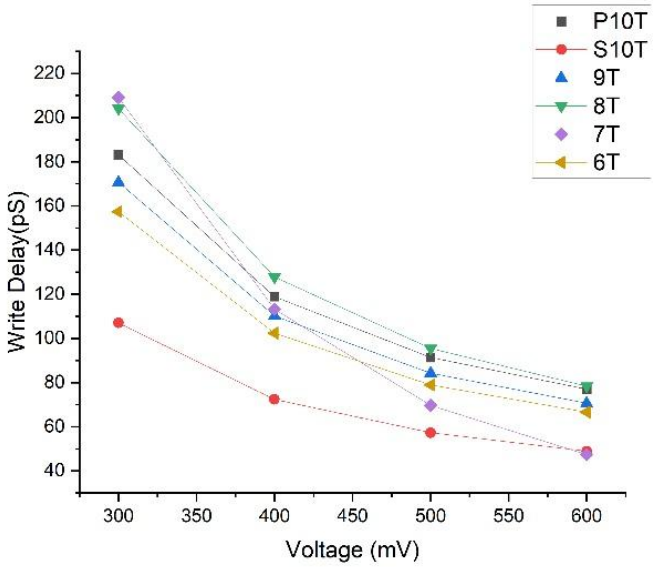

Fig.6.8 write delay at different supply

Conclusion

In as we move towards deep sub micrometer technology as consequences area of integrated circuit gets shrink. So the stability of SRAM cell faces major issue of stability in low supply voltages and deep sub micrometer technology then some effect occurs in CMOS technology i.e. called short channel length effect. To overcome these effect CMOS technology replace with FinFET technology. In 10T cell, loop cutting transistors are utilized to improve the write stability of the cell. Additionally, it reduces the write power dissipation of the cell. The read power dissipation of the cell is also reduced due to single ended structure. The read decoupled structure improves read stability of cell. It concludes that this cell is suitable for low power applications .In this work comparative analysis of conventional 6T based SRAM with FinFET SRAM for 45nm technology and 18nm technology respectively in Cadence virtuoso tool. In FinFET reduction of power and improve the stability as compared to CMOS. In this wrk I have simulated different FinFET based SRAM cells and compared with proposed FinFET based 10T SRAM cell. RSNM is increased with a factor of 1.91 times and 1.53 times as compared to standard 6T and 8T SRAM cells. Write static noise margin is enhanced with a factor of 1.41 times and 1.30 times as reference to conventional 6T and 8T SRAM cells. It has been observed that read power reduces by 62.14% and 45.15% as of conventional 6T and 8T SRAM cells.In addition to this, write power is also significantly reduced by 97.12% and 67.4% as reference to 6T and 8T SRAM cells. Read access time i.e. 1.21 times and 1.11 times has been noticed in proposed cell as compared to other considered 6T and 8T SRAM cells. Write access time of proposed 10T SRAM cell is degraded with the factor of 1.16 times as of 6T SRAM cell whereas it is improved with the factor of .89 times as of 8T SRAM cell.

I have observed improvement of various performance characteristics like RSNM, WSNM, read delay and read power compared to considered 6T,7T,8T,9T, and S10T SRAM cells. FinFET based SRAM cell may be a suitable choice for ultra low power applications. In this compare analysis RSNM, WSNM ,Read power and read delay improved as compared to considered 6T,7T,8T,9T and S10T SRAM cells.

Future Scope

Device Performance can be improved through the change in circuit topology in two ways. The first way by the change in SRAM cell topology which we have already done and the second way is by topology change in other peripherals like reading and write circuitry of SRAM architecture. There is still a wide scope in improvement of topologies in terms of parameters like Delay, power dissipation. SNM etc. It further depends upon the requirement of applications and choice of designer. Needless to say it is of utmost requirement to take care of tradeoff parameters and mismatch values. This work also points towards requirements of statistical parameters and more emphasis towards variation tolerance. Memory design is still an open ended concept with the advent of new parameters viz. PDAP (power delay Area product), normalized equivalents etc. So, future work is to designing of other peripheral to design efficient SRAM Architecture.

References

[1] Taizhi Liu, Chang-Chih Chen, Woongrae Kim, Linda Milor, "Comprehensive reliability and aging analysis on SRAMs within microprocessor systems", Microelectronics Reliability, Volume 55, Issues 9–10,2015, Pages 1290-1296

[2] Tu, Ming-Hsien, et al. "Single-ended sub threshold SRAM with asymmetrical write/read-assist." IEEE Transactions on Circuits and Systems I: Regular Papers 57.12 (2010): 3039-3047.

[3] Sagar Mukherjee, Arka Dutta, Swarnil Roy, Kalyan Koley, Chandan Kumar Sarkar, Impact of lateral straggle on analog and digital circuit performance using independently driven underlap DG-MOSFET, Microelectronics Journal, Volume 46, Issue 11, 2015, Pages1082-1090,

[4] N. Gong, S. A. Pourbakhsh, X. Chen, X. Wang, D. Chen and J. Wang, "SPIDER: Sizing-Priority-Based Application-Driven Memory for Mobile Video Applications," in IEEE Transactions on Very Large Scale Integration (VLSI) Systems, vol. 25, no. 9, pp. 2625-2634, Sept. 2017.

[4] R. Saeidi, M. Sharifkhani and K. Hajsadeghi, "A Subthreshold Symmetric SRAM Cell With High Read Stability," in IEEE Transactions on Circuits and Systems II: Express Briefs, vol. 61, no. 1, pp. 26-30, Jan. 2014.

[5] Jyoti Yadav, Toshiyanka Goswami, P.Bhatnagar, S. Brila, and Neeraj Kr. Shukla, "A Roadmap on the Low Power Static Random Access Memory Design Topologies", International Journal of Scientific & Engineering Research, Volume 5, Issue 2, February 2014

[6] Hong Zhu et al., "A Comprehensive Comparison of Data StabilityEnhancement Techniques With Novel NanoscaleSRAM Cells Under Parameter Fluctuations", IEEE Transactions on Circuits And Systems—I: Regular Papers, Vol. 61, No. 5, May 2014.

[7] S. Pal and A. Islam, "9-T SRAM Cell for Reliable Ultralow-Power Applications and Solving Multibit Soft-Error Issue," in *IEEE Transactions on Device and Materials Reliability*, vol. 16, no. 2, pp. 172-182, June 2016

[8]N. E. Alias, A. Hamzah, M. L. Peng Tan, U. U. Sheikh and M. A. Riyadi, "Low-Power And High Performance Of An Optimized FinFET Based 8T SRAM Cell Design," 2019 6th International Conference on Electrical Engineering, Computer Science and Informatics (EECSI), Bandung, Indonesia, 2019, pp. 66-70, doi: 10.23919/EECSI48112.2019.8976925.

[9]H. Farkhani, A. Peiravi, J. M. Kargaard and F. Moradi, "Comparative study of FinFETs versus 22nm bulk CMOS technologies: SRAM design perspective", Proc. 27th IEEE Int. Syst.-on-Chip Conf. (SOCC), pp. 449-454, 2014.

[10]L. M. Dani, G. Singh, M. Kaur, "FinFET based 6T SRAM Cell for Nanoscaled Technologies", International Journal of Computer Applications, Vol.127, No.13, October 2015

[11]H. Bu, "FinFET technology a substrate perspective", *Proc. IEEE Int. SOI Conf. (SOI)*, pp. 1-27, Oct. 2011

[12] A. A. Kumar and A. Chalil, "Performance Analysis of 6T SRAM Cell on Planar and FinFET Technology," 2019 International Conference on Communication and Signal Processing (ICCSP), Chennai, India, 2019, pp. 0375-0379, doi: 10.1109/ICCSP.2019.8697928.

[13] S. Nakata, H. Hanazono, H. Makino, H. Morimura, M. Miyama and Y. Matsuda, "Increase in Read Noise Margin of Single-Bit-Line SRAM Using Adiabatic Change of Word Line Voltage," in IEEE Transactions on Very Large Scale Integration (VLSI) Systems, vol. 22, no. 3, pp. 686-690, March 2014.

[14]Gupta, V., Khandelwal, S., Raj, B., & Gupta, R. D. (2015). *Leakage current reduction in finfet based 6T SRAM cell for minimizing power dissipation in nanoscale memories. 2015 5th Nirma University International Conference on Engineering (NUiCONE).* doi:10.1109/nuicone.2015.7449596

[15]Kumar, Aswathy A., and Anu Chalil. "Performance Analysis of 6T SRAM Cell on Planar and FinFET Technology." 2019 International Conference on Communication and Signal Processing (ICCSP). IEEE, 2019.

[16]Ensan, Sina Sayyah, et al. "A low-power single-ended SRAM in FinFET technology." AEU-International Journal of Electronics and Communications 99 (2019): 361-368

[17]Kim, Young Bok, Yong-Bin Kim, and Fabrizio Lombardi. "Low power 8T SRAM using 32nm independent gate FinFET technology." 2008 IEEE International SOC Conference. IEEE, 2008.

[18]Pahuja, H., Tyagi, M., Panday, S., & Singh, B. (2018). A novel single-ended 9T FinFET sub-threshold SRAM cell with high operating margins and low write power for low voltage operations. Integration, the VLSI Journal, 60, 99–116. D

[19] Bagheriye, Leila, et al. "Highly stable, low power FinFET SRAM cells with exploiting dynamic back-gate biasing." Integration 65 (2019): 128-137.

[20] Almeida, Roberto B., et al. "Analysis of 6 T SRAM cell in sub-45 nm CMOS and FinFET technologies." Microelectronics Reliability 88 (2018): 196-202.

[21] M. Bansal, A. Kumar, P. Singh and R. K. Nagaria, "A Novel 10T SRAM cell for Low Power Applications," 2018 5th IEEE Uttar Pradesh Section International Conference on Electrical, Electronics and Computer Engineering (UPCON), Gorakhpur, 2018, pp. 1-4, doi: 10.1109/UPCON.2018.8596829.

[22] Young Bok Kim, Yong-Bin Kim, and Fabrizio Lombardi. "Low power 8T SRAM using 32nm independent gate FinFET technology." 2008 IEEE International SOC Conference. IEEE, 2008.

[23]Liu, Zhiyu, and Volkan Kursun. "Characterization of a novel nine-transistor SRAM cell." IEEE transactions on very large scale integration (VLSI) systems 16.4 (2008): 488-492.

[24]Sachdeva A., and Tomar V. K., "Design of Low Power Half Select Free 10T Static Random-Access Memory Cell." Journal of Circuits, Systems and Computers (2020): 2150073. https://doi.org/10.1142/S0218126621500730

[25]N. E. Alias, A. Hamzah, M. L. Peng Tan, U. U. Sheikh and M. A. Riyadi, "Low-Power And High Performance Of An Optimized FinFET Based 8T SRAM Cell Design," 2019 6th International Conference on Electrical Engineering, Computer Science and Informatics (EECSI), Bandung, Indonesia, 2019, pp. 66-70, doi: 10.23919/EECSI48112.2019.8976925.

[26]H. Farkhani, A. Peiravi, J. M. Kargaard and F. Moradi, "Comparative study of FinFETs versus 22nm bulk CMOS technologies: SRAM design perspective", Proc. 27th IEEE Int. Syst.-on-Chip Conf. (SOCC), pp. 449-454, 2014.

[27]L. M. Dani, G. Singh, M. Kaur, “FinFET based 6T SRAM Cell for Nanoscaled Technologies”, International Journal of Computer Applications, Vol.127, No.13, October 2015

[28]H. Bu, "FinFET technology a substrate perspective", *Proc. IEEE Int. SOI Conf. (SOI)*, pp. 1-27, Oct. 2011 T Technology," 2019 International Conference on Communication and

Signal Processing (ICCSP), Chennai, India, 2019, pp. 0375-0379, doi: 10.1109/ICCSP.2019.8697928.

[29] H. Banga and D. Agarwal, "Single bit-line 10T SRAM cell for low power and high SNM," 2017 International Conference on Recent Innovations in Signal processing and Embedded Systems (RISE), Bhopal, 2017, pp. 433-438, doi: 10.1109/RISE.2017.8378194.

[30] Yaug BD, Lee-Sup K. A low- power SRAM using hierarchical bit line and local sense amplifiers. IEEE J Solid-State Circuits. 2005;40(6):1366-1376.

[31] Mohammed, Hussain & Kabir, H M Dipu & Alam, S B. (2011). Fast & Low-Power Consuming SRAM Design by Fast Precharging Using Equalizer and Sense Circuit

[32] T. L. Floyd, Digital Fundamentals, 8th ed. Pearson, 2003.

[33] J. M. Rabaey, A. Chandrakasan, and B. Nikolic, Digital Integrated Circuits, A Design Perspective, 2nd ed., ser. Prentice-Hall Electronics and VLSI Series, C. G. Sodini, Ed. Pearson, 20

[34] D. Hodges, H. Jackson, and R. Saleh, Analysis and Design of Digital Integrated Circuits. McGraw-Hill, 2003, ch. Semiconductor Memory Design, pp. 359.

Publications

1. International conference on Micro/Nano electronics Devices, Circuits and system in NIT SILCHAR ,the title of paper is **"A Low Leakage with enhance write margin 10T SRAM cell for IoT applications"**. (Presented: 31 Jan 2021)

2. Advances in International Conference (Virtual Mode) on Simulation, Automation & Smart Manufacturing (SASM 2021) ,the title of paper is "**Design and analysis of FinFET based 10T SRAM Cell for low power applications**".(**Accepted**)

3. Third paper title is "**Performance evolution of FinFET based 10T SRAM cell for IoT based devices". (Submitted)**

DEPARTMENT OF COMPUTER ENGINEERING & APPLICATIONS
INSTITUTE OF ENGINEERING & TECHNOLOGY

B.Tech. IV Year CSE/CCV/DA

Project Report

On

"FACE MASK DETECTOR"

Under the supervision of

Mr. Asheesh Tiwari

Submitted by

1. SHIKHA BANSAL(Sec-D/Univ Roll no.-171500314)

Group No: G-1

Even Semester, 2020-21

ACKNOWLEDGEMENT

We would like to express our sincere gratitude to our mentor **Mr. Asheesh Tiwari** for guiding us. We deeply respect the mentor for his vast knowledge, numerous suggestions, and strong passion to complete this project. Valuable discussions with him not only made our work smooth but also encouraged us to think more professionally in making our applications based project. We also thank all our teaching and non-teaching staff for their support and well wishes. Finally, We would like to express our deepest gratitude to our parents and friends for their encouragement and support.

- SHIKHA BANSAL

Department of Computer Engineering and Applications
GLA University, Mathura
17 km. Stone NH#2, Mathura-Delhi Road, P.O. – Chaumuhan, Mathura – 281406

DECLARATION

I hereby declare that the work which is carried out in the Major Project titled **"Face Mask Detector"** in partial fulfillment of the requirements for the award of the ***Bachelor of Technology*** in Computer Science and Engineering and submitted to the Department of Computer Engineering and Applications, GLA University, Mathura, is an authentic record of my own work carried under the supervision of **Mr. Asheesh Tiwari, Assistant Professor, Dept. of CEA.** The contents of this project report, in full or in parts, have not been submitted to any other Institute or University for the award of any degree.

Sign _____

Name of Candidate: Shikha Bansal
University Roll No.: 171500314

Certificate

This is to certify that the above statements made by the candidate are correct to the best of my knowledge and belief.

Supervisor
Mr. Asheesh Tiwari
Assistant Professor

Project Coordinator
(Dr. Mayank Srivastava)

Program Co-ordinator
(Dr. Rakesh Kumar Gulav)

Date: 19.05.2021

TABLE OF CONTENT

ABSTRACT

After the breakout of the worldwide pandemic COVID-19, there arises a severe need of protection mechanisms. Several guidelines were issued by the World Health Organization (WHO) for protection against the spread of coronavirus. According to WHO, the most effective preventive measure against COVID-19 is wearing a mask in public places and crowded areas. It is very difficult to monitor people manually in these areas. In this project, we will be proposing a transfer learning model to automate the process of identifying the people who are not wearing masks using OpenCV, Keras/TensorFlow, and Deep Learning. To create our face mask detector, we will be training a two-class model of people wearing masks and people not wearing masks. We'll be reviewing the dataset that will be used to train our custom face mask detector and implement a Python script to train a face mask detector on our dataset using Keras and TensorFlow and review the results. Our goal is to train a custom deep learning model to detect whether a person is or is not wearing a mask. At last we will also be implementing our COVID-19 face mask detector in real-time video streams with OpenCV.

CHAPTER 1

INTRODUCTION

1.1 Motivation and Overview

The year 2020 has shown mankind some mind-boggling series of events amongst which the COVID19 pandemic is the most life-changing event which has startled the world since the year began. Affecting the health and lives of masses, COVID-19 has called for strict measures to be followed in order to prevent the spread of disease. From the very basic hygiene standards to the treatments in the hospitals, people are doing all they can for their own and the society's safety; face masks are one of the personal protective equipment. People wear face masks once they step out of their homes and authorities strictly ensure that people are wearing face masks while they are in groups and public places.

To monitor that people are following this basic safety principle, a strategy should be developed. A face mask detector system can be implemented to check this. Face mask detection means to identify whether a person is wearing a mask or not. The first step to recognize the presence of a mask on the face is to detect the face, which makes the strategy divided into two parts: to detect faces and to detect masks on those faces. Face detection is one of the applications of object detection and can be used in many areas like security, biometrics, law enforcement and more. There are many detector systems developed around the world and being implemented. However, all this science needs optimization; a better, more precise detector, because the world cannot afford any more increase in corona cases.

1.2 Aim and Objective

The goal of the project is to build a real-time system to detect whether the person on the webcam is wearing a mask or not. We will train the face mask detector model using Keras and OpenCV. Since we are using the MobileNetV2 architecture, it's also computationally efficient and thus making it easier to deploy the model to embedded systems (Raspberry Pi, Google Coral, etc.). This system can therefore be used in real-time applications which require face-mask detection for safety purposes due to the outbreak of Covid-19. This project can be integrated with embedded systems for application in airports, railway stations, offices, schools, and public places to ensure that public safety guidelines are followed.

1.3 Scope

In the present scenario due to Covid-19, almost every one of us tends to wear a face mask. It becomes increasingly necessary to check if the people in the crowd wear face masks in most public gatherings such as Malls, theaters, Parks. Since there are no efficient face mask detection applications which are now in high demand for transportation means, densely populated areas, residential districts, large-scale manufacturers and other enterprises to ensure safety. This development of an AI solution to detect if the person is wearing a face mask and allow their entry would be of great help to the society.

Fig.1 People with mask and no masks

CHAPTER 2

SOFTWARE REQUIREMENT ANALYSIS

2.1 Deep Learning

Deep learning is one of the only methods by which we can overcome the challenges of feature extraction. This is because deep learning models are capable of learning to focus on the right features by themselves, requiring little guidance from the programmer. Basically, deep learning mimics the way our brain functions i.e. it learns from experience. As you know, our brain is made up of billions of neurons that allows us to do amazing things. Even the brain of a one year old kid can solve complex problems which are very difficult to solve even using supercomputers. For example:

- Recognize the face of their parents and different objects as well.
- Discriminate different voices and can even recognize a particular person based on his/her voice.
- Draw inference from facial gestures of other persons and many more.

Actually, our brain has sub-consciously trained itself to do such things over the years. Deep learning uses the concept of artificial neurons that functions in a similar manner as the biological neurons present in our brain. Therefore, we can say that Deep Learning is a subfield of machine learning concerned with algorithms inspired by the structure and function of the brain called artificial neural networks.

Now, let us take an example to understand it. Suppose we want to make a system that can recognize faces of different people in an image. If we solve this as a typical machine learning problem, we will define facial features such as eyes, nose, ears etc. and then, the system will identify which features are more important for which person on its own.

Now, deep learning takes this one step ahead. Deep learning automatically finds out the features which are important for classification because of deep neural networks, whereas in case of Machine Learning we had to manually define these features.

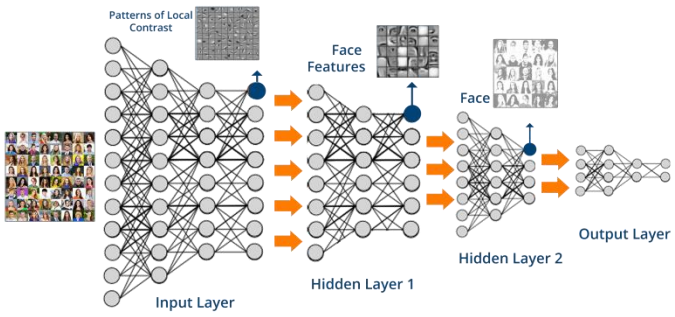

Fig. 2: Face Recognition using Deep Networks

As shown in the image above Deep Learning works as follows:

- At the lowest level, network fixates on patterns of local contrast as important.
- The following layer is then able to use those patterns of local contrast to fixate on things that resemble eyes, noses, and mouths
- Finally, the top layer is able to apply those facial features to face templates.
- A deep neural network is capable of composing more and more complex features in each of its successive layers.

Have you ever wondered how Facebook automatically labels or tags all the people present in an image uploaded by you? Well, Facebook uses Deep Learning in a similar fashion as stated in the above example. Now, you would have realized the capability of Deep Learning and how it can outperform Machine Learning in those cases where we have very little idea about all the features that can affect the outcome. Therefore, Deep networks can overcome the drawback of Machine Learning by drawing inferences from data sets consisting of input data without proper labeling.

2.2 Convolution Neural Network (CNN)

How Does A Computer Read an Image?

Consider this image of the New York skyline, upon first glance you will see a lot of buildings and colors. So how does the computer process this image?

The image is broken down into 3 color-channels which are Red, Green and Blue. Each of these color channels are mapped to the image's pixel.

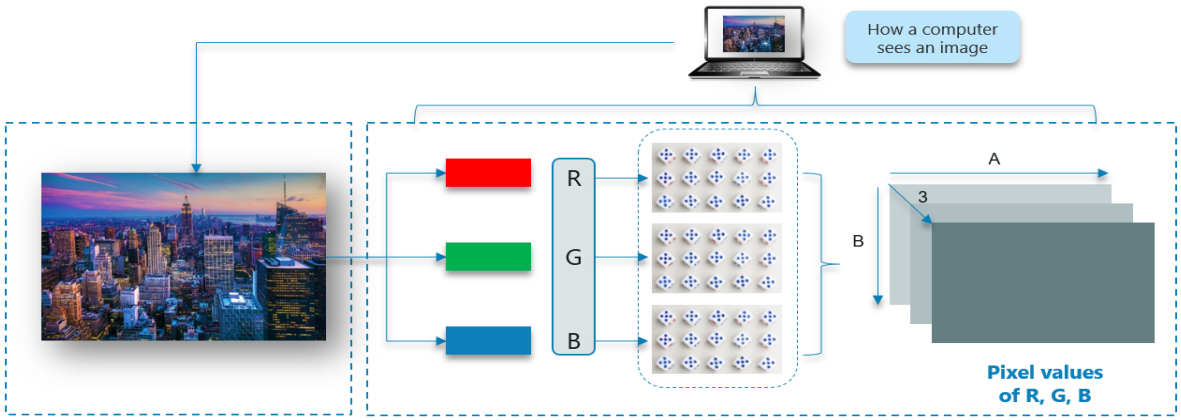

Then, the computer recognizes the value associated with each pixel and determines the size of the image.

However, for black-white images, there is only one channel and the concept is the same.

Why Not Fully Connected Networks?

We cannot make use of fully connected networks when it comes to Convolutional Neural Networks, here's why!

Consider The following image:

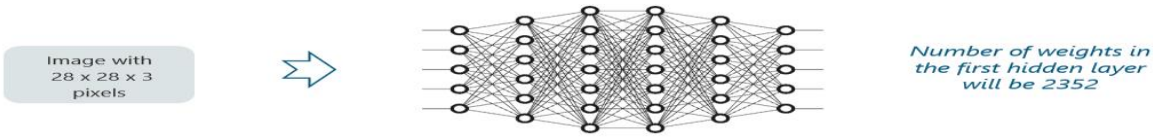

Here, we have considered an input of images with the size 28x28x3 pixels. If we input this to our Convolutional Neural Network, we will have about 2352 weights in the first hidden layer itself.

But this case isn't practical. Now, take a look at this:

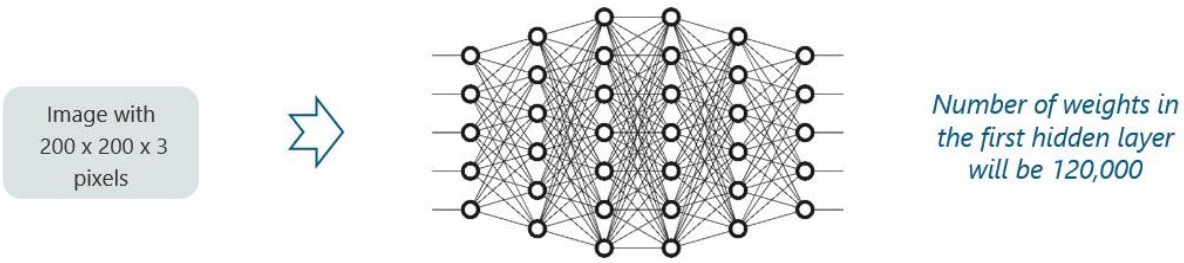

Any generic input image will at least have 200x200x3 pixels in size. The size of the first hidden layer becomes a whopping 120,000. If this is just the first hidden layer, imagine the number of neurons needed to process an entire complex image-set.

This leads to overfitting and isn't practical. Hence, we cannot make use of fully connected networks.

What Are Convolutional Neural Networks?

Convolutional Neural Networks, like neural networks, are made up of neurons with learnable weights and biases. Each neuron receives several inputs, takes a weighted sum over them, passes it through an activation function and responds with an output.

The whole network has a loss function and all the tips and tricks that we developed for neural networks still apply on Convolutional Neural Networks.

Pretty straightforward, right?

Neural networks, as its name suggests, is a machine learning technique which is modeled after the brain structure. It comprises a network of learning units called neurons.

These neurons learn how to convert input signals (e.g. picture of a cat) into corresponding output signals (e.g. the label "cat"), forming the basis of automated recognition.

Let's take the example of automatic image recognition. The process of determining whether a picture contains a cat involves an activation function. If the picture resembles prior cat images the neurons have seen before, the label "cat" would be activated.

Hence, the more labeled images the neurons are exposed to, the better it learns how to recognize other unlabelled images. We call this the process of training neurons.

How Do Convolutional Neural Networks Work?

There are four layered concepts we should understand in Convolutional Neural Networks:

1. Convolution,
2. ReLu,
3. Pooling and
4. Full Connectedness (Fully Connected Layer).

Let's begin by checking out a simple example:

Example of CNN:

Consider the image below:

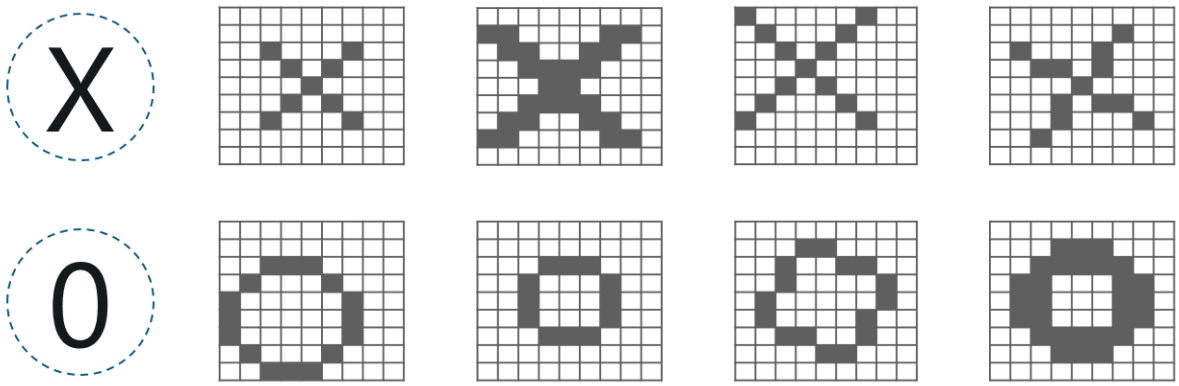

Here, there are multiple renditions of X and O's. This makes it tricky for the computer to recognize. But the goal is that if the input signal looks like previous images it has seen before, the "image" reference signal will be mixed into, or convolved with, the input signal. The resulting output signal is then passed on to the next layer.

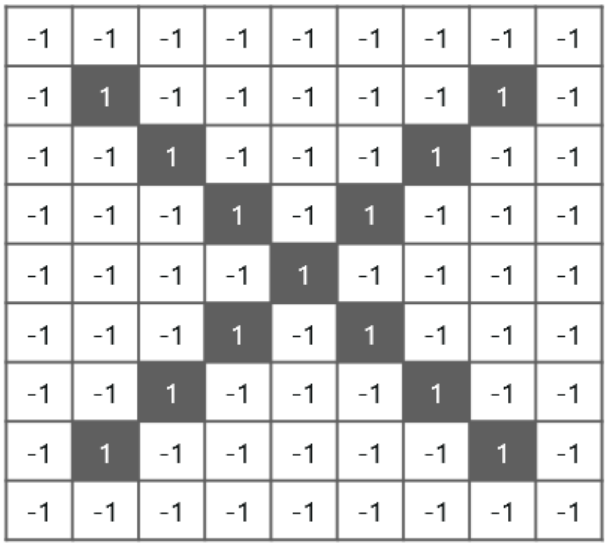

So, the computer understands every pixel. In this case, the white pixels are said to be -1 while the black ones are 1. This is just the way we've implemented to differentiate the pixels in a basic binary classification.

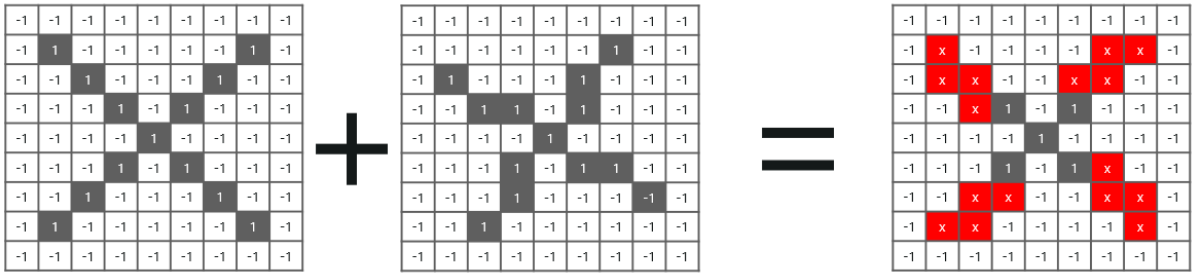

Now if we would just normally search and compare the values between a normal image and another 'x' rendition, we would get a lot of missing pixels.

So, how do we fix this?

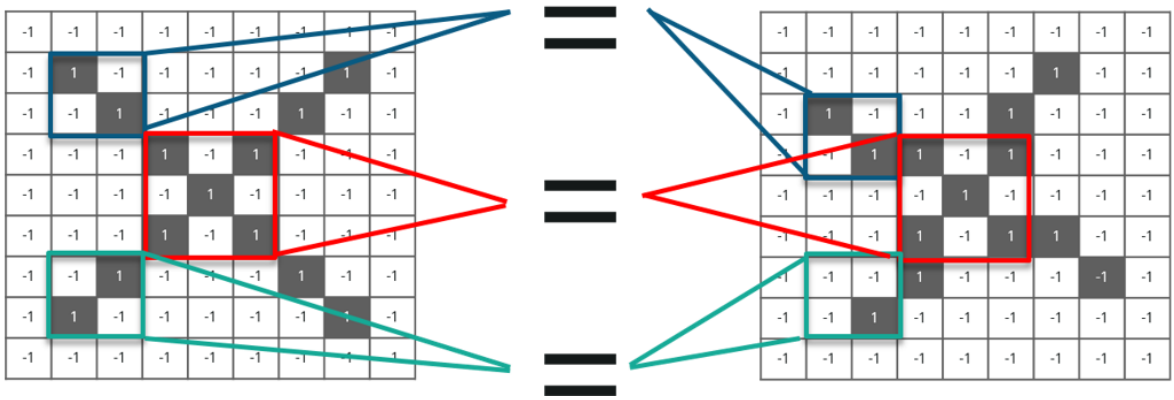

We take small patches of the pixels called filters and try to match them in the corresponding nearby locations to see if we get a match. By doing this, the Convolutional Neural Network gets a lot better at seeing similarity than directly trying to match the entire image.

Convolution Of An Image

Convolution has the nice property of being translational invariant. Intuitively, this means that each convolution filter represents a feature of interest (e.g pixels in letters) and the Convolutional Neural Network algorithm learns which features comprise the resulting reference (i.e. alphabet).

We have 4 steps for convolution:

- Line up the feature and the image
- Multiply each image pixel by corresponding feature pixel
- Add the values and find the sum
- Divide the sum by the total number of pixels in the feature

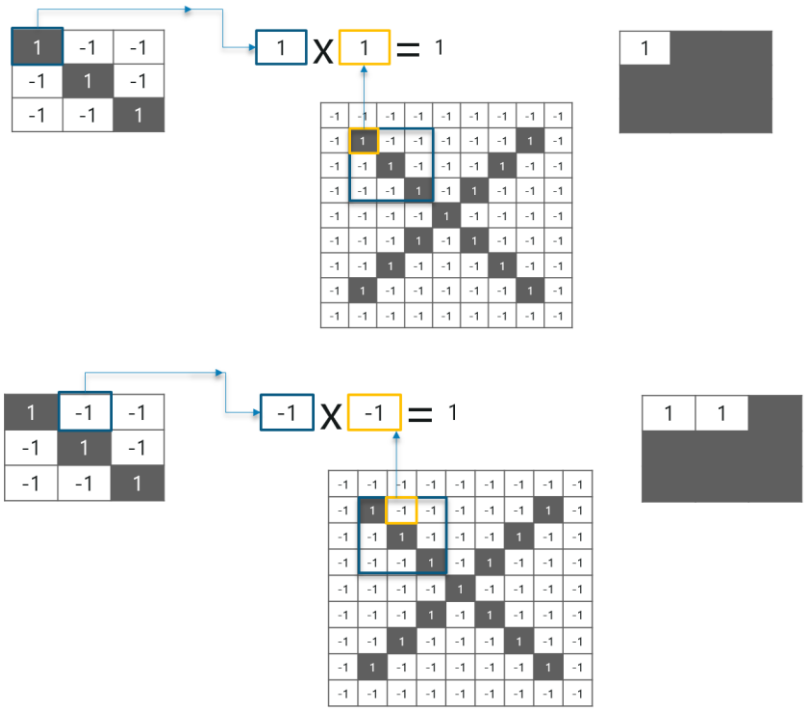

Consider the above image – As you can see, we are done with the first 2 steps. We considered a feature image and one pixel from it. We multiplied this with the existing image and the product is stored in another buffer feature image.

1	-1	-1
-1	1	-1
-1	-1	1

$$\frac{1+1+1+1+1+1+1+1+1}{9} = 1$$

1	1	1
1	1	1
1	1	1

-1	-1	-1	-1	-1	-1	-1	-1	-1
-1	1	-1	-1	-1	-1	-1	1	-1
-1	-1	1	-1	-1	-1	1	-1	-1
-1	-1	-1	1	-1	1	-1	-1	-1
-1	-1	-1	-1	1	-1	-1	-1	-1
-1	-1	-1	1	-1	1	-1	-1	-1
-1	-1	1	-1	-1	-1	1	-1	-1
-1	1	-1	-1	-1	-1	-1	1	-1
-1	-1	-1	-1	-1	-1	-1	-1	-1

With this image, we completed the last 2 steps. We added the values which led to the sum. We then divide this number by the total number of pixels in the feature image. When that is done, the final value obtained is placed at the center of the filtered image as shown below:

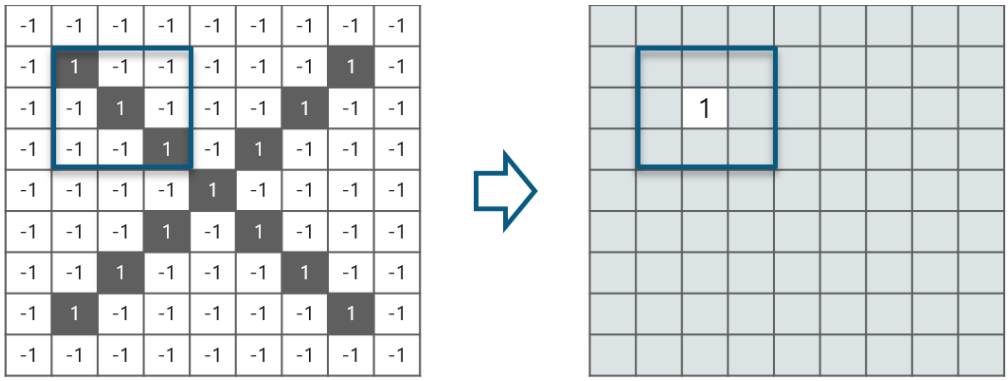

Now, we can move this filter around and do the same at any pixel in the image. For better clarity, let's consider another example:

1	-1	-1
-1	1	-1
-1	-1	1

$$\frac{1+1-1+1+1+1-1+1+1}{9} = .55$$

-1	-1	-1	-1	-1	-1	-1	-1	-1
-1	1	-1	-1	-1	-1	-1	1	-1
-1	-1	1	-1	-1	-1	1	-1	-1
-1	-1	-1	1	-1	1	-1	-1	-1
-1	-1	-1	-1	1	-1	-1	-1	-1
-1	-1	-1	1	-1	1	-1	-1	-1
-1	-1	1	-1	-1	-1	1	-1	-1
-1	1	-1	-1	-1	-1	-1	1	-1
-1	-1	-1	-1	-1	-1	-1	-1	-1

1	1	-1
1	1	1
-1	1	1

As you can see, here after performing the first 4 steps we have the value at 0.55! We take this value and place it in the image as explained before. This is done in the following image:

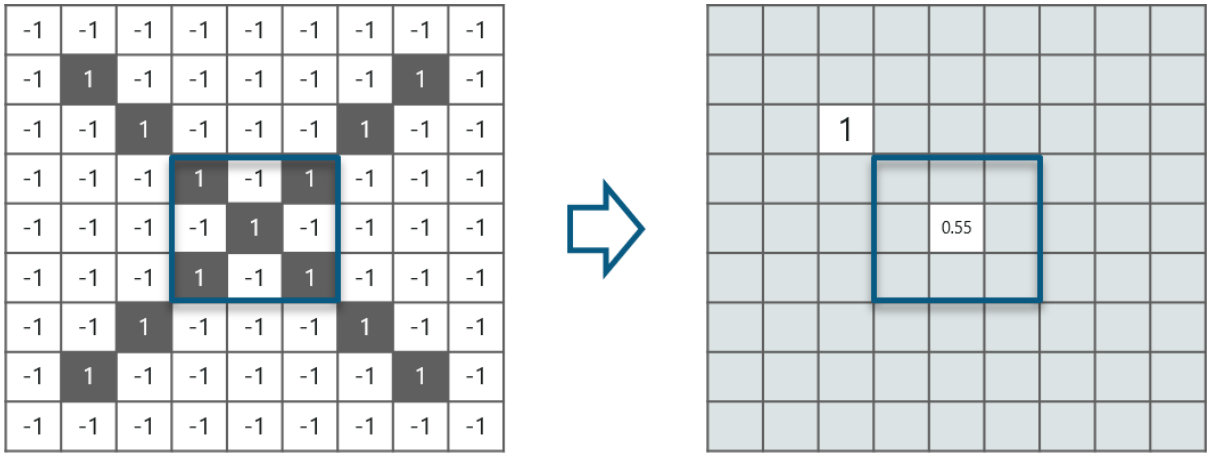

Similarly, we move the feature to every other position in the image and see how the feature matches that area. So after doing this, we will get the output as:

0.77	-0.11	0.11	0.33	0.55	-0.11	0.33
-0.11	1.0	-0.11	0.33	-0.11	0.11	-0.11
0.11	-0.11	1.0	-0.33	0.11	-0.11	0.55
0.33	0.33	-0.33	0.55	-0.33	0.33	0.33
0.55	-0.11	0.11	-0.33	1.00	-0.11	0.11
-0.11	0.11	-0.11	0.33	-0.11	1.00	-0.11
0.33	-0.11	0.55	0.33	0.11	-0.11	0.77

Here we considered just one filter. Similarly, we will perform the same convolution with every other filter to get the convolution of that filter.

The output signal strength is not dependent on where the features are located, but simply whether the features are present. Hence, an alphabet could be sitting in different positions and the Convolutional Neural Network algorithm would still be able to recognize it.

ReLU Layer

ReLU is an activation function. But, what is an activation function?

Rectified Linear Unit (ReLU) transform function only activates a node if the input is above a certain quantity, while the input is below zero, the output is zero, but when the input rises above a certain threshold, it has a linear relationship with the dependent variable.

Consider the below example:

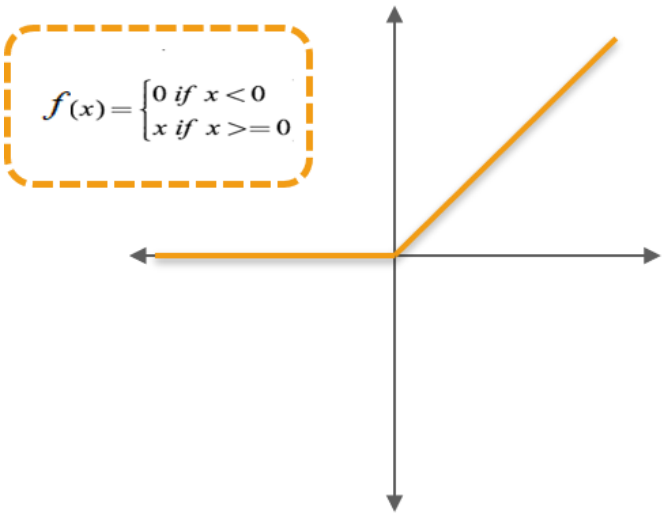

We have considered a simple function with the values as mentioned above. So the function only performs an operation if that value is obtained by the dependent variable. For this example, the following values are obtained:

x	*f(x)=x*	F(x)
-3	*f(-3) = 0*	0
-5	*f(-5) = 0*	0
3	*f(3) = 3*	3
5	*f(5) = 5*	5

Why do we require ReLU here?

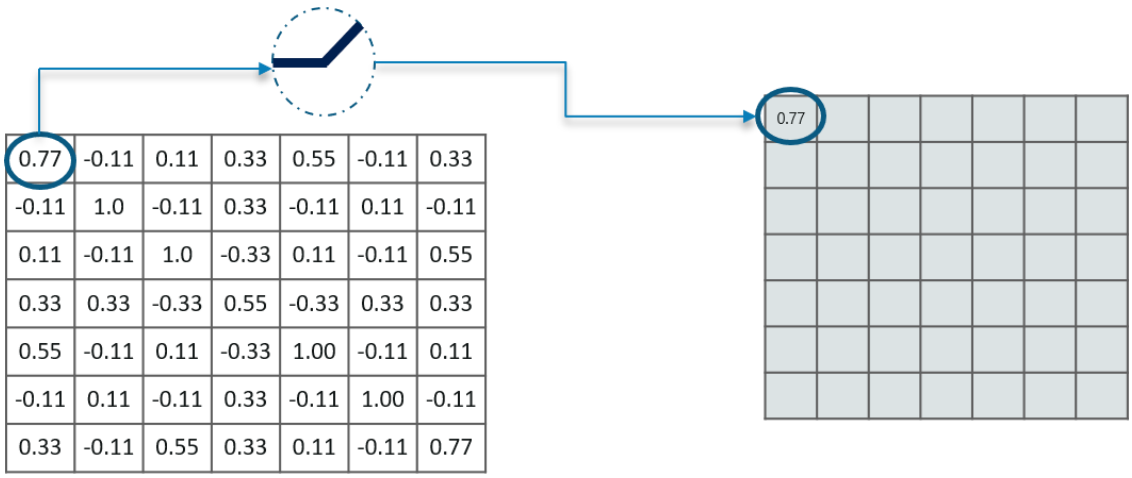

The main aim is to remove all the negative values from the convolution. All the positive values remain the same but all the negative values get changed to zero as shown below:

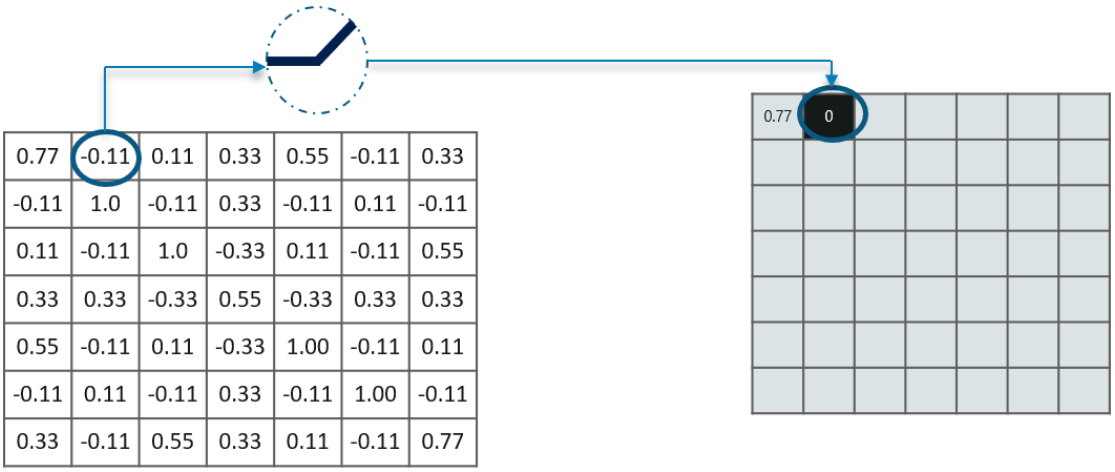

0.77	-0.11	0.11	0.33	0.55	-0.11	0.33
-0.11	1.0	-0.11	0.33	-0.11	0.11	-0.11
0.11	-0.11	1.0	-0.33	0.11	-0.11	0.55
0.33	0.33	-0.33	0.55	-0.33	0.33	0.33
0.55	-0.11	0.11	-0.33	1.00	-0.11	0.11
-0.11	0.11	-0.11	0.33	-0.11	1.00	-0.11
0.33	-0.11	0.55	0.33	0.11	-0.11	0.77

So after we process this particular feature we get the following output:

0.77	-0.11	0.11	0.33	0.55	-0.11	0.33
-0.11	1.0	-0.11	0.33	-0.11	0.11	-0.11
0.11	-0.11	1.0	-0.33	0.11	-0.11	0.55
0.33	0.33	-0.33	0.55	-0.33	0.33	0.33
0.55	-0.11	0.11	-0.33	1.00	-0.11	0.11
-0.11	0.11	-0.11	0.33	-0.11	1.00	-0.11
0.33	-0.11	0.55	0.33	0.11	-0.11	0.77

0.77	0	0.11	0.33	0.55	0	0.33
0	1.00	0	0.33	0	0.11	0
0.11	0	1.00	0	0.11	0	0.55
0.33	0.33	0	0.55	0	0.33	0.33
0.55	0	0.11	0	1.00	0	0.11
0	0.11	0	0.33	0	1.00	0
0.33	0	0.55	0.33	0.11	0	1.77

Now, similarly we do the same process to all the other feature images as well:

0.77	-0.11	0.11	0.33	0.55	-0.11	0.33
-0.11	1.0	-0.11	0.33	-0.11	0.11	-0.11
0.11	-0.11	1.0	-0.33	0.11	-0.11	0.55
0.33	0.33	-0.33	0.55	-0.33	0.33	0.33
0.55	-0.11	0.11	-0.33	1.00	-0.11	0.11
-0.11	0.11	-0.11	0.33	-0.11	1.00	-0.11
0.33	-0.11	0.55	0.33	0.11	-0.11	0.77

0.77	0	0.11	0.33	0.55	0	0.33
0	1.00	0	0.33	0	0.11	0
0.11	0	1.00	0	0.11	0	0.55
0.33	0.33	0	0.55	0	0.33	0.33
0.55	0	0.11	0	1.00	0	0.11
0	0.11	0	0.33	0	1.00	0
0.33	0	0.55	0.33	0.11	0	1.77

0.33	-0.55	0.11	-0.11	0.11	-0.55	0.33
-0.55	0.55	-0.55	0.33	-0.55	0.55	-0.55
0.11	-0.55	0.55	-0.11	0.55	-0.55	0.11
-0.11	0.33	-0.77	1.00	-0.77	0.33	-0.11
0.11	-0.55	0.55	-0.77	0.55	-0.55	0.11
-0.55	0.55	-0.55	0.33	-0.55	0.55	-0.55
0.33	-0.55	0.11	-0.11	0.11	-0.55	0.33

0.33	0	0.11	0	0.11	0	0.33
0	0.55	0	0.33	0	0.55	0
0.11	0	0.55	0	0.55	0	0.11
0	0.33	0	1.00	0	0.33	0
0.11	0	0.55	0	0.55	0	0.11
0	0.55	0	0.33	0	0.55	0
0.33	0	0.11	0	0.11	0	0.33

0.33	-0.11	0.55	0.33	0.11	-0.11	0.77
-0.11	0.11	-0.11	0.33	-0.11	1.00	-0.11
0.55	-0.11	0.11	-0.33	1.00	-0.11	0.11
0.33	0.33	-0.33	0.55	-0.33	0.33	0.33
0.11	-0.11	1.00	-0.33	0.11	-0.11	0.55
-0.11	1.00	-0.11	0.33	-0.11	0.11	-0.11
0.77	-0.11	0.11	0.33	0.55	-0.11	0.33

Inputs from the convolution layer can be “smoothened” to reduce the sensitivity of the filters to noise and variations. This smoothing process is called subsampling and can be achieved by taking averages or taking the maximum over a sample of the signal.

Pooling Layer

In this layer we shrink the image stack into a smaller size. Pooling is done after passing through the activation layer. We do this by implementing the following 4 steps:

- Pick a window size (usually 2 or 3)
- Pick a stride (usually 2)
- Walk your window across your filtered images
- From each window, take the maximum value

Let us understand this with an example. Consider performing pooling with a window size of 2 and stride being 2 as well.

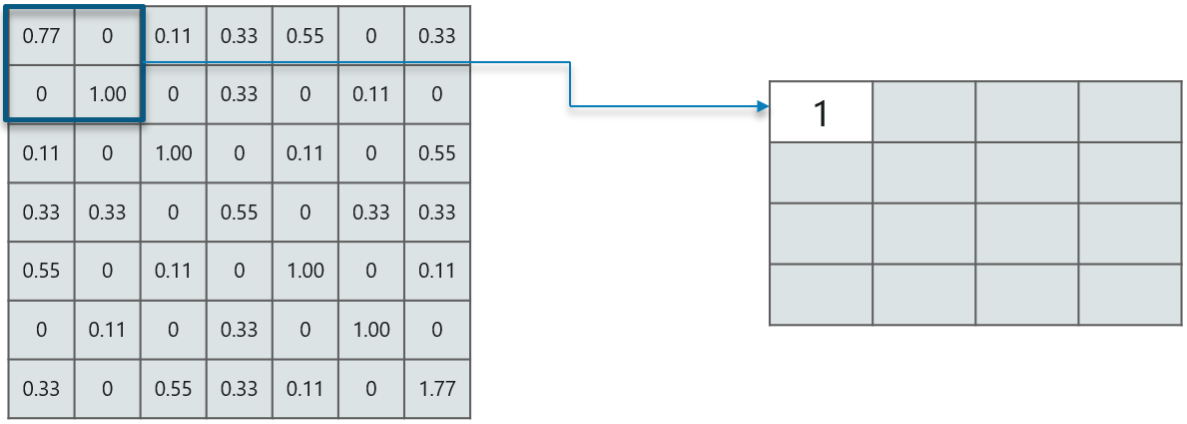

So in this case, we took window size to be 2 and we got 4 values to choose from. From those 4 values, the maximum value there is 1 so we pick 1. Also, note that we started out with a 7×7 matrix but now the same matrix after pooling came down to 4×4.

But we need to move the window across the entire image. The procedure is exactly the same as above and we need to repeat that for the entire image.

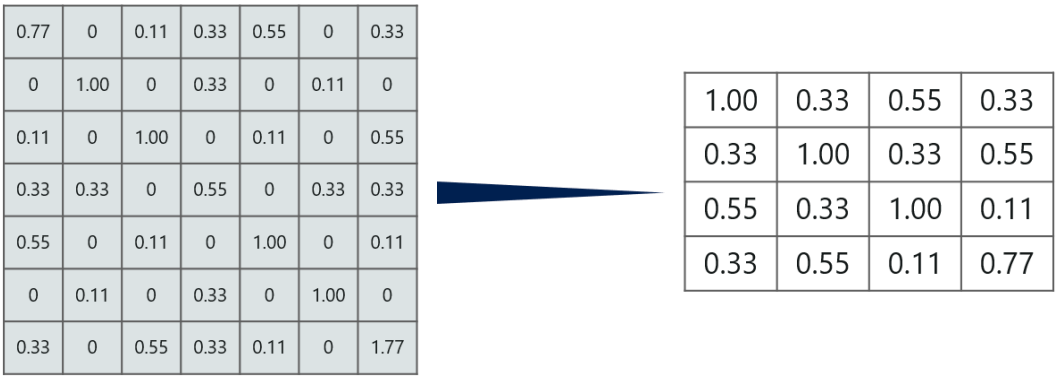

Do note that this is for one filter. We need to do it for 2 other filters as well. This is done and we arrive at the following result:

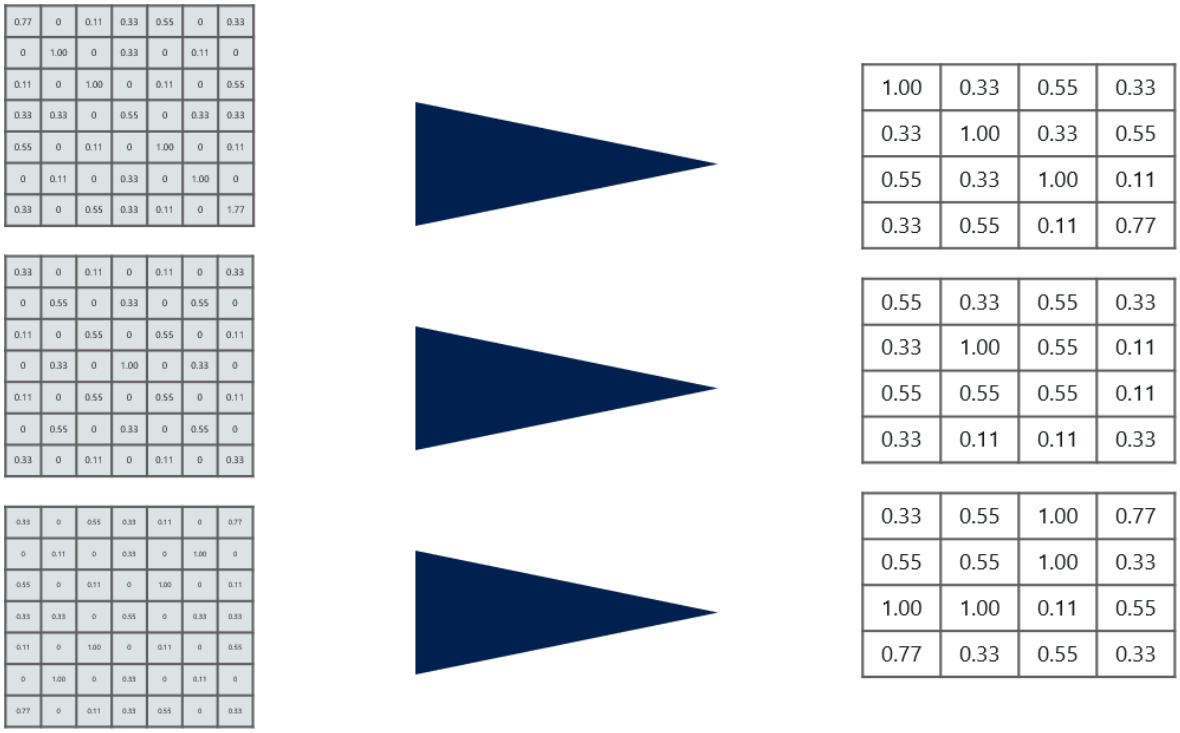

1.00	0.33	0.55	0.33
0.33	1.00	0.33	0.55
0.55	0.33	1.00	0.11
0.33	0.55	0.11	0.77

0.55	0.33	0.55	0.33
0.33	1.00	0.55	0.11
0.55	0.55	0.55	0.11
0.33	0.11	0.11	0.33

0.33	0.55	1.00	0.77
0.55	0.55	1.00	0.33
1.00	1.00	0.11	0.55
0.77	0.33	0.55	0.33

Well the easy part of this process is over. Next up, we need to stack up all these layers!

Stacking Up The Layers

So to get the time-frame in one picture we're here with a 4×4 matrix from a 7×7 matrix after passing the input through 3 layers – Convolution, ReLU and Pooling as shown below:

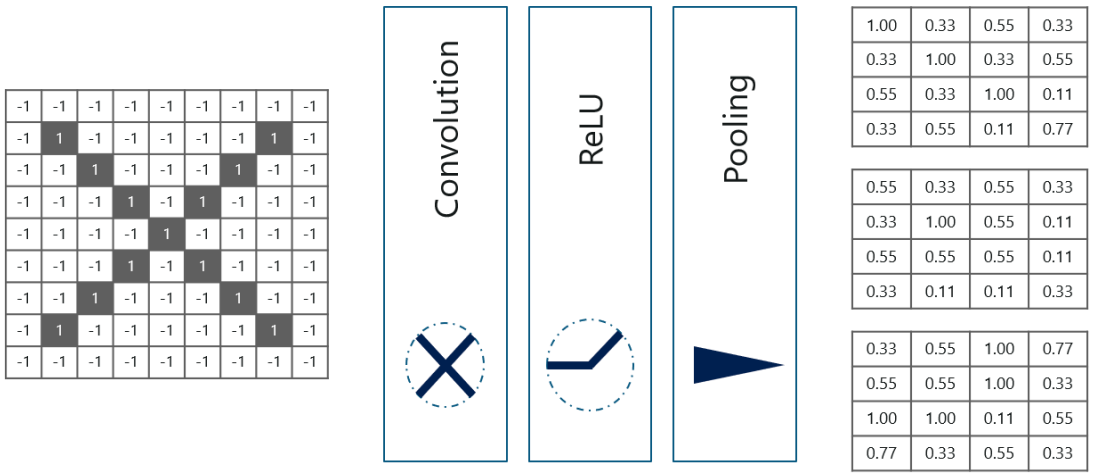

1.00	0.33	0.55	0.33
0.33	1.00	0.33	0.55
0.55	0.33	1.00	0.11
0.33	0.55	0.11	0.77

0.55	0.33	0.55	0.33
0.33	1.00	0.55	0.11
0.55	0.55	0.55	0.11
0.33	0.11	0.11	0.33

0.33	0.55	1.00	0.77
0.55	0.55	1.00	0.33
1.00	1.00	0.11	0.55
0.77	0.33	0.55	0.33

But can we further reduce the image from 4×4 to something lesser?

Yes, we can! We need to perform the 3 operations in an iteration after the first pass. So after the second pass we arrive at a 2×2 matrix as shown below:

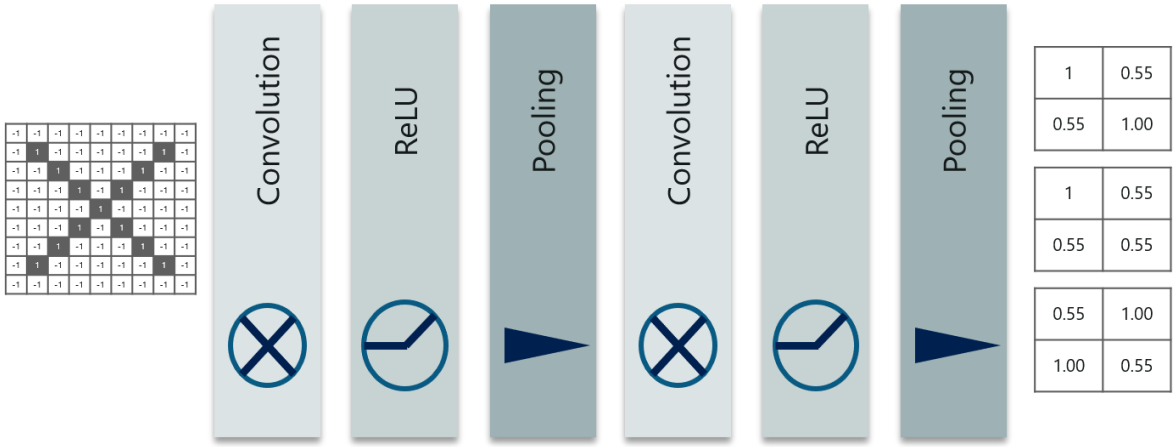

The last layers in the network are fully connected, meaning that neurons of preceding layers are connected to every neuron in subsequent layers.

This mimics high level reasoning where all possible pathways from the input to output are considered.

Also, a fully connected layer is the final layer where the classification actually happens. Here we take our filtered and shrinked images and put them into one single list as shown below:

1	0.55
0.55	1.00

1	0.55
0.55	0.55

0.55	1.00
1.00	0.55

1.00
0.55
0.55
1.00
1.00
0.55
0.55
0.55
0.55
1.00
1.00
0.55

So next, when we feed in, ‘X’ and ‘O’ there will be some element in the vector that will be high. Consider the image below, as you can see for ‘X’ there are different elements that are high and similarly, for ‘O’ we have different elements that are high:

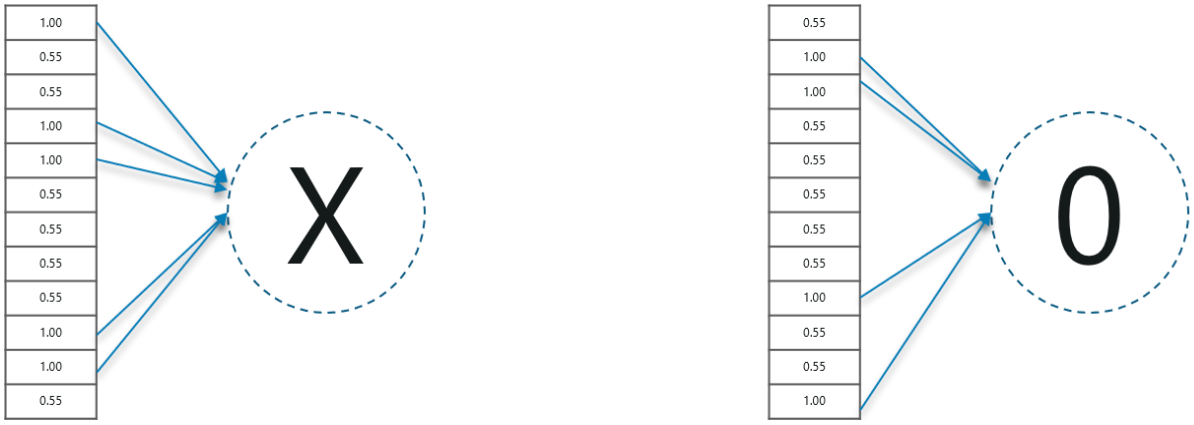

Well, what did we understand from the above image?

When the 1st, 4th, 5th, 10th and 11th values are high, we can classify the image as 'x'. The concept is similar for the other alphabets as well – when certain values are arranged the way they are, they can be mapped to an actual letter or a number which we require, simple right?

Prediction Of Image Using Convolutional Neural Networks – Fully Connected Layer

At this point in time, we're done training the network and we can begin to predict and check the working of the classifier. Let's check out a simple example:

0.9
0.65
0.45
0.87
0.96
0.73
0.23
0.63
0.44
0.89
0.94
0.53

In the above image, we have a 12 element vector obtained after passing the input of a random letter through all the layers of our network.

But, how do we check to know what we've obtained is right or wrong?

We make predictions based on the output data by comparing the obtained values with the list of 'x and 'o'!

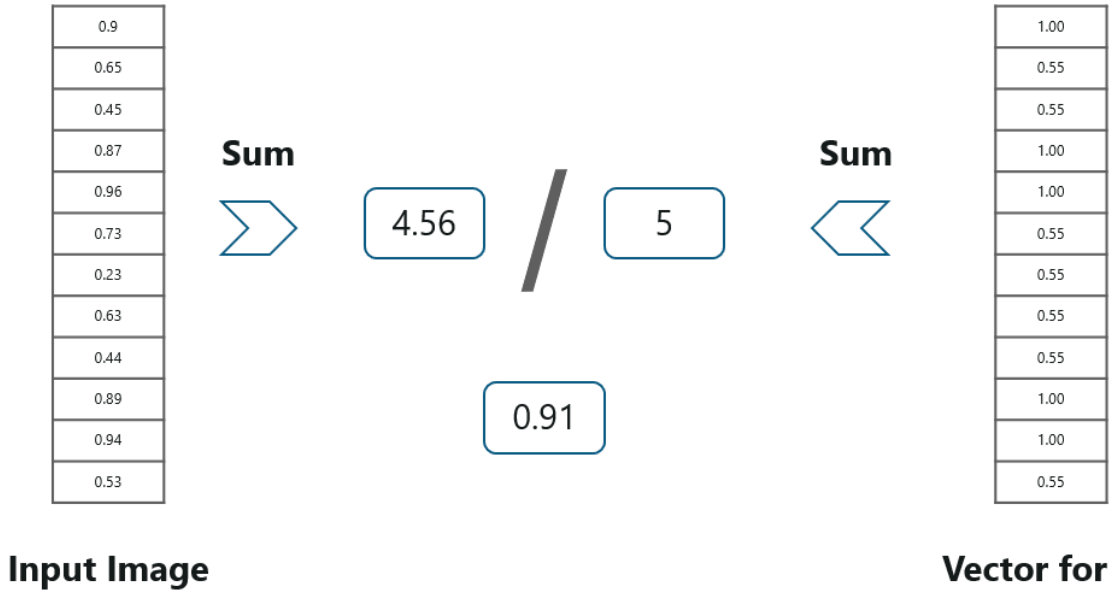

Well, it is really easy. We just added the values we found out as high (1st, 4th, 5th, 10th and 11th) from the vector table of X and we got the sum to be 5. We did the exact same thing with the input image and got a value of 4.56.

When we divide the value we have a probability match to be 0.91! Let's do the same with the vector table of 'o' now:

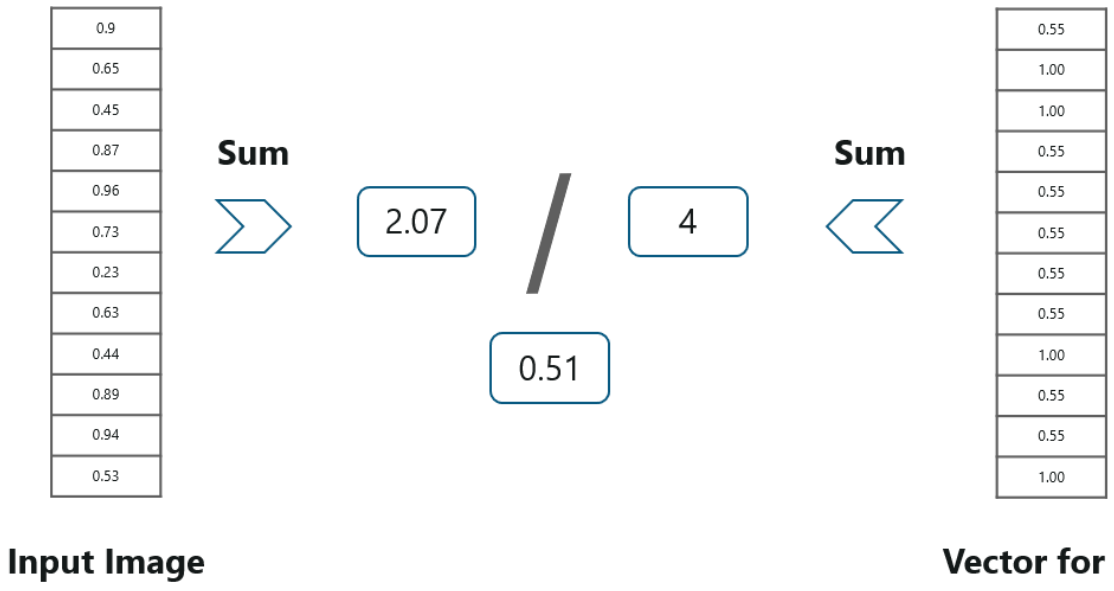

We have the output as 0.51 with this table. Well, probability being 0.51 is less than 0.91, isn't it?

So we can conclude that the resulting input image is an 'x'!

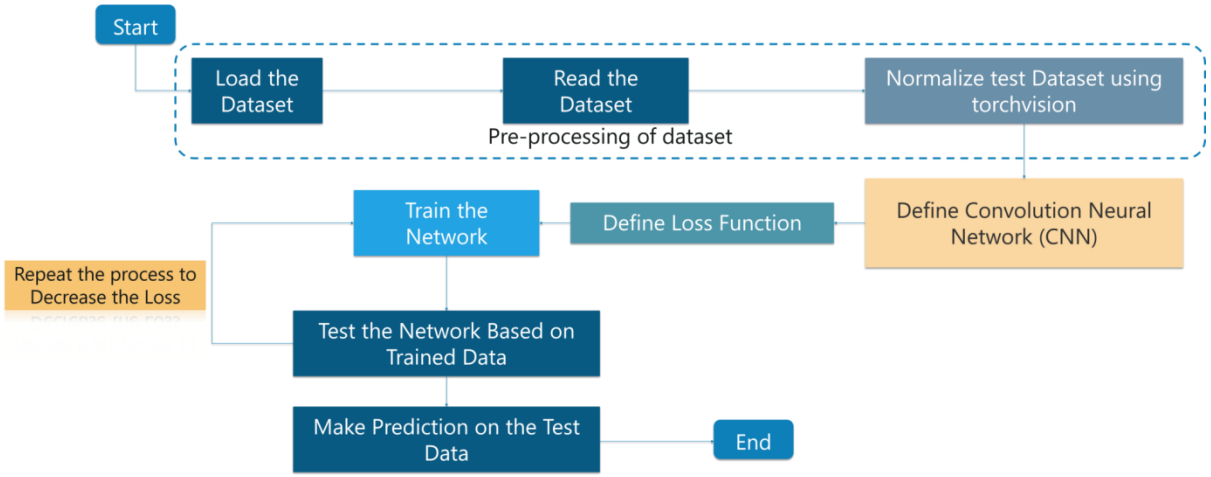

2.3 OpenCV

OpenCV is a Python library which is designed to solve computer vision problems. OpenCV was originally developed in 1999 by Intel but later it was supported by Willow Garage.

OpenCV supports a wide variety of programming languages such as C++, Python, Java etc. Support for multiple platforms including Windows, Linux, and MacOS.

OpenCV Python is nothing but a wrapper class for the original C++ library to be used with Python. Using this, all of the OpenCV array structures get converted to/from NumPy arrays.

This makes it easier to integrate it with other libraries which use NumPy. For example, libraries such as SciPy and Matplotlib.

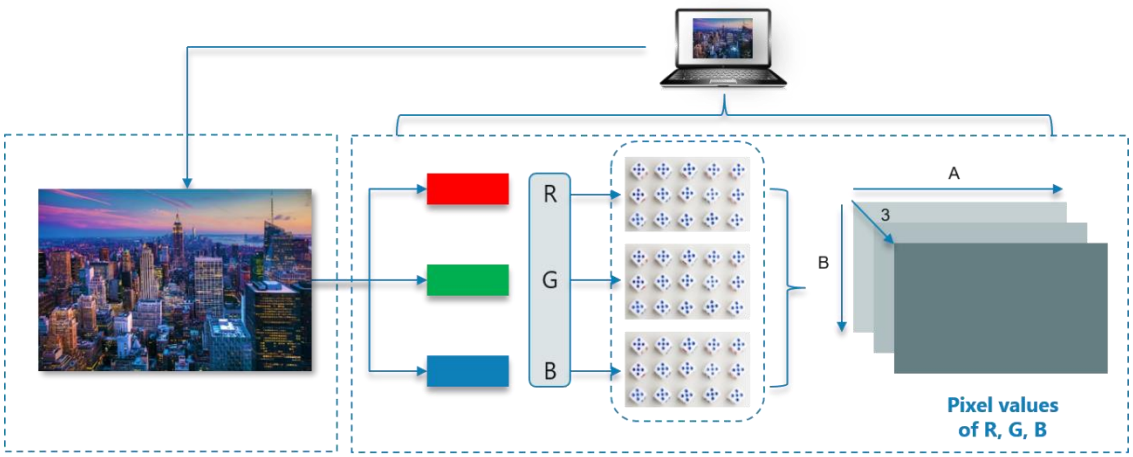

Step 1: Considering our prerequisites, we will require an image, to begin with. Later we need to create a cascade classifier which will eventually give us the features of the face.

Step 2: This step involves making use of OpenCV which will read the image and the features file. So at this point, there are NumPy arrays at the primary data points.

All we need to do is to search for the row and column values of the face NumPy ndarray. This is the array with the face rectangle coordinates.

Step 3: This final step involves displaying the image with the rectangular face box.

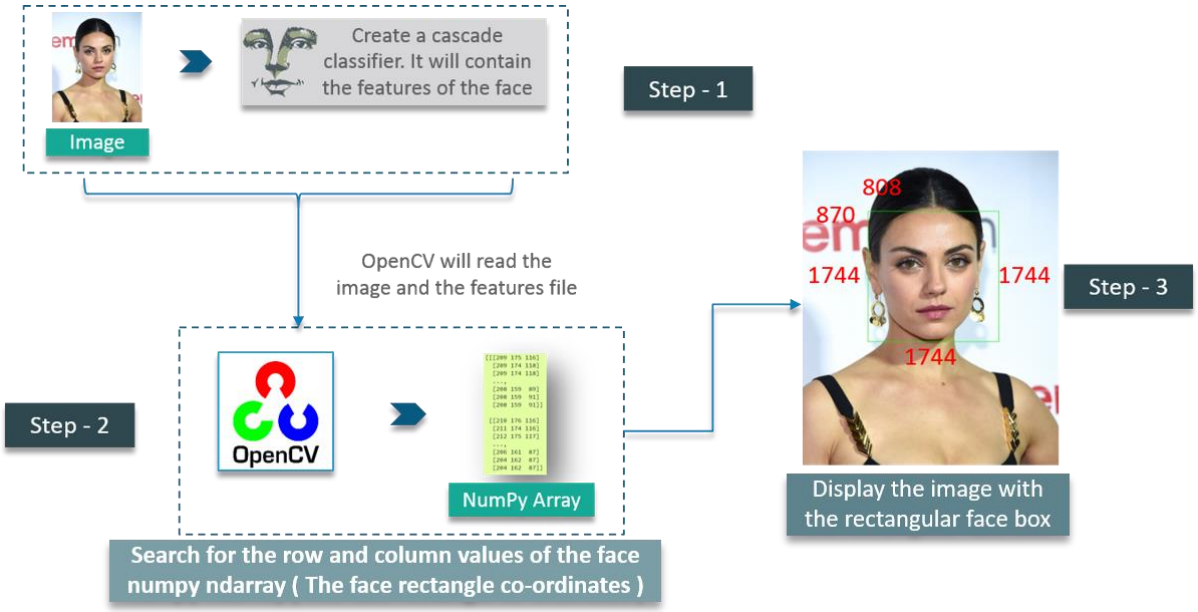

First, we create a CascadeClassifier object to extract the features of the face as explained earlier. The path to the XML file which contains the face features is the parameter here.

The next step would be to read an image with a face on it and convert it into a black and white image using COLOR_BGR2GREY. Followed by this, we search for the coordinates for the image. This is done using detectMultiScale. It's the coordinates for the face rectangle. The scaleFactor is used to decrease the shape value by 5% until the face is found. So, on the whole – Smaller the value, greater is the accuracy.

Finally, the face is printed on the window.

2.4 Tensor Flow

Tensor Flow is Google's Open Source Machine Learning Framework for dataflow programming across a range of tasks. Nodes in the graph represent mathematical operations, while the graph edges represent the multi-dimensional data arrays (tensors) communicated between them.

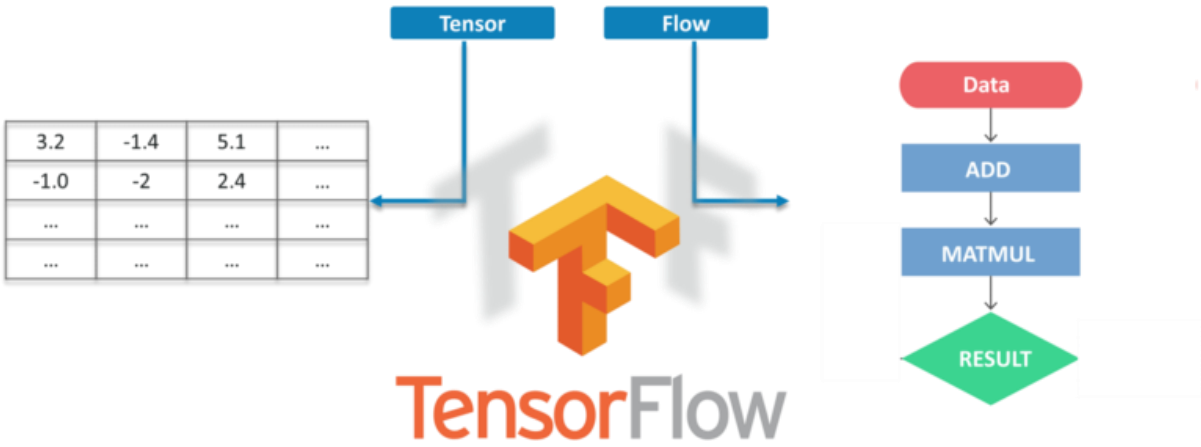

Tensors are just multidimensional arrays, an extension of 2-dimensional tables to data with a higher dimension. There are many features of TensorFlow which makes it appropriate for Deep Learning.

CHAPTER 3

DESIGN AND ANALYSIS

In this project, our two-phase COVID-19 face mask detector, computer vision/deep learning pipeline will be implemented. Reviewing the dataset used to train our custom face mask detector, then implementing a Python script to train a face mask detector on our dataset using Keras and TensorFlow.

Python script is used to train the face mask detector and review the results. After the trained COVID-19 face mask detector, we'll proceed to implement two more additional Python scripts used to:

1. Detect COVID-19 face masks in images.
2. Detect face masks in real-time video streams.

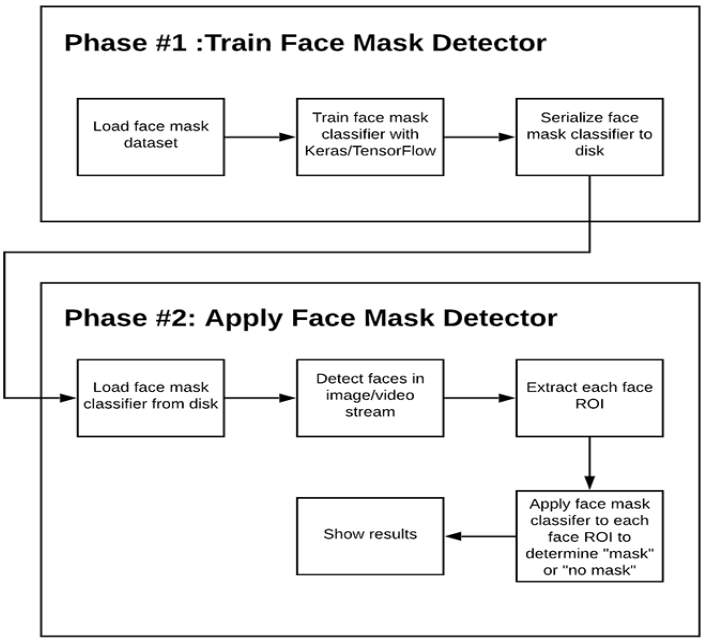

Figure 1: Phases and individual steps for building a COVID-19 face mask detector with computer vision and deep learning using Python, OpenCV, and TensorFlow/Keras.

In order to train a custom face mask detector, we need to break our project into two distinct phases, each with its own respective sub-steps (as shown by Figure 1 above):

1. **Training:** Here we'll focus on loading our face mask detection dataset from disk, training a model (using Keras/TensorFlow) on this dataset, and then serializing the face mask detector to disk
2. **Deployment:** Once the face mask detector is trained, we can then move on to loading the mask detector, performing face detection, and then classifying each face as with_mask or without_mask

Our COVID-19 face mask detection dataset -

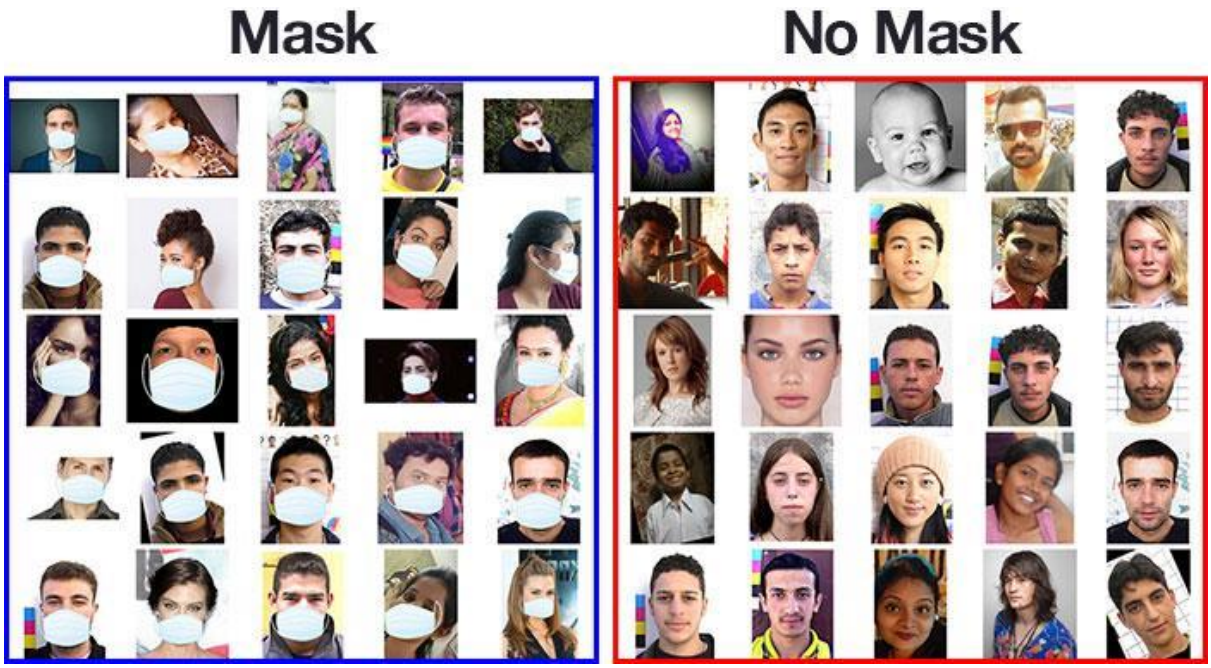

Figure 2: A face mask detection dataset consists of "with mask" and "without mask" images. We will use the dataset to build a COVID-19 face mask detector with computer vision and deep learning using Python, OpenCV, and TensorFlow/Keras.

This dataset consists of 1,376 images belonging to two classes:

- with_mask: 690 images
- without_mask: 686 images

Our goal is to train a custom deep learning model to detect whether a person is or is not wearing a mask.

How was our face mask dataset created?

1. Taking normal images of faces
2. Then creating a custom computer vision Python script to add face masks to them, thereby creating an artificial (but still real-world applicable) dataset

Facial landmarks allow us to automatically infer the location of facial structures, including:

- Eyes
- Eyebrows
- Nose
- Mouth
- Jawline

To use facial landmarks to build a dataset of faces wearing face masks, we need to first start with an image of a person not wearing a face mask:

Figure 3: To build a COVID-19/Coronavirus pandemic face mask dataset, we'll first start with a photograph of someone not wearing a face.

From there, we apply face detection to compute the bounding box location of the face in the image:

Figure 4: The next step is to apply face detection. Here we've used a deep learning method to perform face detection with OpenCV.

Once we know where in the image the face is, we can extract the face Region of Interest (ROI):

Figure 5: The next step is to extract the face ROI with OpenCV and NumPy slicing.

And from there, we apply facial landmarks, allowing us to localize the eyes, nose, mouth, etc.:

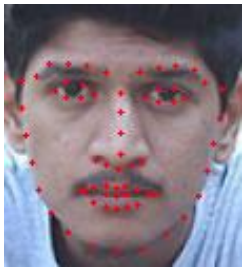

Figure 6: Then, we detect facial landmarks using dlib so that we know where to place a mask on the face.

Next, we need an image of a mask (with a transparent background) such as the one below:

Figure 7: An example of a COVID-19/Coronavirus face mask/shield. This face mask will be overlaid on the original face ROI automatically since we know the face landmark locations.

This mask will be automatically applied to the face by using the facial landmarks (namely the points along the chin and nose) to compute where the mask will be placed.

The mask is then resized and rotated, placing it on the face:

Figure 8: In this figure, the face mask is placed on the person's face in the original frame. It is difficult to tell at a glance that the COVID-19 mask has been applied with computer vision by way of OpenCV and dlib face landmarks.

We can then repeat this process for all of our input images, thereby creating our artificial face mask dataset:

Figure 9: An artificial set of COVID-19 face mask images. This set will be part of our “with mask” / “without mask” dataset for COVID-19 face mask detection with computer vision and deep learning using Python, OpenCV, and TensorFlow/Keras.

However, there is a caveat we should be aware of when using this method to artificially create a dataset!

If we use a set of images to create an artificial dataset of people wearing masks, then we cannot “reuse” the images without masks in your training set — we still need to gather non-face mask images that were not used in the artificial generation process!

If we include the original images used to generate face mask samples as non-face mask samples, out model will become heavily biased and fail to generalize well. Avoid that at all costs by taking the time to gather new examples of faces without masks.

CHAPTER 4

PROJECT STRUCTURE

Three image examples are provided so that we can test the static image mask detector. In this project, we will use three Python scripts:

- train_mask_detector.py: Accept our input data set and fine-tune MobileNetV2 to create our mask_detector.model. At the same time, a training history graph containing the accuracy/loss curve is produced.
- detect_mask_image.py: Perform mask detection using static images.
- detect_mask_video.py: use camera stream.

4.1 Implementing our COVID-19 face mask detector training script with Keras and TensorFlow

To accomplish this task, we'll be fine-tuning the MobileNet V2 Architecture, a highly efficient architecture that can be applied to embedded devices with limited computational capacity (ex., Raspberry Pi, Google Coral, NVIDIA Jetson Nano, etc.).

ARCHITECTURE

MobileNetV2 builds upon the ideas from MobileNetV1 , using depthwise separable convolution as efficient building blocks. However, V2 introduces two new features to the architecture: (1) linear bottlenecks between the layers, and (2) shortcut connections between the bottlenecks1. The basic structure is shown below.

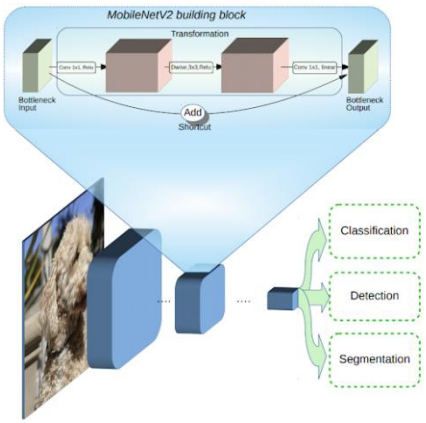

MobileNetV2 Architecture

The typical MobilenetV2 architecture has as many layers listed below, In keras/Tensor Flow we can use the models library in to create the MobileNetV2 model instead of defining/building our own model.

The weights of each layer in the model are predefined based on the ImageNet dataset. The weights indicate the padding, strides, kernel size, input channels and output channels.

Input	Operator	t	c	n	s
$224^2 \times 3$	conv2d	-	32	1	2
$112^2 \times 32$	bottleneck	1	16	1	1
$112^2 \times 16$	bottleneck	6	24	2	2
$56^2 \times 24$	bottleneck	6	32	3	2
$28^2 \times 32$	bottleneck	6	64	4	2
$14^2 \times 64$	bottleneck	6	96	3	1
$14^2 \times 96$	bottleneck	6	160	3	2
$7^2 \times 160$	bottleneck	6	320	1	1
$7^2 \times 320$	conv2d 1x1	-	1280	1	1
$7^2 \times 1280$	avgpool 7x7	-	-	1	-
$1 \times 1 \times 1280$	conv2d 1x1	-	k	-	

Why choose MobileNetV2?

Based on ImageNet dataset MobileNetV2 outperforms MobileNetV1 and ShuffleNet (1.5) with comparable model size and computational cost. And also it will perform well for the smaller dataset.

Network	Top 1	Params	MAdds	CPU
MobileNetV1	70.6	4.2M	575M	113ms
ShuffleNet (1.5)	71.5	**3.4M**	292M	-
ShuffleNet (x2)	73.7	5.4M	524M	-
NasNet-A	74.0	5.3M	564M	183ms
MobileNetV2	**72.0**	**3.4M**	**300M**	**75ms**
MobileNetV2 (1.4)	**74.7**	6.9M	585M	**143ms**

Model Overwritten

MobileNetV2 was chosen as an algorithm to build a model that could be deployed on a mobile device. A customized fully connected layer which contains four sequential layers on top of the MobileNetV2 model was developed. The layers are

1.Average Pooling layer with 7×7 weights

2.Linear layer with ReLu activation function

3.Dropout Layer

4.Linear layer with Softmax activation function with the result of 2 values.

The final layer softmax function gives the result of two probabilities each one represents the classification of “mask” or “not mask”.

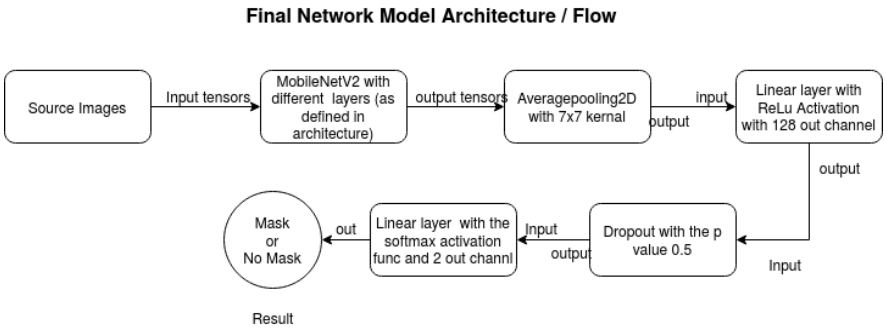

Accuracy Overview

The data set has been divided into two sets, likely a training and validation set. The accuracy of image classifier over the training set vs validation.

Deploying our face mask detector to embedded devices could reduce the cost of manufacturing such face mask detection systems, hence why we choose to use this architecture.

TRAINING SCRIPT:

STEP 1:

Using Keras and TensorFlow to train the classifier to automatically detect whether a person is wearing a mask by importing the following libraries.

```
In [1]: import numpy as np
        import os
        import matplotlib.pyplot as plt

        from imutils import paths

        from tensorflow.keras.applications import MobileNetV2
        from tensorflow.keras.layers import AveragePooling2D
        from tensorflow.keras.layers import Dropout
        from tensorflow.keras.layers import Flatten
        from tensorflow.keras.layers import Dense
        from tensorflow.keras.layers import Input
        from tensorflow.keras.models import Model
        from tensorflow.keras.optimizers import Adam
        from tensorflow.keras.applications.mobilenet_v2 import preprocess_input

        from tensorflow.keras.preprocessing.image import ImageDataGenerator
        from tensorflow.keras.preprocessing.image import img_to_array
        from tensorflow.keras.preprocessing.image import load_img
        from tensorflow.keras.utils import to_categorical
        from sklearn.preprocessing import LabelBinarizer
        from sklearn.model_selection import train_test_split
        from sklearn.metrics import classification_report
```

Fig 4.1 Importing all the necessary python libraries

The main purpose of the above import is:

- Data Augmentation.
- Load the MobilNetV2 classifier (we will fine-tune the model using pre-trained ImageNet weights)
- Building a new fully-connected(FC) head.
- Pretreatment(Preprocessing).
- Loading image data

***We use "scikit-learn (sklearn)" to binarize the class labels, segment the data set, and print the classification report.**

***The "imutils" path implementation will help us find and list images in the data set. We will use "matplotlib" to draw the training curve.**

STEP 2:

Next, we analyze some command line parameters and start the script from the terminal:

--dataset: The path of the input dataset of faces and faces with masks

--plot: output the path of the training history plot, it will be generated using matplotlib

--model: The path of the generated serialized mask classification model

At this point, we are ready to load and pre-process the training data:

```
In [4]: data=[]
        labels=[]

        for i in imagePaths:
            label=i.split(os.path.sep)[-2]
            labels.append(label)
            image=load_img(i,target_size=(224,224))
            image=img_to_array(image)
            image=preprocess_input(image)
            data.append(image)
```

```
In [5]: data
```

```
Out[5]: [array([[[ 0.60784316,  0.5921569 ,  0.6313726 ],
                 [ 0.60784316,  0.5921569 ,  0.6313726 ],
                 [ 0.6       ,  0.58431375,  0.62352943],
                 ...,
                 [ 0.33333337,  0.3411765 ,  0.37254906],
                 [ 0.33333337,  0.3411765 ,  0.37254906],
                 [ 0.33333337,  0.3411765 ,  0.37254906]],

                [[ 0.6       ,  0.58431375,  0.62352943],
                 [ 0.6       ,  0.58431375,  0.62352943],
                 [ 0.62352943,  0.60784316,  0.64705884],
                 ...,
                 [ 0.33333337,  0.3411765 ,  0.37254906],
                 [ 0.33333337,  0.3411765 ,  0.37254906],
                 [ 0.33333337,  0.3411765 ,  0.37254906]],

                [[ 0.5921569 ,  0.5764706 ,  0.6156863 ],
                 [ 0.5921569 ,  0.5764706 ,  0.6156863 ],
```

In this block, we are:

- Grabbing all of the imagePaths in the dataset.
- Initializing data and labels lists.
- Looping over the imagePaths and loading + pre-processing images. Pre-processing steps include resizing to 224×224 pixels, conversion to array format, and scaling the pixel intensities in the input image to the range [-1, 1] Appending the pre-processed image and associated label to the data and labels lists, respectively.
- Ensuring our training data is in NumPy array format.

STEP 3: Next, we encode our labels, partition our dataset, and prepare for DATA AUGMENTATION:

```
# perform one-hot encoding on the labels
lb = LabelBinarizer()
labels = lb.fit_transform(labels)
labels = to_categorical(labels)

# partition the data into training and testing splits using 80% of
# the data for training and the remaining 20% for testing
(trainX, testX, trainY, testY) = train_test_split(data, labels,
    test_size=0.20, stratify=labels, random_state=42)

# construct the training image generator for data augmentation
aug = ImageDataGenerator(
    rotation_range=20,
    zoom_range=0.15,
    width_shift_range=0.2,
    height_shift_range=0.2,
    shear_range=0.15,
    horizontal_flip=True,
    fill_mode="nearest")
```

Fig 4.3. Partitioning the data into training and testing and constructing image generator for data augmentation

STEP 4: Then one-hot encode our class labels, meaning that our data will be in the following format:

```
$ python  train_mask_detector.py --dataset  dataset
[INFO] loading images...
-> (trainX, testX, trainY, testY) = train_test_split(data, labels,
(Pdb) labels[500:]
array([[1., 0.],
       [1., 0.],
       [1., 0.],
       ...,
       [0., 1.],
       [0., 1.],
       [0., 1.]], dtype=float32)
```

Fig 4.4: Labelling the dataset into array

Now, each element of our label array consists of an array in which only one index is “hot” (i.e., 1).Using scikit-learn’s convenience method, this code segments our data into 80% training and the remaining 20% for testing.During training, we’ll be applying on-the-fly mutations to our images in an effort to improve generalization. This is known as data augmentation, where the random rotation, zoom, shear, shift, and flip parameters are established. We’ll use the aug object at training time.

STEP 5: But first, we need to prepare MobileNetV2 for fine-tuning:

```
In [17]: aug=ImageDataGenerator(rotation_range=20,zoom_range=0.15,width_shift_range=0.2,height_shift_range=0.2,shear_range=0.15,horizontal

In [18]: baseModel=MobileNetV2(weights='imagenet',include_top=False,input_tensor=Input(shape=(224,224,3)))

WARNING:tensorflow:From E:\Applications\New folder (2)\lib\site-packages\tensorflow\python\ops\init_ops.py:1251: calling Varian
ceScaling.__init__ (from tensorflow.python.ops.init_ops) with dtype is deprecated and will be removed in a future version.
Instructions for updating:
Call initializer instance with the dtype argument instead of passing it to the constructor

E:\Applications\New folder (2)\lib\site-packages\keras_applications\mobilenet_v2.py:294: UserWarning: `input_shape` is undefine
d or non-square, or `rows` is not in [96, 128, 160, 192, 224]. Weights for input shape (224, 224) will be loaded as the defaul
t.
  warnings.warn('`input_shape` is undefined or non-square, '

In [19]: baseModel.summary()

Model: "mobilenetv2_1.00_224"
__________________________________________________________________________________________________
Layer (type)                    Output Shape         Param #     Connected to
==================================================================================================
input_1 (InputLayer)            [(None, 224, 224, 3) 0
__________________________________________________________________________________________________
Conv1_pad (ZeroPadding2D)       (None, 225, 225, 3)  0           input_1[0][0]
__________________________________________________________________________________________________
Conv1 (Conv2D)                  (None, 112, 112, 32) 864         Conv1_pad[0][0]
__________________________________________________________________________________________________
bn_Conv1 (BatchNormalization)   (None, 112, 112, 32) 128         Conv1[0][0]
__________________________________________________________________________________________________
Conv1_relu (ReLU)               (None, 112, 112, 32) 0           bn_Conv1[0][0]
__________________________________________________________________________________________________
expanded_conv_depthwise (Depthw (None, 112, 112, 32) 288         Conv1_relu[0][0]
__________________________________________________________________________________________________
expanded_conv_depthwise_BN (Bat (None, 112, 112, 32) 128         expanded_conv_depthwise[0][0]
__________________________________________________________________________________________________
expanded_conv_depthwise_relu (R (None, 112, 112, 32) 0           expanded_conv_depthwise_BN[0][0]
```

Fine-tuning setup is a three-step process:

1. Load MobileNet with pre-trained ImageNet weights, leaving the head of the network.
2. Construct a new FC head, and append it to the base in place of the old head.
3. Freeze the base layers of the network. The weights of these base layers will not be updated during the process of backpropagation, whereas the head layer weights will be tuned.

STEP 6: Train COVID-19 mask detector

Now, to train the mask detector using Keras, TensorFlow and Deep Learning.:

Here, I've specified hyperparameter constants including the initial learning rate, number of training epochs, and batch size.

In [23]:
```
learning_rate=0.001
Epochs=20
BS=12

opt=Adam(lr=learning_rate,decay=learning_rate/Epochs)
model.compile(loss='binary_crossentropy',optimizer=opt,metrics=['accuracy'])

H=model.fit(
    aug.flow(train_X,train_Y,batch_size=BS),
    steps_per_epoch=len(train_X)//BS,
    validation_data=(test_X,test_Y),
    validation_steps=len(test_X)//BS,
    epochs=Epochs
)


model.save(r'C:\Users\This pc\Desktop\Face mask detector\mobilenet_v2.model')
```

```
Epoch 1/20
WARNING:tensorflow:From E:\Applications\New folder (2)\lib\site-packages\tensorflow\python\ops\math_grad.py:1250: add_dispatch_
support.<locals>.wrapper (from tensorflow.python.ops.array_ops) is deprecated and will be removed in a future version.
Instructions for updating:
Use tf.where in 2.0, which has the same broadcast rule as np.where
87/87 [==============================] - 135s 2s/step - loss: 0.4862 - acc: 0.7834 - val_loss: 0.1413 - val_acc: 0.9582
Epoch 2/20
87/87 [==============================] - 135s 2s/step - loss: 0.2316 - acc: 0.9086 - val_loss: 0.1199 - val_acc: 0.9544
Epoch 3/20
87/87 [==============================] - 137s 2s/step - loss: 0.2143 - acc: 0.9153 - val_loss: 0.0586 - val_acc: 0.9810
Epoch 4/20
87/87 [==============================] - 138s 2s/step - loss: 0.1646 - acc: 0.9317 - val_loss: 0.0530 - val_acc: 0.9734
Epoch 5/20
87/87 [==============================] - 138s 2s/step - loss: 0.1396 - acc: 0.9451 - val_loss: 0.0536 - val_acc: 0.9696
Epoch 6/20
87/87 [==============================] - 140s 2s/step - loss: 0.1903 - acc: 0.9172 - val_loss: 0.0358 - val_acc: 0.9848
Epoch 7/20
87/87 [==============================] - 140s 2s/step - loss: 0.1533 - acc: 0.9349 - val_loss: 0.0535 - val_acc: 0.9734
```


```
87/87 [==============================] - 138s 2s/step - loss: 0.1646 - acc: 0.9317 - val_loss: 0.0530 - val_acc: 0.9734
Epoch 5/20
87/87 [==============================] - 138s 2s/step - loss: 0.1396 - acc: 0.9451 - val_loss: 0.0536 - val_acc: 0.9696
Epoch 6/20
87/87 [==============================] - 140s 2s/step - loss: 0.1903 - acc: 0.9172 - val_loss: 0.0358 - val_acc: 0.9848
Epoch 7/20
87/87 [==============================] - 140s 2s/step - loss: 0.1533 - acc: 0.9349 - val_loss: 0.0535 - val_acc: 0.9734
```


```
Epoch 8/20
87/87 [==============================] - 147s 2s/step - loss: 0.1560 - acc: 0.9333 - val_loss: 0.0301 - val_acc: 0.9886
Epoch 9/20
87/87 [==============================] - 141s 2s/step - loss: 0.1793 - acc: 0.9288 - val_loss: 0.0404 - val_acc: 0.9886
Epoch 10/20
87/87 [==============================] - 141s 2s/step - loss: 0.1480 - acc: 0.9394 - val_loss: 0.0461 - val_acc: 0.9772
Epoch 11/20
87/87 [==============================] - 142s 2s/step - loss: 0.1293 - acc: 0.9442 - val_loss: 0.0450 - val_acc: 0.9848
Epoch 12/20
87/87 [==============================] - 159s 2s/step - loss: 0.1669 - acc: 0.9326 - val_loss: 0.0349 - val_acc: 0.9848
Epoch 13/20
87/87 [==============================] - 163s 2s/step - loss: 0.1540 - acc: 0.9403 - val_loss: 0.0408 - val_acc: 0.9810
Epoch 14/20
87/87 [==============================] - 155s 2s/step - loss: 0.1626 - acc: 0.9249 - val_loss: 0.0547 - val_acc: 0.9734
Epoch 15/20
87/87 [==============================] - 154s 2s/step - loss: 0.1415 - acc: 0.9394 - val_loss: 0.0341 - val_acc: 0.9886
Epoch 16/20
87/87 [==============================] - 165s 2s/step - loss: 0.1322 - acc: 0.9387 - val_loss: 0.0665 - val_acc: 0.9620
Epoch 17/20
87/87 [==============================] - 161s 2s/step - loss: 0.1530 - acc: 0.9371 - val_loss: 0.0739 - val_acc: 0.9658
Epoch 18/20
87/87 [==============================] - 177s 2s/step - loss: 0.1194 - acc: 0.9557 - val_loss: 0.0645 - val_acc: 0.9658
Epoch 19/20
87/87 [==============================] - 160s 2s/step - loss: 0.1395 - acc: 0.9471 - val_loss: 0.0471 - val_acc: 0.9772
Epoch 20/20
87/87 [==============================] - 157s 2s/step - loss: 0.1173 - acc: 0.9509 - val_loss: 0.0415 - val_acc: 0.9810
```

In [24]:
```
predict=model.predict(test_X,batch_size=BS)
predict=np.argmax(predict,axis=1)
print(classification_report(test_Y.argmax(axis=1),predict,target_names=lb.classes_))
```

```
                    precision    recall  f1-score   support

   train/with_mask       0.96      1.00      0.98       132
train/without_mask       1.00      0.96      0.98       131

          accuracy                           0.98       263
         macro avg       0.98      0.98      0.98       263
      weighted avg       0.98      0.98      0.98       263
```

Fig 4.6: Training the mask detector

STEP 7: Our last step is to draw the accuracy and loss curve:

```
In [29]: # plot the training loss and accuracy

N=Epochs
plt.style.use("ggplot")
plt.figure()
plt.plot(np.arange(0, N), H.history["loss"], label="train_loss")
plt.plot(np.arange(0, N), H.history["val_loss"], label="val_loss")
plt.plot(np.arange(0, N), H.history["acc"], label="train_acc")
plt.plot(np.arange(0, N), H.history["val_acc"], label="val_acc")
plt.title("Training Loss and Accuracy")
plt.xlabel("Epoch #")
plt.ylabel("Loss/Accuracy")
plt.legend(loc="lower left")
plt.savefig(r'C:\Users\This pc\Desktop\Face mask detector\plot_v2.png')
```

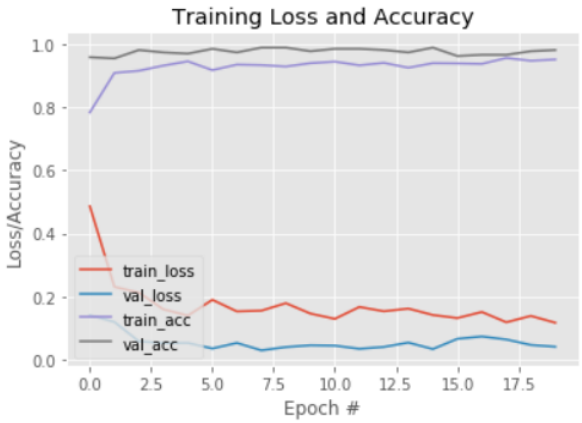

Fig 4.7: Training vs Validation Accuracy

As, we are obtaining ~99% accuracy on our test set.

*Looking at Figure, we can see there are little signs of overfitting, with the validation loss lower than the training loss.

CHAPTER 5

IMPLEMENTATION

Implementing our COVID-19 face mask detector for images with OpenCV

STEP 1: Now that our face mask detector is trained, the next steps will be :

1. Load an input image from disk
2. Detect faces in the image
3. Apply our face mask detector to classify the face as either “with_mask”or “without_mask”.

```
In [1]: from tensorflow.keras.applications.mobilenet_v2 import preprocess_input
        from tensorflow.keras.preprocessing.image import img_to_array
        from tensorflow.keras.models import load_model
        import numpy as np
        import cv2
        import os
```

Fig.5.1 Our driver script requires three TensorFlow/Keras imports to (1) load our MaskNet model and (2) pre-process the input image. OpenCV is required for display and image manipulations.Next, we’ll load both our face detector and face mask classifier models.

```
In [2]: prototxtPath=os.path.sep.join([r'C:\Users\This pc\Desktop\Face mask detector\Mask-Detection-and-Recognition-using-Deep-Learning-K
        weightsPath=os.path.sep.join([r'C:\Users\This pc\Desktop\Face mask detector\Mask-Detection-and-Recognition-using-Deep-Learning-Ke

In [3]: prototxtPath
Out[3]: 'C:\\Users\\This pc\\Desktop\\Face mask detector\\Mask-Detection-and-Recognition-using-Deep-Learning-Keras-master\\deploy.proto
        txt'

In [4]: weightsPath
Out[4]: 'C:\\Users\\This pc\\Desktop\\Face mask detector\\Mask-Detection-and-Recognition-using-Deep-Learning-Keras-master\\res10_300x30
        0_ssd_iter_140000.caffemodel'

In [5]: net=cv2.dnn.readNet(prototxtPath,weightsPath)

In [ ]:

In [6]: model=load_model(r'C:\Users\This pc\Desktop\Face mask detector\Mask-Detection-and-Recognition-using-Deep-Learning-Keras-master\mo

        WARNING:tensorflow:From E:\Applications\New folder (2)\lib\site-packages\tensorflow\python\ops\init_ops.py:97: calling GlorotUn
        iform.__init__ (from tensorflow.python.ops.init_ops) with dtype is deprecated and will be removed in a future version.
```

STEP 2: The next step is to load and preprocess an input image:

```
In [7]: image=cv2.imread(r'C:\Users\This pc\Desktop\Face mask detector\Mask-Detection-and-Recognition-using-Deep-Learning-Keras-master\ma
```

```
In [8]: image
```

```
Out[8]: array([[[249, 249, 249],
                [246, 246, 246],
                [244, 244, 244],
                ...,
                [248, 248, 248],
                [212, 212, 212],
                [231, 231, 231]],

               [[245, 245, 245],
                [247, 247, 247],
                [247, 247, 247],
                ...,
                [247, 247, 247],
                [212, 212, 212],
                [231, 231, 231]],

               [[241, 241, 241],
                [248, 248, 248],
                [249, 249, 249],
                ...,
                [247, 247, 247],
                [211, 211, 211],
                [230, 230, 230]],

               ...,

               [[  1,   0,   4],
                [  4,   0,  12],
```

```
In [9]: (h,w)=image.shape[:2]
```

```
In [10]: (h,w)
```

```
Out[10]: (499, 821)
```

```
In [11]: blob=cv2.dnn.blobFromImage(image,1.0,(300,300),(104.0,177.0,123.0))
```

```
In [12]: blob
```

```
Out[12]: array([[[[ 142.,  138.,  116., ...,  142.,  143.,  110.],
                  [ 143.,  127.,  117., ...,  142.,  142.,  109.],
                  [ 143.,  117.,  118., ...,  142.,  142.,  108.],
                  ...,
                  [ 132.,  148.,  145., ...,  120.,    5., -100.],
                  [-100., -102., -101., ..., -101., -102., -102.],
                  [-101., -102., -101., ...,  -11., -103., -103.]],

                 [[  69.,   65.,   43., ...,   69.,   70.,   37.],
                  [  70.,   54.,   44., ...,   69.,   69.,   36.],
                  [  70.,   44.,   45., ...,   69.,   69.,   35.],
                  ...,
                  [  65.,   71.,   68., ...,   47.,  -70., -174.],
                  [-177., -176., -177., ..., -177., -175., -175.],
                  [-177., -176., -177., ...,  -97., -176., -176.]],

                 [[ 123.,  119.,   97., ...,  123.,  124.,   91.],
                  [ 124.,  108.,   98., ...,  123.,  123.,   90.],
                  [ 124.,   98.,   99., ...,  123.,  123.,   89.],
                  ...,
                  [ 120.,  127.,  126., ...,  101.,  -11., -116.],
                  [-112., -118., -114., ..., -120., -121., -121.],
                  [-112., -118., -114., ...,  -78., -122., -122.]]]], dtype=float32)
```

```
In [13]: blob.shape
```

```
Out[13]: (1, 3, 300, 300)
```

```
In [14]: net.setInput(blob)
         detections=net.forward()
```

```
In [15]: detections
```

```
Out[15]: array([[[[0.        , 1.        , 0.99477947, ..., 0.28274554,
                   0.9131958 , 0.6661748 ],
                  [0.        , 1.        , 0.92867446, ..., 0.2875712 ,
                   0.25532252, 0.6736033 ],
                  [0.        , 1.        , 0.46425745, ..., 0.21960367,
                   0.62674445, 0.6146078 ],
                  ...,
                  [0.        , 0.        , 0.        , ..., 0.        ,
                   0.        , 0.        ],
                  [0.        , 0.        , 0.        , ..., 0.        ,
                   0.        , 0.        ],
                  [0.        , 0.        , 0.        , ..., 0.        ,
                   0.        , 0.        ]]]], dtype=float32)
```

STEP 3: Upon loading our image from disk, we make a copy and grab frame dimensions for future scaling and display purposes. Pre-processing is handled by OpenCV BlobFormImage Function. As shown in the parameters, we resize to 300×300 pixels and perform mean subtraction. Then perform face detection to localize where in the image all faces are.

After knowing the predicted position of each face, we will ensure that they meet the threshold before the confidence extraction of faceROIs:

```
In [16]: #loop over the detections
         for i in range(0,detections.shape[2]):
             confidence=detections[0,0,i,2]


             if confidence>0.5:
                 #we need the X,Y coordinates
                 box=detections[0,0,i,3:7]*np.array([w,h,w,h])
                 (startX,startY,endX,endY)=box.astype('int')

                 #ensure the bounding boxes fall within the dimensions of the frame
                 (startX,startY)=(max(0,startX),max(0,startY))
                 (endX,endY)=(min(w-1,endX), min(h-1,endY))


                 #extract the face ROI, convert it from BGR to RGB channel, resize it to 224,224 and preprocess it
                 face=image[startY:endY, startX:endX]
                 face=cv2.cvtColor(face,cv2.COLOR_BGR2RGB)
                 face=cv2.resize(face,(224,224))
                 face=img_to_array(face)
                 face=preprocess_input(face)
                 face=np.expand_dims(face,axis=0)

                 (mask,withoutMask)=model.predict(face)[0]

                 #determine the class label and color we will use to draw the bounding box and text
                 label='Mask' if mask>withoutMask else 'No Mask'
                 color=(0,255,0) if label=='Mask' else (0,0,255)

                 #include the probability in the label
                 label="{}: {:.2f}%".format(label,max(mask,withoutMask)*100)

                 #display the label and bounding boxes
                 cv2.putText(image,label,(startX,startY-10),cv2.FONT_HERSHEY_SIMPLEX,0.45,color,2)
                 cv2.rectangle(image,(startX,startY),(endX,endY),color,2)


         cv2.imshow("OutPut",image)
         cv2.waitKey(0)
         cv2.destroyAllWindows()
```

Fig 5.3: Running the facial ROI through our MaskNet model:

In this block, we:

- Extract the face ROI via NumPy slicing.
- Pre-process the ROI the same way we did during training.
- Perform mask detection to predict with_mask or without_mask.

STEP 4 : From here, the result will be annotated and displayed!

* First, we determine the class label based on probabilities returned by the mask detector model and assign an associated color for the annotation. The color will be “green” for with_mask and “red” for without_mask. We then draw the label text (including class and probability), as well as a bounding box rectangle for the face, using OpenCV drawing functions.

Once all detections have been processed, it displays the output image.

USE CASES

1 . Let’s try an image, this one of a person *wearing* a face mask:

Fig 4.4: Is our PM wearing a COVID-19/Coronavirus face mask in public? Yes, he is and our computer vision and deep learning method using Python, OpenCV, and TensorFlow/Keras has made it possible to detect the presence of the mask automatically.

2 . Let's try another image, this one of a person *not* wearing a face mask:

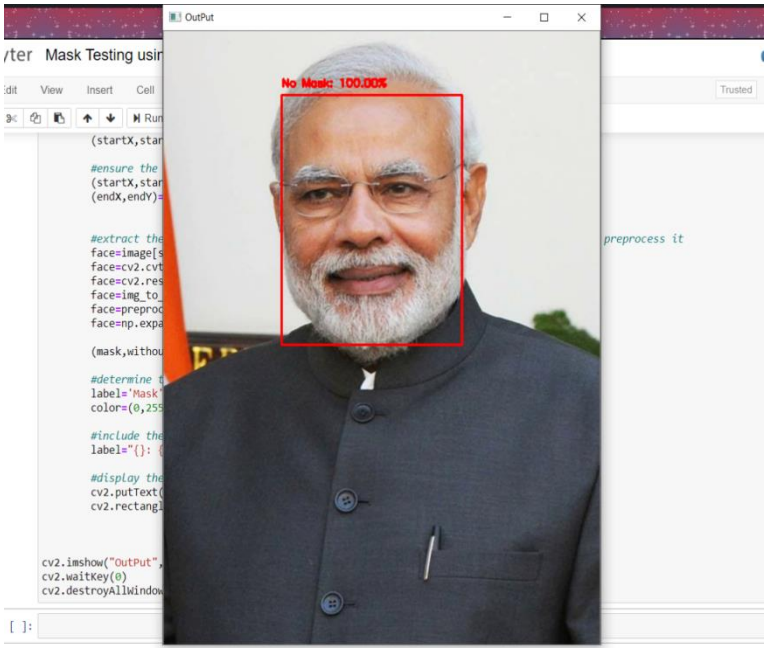

Fig 4.5: Our PM is not wearing a COVID-19 face mask in this picture. Using Python, OpenCV, and TensorFlow/Keras, our system has correctly detected "No Mask" for the face.

3 . Let's try an image, this one of multiple persons *wearing* a face mask:

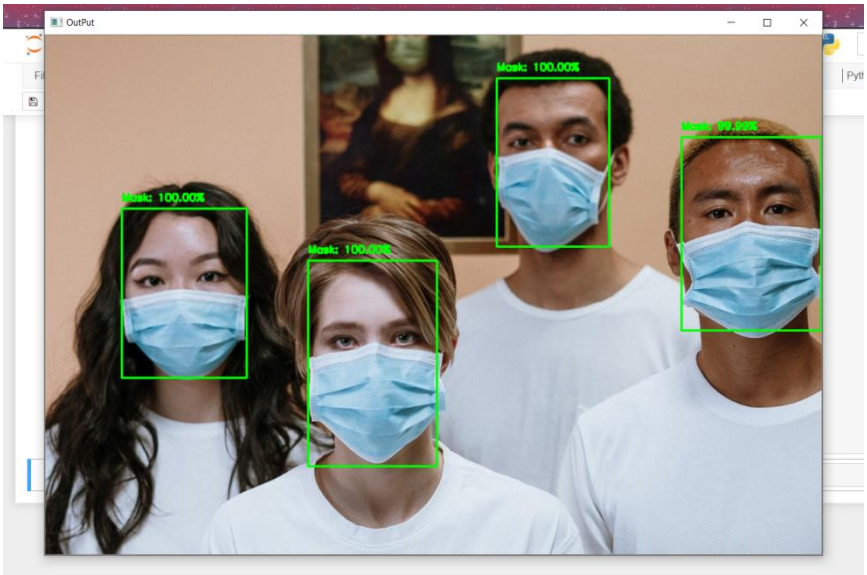

Fig 4.6: These people are wearing a COVID-19 face mask in this picture. Using Python, OpenCV, and TensorFlow/Keras, our system has correctly detected "Mask" for multiple faces.

4. Let's try another image, this one of multiple persons *wearing* and *not wearing* a face mask:

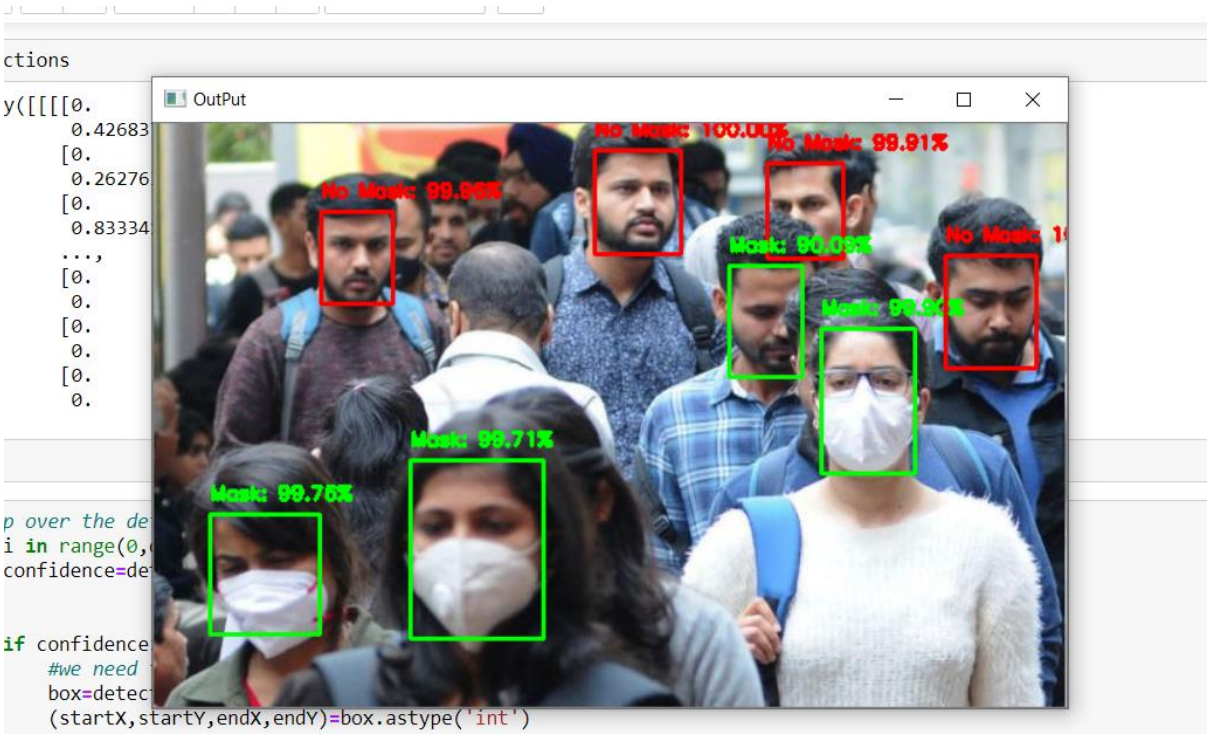

Fig 4.6: Some people are wearing and some not wearing a COVID-19 face mask in this picture. Using Python, OpenCV, and TensorFlow/Keras, our system has correctly detected "Mask" and "No Mask" for multiple faces.

CHAPTER 5

DETAILS AND SUMMARY

5.1 Improvements

As we can see from the results sections above, our face mask detector is working quite well despite:

1. Having limited training data
2. The with_mask class being artificially generated.

To improve our face mask detection model further, we should gather actual images (rather than artificially generated images) of people wearing masks.

While our artificial dataset worked well in this case, there's no substitute for the real thing.

Secondly, we should also gather images of faces that may "confuse" our classifier into thinking the person is wearing a mask when in fact they are not — potential examples include shirts wrapped around faces, bandana over the mouth, etc.

All of these are examples of something that could be confused as a face mask by our face mask detector.

Finally, we should consider training a dedicated two-class object detector rather than a simple image classifier.

Our current method of detecting whether a person is wearing a mask or not is a two-step process:

1. Step 1: Perform face detection.
2. Step 2: Apply our face mask detector to each face.

The problem with this approach is that a face mask, by definition, obscures part of the face. If enough of the face is obscured, the face cannot be detected, and therefore, the face mask detector will not be applied.

To circumvent that issue, a two-class object detector can be trained that consists of a with_mask and without_mask class. Combining an object detector with a dedicated with_mask class will allow improvement of the model in two respects.

First, the object detector will be able to naturally detect people wearing masks that otherwise would have been impossible for the face detector to detect due to too much of the face being obscured.

Secondly, this approach reduces our computer vision pipeline to a single step — rather than applying face detection and then our face mask detector model, all we need to do is apply the object detector to give us bounding boxes for people both with_mask or without_mask in a single forward pass of the network.

Not only is such a method more computationally efficient, it's also more "elegant" and end-to-end.

5.2 Summary

To create a COVID-19 face mask detector using OpenCV, Keras/TensorFlow, and Deep Learning.We trained a two-class model of people wearing masks and people not wearing masks.

We fine-tuned MobileNetV2 on our mask/no mask dataset and obtained a classifier that is ~99% accurate.

We then took this face mask classifier and applied it to images Detecting faces in images by:

1. Extracting each individual face
2. Applying our face mask classifier

Our face mask detector is accurate, and since we used the MobileNetV2 architecture, it's also computationally efficient, making it easier to deploy the model to embedded systems (Raspberry Pi, Google Coral, Jetson, Nano, etc.).

REFERENCES

- https://www.edureka.co/blog/what-is-deep-learning
- https://www.edureka.co/blog/python-opencv-tutorial/
- https://towardsdatascience.com/covid-19-face-mask-detection-using-tensorflow-and-opencv-702dd833515b
- https://www.edureka.co/blog/convolutional-neural-network/

STUDY OF TRAFFIC FLOW AND NOISE POLLUTION RELATED IT

A Project thesis for the successful evaluation of project works for the award of degree of

Master of Technology

In

Transportation Engineering

SUBMITTED BY

Pankaj Kumar Sharma

UNDER THE GUIDANCE OF

Mr. Atul Soni

CIVIL ENGINEERING DEPARTMENT

GLA UNIVERSITY, MATHURA(U.P.)

2019-2021

GLA UNIVERSITY, MATHURA

DECLARATION

I hereby declare that the work which is being presented in the M.Tech Project **"Study of Traffic flow and Noise Pollution related it"**, in the partial fulfillment of the requirement for award of Master of Technology in Transportation Engineering and submitted to the Department of Civil Engineering of GLA University, Mathura is an authentic record of my own work carried under supervision Mr. Atul Soni Sir.

Date: 01.06.21
Place: Mathura

Pankaj

Pankaj Kumar Sharma

GLA UNIVERSITY, MATHURA

CERTIFICATE

The undersigned is to certify that **Pankaj Kumar Sharma** is registered for the M.Tech (Transportation Engineering) programme in Department of Civil Engineering.

I hereby informed that the thesis entitled Project **"Study of Traffic Flow and Noise pollution related it"** be accepted for the partial fulfillment of the requirements for evaluation and award of the M.Tech degree.

Date : 01.06.21

Mr. Atul Soni

(Project Guide)

Professor & Head
Department of Civil Engineering
Institute of Engineering & Technology
GLA University, Mathura-281406

ACKNOWLEDGEMENT

I would like to express my sincere gratitude to my Supervisor and Guide, Asst. Professor **Mr. Atul Soni Sir** of Civil Engineering Department, GLA University (Mathura) for their excellent guidance, constant inspiration, and motivation and above all for their ever attitude that enabled me in carrying up this thesis in the current form.

I also wish to express my deep sense of gratitude to **Prof. (Dr.) Sudhir Goyal, HOD,** Civil Engineering Department, GLA University (Mathura), for providing me an opportunity to work on this project and respected departmental facilities.

I also greatly thankful to all the staff members of the Civil Engineering Department and my entire well-wishers, friends and classmates for their inspiration and help. A special thanks to Asst. Professor **Mr. Atul Soni Sir, Dr. Kunwar Raghvendra Sir and Payal Dubey Mam** for their valuable efforts in solving my problems with great pleasure.

Civil Engineering Department
GLA University (Mathura)

Pankaj Kumar Sharma

ABSTRACT

Noise pollution is an unwelcome result of urbanization and industrialization. Despite the fact that it is undetectable, this unwanted or excessive sound causes enormous harm to humans and has a negative impact on our environment. Among the noise sources with which we deal on a daily basis, transportation noise is likely the fastest-growing and most difficult to avoid. The main objective of this research to calculate Traffic Noise and Traffic Volume on NH-19 in Mathura Uttar Pradesh.

The study includes the areas (i) GLA University, Mathura, (ii) Govardhan Chauraha, (iii) Township Mathura. The study is conducted using Sound Level Meter SLM 100 type 2 and DSLR Camera using for Traffic study. The results were compared with WHO guidelines, which states that the noise level should not exceed 70dB. Due to more traffic on NH-19 causing increasing in traffic noise. The noise level lies between 65dB to 95dB, which is more as compare to WHO guidelines. The impact can be harmful to the people and surrounded environment. Hence, it can cause disease such as concentration difficulty, irritation, annoyance and are most prominent disorders due to continuous traffic noise.

KEYWORDS: Transportation, Noise pollution, Traffic Volume, Sound Level meter.

Table of Contents

List of Tables

List of Figures

CHAPTER - 1
INTRODUCTION

1.1 BACKGROUND

The vibrations in the air that reach our ears are referred to as sound. India is a developing country, which has several environmental issues like air pollution, water pollution and noise pollution [1]. Noise pollution, which is primarily a result of high human population density and a developed industrial state, is now widely acknowledged as a severe threat to urban quality of life. Even in industrialized countries, it is becoming a more constant and undetectable form of air pollution. Noise pollution is unsustainable because it has both direct and indirect health effects[out]. Noise is a common component of the environment, originating from transportation, industry, and neighbors [2]. Traffic noise is one of the most significant sources of noise pollution that has a negative impact on human health [3]. The Ministry of Environment and Forests of the Government of India has issued a notification about permissible noise levels. According to the WHO, the noise pollution creates some human health issues like sleeping disorder, hearing problem, and also headache problem. Due to the poor sleeping there are many chances of accidents [4]. For several urban areas, permissible noise limits have been established. The most recent, the Noise Pollution (Regulation and Control) Rules 2000, which were published in February 2000, explicitly categorized our surroundings into four categories and established the allowed noise limits for each category separately for day and night time.

Different sources and their contribution into Noise Pollution:

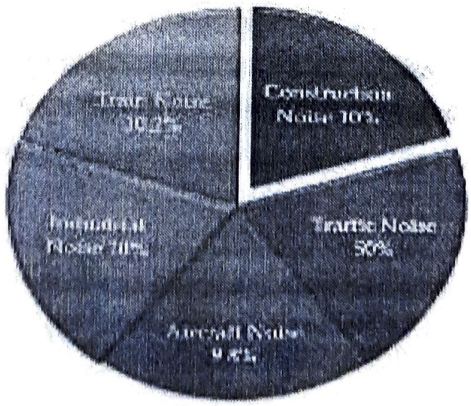

Fig.1 Different sources and their contribution into Noise Pollution
(Source: https://brainly.in/question/11759804?tbs_match=2)

1.2 IMPORTANCE OF STUDY

Mathura is a city in India's Uttar Pradesh state. It's about 55 kilometers north of Agra and 145 kilometers south of Delhi. It is one of India's most well-known pilgrimage destinations and the birthplace of Lord Krishna, an ancient Hindu deity.

The town is one of India's oldest and is well-known for its rich culture and customs. Mathura is home to numerous tourist attractions, pilgrimage sites, and temples. So the city experiences a high number of traffic. Due to the higher traffic volume at several intersections on NH19 (previously known as NH2), There will be a lot of traffic noise, which needs to be addressed.

1.3 OBJECTIVE

These are the following primary goals of this research: -

- To calculate the traffic flow in Mathura City on NH44.
- To assess and quantify traffic noise level L_{min}, L_{max} and L_{eq}.
- Effect of road traffic related noise pollution on human health on NH44.

1.4 STUDY FRAMEWORK

Chapter 1: Introduction is to inform the audience about the study's context. This section also includes a statement of the problem and a list of the objectives that must be met throughout the research.

Chapter 2: Literature Review provides a brief demonstration of noise pollution and its effects on the environment. It also includes articles from the past and present on the subject of noise pollution.

Chapter 3: The current study highlights and investigates noise pollution in Mathura. The noise review that was directed in Mathura also acknowledged for the measuring techniques that were used.

CHAPTER - 2
LITERATURE REVIEW

2.1 INTRODUCTION

This section gives the audience a brief introduction to environmental noise and noise pollution. The reasons for activity noise are investigated, as well as the impact of noise on human beings.

2.2 GENERAL

Increased traffic flow on the road not only causes congestion, but it also contributes to air and noise pollution. Noise is produced not just by passing motor vehicles, but also by friction between the road and vehicle tires, as well as vehicle horns [5]. These noises can be tolerated by society to some extent, in the sense that the sound does not cause a disturbance of comfort but it also other disturbance to the community, but the sounds produced by transportation vehicles at a higher level can already be classified as an annoyance known as noise pollution [6]. When compared to other factors such as pollution or congestion, noise from traffic becomes the standard of irritation for disturbed persons. According to study conducted in Montreal, there is a link between highway traffic noise levels and overall ambient noise [7]. Several factors are known to influence such noise, one of which is the distance from the noise source. Noise disturbance is strongly influenced by the distance to the main road and the type of road [8]. The distance from the noise source has a considerable effect on the noise level, which lowers to a constant tendency of the noise level as the distance increases [9]. In the previous study, the researcher used the microphone, tape recorder to measure the traffic noise level on the road [10]. Also questionnaire based survey was used in the previous study to measure the traffic noise [11].

SLM (Sound level Meter) is also used for measure the noise level. For comparison of the traffic noise with traffic volume, we used the video recorder camera to collect the traffic volume data. After collection of the traffic volume data, we relate this data with traffic noise data and check how does increasing in traffic volume increase traffic noise. The noise pollution from vehicles is a potential health hazard. Rapid urbanization and exponential traffic increase have compounded the problem because it is a worldwide danger. The population living near busy

traffic lanes is constantly exposed to sound levels that exceed the allowed limits. According to the findings of many researches, vehicle-produced noise pollution causes a variety of health concerns, including Irritation and annoyance, sleep disruptions, cardiovascular illness, stroke risk, diabetes, hypertension, and hearing loss are all caused by traffic noise. Work performance suffers as a result of it [12]. Maybe most paramount has been the predictable resignation to engineering and the perpetually-expanding development of high-thickness improvements, the reason being that for every last improvement:

1) There is an increment in the amount of vehicles.

2) Noise, dissimilar to air and water pollution, can't be outwardly decided and takes off no unmistakable record of its vicinity.

3) Noise is innately a specialized issue which the standard national has extraordinary trouble in understanding. While humankind does not comprehend the complex make-up of noise pollution, it is by the by evident that noise is a type of pollution that is requests therapeutic activity by government.

2.3 CAUSES OF TRAFFIC NOISE

Vehicle expansion is the backbone of economic development. But it produces more noise pollution. India's automotive industry is the world's second fastest expanding. Currently, the country produces around 8 million vehicles each year. The country has 121.63 million registered motor cars in 2009, with a motorization rate of 22 automobiles per 1000 people [13]. Noise originates from a variety of causes, one of which being transportation. There are three causes of noise: (a) the friction between the vehicle's tyres and the road. (b) The friction between the vehicle tyres and the road. (c) Heavy vehicle engine (exhaust).

The amount of highway traffic noise is determined by:

(a) Traffic speed (b) Traffic volume

2.4 IMPACT OF NOISE ON HUMAN BEINGS

Physical impact of noise:

High-intensity noise can harm our hearing, either temporarily or permanently. These injuries have a well-understood science. Noise-induced hearing loss can occur in a variety of scenarios when the level of sound is high. Given the wide range of human ear sensitivity to noise, this

could result in hearing loss. And the dangerous character of a noisy environment is referred to as "damage risk." When the corresponding sound level is less than 75dB over an 8-hour exposure period, the danger is considered insignificant.

Physiological impact of noise:

Noise can create momentary stress reactions (such as an increase in heart rate and blood pressure) as well as have harmful impacts on our coordination and respiratory systems. Long-term exposure to noise can result in a permanent elevation in blood pressure [14]. A few studies comparing the physiological behavior of persons who live on noisy streets to those who live on quiet streets have been conducted on the general public. The findings indicate that persons who live on a loud street had higher blood pressure [15].

2.5 INDIAN STANDARDS FOR AMBIENT NOISE LEVELS

The Ministry of Environment and Forests of the Government of India has issued Noise Level Standards and Guidelines under the Environment (protection) Rules 1986, also known as Noise Pollution (Regulation and Control) Rules 2000, in recognition of the necessity to control and regulate noise levels. The following are the specific rules-based standards:

Table 1 Indian Standards for ambient noise levels

Area Code	Category of Area Limits dB(A), L_{eq}	Day	Night
A	Industrial area	75	70
B	Commercial area	65	55
C	Residential area	55	45
D	Silence Zone	50	40

2.6 WHO STANDARDS FOR AMBIENT NOISE LEVELS

To avoid noise-induced hearing loss, the US Environmental Protection Agency (EPA) and the World Health Organization (WHO) suggest that environmental noises be kept below 70 decibels for 24 hours (75 decibels for 8 hours).

CHAPTER - 3
METHODOLOGY

3.1 GENERAL

This chapter describes the procedure for doing the noise assessment in Mathura. There are also diagrams of the instruments used during noise measurements as well as specific measuring spots.

3.2 STUDY AREA

The current research took place between 20th Oct 2020 and 25th Dec 2020. GLA University, Goverdhan Chauraha and Mathura Township were chosen as the study locations for traffic volume and air quality. According to their medical histories and recent studies, the impact of noise pollution on people's health was investigated.

3.2.1 GLA University

In Mathura, Uttar Pradesh, it is one of the top-ranked institute centres. Around 130,000 students apply to this university each year. This university's growing popularity has resulted in increased traffic noise pollution.

3.2.2 Govardhan Chauraha

This is one of the city's most important locations. The area is quite packed, with dozens of street merchants. This location is mostly a commercial district with some institutional land use. This is the intersection of National Highway 19 and the city of Mathura. Also there is a big market here. Due to the large traffic volume, there is more noise pollution.

3.2.3 Mathura Township

This location is famous due to Mathura Oil Refinery. Also there are many residential colonies and big shopping malls near this. So there is more noise pollution.

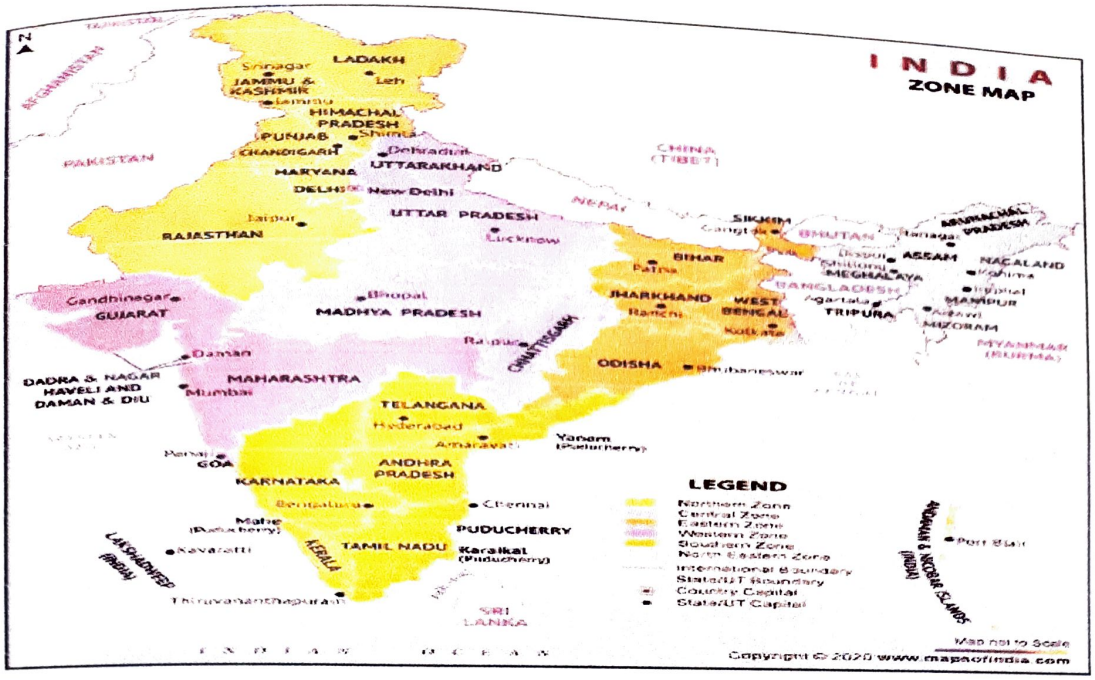

Fig.2 Map of India

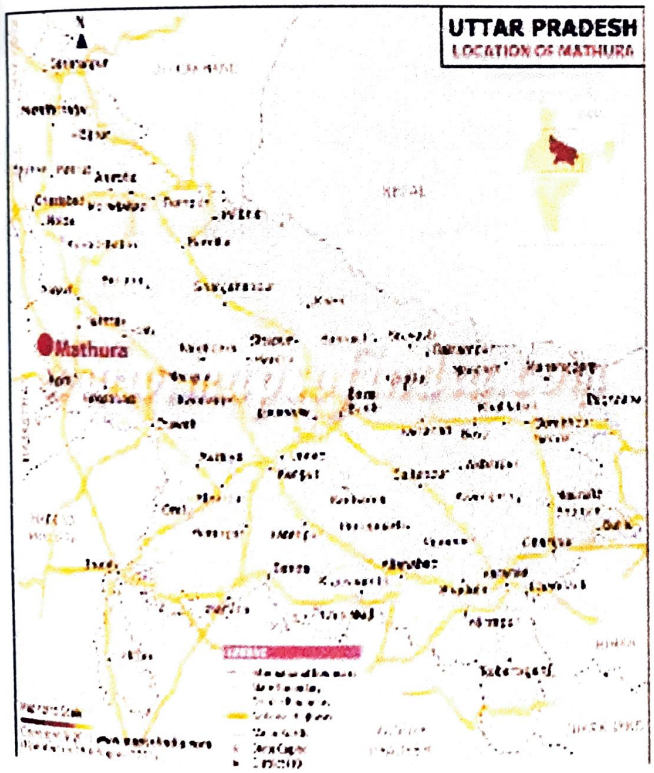

Fig.3 Map of Uttar Pradesh

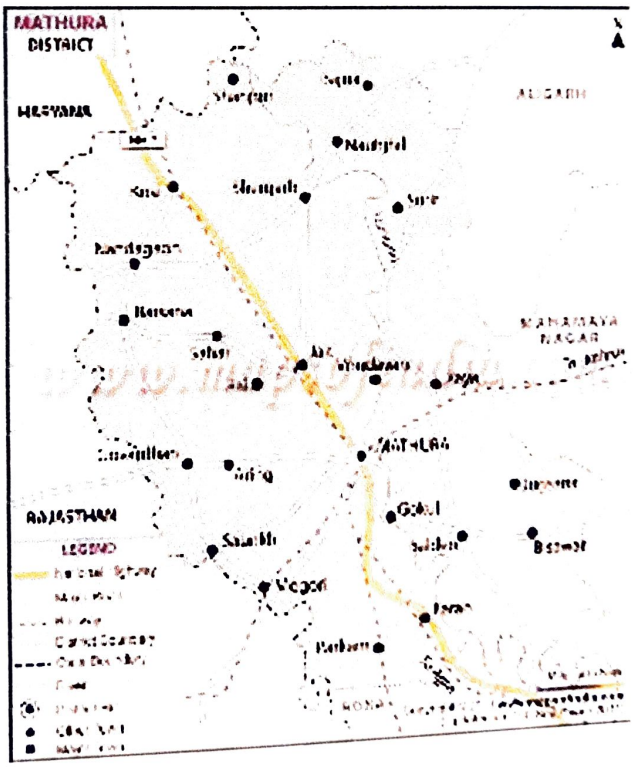

Fig.4 Map of Mathura

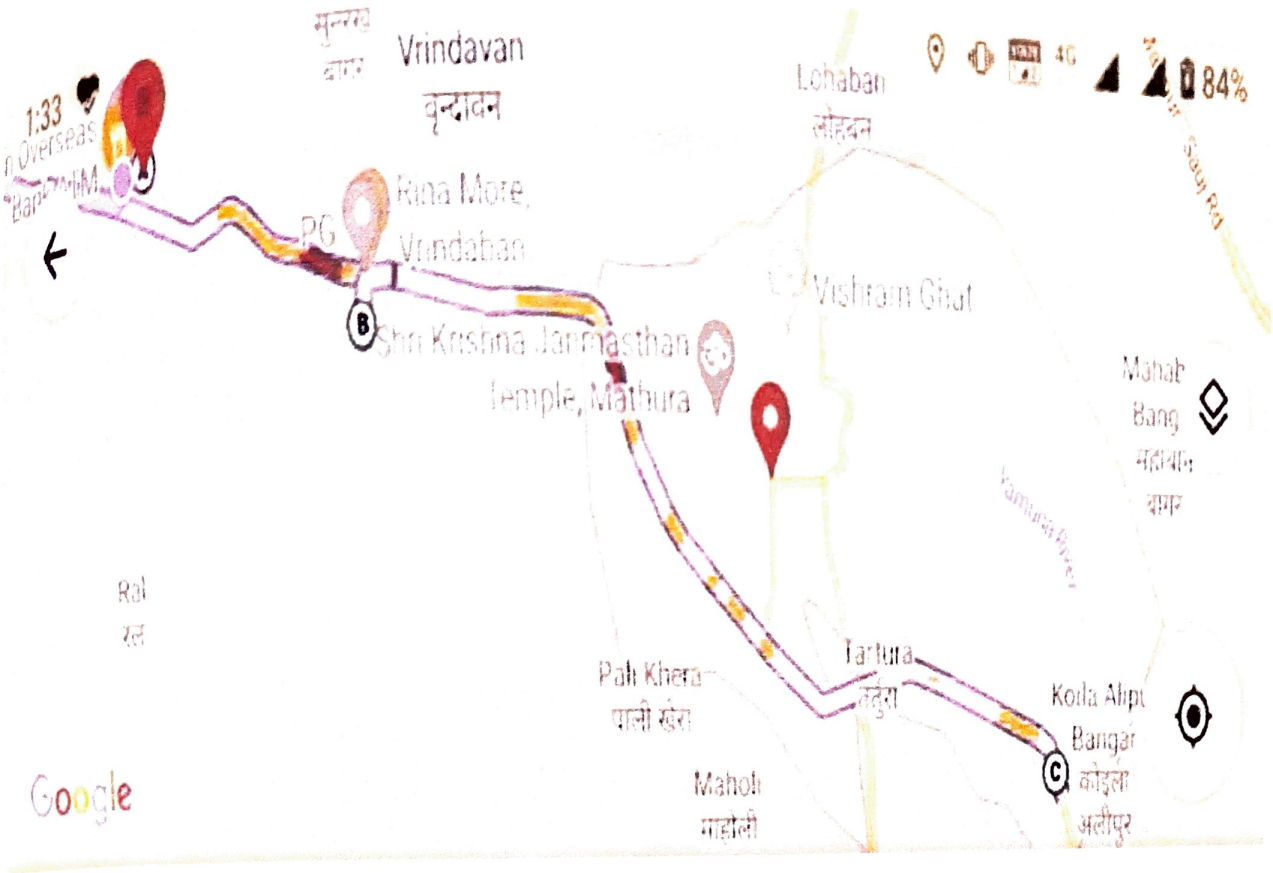

Fig.5 Locations of Site

3.3 STUDY OF TRAFFIC VOLUME

In this research traffic volume was estimated with the help of DSLR Camera video recording on peak hour basis from morning (8:00 to 10:00 AM), in the noon (1:00 to 3:00 PM) and in the evening (6:00 to 8:00 PM). The traffic volume was calculated by measuring the number of vehicles on either side of the road.

Fig. 6 DSLR Camera EOS 80D

3.4 STUDY OF TRAFFIC NOISE

A sound level meter is a basic prerequisite for noise analysis. It is programmed to evaluate the loudness sensitivity level of human ear and provides the noise intensity level with required repeatable observations. To compute the equivalent level, maximum level and minimum level of noise. In this study sound level meter 100 (Type-II) is used. In which frequency weighing —Al type and time weighing SLOW and FAST mode provided as per requirements of (IS 15575(Part-1) 2005).

Fig. 7 Sound Level Meter 100 (Type-II)

3.5 DATA COLLECTION

- The noise and the traffic volume at the specified location are noted for weekdays and weekends
- In the specified locations sound level was taken either at the separator or on bank of the road.
- The sound pressure level and traffic volume at a specified location were noted for 2hr for 3 times during the day (e.g morning, noon, evening).

Fig. 8 Traffic Noise data collection at the Study area

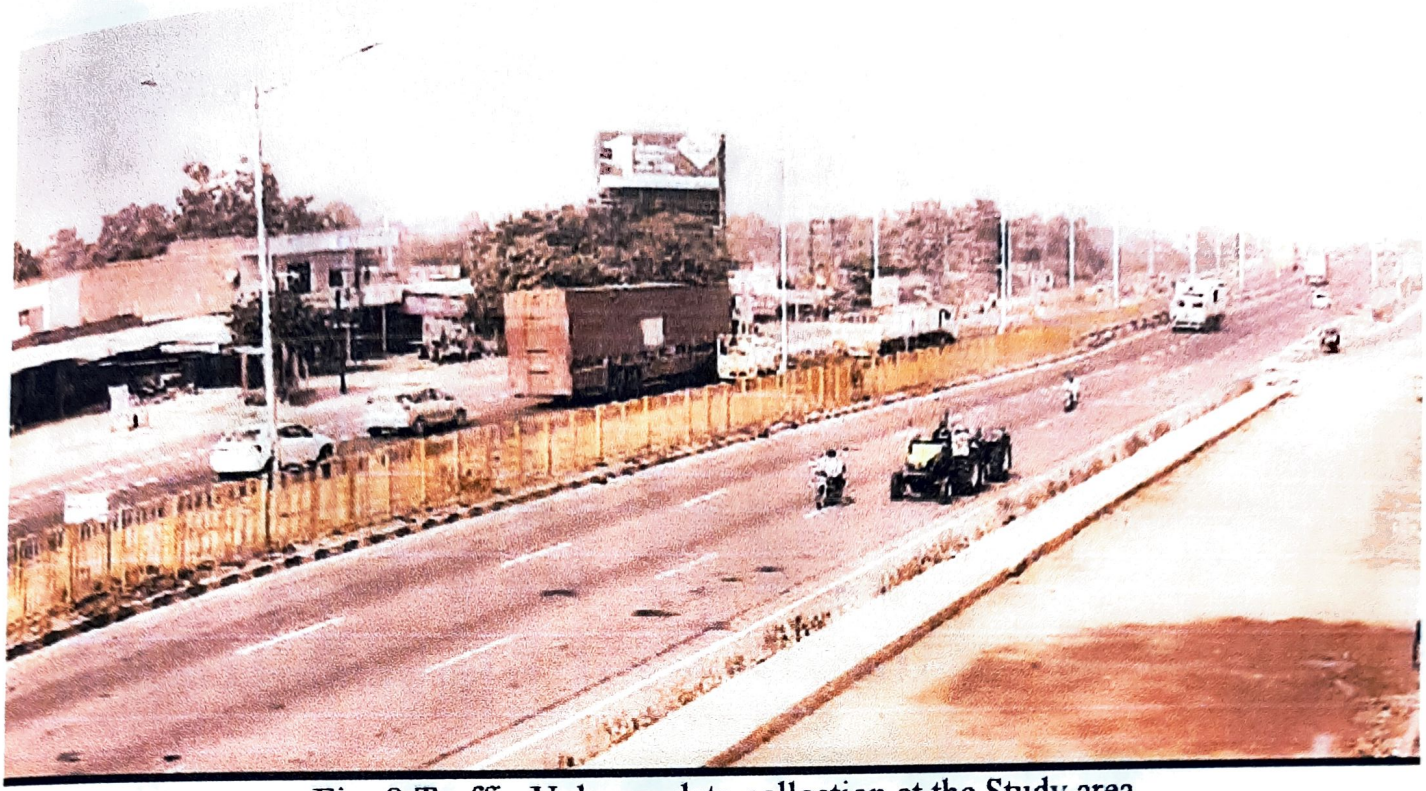

Fig. 9 Traffic Volume data collection at the Study area

CHAPTER - 4
RESULTS AND OBSERVATIONS

DATA COLLECTED:

Traffic volume data is collected on the selected locations with the help of DSLR camera. And the traffic noise is measured with the help of SLM 100.

Table.2 Traffic Volume and Traffic Noise level at Location I (GLA University) on Weekdays

Day	Time	L_{min}(dB)	L_{eq}(dB)	L_{max}(dB)	Traffic Vol. (Veh/Hr)
Mon	Mor (8-10AM)	65.06	71.64	80.15	2654
	Noon (1-3PM)	65.47	71.59	79.84	2367
	Eve (6-8PM)	60.48	67.65	79.11	2397
Tue	Mor (8-10AM)	65.07	70.61	79.67	2481
	Noon (1-3PM)	65.86	71.8	80.87	2295
	Eve (6-8PM)	61.02	69.31	78.62	2413
Wed	Mor (8-10AM)	64.91	71.07	81.92	2592
	Noon (1-3PM)	65.56	70.97	80.54	2343
	Eve (6-8PM)	62.11	69.38	79.23	2478
Thu	Mor (8-10AM)	63.84	70.35	81.59	2589
	Noon (1-3PM)	64.99	70.22	80.32	2314
	Eve (6-8PM)	61.5	68.41	78.39	2477
Fri	Mor (8-10AM)	65.93	71.87	81.44	2401
	Noon (1-3PM)	65.97	70.33	80.12	2288
	Eve (6-8PM)	60.25	67.90	78.02	2398

Graph 1. Traffic Volume at Location I (GLA University) on Weekdays

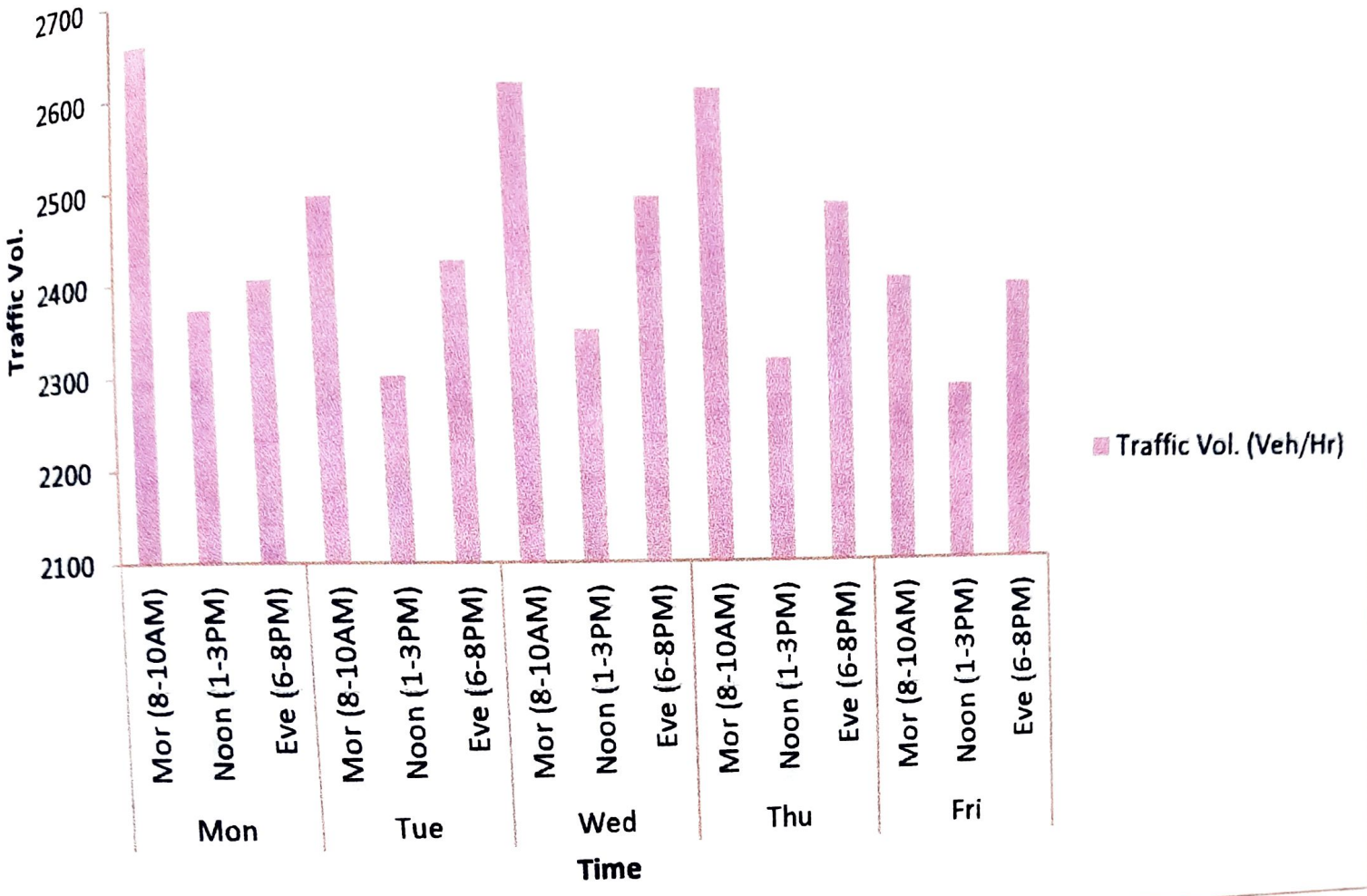

Graph 2. Traffic Noise level at Location I (GLA University) on Weekdays

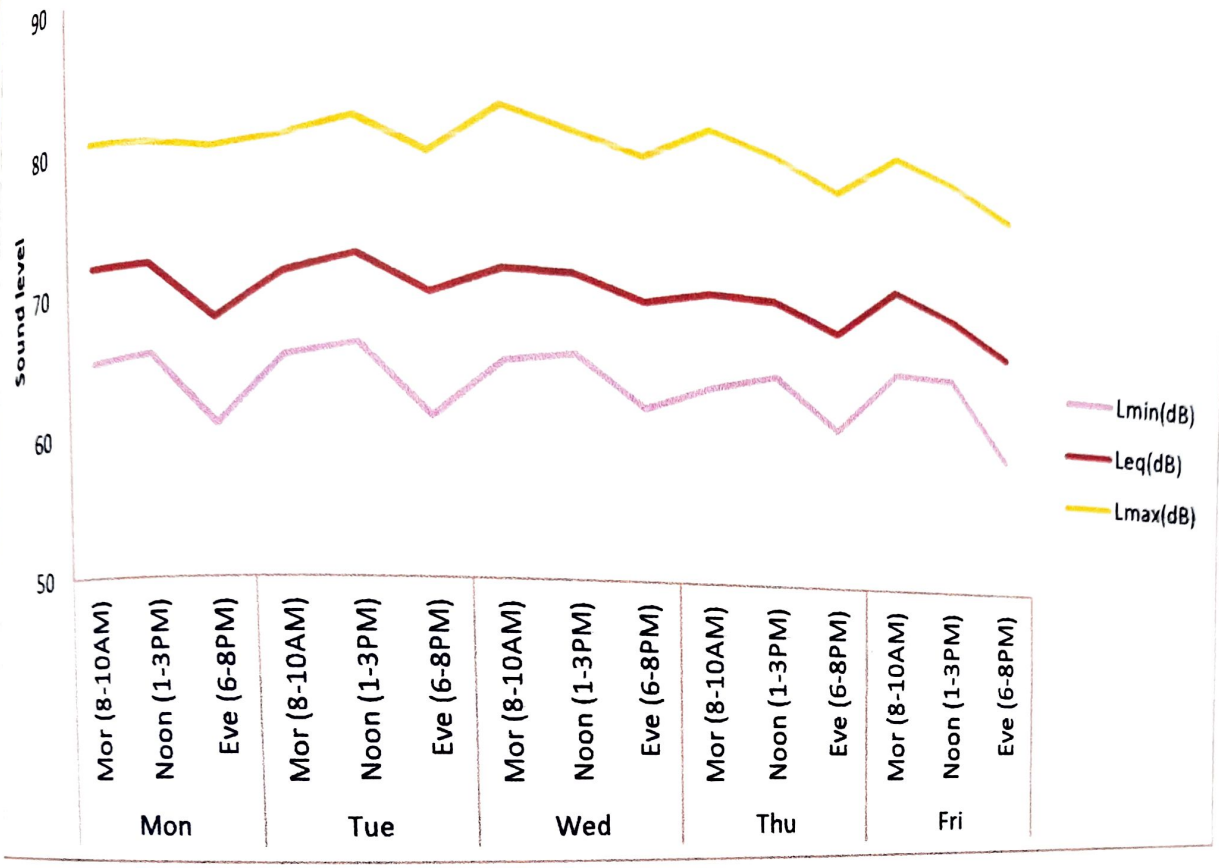

Table. 2 represents the data of Traffic Volume and Traffic Noise at location I (GLA University, Mathura) on Weekdays. And the Graph. 1 and 2 plotted for Traffic Volume and Traffic Noise respectively. From the graph we observed that Noise level during morning is very high as compare to noon and evening because the Traffic Volume is more in the morning. The average traffic volume at this location is something 2500 veh/hr. And the Noise level lies between 60-82dB, which is more as compare to WHO guidelines. Because the Noise limit for silent zone is 50-60dB.

Table.3 Traffic Volume and Traffic Noise level at Location I (GLA University) on Weekends

Day	Time	L_{min}(dB)	L_{eq}(dB)	L_{max}(dB)	Traffic Vol. (Veh/Hr)
Sat	Mor (8-10AM)	62.43	70.14	78.92	2292
	Noon (1-3PM)	62.65	71.59	78.12	2074
	Eve (6-8PM)	59.40	66.05	75.33	2367
Sun	Mor (8-10AM)	59.84	68.78	76.19	2177
	Noon (1-3PM)	60.19	69.50	77.37	2052
	Eve (6-8PM)	57.94	65.80	74.62	2278

Table. 3 represents the data of Traffic Volume and Traffic Noise at location I (GLA University, Mathura) on Weekends. The Traffic Volume on Weekend is less as compare to Weekdays. And also the Noise level on weekends is less as compare to other days. The Traffic Volume on Weekends is about 2000-2300 veh/hr. The minimum Noise level is 57dB observed here.

Graph 3. Traffic Volume at Location I (GLA University) on Weekends

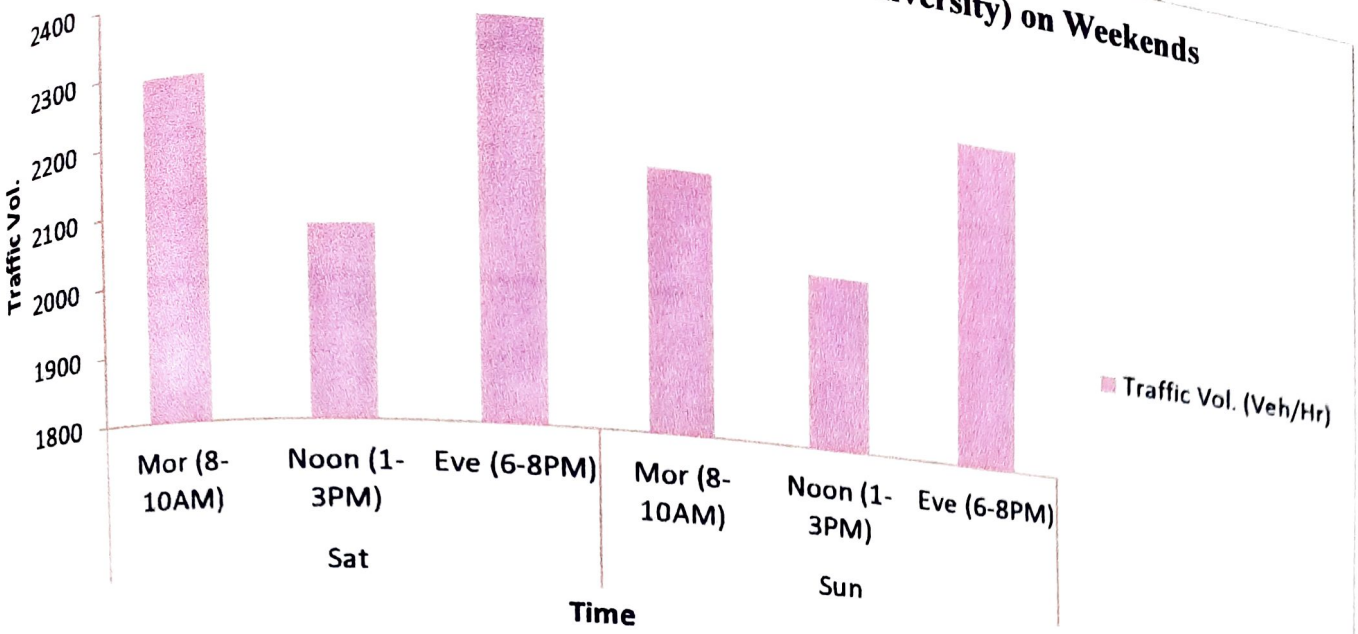

Graph 4. Traffic Noise level at Location I (GLA University) on Weekends

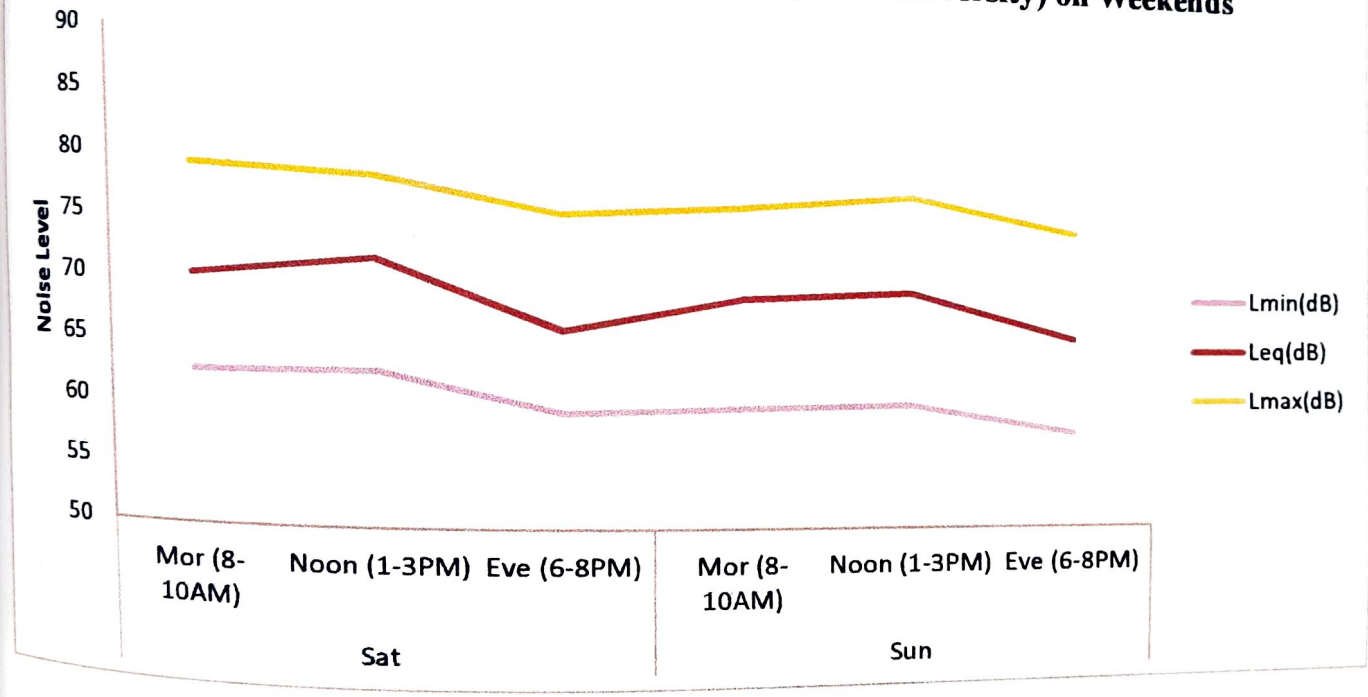

Graph 3 and 4 is the representation of Traffic Volume and Traffic Noise data at location I (GLA University) on Weekend. The Noise level in the noon is more as compare to morning and evening because there is less Traffic volume in the morning.

Table.4 Traffic Volume and Traffic Noise level at Location II (Govardhan Chauraha) on Weekdays

Day	Time	L_{min}(dB)	L_{eq}(dB)	L_{max}(dB)	Traffic Vol. (Veh/Hr)
Mon	Mor (8-10AM)	71.98	82.75	94.03	5388
	Noon (1-3PM)	70.69	80.01	91.22	5167
	Eve (6-8PM)	72.67	83.45	94.53	5352
Tue	Mor (8-10AM)	71.47	82.02	93.39	5356
	Noon (1-3PM)	68.42	81.56	90.01	5127
	Eve (6-8PM)	73.26	82.95	93.89	5298
Wed	Mor (8-10AM)	70.52	80.98	92.09	5176
	Noon (1-3PM)	70.41	79.76	90.94	5082
	Eve (6-8PM)	72.04	82.11	92.23	5234
Thu	Mor (8-10AM)	71.92	82.01	93.24	5223
	Noon (1-3PM)	70.87	80.95	91.11	4955
	Eve (6-8PM)	73.21	83.84	93.04	5278
Fri	Mor (8-10AM)	70.56	80.98	91.16	4948
	Noon (1-3PM)	70.34	79.64	89.54	4688
	Eve (6-8PM)	71.06	81.77	91.81	5043

Graph 5. Traffic Volume at Location I I(Govardhan Chauraha) on Weekdays

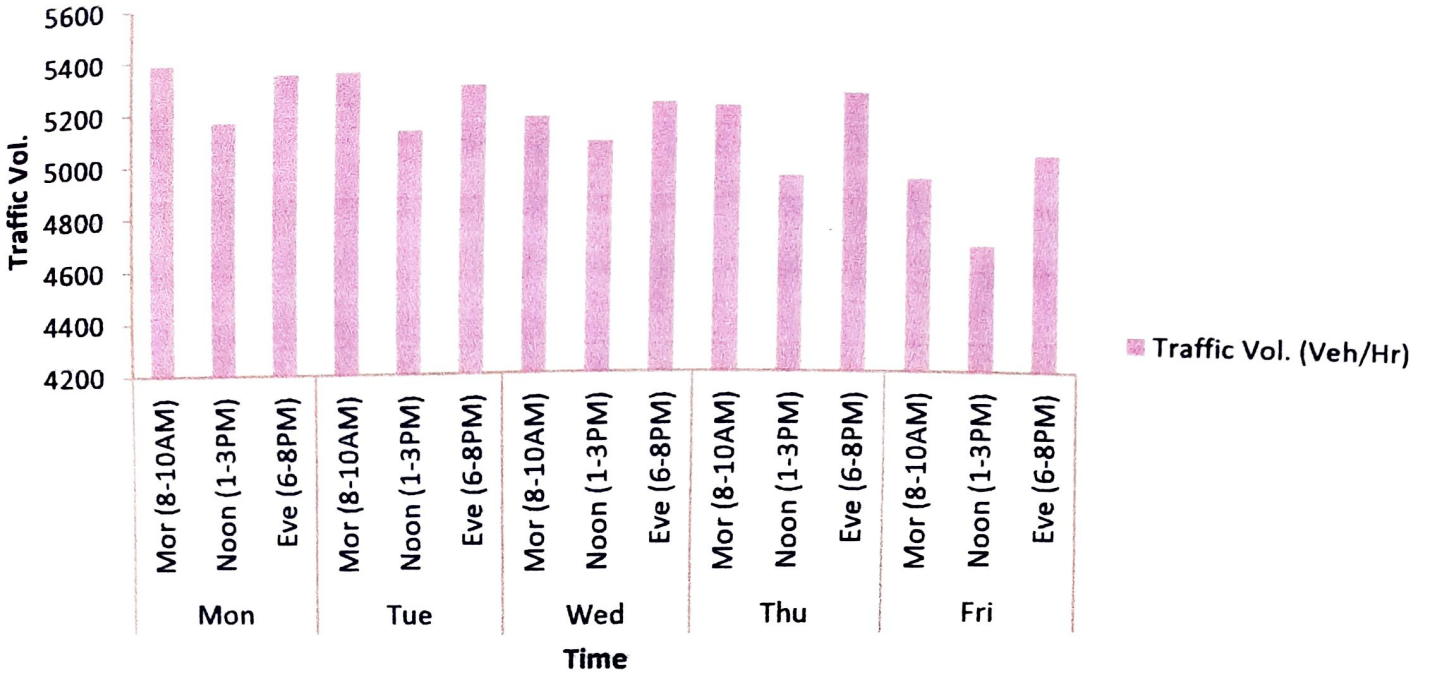

Graph 6. Traffic Noise level at Location II (Govardhan Chauraha) on Weekdays

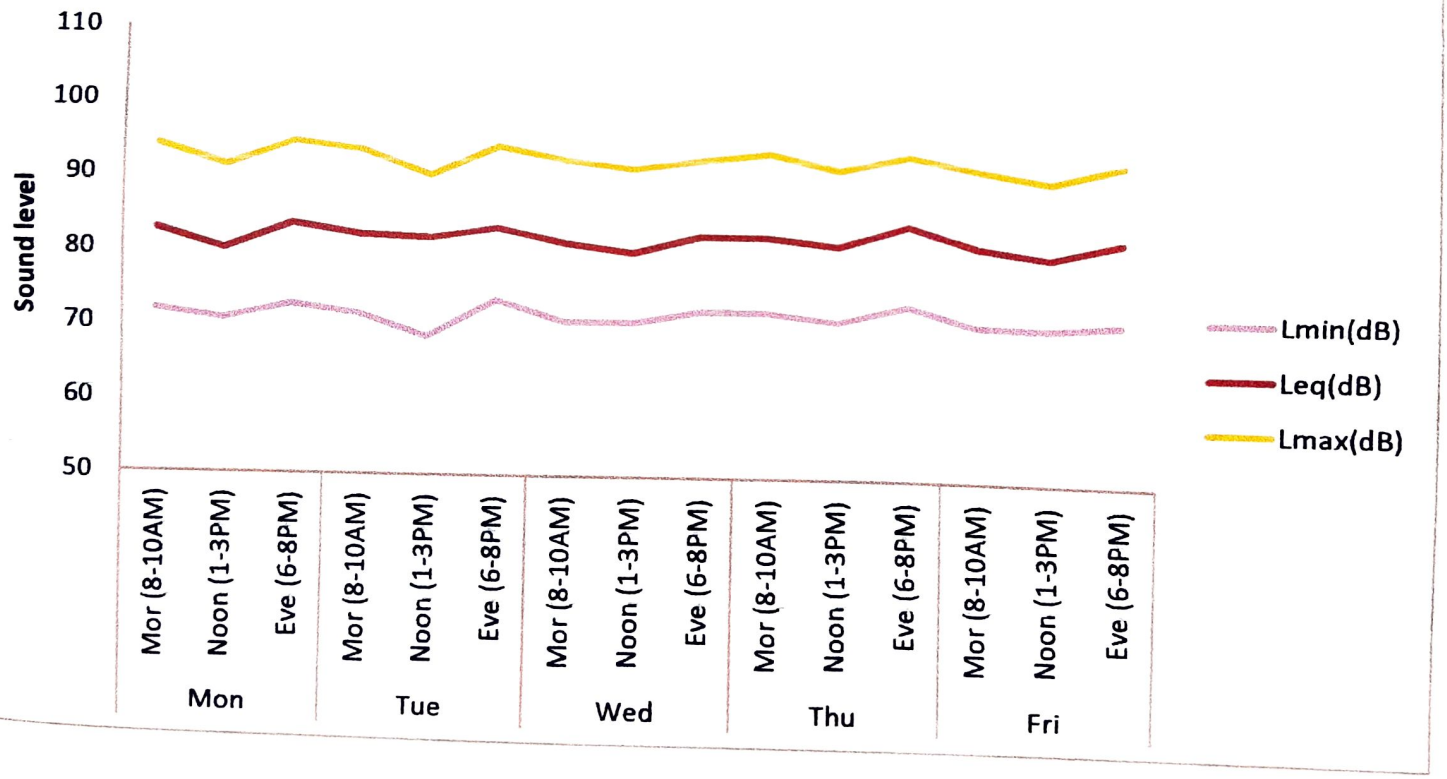

Table. 4 represents the data of Traffic Volume and Traffic Noise at location II (Govardhan Chauraha) on Weekdays. And the Graph.5 and 6 plotted for Traffic Volume Traffic Noise respectively. From the graph we observed that Noise level during morning is very high as compare to noon and evening because the Traffic Volume is more in the morning. And the Noise level lies between 70-95dB, which is more as compare to WHO guidelines. Because the Noise limit for Urban residential zone is 70dB.

Table.5 Traffic Volume and Traffic Noise level at Location II (Govardhan Chauraha) on Weekends

Day	Time	L_{min}(dB)	L_{eq}(dB)	L_{max}(dB)	Traffic Vol. (Veh/Hr)
Sat	Mor (8-10AM)	68.96	79.55	89.21	4872
	Noon (1-3PM)	67.95	77.79	87.99	4499
	Eve (6-8PM)	69.08	80.49	89.76	4995
Sun	Mor (8-10AM)	66.15	76.64	86.39	4256
	Noon (1-3PM)	65.78	75.16	86.28	4077
	Eve (6-8PM)	68.34	79.17	88.04	4467

Table. 5 shows the data of Traffic Volume and Traffic Noise at location II (Govardhan Chauraha) on Weekends. The Traffic Volume on Weekend is about 4000-5000 veh/hr. This intersection has more Traffic Volume because this is the main intersection of the Mathura city. But there is no more effect of weekend on Traffic.

Graph 7. Traffic Volume at Location II (Govardhan Chauraha) on Weekends

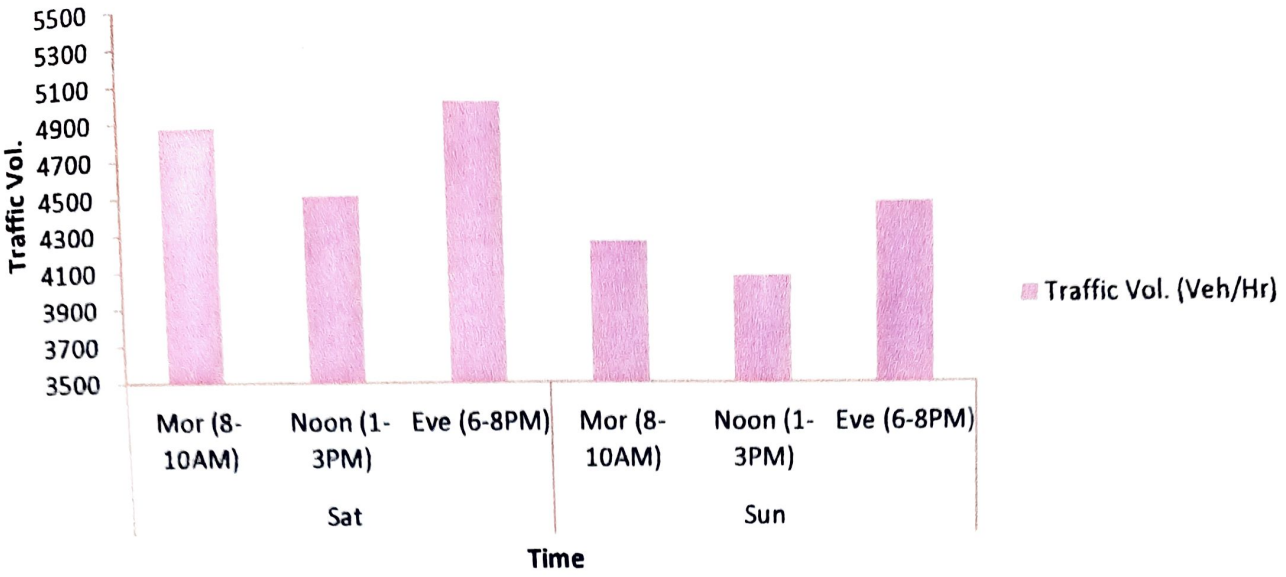

Graph 8. Traffic Noise level at Location II(Govardhan Chauraha) on Weekends

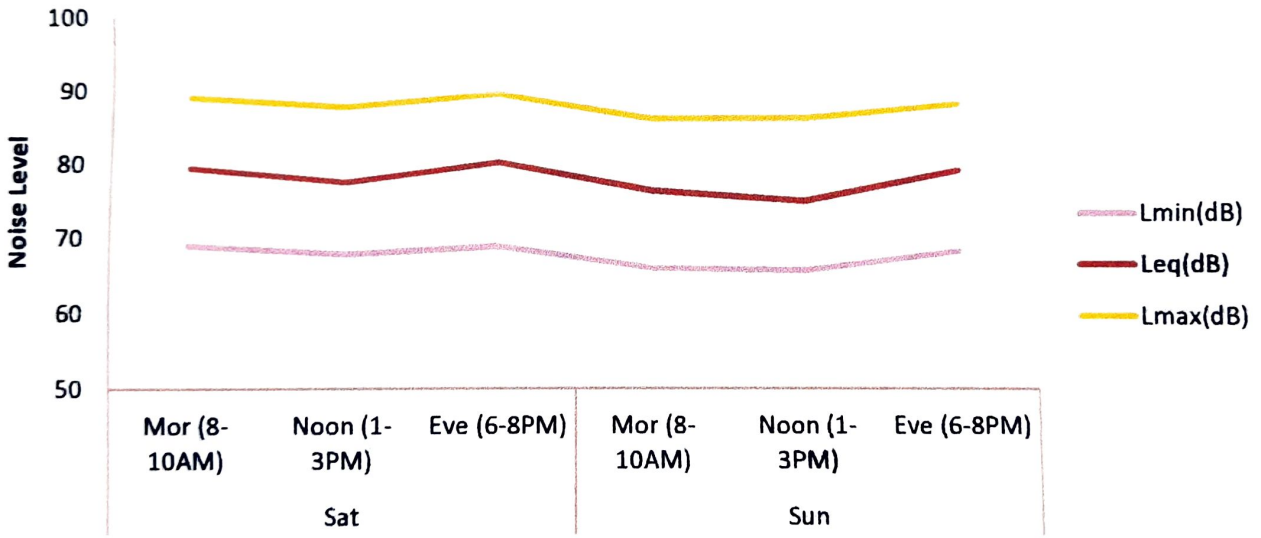

Graph 7 & 8 is the representation of Traffic Volume and Traffic Noise data at location II (Govardhan Chauraha) on Weekend. The Noise level in the evening is more as compare to morning and noon.

Table.6 Traffic Volume and Traffic Noise level at Location II (Mathura Township) on Weekdays

Day	Time	L_{min}(dB)	L_{eq}(dB)	L_{max}(dB)	Traffic Vol. (Veh/Hr)
Mon	Mor (8-10AM)	67.12	75.33	84.66	3812
	Noon (1-3PM)	66.55	74.91	84.12	3775
	Eve (6-8PM)	68.54	76.29	83.91	3834
Tue	Mor (8-10AM)	66.86	74.44	83.76	3799
	Noon (1-3PM)	65.41	73.27	82.98	3752
	Eve (6-8PM)	67.08	77.41	85.27	3864
Wed	Mor (8-10AM)	66.73	74.54	83.76	3784
	Noon (1-3PM)	65.32	72.16	81.74	3695
	Eve (6-8PM)	66.88	75.49	83.33	3801
Thu	Mor (8-10AM)	64.12	74.75	82.45	3578
	Noon (1-3PM)	65.93	75.87	81.98	3521
	Eve (6-8PM)	66.88	74.04	82.19	3697
Fri	Mor (8-10AM)	64.96	75.49	82.16	3565
	Noon (1-3PM)	63.55	73.97	80.87	3605
	Eve (6-8PM)	66.34	74.86	81.05	3785

Graph 9. Traffic Volume at Location III (Township Mathura) on Weekdays

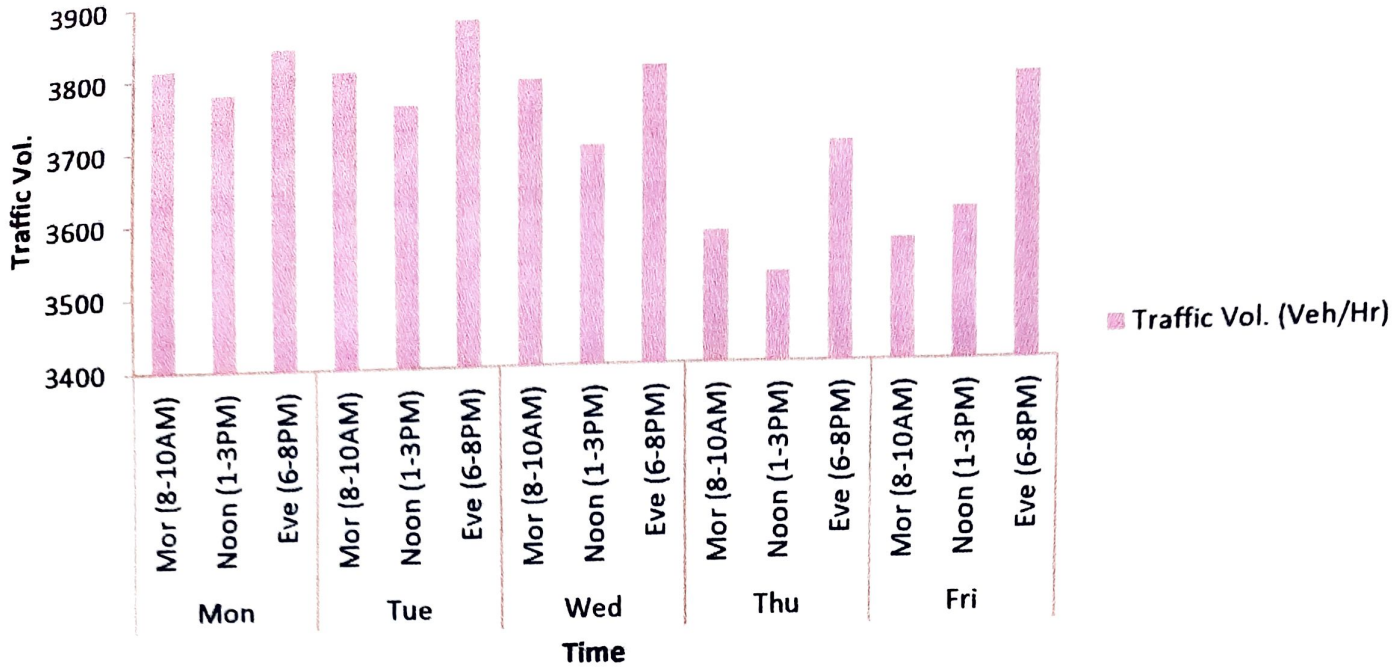

Graph 10. Traffic Noise level at Location III (Township Mathura) on Weekdays

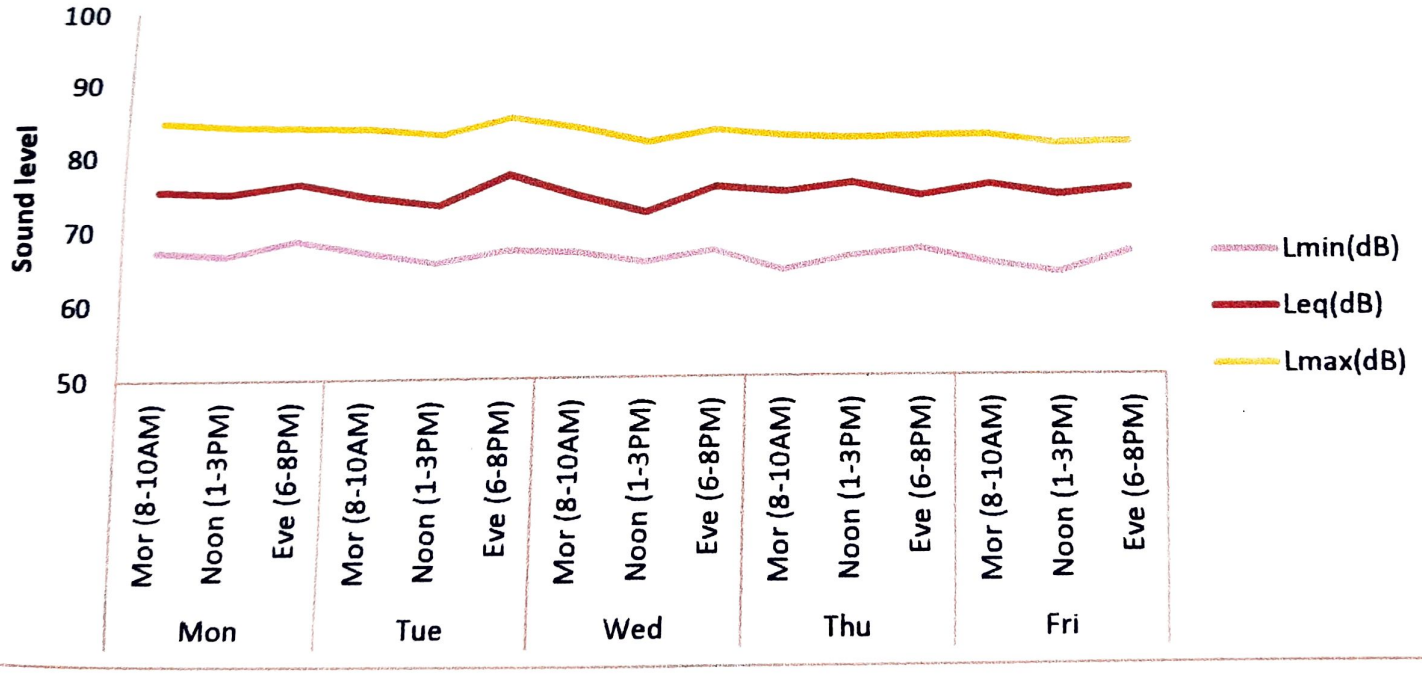

Table. 6 represents the data of Traffic Volume and Traffic Noise at location III (Mathura Township) on Weekdays. And the Graph. 9 and 10 represent the Traffic Volume and Traffic Noise. From the graph we observed that there is no significant changes in the Traffic Volume and Traffic Noise on all weekdays. The minimum Noise level is 63dB and the maximum Noise level is 87dB. And the average Traffic Volume is about 3750 veh/hr.

Table.7 Traffic Volume and Traffic Noise level at Location III (Mathura Township) on Weekends

Day	Time	L_{min}(dB)	L_{eq}(dB)	L_{max}(dB)	Traffic Vol. (Veh/Hr)
Sat	Mor (8-10AM)	63.35	73.61	82.16	3441
	Noon (1-3PM)	62.97	72.92	81.97	3295
	Eve (6-8PM)	63.71	74.87	84.59	3381
Sun	Mor (8-10AM)	64.92	73.95	82.98	3167
	Noon (1-3PM)	61.18	72.03	83.47	3256
	Eve (6-8PM)	62.75	73.17	83.90	3135

Table.7 represents the Traffic Volume and Traffic Noise data on location III (Mathura Township) on Weekend. The Traffic Volume at this location on weekend is about 3300 veh/hr. which is less as compare to weekdays and the Noise level lies between 60-85dB.

Graph 11. Traffic Volume at Location III (Township Mathura) on Weekends

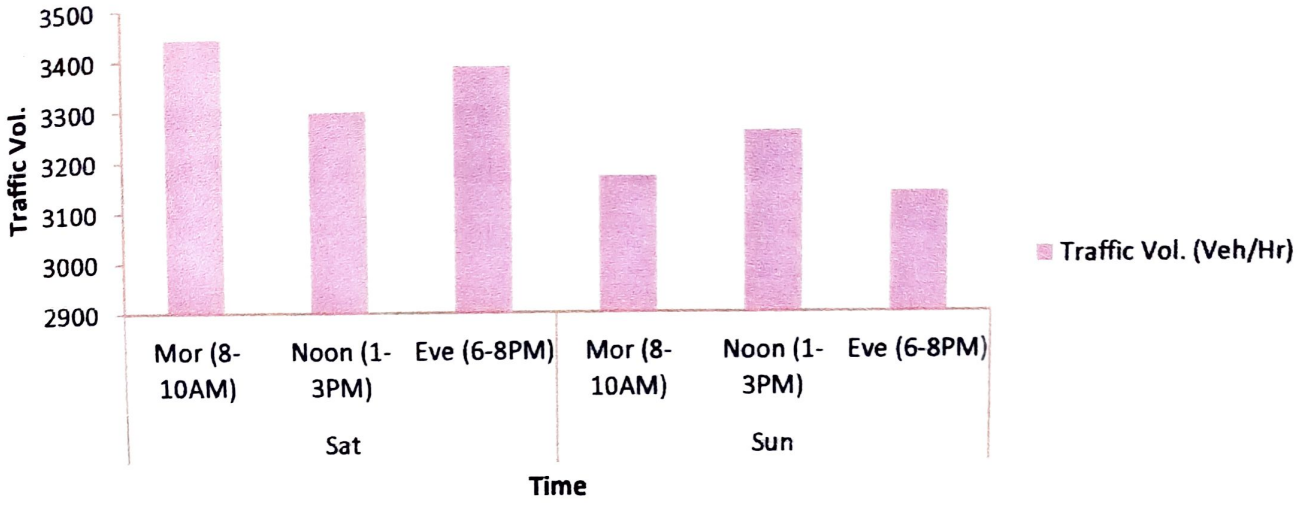

Graph 12. Traffic Noise level at Location III (Township Mathura) on Weekends

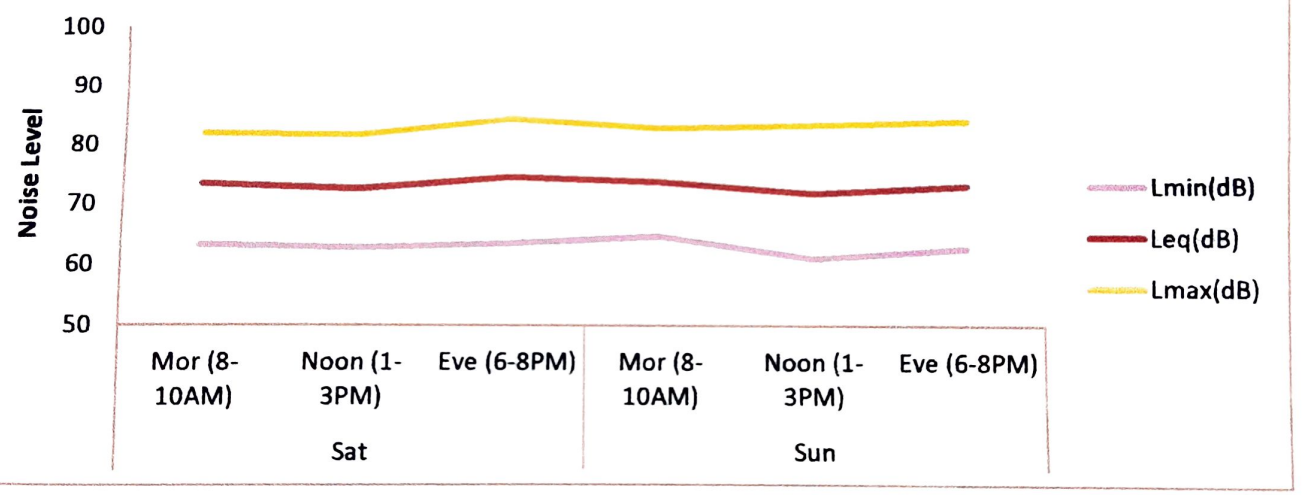

Graph 11 & 12 is the graphical representation of Table 7 data. There are no more significant changes in the Traffic Volume and Traffic Noise during morning, noon and evening. Noise level is less only on Sunday at noon.

COMPARISION WITH STANDARD NOISE VALUE

The maximum equivalent sound level of noise at location I on is Leq =71dB, is more than Leq = 60 dB so that, this area is not suitable for human hearing as the recommended noise value by WHO.

The maximum equivalent sound level of noise at location II is Leq =84dB, is more than Leq = 70 dB so that, this area is not suitable for human hearing as the recommended noise value by WHO.

The maximum equivalent sound level of noise at location III is Leq =75dB, is more than Leq = 75 dB so that, this area is not suitable for human hearing as the recommended noise value by WHO.

CHAPTER - 5

CONCLUSION

Result of this study clearly described that the noise level at these locations has exceeded the noise level limit set by WHO (World Health Organization) which is 70dB for Urban residential and 50-60dB for Residential zone. The noise level at location (ii) is more as compare to noise level at location (i) and location (iii), because the traffic volume is more at this location. But the noise level during morning time was more than evening and noon, this is because of high volume of traffic is experienced in the morning. Based on the data presented in this study, it could be concluded that out-of-order machinery and increased traffic density cause noise pollution affecting the human health in different ways as noise is equally distributed in whole the city. Furthermore, it will cause long term disease and at times non curable such as deafness. Hence, protective measures must be taken. Also, Mathura may be exposed to noise levels that put them at risk of being highly annoyed or having high levels of lack in concentration, sleep disturbance, irritation in behaviour etc. Increase the awareness regarding noise-induced hearing loss and regular check-up implementation is highly recommended. The people having higher education and income level are much aware of the health impact due to traffic noise. Marital status was found to be significantly affecting the annoyance level caused by traffic noise. Traffic noise was found to be interfering with daily activities such as resting, reading, communication, etc.

References

1. Sahoo, S. (2014). Analysis of traffic noise. 37.

2. Agarwal, S., & Swami, B. L. (2010). Status of ambient noise levels in Jaipur city. Environment Conservation Journal, 11, 105–108.

3. 3. Pathak, V., Tripathi, B. D., & Mishra, V. kumar. (2008). Evaluation of traffic noise pollution and attitudes of exposed individuals in working place.

4. Mangalekar, S. B., Jadhav, A. S., & Raut, P. D. (2012). Study of Noise Pollution in Kolhapur City , Maharashtra , India Abstract : Online, 2(1), 65–66

5. Malkamah, S., "Hubungan antara Volume, Kecepatan, Komposisi Kendaraan dan Tingkat Kebisingan di Jalan Raya", MSTT-UGM, Yogyakarta-Indonesia, 1992.

6. Djalante, S., "Analisis Tingkat Kebisingan Di Jalan Raya Yang Menggunakan Alat Pemberi Isyarat Lalu Lintas (APIL) (Studi Kasus: Simpang Ade Swalayan)", Jurnal SMARTek, vol. 8, no. 4, pp. 280-300, 2010.

7. Ragettli, M. S., Goudreau, S., Plante, C., Perron, S., Fournier, M., & Smargiassi, A., "Annoyance from Road Traffic, Trains, Airplanes and from Total Environmental Noise Levels", International Journal of Environmental Research and Public Health, 13(1), pp. 90, 2016.

8. Birk, M., Ivina O., von Klot S., Babisch W., & Heinrich J., "Road Traffic Noise: Self-Reported Noise Annoyance Versus GIS Modelled Road Traffic Noise Exposure", J Enviro Monit, vol. 13, no. 11, pp. 3237-3245, 2011.

9. Saad, A.Q. & Arwa, A., "Effect Of Distance From Road Intersection On Developed Traffic Noise Levels", Canadian Journal of Civil Engineering, vol. 31, no. 4, pp. 533-538, 2004.

10. Radam, I. F., & Heriyatna, E. (2018). A Correlation Analysis of Noise Level and Traffic Flow : Case of One Way Road in Banjarmasin. 06(02), 60–64.

11. Ur, Z., Farooqi, R., Sabir, M., Latif, J., Aslam, Z., Ahmad, H. R., Ahmad, I., Imran, M., & Ili, P. (2019). Assessment of noise pollution and its effects on human health in industrial hub of Pakistan.

12. Singh D, Kumari N, Sharma P. A review of adverse effects of road traffic noise on human health. Fluctuation and Noise Letters. 2018 Mar 18;17(01):1830001.

13. Yusuf, Shahid, ed. Innovative East Asia: the future of growth. World Bank Publications, 2003.

14. Passchier-Vermeer, W., & Passchier, W. F. (2000). Noise exposure and public health. Environmental health perspectives, 108(suppl 1), 123-131.

15. Central Pollution Control Board

16. The Ministry of Environment and Forests of the Government of India

17. World Health Organization

18. Mapsofindia.com

AUTOMATIC VEHICLE ACCIDENT DETECTION AND MESSAGING SYSTEM USING GSM AND GPS MODEM

A Project Report

Submitted in the partial fulfillment of requirement for the award of the

Degree of

BACHELOR OF TECHNOLOGY

IN

ELECTRICAL ENGINEERING

Submitted by

SHIVA MISHRA (181199014)

DIVYANSHU BAGHEL (181199004)

HEMANT SINGH SHEKHAWAT (171100018)

KARTIK KUMAR (171100020)

Under the supervision of

Mr. MAYANK GOYAL

DEPARTMENT OF ELECTRICAL ENGINEERING

INSTITUTE OF ENGINEERING AND THECHNOLOGY

GLA UNIVERSITY, MATHURA – 281404

DECLARATION

We certify that

a. The work contained in this report is original and has been done by us under the guidance of my supervisor(s).

b. We have followed the guidelines provided by the Institute in preparing the report.

c. We have conformed to the norms and guidelines given in the Ethical Code of Conduct of the Institute.

d. Whenever we have used materials (data, theoretical analysis, figures, and text) from other sources, we have given due credit to them by citing them in the text of the report and giving their details in the references. Further, we have taken permission from the copyright owners of the sources, whenever necessary.

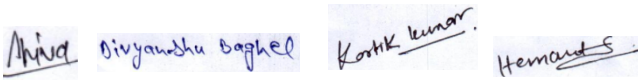

Signature of the Students

CERTIFICATE

This is to certify that Project Report entitled, "**AUTOMATIC VEHICLE ACCIDENT DETECTION AND MESSAGING SYSTEM USING GSM AND GPS MODEM**" which is being submitted by SHIVA MISHRA, DIVYANSHU BAGHEL, KARTIK KUMAR, HEMANT SINGH SHEKHAWAT in partial fulfillment of the requirement for the award of degree B. Tech. in Electrical Engineering and submitted to the department of Electrical Engineering of GLA University, is a record of the candidate own work carried out by him/her under my supervision. The matter embodied in this report is original and has not been submitted for the award of any other degree.

MR. MAYANK GOYAL

Name of the guide

(Assistant Professor)

Date: 15/04/2021

Head of Department
Electrical Engg.
GLA University, Mathur

ACKNOWLEDGEMENT

First and foremost, we would like to thank our Guide of this project Mr. Mayank Goyal for his valuable guidance and advice. He guided us greatly to work in this project. His willingness to motivate us helped tremendously. Besides, we would like to thank the authority of GLA University for providing us with a good environment and facilities to complete this project. It gave us an opportunity to participate and learn about the operation of Automatic Vehicle Accident Detection and Messaging System Using GSM & GPS Modem. Finally, and honorable mention goes to our families and friends for their understanding and support in completing this project. Without help of those mentioned above, this project could not have been completed.

Signature: Shiva

Name : Shiva Mishra

Roll No.:181199014

Date : 14-04-21

signature: Divyanshu Baghel

Name: Divyanshu Baghel

Roll No:181199004

Date: 14-04-21

Signature: Kartik kumar.

Name : Kartik Kumar

Roll No.: 171100018

Date :14-04-21

signature: Hemant S.

Name: Hemant Singh Shekhawat

Roll No: 171100020

Date:14-04-21

Abstract

The always advancing technology has made our day to day lives easier. Since every coin has 2 sides similarly technology has its benefits as well as its disadvantages. The rise in technology has increased the rate of road accidents which causes huge loss of life. The poor emergency facilities available in our country just add to this problem. Our project is going to provide a solution to this problem. According to our project when a vehicle meets with an accident, a sensor situated on the vehicle will detect it immediately and send a message to the microcontroller. The microcontroller then sends the alert message with the help of GSM modem to a police control room or rescue team which will include the location with the help of GPS. Also the alert message containing the location of accident will be send to the relatives of the victim. In case there is no casualty the driver can terminate the alert message by a switch provided in the vehicle. This will save the valuable time of rescue team. Our project is useful for detecting the accident precisely with the help of sensor and microcontroller. Keeping in mind the scope for improvement, we can add a wireless webcam which will capture the images at the time of accident which will help in providing accurate help to the victim as quick as possible. It can be interfaced with vehicle airbag system and a bomb detector.

Contents

CHAPTER III: SYSTEM DESIGN AND FABRICATION

CHAPTER IV: RESULT AND DISCUSSION

CHAPTER V: CONCLUSION AND FUTURE WORK

List of Figures

List of Tables

Chapter I

Introduction

The advent of technology has also increased the traffic hazards and the road accidents. Due to the lack of best emergency facilities available in our country the lives of the people are under high risk. An automatic alarm device for vehicles is introduced in this project which sends the basic information to the medical rescue team within a few seconds of an accident. This device can detect accidents and sends an alert message to rescue teams in significantly less time which will help in saving the lives of the people.

The alert message contains the geographical coordinates, time and angle in which the accident has occurred. In cases where there is no casualty the message can be terminated with the help of a switch in order to avoid wasting the valuable time of the rescue team.

When an accident occurs it is detected with help of a sensor which activates the device, the sensor gives its output to the microcontroller. The microcontroller sends the alert message automatically to the police station and the relatives of the person. The message is sent through the GSM module and the location of the accident is detected with the help of the GPS module. Hence with this project implementation we can detect the position of the vehicle where the accident has occurred so that we can provide the first aid as early as possible.

Background Study

Traffic accidents are a major public issue worldwide nowadays. A huge number of injuries and death as a result of road traffic accident uncovers the story of the global crisis of road safety. According to a statistical projection of traffic fatalities, the most obvious reason of a person's death during accidents is the unavailability of the first aid provision, due to the delay in the information of the accident being reached to the ambulance or to the hospital. The following is the list of patents analyzed before designing the Accident Alert System. It helped us to understand the interfacing of various components used in the project, such as GSM and GPS modems, and also the practical implementation of such projects in real life. The analysis of this report file helped to understand the current technologies prevalent in the field of accident notification system and to find better yet simpler alternatives to modernize such notification systems. The following is the list of patents analyzed before designing the Accident Alert System. It helped us to understand the interfacing of various components used in the project, such as GSM and GPS modems, and also the practical implementation of such projects in real life.

Objectives

The main objective of this work is to design and develop an automatic accident detection and notification systems. Total work can be summarized as:

- Accelerometer sensor is used to detect the accident precisely with the rapid change of acceleration and vibration of the vehicle.
- When a vehicle meets with an accident immediately sensor will detect the signal or if a car rolls over, accelerometer sensor will detect the signal and sends it to microcontroller.
- Microcontroller sends the alert message through the GSM MODEM including the location to police control room or a rescue team.

Literature Review

In countries where the economic status is poor, it becomes crucial for those concerned with developmental policies to adopt appropriate strategies which will ensure that every single unit of money available is used to develop the country in those fields to facilitate a conductive environment for economic development. Road traffic accidents have been recognized as one of the adverse elements which contribute to the suffocation of economic growth in the developing countries, due to the high cost related to them, hence causing social and economic concern. So, Traffic safety is an important key and plays an integral role in sustainable transportation development.

Now days, the main negative impacts of modern road transportation systems are injuries and deaths in road accidents. The success of traffic safety and highway improvement programs hinges on the analysis of accurate and reliable traffic accident data. This study discusses the present state of traffic accident information on NH 47 Gandhipuram to Avinashi and NH-209 from Gandhipuram to Annur, Coimbatore District. It shall also discuss the Identification of high rate accident Locations by using GIS Software and safety deficient areas on the highway. Remedial measures and provisions for traffic safety are suggested for reducing the risk of accidents in black spots.

Citation classics offer an outlook on those papers that have attracted great and historical interest by a research community and that could be also considered the basis of the research field. A new approach, which is called H-Classics, has been developed to identify such highly cited papers. It is based on the H-index and is sensitive to both the own characteristics of the corresponding research discipline and its evolution.

The present study provides a useful insight into the development of intelligent transport systems research fields revealing those scientific actors (authors, countries, and institutions) that have made the biggest research contribution to its development.

Chapter-II

Theory of the Project

Introduction

Consider a busy city scenario, where we have peak morning and evening hours. In peak hours, half of the city population rush to/from workplaces using public or private transportations or a highway scenario with different speed lanes. In each scenario, it is important to detect an accident if it occurs and report to an emergency alert center about an incident with additional information of the location.

Accident Detection Module

To detect an accident on road, first we need to know the all events that we can assume in case of accident. Here are three major events that can help in accident detection.

Collision: A vehicle can collide with other vehicle or any other solid object, as a result driver or passenger inside the vehicle can get injuries.
Roll-over: A vehicle may roll-over when an incident occurs. This is one of the dangerous events that may end-up with the several injuries or death of passengers including drivers.
Speed: If accident happens, the vehicle would stop suddenly. In normal situation, if brakes are applied on the vehicle, it takes a certain amount of time and travel few feet before coming to the stationary position depending upon the speed of the vehicle.

Methodology

We have divided our whole project work with seven phases of our project. Using the Waterfall model, we have completed our project very readily. The waterfall model is a sequential process to solve any problem to develop any system it should arrange the whole work in the segment so that accuracy can be provided. We used the waterfall model in our system because it is seven stage attributes and feedback opportunity system the characteristics of our workflow is it can return to previous steps. If we want to modify our system at any point according to equipment so we will do it depends on our requirement. In this workflow, each phase must be completed completely before the next steps may begin.

Waterfall Model of Methodology

This project has been completed by following strategy, which is given below:

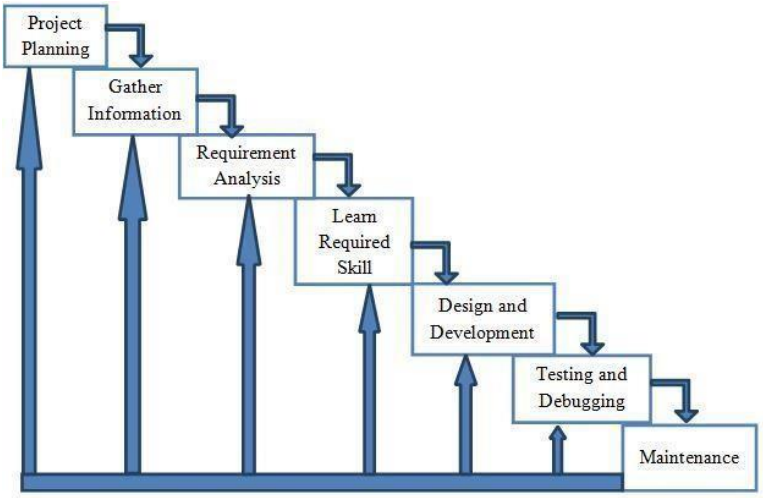

Figure 2.1 Waterfall model of the project

Description of Methodology

Full work has been divided into seven parts. The work is done part by part.

Project Planning: We seek for some problems in our real life. Then we found this problem and planned to solve the problem.
Gather Information: We read some research papers related to accident detection problem. We search on the internet to find solutions.
Requirement Analysis: We use Arduino Uno, GPS, GSM, Accelerometer, ultrasonic sensor, LCD Display, transformer, voltage regulator IC, Buzzer, Vero board, capacitor, Diode, resistor, etc.
Learn Required Skill: To complete the project, we learned C++ language, Arduino Uno language, hardware connection.
Design and Development: We developed a device which the system communicates with the web server through GPS communication via a GSM. It will send the vehicle location's latitude and longitude data to the web server upon user request or after detection of the accident.
Testing and Debugging: Final module testing aims to demonstrate correctness, whereas testing during debugging is primarily aimed at locating errors.
Maintenance: Hardware project maintenance presents the full scope and understanding how to function should operate and be managed in an implementation area. Actions necessary for retaining or restoring a piece of equipment, machine, or system to the specified operable condition to achieve its maximum useful life. It includes corrective maintenance and preventive maintenance.

Requirement Analysis

Requirements analysis also called requirements engineering, is the process of determining user expectations for a new or modified product. These features, called requirements, must be quantifiable, relevant and detailed. In software engineering, such requirements are often called functional specifications. Requirements analysis is an important aspect of project management.

Hardware Requirements

- Arduino UNO
- GSM Module (SIM900A)
- GPS Module (SIM28ML)
- Accelerometer (ADXL335)
- Breadboard
- 16 *2 LCD Display
- Resistor
- Jumper wire
- Power supply

Software Requirements

- Arduino Uno
- Language C++

Arduino UNO

Figure 2.2 Arduino Uno

Arduino Uno is a microcontroller board based on the ATmega328P (datasheet). It has 14 digital input/output pins (of which 6 can be used as PWM outputs), 6 analog inputs, a 16 MHz quartz crystal, a USB connection, a power jack, an ICSP header and a reset button. It contains everything needed to support the microcontroller; simply connect it to a computer with a USB cable or power it with an AC-to-DC adapter or battery to get started. You can tinker with your UNO without warring too much about doing something wrong, worst case scenario you can replace the chip for a few dollars and start over again. "Uno" means one in Italian and was chosen to mark the release of Arduino Software (IDE) 1.0. The Uno board and version 1.0 of Arduino Software (IDE) were the reference versions of Arduino, now evolved to newer releases.

The Uno board is the first in a series of USB Arduino boards, and the reference model for the Arduino platform; for an extensive list of current, past or outdated boards see the Arduino index of boards. Arduino is an open-source platform used for building electronics projects.

Arduino consists of both a physical programmable circuit board (often referred to as a microcontroller) and a piece of software, or IDE (Integrated Development Environment) that runs on your computer, used to write and upload computer code to the physical board. The Arduino IDE uses a simplified version of C++, making it easier to learn to program. Finally, Arduino provides a standard form factor that breaks out the functions of the micro-controller into a more accessible package.

Features of Arduino:

- Arduino boards are able to read analog or digital input signals from different sensors and turn it into an output such as activating a motor, turning LED on/off, connect to the cloud and many other actions.

- You can control your board functions by sending a set of instructions to the microcontroller on the board via Arduino IDE (referred to as uploading software).

- Unlike most previous programmable circuit boards, Arduino does not need an extra piece of hardware (called a programmer) in order to load a new code onto the board. You can simply use a USB cable.

- Additionally, the Arduino IDE uses a simplified version of C++, making it easier to learn to program.

- Finally, Arduino provides a standard form factor that breaks the functions of the micro-controller into a more accessible package.

Specifications

Name	Specification
Microcontroller	ATmega328P
Operating Voltage	5V
Input Voltage (recommended)	7-12V
Digital I/O Pins	14 (of which 6 provide PWM output)
PWM Digital I/O Pins	6
Analog Input Pins	6
DC Current per I/O Pin	20 mA
DC Current for 3.3V Pin	50 mA
Flash Memory	32 KB (ATmega328P) of which 0.5 KB used by boot loader
SRAM	2 KB (ATmega328P)
EEPROM	1 KB (ATmega328P)
Clock Speed	16Hz

Table 1 Arduino Uno Specifications

GSM Module (SIM900A)

Figure 2.3 GSM Module (SIM900A)

GSM is a mobile communication modem; it is stands for global system for mobile communication (GSM). The idea of GSM was developed at Bell Laboratories in 1970. It is widely used mobile communication system in the world. GSM is an open and digital cellular technology used for transmitting mobile voice and data services operates at the 850MHz, 900MHz, 1800MHz and 1900MHz frequency bands.GSM system was developed as a digital system using time division multiple access (TDMA) technique for communication purpose. A GSM digitizes and reduces the data, then sends it down through a channel with two different streams of client data, each in its own particular time slot. The digital system has an ability to carry 64 kbps to 120 Mbps of data rates. There are various cell sizes in a GSM system such as macro, micro, Pico and umbrella cells. Each cell varies as per the implementation domain.

There are five different cell sizes in a GSM network macro, micro, Pico and umbrella cells. The coverage area of each cell varies according to the implementation environment.

Working of GSM Module:

GSM is mix of TDMA (Time Division Multiple Access), FDMA (Frequency Division Multiple Access) and Frequency jumping. At first, GSM utilize two recurrence groups of 25 MHz width: 890 to 915 MHz recurrence band for up-connection and 935 to 960 MHz recurrence for down-interface. Later on, two 75 MHz band were added. 1710 to 1785 MHz for up-connection and 1805 to 1880 MHz for down-interface. Up-interface is the connection from ground station to a satellite and down-connect is the connection from a satellite down to at least one ground stations or recipients. GSM isolates the 25 MHz band into 124 channels each having 200 KHz width and staying 200 KHz is left unused as a gatekeeper band to keep away from impedance.

Control channels: These are primary control directs in GSM:

BCH (Broadcast Channel): It is for down-connect as it were. It has following sorts –

BCCH (Broadcast Control Channel): It communicates data about the serving cell.

SCH (Synchronization channel): Carries data like casing number and BSIC (Base Station Identity Code) for outline synchronization.

FCCH (Frequency Correction Channel): Enable MS to synchronize to recurrence

CCCH (Common Control Channel): It has following sorts –

RACH (Random Access Channel): Used by MS when making its first admittance to organize. It is for up-interface as it were.

AGCH (Access Grant Channel): Used for affirmation of the entrance endeavor sent on RACH. It is for down-connect as it were.

PCH (Paging Channel): Network page the MS, if there is an approaching call or a short message. It is for down-interface as it were.

DCCH (Dedicated Control Channel): It is for both up-connect and down-interface. It has following sorts –

SDCCH (Stand-alone Dedicated Control Channel): It is utilized for call arrangement, verification, encoding area update and SMS.

SACCH (Slow Associated Control Channel): Used to move signal while MS have continuous discussion on subject or while SDCCH is being utilized.

FACCH (Fast Associated Control Channel): It is utilized to send quick message like hand over message.

Specifications

Name	Specifications
Power Input	3.4V to 4.5V
Operating Frequency	EGSM900 and DCS1800
Operating Temperature	-30ºC to +80ºC
Storage Temperature	-5ºC to +90ºC
Transmitting Power Range	2V for EGSM900 and 1W for DCS1800
Data Transfer Link	Download: 85.6kbps, Upload:42.8kbps
SMS	MT, MO, CB, Text and PDU mode.
Antenna Support	Available
Audio Input/output	Available
Serial Port	I2C and UART
Serial Debug Port	Available

Table 2 GSM Module Specification

Features of GSM Module:

- Improved spectrum efficiency
- International roaming
- Compatibility with integrated services digital network(ISDN)
- Support for new services.
- SIM phonebook management
- Fixed dialing number (FDN)
- Real time clock with alarm management
- High-quality speech
- Uses encryption to make phone calls more secure
- Short message service(SMS)

Applications of GSM Module

- Cellular Communication
- Robotics
- Mobile Phone Accessories
- Servers
- Computer Peripherals
- Automobile
- USB Dongle

GPS Module (SIM28ML)

Figure 2.4 GPS Module (SIM28ML)

GPS is a navigation technology which, by use of satellites, tells the precise information about a location. Basically a GPS system consists of group of satellites and well developed tools such as receiver. The system, however, should comprise at least four satellites. Each satellite and the receiver are equipped with stable atomic clock. The satellite clocks are synchronized with each other and ground clocks. GPS receiver also has a clock but it is not synchronized and is not stable (less stable).

Any deviation of actual time of satellites from ground clock should be corrected daily. Four unknown quantities (three coordinates and clock deviation from satellite time) are required to be computed from the synchronized network of satellites and the receiver. The work of the GPS receiver is to receive signals from the network of satellites to compute three basic unknown equations of time and position.

Working of GPS Module:

All GPS (which represents Global Positioning System) units work in a similar fundamental way. The GPS network is comprised of 24 satellites that circle the earth in exact, predefined directions while broadcasting radio signals that contain information about the satellite's exact area. Each satellite's circle and going with radio sign is extraordinary.

GPS recipients are designed to:

1. Acknowledge the approaching signs from the different satellites.

2. Analyze the area information and its transmission time.

3. Utilize this data to locate the beneficiary's exact area.

The GPS gadget needs in any event three signs to decide its situation in two-dimensional space and at any rate four signs to decide its area in three-dimensional space.

Contingent upon area, season of day, and the presence or nonappearance of designs that may hinder the sign, we can anticipate that a receiver should follow upwards of eight satellites out of the blue.

Arduino GPS Capabilities:

In light of your area information, GPS recipients can decide time and distance to another area, your bearing, even your speed/pace of movement (by contrasting ongoing changes in area and an opportunity to move starting with one then onto the next). This is all with a solitary GPS unit working alone.

At the point when you start to add custom programming and different GPS-empowered gadgets to the condition, the potential outcomes increase dramatically. For example, by utilizing two GPS-empowered gadgets couple (like an Arduino and a cell phone), you can analyze or communicate the area information of both to perform undertakings, for example,

- Find a lost pet

- Monitor a kid returning home from school

- Make your cooler chase after you at the excursion (advantageous and an incredible gathering stunt)

You can utilize speed and area data to improve wearable's by following your course as well as your speed over the long run (a particularly valuable expansion for sprinters).

On the off chance that your undertakings include exact information about the area, heading, or speed of at least one items, figuring out how to work with GPS modules will be a major assistance in acknowledging them.

The most effective method to Connect GPS Module to Arduino
Associating GPS units to Arduino will not take long, since the GPS units are prepared to yield sequential information and the Arduino has a few distinct approaches to get sequential data. Follow these means to interface these gadgets.

1. Start by choosing the correct GPS module. Since not all the Arduino pins are voltage-directed, ensure you've picked a GPS unit with a proper force supply, or one that has its own controller to guarantee that the Arduino will not harm it (for example, the yield of a 5V board can harm an unregulated 3.3V GPS).

2. When you have a viable GPS beneficiary, associate it to a 5V force from the Arduino and a ground pin. Associate the RX and TX pins on the GPS to sequential pins on the Arduino.

3. Utilize the Arduino's chronic screen to ensure the GPS is yielding information. Know that numerous GPS modules have long "cool beginning" times, so be patient and allow it a little while before you conclude whether it's associated accurately.

The underlying sequential yield will appear as though gibberish; however it's the local language of the GPS organization.

Ordinarily, you'll see lines that start $GPXXX where "XXX" are three different letters.
These letter codes build up that its GPS information and they give data about what sort of information is being coded (assessed position, speed, and so on)

The letter code is trailed by a series of numbers that address, all together:

- Timestamp

- Latitude

- Longitude

- Quality of the sign (remedied/uncorrected, and so on)

- Number of satellites utilized in the arrange

- Information about elevation

- Any adjustments

All alone, this crude information (called NMEA information, from a standard which went before the creation of GPS and is right now the norm for all GPS units) isn't effectively clear or supportive to the normal client. In any case, introducing an Arduino GPS library like the Tiny GPS Library will change the crude information into comprehensible data in an organization like this:

Area: LATITUDE, LONGITUDE Date/Time: XX/XX/XXXX XX: XX: XX.XX

As should be obvious, the information will currently show as clear arranges, time-stepped with the day, month, year, and time down to hundredths of a second.

Specifications

Name	**Specification**
Receiver Type	22 tracking/66 acquisition channel GPS receiver GPS L1, C/A Code
Operation Temperature	-40 degrees C ~ +85 degrees C
Power Supply	2.8 ~ 4.3V
Backup Power	2.0 V ~ 4.3V
Power Consumption	Acquisition 17mA, Tracking 16mA, Back up 8uA
Antenna Type	Active and Passive

Table 3 GPS Module Specification

Features of GPS Module

- Support GPS/GLONASS/Galileo/QZSS
- Support EASYTM self-generated orbit prediction
- Support EPOTM orbit prediction
- Support SBAS ranging (WAAS, EGNOS, GAGAN, MSAS)
- Support Jamming removing function
- Low-noise amplifier has been integrated

Applications of GPS Module

- Astronomy
- Automated vehicles
- Car location
- Cellular telephony
- Disaster relief and other emergency services

Accelerometer

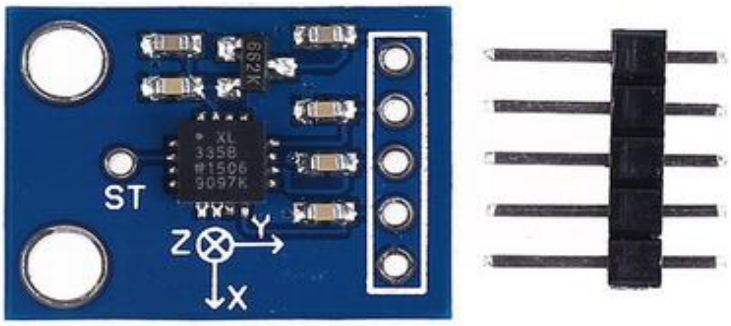

Figure 2.5 Accelerometer

Accelerometer (when all is said and done) is an electromechanical gadget that estimates the quickening powers. These powers can be dynamic like any vibrations to the accelerometer or static like the consistent power following up on the body because of gravity. Accelerometer works in various manners. One such route is by utilizing piezoelectric impact this contains a gem like infinitesimal structures which produces voltages when the accelerative powers follow up on it**.**

The ADXL335 gives total 3-pivot speeding up estimation. This module estimates increasing speed inside range ±3g in the x, y and z pivot. The yield signals are simple voltages which are relative to the increasing speed. It contains a poly-silicon surface-small scale machined sensor and sign moulding hardware. As in Fig. 6 (b), speeding up avoids the moving mass and unbalances the differential capacitor which brings about a sensor yield voltage plentifulness that is relative to the increasing speed. Stage delicate demodulation procedures are then used to decide the size and bearing of the increasing speed.

Specifications

Name	Specification
Operating Voltage	1.8V – 3.6V
Operating Current	350μA (typical)
Sensing Range	±3g (Full Scale)
Temperature Range	−40 to +85°C
Sensing axis	3 axis
Sensitivity	270 to 330mV/g (Ratio metric)
Shock Resistance	Up to 10,000g
Dimension	4mm x 4mm x 1.45mm

Table 4 Accelerometer Specification

Pin Description of accelerometer

VCC	Pin provides power for the accelerometer which can be connected to 5V on the Arduino.
X-Out	pin outputs analog voltage proportional to acceleration exerted on X axis
Y-Out	pin outputs analog voltage proportional to acceleration exerted on Y axis
Z-Out	Pin outputs analog voltage proportional to acceleration exerted on Z axis.
GND	pin is connected to GND on Arduino
ST(Self-Test)	pin controls the self-test feature

Table 5 Pin Description of accelerometer

LCD Display (16×4)

Figure 2.6 LCD 16×4 Display

A 16 x 4 character LCD display with white text on a vivid blue backlit LCD. The pictures don't do justice to the bright blue background with clear white text of these display.4 lines of 16 characters. Standard Hitachi HD44780 compatible interface for easy connection
To microcontrollers.

Dimensions

- Width 3.45 inches(87mm)
- Height 2.35 inches(60mm)
- Display view size 62mm x26mm

Characters of LCD Display16x4

- Character LCD16x4
- 5x8 dots includes cursor
- Built-in controller (ST7066 or Equivalent)
- +5V power supply (Also available for+3V)
- WG16032D3 optional for +3V power supply
- 1/16 duty cycle
- LED can be driven by PIN1, PIN2, PIN15, PIN16 or A andK

Interface Pin Function

Pin No.	Symbol	Description
1	Vss	Ground
2	VDD	Power supply for logic
3	Vo	Contrast Adjustment
4	Rs	Data/ Instruction select signal
5	R/W	Read/Write select signal
6	E	Enable signal
7-14	DB0~DB7	Data bus line
15	A	Power supply for B/L +
16	K	Power supply for B/L -

Table 6 LCD Interface Pin description

Features of 16×4 LCD Module

- Operating Voltage is 4.7 V to 5.3V
- Current consumption is 1 mA without backlight
- Alphanumeric LCD display module meaning can display alphabets and numbers
- Consists of two rows and each row can print 16characters.
- Each character is built by a 5×8-pixelbox
- Can work on both 8-bit and 4-bitmode
- It can also display any custom generated characters
- Available in Green and Blue Backlight.

Breadboard

Figure 2.7 Breadboard

A breadboard is a widely used tool to design and test circuit. You do not need to solder wires and components to make a circuit while using a bread board. It is easier to mount components & reuse them. Since, components are not soldered you can change your circuit design at any point without any hassle. It consist of an array of conductive metal clips encased in a box made of white ABS plastic, where each clip is insulated with another clips. There are a number of holes on the plastic box, arranged in a particular fashion. A typical bread board layout consists of two types of region also called strips. Bus strips and socket strips. Bus strips are usually used to provide power supply to the circuit. It consists of two columns, one for power voltage and other for ground.

Socket strips are used to hold most of the components in a circuit. Generally it consists of two sections each with 5 rows and 64 columns. Every column is electrically connected from inside.

Features and Specifications

- 2 Distribution Strips, 200 tie-points
- 630 tie-points in IC/ circuit areas
- ABS plastic with color legend
- Dimension: 6.5*4.4*0.3 inch
- Hole/Pitch Style: Square wire holes (2.54mm)
- ABS heat Distortion Temperature: 84° C (183° F)
- Rating: 300/3 to 5Amps
- Insulation Resistance : 500MΩ / DC500V
- Withstanding Voltage : 1,000V AC / 1 minute
- Insertion Wire Size: 21 to 26 AWG wire

Advantages of Breadboard:

- It has easy to quick to check for easy and complex circuits both and it has easily verified circuits at the initial stage, so it can save time.
- Quick to check component around.
- It is easy to adjust.
- It is flexible.
- No drilling holes.
- No soldering required.
- It can be debugged easily.
- A solder less connection makes it reusable.
- Cheap and connections can be changed.

Jumper Wire

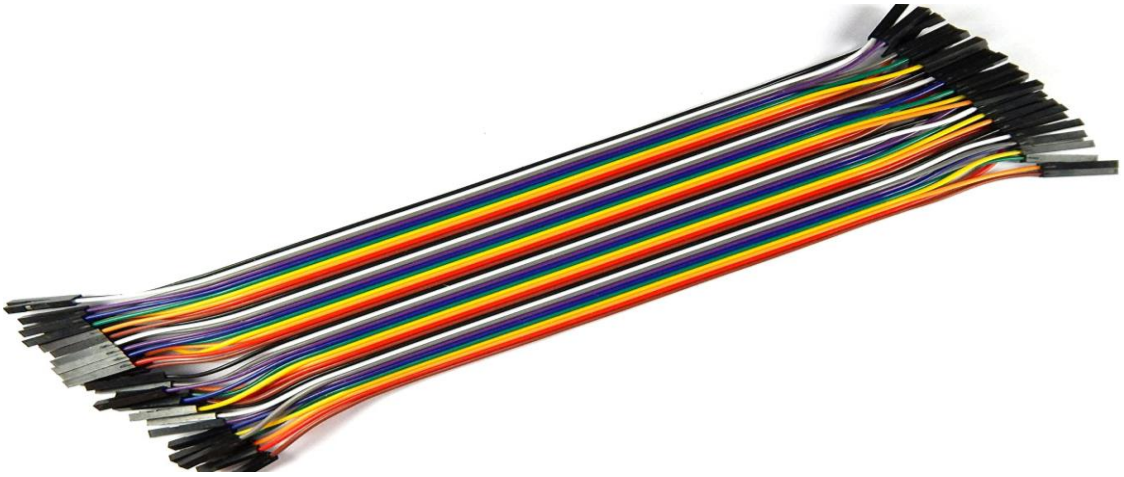

Figure 2.8 Connecting Wires

A wire is a single, usually cylindrical, flexible strand. Wires are used to bear carry electricity and telecommunications signals. Standard sizes are determined by various wire gauges. The term wire is also used more loosely to refer to a bundle of such strands, as in 'multi-stranded wire', which is more correctly termed a wire rope in mechanics, or a cable in electricity. Although usually circular in cross-section, the wire can be made in square, hexagonal, flattened rectangular or other cross-sections, either for decorative purposes or for technical purposes such as high-efficiency voice coils in loudspeakers. Edge-wound coil springs, such as the Slinky toy, are made of special flattened wire.

Chapter-III

System Design and Fabrication

Introduction

In this chapter fully discuss about the project design and fabrication. A general block diagram has been developed and implement according diagram. Here we described overall project description, implementation procedure and working principle. Total project flow chart is also available in this chapter.

Block Diagram

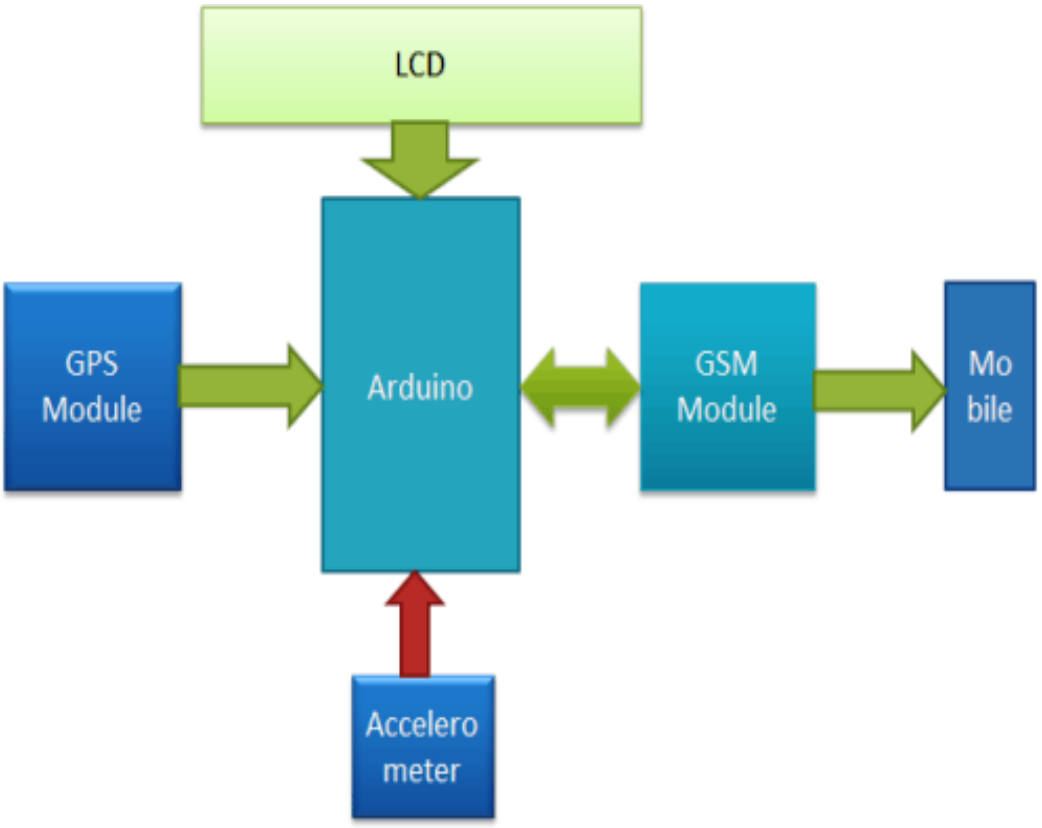

Figure 3.1 Block diagram of vehicle accident detection

Working Explanation

In this project, Arduino is used for controlling whole the process with a GPS Receiver and GSM module. GPS Receiver is used for detecting coordinates of the vehicle, GSM module is used for sending the alert SMS with the coordinates and the link to Google Map. Accelerometer namely ADXL335 is used for detecting accident or sudden change in any axis. And an optional 16x2 LCD is also used for displaying status messages or coordinates. We have used GPS Module SIM28ML and GSM Module SIM900A.

When we are ready with our hardware after programming, we can install it in our vehicle and power it up. Now whenever there is an accident, the car gets tilt and accelerometer changes his axis values. These values read by Arduino and checks if any change occurs in any axis. If any change occurs then Arduino reads coordinates by extracting $GPGGA String from GPS module data (GPS working explained above) and send SMS to the predefined number to the police or ambulance or family member with the location coordinates of accident place. The message also contains a Google Map link to the accident location, so that location can be easily tracked. When we receive the message then we only need to click the link and we will redirect to the Google map and then we can see the exact location of the vehicle. Speed of Vehicle, in knots (1.852 KPH), is also sent in the SMS and displayed on the LCD panel.

Circuit Diagram

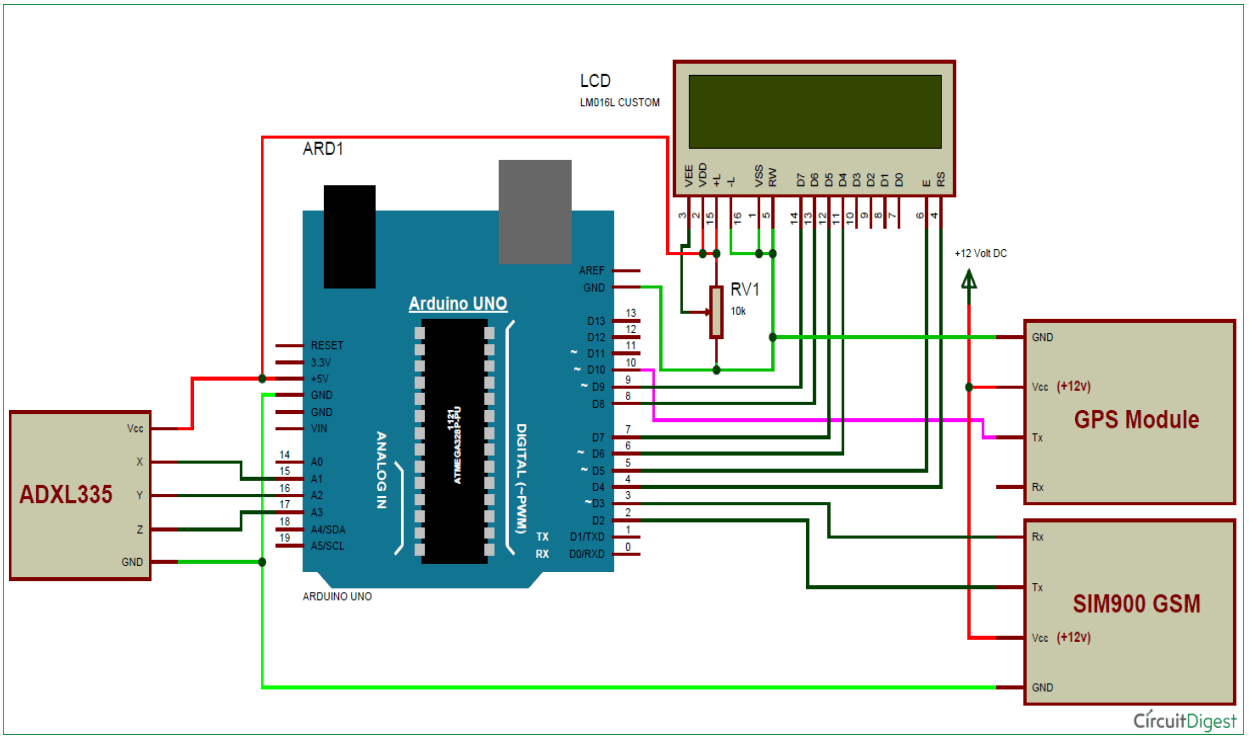

Figure 3.2 Circuit diagram of vehicle accident detection

Circuit Explanation

Circuit Connections of this Vehicle Accident Alert System Project is simple. Here Tx pin of GPS module is directly connected to digital pin number 10 of Arduino. By using Software Serial Library here, we have allowed serial communication on pin 10 and 11, and made them Rx and Tx respectively and left the Rx pin of GPS Module open. By default Pin 0 and 1 of Arduino are used for serial communication but by using the Software Serial library, we can allow serial communication on other digital pins of the Arduino. 12 Volt supply is used to power the GPS Module.

GSM module's Tx and Rx pins of are directly connected to pin D2 and D3 of Arduino. For GSM interfacing, here we have also used software serial library. GSM module is also powered by 12v supply. An optional LCD's data pins D4, D5, D6, and D7 are connected to pin number 6, 7, 8, and 9 of Arduino. Command pin RS and EN of LCD are connected with pin number 4 and 5 of Arduino and RW pin is directly connected with ground. A Potentiometer is also used for setting contrast or brightness of LCD.

An Accelerometer is added in this system for detecting an accident and its x,y, and z-axis ADC output pins are directly connected to Arduino ADC pin A1, A2, and A3.

System Description

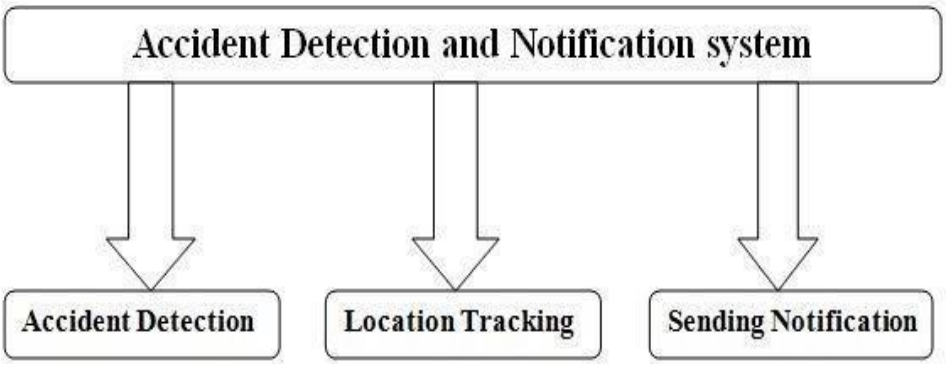

Figure 3.3 system description models

The project is divided into three phases. They are.

Accident Detection:
An Accelerometer sensor senses the accident when the vehicles are fallen down detection x, y, z. initially the angle of the vehicle is zero degree and it could be increase 360 degrees towards any axis. If the angle of the vehicle rises in any direction exceeds our threshold value, the accelerometer considers the situation as an accident. The threshold value in X and Y axis are 320 and 320, respectively. The sensor has sent the signal to the microcontroller.

Location Tracking:
The GPS sensor can detect the current location of the vehicle. In our proposed system we use the GPS device to find the exact accident location. When microcontroller receives any signal of accident it requests for current location of accident spot to the GPS. The GPS sends the location of accident spot to the microcontroller.

Sending Notification:
With accident location link GSM sends text message to the hospital and police control room. The hospital and police control room will get a message along with the map link which will contain the exact latitude and longitude details of the location. In the same time, nearest police station receives an accident occurs message with link Google map. With the help of these details, the ambulance can take the shortest route to the accident location and reduce the time to save the victim.

Hardware Implementation

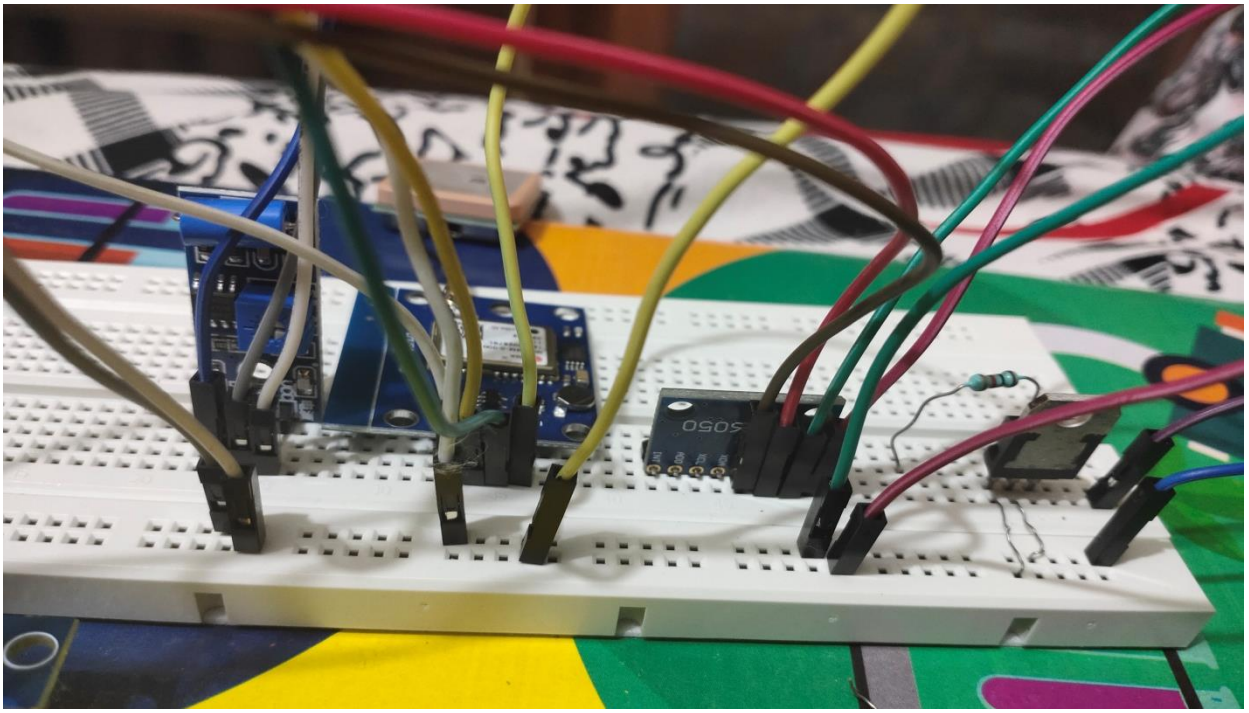

Figure 3.4 Hardware of vehicle accident detection

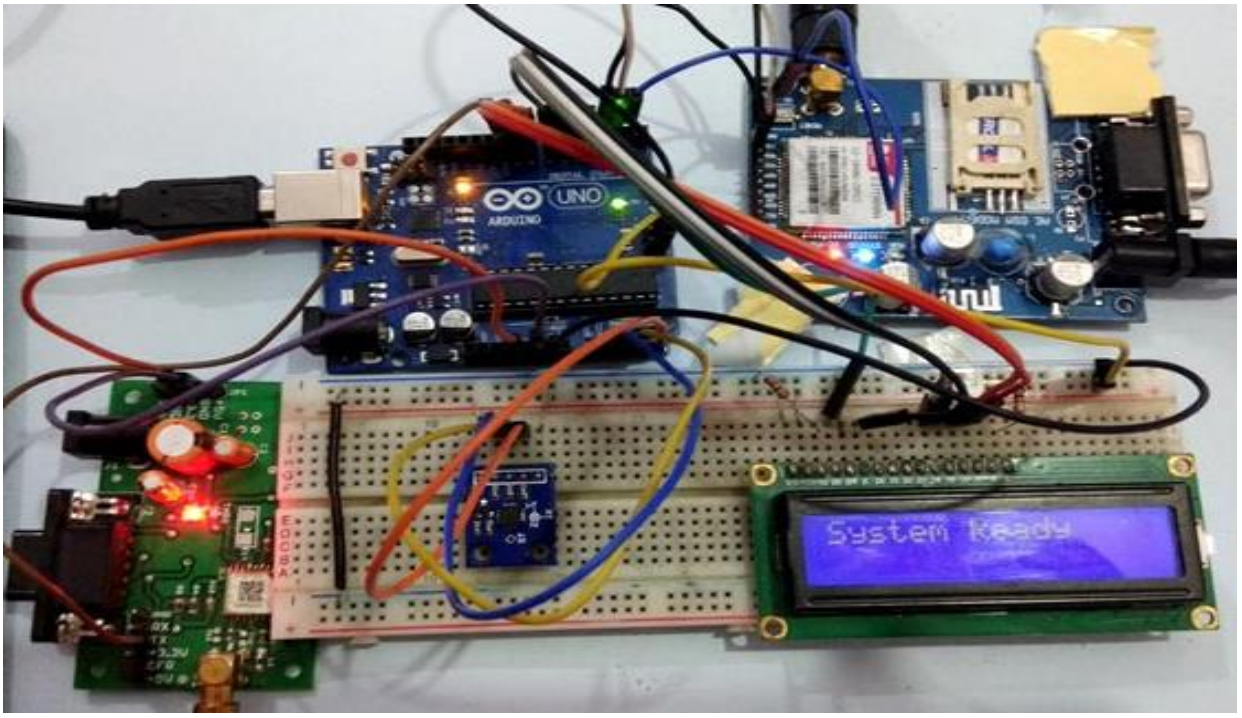

Figure 3.5 Hardware of vehicle accident detection using Accelerometer

AT Command:

AT means ATTENTION. This command is used to control GSM module. There are some commands for calling and messaging that we have used in many of our previous GSM projects with Arduino. For testing GSM Module we used AT command. After receiving AT Command GSM Module respond with OK. It means GSM module is working fine.

Below is **some AT commands** we used here in this project:

```
ATE0 For echo off
AT+CNMI=2,2,0,0,0  <ENTER>       Auto opened message Receiving.  (No need to
open message)
ATD<Mobile Number>; <ENTER>      making a call (ATD+919610126059;\r\n)
AT+CMGF=1 <ENTER>                Selecting Text mode
AT+CMGS="Mobile Number" <ENTER> Assigning recipient's mobile number
>>Now we can write our message
>>After writing message
Ctrl+Z  send message command (26 in decimal).
ENTER=0x0d in HEX
```

Programming Explanation*:*

Complete Program has been given below ; here we are explaining its various functions in brief.
First we have included all the required libraries or headers files and declared various variables for calculations and storing data temporary.
After this, we have created a function ***void initModule(String cmd, char *res, int t)*** to initialize the GSM module and checking its response using AT commands.

```
void initModule(String cmd, char *res, int t)
{
  while(1)
  {
    Serial.println(cmd);
    Serial1.println(cmd);
    delay(100);
    while(Serial1.available()>0)
    {
       if(Serial1.find(res))
       {
        Serial.println(res);
        delay(t);
        return;
       }

       else
       {
        Serial.println("Error");
       }
    }
    delay(t);
  }
}
```

After this, in ***void setup ()*** function, we have initialized hardware and software serial communication, LCD, GPS, GSM module and accelerometer.

```
void setup()
{
  Serial1.begin(9600);
  Serial.begin(9600);
  lcd.begin(16,2);
  lcd.print("Accident Alert  ");
  lcd.setCursor(0,1);
  lcd.print("     System     ");
  delay(2000);
  lcd.clear();
  .... ......
  ...... .....
```

Accelerometer calibration process is also done in *setup* loop. In this, we have taken some samples and then find the average values for the x-axis, y-axis, and z-axis. And store them in a variable. Then we have used these sample values to read changes in accelerometer axis when vehicle gets tilt (accident).

```
lcd.print("Callibrating ");
  lcd.setCursor(0,1);
  lcd.print("Acceleromiter");
  for(int i=0;i<samples;i++)
  {
    xsample+=analogRead(x);
    ysample+=analogRead(y);
    zsample+=analogRead(z);
  }

  xsample/=samples;
  ysample/=samples;
  zsample/=samples;

  Serial.println(xsample);
  Serial.println(ysample);
  Serial.println(zsample);
```

After this, in the *void loop()* function, we have read accelerometer axis values and done a calculation to extract changes with the help of samples that are taken in Calibration. Now if any changes are more or less then defined level then Arduino sends a message to the predefined number.

```
void loop()
{
    int value1=analogRead(x);
    int value2=analogRead(y);
    int value3=analogRead(z);

    int xValue=xsample-value1;
    int yValue=ysample-value2;
    int zValue=zsample-value3;
```

```
Serial.print("x=");
Serial.println(xValue);
Serial.print("y=");
Serial.println(yValue);
Serial.print("z=");
Serial.println(zValue);
..... .....
........ ...
```

Here we have also created some other function for various purposes like ***void gpsEvent()*** to get GPS coordinates, ***void coordinate2dec()*** for extracting coordinates from the GPS string and convert them into Decimal values, ***void show_coordinate()*** for displaying values over serial monitor and LCD, and finally the ***void Send()*** for sending alert SMS to the predefined number.

Complete code is given below; you can check all the functions in the code.

Complete Program

```
#include<SoftwareSerial.h>
SoftwareSerial Serial1(2,3); //make RX arduino line is pin 2, make TX arduino line is pin 3.
SoftwareSerial gps(10,11);
#include<LiquidCrystal.h>
LiquidCrystal lcd(4,5,6,7,8,9);

#define x A1
#define y A2
#define z A3

int xsample=0;
int ysample=0;
int zsample=0;

#define samples 10

#define minVal -50
#define MaxVal 50

int i=0,k=0;
int  gps_status=0;
float latitude=0;
float logitude=0;
String Speed="";
String gpsString="";
char *test="$GPRMC";

void initModule(String cmd, char *res, int t)
{
  while(1)
  {
    Serial.println(cmd);
    Serial1.println(cmd);
    delay(100);
    while(Serial1.available()>0)
    {
      if(Serial1.find(res))
      {
       Serial.println(res);
       delay(t);
       return;
      }

      else
      {
       Serial.println("Error");
      }
    }
    delay(t);
```

```
  }
}

void setup()
{
  Serial1.begin(9600);
  Serial.begin(9600);
  lcd.begin(16,2);
  lcd.print("Accident Alert  ");
  lcd.setCursor(0,1);
  lcd.print("     System     ");
  delay(2000);
  lcd.clear();
  lcd.print("Initializing");
  lcd.setCursor(0,1);
  lcd.print("Please Wait...");
  delay(1000);

  Serial.println("Initializing....");
  initModule("AT","OK",1000);
  initModule("ATE1","OK",1000);
  initModule("AT+CPIN?","READY",1000);
  initModule("AT+CMGF=1","OK",1000);
  initModule("AT+CNMI=2,2,0,0,0","OK",1000);
  Serial.println("Initialized Successfully");
  lcd.clear();
  lcd.print("Initialized");
  lcd.setCursor(0,1);
  lcd.print("Successfully");
  delay(2000);
  lcd.clear();
  lcd.print("Callibrating ");
  lcd.setCursor(0,1);
  lcd.print("Acceleromiter");
  for(int i=0;i<samples;i++)
  {
    xsample+=analogRead(x);
    ysample+=analogRead(y);
    zsample+=analogRead(z);
  }

  xsample/=samples;
  ysample/=samples;
  zsample/=samples;

  Serial.println(xsample);
  Serial.println(ysample);
  Serial.println(zsample);
  delay(1000);

  lcd.clear();
```

```
  lcd.print("Waiting For GPS");
  lcd.setCursor(0,1);
  lcd.print("     Signal    ");
  delay(2000);
  gps.begin(9600);
  get_gps();
  show_coordinate();
  delay(2000);
  lcd.clear();
  lcd.print("GPS is Ready");
  delay(1000);
  lcd.clear();
  lcd.print("System Ready");
  Serial.println("System Ready..");
}

void loop()
{
    int value1=analogRead(x);
    int value2=analogRead(y);
    int value3=analogRead(z);

    int xValue=xsample-value1;
    int yValue=ysample-value2;
    int zValue=zsample-value3;

    Serial.print("x=");
    Serial.println(xValue);
    Serial.print("y=");
    Serial.println(yValue);
    Serial.print("z=");
    Serial.println(zValue);

    if(xValue < minVal || xValue > MaxVal  || yValue < minVal || yValue > MaxVal  || zValue <
minVal || zValue > MaxVal)
    {
      get_gps();
      show_coordinate();
      lcd.clear();
      lcd.print("Sending SMS ");
      Serial.println("Sending SMS");
      Send();
      Serial.println("SMS Sent");
      delay(2000);
      lcd.clear();
      lcd.print("System Ready");
    }
}

void gpsEvent()
{
```

```
 gpsString="";
 while(1)
 {
  while (gps.available()>0)           //Serial incoming data from GPS
  {
   char inChar = (char)gps.read();
    gpsString+= inChar;                    //store incoming data from GPS to temparary string str[]
    i++;
   // Serial.print(inChar);
    if (i < 7)
    {
     if(gpsString[i-1] != test[i-1])         //check for right string
     {
       i=0;
       gpsString="";
     }
    }
   if(inChar=='\r')
   {
    if(i>60)
    {
      gps_status=1;
      break;
    }
    else
    {
      i=0;
    }
   }
  }
   if(gps_status)
    break;
  }
}

void get_gps()
{
  lcd.clear();
  lcd.print("Getting GPS Data");
  lcd.setCursor(0,1);
  lcd.print("Please Wait.....");
   gps_status=0;
   int x=0;
   while(gps_status==0)
   {
    gpsEvent();
    int str_lenth=i;
    coordinate2dec();
    i=0;x=0;
    str_lenth=0;
```

```
  }
}

void show_coordinate()
{
   lcd.clear();
   lcd.print("Lat:");
   lcd.print(latitude);
   lcd.setCursor(0,1);
   lcd.print("Log:");
   lcd.print(logitude);
   Serial.print("Latitude:");
   Serial.println(latitude);
   Serial.print("Longitude:");
   Serial.println(logitude);
   Serial.print("Speed(in knots)=");
   Serial.println(Speed);
   delay(2000);
   lcd.clear();
   lcd.print("Speed(Knots):");
   lcd.setCursor(0,1);
   lcd.print(Speed);
}

void coordinate2dec()
{
 String lat_degree="";
   for(i=20;i<=21;i++)
     lat_degree+=gpsString[i];

 String lat_minut="";
    for(i=22;i<=28;i++)
     lat_minut+=gpsString[i];

 String log_degree="";
   for(i=32;i<=34;i++)
     log_degree+=gpsString[i];

 String log_minut="";
   for(i=35;i<=41;i++)
     log_minut+=gpsString[i];

   Speed="";
   for(i=45;i<48;i++)          //extract longitude from string
     Speed+=gpsString[i];

    float minut= lat_minut.toFloat();
    minut=minut/60;
    float degree=lat_degree.toFloat();
    latitude=degree+minut;
```

```
    minut= log_minut.toFloat();
    minut=minut/60;
    degree=log_degree.toFloat();
    logitude=degree+minut;
}

void Send()
{
  Serial1.println("AT");
  delay(500);
  serialPrint();
  Serial1.println("AT+CMGF=1");
  delay(500);
  serialPrint();
  Serial1.print("AT+CMGS=");
  Serial1.print("");
  Serial1.print("9821757249");    //mobile no. for SMS alert
  Serial1.println("");
  delay(500);
  serialPrint();
  Serial1.print("Latitude:");
  Serial1.println(latitude);
  delay(500);
  serialPrint();
  Serial1.print(" longitude:");
  Serial1.println(logitude);
  delay(500);
  serialPrint();
  Serial1.print(" Speed:");
  Serial1.print(Speed);
  Serial1.println("Knots");
  delay(500);
  serialPrint();
  Serial1.print("http://maps.google.com/maps?&z=15&mrt=yp&t=k&q=");
  Serial1.print(latitude,6);
  Serial1.print("+");              //28.612953, 77.231545   //28.612953,77.2293563
  Serial1.print(logitude,6);
  Serial1.write(26);
  delay(2000);
  serialPrint();
}

void serialPrint()
{
 while(Serial1.available()>0)
 {
   Serial.print(Serial1.read());
 }
}
```

Chapter-IV

Result and Discussion

This chapter contains the results obtained and discussion about the full project. We have also covered discussions about advantages, limitation, application and estimated cost of the current version of the vehicle accident detection.

Results and Discussions

The results include the successful operation of an automatic accident detection and notification systems. This system can detect the accident and then alert the nearest police station and medical assist center to provide emergency medical aid to accident victim.
Actually which types of sensor have been used in this project discuss it given bellow:

Limitations of the System

1. It does not work without network.
2. It does not work when mobile is damage

Angle of Rotation Accelerometer Sensor (ADXL335)

Now let's find a complete angle of rotation (0° to 360°) around X, Y, Z axis, which we can also callas,

Roll - Angle of rotation along the X-axis
Pitch - Angle of rotation along the Y-axis
Yaw - Angle of rotation along the Z-axis

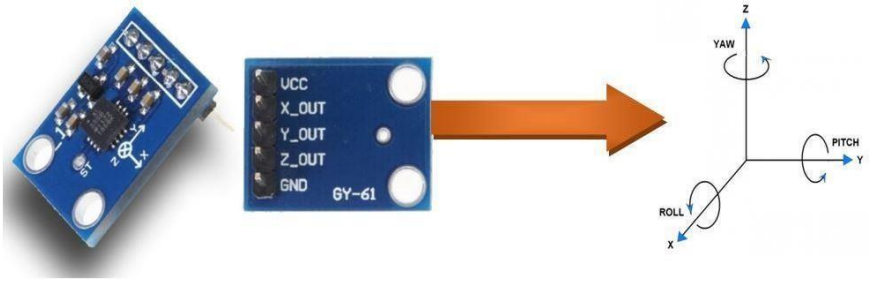

Figure 4.1 Angle of Rotation Accelerometer Sensor (ADXL335)

Angles Calculation of Accelerometer Sensor (ADXL335)

Angle of inclination means by how much angle the device is tilted from its plane of surface. Angle of inclination is shown in below figure.
To calculate angle of inclination of X, Y, Z axis from its reference, we need to use below formulas.

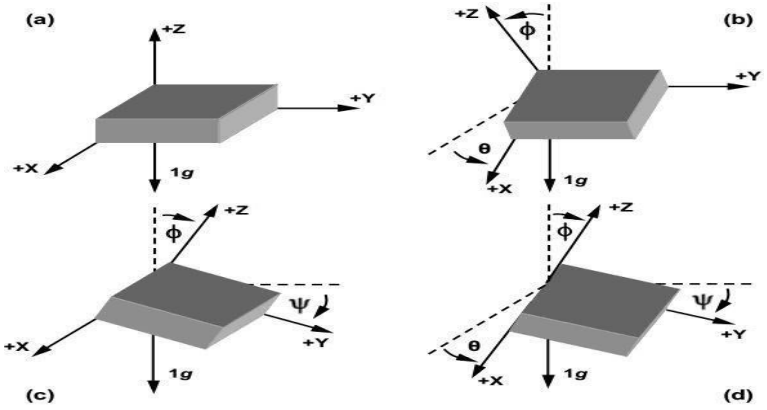

Figure 4.1.1 Angles calculation of Vibration Sensor (ADXL335)

We can calculate angle of inclination or tilt by using X, Y, Z's value. Also, we can calculate Roll, Pitch and Yaw angles with respect to X, Y and Z axis. So first we need to convert 10- bit ADC values into g unit. As per ADXL335 datasheet maximum voltage level at 0g is 1.65V and sensitivity scale factor of 330m.V/g.

$$Aout = \frac{\frac{\text{ADC value} \times \text{Vref}}{1024} - \text{Voltage Level at 0g}}{\text{Sensitivity Scale Factor}}$$

Above formula gives us acceleration values in g unit for X, Y and Z axis as,
Axout= (((X axis ADC value * Vref) / 1024) – 1.65) / 0.330 Ayout= (((Y axis ADC value * Vref) / 1024) – 1.65) / 0.330 Azout= (((Z axis ADC value * Vref) / 1024) – 1.65) / 0.330

Frequency response of Accelerometer sensor (ADXL335)

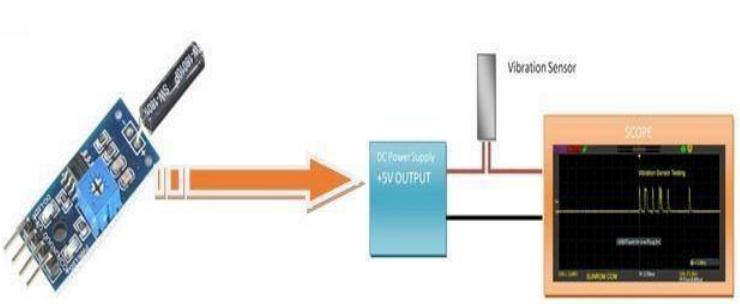

Figure 4.2 Frequency response of accelerometer sensor (ADXL335)

Sensor is made up of a small spring mechanism, which makes the contact ON when the applied vibration force is at above a certain threshold. It has two legs coming out of it. Normally the two terminals are insulated by a resistance value more than 10MOhm. When someone applies vibratory force on the switch, spring inside the switch vibrates and makes a momentary short circuit between the two terminals. Internal spring mounted system to detect vibration. As spring system moves it contacts with the outer wall and generates output voltage.

Experimental Results

The intelligent accident detection and notification system has been tested in 20 different places in different cities of India. We tested our system in sloping, uneven, curved highways for various degrees of angles. If the degree of angles in X or Y axis exceeded 310 and 340 degree, respectively for any case, the system detected it as an accident. If any vehicle reached within 5 cm, the system detected a possibility of crash. As the system has tested in highways there are lower possibilities of reaching any object, living being within 5 cm of the vehicle body. Table I listed the test results of the accident detection, exact location tracking and sending a notification message. On the basis of the experimental data listed in Table 1, we evaluate system performance.

The system performance is divided into three sections:
(1) Accident detection accuracy,
(2) Location tracking accuracy,
(3) Notification sending accuracy.

1) <u>Accident Detection Accuracy</u>: Accident detection accuracy, DA is defined by

$$D_A = \frac{TP_A}{TP_A + FN_A}$$

Where, TPA and FNA denote correct detection of accident and incorrect detection of accident, respectively.

2) Location Tracking Accuracy: Location tracking accuracy, TL is defined by

$$T_L = \frac{TP_L}{TP_L + FN_L}$$

Where, TP_L and FN_L denote correct tracking of location and incorrect tracking of location, respectively.

Place No.	Accident Detection Status	Exact Location Tracking Status	Notification Sending Status
1	Yes	Yes	Yes
2	Yes	Yes	Yes
3	Yes	Yes	Yes
4	Yes	Yes	Yes
5	Yes	Yes	Yes
6	No	Yes	Yes
7	Yes	Yes	Yes
8	Yes	Yes	Yes
9	Yes	No	Yes
10	Yes	Yes	Yes
11	Yes	Yes	Yes
12	Yes	Yes	Yes
13	Yes	Yes	Yes
14	Yes	Yes	Yes
15	Yes	No	Yes
16	Yes	Yes	Yes
17	Yes	Yes	Yes
18	Yes	Yes	Yes
19	Yes	Yes	Yes
20	Yes	Yes	Yes

Table 7 Experimental Result

3) Notification Sending Accuracy:

Notification Sending accuracy, SN is defined by

$$S_N = \frac{TP_N}{TP_N + FN_N}$$

Where, TPN and FNN denote successful sending of notification and unsuccessful sending of notification in specified phone numbers, respectively. Our proposed intelligent accident detection and notification system provide 95% accident detection accuracy, 90% exact location tracking accuracy and 100% successful notification sending accuracy in nearby hospital and police station.

Advantages of the System

- Portable and easy tousle.
- It is easy to design and manufacture as all the components are easily available.
- It is portable and hence can be placed anywhere.
- Due to wireless communication data rate is faster.
- No need for lengthy wires.
- Easy to control
- Easy to maintain and repair

- Efficient and low-cost design
- Low power consumption
- The programming of the Arduino is easy.
- Can be modified easily.

Applications of the System

- It can be widely used in all types of vehicle for automatic accident detection and sending notification to the nearest police station and medical assist center.
- It can be used to track the stolen vehicle.

Estimated Cost of the System

S.No.	Particulars	Quantity	Unit Price (in BDT)	Total Price (in BDT)
1	Arduino UNO	1	350	350
2	GPS Module	1	900	900
3	GSM Module	1	1159	1159
4	Accelerometer Sensor	1	250	250
5	LCD Display	1	211	211
6	Jumper Wire	As per need	1	50
Total				2920

Table 8 Estimated Cost of the system

Chapter-V

Conclusion and Future Work

Conclusion

This project presents vehicle accident detection and alert system with SMS to the user defined mobile numbers. The GPS tracking and GSM alert based algorithm is designed and implemented. The proposed vehicle accident detection system can track geographical information automatically and sends an alert SMS regarding accident. The system is successfully implemented and tested. After the detailed experiment, it is observed that this system is efficient and reliable.

Future Works

This system could be more reliable and useable if we develop or add some other features and systems. They are as follows:

- The Accident Alert System is a versatile system which can be modified to work with many other embedded circuits in vehicles to provide a number of applications.
- The Accident Alert System can be interfaced with the Air Bag system, which provides security to the driver in case of an accident.
- The circuit can be used for parking assistance in vehicles with slight modifications.
- A Proximity sensor can be added to the circuit, which would alert the driver by beeping a buzzer if the driver is about to collide with the vehicle in front.
- The presence of GSM modem makes it possible to track the vehicle in case of theft.
- The GPS modem makes it possible to make route navigation possible.
- A warning light or a loud horn can be interfaced with the circuit which is turned on in case of an accident, which draws the attention of the people nearby to the site of the accident.

This frame can be additionally created to distinguish alcohol driver. Signs of drinking Expenses can be sent to family members/crisis. Numbers to ensure that the driver is not driving when he was drunk. The other expands to this frame can be a rest level recognize. This can be used to show the sluggishness and the rest of the level the driver is away from him elsewhere when driving a vehicle drowsy and keep in this way strategic distance from further causality.

REFERENCES

1. https://www.ijert.org/automatic-vehicle-accident-detection-and-messageing-system
2. https://www.researchgate.net/publication/338157166_Automatic_Vehicle_Accident_Detection_and_Messaging_System_Using_GPS_and_GSM_Module
3. https://www.academia.edu/41661155/Automatic_Vehicle_Accident_Detection_and_Messaging_System_Using_GSM_and_GPS_Module
4. https://www.ncbi.nlm.nih.gov/pmc/articles/PMC6540187/
5. https://www.engineersbazaar.in/gps-receiver-and-gps-tracker.html
6. https://components101.com/wireless/sim900a-gsm-module
7. https://components101.com/microcontrollers/arduino-uno

Study of Mechanical Properties Improvement Using Equal-Channel Angular Pressing (ECAP) of Al6063: Experimental and Simulation

A thesis submitted in partial fulfilment of the requirements for the award of the degree of

Master of Technology

in

Mechanical Engineering (Production)

Submitted by

Akash Gupta

Roll No: 198120002

12-B Status from UGC

Department of Mechanical Engineering

Institute of Engineering & Technology

GLA. University

Mathura-281406, INDIA

JULY, 2021

Dedicated

To

My Beloved Maa Papa

And

My Teachers

Declaration

I hereby declare that the work which is being presented in the M. Tech Thesis Study of **"Mechanical Properties Improvement Using Equal-Channel Angular Pressing (ECAP) of Al6063: Experimental and Simulation",** is in partial fulfillment of the requirements for the award of the Master of Technology in Mechanical Engineering (Production) and submitted to the Department of Mechanical Engineering, GLA University, Mathura, is an authentic record of my own work carried under the supervision of **Dr. Kuldeep Kumar Saxena.**

In full or in parts, the contents of this thesis have not been submitted to any other Institute or University for the award of any degree and are free from plagiarism.

Signature of Candidate:

Name of Candidate: Akash Gupta

Roll. No. 198120002

GLA UNIVERSITY MATHURA
Accredited with A Grade by NAAC

CERTIFICATE

This is to certify that Akash Gupta roll no. 198120002 is working on the work embodied in the thesis entitled **"Mechanical Properties Improvement Using Equal-Channel Angular Pressing (ECAP) of Al6063: Experimental and Simulation",** is his original endeavor carried out under my supervisionand has not been submitted elsewhere for the award of anyother degree.

Signature of

Project Guide:

Date:

Name & designation of Supervisor:

Dr. Kuldeep Kumar Saxena (Associate Professor)
Department of Mechanical EngineeringInstitute of Engineering & Technology
GLA. University
Mathura 281406, India

Prof. PIYUSH SINGHAL
Head, Dept. of Mech. Engg.
GLA University, Mathura

ACKNOWLEDGEMENTS

I want to express my deepest sincere gratitude to my supervisor Dr. Kuldeep Kumar Saxena, Associate Professor, Department of Mechanical Engineering, GLA University, Mathura, for giving me a unique opportunity to work on such an important topic. Their continuous guidance, invaluable suggestions, emotional encouragement, generous help, and necessary acumen are greatly acknowledged. I consider myself fortunate to work under their supervision.

I am grateful to Prof. Piyush Singhal, Head, Department of Mechanical Engineering and Prof. Kamal Sharma, Associate Dean (R&D), GLA University Mathura to their motivations and suggestions in carry out the investigations.

I also like to express my gratitude to Dr. Vijay Kumar Dwivedi (Associate Professor) and Dr. Manoj Kumar Agrawal (Associate Professor) at GLA University, Mathura, for providing valuable suggestions and help concerning this research work.

Last but not least, I place a deep sense of gratitude to my family members and my friends, who have been a constant source of inspiration during this research work.

Finally, I also like to thank all the persons who helped me directly or indirectly in carrying out this research work.

July 2021 **Akash Gupta**

CONTENTS

Table of Contents

List of Figures

List of Tables

We do not inherit the Earth from our Ancestors;
We borrow it from our next generation.

CHAPTER 1

INTRODUCTION

Human is the inquisitive animal on the planet. Altogether, they discovered terrific things on this planet and up in space. One of the utmost discoveries of humans is Material Science. A tiny drop of that science is discussed in this study. As the world grows, the need for new enhanced, refine material is increased. However, there are some questions to be answered: (i) How to refine the grain size of materials, which are stronger, more ductile? (ii) How to use SPD techniques like equal-channel angular pressing for deforming materials? (iii) How to identify the plastic-deformation zone in ECAP? (iv) How to identify the influence of ultra-fine grains on the mechanical properties? (v) How deformation techniques like ECAP can efficiently use? (vi) How can simulation help in overcoming the limitation of experimental studies of the deformation process? To achieve these objectives, experimental and simulation-based studies were performed. The sole purpose of this study is to give the precise answer to these questions.

1.1. Severe Plastic Deformation

One of the best methods of enhancing the material properties generally embroils the change in the microstructure of metals and their alloy to obtain the desired property for a particular task or application. Grain size is the main characteristic of microstructure that is highly manipulated to enhance metals and alloy properties. The fact that "the lesser the grain size, the higher the strength" of that particular material. The research of Hall [1] and Petch [2], insight the attention towards the material with ultra-fine grain size. The Hall-Petch equation states, yield strength and fracture toughness depend directly on the grain size [3,4]. The Hall-Petch equation and the mathematical relation between yield stress and grain size are shown in equation (1.1) [5]. Where σ_y denotes yield stress, σ_o and k_y denotes material constraints, and d denotes the average grain size or diameter on an average basis.

$$\sigma y = \sigma o + \frac{ky}{d} \tag{1.1}$$

So, the easiest way of improving the strength of the metals is to make the grain size as more minor as conceivable and increase the number of grain boundaries. Smaller grains have the higher surface area to volume ratios, implying a higher grain boundary to dislocation ratio. Higher

the number of grain boundary means the high strength of the material [3]. Vapor deposition, rapid solidification, high-energy ball milling, and extreme plastic deformation are all techniques for generating ultra-fine grain size [4].

For decades, severe plastic deformation widely used to achieve superior mechanical properties such as good strength, high ductility, higher superplasticity, low friction coefficient, excellent wear resistance, extended fatigue life cycle, and corrosion resistance, as well as ultra-fine grain materials. [6]. Most known SPD method like Equal-Channel Angle Pressing (ECAP), high-pressure torsion (HPT), multi-directional forging (MDF), sandglass extrusion (SE), repetitive corrugation and straightening (RCS), twist extrusion (TE), constrained groove pressing (CGP) and accumulated roll-bonding (ARB), attract researchers to dedicate their time and energy to this field [7]. Since the materials generated by SPD methods are impervious to porosity and contamination, they offer the potential for both fundamental theory and engineering application. Even though the SPD technique purposefully provided microstructure refinement, it could not generate the necessary uniform refined structure effectively.

Present SPD methods have some limitations like demanding or specific tools, high cost, difficult process, and last but not least, complexity in industrialization and automation for mass production. In the recent past, SPD methods have emerged for commercial application from laboratory interest. So, efforts have been made to simplify, modify, and innovate the SPD techniques to obtain these unique properties commercially. Some of new and hybrid SPD techniques are, multi-pass coin-forging (MCF) [8], cons-hearing pressing [9], continuous confined strip shearing (C2S2) [10], equal channel multi-angular pressing (ECMAP) [11], rotary-die ECAP [12], cross-ECAP [13], T-shaped ECAP [14,15], CONFORM process [16], multi-pass ECAP [17], torsional-equal channel angular pressing (T-ECAP) [18], incremental ECAP (I-ECAP) [19] and repetitive side extrusion process (RSEP) [20].

1.2. Equal-Channel Angular Pressing

Plastic deformation in a workpiece can be achieved by different processes like rolling, drawing, or extrusion in the metal-forming industry. Such a process helps in grain refinement and enhanced material strength, generally with a loss of ductility. It is known that increasing plastic deformation for producing ultra-fine grains in metals and composites affects the mechanical

properties [21]. SPD has many techniques for this purpose, but High-pressure Torsion (HPT) [22] and Equal-Channel Angular Pressing (ECAP) [23] have the higher capability of improving both the strength and ductility. The major problem in the High-pressure Torsion technique is that it is only capable of deforming tiny samples. (e.g., 12×20×1 mm) [22]. On the other hand, Equal-Channel Angular Pressing has the ability to deform massive nonporous billets. (e.g., 60×120 mm in diameter and length, respectively) [24]. ECAP generates very high stresses without altering the billet's geometric form since the billet can be pushed repeatedly from a die with two equal-cross-section interconnecting channels [25]. So, materials deformed by ECAP will give many benefits, advantages to the engineering applications. Equal-channel angular pressing (ECAP) or Equal-channel angular extrusion (ECAE) was initially developed in the formerly USSR by V. M. Segal in 1977 [26]. A good ECAP deformation may be accomplished by modifying the effect of processing factors (die shape, process temperature and route, induced strain, deformation rate, and back-pressure) and starting material characteristics (composition, stress, grain size, texture) [27].

In the ECAP method, a sample, either rectangular or cylindrical shape placed in the die channel with sufficient lubrication and then pressed with force by a plunger into the second channel with the same cross-section that has a certain angle with the first channel, this angle knew as ECAP die channel angle and represented by ∅. The coarse grains of the billet are converted into ultra-fine grains due to simple shear at the exit of the die channel. For better refinement of grain size, several such ECAP passes are required depending upon material characteristics, pressing temperature, pressing temperature, and other factors. Some advantages and limitations of the ECAP process are listed below.

Advantages

- Grain Refinement, from coarse-grains to ultra-fine grains (UFG)
- Improve hardness of the billet
- Increase toughness of the material
- Increase strength of the material
- ECAP also improve the conductivity of the material

Problems with ECAP

1) Cracks and defects in pressed billets
2) Currently, ECAP is a low-productive process.
3) Processing cost is relatively high due to the requirement of several passes

1.3. Finite Element Method

The finite Element Method (FEM) is broadly used to solve numerical equations in engineering and mathematical modeling. The general areas where FEM is applicable are conventional areas of structural analysis, heat transfer, fluid flow, mass transport, and electro-magnetic potential. It is a numerical technique for solving differential and partial equations in two or three dimensions. FEM divided a significant problem into some smaller parts known as *finite elements*. The division of a significant problem into smaller parts have many benefits [28]:

- Precise demonstration of complex geometry
- The enclosure of different material properties
- An easy demonstration of the entire explanation

The finite element method has a practical application called Finite Element Analysis (FEA) to understand real-life problems in a computer simulation. FEA uses the mesh generation method for dividing one significant problem into finite elements using computer software. Much such software (e.g., DEFORM) provides automatic numerical calculation and simulation of different processes. DEFORM-3D is a cost-effective and practical system for forecasting material flow in commercial forming processes. It is capable of forecasting material flow and thermal behavior in massive deformations with remarkable accuracy. Besides, most FEM-based software DEFORM-3D provides an easy and very accurate graphical representation of obtaining data. There are three significant phases in DEFORM-3D, (i) pre-processor, (ii) simulation module, and (iii) post-processor. In addition, DEFORM-3D has an automatic mesh generation (AMG) method for generating new mesh elements during simulation.

1.4. Aluminum Alloy

The use of light-weighted mechanical materials has increased over the last decades. Especially the demand for such material in the automobile and aerospace industries is very high. Aluminum (Al) alloys have gained widespread recognition in these applications due to their lightweight nature, ease of machining, and energy-efficient low power usage. Al alloys have a broad variety of uses, from construction to aerospace industries. Specifically, Aluminum alloy 6063 (Al6063) is generally used in construction, transportation, automobile, and aerospace industries [29]. Al6063 has many superior properties like weldability, formability, machinability, and good corrosion resistance [30,31]. However, implementing Al6063 as a high-performance material for use in chemical and aerospace industries requires improving the core strength, elasticity, and wear resistance of Al6063. Fatigue failures are a severe concern, particularly in applications subjugated to fluctuating loads, like aircraft structures exposed to aerodynamic loads.

1.5. Present Work: Aim & Scope

Al6063 has many advantages like light-weighted and corrosion resistance and is suitable in many applications like construction, transportation, and automobile industries. However, because of its limited mechanical properties, it is challenging to used Al6063 for very high strength applications like on the outer body of planes where atmospheric pressure is very high. Therefore, there is a need to investigate some new methods for enhancing the mechanical strength of aluminum alloys for very high strength applications.

The impact of processing temperature and the number of ECAPed passes with a 120° channel angle and a 30° die corner angle on the mechanical and microstructural characteristics of Al6063 are investigated in this research. This study is a combination of experimental work and a FEM simulation study. The specific objectives are to;

1) Investigate the effect of the number of ECAPed passes on mechanical and microstructural properties
2) Investigate the effect of ECAP processing temperature on mechanical and microstructural properties
3) Study the improvement in hardness of Al6063
4) Investigate variation in strain and stress during the ECAP process.

CHAPTER 2

LITERATURE REVIEW

2.1. Material

A range of materials had been studied under the ECAP technology. Table 1 shows such studies, with novel properties (grain size and mechanical properties) of pure metals (like copper, aluminum, titanium, and tungsten) [24,32–37], processed with ECAP technology. In table 2, aluminum alloy and its composites related study [9, 20-34]. The overall conclusion of all the studies for different materials is that equal-channel angular pressing gives considerable grain refinement, increases the ductility or superplastic behavior, and increases the hardness and toughness of the given material.

Table 1 - Microstructures and mechanical characteristics of pure metals such as copper, aluminum, titanium, and tungsten produced through the ECAP process.

Metal	Reference	Grain size (μm)	Microstructure	Properties
Copper	[24,33]	0.26	Low-angle grain boundaries Fine grains	Vickers hardness = 136 (45) *; RA = 43%
Copper	[34]	0.20	Equiaxed grains with high-angle grain boundaries	Yield Strength = 460 MPa (240 MPa) elongation = 860%
Copper	[35]	0.1	Dislocation free grains	Yield Strength = 400 MPa Ultimate Tensile Strength = 510 MPa
Aluminum	[36]	1 (room temperature, $6B_C$)	Constant equiaxed	elongation = 27%; Yield Strength = 200 MPa (150 MPa)
Titanium	[37]	0.30	Constant equiaxed (4Bc); high-angle grain boundaries	elongation = 14%,
Tungsten	[32]	1 (70 - 75) (8C)	As-received: Polygonised dislocations ECAP, 4C: serrated grain boundaries, elongated ECAP, 8C: equiaxed, dislocation free	Vickers hardness = 6.2 GPa (5.5 GPa)
* The values in brackets are for as-received material; A, B_c, or C are ECAP routes;				

Table 2 - Microstructures and mechanical characteristics of Al alloys produced through the ECAP process.

Material	Reference	Grain size (μm)	Microstructure	Properties
Al5056	[38]	0.30 at 4C, 150 °C	Low-angle grain boundaries	Fatigue testing: N = 107 (σ_a = 120 MPa) *
Al5056	[39]	0.22 at 140 °C 15 - 30 at 200 °C	Low-angle grain boundaries After annealing: high-angle grain boundaries	Yield strength increases 3 times
Al2024	[40]	0.6	Route A: elongated Route B: isotropic, spherical	Increased hardness by two times
Al6061	[41]	0.21-0.42 at 110 °C; 8BA	Elongated, misoriented grains	Hardness = 97 HB; ultimate-tensile stress = 400 MPa (310 MPa); elongation = 11 % (12 %)
Al6061	[42]	0.60	Randomness and irregularity in grains	Yield strength increases 2 times; elongation = 150%, 200 °C at 10-3/s; hardness ~ 1,300 MPa (650 MPa);
* The values in brackets are for as-received material; RT - room temperature; A, Bc, or C are ECAP routes;				

The remarkable combination of the ductility and strength was gained for pure copper after sixteen ECAPed passes [35]. However, the fatigue behavior of the ultra-fine grains of copper [33] is endangered to low-cycle fatigue and shows a smaller life than the coarse-grains material. Pure titanium (Ti) gains strength at room temperature [37]. ECAPed deformation on pure aluminum at room temperature [36] shows the uniformity in equiaxed grains and increases the yield strength (YS).

2.1.1. Aluminum Alloys

Aluminum alloys have properties like medium tensile strength, excellence in corrosion resistance, and welding with high ductility [43,44]. The raw form of aluminum alloys can be used in high pressure, high strength applications like automobile, aerospace industries, chemical industries, and marine industries. However, the cast form of aluminum alloy can be used in food industries (for handling), dairy industries, and transportation. The strength of aluminum alloys can increase by adding magnesium (Mg) through Solid Solution Strengthening (SSS). It is well known that magnesium has excellent solid solubility in aluminum. For obtaining a high strength level in aluminum alloys, a high composition of magnesium is required. However, such high composition may cause problems during alloys processing and can lead the alloy to stress cracking [45].

2.1.2. ALUMINIUM 6063 ALLOY

Al-6063 is an easily accessible aluminum alloy in the metal industry. Many aluminum production industries highly produce the alloy at reasonable prices for different applications like automobiles, aircrafts, pipes, fittings, furniture making, agricultural and irrigation purposes [46]. Other than aluminum, magnesium and silicon are the significant elements of Al6063, whereas copper, zinc, iron, manganese, titanium, and chromium are the minor alloying element. Mg and Si are presented in the ratio required to form an intermetallic compound. Al-6063 has an average alloy strength with decent welding ability, formability, machinability, heat treatability, and corrosion resistance. The physical, mechanical, and thermal properties of Al6063 are shown in Table 3.

Table 3 - Properties of Al-6063 alloy

Properties	**Value**
Ultimate Tensile Strength	152 MPa
Yield Strength	118 MPa
Hardness Webster Hardness Tester (Model B)	8° to 10°
Modulus of elasticity	69 GPa
Density	2.71 g/cm3
Melting Point	600-650 °C
Specific Heat between 0-100°C	879 J/Kg °C
Thermal expansion conductivity 25°C	201W/m °C
Electrical resistivity at 20°C	0.033μΩm

2.2. Plastic Deformation

Plastic deformation is a process in metal forming in which metal and alloy are permanently deformed when the material undergoes the tensile, compressive, bending, or torsion stresses, and it surpasses the yield point and elastic limit of the material [47,48]. This resulted in elongation, compression, buckling, bending, or twisting in the material without any fracture in the sample body [49]. Taylor [50], Orowan [51], and Polanyi [52], among others, introduced and established the idea of plastic deformation. Their work made plastic deformation more understandable. These studies set the path for more research and attention to this field of materials science.

Researchers can characterize mechanical characteristics such as tensile strength, yield strength, ductility, resilience, and toughness using plastic deformation [53]. Hardness measures are also heavily influenced by the idea of plastic deformation. These characteristics are beneficial

in assessing the ability of metals to be employed in specific applications based on the standards required. Different processes of deformation occur in crystalline and amorphous materials. Dislocation movement, commonly known as slip, is the essential element of plastic deformation in crystalline materials. This is most common along close-packed lattice planes because of the low energy needed for dislocation motion in such areas [48]. The dislocation line is stated to proceed through the crystal until it reaches the end of the crystal, resulting in a visible step known as slip bands, and slip happens in the (111) close-packed plane without any noticeable alterations in the crystal structure [48]. Twinning is another unique technique. When the crystal lattice kinks, it creates a mirror copy of the crystalline structure across the twin boundary. The process of deformation while twining generates a significant change in the material's crystal structure.

Plastic deformation is highly helpful during material processing for applications like sheet metal stamping, SPD, hot isostatic pressing, foaming, and forging, and others [54]. Recent research done by [55] looked at the formability, quench ability, and heating of hot-stamped ultra-high-strength steel components. The research done by Zhutao et al. [56], assessing the formability of sheet metals under hot stamping circumstances using a unique biaxial testing method and a new materials model, is another proof of plastic deformation in hot stamping for diverse applications. Besson et al. [57] performed hot isostatic pressing on pure alumina and discovered that the resulting grain growth was produced by point defects and dislocation loops, residues of plastic deformation.

2.3. Severe plastic deformation

Severe Plastic Deformation (SPD) is described as a metal forming process in which high plastic stresses are placed on the metals and alloys during the process in order to obtain ultra-fine grained (UFG) metals with higher strength [58]. Five approaches for improving metal strength using the idea of SPD have been addressed in the literature [59].

- Accumulated roll bonding (ARB),
- Asymmetric rolling (AR),
- High pressure torsion (HPT),
- Receptive corrugation and straightening (RCS),
- Equal channel angular pressing (ECAP).

2.3.1. Asymmetric rolling

Asymmetric rolling is an SPD technique used for plastically deform samples to create ultra-fine grained materials with higher strength. Asymmetric rolling has also been used in various investigations to investigate specific characteristics in a variety of materials. Figure 1 depicts this technique and cumulative roll bonding schematically. According to Verlinden et al., [4], asymmetric rolling is often determined by the component of shear on the metal sheet or sample surface. Rolls with various diameters or equal diameters with variable rotational speeds are typically utilized to get better outcomes (Figure 1). The progressive formation of the new microstructure of the samples during this phase is generally attributable to the simultaneous action of shear and compression [4]. Chen et al. [60] perform a finite element modeling on crystal plasticity for each grain as well as for the entire specimen during asymmetric rolling. The deformation behavior investigated were inhomogeneous material flow, and a decrease in roll force and contact press as grain size rose for constant-sized specimens.

A recent study examined the microstructure's through-thickness gradient as a function of asymmetric hot rolling process parameters in a high manganese non-magnetic steel [61]. According to the paper, the shear strain distributions were studied using a 2D FE approach. After refining, the surface layer and core had austenitic grain sizes of around 5 nm and 9 nm, respectively. As a result, the tensile strength increases [61]. Asymmetric rolling reduces grain size in varieties of materials, improving mechanical characteristics as a result.

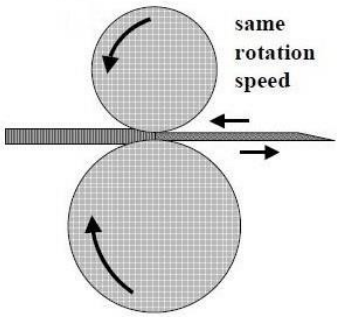

Figure 1: Asymmetric Rolling [4].

2.3.2. Repetitive corrugation and straightening

The RCS is another type of SPD that may be utilized to generate fine-grained structures in bulk metallic sheets or plates (Figure 2) [62–66]. The setup is typically composed of two corrugated dies and two rolls that distort the material. A sample is bent and repeatedly straightened without causing significant changes in its sizes, imparting several stresses into the material and refining the grains.

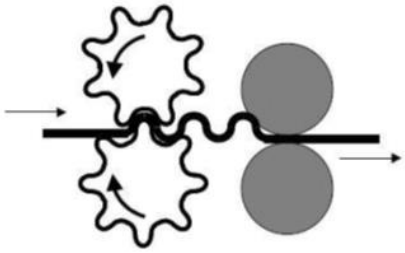

Figure 2: Illustration of continuous repetitive corrugation strengthening [4]

Huang et al. [62] reported that after applying the responsive corrugation and straightening technique to bulk nanostructured materials, the grain size of the samples examined decreased on average in all directions. The grains were equiaxed in all three dimensions with no apparent elongation, and TEM studies revealed a high density of dislocations and highly strained grains (Figure 3) [62,66].

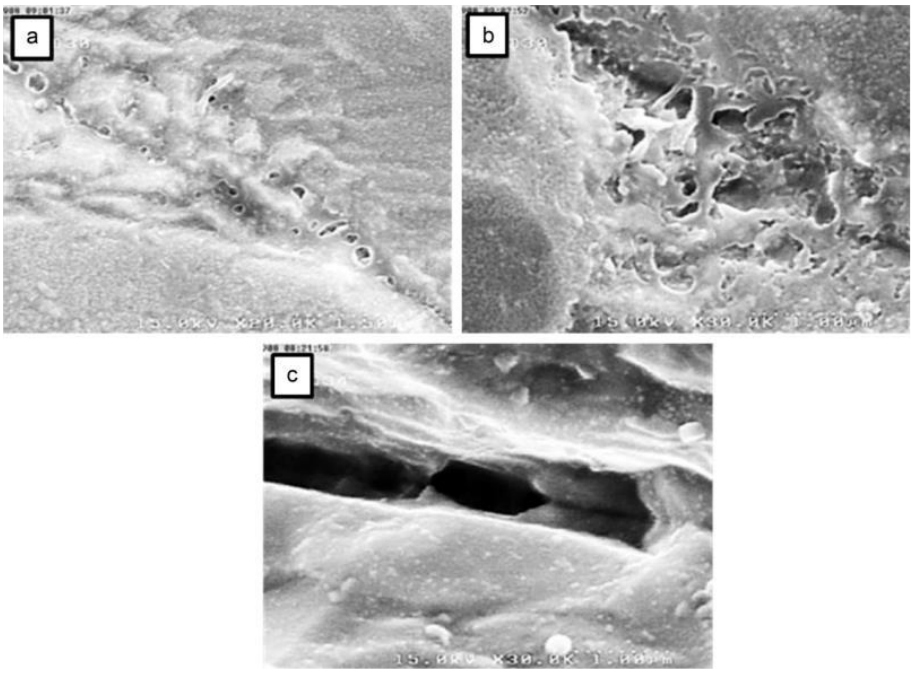

Figure 3: TEM images of bulk nanostructured materials after the RCS [62].

After 18 RCS cycles, the continuous RCS machine-generated bulk nanostructured materials from the original samples, unfortunately, fractures were seen on the surface of the workpiece after the 18 cycles, indicating that the number of RCS cycles that may be applied to a workpiece is limited [62,66]. It was claimed that the RCS machine was not intended to generate sufficient plastic strain each cycle to produce efficient grain refining at the time. Additionally, Huang et al. [62] experimented with a discontinuous RCS design, demonstrating increased grain refinement capacity.

However, Thangapandian et al. [64] utilized various corrugated die profiles and die settings to achieve consistent grain refinement in materials. In practice, an RCS technique was utilized on Al-Mg alloy through three distinct corrugations die profiles: semi-circular groove, V-groove, and flat groove (Figure 4). After this procedure, straightening was performed to determine the maximum number of passes possible before the surface fractures [64].

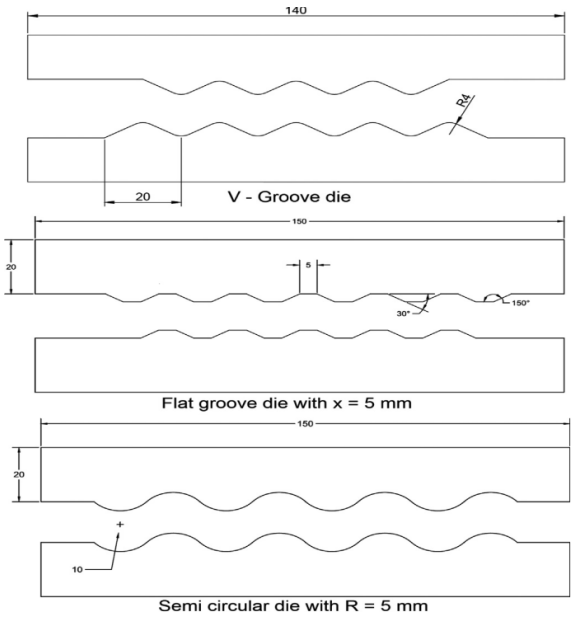

Figure 4: The three corrugation dies, shown in (i) V–groove, (ii) Flat groove, and (iii) Semi-circular Die [64].

The research found that the most significant number of passes was obtained when the material was deformed using a semi-circular die, namely 15 passes. As a result of the lack of sharp edges and the induction of relatively low strain, no surface cracking was detected [64,66]. The semi-circular and flat groove dies were very efficient in refining grains uniformly [64]. The average grain size was about 20 μm, and in both instances, the tensile strength and hardness improved as the number of passes increased in all dies utilized. The flat grooved Die was found to be the most effective method for obtaining the highest hardness and tensile strength values [64].

Two alloys, Al-Cu and Al-Cu-Si, were plastically deformed in up to four passes using a continuous repeating corrugation and straightening facility. Hardness measures revealed significant increases throughout the whole length of the two alloys examined; however, hardness was enhanced further when samples were rotated 90 degrees between successive passes, and the homogeneity of the test samples was also enhanced significantly [65]. The focus in this research was not on the kind of Die used but on how the continuous RCS process enhanced the mechanical characteristics and uniformity of the test samples. The continuous and discontinuous RCS processes have been effectively utilized for grain refinement of test materials, and the degree of grain refinement is highly dependent on a few process modifications.

2.3.3. High pressure torsion (HPT)

Torsion under high pressure is also a kind of severe plastic deformation used to generate plastic strain in materials to create ultra-fine-grained materials (Figure 5). It is a metal processing technique that involves the application of compressive force and concomitant straining on samples. Numerous research on this technique has been performed, with varied results.

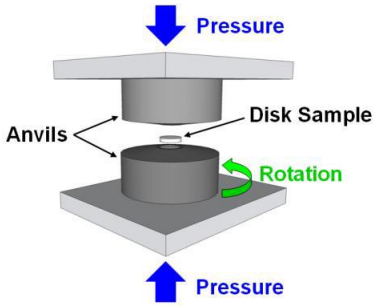

Figure 5: High-pressure torsion

Wei et al. [67] presented a study in which they sought to shed light on how the textural processes developed when HPT was employed on a nickel single crystal [67]. Crystal plasticity simulations and experiments revealed a steady-state stage with stable crystallographic orientations, with dominant slip acting as the primary source of slip mechanisms [67]. However, in another research conducted by Korneva et al. [68], the impact of HPT on the microstructure of Cu-36 wt.% Sn was investigated, and a rise in dislocation density and grain refinement was found in the sample, even though the macroscopic form remained the same [68]. This demonstrated the effective conversion of the Cu-36 wt.% Sn microstructure into ultra-fine grains with greater strength than the original condition.

Additionally, recent research by Khajouei-Nezhad et al. [69] revealed that coarse-grained aluminum powder containing 99.5 wt. Percent encountered a semi-constrained state due to the powder holder's interior wall expansion during HPT [69]. After four turns of HPT, a relative density of 99.83 percent was obtained, and the grain size decreased while the dislocation density increased as the number of HPT turns increased. The smallest grain size (0.41 μm) and highest dislocation density (6.8×10^{14} m^{-2}) were obtained around the edges of discs subjected to four turns [69]. Tensile experiments performed on Al powder consolidation after four rounds of HPT revealed a high UTS (~373 MPa) and increased ductility (~22%), indicating that the connection

between yield strength and grain size agrees with the Hall-Petch equation (1.1). This research shows the ability to treat consolidated aluminum powder with excellent strength and ductility using the HPT method [69]. Whereas, earlier study by Wei et al. [67] focused on texture evolution, the subsequent studies by Korneva et al. [68] and Khajouei-Nezhad et al. [69] focused on grain refinement and dislocation density evolution in order to improve the mechanical properties of the test samples as a result of high-pressure torsion processes.

2.3.4. Equal channel angular pressing

Equal channel angular pressing (ECAP) is used to deform materials. A sample is fed through a die at a specified pace and then deformed by shear. Equal-Channel Angular Pressing (ECAP) shows the capability to produce ultra-fine grain-sized materials without changing the cross-section because that is the lone approach to improving mechanical properties [59,70–73]. This technique produces a large amount of true strain on the grains and delivers recrystallization at a specific temperature range [74].

Many metals and alloys have been researched, and a significant improvement in the mechanical properties with ultra-fine grain size by the ECAP technique has been reported [67,75–80]. Temperature, friction between die walls and billet, die and corner angle, plunger speed, pressing route, and the number of passes affect the resulting properties. The equivalent strain reported after the 'N' number of ECAP passes can be calculated from equation (2.1) [81]

$$E = \frac{N}{\sqrt{3}}\left[2\ cot\ \left(\frac{\varphi+\emptyset}{2}\right) + \varphi\ cosec\left(\frac{(\varphi+\emptyset)}{2}\right)\right] \quad (2.1)$$

There are so many parameters that affect the net results of the ECAP process in different ways, and it is not easy to study all of them. Although, many researchers in the past worked on ECAP to find optimal parameters [58,82–89]. Damavandi et al. [90] studied the microstructural evolution and the texture behavior of ECAPed samples of Al-Si-Cu alloy. They found that a maximum drop in grain size due to recrystallization is shown after only one pass. Further, they concluded that texture evolution has no remarkable effect on the strengthening of the aluminum alloy. Texture evolution also shows that with the increment in the number of passes, the strength of A*1 and A*2 components was improved while B and C components became more stable.

In another study, Sunil et al. [91,92] stated that due to age hardening, Mg_2Si precipitates were observed in SEM images, which are helpful to increase both hardness and tensile strength of Al6063. For improving hardness and refinement of grains, all three parameters, such as the number of passes, processing temperature, and die angle, are contributed equally. However, processing temperature increases the grain size due to the diffusion process and allows recrystallization. Yuan et al. [93] found that grains of Al-Mg alloy are elongated after four passes and had the majority of by high angle grain boundaries (HAGB's) in the extrusion direction. Electron back-scatter diffraction images showed the formation of new equiaxed and subgrains and LAGBs aligned in the elongated coarse HAGB grains. They thus concluded that Grain boundary (GB) strength and precipitation strength are both responsible for high billet strength after the ECAP process. Guzide et al. [74] conducted an analytical and experimental study on optimizing ECAP parameters to increase the strength of Al-Zn-Mg alloy. They found that the desired strength was achieved after eight passes by following route Bc at 100 °C temperature. Further results showed that processing temperature has more influence on the grain size. They also found that as the process temperature increases, the friction between HAGBs and formed new equiaxed grains decreases with increased grain size. Although, the influence of temperature on hardness is insignificant.

Maged et al. [83] performed a cold ECAP process to obtain desired mechanical properties with UFG size. The microstructural results showed the evolution of grains from a coarse structure to elongated structure and then progressing to equiaxed, refined grains to a finally ultra-fine grain structure with an average grain size of 103 nm after six ECAP passes. Hardness, tensile strength, and yield strength improved from the very first ECAPed pass and, after six passes, resulted in excellent improvement in these mechanical properties. Omer et al. [94] performed the ECAP process on Al matrix composite with graphene reinforcement with different weight percentages (0.1,0.2,0.3, and 0.6 wt. %), all the samples were subjected to the ECAP process. Two die angles, 120° and 90°, were chosen with different process temperatures and ECAP routes—samples with 0.1 and 0.2 wt. % showed outstanding improvement in mechanical, thermal, and electrical properties. Samples that contained graphene more than 0.3 of wt. % was difficult for the ECAP process, and some cracks and brittle fractures were observed while processing. Results showed that after a specific temperature, the effect of ECAP is reduced with the increment of temperature due to the recrystallization of grains. With a 90° die angle, the strength values of

samples were more than 120° die angle, but the chances of cracking or brittle fracture in samples are higher in the 90° die angle.

2.4. Mechanisms of grain refinement during equal channel angular pressing

According to the above explanation, equal channel angular pressing efficiently causes grain refining and ultimately increases the strength of materials under favourable circumstances. Numerous models have been suggested to account for the processes behind grain refining during the ECAP. The majority of these suggested models are often reliant on the crystal structure of the metals involved. That is, the metal's structure is either face center cubic (FCC), body center cubic (BCC), or hexagonal closed pack (HCP).

Segal [95], a pioneer of ECAP, presented a grain refinement model heavily reliant on shear bands and subgrain rotation. In one of his studies, he concluded that the development of induced shear planes in materials as a consequence of successive passes and rotating strain accommodation modes is utilized to define grain refinement for various processing methods [95]. In an another study, Shin et al. [96] investigated low-carbon steel with a BCC structure composed of iron-0.15 wt. percent, carbon–0.25 wt. percent, silicon–1.1 wt. percent. When processing method C was employed, it was suggested that shear bands formed for the odd number of passes, while an even number of passes was believed to play a role in restoring the originally equiaxed grain structure. During the first pressing stage, sub-micrometer order ferrite grains were produced by activating several slip systems belonging to the {110} <111> and {112} <111> slip system families, and as the number of passes rose, the number of HAGBs grew as well. These high-angle boundaries were formed as a consequence of subgrain rotation along serrated boundaries [95,96]. This implies that, depending on the processing route and the crystallographic structure of the material being processed, various slip systems are triggered throughout the process to induce the material's grain refinement. Zhu and Lowe [97] also made a similar claim when they investigated the processes of grain refinement in aluminum alloys with an FCC crystalline structure. After reviewing prior research on the processes, they asserted that owing to aluminum's high stacking fault energy, and dislocation slip happens more often on the {111} planes for Al alloys, which is the sole deformation process. Typically, the {111} planes form a tetrahedron, with any two sides crossing at a 70.5° angle, which is critical for the ECAP. According to the theory advanced in this article, the closer the angle between the texture plane and the shear plane is to 70.5°, the more

precise the specification for defining grain refinement efficacy is. This is the angle formed by two FCC aluminum {111} tetrahedron planes (Figure 6) [97]. As a result, the same holds for grain refining of any aluminum alloys having an FCC crystal structure.

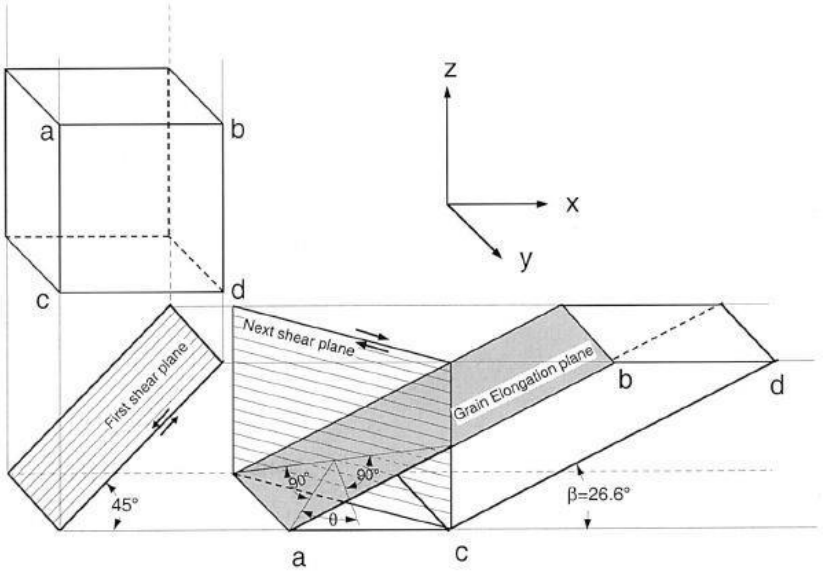

Figure 6: For ECAP routes BC or BA, the orientation connection between the first pass's grain elongation plane and the second pass's shear plane. The angle formed by the grain elongation plane and the following shear plane is denoted by θ [97].

As shown by the previous discussions, ECAP has been utilized to purify grains of various metals under a variety of different circumstances. However, the effectiveness of ECAP is usually contingent upon a variety of variables, some of which are described in the following section.

2.5. Die Geometry

One of the variables affecting the impact of ECAP on the materials or samples being plastically deformed is the die geometry. According to Kim et al. [98], shear deformation often occurs at the bend between the intake and outlet channels, defined by the inner or channel angle, typically denoted by $\emptyset$, and the outside or corner angle, often denoted by φ. Inner or channel angle refers to the angle formed by two channels, which is typically between 0° and 180° [98]. The corner or outside angle is formed by the upper and lower channels (Figure 7).

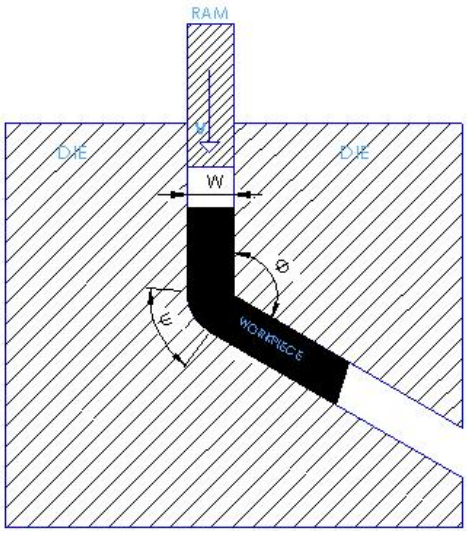

Figure 7: The schematic sketch of the ECAP die.

Two dies with the same channel angle (Ø= 90°), but corner angles (φ) of 0° and 90° were utilized to simulate an ECAP process [98]. After doing a finite element method (FEM) study, it was shown that the round corner angle (φ= 90°) not only reduced shear deformation but also enhanced strain inhomogeneity after one simulated pass. This essentially means that a corner angle of 0° causes the sample to undergo more significant shear deformation and enhances the sample's strain homogeneity. Ponce-Pena et al. [99] used a similar FEM analysis to study the impact of die geometry on the deformation homogeneity of ECAP samples. They examined six different dies (Figure 8) and their impact on deformation homogeneity. However, this research took into account various friction coefficients (μ = 0, μ= 0.05, μ= 0.1) in each of these instances [99].

The FEM study revealed that when the redesigned ECAP die (die 4) was utilized, the tensile stress state was decreased, and the compression state enlarged. The research found that the shape of the Die has a significant effect on deformation homogeneity, resulting in a more uniform distribution of shear deformation on die 4 with a coefficient of friction of 0.05 (Figure 9) [99]. As a result, the die shape may be modified in various ways to increase the amount of strain applied to the ECAP samples and enhance deformation uniformity.

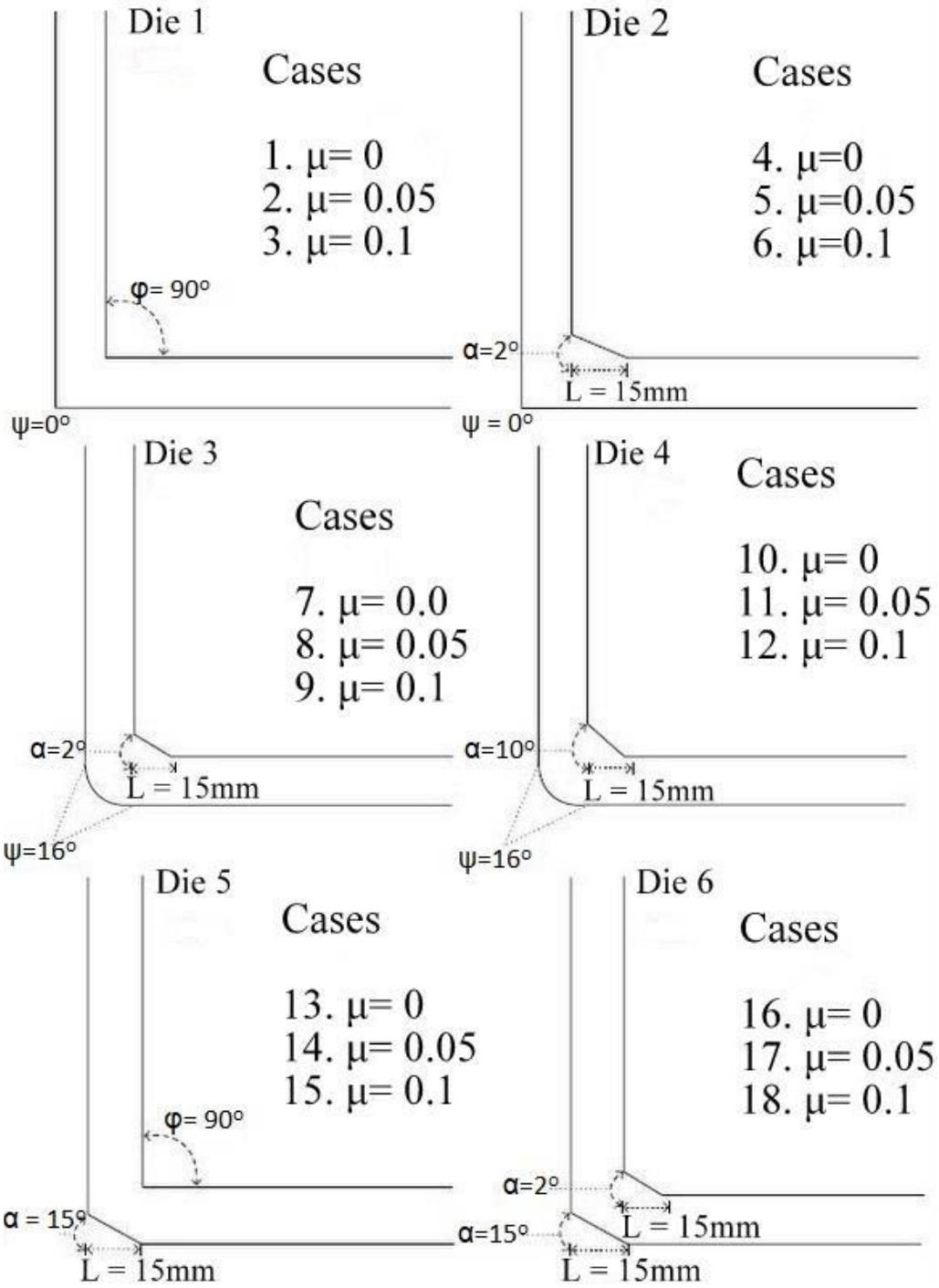

Figure 8: Schematic of the six different dies used in the study [99].

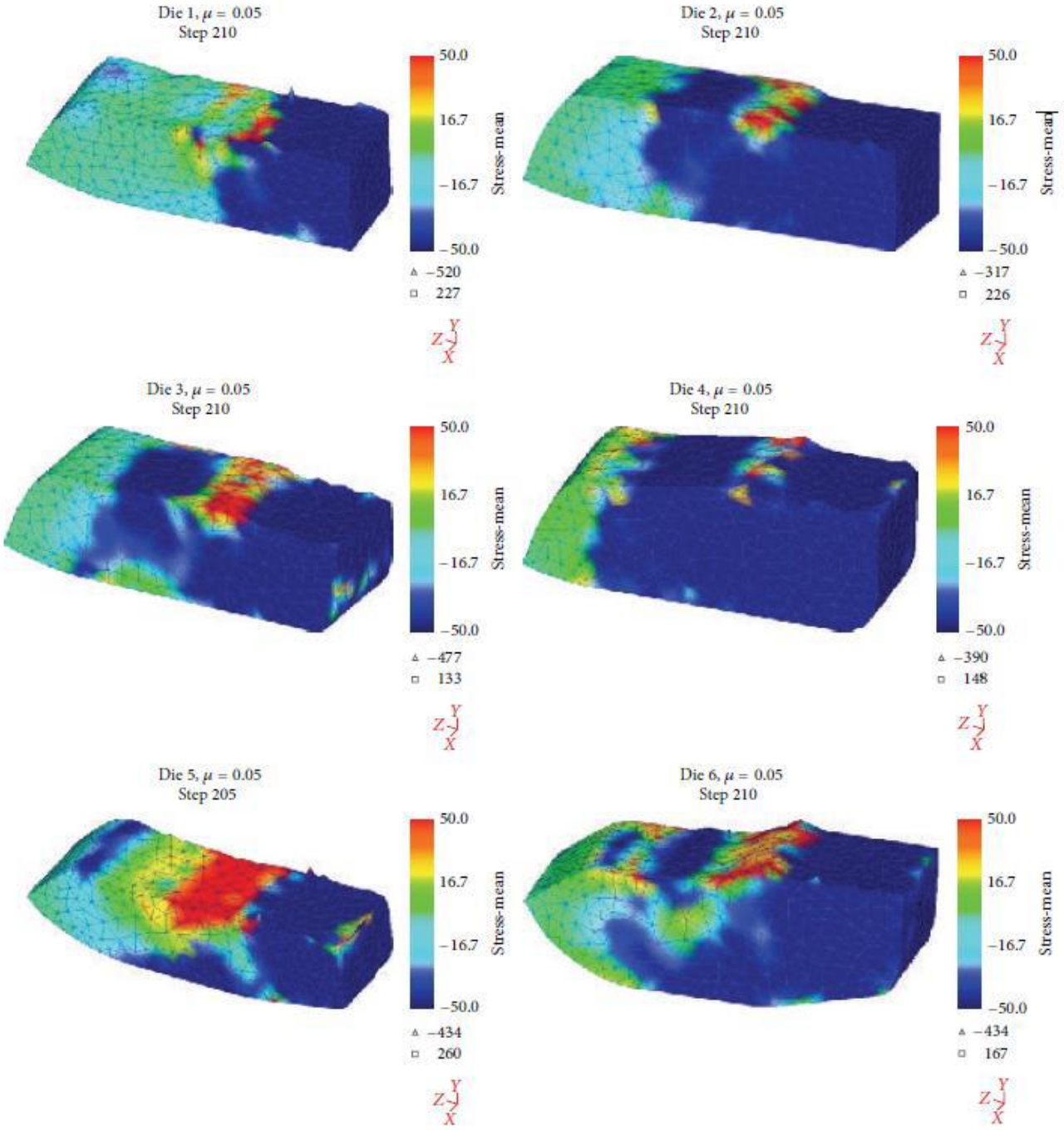

Figure 9: FEM mages showing shear deformation for the different dies. [99]

2.6. Processing routes

There are four pressing routes for the ECAP process, as shown in Figure 10 [100]. There is no change in rotation angle during the ECAP passes of a billet in Route A. After each pass on route BA, the rotation angle direction is changed by 90°. On odd-numbered passes of route BA, the workpiece turned 90° clockwise, and 90° counterclockwise on even number passes. On route BC, the billet turned 90 degrees with each pass in the same direction, clockwise or counterclockwise. On route C, the billet is rotated 180 degrees with each pass.

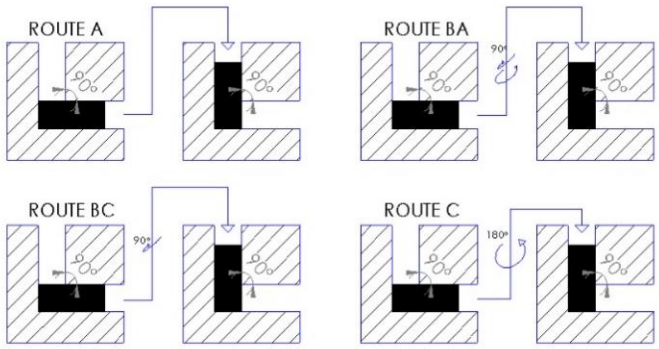

Figure 10: Four different processing routes for ECAP

Several studies have examined the deformation pathways to optimize grain refinement during the ECAP process to see how they influence the microstructural changes after the procedure [83–89]. Although the processing methods had no evident impact on the microhardness of the samples, route Bc was found to be the most efficient in terms of grain refinement, producing equiaxed grains with an average size of 260 nm, while routes BA and C produced elongated grains [101]. This statement is entirely compatible with the findings of Rifai et al. study [102].

2.7. Temperature

The temperature during the pressing process may be adjusted to get various outcomes, as shown in the following studies. Yamashita et al. [103] conducted one of the first comprehensive studies on the effect of temperature on the ECAP process. Three distinct materials were pressed from room temperature to 573K in this study: pure Al, Al-3% Mg alloy, and Al-3% Mg-0.2% Sc alloy. A thermocouple was inserted into a horizontally bored hole about 5mm from the channel wall's shearing plane. Each specimen was examined twice throughout the process. One was heated before being placed in the Die and then kept at that temperature for about ten minutes before

pressing. The second specimen was heated to a temperature close to that of the first in a separate furnace before being placed into the Die for pressing. Three main implications may be taken from the tests' results:

a) At equilibrium, the grain size grew in lockstep with the temperature rise (Figure 11)
b) Following an examination of the SAED patterns, it was concluded that the number of LAGBs increased with increasing temperature. According to the study, this increased regaining rate at higher temperatures resulted in dislocations being progressively eliminated while the number of dislocations absorbed into the sub-grain walls decreased.
c) The highest conversion of LAGBs occurred at about 473 K for pure Al and about 573 K for the Al-3 wt.% Mg alloy. However, no transition of LAGBs was seen in the Al-3 wt.% Mg-0.2 wt.% Sc alloy [103].

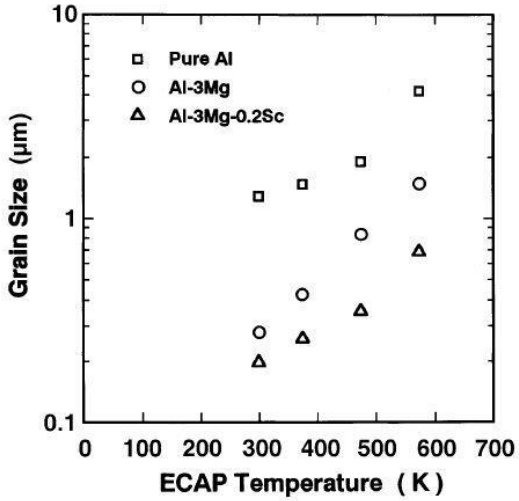

Figure 11: Grain size against the pressing temperature after the ECAP of Al, Al-3%Mg, and Al-3%Mg-0.2%Sc [103].

Shaeri et al. [104] utilized the Al-7075 alloy, which has 5.7wt. % zinc, 2.65wt. % magnesium, 1.5wt. % copper, and 0.21wt. % chromium. 7×7×50 mm^3 samples were heated in solution at 470 °C for about 1 hour and then quenched in water to produce a supersaturated solid solution (SSS). Immediately after water quenching, ECAP performs so that cracks are not formed. After that, the specimens were treated at room temperature (RT) and 120 °C in three passes and 150 °C and 180 °C in up to four passes. Following investigations, the following conclusions can

be drawn about the impact of raising the ECAP temperature on the microstructure development during ECAP of Al-7075 alloy:

a) The grain size increased.
b) There were more equiaxed grain forms present
c) The percentage of high angle borders decreased significantly (HABs).
d) The precipitation rate increased.

2.8. Finite Element Method (FEM)

The finite Element Method (FEM) is a handy tool for analyzing and optimizing material deformation behavior using different deformation techniques [105]. In recent years, the finite element method has been effectively used to evaluate the influence of ECAP process parameters on the distribution of state variables [106–111]. Moreover, FEM also helps overcome practical limitations such as cost implication and processing time, making it challenging to conduct bulk experimental studies. In such situations, numerical simulation techniques [100,105–108] make the investigation process more convenient. Several investigations focus on the influence of die angle (Φ) and channel corner angle (ψ) deformation behavior. Mathieu et al. [110] presented a novel die design to reduce the deformation load for processing various materials. Shunqi Wang et al. [111] provided further improvements and modifications for increasing the number of passes without any permanent deformation of dies.

CHAPTER 3

Materials and Methodology

3.1. Materials

Aluminium alloy-6063 (Al6063) is used as the billet material, and Molybdenum Disulfide (MoS_2) is used for lubrication during the ECAP process for this study. Al6063 was chosen due to high demand in the market and good formability. Other than Aluminium (Al), Magnesium (Mg) and Silicon (Si) are the two significant elements in the alloy, and table 4 shows the different alloying elements with their weight percentage (wt. %).

Table 4 - Composition of Al-6063.

Element	Si	Mg	Fe	Cu	V	Zn	Ti	Cr	Al
Wt. %	0.6	0.6	0.3	0.05	0.01	0.1	0.01	0.01	Balance

Cylindrical-shaped billets were used for the ECAP process, having a diameter of 9.5 mm and length 54 mm. Before the ECAP process, all billets went for an annealing process for 30 minutes at 350 °C followed by furnace cooling (approx. 24 hrs.). Molybdenum disulfide (MoS_2), a widely known lubricant for metal processing, and was utilized to significantly decrease friction between the die channel walls and billet during ECAP.

3.2. Equal-Channel Angular Pressing (ECAP) Process

ECAP is an SPD technique used for deform Al6063 billets. The ECAP die, plunger, and the ultimate tensile machine (UTM) are shown in Figure 12. This process is carried out by pressing billet (cylindrical or rectangular) through the two-equal channels of die having an intersecting or die angle (Φ) with channel corner angle (ψ). The billet is pressed with the help of the plunger. As the billet starts moving in the channel, it goes to shear while regaining the original cross-section after the corner or bend. Several such passes are required to achieve the desired results.

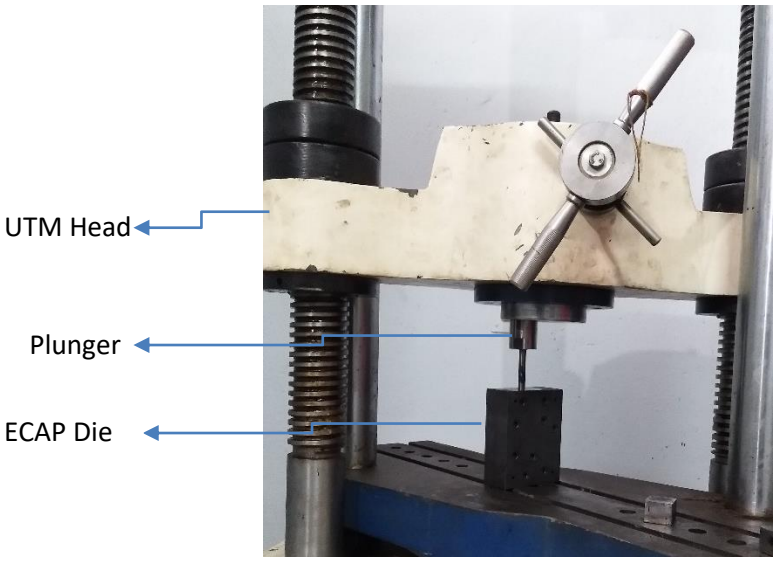

Figure 12: Process Components

Route Bc was selected for all ECAPed passes. On route BC, the billet turned 90 degrees with each pass in the same direction, clockwise or counterclockwise. Table 5 shows the ECAP parameters and their corresponding levels employed for this study. The process was carried out on two different processing temperatures (i) room temperature (RT) (ii) elevated temperature of 250 °C (ET). Three samples for each temperature were processed with three different numbers of passes, one pass (1p), three continuous passes (3p), and six continuous passes (6p). The die angle ($\emptyset$) and the die corner angle (φ) remain constant throughout the process at 120° and 30°, respectively.

Table 5 - ECAP process parameters and associated levels chosen for this research.

Number of Passes	**Temperature**	
	Room Temperature	250 °C
1	R1	E1
3	R3	E3
6	R6	E6

3.3. Methodology

The complete study is divided into two parts: (i) experiment (ii) simulations. Figure 13 shows the process flow chart from sample billets to testing to simulation and then finally results. In the experimental part, the actual practical process of ECAP performs. 9.5×54 mm size cylindrical billet was used for deformation. ECAP die having 120°, and 30° die channel angle and channel corner angle were used for the process. Before the deformation process, the billets' annealing was done for 3 hours at 350 °C, followed by furnace cooling. Two samples were taken for each process parameter to maintain accuracy. The Molybdenum (MoS_2) lubricant was used on the walls of the die channel, plunger, and billets for reducing fractions during the process. Die, plunger, and billet (inside the Die) were manually fixed on UTM. Then UTM head applied force with a constant speed of 1 mm/sec so the billet could deform. For elevated temperature, the billets and die were heated first at 250 °C. Then the ECAP process was performed. After all the ECAP passes, testing of material was conducted. The simulation part of the study consists of the finite element simulation of the ECAP process with the same process parameter as the experiment. In this study, the finite element method (FEM) based 3D model was used to simulate the ECAP process on Al6063 and obtain various load distribution curves and effective strain. The numerical simulation is carried on the DEFORM-3D v10.0.

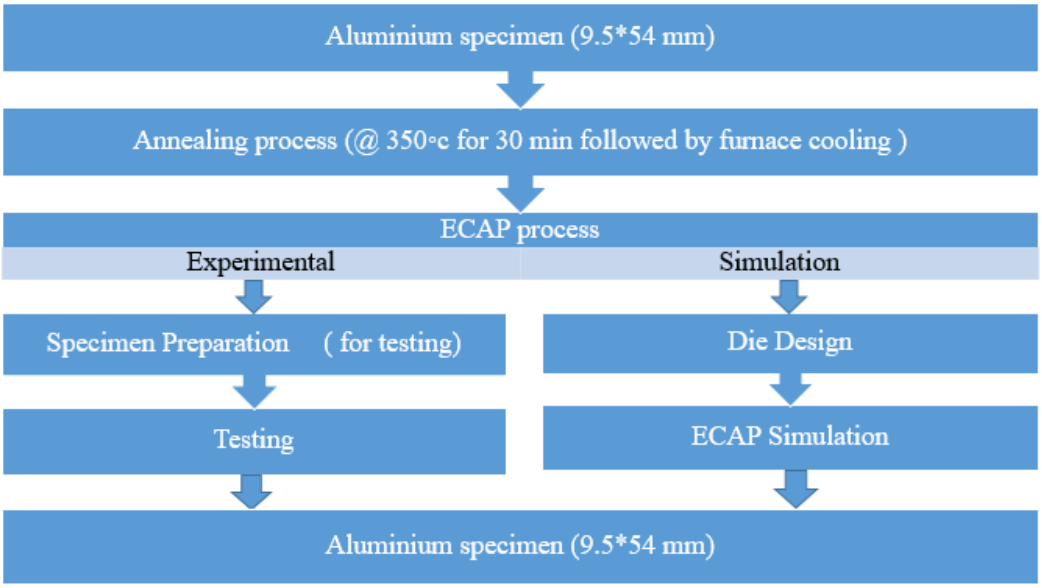

Figure 13: Process Flow Chart

3.4. Specimen Preparation

The billets of size 9.5 mm in diameter and 54 mm in length were cut from the rod of Al6063. After processing, hardness value and microstructure were studied. The test specimens were cut from the ECAPed samples in the direction parallel to the deformation axis. After cutting, surface finish, cloth polish, and etching were done before the final investigation of the surface. The final microstructures were characterized by Electron Back Scattered Diffraction (EBSD) attached to a FEG-SEM (Make: Hitachi; Model: Su-70) using Channel 5™ Software (Oxford Instruments, UK). For EBSD investigations, the samples were polished by electropolishing using a mixture of perchloric acid and ethanol as electrolytes (1:9) at 20V and -30°C (using Liquid N2) for 20 sec.

3.4.1. Surface Finish and Polishing

The samples were polished using emery paper of different grit sizes, ranging from 220 to 2000. Final polishing was conducted using a double-disk polishing machine with the diamond paste of three different grades, D6 μm, D3 μm, and D1 μm.

3.4.2. Etching

Etching was used to reveal the alloy's microstructure using Keller's etchant (25 ml of hydrochloric acid, 25 ml of nitric acid, 25 ml of methanol, and two drops of hydrofluoric acid). The soaking time for etching was 40-50 sec, followed by a water bath and dried using a dryer.

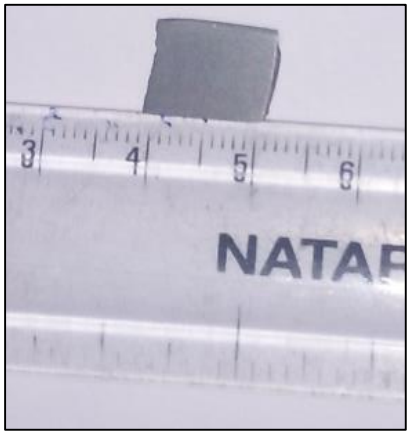

Figure 14: Prepared specimen for microstructure and hardness test

3.5. Simulation

The numerical simulation is carried on the DEFORM-3D v10.0. DEFORM-3D is a FEM-based package to analyze different complex metal forming and machining processes. There are three significant phases in DEFORM-3D, (i) pre-processor, (ii) simulation module, and (iii) post-processor.

The pre-processor is generating a database file in which forming parts are created and assembled. All the inputs like material details, object description, simulation controls are placed in the pre-processor. The pre-processing step of DEFORM-3D includes several steps. The first is to upload all the required geometries and check them. The second step was to assign material characteristics of the billet. Al6063 was used as the deform material, and all the related material characteristics were directly imported from DEFORM material library. In the third step, the billet meshed into 50000 four-node elements. Suppose elements became too distorted during simulation, the elements automatically re-meshed. The 4^{th} step in pre-processing is for assigning the movement control to the plunger. Lastly, boundary conditions and coefficient of friction between Die, workpiece, and plunger were assigned. Boundary conditions were automatically generated. Figure 15 shows the assembly of the workpiece, die, and plunger. Table 6 shows the simulation parameters used in this study.

After the pre-processor, the second part comes, i.e., the simulation module where all the needy calculation is done by the FEM tool. The simulation module reads the simulation controls in the database file, implements calculations, and finally adds the solution in the database file. DEFORM-3D has an automatic mesh generation (AMG) system for generating new mesh elements during simulation. Postprocessor is the last part that provides graphs and data obtained from simulation. It also allows visualizing the whole process step by step.

Table 6 - Simulation Parameters.

Sl. No.	Simulation parameter	Value
1	Diameter of Cylinder	9.5 mm
2	Length of Cylinder	54 mm
3	Coefficient of friction	0.08 (Default)
4	Cylinder Temperature (@ room)	20 °C
5	Cylinder Temperature (for elevated)	250 °C
6	Upper and lower dies temperature (for elevated)	250 °C
7	Punch dimensions	10×60 mm
8	Movement Speed	1 mm/sec
9	Conventional coefficient (for elevated)	0.02 N/ s.mm. °C
10	Heat transfer coefficient (for elevated)	5 N/ s.mm. °C

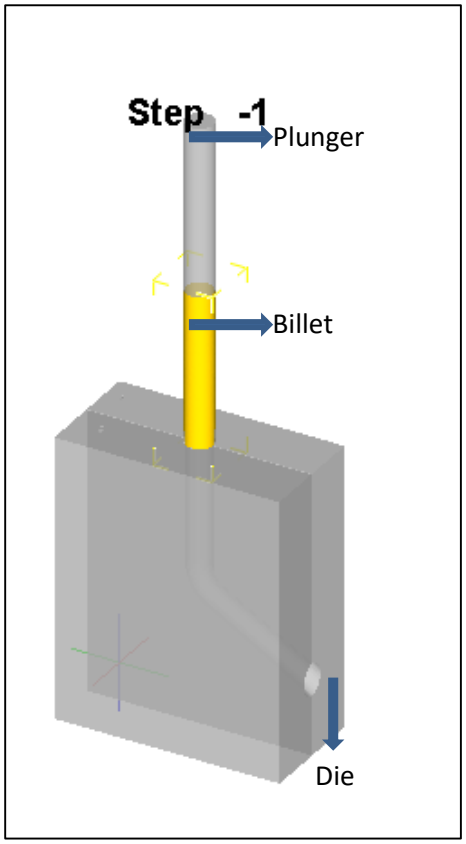

Figure 15: Assembly of the workpiece, die, and plunger

3.5.1. Die Design

The Die is designed in 3D CAD package SolidWorks V.2017. The Die is designed in two halves. Cross-section of each half 100×80×20 mm with an angular channel having 120° die angle (Φ) and 30° channel corner angle (ψ). The geometry of Die was saved in dot stereolithography (.stl) format that is compatible with DEFORM-3D. The billet and plunger were directly designed in DEFORM-3D. The diameter and length of the billet were 9.5×54 mm, respectively. The diameter and length of the plunger were 10×60 mm, respectively. Figure 16 (a) shows the die assembly after one ECAP pass with deform billet inside it; figure 16 (b) enlarge the image of deform billet.

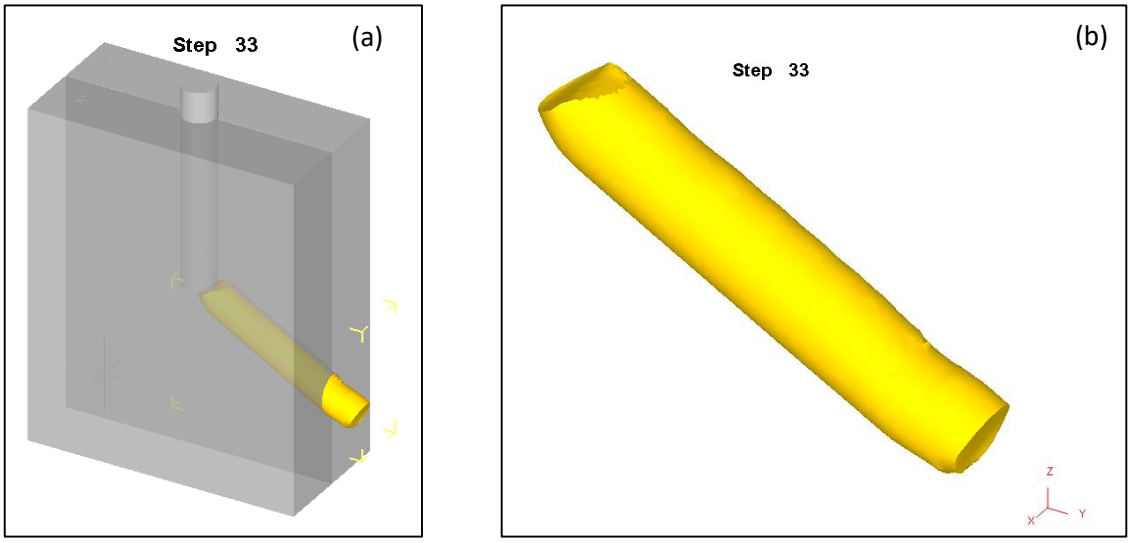

Figure 16: (a) the die assembly after one ECAP pass with deform billet inside it, (b) enlarge the image of deform billet.

CHAPTER 4

Results and Discussions

In this chapter, the results obtained from the hardness, optical microscopy, electron back-scattered diffraction (EBSD), and the simulation investigations will be described in detail.

4.1. Microhardness

Micro Hardness (HV) is measured for all the ECAPed samples perpendicular to the deformation direction with 100g of the test load. HV is measured on four different points on the axis for better results. The average HV values of different samples and standard deviation (SD) are shown in Figure 17. R1, R3, and R6 are the samples with one pass, three passes, six passes at room temperature. E1, E3, and E6 are the samples with one pass, three passes, six passes at elevated temperature, i.e., 250 °C, respectively. It can be seen that the hardness values start increasing from the first pass. From the HV values, the maximum hardness value, i.e., 85 HV, is observed from the sixth continuous pass specimen deformed at room temperature, i.e., 85 HV. However, the sample with one ECAPed pass shows the maximum growth of 83.40% in hardness value at room temperature. After one pass of ECAP, the rate of increasing hardness value decreases. After one or two passes, almost all the grains are equiaxed and elongated, and there is a minor gap left between the grain boundary. The column graphs show that hardness obtained from room temperature is far better than the hardness obtained from elevated temperature. This is because recrystallization starts as the temperature increases—also, elevated temperatures to larger grain size due to the grain growth process. The maximum growth of hardness in samples processed at elevated temperature is 17.13% at the third pass. However, the Hardness value decreases at the sixth pass at 250 °C, due to continuous heating of sample six times, and after a certain temperature point, the effect of ECAP starts decreasing as the temperature increases. In Figure 17, the upper right-hand corner shows the indentation mark on the sample processed at elevated temperature with one pass, and the magnification is 10 microns with a test load of 100g.

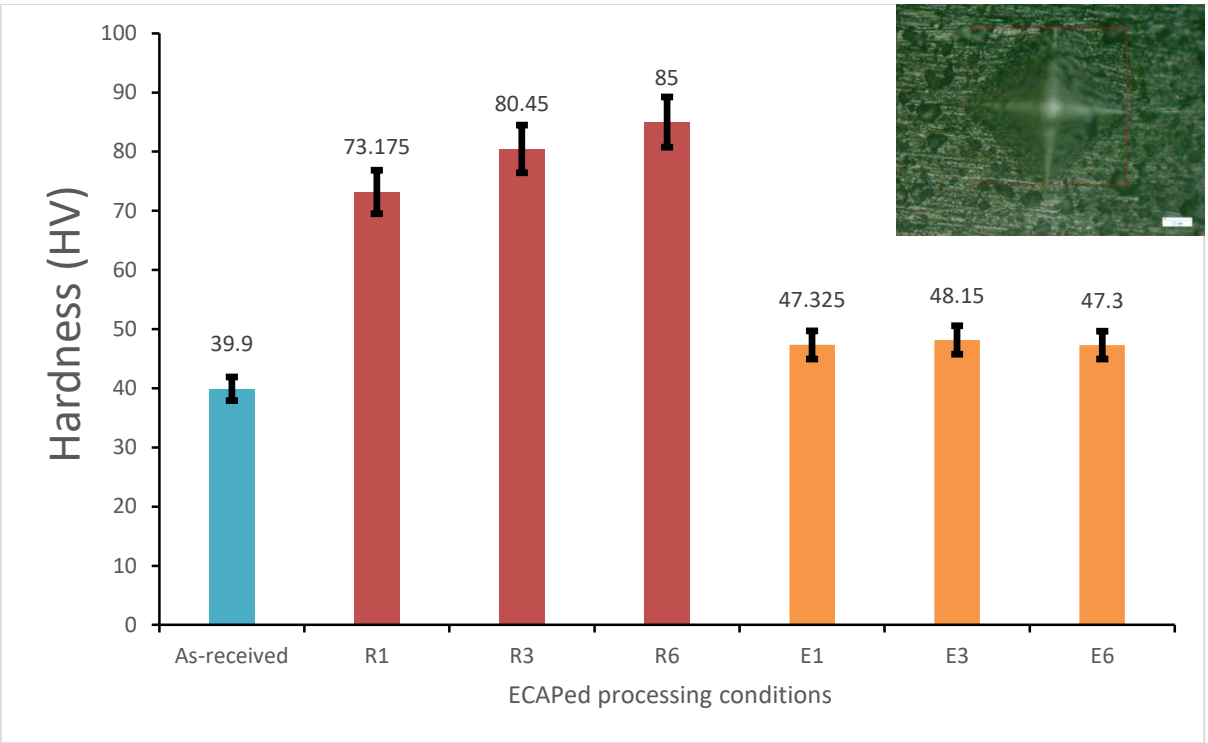

Figure 17: Hardness value at different level, blue shows initial hardness, red and orange column shows the hardness of ECAPed processed samples at room temperature and at 250°C respectively, In the corner Indentation of Hardness test on E1 sample

4.2. Optical Microscopy

The images obtained from an optical microscope with a 20 X magnification zoom are shown in Figure 18. Figure 18(a-c) shows the microstructure of samples processed at room temperature with first, third, and sixth ECAP pass, respectively. Similarly, Figure 18(d-f) has the microstructure of samples processed at elevated temperature with first, third, and sixth ECAP pass, respectively. The microstructure of the as-received sample is shown in Figure 18 (g). Primarily, the as-received Al-6063 have some coarse grain-like structure and an imprecise orientation. With the start of the deformation process and increment in the number of passes, elongation of grain in extruded direction can be observed, which then, in the end, finally converts into ultra-fine grains (UFG). As the number of passes increases, the formation of subgrains also increases due to large deformation and dislocations. However, reduction in grain, equiaxed grain formation, and grain orientation are the main reasons for forming sub-grains. Some shear bands are also visual in all samples. There is a stable growth of the density of shear bands inside the samples because of the ECAP process route BC. In this route, the sample routed 90° with every pass. Shear bands are

frequent observations of confined strain in the samples and signify grain refinement [53]. Each shear band is supposed to have many dislocation cells, which were linked beside the route of the shear band [112], and the contact of the shear and slip bands origins the growth of the grains at the sub-micron level is the ultimate reason behind the grain refinement.

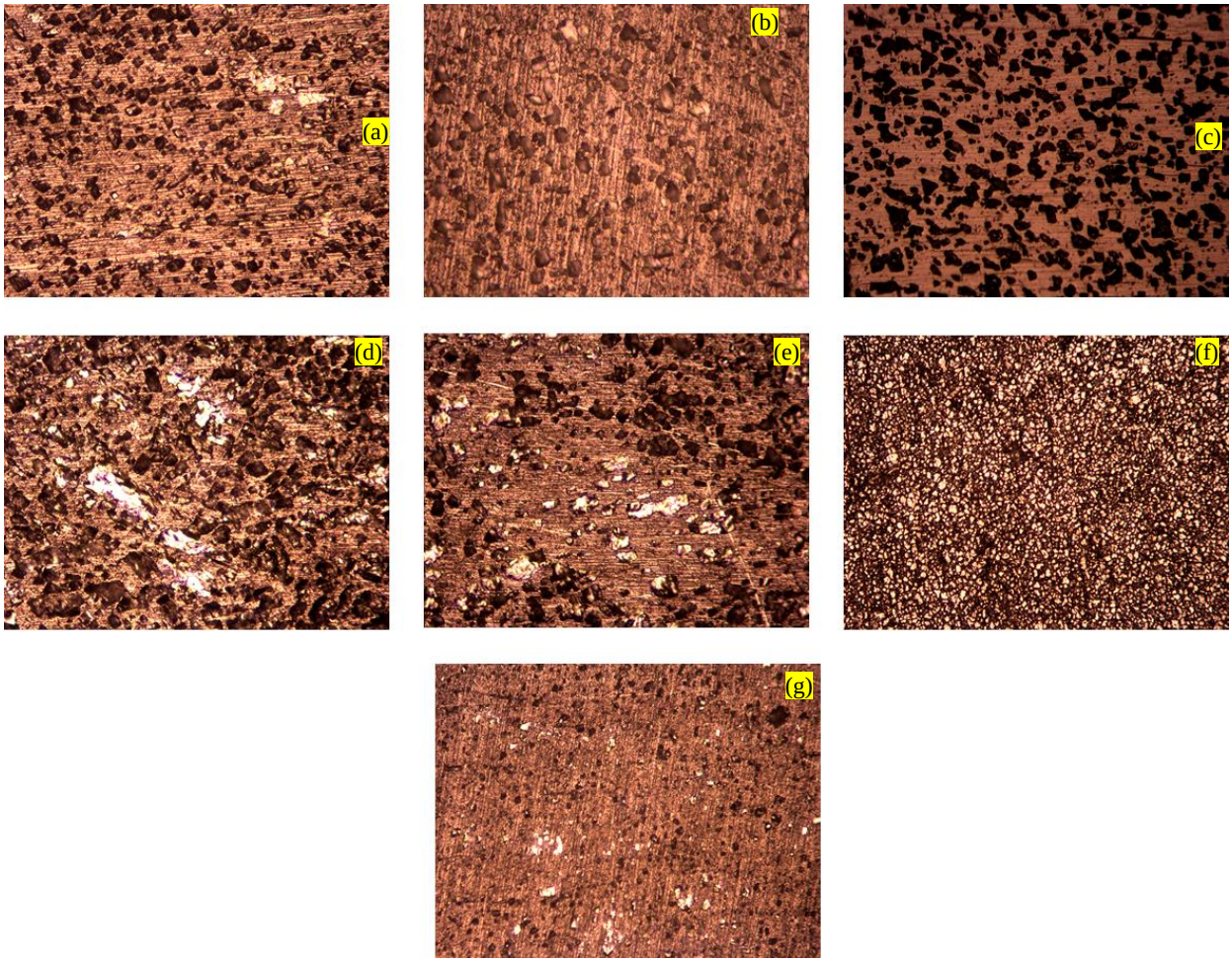

Figure 18: Optical Microstructure with 20X magnification, (a), (b), and (c) shows the microstructure of ECAPed sample with first, third, and sixth pass at room temperature, (d), (e), and (f) shows the microstructure of ECAPed sample with first, third and sixth pass at 250 °C and (g) shows the microstructure of initial sample, respectively.

4.3. Electron back-scattered diffraction (EBSD) analysis:

Earlier in this research, hardness value (HV) improved strength with an increasing number of passes. To better understand the role of temperature in the ECAP process, the sample with one pass at elevated temperature (250 °C) is observed under Electron back-scattered diffraction (EBSD). EBSD data includes the information about grain orientation map, inverse pole figure, and average distribution of misorientation angles shown in Figure 19 (a, b) and Figure 20, respectively.

As SPD occurs, there is an interface among the dislocations in the metal and the movement in grain boundaries. Grain boundaries generally hamper the movement of dislocations in metals besides the slip planes [90]. Figure 19 shows the grain elongation in the direction of deformation. It can be observed that some ultra-fine equiaxed grains or sub-grains are also visible along with HAGBs. It is observed from Figure 20 and there is a dominance of Low Angle Grain Boundaries (LAGBs) with an insignificant presence of High Angle Grain Boundaries (HAGBs). LAGBs are 91.06%, where HAGBs are only 8.9%. This is because of two main reasons: the formation of new equiaxed grains and sub-grains with LAGBs aligned in the elongated coarse HAGB grains. This happens after each ECAP pass. The second and most important reason is process temperature, i.e., as the process temperature increases, the friction in HAGBs and formed new equiaxed grains with increased grain size decreases. The average grain size of this particular sample, deformed with the first pass at elevated temperature, is ~20 μm. Thus it can be concluded that the influence of process temperature on grain size is excellent.

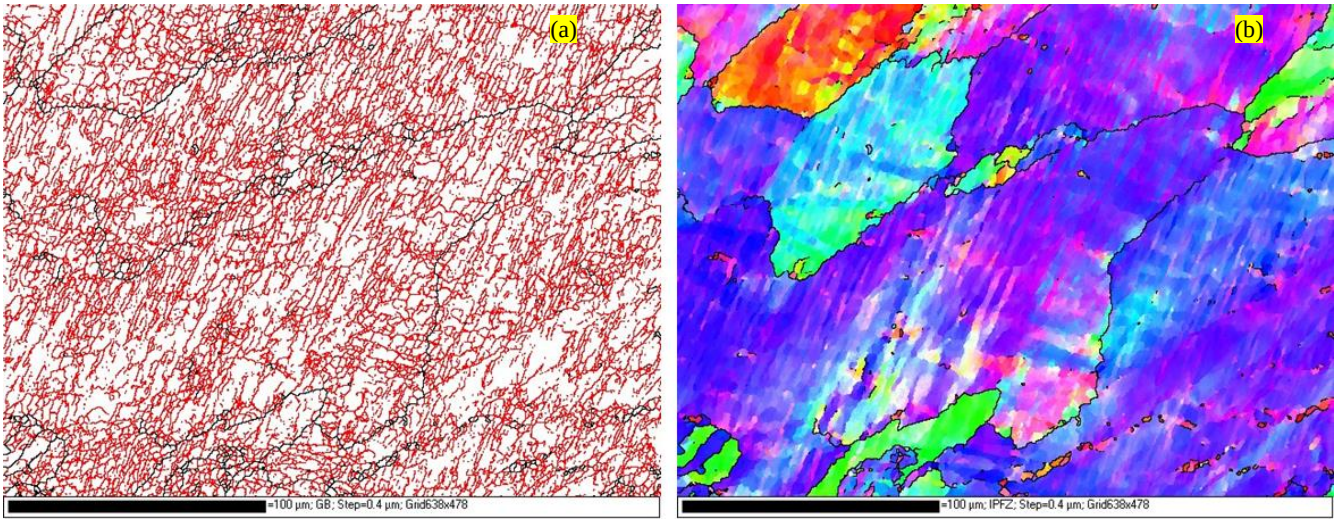

Figure 19: EBSD images of ECAPed sample with one pass at elevated temperature (a) Grain orientation map (b) inverse pole figure

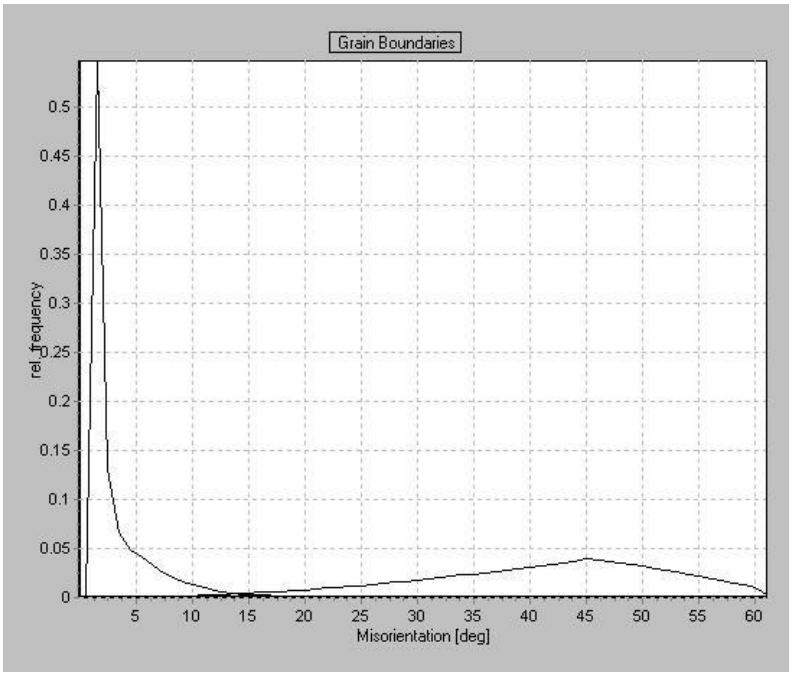

Figure 20: Average distribution of misorientation angles

4.4. Effective Strain Distribution

The simulation results of Effective strain distribution of the billet after 1st, 2nd, 3rd, 4th, 5th, and 6th ECAP pass at room temperature and elevated temperature shown in figure 21 and figure 22, respectively. In figure 21 and figure 22, the effective strain distribution contours become more homogenous as the number of passes increases indicates the small grain size. The trend of strain distribution shows plastic distribution is homogeneous in the extrusion direction for both the temperature. It also helps in achieving better mechanical properties. From the figures, the distribution trend is mostly occurring at the top part of the billets, where the force applied by the plunger is more. Figure 21(f), the sixth ECAPed pass at room temperature, records the highest strain distribution throughout the billet and the primary distribution of strain occurs at the head of the billet. A new trend of strain distribution is also observed in figure 21 (a, c, e), where the number of passes is odd shows the low effective strain compared to figure 21 (b, d, f), where the number of passes is even number. This can be because of the effect of route BC, where the billet rotated 90° clockwise every time. The influence of elevated temperature can be seen in figure 22. As the ECAP passes increase at the elevated temperature, the effective strain becomes better. Similar strain trends at room temperature are also shown in the numerical result of Niu et al., where homogeneous plastic deformation is seen in both vertical and horizontal directions [113].

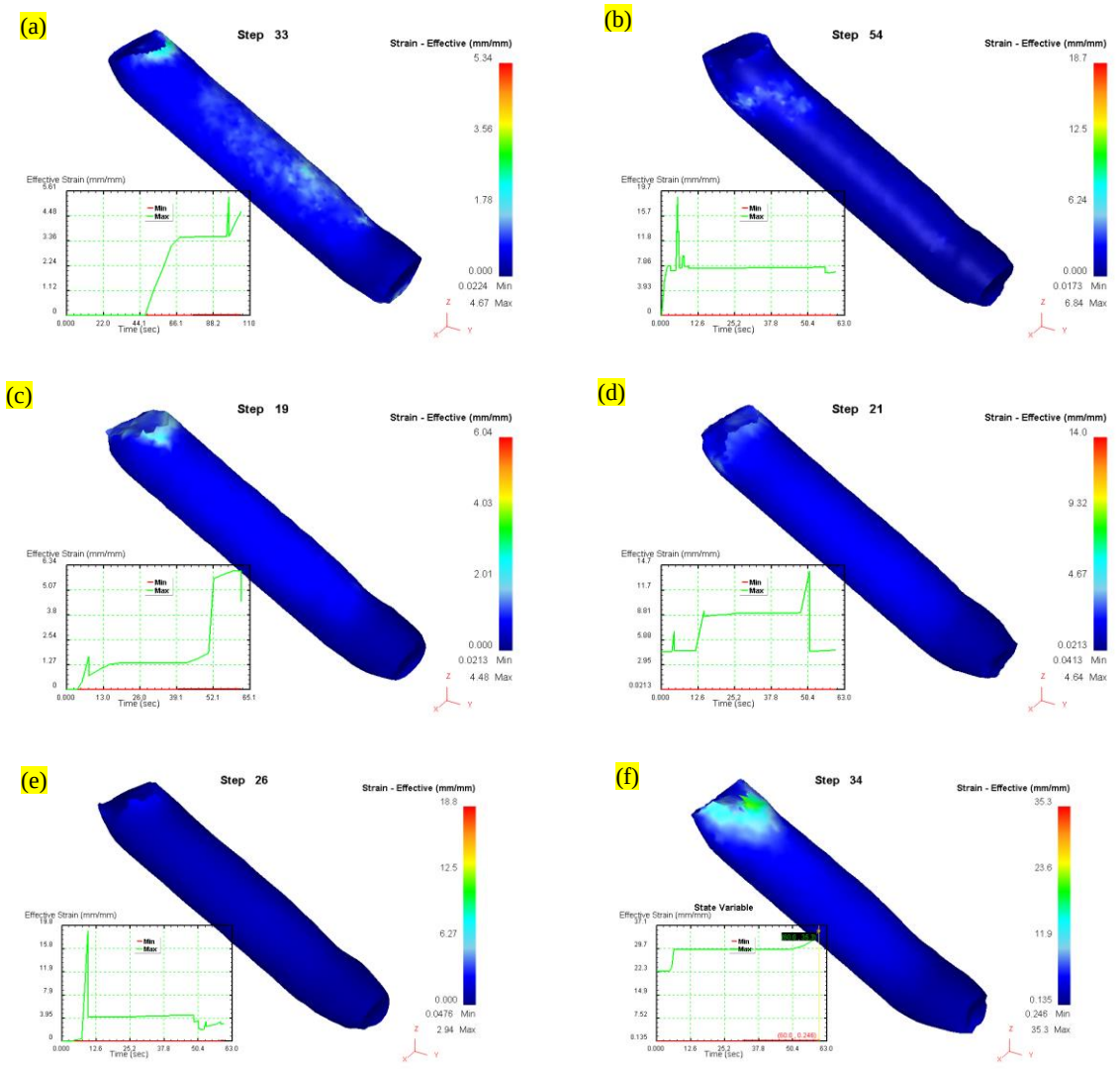

Figure 21: Effective strain distribution at room temperature with (a) 1, (b) 2, (c) 3, (d) 4, (e) 5, and (f) 6, number of ECAP passes

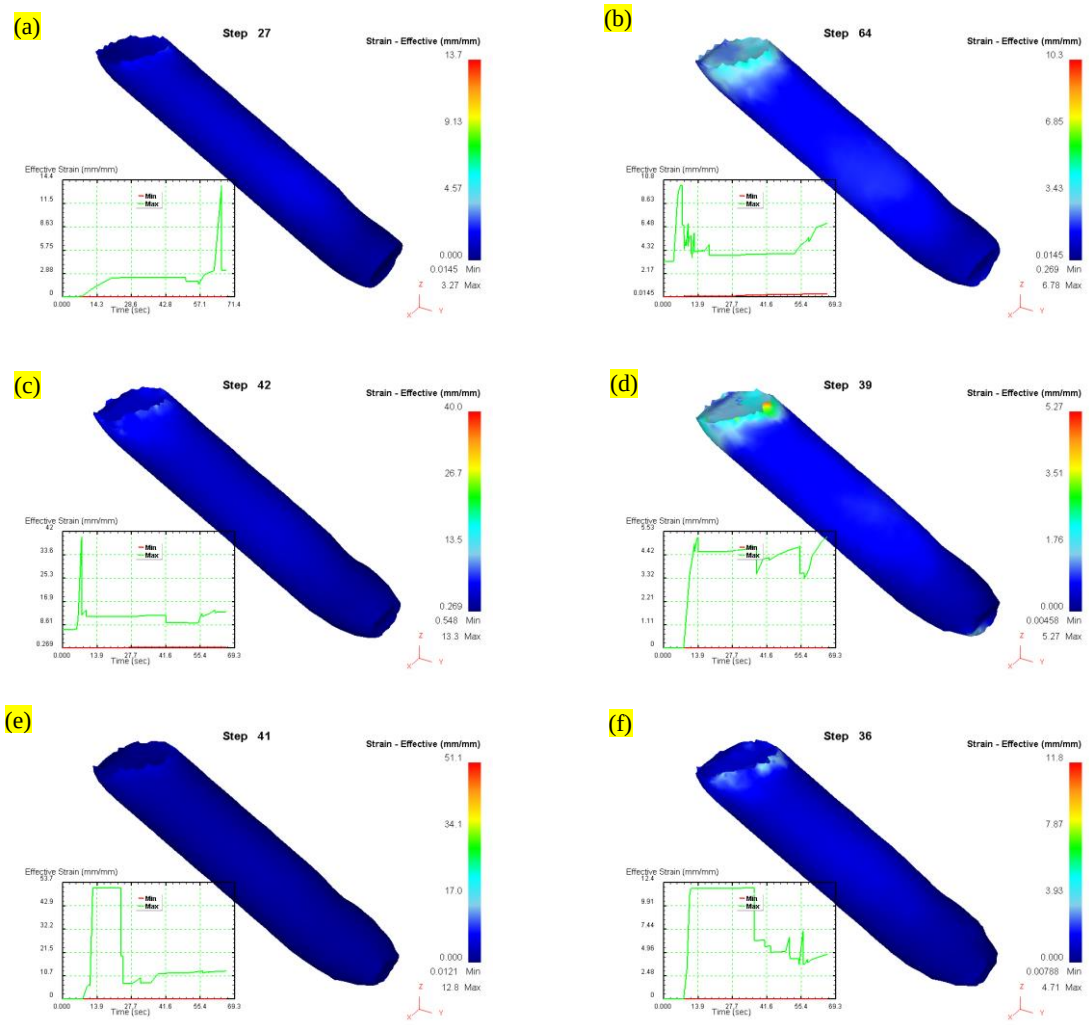

Figure 22: Effective strain distribution at elevated temperature (250 °C) with (a) 1, (b) 2, (c) 3, (d) 4, (e) 5, and (f) 6, number of ECAP passes

4.5. Effective stress Distribution

Figure 23 (a-f) and figure 24 (a-f) show the trends of effective stress induced during the first to sixth ECAPed pass at room temperature and elevated temperature, respectively. It is observed that the stress distribution shows a gradient variation until the billets enter the deformation zone. The stress is primarily induced in the top of the billet and corner region of the channel (also known as the deformation zone). The second ECAP pass of billet shows the maximum stress for both temperatures, i.e., room temperature and elevated temperature shown in figure 23 (b) and figure 24 (b), respectively. After that, no significant change in effective stress is shown. Effective stress at elevated temperature is more petite than effective stress at room temperature because high temperature increases the ductility of aluminum billet. Some similar stress distribution is also reported by Niu et al. [113]

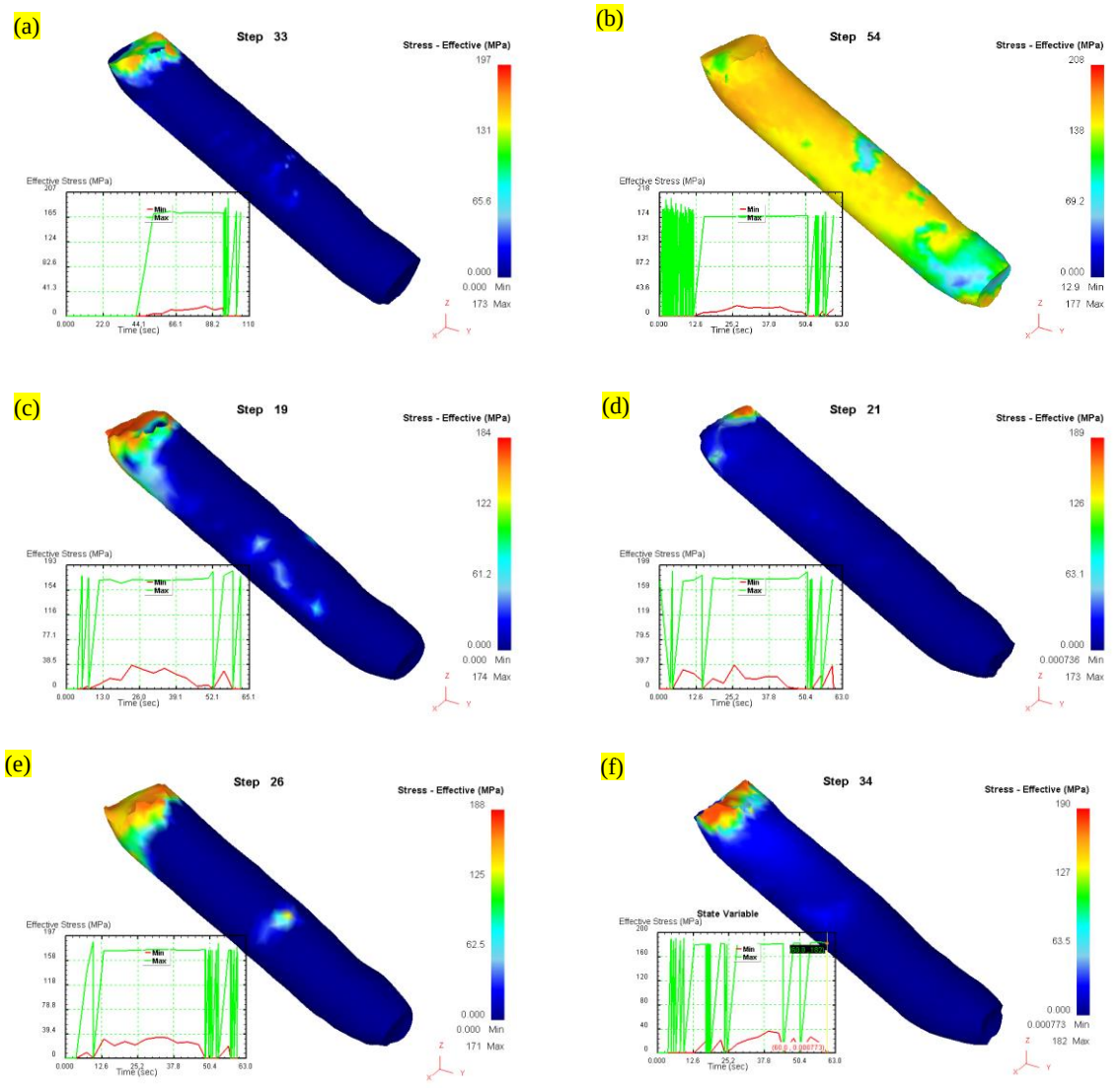

Figure 23: Effective stress distribution at room temperature with (a) 1, (b) 2, (c) 3, (d) 4, (e) 5, and (f) 6, number of ECAP passes

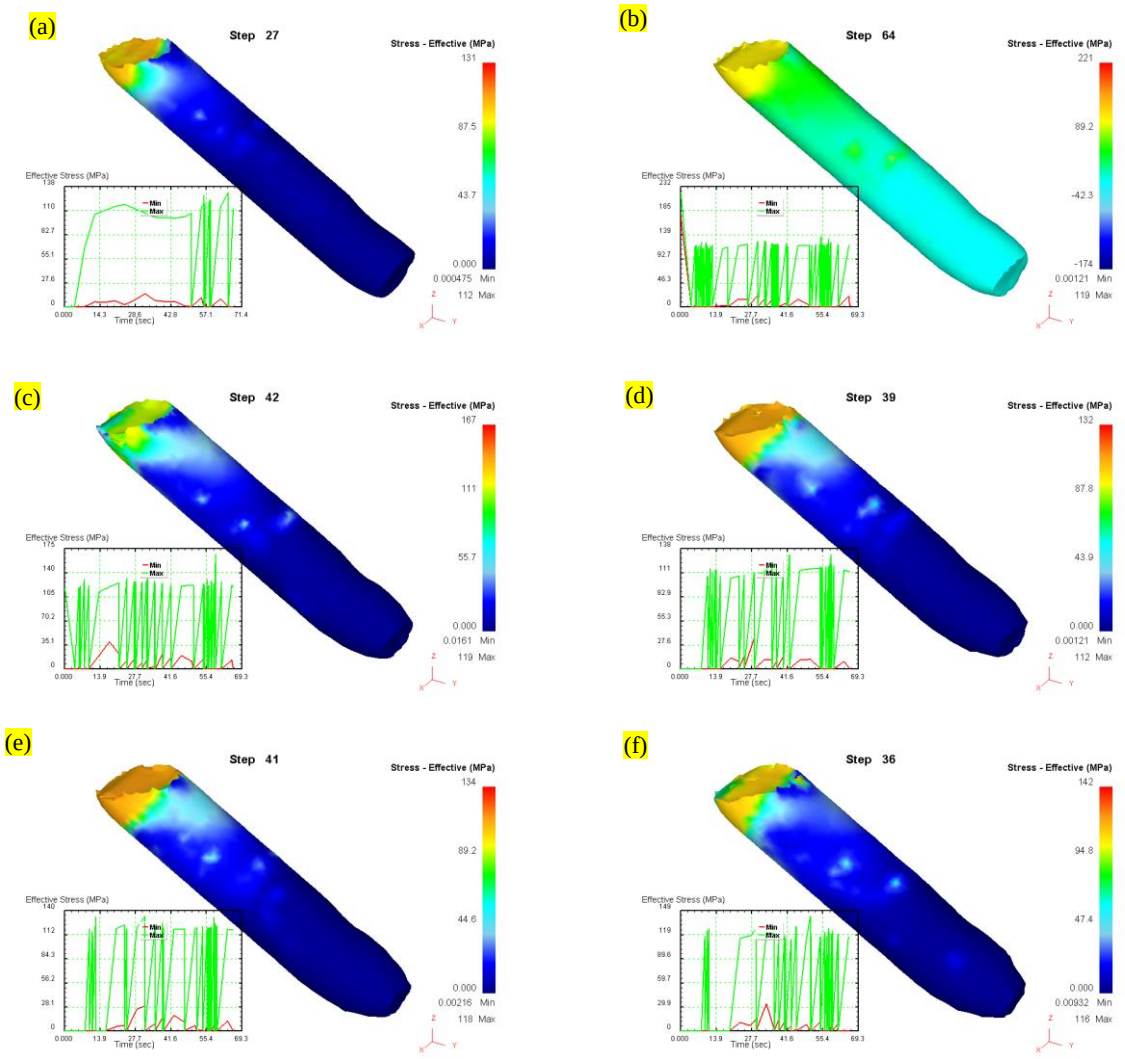

Figure 24: Effective stress distribution at elevated temperature with (a) 1, (b) 2, (c) 3, (d) 4, (e) 5, and (f) 6, number of ECAP passes

4.6. Extrusion Load

Figure 25 shows the load (N) graph of different ECAPed passes (from the first pass to sixth) during the ECAP process at room temperature and elevated temperature, respectively. The extrusion load starts increasing as the billet passes the corner of the die channel or deformation zone, and after reaching maximum value, the loads decrease gradually and become steady. The load at room temperature increases up to 11 KN and increases up to 20 KN for elevated temperature. Fluctuations in load vs. time curves are shown during the simulation process, and these fluctuations are recognizing because of changes in contact friction between billet and channel walls. Therefore, it can be concluded that a sufficient amount of lubricant in die channel during the experimental process may decrease the overall extrusion load and help improve Die and plunger life. From graph in figure 25, it can be concluded that extrusion load at 250 °C is more prominent than at room temperature. The load curves present in this study show no bend and shear stages at the higher peak of load. Such bend is previously noted in different studies [114–116]. The die corner angle (φ) plays a major role in the behavior of load vs time curves [117]. If the value of φ is more than or equal to the 40° it can affects the behavior and peak load of load vs. time curves [115].

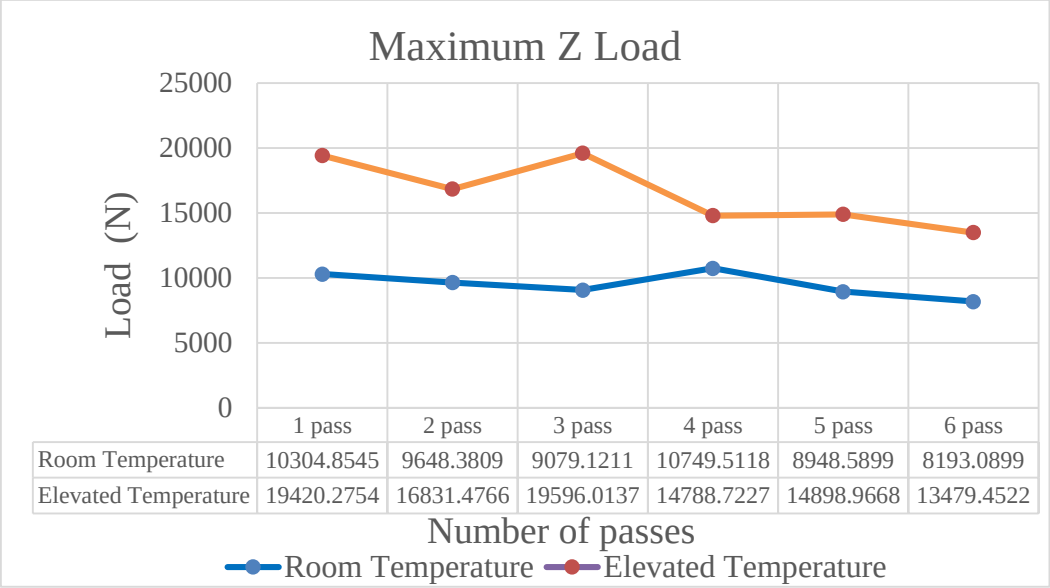

Figure 25: Load (N) graph with 1-6 number of ECAP passes at room temperature in blue and elevated temperature in orange

CHAPTER 5

Conclusion

In this work, Al-6063 was subjected to SPD using the ECAP technique for two different processing temperatures. A finite element method based on computer simulation is beneficial to understand the effect of processing temperature on the ECAP process. Results obtained from different specimen tests are discussed in this study. From the results and discussion, the following conclusions can be drawn:

- ECAP up to six passes increased hardness at room temperature from 39.9 HV to 85 HV. However, after the sixth pass at 250 °C, the hardness decreases due to continuous heating of the material.
- Maximum hardness value with growth of 83.39% is observed at room temperature after the first pass (73.175 HV) and then hardness is not increased much. Hardness values at room temperature are better than hardness values at elevated temperatures.
- Optical micrographs show ECAP's effect, elongated grains are observed. As the number of passes increases, sub-grain formation also increases due to large deformation and dislocation.
- The average grain size of the sample with one pass at elevated temperature is ~20 μm.
- The effective strain distribution contours become more homogenous as the number of passes increases helps increase mechanical properties.
- The effective stress is reduced at deformation zone as a function of temperature.
- Extrusion load increases as the billet passes from the deformation zone and progressively decreases after reaching the maximum amount.
- The simulation result shows that using significant amount of lubricant in the experimental process can help in reducing the overall extrusion load of the ECAP process.

REFERENCES

[1] E.O. Hall, The lüders deformation of mild steel, Proc. Phys. Soc. Sect. B. (1951). https://doi.org/10.1088/0370-1301/64/12/109.

[2] N.J. Petch, The cleavage strength of polycrystals, J. Iron Steel InstInst. (1953).

[3] M. Gedeon, Grain Size and Material Strength, Tech. Tidbits. (2010).

[4] B. VERLINDEN, Severe plastic deformation of metals, Metal. Metall. (2005). https://doi.org/10.30544/380.

[5] L. Olejnik, A. Rosochowski, Methods of fabricating metals for nano-technology, Bull. Polish Acad. Sci. Tech. Sci. (2005).

[6] R.Z. Valiev, Y. Estrin, Z. Horita, T.G. Langdon, M.J. Zehetbauer, Y.T. Zhu, Producing bulk ultrafine-grained materials by severe plastic deformation, JOM. (2006). https://doi.org/10.1007/s11837-006-0213-7.

[7] Z. Xie, J. Xie, Y. Hong, X. Wu, Influence of processing temperature on microstructure and microhardness of copper subjected to high-pressure torsion, Sci. China Technol. Sci. 53 (2010) 1534–1539. https://doi.org/10.1007/s11431-010-3157-7.

[8] A.K. Ghosh, W. Huang, Severe Deformation Based Process for Grain Subdivision and Resulting Microstructures, in: Investig. Appl. Sev. Plast. Deform., 2000. https://doi.org/10.1007/978-94-011-4062-1_4.

[9] Y. Saito, H. Utsunomiya, H. Suzuki, T. Sakai, Improvement in the r-value of aluminum strip by a continuous shear deformation process, Scr. Mater. (2000). https://doi.org/10.1016/S1359-6462(00)00349-3.

[10] J.C. Lee, H.K. Seok, J.H. Han, Y.H. Chung, Controlling the textures of the metal strips via the continuous confined strip shearing(C2S2) process, Mater. Res. Bull. (2001). https://doi.org/10.1016/S0025-5408(01)00557-8.

[11] H.S. Kim, Finite element analysis of deformation behaviour of metals during equal channel multi-angular pressing, Mater. Sci. Eng. A. (2002).

https://doi.org/10.1016/S0921-5093(01)01793-2.

[12] Y. Nishida, H. Arima, J.C. Kim, T. Ando, Rotary-die equal-channel angular pressing of an Al - 7 mass% Si - 0.35 mass% Mg alloy, Scr. Mater. (2001). https://doi.org/10.1016/S1359-6462(01)00985-X.

[13] C.Y. Chou, S.L. Lee, J.C. Lin, C.M. Hsu, Effects of cross-channel extrusion on the microstructures and superplasticity of a Zn-22 wt.% Al eutectoid alloy, Scr. Mater. (2007). https://doi.org/10.1016/j.scriptamat.2007.04.029.

[14] B. Talebanpour, R. Ebrahimi, K. Janghorban, Microstructural and mechanical properties of commercially pure aluminum subjected to Dual Equal Channel Lateral Extrusion, Mater. Sci. Eng. A. (2009). https://doi.org/10.1016/j.msea.2009.07.040.

[15] V.S. Rao, B.P. Kashyap, N. Prabhu, P.D. Hodgson, T-shaped equi-channel angular pressing of Pb-Sn eutectic and its tensile properties, Mater. Sci. Eng. A. (2008). https://doi.org/10.1016/j.msea.2007.09.004.

[16] Y.H. Kim, J.R. Cho, K.S. Kim, H.S. Jeong, S.S. Yoon, Study of the application of upper bound method to the CONFORM process, J. Mater. Process. Technol. (2000). https://doi.org/10.1016/S0924-0136(99)00366-0.

[17] E. Cerri, P.P. De Marco, P. Leo, FEM and metallurgical analysis of modified 6082 aluminium alloys processed by multipass ECAP: Influence of material properties and different process settings on induced plastic strain, J. Mater. Process. Technol. (2009). https://doi.org/10.1016/j.jmatprotec.2008.04.013.

[18] B. Mani, M. Jahedi, M.H. Paydar, A modification on ECAP process by incorporating torsional deformation, Mater. Sci. Eng. A. (2011). https://doi.org/10.1016/j.msea.2011.02.015.

[19] A. Rosochowski, L. Olejnik, Finite element analysis of two-turn Incremental ECAP, Int. J. Mater. Form. (2008). https://doi.org/10.1007/s12289-008-0108-y.

[20] A. Azushima, K. Aoki, Properties of ultrafine-grained steel by repeated shear deformation of side extrusion process, Mater. Sci. Eng. A. (2002). https://doi.org/10.1016/S0921-

5093(02)00005-9.

[21] V.M. Segal, V.I. Reznikov, A.E. Drobyshevskii, V.I. Kopylov, Plastic Metal Working by Simple Shear., Izv. Akad. Nauk SSSR. Met. (1981).

[22] R. Hill, Studies in large plastic flow and fracture, J. Mech. Phys. Solids. (1953). https://doi.org/10.1016/0022-5096(53)90019-2.

[23] R.Z. Valiev, A. V. Korznikov, R.R. Mulyukov, Structure and properties of ultrafine-grained materials produced by severe plastic deformation, Mater. Sci. Eng. A. (1993). https://doi.org/10.1016/0921-5093(93)90717-S.

[24] S. Ferrasse, V.M. Segal, K.T. Hartwig, R.E. Goforth, Development of a submicrometer-grained microstructure in aluminum 6061 using equal channel angular extrusion, J. Mater. Res. (1997). https://doi.org/10.1557/JMR.1997.0173.

[25] V.M. Segal, K.T. Hartwig, R.E. Goforth, In situ composites processed by simple shear, Mater. Sci. Eng. A. (1997). https://doi.org/10.1016/s0921-5093(96)10539-6.

[26] V. Segal, R.E. Goforth, T.K. Hartwig, Apparatus and method for deformation processing of metals, ceramics, plastics and other materials, 5400633, 1977. https://hdl.handle.net/1969.1/176516 (accessed June 8, 2021).

[27] M. Furukawa, Z. Horita, M. Nemoto, T.G. Langdon, Review: Processing of metals by equal-channel angular pressing, J. Mater. Sci. 36 (2001) 2835–2843. https://doi.org/10.1023/A:1017932417043.

[28] J.N. Reddy, An Introduction to The Finite Element Method Department of Mechanical Engineering (SOLUTIONS), Mech. Eng. (2005).

[29] H.Y. Li, C.T. Zeng, M.S. Han, J.J. Liu, X.C. Lu, Time-temperature-property curves for quench sensitivity of 6063 aluminum alloy, Trans. Nonferrous Met. Soc. China (English Ed. (2013). https://doi.org/10.1016/S1003-6326(13)62426-7.

[30] J. Nemati, G.H. Majzoobi, S. Sulaiman, B.T.H.T. Baharudin, M.A. Azmah Hanim, Effect of equal channel angular extrusion on Al-6063 bending fatigue characteristics, Int. J.

Miner. Metall. Mater. (2015). https://doi.org/10.1007/s12613-015-1085-z.

[31] S. Natarajan, R. Narayanasamy, S.P. Kumaresh Babu, G. Dinesh, B. Anil Kumar, K. Sivaprasad, Sliding wear behaviour of Al 6063/TiB2 in situ composites at elevated temperatures, Mater. Des. (2009). https://doi.org/10.1016/j.matdes.2008.09.037.

[32] V. V. Stolyarov, Y.T. Zhu, T.C. Lowe, R.K. Islamgaliev, R.Z. Valiev, Two step SPD processing of ultrafine-grained titanium, Nanostructured Mater. (1999). https://doi.org/10.1016/S0965-9773(99)00384-0.

[33] M. Furukawa, Z. Horita, M. Nemoto, T.G. Langdon, The use of severe plastic deformation for microstructural control, Mater. Sci. Eng. A. (2002). https://doi.org/10.1016/S0921-5093(01)01288-6.

[34] S.R. Agnew, J.R. Weertman, The influence of texture on the elastic properties of ultrafine-grain copper, Mater. Sci. Eng. A. (1998). https://doi.org/10.1016/s0921-5093(97)00504-2.

[35] R.Z. Valiev, I. V. Alexandrov, Y.T. Zhu, T.C. Lowe, Paradox of strength and ductility in metals processed by severe plastic deformation, J. Mater. Res. (2002). https://doi.org/10.1557/JMR.2002.0002.

[36] R.Z. Valiev, Recent developments of SPD processing for fabrication of bulk nanostructured materials, in: TMS Annu. Meet., 2002. https://doi.org/10.1002/9781118804537.ch37.

[37] E. V. Kozlov, A.N. Zhdanov, L.N. Ignatenko, N.A. Popova, Y.F. Ivanov, N.A. Koneva, Structural evolution of ultrafine-grained copper and copper-based alloy during plastic deformation, in: TMS Annu. Meet., 2002. https://doi.org/10.1002/9781118804537.ch48.

[38] E. Bagherpour, M. Reihanian, N. Pardis, R. Ebrahimi, T.G. Langdon, Ten years of severe plastic deformation (SPD) in Iran , part I : equal channel angular pressing (ECAP), Iran. J. Mater. Form. (2018).

[39] M. Mabuchi, H. Iwasaki, K. Higashi, Microstructure and mechanical properties of 5056 Al alloy processed by equal channel angular extrusion, Nanostructured Mater. (1997). https://doi.org/10.1016/S0965-9773(98)00032-4.

[40] P.L. Sun, P.W. Kao, C.P. Chang, The effect of strain per pass on the microstructure developed in aluminum processed by equal channel angular extrusion, in: TMS Annu. Meet., 2002. https://doi.org/10.1002/9781118804537.ch4.

[41] K. Matsuki, T. Aida, T. Takeuchi, J. Kusui, K. Yokoe, Microstructural characteristics and superplastic-like behavior in aluminum powder alloy consolidated by equal-channel angular pressing, Acta Mater. (2000). https://doi.org/10.1016/S1359-6454(00)00061-6.

[42] T. Lokesh, U.S. Mallik, Effect of Equal Channel Angular Pressing on the Microstructure and Mechanical Properties of Al6061-SiCp Composites, in: IOP Conf. Ser. Mater. Sci. Eng., 2016. https://doi.org/10.1088/1757-899X/149/1/012119.

[43] J.R. Davis, Alloying. Understanding the basics: Aluminum and Aluminum Alloys, 2001.

[44] S. Toros, F. Ozturk, I. Kacar, Review of warm forming of aluminum-magnesium alloys, J. Mater. Process. Technol. (2008). https://doi.org/10.1016/j.jmatprotec.2008.03.057.

[45] S. Lathabai, P.G. Lloyd, The effect of scandium on the microstructure, mechanical properties and weldability of a cast Al-Mg alloy, Acta Mater. (2002). https://doi.org/10.1016/S1359-6454(02)00259-8.

[46] H. Zhang, M.W. Chen, K.T. Ramesh, J. Ye, J.M. Schoenung, E.S.C. Chin, Tensile behavior and dynamic failure of aluminum 6092/B4C composites, Mater. Sci. Eng. A. (2006). https://doi.org/10.1016/j.msea.2006.06.055.

[47] K. Nguyen, M. Zhang, V.J. Amores, M.A. Sanz, F.J. Montáns, Computational modeling of dislocation slip mechanisms in crystal plasticity: A short review, Crystals. (2021). https://doi.org/10.3390/cryst11010042.

[48] B. Gurrutxaga–Lerma, J. Verschueren, A.P. Sutton, D. Dini, The mechanics and physics of high-speed dislocations: a critical review, Int. Mater. Rev. (2021). https://doi.org/10.1080/09506608.2020.1749781.

[49] M. Ciemiorek, M. Orłowska, M. Lewandowska, Ultrafine-Grained Plates and Sheets: Processing, Anisotropy and Formability, Adv. Eng. Mater. (2020). https://doi.org/10.1002/adem.201900666.

[50] G.. Taylor, The Mechanism of Plastic Deformation of Crystals ., Proc. R. Soc. A Math. Phys. Eng. Sci. (1934).

[51] E. Orowan, A type of plastic deformation new in metals, Nature. (1942). https://doi.org/10.1038/149643a0.

[52] M. Polanyi, Über eine Art Gitterstörung, die einen Kristall plastisch machen könnte, Zeitschrift Für Phys. (1934). https://doi.org/10.1007/BF01341481.

[53] W.D.D. Callister, Materials science and engineering : An introduction, 10th australia and new zealand edition, 2019.

[54] V. Segal, Review: Modes and processes of severe plastic deformation (SPD), Materials (Basel). (2018). https://doi.org/10.3390/ma11071175.

[55] K. Mori, P.F. Bariani, B.A. Behrens, A. Brosius, S. Bruschi, T. Maeno, M. Merklein, J. Yanagimoto, Hot stamping of ultra-high strength steel parts, CIRP Ann. - Manuf. Technol. (2017). https://doi.org/10.1016/j.cirp.2017.05.007.

[56] Z. Shao, N. Li, J. Lin, T. Dean, Formability evaluation for sheet metals under hot stamping conditions by a novel biaxial testing system and a new materials model, Int. J. Mech. Sci. (2017). https://doi.org/10.1016/j.ijmecsci.2016.11.022.

[57] J. Besson, M. Abouaf, Grain growth enhancement in alumina during hot isostatic pressing, Acta Metall. Mater. (1991). https://doi.org/10.1016/0956-7151(91)90004-K.

[58] K.K. Saxena, k. Basanth Kumar, A. Gupta, Effect of processing parameters on equal-channel angular pressing of aluminum alloys: An overview, Mater. Today Proc. (2021). https://doi.org/10.1016/j.matpr.2021.02.303.

[59] A. Gupta, B. Chandrasekhar, K.K. Saxena, Effect of Equal-channel angular pressing on mechanical Properties: An overview, Mater. Today Proc. (2021). https://doi.org/10.1016/j.matpr.2021.02.317.

[60] S.D. Chen, X.H. Liu, L.Z. Liu, Grain statistics effect on deformation behavior in asymmetric rolling of pure copper foil by crystal plasticity finite element model, Trans.

Nonferrous Met. Soc. China (English Ed. (2015). https://doi.org/10.1016/S1003-6326(15)63972-3.

[61] B. Ma, C. Li, J. Wang, B. Cai, F. Sui, Influence of asymmetric hot rolling on through-thickness microstructure gradient of Fe–20Mn–4Al–0.3C non-magnetic steel, Mater. Sci. Eng. A. (2016). https://doi.org/10.1016/j.msea.2016.06.047.

[62] J. Huang, Y.T. Zhu, D.J. Alexander, X. Liao, T.C. Lowe, R.J. Asaro, Development of repetitive corrugation and straightening, Mater. Sci. Eng. A. (2004). https://doi.org/10.1016/S0921-5093(03)00114-X.

[63] H. Abolfathi, H.R. Jafarian, H. Arabi, N. Park, A.R. Eivani, Microstructural development and its effects on tensile properties of a high Ni TRIP steel produced by repetitive corrugation and straightening via rolling (RCSR), J. Mater. Res. Technol. (2020). https://doi.org/10.1016/j.jmrt.2019.12.059.

[64] N. Thangapandian, S. Balasivanandha Prabu, K.A. Padmanabhan, Effects of die profile on grain refinement in Al-Mg alloy processed by repetitive corrugation and straightening, Mater. Sci. Eng. A. (2016). https://doi.org/10.1016/j.msea.2015.09.051.

[65] S.C. Pandey, M.A. Joseph, M.S. Pradeep, K. Raghavendra, V.R. Ranganath, K. Venkateswarlu, T.G. Langdon, A theoretical and experimental evaluation of repetitive corrugation and straightening: Application to Al-Cu and Al-Cu-Sc alloys, Mater. Sci. Eng. A. (2012). https://doi.org/10.1016/j.msea.2011.11.070.

[66] B.R. Sunil, Repetitive Corrugation and Straightening of Sheet Metals, Mater. Manuf. Process. (2015). https://doi.org/10.1080/10426914.2014.973600.

[67] P. Wei, C. Lu, K. Tieu, L. Su, G. Deng, W. Huang, A study on the texture evolution mechanism of nickel single crystal deformed by high pressure torsion, Mater. Sci. Eng. A. (2017). https://doi.org/10.1016/j.msea.2016.11.098.

[68] A. Korneva, B. Straumal, R. Chulist, A. Kilmametov, P. Bała, G. Cios, N. Schell, P. Zięba, Grain refinement of intermetallic compounds in the Cu-Sn system under high pressure torsion, Mater. Lett. (2016). https://doi.org/10.1016/j.matlet.2016.05.059.

[69] M. Khajouei-Nezhad, M.H. Paydar, R. Ebrahimi, P. Jenei, P. Nagy, J. Gubicza, Microstructure and mechanical properties of ultrafine-grained aluminum consolidated by high-pressure torsion, Mater. Sci. Eng. A. (2017). https://doi.org/10.1016/j.msea.2016.11.076.

[70] A.R. Eivani, H.R. Mirzakoochakshirazi, H.R. Jafarian, Investigation of joint interface and cracking mechanism of thick cladding of copper on aluminum by equal channel angular pressing (ECAP), J. Mater. Res. Technol. (2020). https://doi.org/10.1016/j.jmrt.2020.01.075.

[71] R. Procházka, P. Sláma, J. Dlouhỳ, P. Konopík, Z. Trojanová, Local mechanical properties and microstructure of EN AW 6082 aluminium alloy processed via ECAP-conform technique, Materials (Basel). (2020). https://doi.org/10.3390/ma13112572.

[72] L. Winter, K. Hockauf, S. Winter, T. Lampke, Equal-channel angular pressing influencing the mean stress sensitivity in the high cycle fatigue regime of the 6082 aluminum alloy, Mater. Sci. Eng. A. 795 (2020). https://doi.org/10.1016/j.msea.2020.140014.

[73] K.M. Agarwal, R.K. Tyagi, K.K. Saxena, Deformation analysis of Al Alloy AA2024 through equal channel angular pressing for aircraft structures, Adv. Mater. Process. Technol. (2020) 1–15. https://doi.org/10.1080/2374068X.2020.1834756.

[74] G.M. Lule Senoz, T.A. Yilmaz, Optimization of Equal Channel Angular Pressing Parameters for Improving the Hardness and Microstructure Properties of Al–Zn–Mg Alloy by Using Taguchi Method, Met. Mater. Int. (2020). https://doi.org/10.1007/s12540-020-00730-9.

[75] M.J. Qarni, G. Sivaswamy, A. Rosochowski, S. Boczkal, Effect of incremental equal channel angular pressing (I-ECAP) on the microstructural characteristics and mechanical behaviour of commercially pure titanium, Mater. Des. (2017). https://doi.org/10.1016/j.matdes.2017.03.015.

[76] V.M. Segal, Materials processing by simple shear, Mater. Sci. Eng. A. (1995). https://doi.org/10.1016/0921-5093(95)09705-8.

[77] S. Upadhyay, K.K. Saxena, Effect of Cu and Mo addition on mechanical properties and microstructure of grey cast iron: An overview, in: Mater. Today Proc., 2019. https://doi.org/10.1016/j.matpr.2020.02.524.

[78] S. Kadiyan, B.S. Dehiya, Effects of severe plastic deformation by ECAP on the microstructure and mechanical properties of a commercial copper alloy, Mater. Res. Express. 6 (2019). https://doi.org/10.1088/2053-1591/ab4a44.

[79] Equal Channel Angular Pressing: A Novel Technique for the Production of Ultra Fine Grained Structure in Materials– A Mini Review, Int. J. Mod. Stud. Mech. Eng. (2017). https://doi.org/10.20431/2454-9711.0301002.

[80] N. Sadasivan, S. Madhu, M. Balasubramanian, Acute angle ECAP die with modification for punchless back pressure provider, in: Mater. Today Proc., Elsevier Ltd, 2020: pp. 1228–1232. https://doi.org/10.1016/j.matpr.2019.11.332.

[81] Y. Iwahashi, Z. Horita, M. Nemoto, T.G. Langdon, The process of grain refinement in equal-channel angular pressing, Acta Mater. (1998). https://doi.org/10.1016/S1359-6454(97)00494-1.

[82] P. Minárik, R. Král, J. Pešička, F. Chmelík, Evolution of mechanical properties of LAE442 magnesium alloy processed by extrusion and ECAP, J. Mater. Res. Technol. 4 (2015). https://doi.org/10.1016/j.jmrt.2014.10.012.

[83] M. Elhefnawey, G.L. Shuai, Z. Li, M. Nemat-Alla, D.T. Zhang, L. Li, On achieving superior strength for Al–Mg–Zn alloy adopting cold ECAP, Vacuum. (2020). https://doi.org/10.1016/j.vacuum.2020.109191.

[84] C. Xu, S. Schroeder, P.B. Berbon, T.G. Langdon, Principles of ECAP-Conform as a continuous process for achieving grain refinement: Application to an aluminum alloy, Acta Mater. (2010). https://doi.org/10.1016/j.actamat.2009.10.044.

[85] M.N. Gajanan, S. Narendranath, S.S.S. Kumar, Influence of ECAP processing routes on microstructure mechanical properties and corrosion behavior of AZ80Mg alloy, in: AIP Conf. Proc., American Institute of Physics Inc., 2019. https://doi.org/10.1063/1.5093834.

[86] S. Surendarnath, R. Subbiah, K. Sankaranarayanasamy, B. Ravisankar, Finite Element Simulation of Pure Aluminum Processed by ECAP Using New Die Design, in: Mater. Today Proc., Elsevier Ltd, 2017: pp. 2544–2553. https://doi.org/10.1016/j.matpr.2017.02.108.

[87] K.M. Agarwal, R.K. Tyagi, V. Saxena, K.K. Choubey, Mechanical behaviour of Aluminium Alloy AA6063 processed through ECAP with optimum die design parameters, Adv. Mater. Process. Technol. (2021). https://doi.org/10.1080/2374068X.2021.1878705.

[88] S.K. Iyappan, S. Karthikeyan, K. Ravikumar, S. Makkar, K. Rutvi Uday, M. R. V, Mechanical Properties and Machinability of Aluminium and Aluminium-Silicon Carbide Composites Processed by Equal Channel Angular Pressing (ECAP), Adv. Mater. Process. Technol. (2020). https://doi.org/10.1080/2374068X.2020.1833402.

[89] S. Sulaiman, J. Nemati, G.H. Majzoobi, M. AlJermi, Experimental and numerical study of high strain rate property of pure copper processed by ECAE method, Adv. Mater. Process. Technol. (2019). https://doi.org/10.1080/2374068X.2019.1616416.

[90] E. Damavandi, S. Nourouzi, S.M. Rabiee, R. Jamaati, J.A. Szpunar, EBSD study of the microstructure and texture evolution in an Al–Si–Cu alloy processed by route A ECAP, J. Alloys Compd. (2021). https://doi.org/10.1016/j.jallcom.2020.157651.

[91] S. Kadiyan, B.S. Dehiya, R.K. Garg, P. Kamiya, M. Saini, A Statistical Method to Predict the Hardness and Grain Size After Equal Channel Angular Pressing of AA-6063 with Intermediate Annealing, Arab. J. Sci. Eng. (2020). https://doi.org/10.1007/s13369-020-04999-1.

[92] S. Kadiyan, B.S. Dehiya, R.K. Garg, P. Kamiya, M. Saini, A Statistical Method to Predict the Hardness and Grain Size After Equal Channel Angular Pressing of AA-6063 with Intermediate Annealing, Arab. J. Sci. Eng. (2021). https://doi.org/10.1007/s13369-020-04999-1.

[93] T. Yuan, J. Jiang, A. Ma, Y. Wu, Y. Yuan, C. Li, Simultaneously improving the strength and ductility of an Al-5.5Mg-1.6Li-0.1Zr alloy via warm multi-pass ECAP, Mater. Charact. (2019). https://doi.org/10.1016/j.matchar.2019.03.043.

[94] Ö. Güler, N. Bağcı, S.H. Güler, C.A. Canbay, H. Safa, T.A. Yılmaz, M. Taşkın, The effect of equal-channel angular pressing (ECAP) on the properties of graphene reinforced aluminium matrix composites, J. Compos. Mater. (2020). https://doi.org/10.1177/0021998320979040.

[95] V.M. Segal, Equal channel angular extrusion: From macromechanics to structure formation, Mater. Sci. Eng. A. (1999). https://doi.org/10.1016/s0921-5093(99)00248-8.

[96] D.H. Shin, I. Kim, J. Kim, K.T. Park, Grain refinement mechanism during equal-channel angular pressing of a low-carbon steel, Acta Mater. (2001). https://doi.org/10.1016/S1359-6454(01)00010-6.

[97] Y.T. Zhu, T.C. Lowe, Observations and issues on mechanisms of grain refinement during ECAP process, Mater. Sci. Eng. A. (2000). https://doi.org/10.1016/S0921-5093(00)00978-3.

[98] H.S. Kim, P. Quang, M.H. Seo, S.I. Hong, K.H. Baik, H.R. Lee, D.M. Nghiep, Process modelling of equal channel angular pressing for ultrafine grained materials, in: Mater. Trans., 2004. https://doi.org/10.2320/matertrans.45.2172.

[99] P. Ponce-Peña, E. López-Chipres, E. García-Sánchez, M.A. Escobedo-Bretado, B.X. Ochoa-Salazar, M.A. González-Lozano, Optimized design of an ECAP die using the finite element method for obtaining nanostructured materials, Adv. Mater. Sci. Eng. (2015). https://doi.org/10.1155/2015/702548.

[100] V. V. Stolyarov, Y.T. Zhu, T.C. Lowe, R.Z. Valiev, Microstructure and properties of pure Ti processed by ECAP and cold extrusion, Mater. Sci. Eng. A. (2001). https://doi.org/10.1016/S0921-5093(00)01884-0.

[101] V. V. Stolyarov, Y. Theodore Zhu, I. V. Alexandrov, T.C. Lowe, R.Z. Valiev, Influence of ECAP routes on the microstructure and properties of pure Ti, Mater. Sci. Eng. A. (2001). https://doi.org/10.1016/S0921-5093(00)01411-8.

[102] M. Rifai, H. Miyamoto, H. Fujiwara, The Effect of ECAP Deformation Route on Microstructure, Mechanical and Electrochemical Properties of Low CN Fe-20%Cr Alloy,

Mater. Sci. Appl. (2014). https://doi.org/10.4236/msa.2014.58059.

[103] A. Yamashita, D. Yamaguchi, Z. Horita, T.G. Langdon, Influence of pressing temperature on microstructural development in equal-channel angular pressing, Mater. Sci. Eng. A. (2000). https://doi.org/10.1016/S0921-5093(00)00836-4.

[104] M.H. Shaeri, M. Shaeri, M. Ebrahimi, M.T. Salehi, S.H. Seyyedein, Effect of ECAP temperature on microstructure and mechanical properties of Al-Zn-Mg-Cu alloy, Prog. Nat. Sci. Mater. Int. (2016). https://doi.org/10.1016/j.pnsc.2016.03.003.

[105] A. Gupta, D. Kundalkar, K.K. Saxena, Investigation on deformation of Inconel alloy 751, Mater. Today Proc. (2021). https://doi.org/10.1016/j.matpr.2021.01.959.

[106] M. Vishnoi, S. Senthil Murugan, A.N. Veerendra Kumar, T.G. Mamatha, Analysis of plastic deformation of A16063, Magnesium AZ91C and commercially used Titanium alloys using ECAP, in: Mater. Today Proc., 2019. https://doi.org/10.1016/j.matpr.2019.08.185.

[107] H.S. Kim, M.H. Seo, S.I. Hong, Plastic deformation analysis of metals during equal channel angular pressing, in: J. Mater. Process. Technol., 2001. https://doi.org/10.1016/S0924-0136(01)00710-5.

[108] M.S. Ghazani, A. Fardi-Ilkhchy, B. Binesh, Finite element simulation of the T-shaped ECAP processing of round samples, Mater. Res. Express. (2018). https://doi.org/10.1088/2053-1591/aac1f4.

[109] M.F.X. Wagner, N. Nostitz, S. Frint, P. Frint, J. Ihlemann, Plastic flow during equal-channel angular pressing with arbitrary tool angles, Int. J. Plast. (2020). https://doi.org/10.1016/j.ijplas.2020.102755.

[110] J.P. Mathieu, S. Suwas, A. Eberhardt, L.S. Tóth, P. Moll, A new design for equal channel angular extrusion, J. Mater. Process. Technol. (2006). https://doi.org/10.1016/j.jmatprotec.2005.11.007.

[111] S. Wang, W. Liang, Y. Wang, L. Bian, K. Chen, A modified die for equal channel angular pressing, J. Mater. Process. Technol. (2009).

https://doi.org/10.1016/j.jmatprotec.2008.07.022.

[112] R.Z. Valiev, T.G. Langdon, Principles of equal-channel angular pressing as a processing tool for grain refinement, Prog. Mater. Sci. (2006). https://doi.org/10.1016/j.pmatsci.2006.02.003.

[113] X. Niu, C. Wang, K.C. Chan, H. Wang, S. Feng, Study of numerical simulation during ECAP processing of can based on smooth particle hydrodynamics, Complexity. (2019). https://doi.org/10.1155/2019/8373712.

[114] A. V. Nagasekhar, S.C. Yoon, J.H. Yoo, S.Y. Kang, S.C. Baik, M.I.A. El Aal, H.S. Kim, Plastic flow and strain homogeneity of an equal channel angular pressing process enhanced through forward extrusion, in: Mater. Trans., 2010. https://doi.org/10.2320/matertrans.M2009407.

[115] I. Balasundar, M. Sudhakara Rao, T. Raghu, Equal channel angular pressing die to extrude a variety of materials, Mater. Des. (2009). https://doi.org/10.1016/j.matdes.2008.06.057.

[116] H.S. Kim, Finite element analysis of equal channel angular pressing using a round corner die, Mater. Sci. Eng. A. (2001). https://doi.org/10.1016/S0921-5093(01)01188-1.

[117] M.I. Abd EL AAL, 3D FEM simulations and experimental validation of plastic deformation of pure aluminum deformed by ECAP and combination of ECAP and direct extrusion, Trans. Nonferrous Met. Soc. China (English Ed. (2017). https://doi.org/10.1016/S1003-6326(17)60155-9.

LIST OF PUBLICATIONS

[1] ***Akash Gupta,*** *K. K. Saxena. Ajaya Bharti, L. Jayahari, Kanwal Chadha, Prudvi Reddy Paresi,* ***"Influence of ECAP Processing Temperature and Number of Passes on Hardness and Microstructure of Al6063"****, Advances in Materials and Processing Technologies (T & F), 2021 (Accepted –In press),* ***Scopus Indexed Journal.***

[2] *Kuldeep K. Saxena, K. Basanth Kumar,* ***Akash Gupta****;* ***Effect of processing parameters on equal-channel angular pressing of aluminum alloys: An overview****, Materials Today: Proceedings, 2021, Vol 45, Part 6, Pages 5551-5559, https://doi.org/10.1016/j.matpr.2021.02.303.*

[3] ***Akash Gupta****, Balla Chandrasekhar, Kuldeep K. Saxena;* ***Effect of Equal-channel angular pressing on mechanical Properties: An Overview,*** *Materials Today: Proceedings, 2021, Vol. 45, Part 6, Pages 5602-5607, https://doi.org/10.1016/j.matpr.2021.02.317*

[4] ***Akash Gupta,*** *Deepak Kundalkar, Kuldeep K. Saxena;* ***Investigation on deformation of Inconel alloy 751****, Materials Today: Proceedings, 2021, Vol 45, Part 6, Pages 5377-5380, https://doi.org/10.1016/j.matpr.2021.01.959*

MINI RESEARCH PROJECT REPORT

ON

"STUDY OF WORKING CAPITAL MANAGEMENT OF DOMINOS PIZZA, INC"

SUBMITTED TO

"BACHELOR OF BUSINESS ADMINISTRATION" (HONOURS)"

Session 2021-22

Submitted by:

PRASHANT GOYAL

Student of BBA (H)

Roll No.:194700072

Supervised by:

DR. PRATEEK KUMAR BANSAL

Asst. Professor -Dept. of Mgmt

GLA University, Mathura

GLA UNIVERSITY
MATHURA

Accredited with A Grade by NAAC

CERTIFICATE

This is to certify that the mini research project report entitled **"A STUDY ON WORKING CAPITAL MANAGEMENT"**, is submitted by Mr./Ms **PRASHANT GOYAL**, student of **BBA (H)** of "Institute of Business Management", GLA University, Mathura, under my supervision for the Session 2020-21.

Place: Mathura

(DR. PRATEEK KUMAR BANSAL)

Name & Signature of Supervisor

DECLARATION

I **Prashant Goyal,** student of BBA (H) Session 2020-21, Batch 2019-22 hereby declare that my work entitled **"Study of working capital management of Domino's Pizza, Inc."** is the outcome of genuine efforts done by me under the able guidance of **Dr. Prateek Kumar Bansal**. and being submitted to "Institute of Business Management", GLA University, Mathura as Mini research project report for the session 2020-21.

Place: Mathura

Date: .....

Prashant Goyal

Name: PRASHANT GOYAL

Course: BBA (H)

University Roll No.194700072

3

TABLE OF CONTENTS

Chapter-1

About the Company

As of 1997 Domino's Pizza, Inc. was the largest pizza delivery company in the world and the world's second largest pizza chain, behind Tricon Restaurant Group's Pizza Hut. Dominos had 4,431 pizza delivery stores in the United States and more than 1,521 units in 59 foreign countries by the end of 1997. Its 1997 sales were $3.16 billion, earning Domino's a place as the two-hundredth largest private company on the *Forbes* Private 500 list. Domino's sells a variety of pizza products, including deep-dish, pan, and thin-crust pizzas, as well as specialty items such as flavored-crust pizzas.

In 1997 Domino's sold over 325 million pizzas, with pepperoni being the most popular topping. The chain used over 27 million pounds of pepperoni that year, as well as over 174 million pounds of part-skim mozzarella cheese and over 3 million pounds of pizza sauce, among other ingredients.

COMPANY FINANCES

Following several difficult years, Domino's annual sales have risen steadily since 1993: $2.2 billion in 1993; $2.5 billion in 1994; $2.6 billion in 1995; and $2.8 billion in 1996. In 1996 the firm saw a 2-percent increase in sales at stores open more than one year. By the end of 1997 Domino's had achieved record sales of almost $3.2 billion, a 14.3-percent increase over 1996. (Because Domino's is a privately held company, it does not issue stock to the public.)

HISTORY

Domino's traces its roots to 1960, when Tom Monaghan and his brother, James, purchased "DomiNick's," a pizza store in Ypsilanti, Michigan. Monaghan borrowed $500 to buy the store, and in 1961 James traded his half of the business to Tom in exchange for a Volkswagen Beetle automobile. Tom Monaghan established the pizza business to support himself while he studied to be an architect. Soon after, however, he dropped out of school to build the business.

By 1965 Tom Monaghan was the sole owner of the company, and he renamed the enterprise Domino's Pizza, Inc. As Domino's grew, its success was attributed to a simple but powerful idea: Monaghan, who had been raised in Catholic orphanages and foster homes, believed that people who ordered pizzas were hungry. To keep them happy a company must not only deliver pizzas, but promise fast delivery. Dominoes went on to guarantee pizza delivery in 30 minutes or less.

That 30-minute delivery philosophy began to blossom in the mid- to late 1970s. In 1967 the first Domino's Pizza franchise store was opened in Ypsilanti, Michigan. The franchising concept helped to dramatically accelerate the company's growth. In 1978 the two-hundredth Domino's store opened, and in 1983 Domino's opened its first international store in Winnipeg, Canada. In that same year the 1,000th Domino's store opened. In 1985 Domino's opened 954 new units, making a total of 2,841.

In 1989 Monaghan stepped down as Domino's president for two years to devote himself to philanthropic work. According to some press reports, the company did not do well during that time, but after Monaghan's return the company was able to restore profitability. In 1992 Domino's began the national roll-out of bread sticks, the company's first national non-pizza menu item. In 1993 Crunchy Thin Crust Pizza was introduced nationwide. In that same year the company dropped its 30-minute delivery guarantee in corporate stores following highly publicized accidents involving Domino's delivery drivers.

In 1994 the first Domino's store in eastern Europe opened in Warsaw, Poland. In that same year the first agreement to develop Domino's in an African country was signed by Specialized Catering Services, Inc. In 1995 Domino's Pizza International division opened its one-thousandth store.

STRATEGY

Domino's basic business strategy has been to offer a limited menu through carryout or delivery only. Until 1992 the company's outlets offered just two products: Domino's Traditional Hand Tossed Pizza and Coca-Cola. Beginning in 1992, however, Domino's began to expand its menu options; during the next five years it added bread sticks, Ultimate Deep Dish Pizza, Crunchy Thin Crust Pizza, Buffalo Wings, Roma Herb Crust Pizza, Garlic Crunch Crust, and Pesto Crust Pizza.

In addition to its corporately owned stores, Domino's operates an extensive franchise network, with independent owners operating Domino's stores. According to the company, over 90 percent of its 1,200 franchisees started with the company as drivers. The company's franchising system provides ownership opportunities only to qualified internal candidates, as of the late 1990s. A candidate is required to have successfully managed and/or supervised a Domino's store for one year, and must have also completed required training courses. External candidates are not considered for full franchise status; however, external investors, approved by Domino's, can become 49-percent owners in a franchise supporting an internal candidate.


Domino's Pizza
Domino's Pizza

About Domino's Pizza, Inc..

- **Ownership:** Domino's Pizza, Inc. is a privately owned company.
- **Officers:** Thomas Monaghan, Pres. & Chmn.; Cheryl A. Batchelder, VP, Marketing & Product Development; Harry Silverman, CFO & VP, Finance & Administration
- **Employees:** 170,000 (1997 est.)
- **Principal Subsidiary Companies:** Domino's Pizza, Inc. operates about 6,000 stores in the United States and 60 other countries. Its main subsidiary is Domino's Pizza International, Inc.
- **Chief Competitors:** Major competitors include the many other pizza chains and fast-food operations in the United States and elsewhere, such as: Bertucci's; Little Caesar's; Papa Gino's; Pizza Hut; and McDonald's.

Chapter-2

Introduction to the topic, Importance & Objectives

Working capital (abbreviated **WC**) is a financial metric which represents operating liquidity available to a business, organization, or other entity, including governmental entities. Along with fixed assets such as plant and equipment, working capital is considered a part of operating capital. Gross working capital is equal to current assets. Working capital is calculated as current assets minus current liabilities. If current assets are less than current liabilities, an entity has a **working capital deficiency**, also called a **working capital deficit** and **Negative Working capital**.

1.1 Classification OF WORKING CAPITAL

Working capital is classified in two ways:

- On the premise on idea
- On the premise of time.

- Based on idea working capital can be named net working capital and net working capital. Based on time, working capital might be named:

- ☐ Permanent or settled working capital.
- ☐ Temporary or variable working capital

Permanent OR FIXED WORKING CAPITAL

Changeless or settled working capital is least sum which is required to guarantee compelling usage of settled offices and for keeping up the course of current resources. Each firm needs to keep up a base level of crude material, work-in-process, completed merchandise and money adjust. This base level of current assets is called changeless or settled working capital as this piece of working is for all time obstructed in current resources. As the business develop the prerequisites of working capital additionally increments because of increment in current resources.

Temporary OR VARIABLE WORKINGCAPITAL

Variable working capital is the measure of working capital which is required to meet the regular needs and some extraordinary situations. Variable working capital can additionally be named regular working capital and exceptional working capital.

ADVANTAGE OF ADEQUATE WORKING CAPITAL

- ***Cash Discounts:***

Sufficient working capital provides a firm to avail to cash discounts on the purchases and hence reduces cost.

- ***Regular Payment of Salaries, Wages and Other Day TO Day Commitments:***

It leads to the satisfaction of the employees and raises the morale of its employees, increases their efficiency, reduces wastage and costs and enhances production and profits.

- ***Exploitation of Favorable Market Conditions:***

In case firm is having sufficient working capital then it can get the favorable market conditions

- ***Ability to Face Crises:***

A concern can face the situation during the depression.

- ***Quick and Regular Return on Investments:***

Sufficient working capital provides a concern to pay quick and regular dividends to its holders and gains confidence of the investors.

INADEQUATE WORKING CAPITAL

Each business concern difficult to have satisfactory measure of working money to maintain its business activities. It ought to have neither repetitive or overabundance working capital nor insufficient. Both overabundance and short working capital positions are terrible for any business.

Hindrances of REDUNDANT OR EXCESSIVE WORKING CAPITAL-

Excessive working capital means perfect assets which procure no benefit for the firm and business can't win the required rate of profit for its ventures.

Redundant working capital prompts pointless acquiring and gathering of inventories.

Excessive working capital suggests unnecessary borrowers and blemished credit strategy which causes higher frequency of awful obligations.

WORKING CAPITAL ANALYSIS

As we know working capital is the life blood of the business. Sufficient amount of working capital is very much essential for the smooth running of the business. The Hence a study of changes in its uses of working capital is necessary to evaluate the efficiency with which the working capital is employed in a business. This involves the need of working capital analysis.

The analysis of working capital can be conducted through a number of devices, such as:

1. Ratio analysis.
2. Fund flow analysis.
3. Budgeting.

MANAGEMENT OF WORKING CAPITAL

Guided by the above criteria, management will use a combination of policies and techniques for the management of working capital. The policies aim at managing the *current assets* (generally cash and cash equivalents, inventories and debtors) and the short-term financing, such that cash flows and returns are acceptable.

- **Cash management**. Identify the cash balance which allows for the business to meet day to day expenses, but reduces cash holding costs.
- **Inventory management**. Identify the level of inventory which allows for uninterrupted production but reduces the investment in raw materials—and minimizes reordering costs—and hence increases cash flow. Besides this, the lead times in production should be lowered to reduce Work in Process (WIP) and similarly, the Finished Goods should be kept on as low level as possible to avoid overproduction—see Supply chain management; Just In Time (JIT); Economic order quantity (EOQ); Economic quantity
- **Debtor's management**. Identify the appropriate credit policy, i.e. credit terms which will attract customers, such that any impact on cash flows and the cash conversion cycle will be offset by increased revenue and hence Return on Capital (or *vice versa*); see Discounts and allowances.
- **Short-term financing**. Identify the appropriate source of financing, given the cash conversion cycle: the inventory is ideally financed by credit granted by the supplier; however, it may be necessary to utilize a bank loan (or overdraft), or to "convert debtors to cash" through "factoring".

Chapter - 3

Research Methodology

Vision and mission:

Vision:

- Our vision is to lead the internet of food in every neighborhood.

Mission:

- Our mission is to redefine convenience by creating inspired food, picked up in three minutes or safely delivered in 10.

Values:

- Treat people as you'd like to be treated.
- Produce the best for less.
- Measure, manage and share what's important.
- Think big and grow.
- Incentivize what you want to change.
- Set the bar high, train, never stop learning.
- Promote from within.
- We are not ordinary, we are exceptional.

SWOT ANALYSIS OF Dominos

STRENGTHS:

Brand Recall: High brand recall due to its regular advertising with taglines such as '30 minutes nahi to free'. Such aggressive marketing has created awareness & a promise for the brand in the market.

Fantastic channel network: With its 9000 franchise & company owned outlets Dominos has extensive network spread over more than 60 countries.

Quick service & deep menu: Quicker than expected service delights the consumers and helps the company to differentiate itself from others. In India Domino's is trying to attract the middle class and lower middle class people who are interested to spend their money on pizza but in low price. Those people are eager to go for an outing in any festival and want cheap and best family restaurant. Domino's would be most preferable.

Low cost alternative: They do not need high class Ambiance or amusement in the shop so the establishment cost is low for the dealers and the price of pizza is very reasonable for the customers.

Healthier alternatives: To combat health awareness among consumers, Dominos is trying to change their dough by having healthier fats, which is done by incorporating more whole wheat into their crusts. The pizza toppings are also becoming healthier, and some pizzerias are introducing salads into their menus.

Efficient supply chain: Due to its efficient supply chain Dominos has made it possible for quicker service so that customers don't have to wait for long. The preference of Dominos is because the customer can have home delivery within 30 minutes. Making a small breakfast at home itself takes 15 minutes.

WEAKNESS:

Operations: Large number of franchised outlets results in difficulty in handling operations. Quality control too becomes challenging. Due to this, some of the Domino's outlets got closed affecting the image of the brand.

Decreasing sales in mature markets: Due to rise in health-conscious population there is decrease in revenue affecting the business as a whole.

Low staff retention: High attrition due to the absence of proper training & development is a major challenge for Dominos. Plus the manpower employed is also unskilled so they quickly change jobs when they cannot adjust to the hectic environment.

Lesser number of eateries: Dominos has more delivery outlets then eating joints which is a problem especially in places like malls and other locations where clearly customers want a sitting place

OPPORTUNITIES:

Market Expansion: Expanding to the developing markets will be beneficial as far as Pizza industry is concerned, as developed markets are maturing. Targeting the developing economies should be the future strategy of the company.

Penetration: Strengthening its outlet network by further penetrating the current market will help Dominos to increase its revenues.

Health-conscious eatables: Introducing health-conscious menu with new flavor additives which is low in fat will result in increasing it revenues in future.

Restaurants: By introducing exclusive Domino's restaurants in cream areas will help the brand with more brand recognition and will also help in getting the customers who like to eat outside in plush restaurants.

THREATS:

Direct and Indirect Competition: Intensive competition from the local & national players like “Pizza hut”, US pizza and more. In fact, Indirect competition is more from the likes of McDonalds and KFC wherein customers prefer burgers over pizza.

Changing Consumer eating habits: With government & NGO’s concentrating more on health awareness, people are becoming more aware of what to consume & what to avoid which is affecting the business of Dominos.

Cost: As the cost of vegetables and raw materials rises, the cost of maintaining the pizza chain also goes up. Plus, competition affects the bottom line of the company. Thus, managing the cash flow becomes difficult.

Topic chosen for the study: Study on working capital management of Domino’s Pizza Inc.

Working capital, otherwise called net working capital, is the distinction between a company's current resources, similar to money, records of sales (clients' unpaid bills) and inventories of crude materials and completed products, and current liabilities, similar to creditor liabilities.

Working Capital = Current Assets - Current Liabilities

In the event that an organization's present resources don't surpass its present liabilities, at that point it might experience difficulty paying back loan bosses or go bankrupt. A declining working capital proportion is a red flag for budgetary experts. They may likewise take a gander at the quick proportion, which is a greater amount of a basic analysis of here and now liquidity since it just incorporates money and money counterparts, attractive ventures and records receivable.

OBJECTIVES OF STUDY:

- ✓ To know liquidity position
- ✓ To see how day to day operations in the company take place
- ✓ To know cash position in the company

IMPORTANCE OF WORKING CAPITAL MANAGEMENT

- ✓ To know liquidity position
- ✓ To know solvency position
- ✓ For day-to-day operation

SCOPE OF THE STUDY:

- ✓ For day to operation
- ✓ To meet its debts
- ✓ To increase sales targets

Chapter-4

Data Analysis and Interpretation

Working Capital is likely to drop to about 305.3 **M** in 2021. Invested Capital is likely to drop to about 4.4 **B** in 2021.

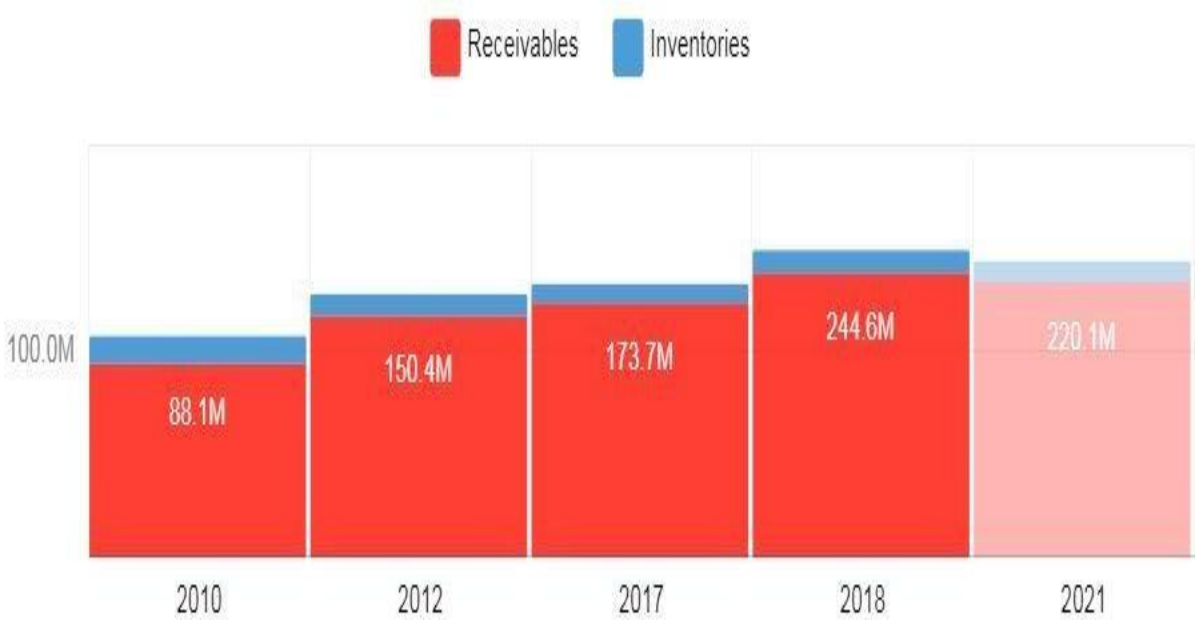

Dominos Working Capital Analysis

Dominos Pizza's Working Capital is a measure of company efficiency and operating liquidity. The working capital is usually calculated by subtracting Current Liabilities from Current Assets. It is an important indicator of the firm ability to continue its normal operations without additional debt obligations.

Current Domino’s Pizza Working Capital

Most of Dominos Pizza's fundamental indicators, such as Working Capital, are part of a valuation analysis module that helps investors searching for stocks that are currently trading at higher or lower prices than their real value. If the real value is higher than the market price, Domino’s Pizza is considered to be undervalued, and we provide a buy recommendation. Otherwise, we render a sell signal.

Dominos Working Capital Driver Correlations

Understanding the fundamental principles of building solid financial models for Domino’s Pizza is extremely important. It helps to project a fair market value of Ford stock properly, considering its historical fundamentals such as Working Capital. Since Dominos Pizza's main accounts across its financial reports are all linked and dependent on each other, it is essential to analyze all possible correlations between related accounts. However, instead of reviewing all of Dominos Pizza's historical financial statements, investors can examine the correlated drivers to determine its overall health. This can be effectively done using a conventional correlation matrix of Dominos Pizza's interrelated accounts and indicators.

Working Capital Historical Pattern

Today, most investors in Domino’s Pizza Stock are looking for potential investment opportunities by analyzing not only static indicators but also various Dominos Pizza's growth ratios. Consistent increases or drops in fundamental ratios usually indicate a possible pattern that can be successfully translated into profits. However, when comparing two companies, knowing each company's working capital growth rates may not be enough to decide which company is a better investment. That's why investors frequently use a static breakdown of Domino’s Pizza working capital as a starting point in their analysis.

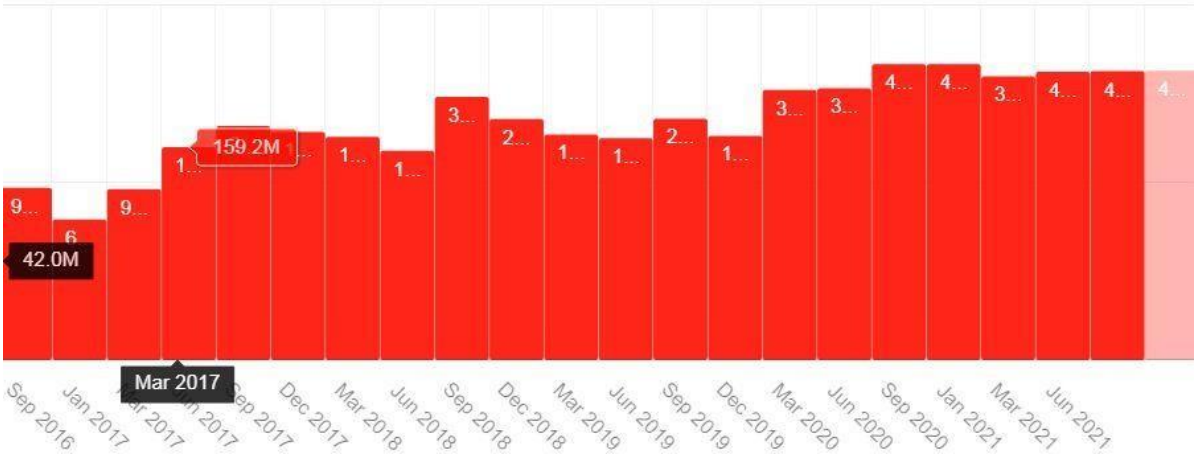

Chapter -5

Findings, Suggestion and Conclusions

FINDINGS:

- **TO KNOW LIQUIDITY POSITION**

Liquidity ratios

Liquidity ratios show the ability of an organization to maintain positive cash flow while satisfying immediate obligations, that is, the availability of cash to pay current debt. It is necessary to maintain optimal liquidity ratios since either low or very high ratios are not favorable (Holmes & Sugden 2008, p. 76). The table below summarizes the liquidity ratios of the company for the past one year.

The current ratio of the company was 1.322. This implies that the current liabilities can be paid off using current assets. However, the quick ratios were quite low. This implies that the current liabilities cannot be paid off using quick assets.

Profitability Ratio

Profitability ratios indicate the earning capacity of an entity. The ratios measure the effectiveness of a company in meeting the profit objectives both in the long run and short run. The ratios show how well a company employs its resources to generate returns. Commonly used profitability ratios comprise of gross profit margin, operating profit margin, net profit margin, the return on asset ratio, and the return on equity. The table below summarizes the profitability ratios of the company for the past one year.

S.NO	Profitability ratios	2012
1	Gross profit margin	36.59%
2	Operating profit margin	17.74%
3	Net profit margin	12.60%
4	Return on assets	16.67%
5	Return on equity	43.09%

TO KNOW CONVERSIONCYCLE

- Domino's Pizza's latest twelve months cash conversion cycle is 15 days.
- Domino's Pizza's cash conversion cycle for fiscal years ending January 2017 to 2021 averaged 11 days.
- Domino's Pizza's operated at median cash conversion cycle of 11 days from fiscal years ending January 2017 to 2021.
- Looking back at the last five years, Domino's Pizza's cash conversion cycle peaked in September 2021 at 15 days.
- Domino's Pizza's cash conversion cycle hit its five-year low in January 2017 of 6 days.
- Domino's Pizza's cash conversion cycle decreased in 2017 (6 days, -12.1%) and increased in 2017 (8 days, +42.4%), 2018 (11 days, +36.3%), 2019 (13 days, +16.7%) and 2021 (15 days, +15.9%).

.

SUGGESTION:

Aletrnative-1: Expanding International Brick and Recommendations of Domino's Pizza: Strategies to Tackle Global Economic Slowdown Case Help Stores

Alternative-2: Introduction of Click and Recommendations of Domino's Pizza: Strategies to Tackle Global Economic Slowdown Case Solution Stores

Alternative-3: Expansion towards International Markets Without closing Domestic Stores

CONCLUSION:

- ✓ Company is performing very effectively which is reflected in the study.
- ✓ With use of advanced technologies in its area, company is providing quality products to its customers.

PROJECT REPORT

on

Phytochemical analysis, Antimicrobial efficacy of leaves of Murraya koenigii (Curry tree)

SUBMITTED TO

DEPARTMENT OF BIOTECHNOLOGY GLA UNIVERSITY, MATHURA

IN PARTIAL FULFILMENT OF THE REQUIREMENTS FOR THE AWARD OF DEGREE IN "BACHELOR OF SCIENCE (HONS.) BIOTECHNOLOGY

SUBMITTED BY

PRAVESH SINGH

B.Sc. (Hons.) Biotechnology (VI Semester)

UNDER THE SUPERVISION OF

Dr. Alok Bhardwaj

Associate Professor Department of Biotechnology G.L.A. University, Mathura

GLA UNIVERSITY
MATHURA
Recognised by UGC Under Section 2(f)

Accredited with A Grade by NAAC

CERTIFICATE

This is to certify that **PRAVESH SINGH** of **B.Sc (H) Biotechnology** has carried out the Project work entitled **"Study of phytochemical analysis and antimicrobial efficacy of leaves of Murray koenigii (curry leaves)"** for the award of B.Sc (H) Biotechnology from Institute of Applied Science and Humanities, GLA University, Mathura under my supervision during session 2020-2021.

Her conduct during this project duration was satisfactory.

(PRAVESH SINGH)

Signature of Student

(Dr. Alok Bhardwaj)

Signature of Supervisor

Date – 15-03-2021

DECLARATION

I, the undersigned hereby declaring that the project report entitled "**Phytochemical analysis, Antimicrobial efficacy of leaves of Murraya koenigii (Curry tree)"** written and submitted by me to the GLA University, Mathura in partial fulfillment of the requirement for the award of degree in "Bachelor of Science (Hons.) biotechnology" under the guidance of Dr. Alok Bhardwaj sir. Further, I declare that I have done my work sincerely and accurately and the conclusions drawn therein are based on the material collected by myself even then if a mistake or an error has crept in, I shall mostly humbly like the readers to point out my errors and guide me for their removal.

PRAVESH SINGH

B.Sc. (Hons.)
BIOTECHNOLOGY GLA
UNIVERSITY

ACKNOWLEDGEMENTS

"It is not possible to prepare a project report without the assistance & encouragement of other people. This one certainly no exception."

Presentation, inspiration, and motivation have always played a central role in any venture's success.

At the very outset of this project. I would like to extend my sincere & heartfelt obligation towards all the personages who have helped me in this endeavor. Without their active guidance, help, corporation & encouragement I would not have made my head away in the project.

First, I would like to express my salutation to **GOD** for giving me the strength, confidence, and morale boost to the successful completion of this report.

Secondly, I earnest wish to express my deepest feeling of gratitude originate from the innermost core of my heart for my internal supervisor **Dr. Alok Bhardwaj** (Associate professor) at the Department of Biotechnology of GLA University, Mathura for his unflinching interest and supervision through provoking discussions and meticulous guidance which enhanced my learning**.**

I'd love to express my sincere thanks and gratitude to **Prof. A.K. Gupta** (Director) GLA University, Mathura.

It is my privilege to express our sincerest regards to our Head of Department, **Dr Shoor Vir Singh,** GLA University, Mathura, INDIA who continuously supporting and helping me.

I'd love to give my humble thanks to all my teachers for providing me, encouragement, guidance, knowledge, timely help me for my entire B.Sc., I would like to express my sincere thanks and gratitude to, **Dr. Vishal Khandelwal**, **Dr. Ajana Goel, Mr. Aditya Saxena, Dr Pradeep Chaudhary, Dr Saurabh Gupta, Dr Kundan Chaubey, Dr Gaurav Pant, Dr Rama Sharma, Mrs. Anuja Mishra, Miss. Preetipal, Mr. Sunil Shakya**, GLA University, Mathura. I just want to thank my friends for their enthusiastic company and assistance during my project. Words fail to express my profound regards to my family members for their affection, encouragement, cooperation, and blessings. Last but not least, for me to my parents are an important inspiration. So, I express my thanks to them with due respect.

PRAVESH SINGH

CONTENT

List of Abbreviations

1. DMSO – Dimethyl Sulfoxide
2. H_2SO_4 – Sulphuric acid
3. $FeCl_3$ - Ferric Chloride
4. Conc. – Concentrated
5. EtOH – Ethyl Alcohol
6. DPPH – 2,2-diphenyl-1-picrylhydrazyl
7. DW – Distilled Water
8. NaOH – Sodium hydroxide
9. MCF- 7 - Michigan Cancer Foundation-7
10. IC50- Half-maximal inhibitory concentration
11. PMK- Petroleum ether extract of Murraya koenigii leaves
12. AMK- Alkaloids separated from petroleum ether extract of Murraya koenigii leaves

13.FBG- Fasting blood glucose

14.TC- Total cholesterol

15.TG- triglycerides

16.HDL- High density lipoprotein

17.SGOT- Serum glutamic oxaloacetic transaminase

18.SGPT- Serum glutamic pyruvic transaminase

LIST OF FIGURES

INTRODUCTION

Murraya koenigii (L.) Spreng. the plant belongs to the family Rutaceae. It is generally known as Kadipatta in Hindi and Curry leaves in English. It is a traditional product widely used as spice and condiment and scrutiny of the literature reveals some notable pharmacological activities of the plant. It is widely distributed over tropical to sub-tropical regions and native to Asia. Among the 14 global species belonging to the genus Murraya, only two, M. koenigii and M. paniculate are available in India.

Basic Morphology of M. koenigii-

Murraya koenigii is a semi-deciduous, unharmed aromatic smell spreading shrub or tree with strong woody stem but slender with the stem which is dark green to brownish, the tree is 4- 8.7 m (13-31 feet) tall, with a trunk up to 81 cm diameter. The diameter of the main stem is 16 cm. In stature cultivated for leaves and hence for roots, stem and bark and seeds because of their traditional medicinal use.[1]

PLANT PARTS WITH THEIR BASIC MORPHOLOGY:

Leaves: Curry leaves are aromatic in nature having a characteristic aroma, leaves of curry leaves are shiny and smooth with paler undersides. Leaves are pinnate, exstipulate, having reticulate venation, and having ovate-lanceolate with an oblique base, with 11-21 leaflets whose size description in each leaflet is 0.79-1.57 inch long & 0.39-0.79 inch broad.

Leaflets are short-stalked alternate gland-dotted and having 0.5cm long petiole. The leaf margins are irregularly serrate. They yield of a bush in approx. found about 480 g in three to four pickings.[2]

Bark: The stem and bark of Murraya keonigii are brown to dark green, with dots on the bark like a small node on it when the bark was peeled of longitudinally under the exposing the white wood underneath; the girth of the main stem is 16cm up to 6 m in height and 15-40cn in diameter.[2]

Flowers: The flowers of curry leaves are small, white fragrant and funnel-shaped, regular, pentamerous, stalked, complete, ebracteate, hypogynous, persistent, inferior, green, corolla, polypetalous, androecium, polyandrous, lanceolate, stigma, bright, sticky, style, short, ovary, inflorescence, a terminal cyme, the diameter of a flower is 1.12cm in fully opened form. The curry tree flowers have a sweet fragrance, bisexual with self- pollination.

Murryaya koenigii (curry leaves) leaves are used as an anti-helminthics, analgesics and digestives, and appetizer in Indian cookery.

M. koenigii (curry leaves) oil used in regular skin care cream or lotion helps by applying it on the affected area to cure skin problems such as pimples, athlete's foot, ringworm, itches, acne, boils and septic of wounds, and burns [2][3]

Murraya koenigii (curry leaves) contains several medically active constituents including a glycoside called koenigine, essential oil, and tannins. It is a warming, strongly aromatic herb that improves appetite and digestion.[3]

The essential oil extracted from *Murraya koenigii (curry leaves)* leaves is utilized in the soap and cosmetic industry for aromatherapy

The medicinal properties of *M. koenigii (curry leaves)* have been accredited to several chemical constituents of different carbazole alkaloids and other important metabolites, like terpenoids, flavonoids, phenolics, carbohydrates, carotenoids, vitamins, and nicotinic acid from different parts of the *M. koenigii* plant.[3][4]

Phytochemical screening of *Murraya koenigii (curry leaves)* leaves shows the presence of some vitamins, phenolic compounds, terpenoids, carbazole alkaloids, and mineral contents such as zinc, calcium, iron, and vanadium, etc.

The pharmacological investigation revealed that Murraya koenigii (curry leaves tree) possess anti-oxidative, hepatoprotective, antimicrobial, antifungal, anti-inflammatory, and nephroprotective activities, anti-diabetic, anti-amnesic, anti-diarrheal, anti-analgesic, anti-inflammatory, anti-pyretic, and several protective effects.

Table 1- Scientific Taxonomical Classification of *M. koenigii*

Kingdom	Plantae
Sub-kingdom	Tracheabionta
Super-division	Spermatophyta
Division	Magnoliophyta
Class	Magnoliospida
Sub-class	Rosidae
Order	Sapindales
Family	Rutaceae
Genus	Murraya
Species	Murraya Koenigii L. Spreng.

Table 2- Common names of *M. koenigii*-

Sanskrit	Girinimba, Surabhinimba
Hindi	Kari patta, Meetha neem
English	Curry leaf
Gujarati	Mitho limbdo
Marathi	Kudianim
Spanish	Hojas de curry
German	Curryblatter
French	Feuille de curry
Tamil	Kaṟivēppilai
Telugu	Karivēpāku

Fig.1- Murraya koenigii plant

1.3 Various uses of plant *M. koenigii*-

There are various studies and biological and microbiological experiments that have shown different and diverse properties and use of the plant M. koenigii. And on the other hand, making it a medicinal and economically important plant. The plant, on the whole, is an ethnomedicinal plant used cosmetically as well as medicinally for decades. The different parts of the plant are used for different medicinal and other uses. Some of the plant parts are listed with their significant uses:

1) Leaves:

They are the parts, that are directly exposed to the sunlight. They also play a vital role in the medical field and in the cosmetic field too, such as:

- Anti-diabetic
- Anti-anemic
- Analgesic
- Anti-Ulcer and purgative
- For flavoring and seasoning
- Cure Bruises and Eruption [4][8]

2) Roots:

The root is a centrally important part of the plant plays a key role in the following medical issues:

- Anti-helminthic
- Cooling agent
- Reduces Inflammation, itching
- To cure Kidney pain, Leukoderma, Blood disorders [5]

3) Stem, bark, and fruit:

Stem, bark, and fruits eventually important part of the plant also play a necessary role in the following medical role:

- Used as Datum for cleaning, strengthen gums, and teeth (stem)
- Hair tonic, Stomachic and Carminative (bark)
- Astringent (fruits) [5][8]

4) Whole plant:

The whole plant is used to cure many human ailments. The ethnobotanical profile shows the following uses:

- Used as Stimulant
- Hair tonic, Blood purifier
- Antidepressant, Antidysentery, Antidiarrheal, Antifungal, Anti-inflammatory
- To cure Diabetes mellitus, Leucoderma, Body aches, Kidney pain, Vomiting.[6][8]

Objective

- Phytochemical analysis of Murraya koenigii.
- Anti-microbial activity of leaves extract of Murraya koenigii.

Review of Literature

2.1- PHYTOCHEMISTRY-

Various phytochemical components in different parts of *Murraya koenigii* are: -

- **Root:** - The roots are analyzed and reported to contain murrayanol, murrayagetin and marmesin-1"-O-rutinoside, three monomeric and five binary carbazole alkaloids named mukoenine-A, B, C and murrastifoline-F, and also found to contain girinimbine, koenoline (1- methoxy-3- hydroxy methyl carbazole). [7][9]

- **Stem: -** The plant stem contains the carbazole alkaloids such as murrayacine, murrayazolidine, murrayazoline, mahanimbine, girinimbine, koenioline and xynthyletin, coumarin galactoside, Carbazole carboxylic acid, glycolipids, Phospholipids, etc. [11]

- **Leaves: -** Murraya koenigii leaves have following compounds- [15][12][13][32][33]

a) **Phenolic compound**- compound 1, C30H50, identified as squalene. Compound 2, C29H50O, mp 134–136°C, identified as β-sitosterol. Compound 3, C29H48O, identified as stigmast-4-en-3-one. Compound 4, C15H26O, mp 60–62°C, identified as selin11-en-4α-ol. Compound 5, C10H12O4, mp 187–188°C, identified as 2-hydroxy-4-methoxy-3,6-dimethylbenzoic acid. Compound 6, C29H50O2, colorless oil. α 25 D +16.0° (c 0.02, CH3OH). UV (CH3OH, λmax, nm): 225, 254, 268, 288. IR (CH3OH, νmax, cm–1): 3327, 1452. HR-ESI-MS m/z 430.2458 [M]+.

b) **Flavonoids**- The UHPLC chromatogram of the identified flavonoid compounds from the curry leaf extract catechin, myricetin and quercetin.

c) **Essential Oils**- *M. koenigii* oil contained 39 compounds of which the major is 3-carene (54.2%) followed by caryophyllene (9.5%). Oil *M. paniculate* contained 58 compounds of which the major is caryophyllene oxide (16.6%), b-caryophyllene (11.8%), spathulenol (10.2%), b-elemene (8.9%), germacrene D (6.9%) and cyclooctene, 4-methylene-6-(1-propenylidene) (6.4%).

Many other phytochemical compounds are reported and are specifically extracted from either the plant part or found commonly in whole of the plant.

2.2 -PHARMACOLOGICAL PROFILE

2.2.1 Antibacterial activity

Different extracts such as ethanolic, aqueous Murraya koenigii leaves were examined for the determination of the inhibition of the growth of different strains of Gram-negative as well as Gram-positive bacteria using the Disc Diffusion assay method. The result demonstrated that all the extracts possessed antibacterial activity against all the bacterial strains on which they were tested upon. The leaf extract of Murraya keonigii showed antibacterial activity against 4 bacterial strains i.e., *E. coli, S. aureus, B. subtelis, and P. aeruginosa* by the method of disc diffusion. The concentration of the extract used in the experiment was 30 mg/disc.

The 3 carbazole alkaloids viz. mahanine, mahanimbicine, and mahanimbine and essential oils from the leaves of *Murraya koenigii* were evaluated for the effects on the growth of five antibiotic-resistant pathogenic bacteria and three tumor cell lines (MCF-7, P388, and Hela). Mahanimbine and essential oil demonstrated potent dose-dependent antibacterial and cytotoxic effects (<=5.0 micro gm/mL). Additionally, significant antitumor activities against MCF- 7, Hela, and P388 cell lines were also noted.[24]

2.2.2 Antioxidant Activity

This property of this plant was studied using the DPPH assay. The antiradical and DNA protective activity of this plant's leaves were investigated in an in vitro environment. The extract quenched the IC50 value of 352.78 μg/ml for the DPPH assay. The result demonstrated a hydroxyl radical scavenging potential of 59.75% at a dose of 100 μg/ml concentration of ethyl acetate extract**.** When the methanolic extract was studied for the free radical scavenging, by DPPH assay the antioxidant activity value for this was found to be IC50 value was 17.0689 μg/ml**.** Among the following extracts hexane, chloroform, and methanol, the methanolic extract showed the highest activity of antioxidant.

Amongst the green leafy vegetable, the total antioxidant activity was the highest in *Murraya koenigii* (2691 micromol of ascorbic acid/gm sample) as compared to that of methanol extracts of Amaranthus sp., *Centella Asiatica*, and *Trigonella foenum graecum*.

Studies conducted by Mitra *et al*. 2012 indicate that the aqueous extracts of *Murraya koenigii* leaf confer significant protection to rat cardiac tissue against cadmium-induced oxidative stress probably due to its antioxidant activity. The alterations seen in the levels of lipid peroxidation, reduced glutathione, protein carbonyl content, changes in the activities of cardiac antioxidant and pro-oxidant enzymes, indicate that cadmium-induced tissue damage was the result of oxidative stress. This antioxidant activity of *Murraya koenigii* could be beneficial to people who are exposed to cadmium either environmentally or occupationally.[24][25]

2.2.3 Anti-nociceptive Activity

Both petroleum ether extracts of *Murraya koenigii* (PMK) and alkaloids separated from PMK i.e. (AMK) significantly decreased the number of acetic acid-induced writhing, increased the latency of paw licking in hot plate method and basal reaction time in tail immersion method in a dose-dependent manner (100 mg and 300 mg/kg p.o). These anti-nociceptive effects were also produced following chronic administration i.e., at the end of 15 days study, suggesting the potential of *Murraya koenigii* to be used as an analgesic.

Furthermore, the methanolic extracts of the dried leaves of *Murraya koenigii* at doses of 100, 200 and 400 mg/kg body weight administered to albino rats caused a significant reduction ($P<0.001$) in the carrageenan-induced paw edema. Its analgesic activity was evidenced by an increase in the reaction time by Eddy's hot plate method and formalin-induced paw licking method, which too was statistically significant ($P<0.05$). These anti-inflammatory and analgesic effects were comparable to standard drug diclofenac (10 mg/kg, p.o.). Hence, results suggest the possible benefit of *Murraya koenigii* in alleviating conditions associated with inflammatory pain.[28][31]

2.2.3 Lipid-lowering Activity

Lipid abnormalities which are frequently seen in diabetes patients result in a significant increase in cardiovascular mortality. Hence, a study conducted by Kesari *et al*. 2007, wherein they evaluated the effect of one-month oral administration of *Murraya koenigii* aqueous leaves extract in normal and streptozotocin (STZ)-induced severe diabetic rats at doses of 300 mg/kg bodyweight on various biochemical parameters.

Results demonstrated that the fasting blood glucose (FBG) of treated animals decreased by 48.2%, total cholesterol (TC) by 30.8%, triglycerides (TG) by 37.1%. *Murraya koenigii* extract increased the HDL-cholesterol levels by 29.4%. Serum alkaline phosphatase values were reduced by 33%, SGOT by 36.7%, and SGPT by 32.2%. Additionally, the serum creatinine levels reduced by 18.2%, and urine sugar values decreased by 75% in the *Murraya koenigii* treated group. Thus, the results indicate that besides lipid-lowering activity the aqueous extract of *Murraya koenigii* also reduced the severity of diabetes and its associated nephropathic complications.[11][32]

2.2.4 Diabetes and its complications

A) *Antidiabetic and islet protective*- *Extracts* of *Murraya koenigii* resulted in pancreatic beta-cell protection and functional pancreatic islets that produce insulin. This was evident by the normalization of plasma insulin and C-peptide levels, indicating endogenous insulin secretion, after treatment in streptozotocin-induced diabetic Swiss mice. Even the histochemical and immunohistochemical analysis suggests an islet protective and insulin productive role. Additionally, extracts of *Murraya koenigii* increased the levels of glucose-6-phosphate dehydrogenase enzyme, normalized hepatic and muscle glycogenesis, resulting in proper glucose utilization. The levels of post-prandial hyperglycemia were also reduced due to the pancreatic and intestinal glucosidase inhibitory activity of the extracts of *Murraya koenigii*.

B) *Immunomodulatory-* The leaf extracts of *Murraya koenigii* not only have anti-diabetic properties but also possess certain effects to regulate immunology related to oxidative stress metabolism. This immunomodulatory and anti-inflammatory activity was evident by interleukin (IL)-2, 4, 10 and tumor necrosis factor-alpha (TNF-alpha) expression.

C) *Nephroprotective And Neuroprotective-* Daily oral administration of aqueous extracts of leaves of *Murraya koenigii* to STZ-induced diabetic male rats (Sprague Dawley strain) for 30 days, produced a significant dose-dependent reduction in serum urea and creatinine levels ($P<0.001$). It also produced tissue regeneration in kidneys as observed from histological studies. Ethanolic extracts of leaves of *Murraya koenigii* increased in grip strength of STZ-induced diabetic rats that developed neuropathy 9 weeks following a single injection of 70 mg/kg i.v streptozotocin (STZ). Prior treatment with *Murraya koenigii* extracts increased the withdrawal time and licking latency in hot plate and tail-flick tests, respectively. This indicates that chronic treatment with *Murraya koenigii* besides decreasing glycemic levels offered neuroprotective benefits.[39][41]

2.2.5 Anticancer Activity

The methanolic extract of *Murraya koenigii* leaves demonstrated a significant increase in the phagocytic index by the rapid removal of carbon particles from the bloodstream. It also demonstrated an increase in the antibody titer against ovalbumin and protection against cyclophosphamide-induced myelosuppression. Thus, *Murraya koenigii* holds promise as an immunomodulatory agent acting by stimulating humoral immunity and phagocytic function. However, these extracts were unable to stimulate cellular immunity.
Furthermore, 3 carbazole alkaloids mahanine, pyrayafoline and murrafoline, showed significant activity against HL-60 cells by inducing apoptosis through of capsase-9/capsase-3 pathway, through mitochondrial dysfunction. [47]

2.2.6 Hepatoprotective

Hydroethanaolic leaf extracts of *Murraya koenigiii* in doses of 200, 400 and 600 mg/kg body weight demonstrated a significant reduction in the levels of alanine aminotransferases, aspartate aminotransferases, alkaline phosphatase, total bilirubin in CCl4-treated hepatotoxic rats. Additionally, *Murraya koenigii* treated rats also resulted in a dose-dependent increase in hepatic superoxide dismutase, catalase, reduced glutathione, and ascorbic acid, and a decrease in lipid peroxidation. Even the microscopic studies revealed minimal CCl4-induced lesions in *Murraya koenigii* treated rats, thus suggesting the hepatoprotective potential of *Murraya koenigii*.
The tannins and carbazole alkaloids from the aqueous extracts exhibited excellent hepatoprotective activity against ethanol-induced hepatotoxicity comparable to standard drug L-ornithine L-aspartate (LOLA).[41][51]

2.2.7 Gastrointestinal disorders

The n-hexane extracts of the seeds of *Murraya koenigii* demonstrated significant inhibitory activity against castor oil-induced diarrhea and PGE2-induced enteropooling in rats. Additionally, a significant decrease in gastrointestinal motility was observed in the charcoal meal test in Wistar rats.[41]

2.2.8 Miscellaneous Activity

Ethanolic extract of fresh leaves of *Murraya koenigii* (MKEE) showed a dose-dependent positive inotropic effect on isolated frog hearts possibly by increasing availability of calcium from extracellular sites.

The activity demonstrated by some of the isolated carbazole alkaloids of *Murraya koenigii* and their derivatives against *Trichomonas gallinae* confirmed that the anti-trichomonal activity of the leaf may be due to its carbazole alkaloids.

The methanol extracts of plants like *Murraya koenigii* is an ideal eco-friendly approach to aid for the control of mosquito species, *Ae*. *aegypti*, and *An*. *stephensi*. The study conducted by Patil *et al*. 2011 concludes that *Murraya koenigii* could be screened as a potential drug for the prevention or treatment of neuroleptic-induced OD. [41][52]

Materials & Method

3.1 Materials-

Soxhlet apparatus, Petri dishes, Eppendorf tubes, Centrifuge tubes, filters, Naphelometer, Vortexer, L-shaped spreader, Inoculating loop, Plant extracts, Bacterial cultures.

Chemicals required- Wagner's reagent, Ferric chloride, Sodium hydroxide, Glacial acetic acid, Molisch's reagent, Ninhydrin, Bromine water, Sulfuric acid, Ammonium hydroxide, Sodium nitroprusside, Million's reagent, Fehling A, Fehling B.

3.2-Collection of *Murraya keonigii* leaves-

Being a semi-deciduous, unharmed aromatic smell spreading shrub or tree with strong woody stem, it is easily available. The plant was collected from outside of G.L.A University. Leaves were detached and cleaning was done two times with running tap water and with distilled water so that all the dust and impurities shall runoff. The weight of wet leaves was taken and recorded. At room temperature leaves were air-dried and crushed by the mixer to get a powdered form, the weight of powder was taken and recorded.

Fig.2 Fresh Leaves.

Fig.3 Dried Leaves.

Fig.4 Crushed leaves.

3.3-Extract preparation-

Extraction was carried out using the Soxhlet apparatus. 25grams (for aqueous) and 29 grams (for ethanol) powdered leaves were taken in the thimble and covered with cotton wool, the thimble having sample was then placed in the extraction jacket and the continuous extraction was carried out by using solvents, double distilled water and methanol each with amount 200 ml. The extraction was carried out till the light color of solvent was seen in the siphon tube. The temperature of Soxhlet was adjusted to 100^{o}C for aqueous extraction and 50^{o}C for ethanol extraction. When the extraction is complete, the thimble is removed and by again switching on the Soxhlet, and the purified solvent was extracted out from the extract which will use further. Put the extract overnight in an incubator on a 200 mm Petri plate and incubate it at 50^{o}C till the solvent evaporate and collect the extract, weigh the obtained extract and store it in a sterile vial and recorded.

a) Aqueous extraction b) Ethanol extraction

Fig.5 – Soxhlet Assembly for extraction

200mg of both aqueous and methanolic extract was taken in a sterilized centrifuged tube. The aqueous extract was dissolved in sterilized DW (500µL). As ethanol extract contains some compound that was insoluble in water, so it was dissolved in 200µL of DMSO (dimethyl sulfoxide) and the rest of the fraction with DW i.e., 300µL to make the final volume 500µL. As DMSO also exhibits antimicrobial activities so the smallest concentration of DMSO was taken to dissolve the extract.

a) The extraction obtained from water

b) The extraction obtained from Ethanol

Fig.6 – Extracts of *Murraya koenigii* leaves

3.4-Preparation of sterile disc- The discs were made with Whatman filter paper using a punching machine. The discs of diameter 0.5cm were stored in a sterilized container. The discs were then sterilized with an autoclave at 121°C for 20 minutes at 15psi pressure.

Fig.7-Sterile discs

3.5-Sterilization of extract –

Both the extracts were sterilized through a syringe filter of pore size 0.45µm. The solution of 500mg/mL was then serial diluted to 250mg/mL, 125mg/mL, 62.5mg/mL and 31.25mg/mL in sterilized Eppendorf tube. The sterilized discs were then loaded with 20µl of the solution of different concentrations of aqueous and methanol extract of *Murraya keonigii* leaves. These discs were then allowed to dry in laminar airflow and were then used as herbal discs.

3.6-Preparation of bacterial suspension and determination of their concentration-

The four bacterial strains (*Escherichia coli, Staphylococcus aureus, Bacillus subtilis, and Pseudomonas aeruginosa)* were inoculated in 100 ml nutrient broth and incubated for 24 hours at 37°C. The incubated broths were then centrifuged at 2700 rpm for 15 minutes to get the pellet and supernatant is removed. The pallets of different bacterial were collected in a different sterilized centrifuge tube and washed 3 times with normal saline. The turbidity of all the bacterial suspensions was matched with a nephelometer and was kept in a sterilized centrifuge tube in the refrigerator.

3.7-Preparation of Nutrient agar plates-

The nutrient agar was made.

Table3-Composition of Nutrient agar (100mL)

Peptone	0.5gm
Beef extract	0.2gm
Sodium chloride	0.5gm
Agar	1.5gm
Ph	7.2

Both the medium was sterilized by autoclaving at 121°C for 20 minutes at 15psi pressure. The sterilized agar medium was poured in sterilized Petri dish under laminar airflow. After the solidification of agar medium Petri dishes were wrapped and stored in the refrigerator.

Fig.8- Nutrient agar plates

3.8-Determination of antibacterial activity-

- The antibacterial activity was carried out using the disc diffusion method. The plates of bacteria *E. coli*, *S.aureus*, *B.subtilis* and *Pseudomonas aeruginosa* were made. The 100µL of each was loaded on the Petri dish and spread using an L-shaped spreader. The discs of different concentrations of both extracts were loaded on plates.

- Ciprofloxacin and Gentamicin discs were taken as a positive control for *E. coli, S.aureus* respectively.

- Disc impregnated with 20 µL of distilled water was taken as a negative control for aqueous extract and disc impregnated with 20 µL of a mixture of DMSO and distilled water (20%) was taken as a negative control for methanol extract.

They then incubated the bacterial plates for 24 hours at 37ºC temperature. Upon incubation, all plates for an inhibition zone were analyzed, and the diameter of these zones was measured in centimeters. All the tests were conducted in a sterile condition.

3.9- Preliminary phytochemical screening of Murraya keonigii:

3.9.1-Alkaloids:

Wagner's test: To few mL of extract, 1 or 2 mL of **Wagner's** reagent were added by the side of the test tube. A prominent brown or yellow precipitate indicated the test as positive.

3.9.2-Saponins:

a) Foam test- 2ml of Water was added to the dry extract and shake vigorously. Foam appearance showed the absence of saponins.

3.9.3-Tannins:

To 2ml of the extract was added and a few drops of 1% $FeCl_3$ was added, the appearance of blue-black precipitate in the solution confirms the test.

3.9.4-Cardiac glycosides:

2mL of plant extracts were treated with 2 mL of glacial acetic acid containing a drop of $FeCl_3$ solution. This was treated with 1 mL of concentrated H_2SO_4. A brown ring obtained at the interface indicates the presence of de-oxy sugar characteristics of cardenolide.

3.9.5-Steroids:

Salkowski test- To the crude extract, chloroform was added followed by the addition of a few drops of concentrated H_2SO_4, shaking well and mix. was allowed to stand for some time. Presence of steroids was confirmed by the appearance of red color at the lower layer while the presence of triterpenoids was confirmed by yellow color layer formation.

3.9.6-Carbohydrates:

a) **Molisch's test**-In a test tube 2ml of the sample was taken and a small amount of Molisch's reagent (∝-naphthol dissolved in EtOH) was mixed. Conc. H_2SO_4 was added slowly through the wall of the test tube, to form a bottom layer. Formation of a bluish-violet ring at the junction confirms the presence of carbohydrates.

3.9.7-Proteins:

a) **Ninhydrin test-** 2ml of the extract was taken in a test tube and boiled with Ninhydrin (indane 1, 2, 3 trione hydrate). The appearance of violet color confirmed the test.

3.9.8- Phenolic compound:

a) **Bromine water test-** To the test solution Bromine Water was added. Presence of yellow precipitate confirms the test.

3.9.10- Iodine:

Using **iodine** to **test** for the presence of **starch** is a common **experiment**. A solution of **iodine** (I_2) and potassium **iodide** (KI) in water has a light orange-brown color. When added to an extract sample, the color changes to a deep blue.

3.9.11- Flavonoids:

2ml of 2% NaOH was added to the extract which produces yellow color which gets disappeared when 2-3 drops of dilute acid are added.

Results

4.1-Collection of plant-

Weight of wet leaves - 250.23gm.

Weight of leave powder – 160.35gm.

4.2-Extract prepared-

Weight of Aqueous extract formed – 5.45gm

Weight of Methanol extract formed– 7.89gm

4.3- Phytochemical Analysis-

The different phytochemicals were analyzed in both Aqueous and Methanolic extract of Murraya koenigii leaves, and the results obtained are as follows:

Sr. No.	PHYTOCHEMICALS	Aqueous Extract	Ethanolic Extract
1.	Alkaloids (Hager's test)	+	+
2.	Glycosides (Legal's test)	+	+
3.	Saponins (Foam test)	-	-
4.	Tannins	+	+
5.	Steroids (Salkowski test)	+	+
6.	Carbohydrates (Molisch's test)	+	+
7.	Proteins (Ninhydrin test)	+	+
8.	Phenolic compounds (Bromine water test)	+	+
9.	Flavonoids	+	+
10.	Iodine test	-	-

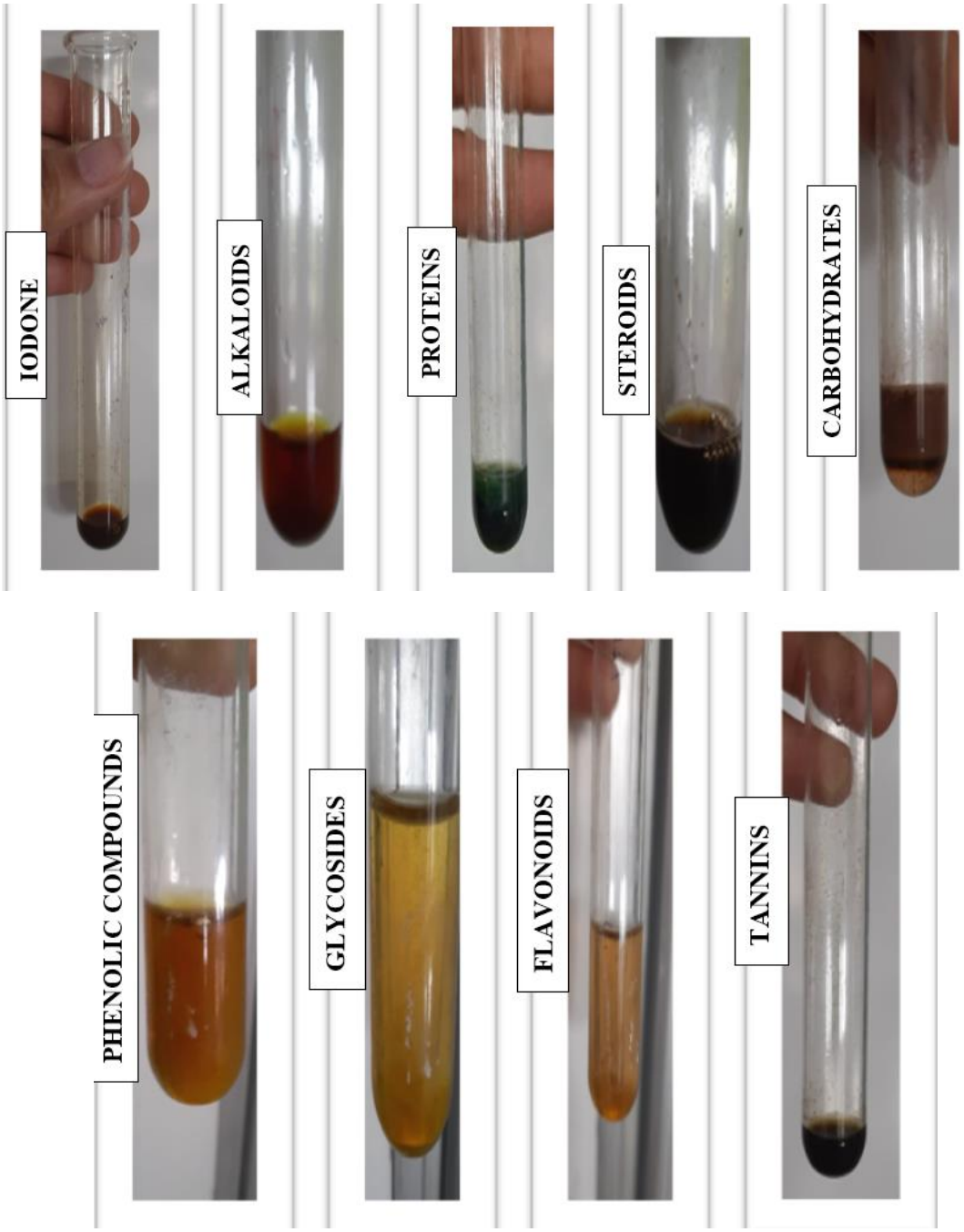

Fig.9 – Phytochemical analysis of the Aqueous extract

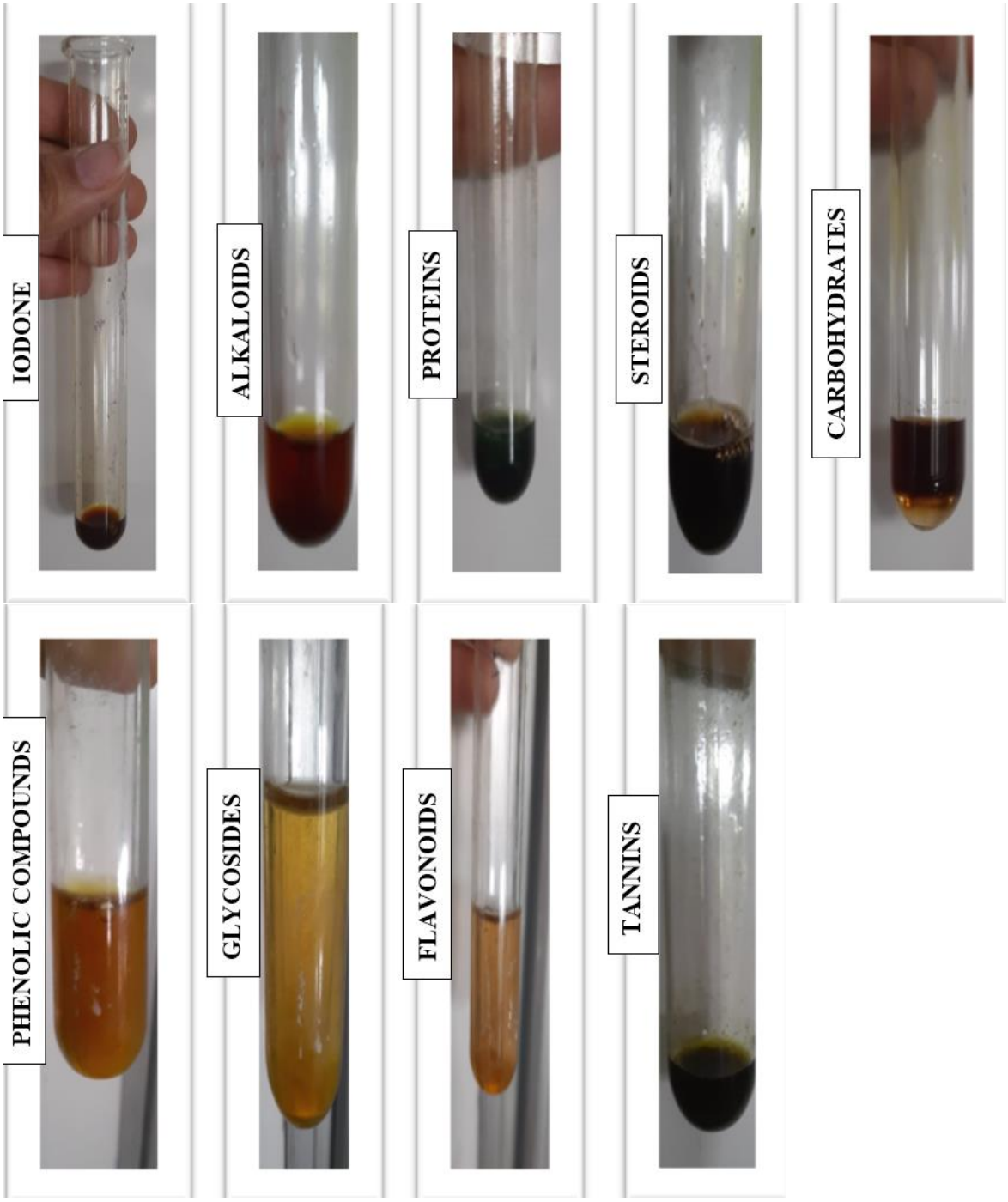

Fig.10 – Phytochemical analysis of Ethanolic extract

4.4-Determination of antibacterial activity-

As the antibacterial activity of *Murraya koenigii* leaves extract (aqueous and ethanol) was conducted against:

- *Escherichia coli*
- *Staphylococcus aureus*
- *Pseudomonas aeruginosa*
- *Bacillus Subtilis*

The disc diffusion method was observed with the following sizes zones of inhibition at different concentration of both the Aqueous as well as Ethanolic extracts for the above-mentioned microorganisms:

4.4.1 Antibacterial activity determination by Aqueous extract:

There were both positive as well as a negative control for the antibacterial activity determination:

- Positive Control – Ciproflaxin (CIP)
- Negative Control – Double Distilled Water

4.4.1.1 Table for inhibition zone size against *E. coli:*

	24 hours
Positive Control	3.0
Negative Control	0.0
0.25 mg/ml	0.7cm
0.50 mg/ml	1.1cm
1.00 mg/ml	1.6cm

4.4.1.2 Table for inhibition zone size against *B. subtilis*:

	24 hours
Positive Control	2.6cm
Negative Control	0.0cm
0.25 mg/ml	0.4cm
0.50 mg/ml	0.5cm
1.00 mg/ml	0.9cm

4.4.1.3 Table for inhibition zone size against *S. aureus*:

	16 hours
Positive Control	2.1cm
Negative Control	0.0cm
0.25 mg/ml	0.6cm
0.50 mg/ml	0.9cm
1.00 mg/ml	1.0cm

4.4.1.4 Table for inhibition zone size against *Pseudomonas:*

	16 hours
Positive Control	2.2cm
Negative Control	0.0cm
0.25 mg/ml	0.5cm
0.50 mg/ml	0.6cm
1.00 mg/ml	0.8cm

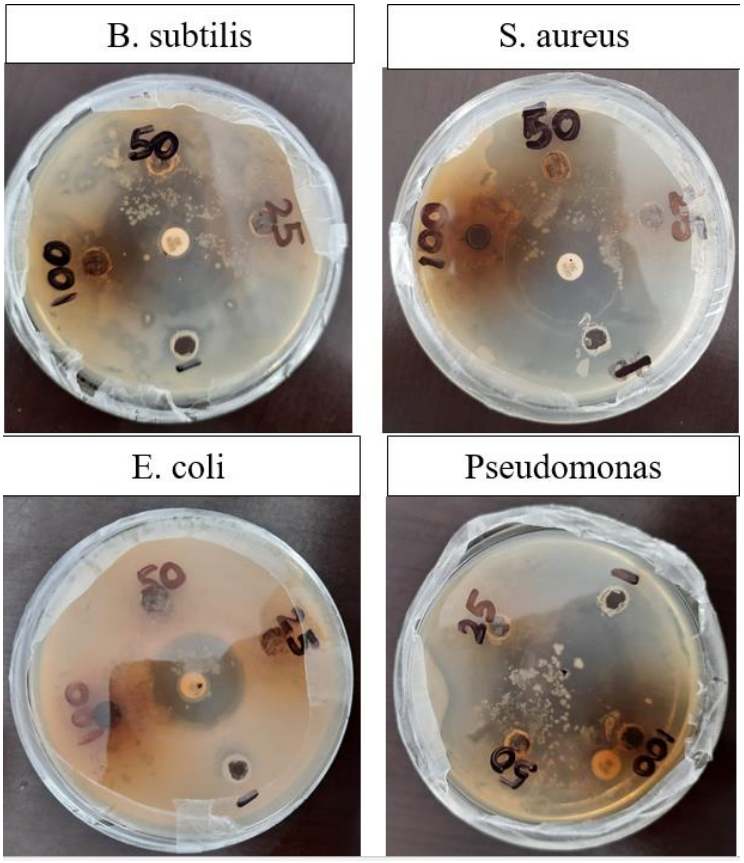

Fig.11 – Antibacterial activity of Aqueous Extract

4.4.2 Antibacterial activity determination by Ethanolic extract:

There were both positive as well as a negative control for the antibacterial activity determination:

- Positive Control – Chloramphenicol
- Negative Control – 1% DMSO

4.4.2.1 Table for inhibition zone size against *E. coli:*

	24 hours
Positive Control	1.6cm
Negative Control	0.0cm
Blank	0.0cm
0.25 mg/ml	0.9cm
0.50 mg/ml	1.0cm
1.00 mg/ml	1.1cm

4.4.2.2 Table for inhibition zone size against *Pseudomonas:*

	24 hours
Positive Control	1.6cm
Negative Control	0.0cm
blank	0.0cm
0.25 mg/ml	0.5cm
0.50 mg/ml	0.7cm
1.00 mg/ml	1.0cm

4.4.2.3 Table for inhibition zone size against *S. aureus:*

	24 hours
Positive Control	3.0cm
Negative Control	0.0cm
blank	0.0cm
0.25 mg/ml	0.6cm
0.50 mg/ml	0.6cm
1.00 mg/ml	0.7cm

4.4.2.4 Table for inhibition zone size against *B. subtilis:*

	24 hours
Positive Control	2.1cm
Negative Control	0.0cm
Blank	0.0cm
0.25 mg/ml	0.6cm
0.50 mg/ml	0.7cm
1.00 mg/ml	0.9cm

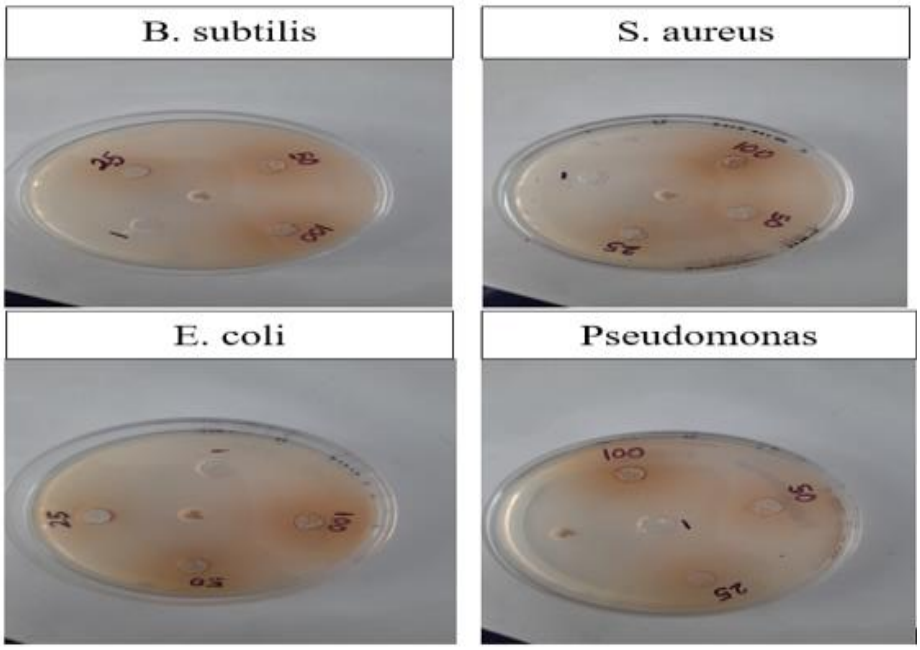

Fig.12 – Antibacterial activity of Ethanolic Extract

Discussion & Conclusion

Murraya koenigii being a medicinally important plant possess antimicrobial activity in leaf extracts, whether it being an Aqueous or Ethanolic extract. There are many reports and research papers that represented the antimicrobial activity of Murraya koenigii in barks, leaves and stems. The leave extract was able to show the antimicrobial effects against the following strain: *E. coli, Pseudomonas aeruginosa, S. aureus and B. subtilis* efficiently.

The present study was observed with the antimicrobial activity of both Aqueous as well as the Ethanolic extracts.

When screened for phytochemical analysis both the extracts gave similar results and showed the absence of Saponins and iodine, and tested positive for the Alkaloids, Flavonoids, Proteins, Carbohydrates, Terpenoids, Glycosides, Tannins, Steroids and Phenolic Compounds.

Summary

Murraya koenigii (L.) Spreng. the plant belongs to the family Rutaceae. It is generally known as Kadipatta in Hindi and Curry leaves in English. Murraya koenigii is a traditional product widely used as spice and condiment and scrutiny of literature reveals some notable pharmacological activities of the plant. It has been tested and revealed that this semi-deciduous, unharmed aromatic smell spreading shrub or tree possessing medicinal properties has a peak potential for pharmacological properties such as possess anti-oxidative, hepatoprotective, antimicrobial, antifungal, anti-inflammatory, and nephroprotective activities, anti-diabetic, anti-amnesic, anti-diarrheal, anti-analgesic, anti-inflammatory, anti-pyretic, and several protective effects.

It has been reported that the plant has several bioactive compounds such as glycosides, alkaloids, steroids, phenolic compounds, carbohydrates, flavonoids, terpenoids and tannins, proteins. As it shows antibacterial, so the experiment was been conducted. The aqueous and ethanol extract was prepared by Soxhlet extraction and the antibacterial was determined by disc diffusion method against *E. coli, S. aureus, Pseudomonas aeruginosa* and *B. subtilis* of *Murraya keonigii* leave extracts. The plant extract shows positive results for *Pseudomonas aeruginosa, B. subtilis, S. aureus and E. coli*.

References

1) MURRAYA KOENIGII (L.) SPRENG-CURRY LEAVES/MITHO NIM- A MIRACLE PLANT -https://www.nepjol.info/index.php/bcj/article/download/36515/28496/

2) Curry leaf (Murraya Koenigii): a spice with medicinal property-https://medcraveonline.com/MOJBM/MOJBM-02-00050.pdf.

3) Curry Tree - Jean-Michel Cousteau Resort Fiji-https://www.fijiresort.com/botanical-tour-51/

4) Journal of Drug Delivery and Therapeutics-https://core.ac.uk/download/pdf/230742557.pdf

5) https://www.ncbi.nlm.nih.gov/pmc/articles/PMC7070712/Medicinal Profile, Phytochemistry, and Pharmacological Activities of *Murraya koenigii* and Its Primary Bioactive Compounds

6) Curry Leaves: Medicinal Uses, Therapeutic Benefits For Hair, Diabetes And Supplements-https://www.netmeds.com/health-library/post/curry-leaves-medicinal-uses-therapeutic-benefits-for-hair-diabetes-and-supplements.

7) Review Article - Universal Journal of Pharmaceutical Research-http://ujpr.org/1-2-rw2.pdf

8) https://www.researchgate.net/publication/235758652_A_REVIEW_ON_MURRAYA_KOENIGII_MULTIPOTENTIAL_MEDICINAL_PLANT.

9) Medicinal Profile, Phytochemistry, and Pharmacological Activities of *Murraya koenigii* and Its Primary Bioactive Compounds-https://www.ncbi.nlm.nih.gov/pmc/articles/PMC7070712/

10) https://pubs.acs.org/doi/abs/10.1021/jf010621r Antioxidative Activity of Carbazoles from *Murraya koenigii* Leaves

11) https://www.ncbi.nlm.nih.gov/pmc/articles/PMC7070712/Medicinal Profile, Phytochemistry, and Pharmacological Activities of *Murraya koenigii* and Its Primary Bioactive Compounds

12) https://www.researchgate.net/publication/291161604_ANTIOXIDANT_ACTIVITY_AND_TOTAL_PHENOLICS_CONTENT_OF_EXTRACTS_FROM_MURRAYA_KOENIGII_CURRY_LEAVES_LAURUS_NOBILIS_BAY_LEAVES_AND_CAMELLIA_SINENSIS_TEA

13) Antioxidant activities of curry leaves (Murayya koenigii) and salam leaves (Eugenia polyantha) https://media.neliti.com/media/publications/174573-EN-antioxidant-activities-of-curry-leaves-m.pdf

14) Ito C. Studies On Medicinal Resources of Rutaceous Plants and Development To Pharmaceutical Chemistry, Natural Med.21 (4): 2000; 117-122

15) Gahlawat DK, Jakhar S, Dahiya P. Murraya koenigii (L.) Spreng: An ethnobotanical, phytochemical and pharmacological review. J Pharmacogn Phytochem 2014; 3:109-19.

16) Srivastava SK, Srivastava SD. New constituents and biological activity of the roots of Murraya Koenigii. Journal of Indian Chemical Society 1993; 70(7):655- 659.

17) Chihiro I, Thoyama Y, Omura M, Kajiura I, Furukawa H. Alkaloid constituents of Murraya koenigii. Isolation and Structure Elucidation of novel binary Carbazolequinones and Carbazole Alkaloids. Chemical and Pharmaceutical Bulletin 1993; 41(12):2096-2100.

18) Joshi BS, Kamat VN, Gawd DH. Structures of Girinimbine, Mahanimbine, Isomahanimbine, Koenimbidine and Murrayacine. Tetrahedron 1970; 26(6):1475- 1482.

19) Cheung KY, Hung K, But PPH, Qian L, Xao YS, Zhang HT et al. Sources of anti-implantation Alkaloid Yuehchukene in the genus Murraya. Journal of Ethnopharmacology 1986; 15(2):195-200.

20) https://www.jmnn.org/article.asp?issn=2278-1870;year=2012;volume=1;issue=2;spage=92;epage=97;aulast=Bhandari#top

21) https://www.researchgate.net/publication/310340726_THE_ANTIBACTERIAL_EFFECT_OF_CURRY_LEAVES_Murraya_Koenigii

22) Nagappan T, Ramasamy P, Wahid ME, Segaran TC, Vairappan CS. Biological activity of carbazole alkaloids and essential oil of Murraya koenigii against antibiotic resistant microbes and cancer cell lines. Molecules 2011; 16:9651-64.
[PUBMED]

23) Kusuma IW, Kuspradini H, Arung ET, Aryani F, Min YH, Kim JS, *et al*. biological activity and phytochemical analysis of three Indonesian medicinal plants, Murraya koenigii, Syzygium polyanthum and Zingiber purpurea. J Acupunct Meridian Stud 2011; 4:75-9.
[PUBMED]

24) Curry leaf (*Murraya koenigii*) or Cure leaf: Review of its curative propertieshttps://www.jmnn.org/article.asp?issn=2278-1870;year=2012;volume=1;issue=2;spage=92;epage=97;aulast=Bhandari

25) Bonde SD, Nemade LS, Patel MR, Patel AA. *Murraya koenigii* (Curry leaf): Ethnobotany, phytochemistry and pharmacology - A review. Int J Pharm Phytopharmacol Res 2011; 1:23-7.

26) Gupta P, Nahata A, Dixit VK. An update on Murraya koenigii spreng: A multifunctional Ayurvedic herb. Zhong Xi Yi Jie He Xue Bao 2011; 9:824-33.

27) Yankuzo H., Ahmed Q.U., Santosa R.I., Akter S.F.U., Talib N.A. Beneficial effect of the leaves of *Murraya koenigii* (Linn.) Spreng (Rutaceae) on diabetes-induced renal damage in vivo. *J. Ethnopharmacol.* 2011; 135:88–94. doi: 10.1016/j.jep.2011.02.020.

28) Husna F., Suyatna F.D., Arozal W., Poerwaningsih E.H. Anti-Diabetic Potential of *Murraya koenigii* (L) and its Antioxidant Capacity in Nicotinamide-Streptozotocin Induced Diabetic Rats. *Drug Res. (Stuttg)* 2018; 68:631–636. doi: 10.1055/a-0620-8210.

29) Amna U., Halimatussakdiah P.W., Saidi N., Nasution R. Evaluation of cytotoxic activity from Temurui (*Murraya koenigii* [Linn.] Spreng) leaf extracts against HeLa cell line using MTT assay. *J. Adv. Pharm. Technol. Res.* 2019; 10:51–55. doi: 10.4103/japtr.JAPTR_373_18.

30) Rautela R., Das G.K., Khan F.A., Prasad S., Kumar A., Prasad J.K., Ghosh S.K., Dhanze H., Katiyar R., Srivastava S.K. Antibacterial, anti-inflammatory and antioxidant effects of Aegle marmelos and *Murraya koenigii* in dairy cows with endometritis. *Livest. Sci.* 2018; 214:142–148. doi: 10.1016/j.livsci.2018.05.015.

31) Nalli Y., Khajuria V., Gupta S., Arora P., Riyaz-Ul-Hassan S., Ahmed Z., Ali A. Four new carbazole alkaloids from *Murraya koenigii* that display anti-inflammatory and anti-microbial activities. *Org. Biomol. Chem.* 2016; 14:3322–3332. doi: 10.1039/C6OB00267F.

32) Murraya koenigii (L.) Spreng: an ethnobotanical, phytochemical and pharmacological review Dheeraj K. Gahlawat, Savita Jakhar and Pushpa Dahiya - https://www.phytojournal.com/vol3Issue3/Issue_sep_2014/31.1.pdf

33) MURRAYA KOENIGII (L.) SPRENG-CURRY LEAVES/MITHO NIM- A MIRACLE PLANT Anant Gopal Singh- https://www.nepjol.info/index.php/bcj/article/download/36515/28496/

34) Murraya koenigii (curry leave)- A review on its potential- https://sphinxsai.com/2015/ph_vol7_no4/1/(566-572)V7N4.pdf

35) Balakrishnan R, Vijayraja D, Jo S-H, Ganesan P, Su-Kim I, Choi D-K. Medicinal profile, phytochemistry, and pharmacological activities of *Murraya koenigii* and its primary bioactive compounds. Antioxidants. 2020;9(2):101.

36) Brar B, Duhan JS, Rakha P. Analgesic activity of various extracts of leaves of *Murraya koenigii* (L.) Spreng. World J Pharm Pharm Sci. 2015;4(10):1255–62.

37) Gahlawat DK, Jakhar S, Dahiya P. *Murraya koenigii* (L.) Spreng: an ethnobotanical, phytochemical and pharmacological review. J Pharmacogn Phytochem. 2014;3(3):109–19.

38) Ghasemzadeh A, Jaafar HZ, Rahmat A, Devarajan T. Evaluation of bioactive compounds, pharmaceutical quality, and anticancer activity of curry leaf (*Murraya koenigii* L.). Evid Based Complement Alternat Med. 2014; 2014:873803. https://doi.org/10.1155/2014/873803.

39) Gupta P, Nahata A, Dixit VK. An update on *Murraya koenigii* spreng: a multifunctional Ayurvedic herb. J Chin Integr Med. 2011;9(8):824–33.

40) Handral HK, Pandith A, Shruthi S. A review on *Murraya koenigii*: multipotential medicinal plant. Asian J Pharm Clin Res. 2012;5(4):5–14.

41) Curry leaf (*Murraya koenigii*) or Cure leaf: Review of its curative properties- https://www.jmnn.org/article.asp?issn=2278-1870;year=2012;volume=1;issue=2;spage=92;epage=97;aulast=Bhandari

42) Husna F, Suyatna FD, Arozal W, Poerwaningsih EH. Anti-diabetic potential of *Murraya koenigii* (L.) and its antioxidant capacity in Nicotinamide-Streptozotocin induced diabetic rats. Drug Res (Stuttg). 2018;68(11):631–6. https://doi.org/10.1055/a-0620-8210.

43) Igara C, Omoboyowa D, Ahuchaogu A, Orji N, Ndukwe M. Phytochemical and nutritional profile of *Murraya koenigii* (Linn) Spreng leaf. J Pharmacogn Phytochem. 2016;5(5):07–9.

44) Iman V, Mohan S, Abdelwahab SI, Karimian H, Nordin N, Fadaeinasab M, Noordin MI, Noor SM. Anticancer and anti-inflammatory activities of girinimbine isolated from *Murraya koenigii*. Drug Des Devel Ther. 2017; 11:103–21. https://doi.org/10.2147/DDDT.S115135.

45) Kumar SR, Loveleena D, Godwin S. Medicinal property of *Murraya koenigii*-a review. Int Res J Biol Sci. 2013;2(9):80–3.

46) Kunwar RM, Mahat L, Acharya RP, Bussmann RW. Medicinal plants, traditional medicine, markets and management in far-West Nepal. J Ethnobiol Ethnomed. 2013; 9:24.

47) Ma QG, Xu K, Sang ZP, Wei RR, Liu WM, Su YL, Yang JB, Wang AG, Ji TF, Li LJ. Alkenes with antioxidative activities from *Murraya koenigii* (L.) Spreng. Bioorg Med Chem Lett. 2016;26(3):799–803. https://doi.org/10.1016/j.bmcl.2015.12.091.

48) Mandal S, Nayak A, Kar M, Banerjee SK, Das A, Upadhyay SN, Singh RK, Banerji A, Banerji J. Antidiarrhoeal activity of carbazole alkaloids from *Murraya koenigii* Spreng (Rutaceae) seeds. Fitoterapia. 2010;81(1):72–4. https://doi.org/10.1016/j.fitote.2009.08.016.

49) Muthu C, Ayyanar M, Raja N, Ignacimuthu S. Medicinal plants used by traditional healers in Kancheepuram District of Tamil Nadu, India. J Ethnobiol Ethnomed. 2006; 2:43.

50) Rajendran MP, Pallaiyan BB, Selvaraj N. Chemical composition, antibacterial and antioxidant profile of essential oil from *Murraya koenigii* (L.) leaves. Avicenna J Phytomed. 2014;4(3):200–14.

51) A REVIEW ON MURRAYA KOENIGII: MULTIPOTENTIAL MEDICINAL PLANT HARISH K HANDRAL1, ANUP PANDITH2 AND SHRUTHI SD3- https://citeseerx.ist.psu.edu/viewdoc/download?doi=10.1.1.460.4397&rep=rep1&type=pdf9

52) Benefits and Uses of Curry Leaves-https://www.healthline.com/nutrition/curry-leaves-benefits#3.-May-have-neuroprotective-properties.

53) A Pharmaceutical Importance of Murraya Koenigii- A Complete Study- https://medicopublication.com/index.php/ijphrd/article/download/11396/10524/21763.

54) Ethnobotany, Phytochemical, Pharmacological Potentials of Murraya koenigii, and Its Health Benefits – A Review- https://www.journalcjast.com/index.php/CJAST/article/view/30902.

55) CURRY LEAVES (Murraya koenigii Linn. Sprengal)- A MIRCALE PLANT- Indian J.Sci.Res.4 (1): 46-52, 2014-https://www.ijsr.in/upload/602447219Microsoft%20Word%20-%20paper%203.pdf

56) PHYTOCHEMICAL ANALYSIS OF MURRAYA KOENIGII IN URBAN AND COASTAL AREA-https://jprsolutions.info/files/final-file-56855166324836.04212274.pdf

57) MURRAYA KOENIGI-A BOON IN DIFFERENT PATHOLOGICAL CONDITIONS- http://ujpr.org/index.php/journal/article/view/29/207, http://doi.org/10.22270/ujpr.v1i2.RW5

G.L.A. UNIVERSITY

B.Ed. [Sem. III]

BATCH-2019-21

SESSION-2020-21

ACTION-RESEARCH FILE

Submitted By

Akanksha Gautam

197000004

Submitted to

Faculty of Education

GLA UNIVERSITY
MATHURA
Recognised by UGC Under Section 2(f)
Accredited with A Grade by NAAC

Faculty of Education

Date-02-12-2020

Certificate

This is to certify that Mr./Ms**. Akanksha Gautam** Roll No. **197000004** of B.Ed. II Year, Session 2020-21 has successfully completed his/her Project under my supervision on **"Low marks due to poor handwriting"**

Jyoti Sharma
Assistant Professor
Faculty of Education

INDEX

Name : Akanksha Class & Section : B. Ed II year

Subject : Action Research Roll No. 197000004

S No.	Topic	Page No.	Date	Signature of Teacher
1.	Action research definition	1	30/10/2020	sgd
2.	Meaning	2	"	
3.	Characteristics	3	"	
4.	Steps	4	"	
5.	Purpose of action research	5	"	
6.	Aims of Research	6	"	
7.	Advantages	7	"	
8.	Scope of research	8	"	
9.	Limitations of research	9	"	
10.	Title of Research	10	1/11/2020	
11.	Introduction	11	"	sgd
12.	Evidence of Research	11	"	
13.	Diagonisis of Problem	12	"	
14.	Action hypothesis	13	8/11/2020	
15.	Execution	14	"	
16.	Analysis	14	"	
17.	Conclusion	16	"	

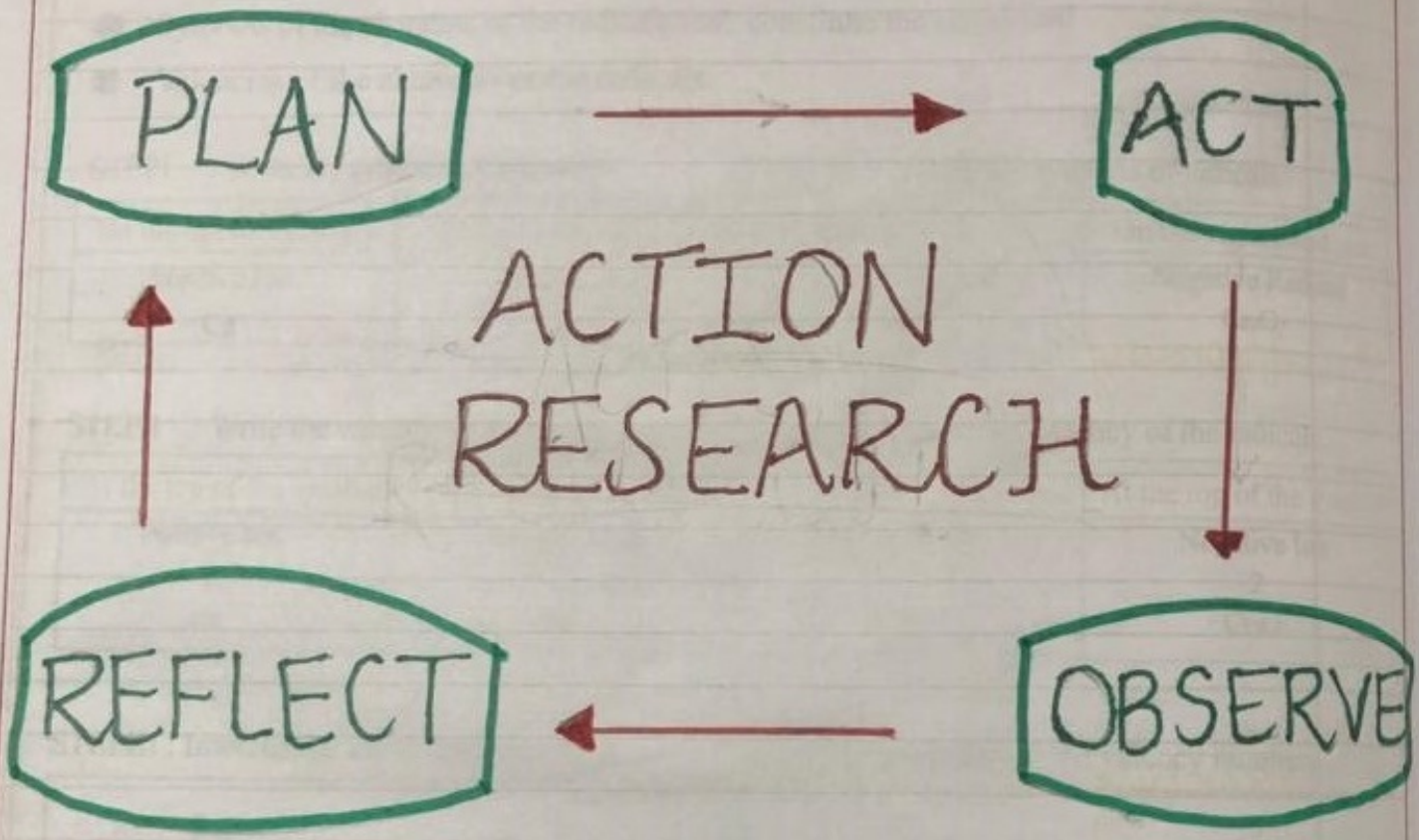
PLAN
ACT
ACTION RESEARCH
REFLECT
OBSERVE

WHAT IS ACTION RESEARCH ?

▶ According to 'Kurt Lewin ;

" Action reasearch is a comparative research on the conditions and effects of various forms of social action and research leading to social action. "

▶ According to Kemmis ;

" Action research is a form of self reflection enquiry that can be utilized by teacher in order to improve the rationality and justice of their own practice, their understanding of these prbctices and situations in which those practices occur. "

Teacher's Signature : _____

MEANING

Action research is a research initiated to solve an immediate problem led by individuals working with others in teams or as part of a "Community of Practice" - to improve the way they solve problems. It is a process of systematic reflection, inquiry and action. It can be traced back to the early works of John Dewey in the year 1920, and Kurt Lewin in the year 1940.

The term action research was coined by Stephen Cary at the teacher's college of Columbia University in the year 1949. The general goal is to create a simple, practical, repeatable process of interactive learning, evaluation and improvement that leads to increasingly better results for schools, teachers and students.

Teacher's Signature : _____

Name of Experiment..... Date..... Page No. 3

Experiment No..... Experiment Result.....

CHARACTERISTICS

1. Concentration on practical issues.
2. An interactive cycle of plan - act - reflect.
3. Emphasis on changes
4. Collaboration with problem solvers.
5. Multiple Data generation methods.
6. Action outcomes plus research outcomes.

Teacher's Signature : _____

Identify the Problem

Devise a Plan

Act to implement your plan

Observe collect and Analyse your Data

Reflect and share

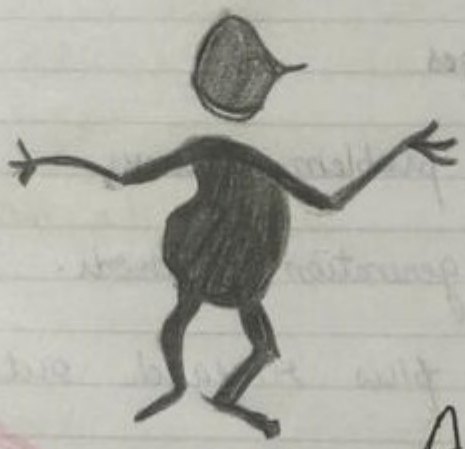

Name of Experiment..... Date..... Page No. 4

Experiment No..... Experiment Result.....

STEPS

1. Selecting a focus.
2. Classifying theories
3. Identifying Research Questions
4. Collecting data
5. Analysing data
6. Reporting results
7. Taking informal actions.

Teacher's Signature : _____

Purpose of Action Research

The main purpose of action research is to identify a problem or area of problem and solve that problem of students to become more motivated learners in a classroom. where there are multiple types of opportunities for learners to achieve success.

Another purpose is to motivate students to be engaged successful learners through a classroom enviornment where they act as a participants of learners.

Teacher's Signature : _____

AIMS OF ACTION RESEARCH

1. To contribute towards whole school improvement :

It means to encourage and assist teachers to conduct action research as a means of affecting positive social and educational change in their environment.

2. To provide opportunities to staff members to become involved in research projects :

The expertise of various staff members can be encouraged for specific projects identified by the teachers.

3. To effect improvement in the personal / professional practice of teachers :

The process of conducting action research has been shown to have positive consequences for the personal and professional development of participants.

Teacher's Signature : _____

4. To provide undergraduate students with opportunities:

The unit provides a perfect condition for undergraduate students to engaged in research.

ADVANTAGES

1. Encourages changes in school.
2. Fosters a democratic approach to education
3. Empower individuals through collaboration on projects.
4. Teachers investigate their own practice in new ways looking deeper in what they and their students actually do and fail to do.
5. Teachers develop a deeper understanding of students teaching learning process and their role in the both education of teachers and students.
6. Action research helps in applying strategies
7. Promote a process of testing new ideas.

Teacher's Signature : _____

Name of Experiment..... Date..... Page No. 8

Experiment No..... Experiment Result.....

SCOPE OF ACTION RESEARCH -

1. Utility of teaching material in classroom.
2. Disciplined related problems.
3. Washroom cleanliness problem.
4. Improvement in teaching method in classrooms.
5. Drinking water related problems.
6. Social problems.
7. Attendance related problems.
8. Homework related problems.
9. Institutional and management related problem in classroom and school environment.
10. Reading and writing related problems of students.

Teacher's Signature : _____

LIMITATIONS OF ACTION RESEARCH

1. It is of local importance.
2. Its conclusion can not be generalised.
3. Its qualitatively less important.
4. Sometimes teacher's feel difficulty in controlling variables due to lack of training.
5. Sometimes teacher unable to observe the problem scientifically and objectively.
6. Teachers feel the lack of direction while doing action research.
7. The nature of action research is basically subjective.
8. This is done only on the real problem of Education.

Teacher's Signature : _____

ACTION RESEARCH

- Title of the Research Problem :
  Low marks due to poor handwriting.
- Name of the Student : Krishna Gautam
- Class of the Student : VI
- School : Romex International School, Mathura
- Name of Research Scholar : Akanksha Gautam
- Time duration : 10 days.

Teacher's Signature : _____

Name of Experiment..... Date..... Page No. 11

Experiment No..... Experiment Result.....

▶ Introduction of the Problem :

How can I improve the handwriting of student named 'Krishna Gautam' of class VII from Romex International School.

Research Scholar Akanksha Gautam discuss on the above mentioned problem with the other students of same class found that student's grade was low as compared to the knowledge and the way this student perform in classroom after discussing and checking some evidence I found the main cause is bad handwriting it is due to many resons on which I researched and try to find out the solution so that child get good marks in exam as he is a good achiever.

▶ Ways of Getting Evidence the Problem -

1. By observing the child in learning hours.
2. By checking answer sheets of the student.
3. By discussing other teachers about his performance in other classes also.

Teacher's Signature : _____

Name of Experiment..... Date..... Page No. 12

Experiment No..... Experiment Result.....

Causes or Diagnosis of the Problem :-

S. No.	Probable Cause	Evidence to confirm by	If I can do Something	Priorities
1.	Lack of Basic writing skill	After checking answer sheets	Yes	1
2.	Slow speed of writing	After conducting a class test	Yes	2
3.	Improper vision	By observing	No	
4.	Lack of language Interpretation	After checking his verbal Knowledge	Yes	3
5.	Due to non-english family background	By observing	No	

Teacher's Signature : _____

Action Hypothesis -

To Improve the handwriting of the student following action I can take :

(1) If I provide worksheet for practice he may improve his handwriting by frequent writing.

(2) If I organise an extra class for students whose writing speed is slow in which group activities for writing purpose only should be given to them in a specific time limit.

(3) If I dictate the content in the classroom so that drill practice of writing after listening takes place and handwriting may improve and also speed maintained.

Teacher's Signature : _____

Name of Experiment..... Date..... Page No. 14

Experiment No..... Experiment Result.....

▶ Design of the research and Execution :

Step 1	Step 2	Step 3
By observing his answer sheets.	1- By providing work sheets in classroom. 2- Involving him in writing activities 3- By dictating content in classroom	After that again observe his handwriting and grades in answer sheets.

▶ Plan Procedure with time target :

S.No	Work	time
1.	By Observing his handwriting in class notebooks and Worksheets	1 week
2.	By conducting class test and writing activities	4 days

▶ Analysis :

1. If I provide regular worksheet for writing, student's handwriting automatically improve after practice.

2. If I involve child in writing activities by dictating content he may improve in

Teacher's Signature : _____

his speed of writing.

3. Continous drill practice by group activities make him motivated to improve and score better.

▶ follow up :

By this action research that child score good marks as well as the teachers of other class / subjects get impressed by his performance in classroom. A self confidence will develop in the student after such achievements.

Teacher's Signature : _____

CONCLUSION

After the completion of Action research on finding the main cause of that child's low grades., research scholar makes various hypothesis and probable causes of the problem and then implementation and after that she gets positive results of handwriting improvement of that child.

As the plan of research scholar successful in her action research that child feels confident and achieve good grades in all subject and become more motivated towards his studies.

This plan of research scholar facilitates other students also to improve their handwriting in exam as well as many other academic areas. They revised all of their topics by writing it again and again. And grades of students in that academic year improved. It also help other teachers to interpret their answers easily and evaluation becomes easy.

Teacher's Signature :

EVALUATION OF ESTROGEN AGONIST DAIDZEIN ON MOTOR DISORDER IN AN OVARIECTOMIZED ANIMAL MODEL OF PARKINSONISM

A THESIS

Submitted
for the award of the degree

of

MASTER OF PHARMACY

in

PHARMACOLOGY

by

AANCHAL VERMA
(Roll no. 198440001)

Under the Supervision of

DR. AHSAS GOYAL

to the

INSTITUTE OF PHARMACEUTICAL RESEARCH
GLA UNIVERSITY, MATHURA- 281406 (U.P.) INDIA
2021

DECLARATION

I hereby declare that

- The work presented in the thesis is original and has been done by myself under the general supervision of my supervisor.
- The work has not been submitted to any other Institution/University for any degree or diploma.
- I have followed the guidelines prescribed by the University in writing the thesis.
- I have followed the norms and guidelines given in the Ethical code of conduct of the University.
- Wherever I have quoted written materials from other sources, I have put them under the quotation marks and given due credit to the sources by citing them and giving the required details in the references.

Mathura **Aanchal Verma**

Date: ……

CERTIFICATE

This is to certify that the work reported in the thesis entitled **"Evaluation of Estrogen Agonist Daidzein on Motor Disorder in an Ovariectomized Animal model of Parkinsonism"** has been carried out by **Ms. Aanchal Verma** under my supervision and guidance at the **Institute of Pharmaceutical Research, GLA University, Mathura, Uttar Pradesh, India** for the award of the degree of **Master of Pharmacy**.

To the best of my knowledge, the contents of this thesis have not formed as a basis for the award of any previous degree to anybody else. I hereby forward his thesis.

Forwarded:

Prof. Meenakshi Bajpai
Institute of Pharmaceutical Research
GLA University, Mathura
(Director)

Dr. Ahsas Goyal
Assistant Professor
Institute of Pharmaceutical Research
GLA University, Mathura
(Supervisor)

23 Years EDUCATIONAL EXCELLENCE

GLA UNIVERSITY MATHURA
Recognised by UGC Under Section 2(f)

Accredited with A Grade by NAAC

12-B Status from UGC

Institutional Animal Ethics Committee (IAEC)

Registration No: 1260/Po/Re/S/09/CPCSEA

Ref No. GLAIPR/CPCSEA/IAEC/2021/P.Col./ R1 Date : 08.09.2021

CERTIFICATE

Certified that the project entitled **"Evaluation of Estrogen Agonist Daidzein on Motor Disorder in an Ovariectomized Animal Model of Parkinsonism"** submitted by **Ms. Aanchal Verma** student M. Pharm 2nd year has been approved by the IAEC in the meeting held on February 20, 2021.

Termination of project : August 30, 2021

No. of animals sanctioned : 36 Female Rats

Meenakshi

Prof. Meenakshi Bajpai

Chairman IAEC

ACKNOWLEDGMENT

First of all, I owe my extreme sense of gratefulness to the **Almighty** for enabling me to reach this so far. When I am thanking Almighty in these blissful moments, I am incapable of expressing my innermost feelings into words. At the time of carrying out such a herculean task, one really finds oneself against a headwind. Research is an arduous task, which despite consistent and dedicated mind with regards to strenuous and hard labor, also requires patience with the benediction and grace of Almighty.

I must offer my most profound gratitude to my supervisor **Dr. Ahsas Goyal**, Assistant Professor, Institute of Pharmaceutical Research, GLA University, Mathura, for finding an appropriate subject at the beginning of the process of writing thesis. He is the gem of institute and like a lighthouse to my small ship in vast ocean of my research work. He offered unreserved help and guidance and led me to finish my thesis step by step. He has been moving spirit behind this uphill task. Without his kind and patient instructions, it was impossible for me to finish the thesis.

I wish to express my heartiest thanks to **Prof. Meenakshi Bajpai,** Director, GLA University, whose inspiring and priceless guidance was a constant source of inspiration for me.

It is my cherished privilege to express my deep sense of gratitude and indebtedness to **Mr. Narayan Das Agrawal,** Chancellor, **Prof. Durg Singh Chauhan,** Pro-Chancellor, **Prof. Phalguni Gupta,** Vice Chancellor, **Prof. Anand Mohan Agrawal,** Pro-Vice Chancellor, **Mr. Neeraj Agrawal,** Chief Executive Officer, **Prof. Anoop Kumar Gupta,** Dean-Academics, **Mr. Ashok Kumar Singh,** Registrar, **Prof. Anirudh Pradhan**, Dean Research, **Prof. Kamal Sharma,** Associate Dean Research, GLA University, for providing me the opportunity and all necessary facilities to accomplish this endeavor successfully.

My sincere gratitude to **Dr. Debapriya Garabadu,** Central University of Punjab, Bhatinda, for providing lab facilities to carry out the biochemical analysis.

All faculty members of the institute have been very kind enough to extend their help at various phases of this research, whenever I approach them.

No research is possible without the library, the center of learning resources. I take this time to express my gratitude to all the library staff for updating me with the latest publications and *e*-resources. I am equally thankful to all the non-teaching staff for extending

help and co-operation in laboratory work. I would like to express my special thanks to animal house attendant for providing me animals timely for research work.

Some friends are never too busy to give us a hand whenever they are needed. I express my sincere love and affection towards my friends.

I would like to dedicate this thesis to my family. The sacrifices you made throughout my years here are simply ineffable. The belief you have in me and the support you gave instilled the values and virtues that see me through on a daily basis. I thank my father, Mr. Ajay Kumar Verma for encouraging me to go for higher studies. I thank my mother, Mrs. Hemlata Verma for her tender loving care and compassion. Amma! Need I tell you that you are the goddess incarnation in our family enhance I dedicate all at your feet. My heartfelt gratitude goes to my sister, Ananya Verma for her ebullient encouragement and moral support. Their love and care for me are my real source of performance whatsoever I am today is due to them only. There is no such word to express my heartiest love to my friends because their unconditional love has been my greatest strength. They believed in me before I believed in myself.

I pay my homage to those experimental animals who have sacrificed their lives in making my endeavor successful. May God grant them eternal peace!

At last but not least, I acknowledge all those who knowingly and unknowingly contributed to making my work easier and a real success.

Above all, I owe it all to almighty God for granting me the wisdom, health, and strength to undertake this research task and enabling me to its completion.

Aanchal Verma

LIST OF ABBREVIATIONS

6-OHDA = 6-hydroxydopamine

ANOVA = Analysis of Variance

Bad = Bcl-2-associated Death Promoter

Bax = Bcl-2-Like Protein 4

Bcl-2 = B-Cell Lymphoma 2

BDNF = Brain-Derived Neurotrophic Factor

CNS = Central Nervous System

COX-2 = Cyclooxygenase-2

CPCSEA = Committee for the Purpose of Control and Supervision of Experiments on Animals

CREB = Camp Response Element-Binding Protein

DA = Dopamine

DMSO = Dimethyl sulphoxide

DOPAC = 3,4 – Dihydroxyphenylacetic acid

EGCG = Epigallocatechin-3 Gallate

ER = Estrogen Receptor

ER = Estrogen Receptor

Eres = Estrogen Reaction Elements

ERK = Extracellular Signal-Regulated Kinase

ERT = Estrogen Replacement Therapy

GPER1 = G Protein-Coupled Estrogen Receptor 1

GPER1 = G Protein-Coupled Estrogen Receptor 1

Gpx = Glutathione Peroxidases

GSH = Glutathione

HPLC = High Performance Liquid Chromatography

HVA = Homovanillic acid

i.p. = Intraperitoneal injection

IAEC = Institutional Animal Ethics Committee

IL-6 = Interleukin-6

JNK = c-Jun Amino-Terminal Kinase

L-dopa = Levodopa

MPTP = 1-methyl-4-phenyl-1,2,3,6-tetrahydropyridine

NADPH = Nicotinamide adenine dinucleotide phosphate

NGF = Nerve Growth Factor

OVX = Ovariectomized

p.o. = Orally

P13K = Phosphatidylinositol-4 5-biphosphate 3-kinase

PD = Parkinson's Disease

PEG = Polyethylene glycol

ROT = Rotenone

SEL = Selegiline

SN = Substantia Nigra

SNpc = Substantia Nigra Pars Compacta

TNF-α = Tumor Necrosis Factor α

LIST OF FIGURES

TABLE OF CONTENTS

ABSTRACT

ABSTRACT

- **Background:** Daidzein is a phytoestrogen that is exclusively found in soybeans and other legumes. It structurally belongs to the class of isoflavones. Rotenone inhibits complex I of the mitochondrial electron transport chain in dopaminergic neurons leading to glutathione (GSH) level reduction and oxidative stress. This study aimed to determine the neuroprotective effects of Daidzein against a Parkinson's disease (PD) model induced by rotenone in female albino Wistar rats.

- **Objective:** Parkinson's disease (PD) is a neurodegenerative disorder characterized by progressive damage of mesencephalic dopaminergic (DA) neurons of the substantia nigra (SN) which leads to motor disabilities and cognitive dysfunction. Evidence suggests that PD affects women less commonly than men, indicating a role for steroid hormones in the preservation of dopaminergic nigrostriatal neurons. It is reported that daidzein, a phytoestrogen and estrogen agonist, shows neuroprotective effects against neuronal death. In this study, we evaluated the effect of daidzein in ovariectomized and Parkinson's disease-induced rats.

- **Methods:** The experiments were carried out on Sham, OVX, OVX+ROT, and OVX+ROT+Daidzein groups of animals. The motor abilities were evaluated using behavioral parameters like actophotometer, rotarod, footprint analysis, bar catalepsy test, narrow beam walk test, open field test and grip strength test.

- **Results:** We found that Parkinson's disease leads to motor disabilities and ovariectomy worsened these disabilities. Whereas treatment with daidzein improved the performances of rats belonging to OVX+ROT group. Daidzein displayed a neuroprotective effect on dopaminergic neurons.
- **Conclusion:** Restorative impact of daidzein on motor dysfunction proves its beneficial effects on the nigrostriatal pathway and striatum.

Keywords: Daidzein, Parkinson's disease, Estrogen, Rotenone, Ovariectomy, Motor disorders

CHAPTER 1

INTRODUCTION

Chapter 1: INTRODUCTION

Parkinson's disease (PD) is the second-most common neurodegenerative disorder characterized by clinical symptoms including postural instability, tremors, rigidity, and bradykinesia [1]. It is caused due to the loss of dopaminergic neurons in the substantia nigra pars compacta (SNpc). As a result, dopamine levels in the striatum decrease [2,3]. According to the global burden of diseases study 2017, the global prevalence of PD was reported to be 8.52 million and the incidence was 1.02 million [4]. The same study estimated that the number of PD cases will double, from approximately 7 million in 2015 to 13 million in 2040, predicting a possible "PD Pandemic" [5]. Different genetic, hormonal, neuroendocrine, and molecular factors contribute to the variations in Parkinson's disease pathogenesis [6]. A population-based study reported that males are 50% more likely to get Parkinson's disease [7]. Other PD prevalence studies also show a steady increase in PD with age and male gender [8]. This information suggests a possible protective role of estrogen against PD.

In postmenopausal women, the high incidence of PD indicates a reduction in estrogen [9]. The correlation between estrogen exposure and PD risk has been investigated in a clinical report [10] and a relationship between the duration of estrogen exposure and PD susceptibility has also been established [11]. Estrogen replacement therapy (ERT) recently became a suitable treatment option for PD in postmenopausal women [12]. Despite the favourable impact of ERT in PD, it possesses undesirable effects, such as the increased risk of breast and endometrial cancer, ischemic disorders, and irregular bleeding [13,14]. They are non-steroidal compounds that closely resemble the effects of endogenous estrogen structurally and functionally without undesired effects. In addition to estrogen, phytoestrogens are also found to exhibit neuroprotective effects [15]. Therefore, phytoestrogens can be used as an alternative therapeutic approach for the development of novel drug treatment for the management of PD.

Daidzein is a potent phytoestrogen that belongs to the class of Isoflavones. It is widely present in Pueraria, nuts, soy, and soy products [16,17]. Daidzein is chemically similar to human estrogen and shows bi-directional activity on estrogen receptors. The effect of Daidzein is shown by estrogen receptor regulation [18]. Moreover, some findings have highlighted the role of daidzein in neuroprotection. It is used in the treatment of cerebral ischemia due to its neuroprotective power [19]. It was able to reduce neuroinflammation and restore the proper cell morphology and functionality by activation of Erβ, downregulating cell death, proinflammatory processes, oxidative stress, and apoptosis [20]. In addition, multiple studies have shown that microbial biotransformation of isoflavones in the intestine has an important impact on their clinical therapeutic effectiveness, like neuroprotection [21]. It is well established that phytochemicals are usually safe for the health when compared with synthetic drugs as they are less toxic and have fewer or mild side effects [22]. Hence, there is an urge to develop a novel treatment for Parkinson's disease using the potential benefits of phytoestrogens.

It has been reported that mitochondrial function inhibitors like pesticides and rotenone produce PD-like outcomes like behavioral defects and nigrostriatal degeneration [23]. Rotenone is a lipophilic compound that is reported to easily cross the blood-brain barrier. Rotenone accumulates in mitochondria and inhibits the complex-I unit of the electron transport chain [24]. Intracranial injection of rotenone in rats resulted in motor dysfunction of rats [25].

In this study, the reformative effects of daidzein on a rotenone-induced experimental model of Parkinson's disease in rats were revealed by measuring motor abilities and biochemical features.

CHAPTER 2

REVIEW OF LITERATURE

Chapter 2: Review of Literature

Parkinson's disease (PD) is a neurodegenerative disorder characterized by incremental depletion of dopaminergic neurons in the substantia nigra pars compacta (SNpc), reduced striatum dopamine levels, and muscle impairments, including bradykinesia, rigidity, and tremor [26]. Several non-motor symptoms including sleep, neurological, neuropsychiatric, autonomic, and sensory disturbances are also observed [27]. Clinical studies have indicated a higher frequency and prevalence of PD in males than in females [28,29]. The cause of most cases of PD is unclear and is possibly due to a range of genetic and environmental risk factors [30]. In vivo studies have also shown the significant beneficial effects of estrogen in shielding the brain from neurodegenerative processes like PD. Efficient drug regimens were mainly accompanied by the enhancement of sufficient dopamine concentrations in the Central Nervous System (CNS). Estrogen lowers the striatal dopamine loss in 1-methyl-4-phenyl-1,2,3,6-tetrahydropyridine (MPTP)-intoxicated mice [31,32] and in 6-hydroxydopamine (6-OHDA)-lesioned rats [33]. Even though studies indicate the beneficial effects of estrogen in PD and perhaps other senile diseases, but due to the unwelcome side effects of estrogen, such as the elevated risk of breast and endometrial cancer and irregular bleeding, many women resort to phytoestrogens as an alternative to hormone replacement therapy (HRT) [34,35].

The neuroprotective effects of phytoestrogens against cell and animal models of PD have been documented in both in vivo and in vitro studies [36,37]. Phytoestrogens have the potential to exhibit weak estrogenic actions to regulate the physiological behaviour of endogenous estrogen by interacting with ERs (estrogen receptors) [38]. While phytoestrogens classification is still uncertain, it is broadly accepted that phytoestrogens can be subdivided into four major categories: flavonoids, lignans, coumestans, and stilbenes [39]. Generally, phytoestrogens are commonly divided into different subclasses: isoflavones, flavonols,

flavanones, flavanols, anthocyanins, flavones, and have potential neuroprotective activity without inducing side effects as HRT does [40–43]. Soy, soy-based food items, and other legumes are abundant in isoflavones, of which genistein and daidzein are the two most common [44]. Exposure to dietary genistein can function similarly to estradiol in increasing striatal dopamine (DA) discharge in preclinical and clinical studies [26,45]. Estrogen is believed to facilitate cell survival in non-neuronal tissues and alleviate brain damage by affecting the expression of Bcl2 [46]. It is a survival factor that can inhibit the death of apoptotic cells. Several shreds of evidence from distinct epidemiological findings and animal models of parkinsonism have demonstrated that estrogen shows the neuroprotective results on dopaminergic neurons by either re-establishing the oxidative state of the cells or by reducing the inflammatory processes correlated with the disorder [47]. Hence, research on phytoestrogens' effects in neurodegenerative conditions such as PD has increased considerably. Here, we review the role of various phytoestrogens in the brain with an emphasis on animal models of PD as well as the mechanisms involved in the neuroprotective effect of estrogen.

ERs regulate estradiol's biochemical actions. Firstly, two nuclear receptors ERα and ERβ belonging to the superfamily, were identified [48]. The ERs are activated when 17β-estradiol binds to the binding domain and by phosphorylation of distinct threonine/serine residues, which cause either homodimerization or heterodimerization of ERs and bind to particular DNA-binding region is known as EREs or estrogen reaction elements found in the target gene promotor area and the transcriptional gene action is either increased or decreased based on the portion of recruited corepressors and coactivators. ERs can modulate genes that are free from ERE by serving as transcription partners on non-ERE locations. Furthermore, 17β-estradiol may bind to ER-associated plasma membrane on ERα and ERβ receptors as microdomains where it interferes with the signalling of neurotransmitters and growth factor

receptors [49–51]. These plasma membrane ERs are mainly accountable for the accelerated cellular events caused by 17β-estradiol. Various signalling pathways such as phosphatidylinositol-4,5-biphosphate 3-kinase (P13K)/ protein kinase B, extracellular signal-regulated kinases (ERK)1/(ERK)2, protein kinase A/cAMP/CREB, mobilization of calcium, and numerous ion channels are responsible for the rapid neurotransmission mediated by estrogen [52,53].

Repeated researches have shown that some phytoestrogens directly bind to ERs but possess a comparatively pooraffinity to 17β-estradiol. The isoflavonoids have the binding ability towards each ER isoforms, leading to gene transcription activation dependent on ER [54,55]. Isoflavones suchas genistein and daidzein belonging to the class offlavonoids have a greater affinity to ERs, especially ERβ.For instance, genistein exhibits a much higher affinity toERβ than ERα [56]. This function of isoflavonoids isunique in its selective binding to ERβ, and it indicates thatvarious 17β-estradiol related effects can be exhibited by these phytoestrogens, which binds with the same affinity toERα and ERβ [57,58].These findings indicate that the phytoestrogens exhibit the desired estrogenicfeatures based on the basic phytoestrogen structure.

The main signalling routes mediated by ERα and ERβ activation were involved in mechanisms related to DA neurons' neuroprotection. Signalling cascades: ERK1/ERK2, Akt/PI3K, and c-Jun amino-terminal kinase (JNK) are known to activate a wide range of transcription factors engaged in the survival of the neurons [59,60]. Adding to this, ER activation-induced expression of some neuroprotective proteins may initiate other neuroprotective signalling pathways. For example, expression of a neurotrophic factor-like BDNF (brain-derived neurotrophic factor) shows a surge following ER activation by raised phosphorylation of CREB and BDNF receptor- (Trk) B (tropomyosin receptor kinase).Intracellularly activated ERα also interacts with neuroprotective signalling cascades

and activates the insulin-like growth factor (IGF)-1 receptor [49,61]. Further, these signaling pathways ERK1/ERK2 and PI3K/Akt trigger antiapoptotic protein production. Some examples of such proteins are Bcl-2, Bcl-xL, and Bcl-W. These neuroprotective signaling cascades also cause the downregulation of apoptosis inducer- Bax and the death promoter-Bad [62]. Several recent studies have suggested that some phytoestrogens belonging to the subclass of flavanoids may cause neuritis growth and hinder neuronal survival by expressing neurotrophic factors, including ERK1/ERK2, PI3K, PKC activation, and CREB neurotrophic signaling pathway [63]. In cultured astrocytes of rats, 22 flavonoids, out of 33 test compounds, have been shown to cause enhanced secretion of neurotrophic factors, including NGF, BDNF, and GDNF. The most effective flavonoids that induced the secretion of these neurotrophic factors are calycosin, isorhamnetin, luteolin, and genistein. Elevated production of neurotrophic factors initiated by these flavonoids was followed by a rise in phosphorylation of the ERα receptor. These outcomes being obstructed by pre-incubation of the astrocytes using an ER antagonist show that certain flavonoids have a clear relationship between an ER-dependent pathway to enhance neurotrophic factor expression [64–67]. These studies show that phytoestrogens play an important role in neuroprotection in Parkinson's disease by modifying neuronal signaling pathways.

Daidzein is an isoflavone, primarily present in soybeans and peanuts, act as ERβ, ERα, and GPER1 agonists [68]. Interestingly, a significant contribution has been made to the daidzein-mediated increased caspase-3 function of intracellular signaling pathways ERβ and GPER1 in hippocampal cultures [69]. This isoflavone barred apoptosis and 6-OHDA-induced cell death in NGF-differentiated PC12 cells and decreased the activity of caspase-3/8 [70]. Daidzein has manifested its neuroprotective activity in BV-2 murine microglial cells by decreasing ROS, NO and subsequently, induced the prostaglandin E2 by microglia through reduction of pro-inflammatory factors' release such as TNF- α, COX-2, iNOS, and IL-6 [71].

CHAPTER 3

MATERIALS AND METHODS

Chapter 3: Materials and Methods

3.1 Experimental Animals

For experimentation, adult female Wistar albino rats (150-200 g weight) were acquired from the central animal house, Institute of Pharmaceutical Research, GLA University, Mathura. All the 36 animals in this experiment were split into six groups of six animals each. The rats were placed in polyacrylic cages and the place was maintained under a 12:12 hours of light/dark cycle, 25 ± 1 °C temperature, and 45%-55% of relative humidity. Throughout the experiment, the animals were fed their standard pellet diet (Lipton India, Ltd., Mumbai) and water as required. The experimental investigation was granted approval by the Institutional Animal Ethics Committee (GLAIPR/CPCSEA/IAEC/2021/P.Col./R01) in accordance with the guidelines of the Committee for the Purpose of Control and Supervision of Experiments on Animals (CPCSEA). Furthermore, during the experiments, the principle of laboratory animal concern (National Research Council (US) Committee for the update of the guide for the care and use of laboratory animals 2011) was followed.

3.2 Chemicals and Reagents

Rotenone, daidzein and selegiline were the chemicals, purchased from Sigma-Aldrich (St. Louis, MO, USA). The rest of the analytical grade reagents and chemicals were obtained from Merck Pvt. Ltd., New Delhi.

3.3 Surgical Procedures

3.3.1 *Ovariectomy*

Ovariectomy was performed through dorsolateral incisions [72]. The animals in the Sham group were subjected to the same procedure but their ovaries were kept intact. Following ovariectomy, vaginal smears were performed for 5 days to confirm the success of the ovariectomy and the cessation of the estrous cycle. In the OVX group, only vehicle (DMSO and PEG) was administered.

3.3.2 *Stereotaxic Injection of Rotenone*

Before surgery, the rats were anesthetized with intraperitoneal administration of a combination of ketamine and xylazine and fixed in a stereotaxic frame (Instruments and Chemicals, Ambala, New Delhi). Rotenone (ROT) was dissolved in DMSO:PEG (1:1) and injected (2µl) at a flow rate of 0.2 l/min into the right substantia nigra pars compacta (SNpc). From the Bregma point, the stereotaxic coordinates were: lateral=0.20, anterio-posterior=0.53, and dorso-ventral=0.75 [73,74].The Sham animals were given 2 µl of a 1:1 mixture of DMSO and PEG into the right SNpc. Further, the animals received proper post-operative care until they were completely recovered.

3.4 Experimental Design

The entire experimental protocol was planned for 14 days (Figure 1). All the animals were acclimatized for 7 days before being randomly divided into six groups, each with six animals. These groups were termed Sham, OVX, OVX+ROT, OVX+D-1+ROT, OVX+D-2+ROT and OVX+ROT+SEL. Rats of all groups were subjected to bilateral ovariectomy. However, the rats of Sham group underwent the same procedure, their ovaries were kept intact. After the surgery, the rats were allowed to recover. Daidzein (50 mg/kg and 100mg/kg, p.o.) [75]and Selegiline (10 mg/kg, i.p.) [76] were administered to OVX+D-1+ROT, OVX+D-1+ROT and OVX+ROT+SEL groups of animals on Day-12 to Day-29 respectively. While ROT was given on Day-16 of the experimental program to all animals of Sham and OVX groups. Experimental animals were subjected to behavioral tests on Day-30 of the protocol. After behavioral tests, rats were sacrificed through cervical dislocation and the brain was micro-dissected into striatum and SNpc and instantly stored at −80 °C for biochemical analysis [74]. For reproducibility, all the biochemical experiments were done twice.

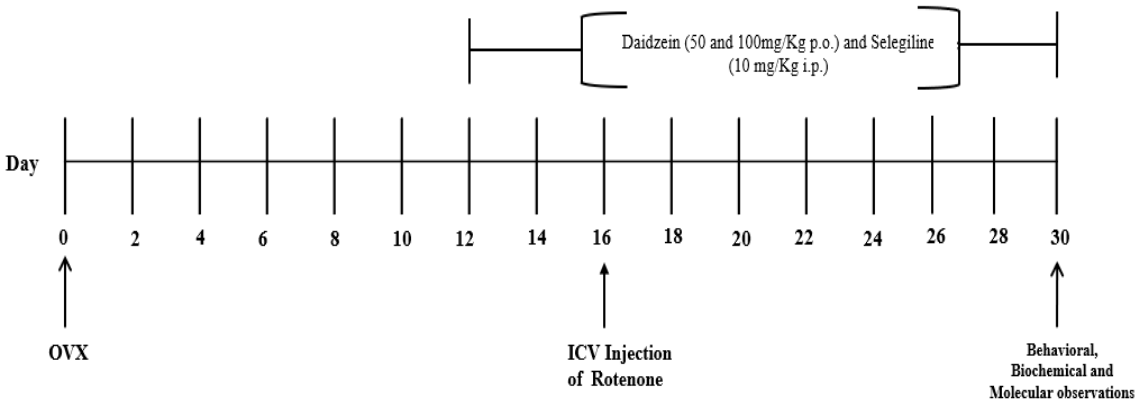

Figure 1: Diagrammatic representation of detailed experimental schedule.

3.5 Behavioural Tests

3.5.1 Narrow Beam Walk Test

Narrow beam walk test was conducted to evaluate the impairment of hind-limb [77]. The number of foot-slips was noted and time taken to cross the beam was measured. The rats were previously trained two times on D-16, 2 hr prior to rotenone injection to cross an uplifted wooden beam. On D-30, the rats were horizontally placed 60 cm above the floor, 120 cm long and 3 cm diameter, to abscond the end of the beam. On the other end of the beam, a dark goal box measuring 25×20×18 cm is present. The rats were evaluated on the 30th day by putting individual rat on the end of the beam and the frequency of hind-paw slips as well as the time taken by the rats to cross the beam were noted. The maximum time sanctioned for the task was 120 s.

3.5.2 *Open Field Test (OFT)*

OFT evaluates locomotor and emotional responses in rats [78]. A wooden open field measuring (60 × 60 cm) with 30 cm high walls was taken. All behavioral variables including total distance covered, immobility time period, the number of rearing, and the number of lines crossed by hindlimb of every rat was recorded for 5 min after being put down in the center of the field. As a measure of total distance travelled and rearing (exploratory activity), grid crosses by hind limb were counted under moderate illumination [79].

3.5.3 *Rotarod Test*

The Rotarod test was used to track animals' motor coordination capability [80]. Animals from all the groups were trained on rotarod apparatus (orchid scientific), prior to the lesioning for five consecutive days with accelerating speed of the rod ranging from 4 to 40 rpm in 10 minutes, until a stable activity was attained. For each test of training, the animals were carefully positioned on the apparatus, opposite the rotating rod, in order to obtain the requisite skilled behavior on the rotating rod, so that a fall could be avoided. The cut-off period was 60 s (considered as the maximum time for rats to remain on the rod). The time was estimated to remain on the spinning rod.

3.5.4 *Bar Catalepsy Test*

Catalepsy bar tests are widely used to evaluate muscular rigidity or catalepsy behavior [81]. This behavior was evaluated by recording the number of latencies used by rats to withdraw one of their forelimbs from a 10 cm bar after being placed in a standing posture in three successive trials. The cut-off time allowed was 60 s.

3.5.5 *Grip Strength Test*

Neuromuscular strength and limb impairment were measured on D-30 by the grip strength test. The apparatus included of a metal wire measuring approximately 90 cm in length and horizontally fixed between two vertical supports at a height of 50 cm [82]. The rat was hung with its forepaws reaching the center of the wire and evaluated using the following scale: 0—fall offs; 1— hangs onto string with both forepaws; 2— same as 1 but seeks to climb on the string; 3—hangs onto string with both forepaws plus one or both hind paws; 4—hangs onto string with all fore paws plus tail wrapped around the string and 5—escapes from apparatus and falls down.

3.5.6 *Actophotometer*

The locomotor activity was assesed using actophotometer (IKON Instrument). It consisted of a square arena where the animal could move freely. It also consisted of a digital counter, photocell, and a light source to measure the locomotor activity of the animal. The movement of an animal cutting a beam of light falling on the photocell as well as count was displayed digitally and recorded. Individual animals were placed in the device, and the overall activity count was monitored at D-30 for 5 min. The locomotor activity was expressed in terms of total photobeam counts/5 min [83].

3.5.7 *Foot Print Analysis*

As an indicator for the animal gait, the footprint patterns (walking tracks) have been calculated. In summary, rats were made to walk along a narrow track (100 cm long, 10 cm wide and with 20 cm high walls), white sheet-covered corridor (leading to a darkened enclosure), leaving a trail of footprints. The animal's fore- and hind-paws were painted in red and green, respectively. To obtain the footprint pattern, rats were trained to walk on a platform lined with white paper. The footprints of the rats were assessed for fore- and hind-paw base width and fore- and hind-paw stride length of the rats [84].

3.6 Biochemical Measurements

3.6.1 Estimation of dopamine and its metabolite levels

The concentration of DA and its metabolites was evaluated in the striatum of all experimental animals using HPLC with an electrochemical detector [85,86].

3.6.2 Estimation of caspase-3 activity

Caspase-3 activity was calculated as an apoptosis indicator. Caspase-3 colorimetric assay kit (Assay Design, Inc. Michigan USA) was used for the estimation. The standard protocol, as specified by the manufacturer, was followed. Caspase 3 activity was measured in unit per mg of tissue weight. The amount of enzyme required to convert one picomole of substrate per minute at 30 ℃ is specified as a unit.

3.6.3 Estimation of glutathione peroxidase (GPx) activity

The glutathione (GSH)/NADPH/glutathione reductase system, reduction of H_2O_2 at 340 nm was used to measure GPx, with a spectrophotometer. The oxidation of glutathione was linked to NADPH oxidation catalyzed by glutathione reductase [87,88]. GPx activity was expressed as µmol oxidized NADPH/min/mg protein.

3.7 Statistical Analysis

The results are displayed in terms of mean and standard deviation. Statistical software GraphPad Prism (Version 6.0) was used for data analysis. One-way ANOVA variance test was performed followed by Tukey's Multiple Comparison Test, used for the analysis of behavioral and biochemical estimations. A *p* value of less than 0.05 was considered as statistically significant.

CHAPTER 4

RESULTS

Chapter 4: Results

4.1 Behavioral Tests

4.1.1 Recuperative Effect of Daidzein (50 mg/kg and 100mg/kg) on Rotenone-Influenced Motor Changes in Narrow Beam Walk Test

Figure 2 displays the action of daidzein on rotenone-influenced behavioral changes in the functions of hind-limb with respect to (A) time required to enter the goal box, (B) number of left hind-paw slips, and (C) number of right hind-paw slips of the rats in the narrow beam walk test. One-way ANOVA showed notable disparities in the transfer time [$F(5, 30) = 28.48$, $p>0.05$] and number of left hind-paw slips [$F(5, 30) = 29.27$, $p>0.05$] in the animal groups but no notable differences were observed in the frequency of right hind-paw slips [$F(5, 30) = 0.82$, $p>0.05$] among the group of animals. Post-hoc analysis revealed that ovariectomy further worsened the motor functions of the rats. Thus, rats of OVX group took longer and rotenone-administered ovariectomized rats took the longest time to cross the beam and showed significantly more foot slips than rats of the sham group. Here, daidzein reduced rotenone-instigated behavioral modifications in rats, similar to selegiline.

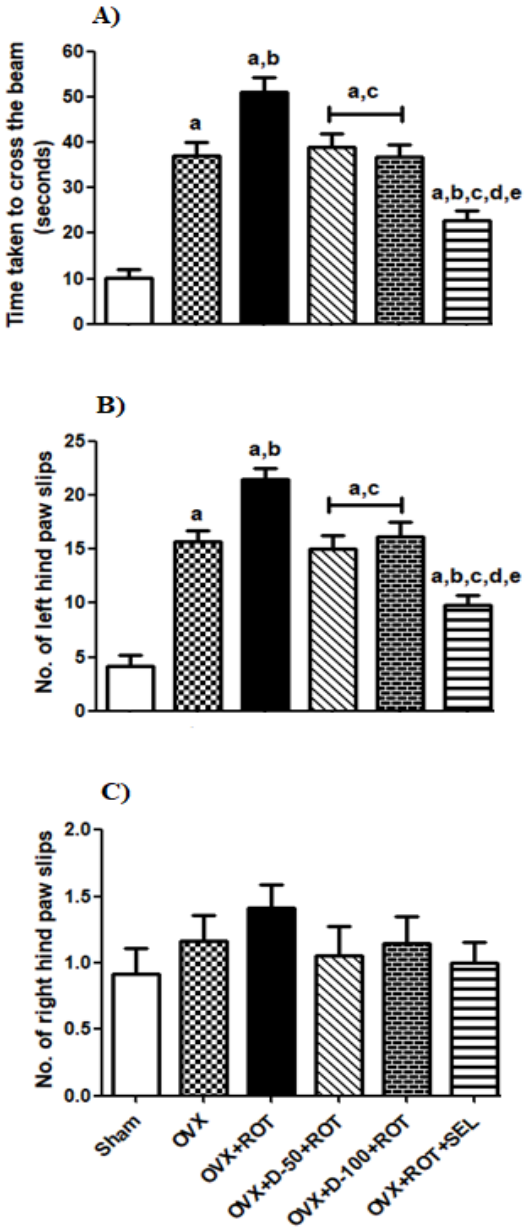

Figure 2: Effect of daidzein (50 and 100 mg/kg) on rotenone-induced variations in (A) time taken to reach into goal box, (B) number of left hind-paw slips and (C) number of right hind-paw slips in narrow beam walk test. All values are expressed as mean±SEM (N=6). $^{a}p<0.05$ compared to Sham, $^{b}p<0.05$ compared to OVX, $^{c}p<0.05$ compared to OVX+ROT, $^{d}p<0.05$ compared to OVX+D-1+ROT, $^{e}p<0.05$ compared to OVX+D-2+ROT (one-way ANOVA followed by Tukey's –Multiple–Comparison Post-hoc test).

4.1.2 Recuperative Effect of Daidzein (50 mg/kg and 100mg/kg) on Rotenone-Influenced Motor Changes in Open Field Test

Figure 3 displays the action of daidzein on behavioral changes induced by rotenone in (A) the distance traveled, (B) total number of lines traversed by the hind-paw, (C) number of rearing, and (D) inactivity period during the open field test. Significant differences in the distance travelled [$F(5, 30) = 30.77$, $p>0.05$], total number of lines traversed by the hind-paw [$F(5, 30) = 44.46$, $p>0.05$], number of rearing [$F(5, 30) = 23.47$, $p>0.05$], and total immobility period [$F(5, 30) = 25.45$, $p>0.05$], were observed among the animal groups, in one-way ANOVA test. Post-hoc analysis displayed that the animals of OVX and OVX+ROT groups showed a decrease in distance traveled, number of rearing, wandering and increased immobility time when compared to the rats of the sham group. Further, daidzein remarkably attenuated rotenone-instigated reduction in total distance traveled, number of rearing and motor activities, and rat's increased immobility time, similar to selegiline.

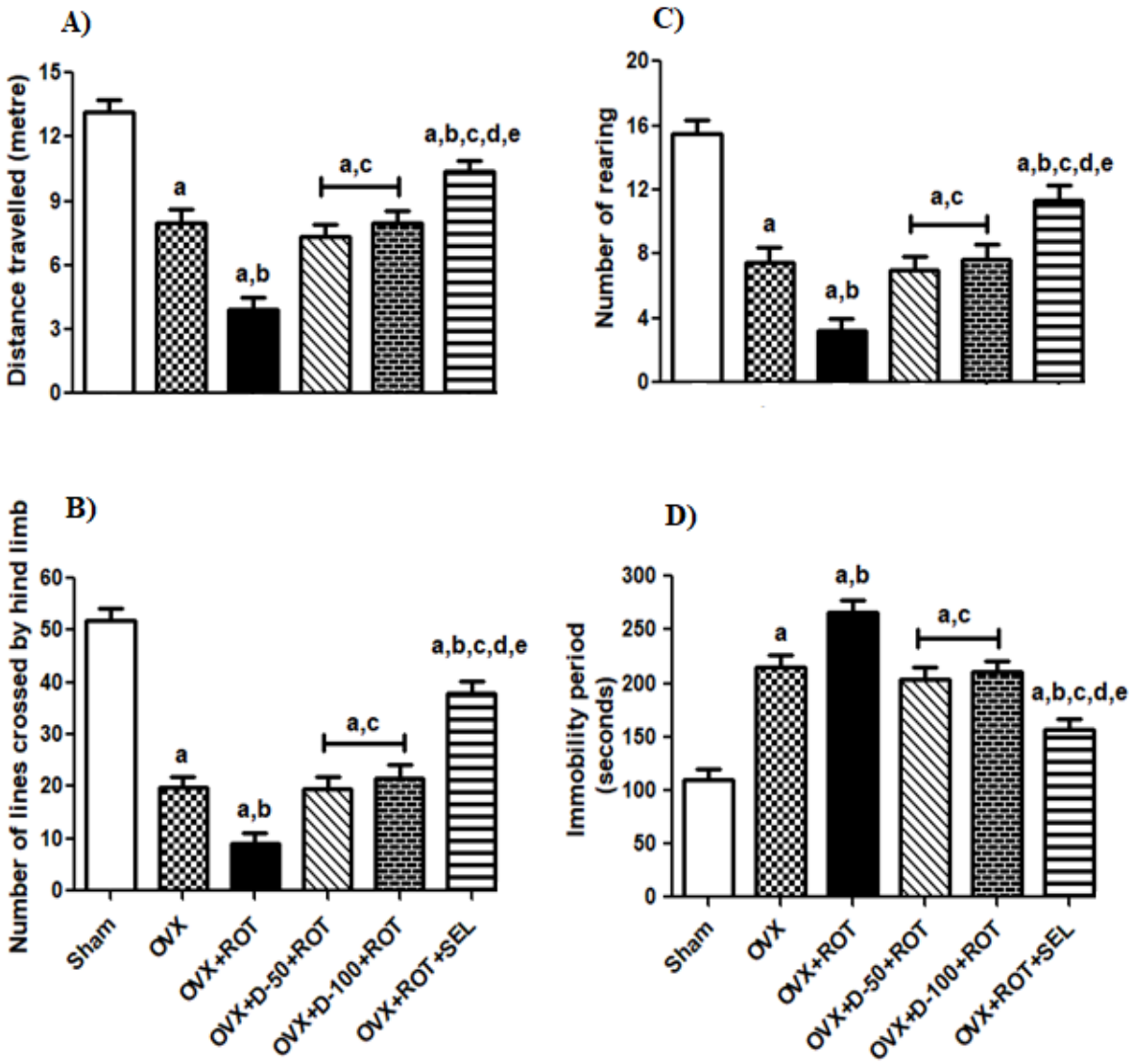

Figure 3: Effect of daidzein (50 and 100 mg/kg) on rotenone-induced variations in (A) total distance travelled, (B) lines traversed by hind limb of rats, (C) number of rearing and (D) inactivity period in open field test. All values are expressed as mean±SEM (N=6). $^{a}p<0.05$ compared to Sham, $^{b}p<0.05$ compared to OVX, $^{c}p<0.05$ compared to OVX+ROT, $^{d}p<0.05$ compared to OVX+D-1+ROT, $^{e}p<0.05$ compared to OVX+D-2+ROT (one-way ANOVA followed by Tukey's –Multiple–Comparison Post-hoc test).

4.1.3 Recuperative Effect of Daidzein (50 mg/kg and 100mg/kg) on Rotenone-Influenced Motor Changes in Retention Time, Grip Strength, Locomotor Activity and Bar Catalepsy Test

Figure 4 shows daidzein's action on rotenone-induced modifications in (A) retention time, (B) scoring in-grip strength test, (C) locomotor activity and (D) cataleptic activity of the animals in bar test during these behavioral tests. In one-way ANOVA, significant differences were noted in retention time [$F(5, 30) = 50.73$, $p>0.05$], score of grip strength test [$F(5, 30) = 30.58$, $p>0.05$], locomotor activity [$F(5, 30) = 24.04$, $p>0.05$] and cataleptic behaviour [$F(5, 30) = 50.22$, $p>0.05$] among the group of animals. Post-hoc analysis unveiled that ovariectomy further deteriorated the behavioral functions of rats. And, rats of OVX group and rotenone-treated rats displayed attenuated retention time, grip strength, and locomotor activity, as well as increased cataleptic behavior when compared to animals of sham group. Daidzein reversed rotenone-induced behavioral modifications in rats in rotarod, bar catalepsy, grip strength, and locomotor activity tests, like selegiline.

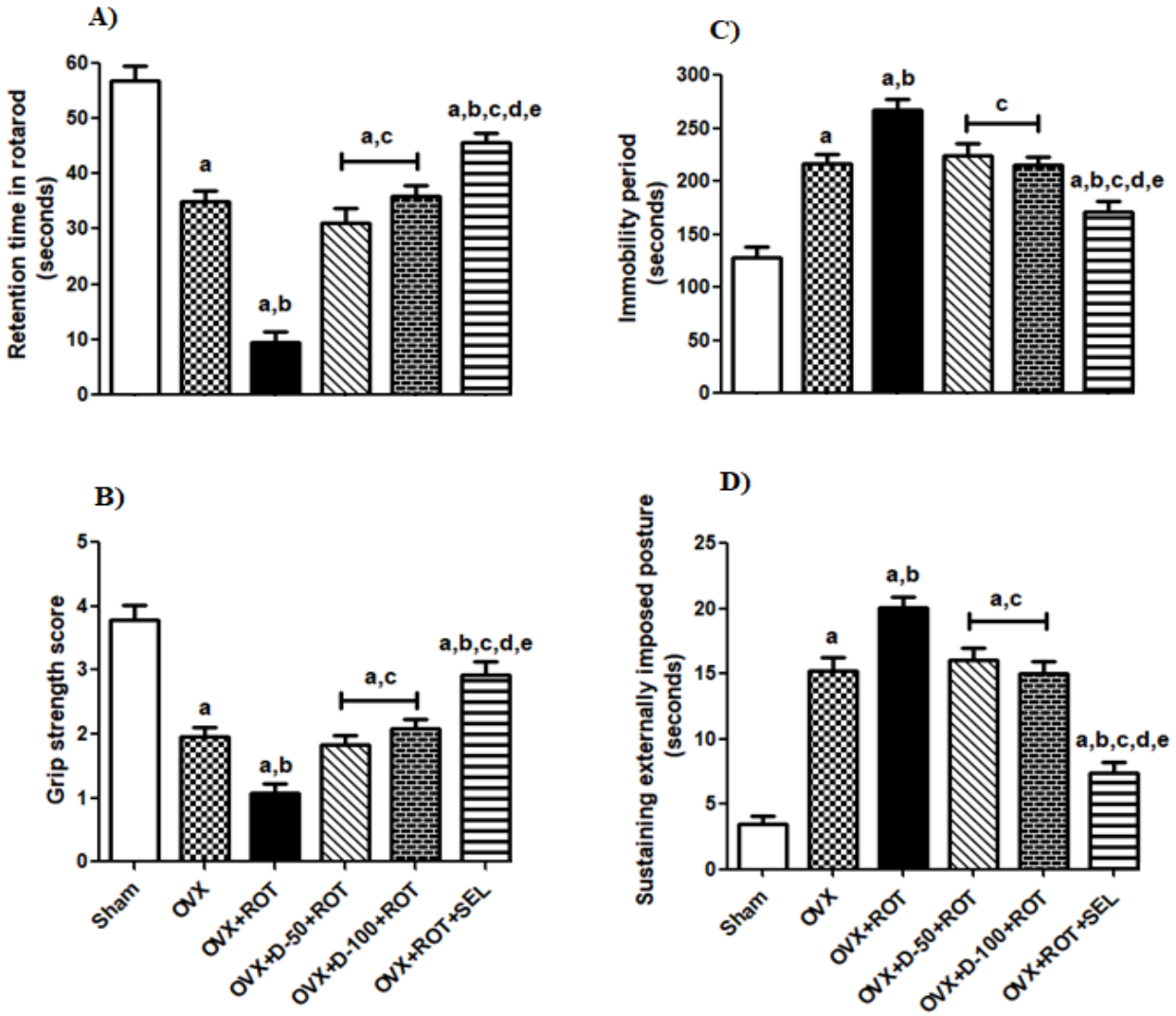

Figure 4: Effect of daidzein (50 and 100 mg/kg) on rotenone-induced variations in (A) retention time in rota rod, (B) score in grip strength test, (C) locomotor activity in actophotometer and (D) cataleptic behaviour in bar catalepsy test. All values are expressed as mean±SEM (N=6). [a]p<0.05 compared to Sham, [b]p<0.05 compared to OVX, [c]p<0.05 compared to OVX+ROT, [d]p<0.05 compared to OVX+D-1+ROT, [e]p<0.05 compared to OVX+D-2+ROT (one-way ANOVA followed by Tukey's –Multiple–Comparison Post-hoc test).

4.1.4 Recuperative Effect of Daidzein (50 mg/kg and 100 mg/kg) on Rotenone-Influenced Motor Changes in Footprint Test

Figure 5 displays the result of daidzein on mean stride length (cm), and the difference in base width (both fore-paw and hind-paw; cm). Statistical analysis revealed that there were remarkable disparities in the (A) stride length of left fore-paw [$F(5, 30) = 28.37$, $p>0.05$] and (B) left hind-paw [$F(5, 30) = 33.95$, $p>0.05$] among the animal groups. However, no significant differences were observed in the (C) base width of fore-paw [$F(5, 30) = 1.10$, $p>0.05$] or (D) hind-paw [$F(5,30) = 1.11$, $p>0.05$] in the groups of animals. Post hoc analysis showed that ovariectomy distorted the gait of animals. Therefore, ovariectomized rats and rotenone-treated rats showed shorter strides on both the fore and hind paws of the left foot, as well as a greater overlap in the rats, when compared to the rats of sham group. Daidzein notably reduced the rotenone-induced reduction in stride length of the fore and hind paws of the left foot of the animals, like selegiline.

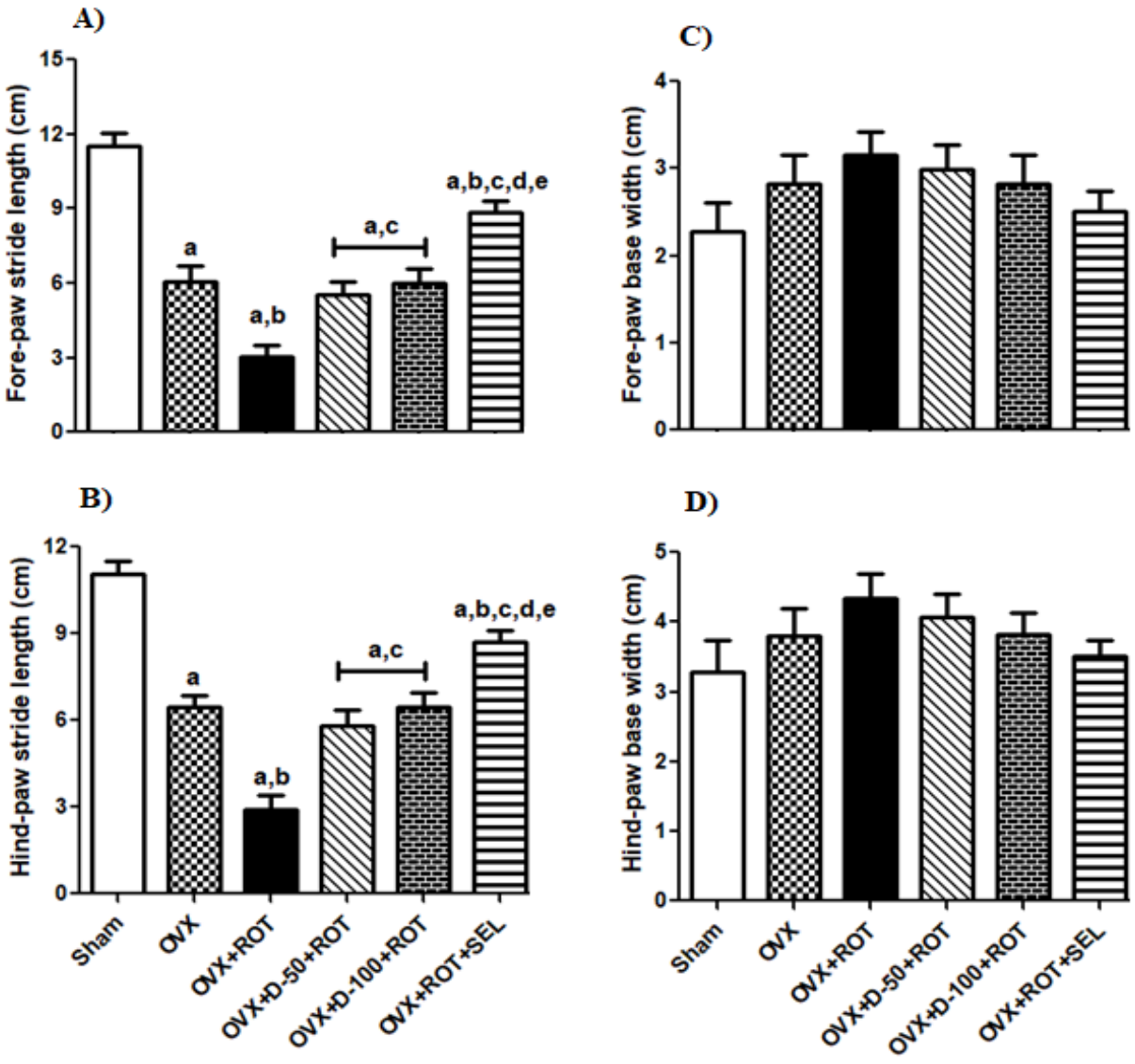

Figure 5: Effect of daidzein (50 and 100 mg/kg) on rotenone-induced variations in (A) left fore-paw stride length (B) left hind-paw stride length (C) fore-paw base width and (D) hind-paw base width in foot print analysis. All values are expressed as mean±SEM (N=6). [a]p<0.05 compared to Sham, [b]p<0.05 compared to OVX, [c]p<0.05 compared to OVX+ROT, [d]p<0.05 compared to OVX+D-1+ROT, [e]p<0.05 compared to OVX+D-2+ROT (one-way ANOVA followed by Tukey's –Multiple–Comparison Post-hoc test).

4.2 Biochemical Tests

4.2.1 Recuperative Effect of Daidzein (50 mg/kg and 100mg/kg) on Rotenone-Influenced Changes in GPx activity and Caspase-3 activity in SNpc

Figure 6 displays the action of daidzein on rotenone-influenced modifictions in (A) GPx activity and (B) Caspase-3 activity, in the SNpc of rats, during these biochemical estimations. Statistical analysis displayed that there was significant difference in the GPx activity [$F(5, 30) = 29.30$, $p>0.05$] and caspase-3 activity [$F(5, 30) = 28.48$, $p>0.05$] in the brains of rats. Furthermore, Post-hoc analysis revealed that ovariectomy significantly increased the nigral caspase-3 activity, and decreased GPx activity, when compared to sham-operated rats. Administration of rotenone resulted in a notable increase in nigral caspase-3 activity as well as notable decrease in GPx activity, on comparison with OVX rats. Treatment with daidzein led to a significant decrease in nigral caspase-3 activity and an increase in GPx activity. Therefore, daidzein significantly improved caspase-3 activity and GPx activity in experimental animals, as selegiline did.

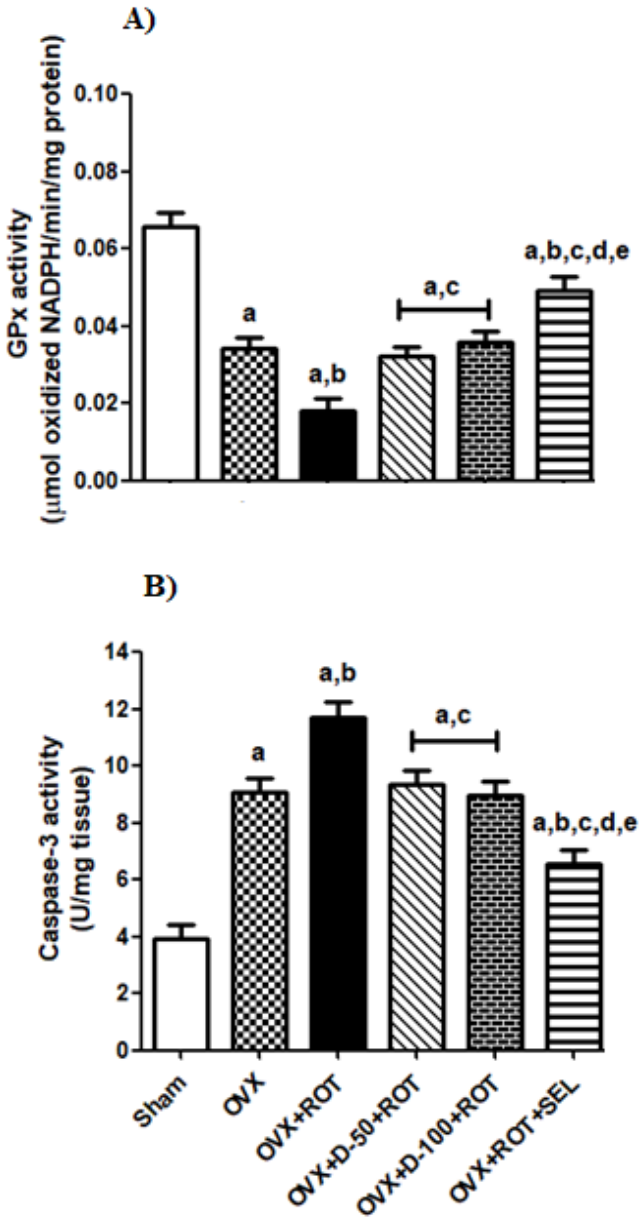

Figure 6: Effect of daidzein (50 and 100 mg/kg) on rotenone-induced variations in (A) GPx activity and (B) Caspase-3 activity. All values are expressed as mean±SEM (N=6). $^{a}p<0.05$ compared to Sham, $^{b}p<0.05$ compared to OVX, $^{c}p<0.05$ compared to OVX+ROT, $^{d}p<0.05$ compared to OVX+D-1+ROT, $^{e}p<0.05$ compared to OVX+D-2+ROT (one-way ANOVA followed by Tukey's –Multiple–Comparison Post-hoc test).

4.2.2 Effect of Daidzein on Striatal DA and its metabolites in SNpc

Figure 7 shows daidzein's action on rotenone-influenced altered dopamine concentration and its metabolites DOPAC and HVA in SNpc of rats. Statistics showcased that there was notable difference in the concentration of (A) Dopamine [$F(5, 30) = 32.89$, $p>0.05$], (B) DOPAC [$F(5, 30) = 31.40$, $p>0.05$] and (C) HVA [$F(5, 30) = 29.60$, $p>0.05$] in the striatum of mice. Post-hoc analysis showed that ovariectomy resulted in a notable decrease in striatal dopamine, DOPAC and HVA concentrations when compared to sham-operated rats whereas rotenone injection led to a significant decrease in striatal dopamine, DOPAC and HVA levels compared to OVX rats. However, treatment with daidzein increased the levels of dopamine and its metabolites, like selegiline.

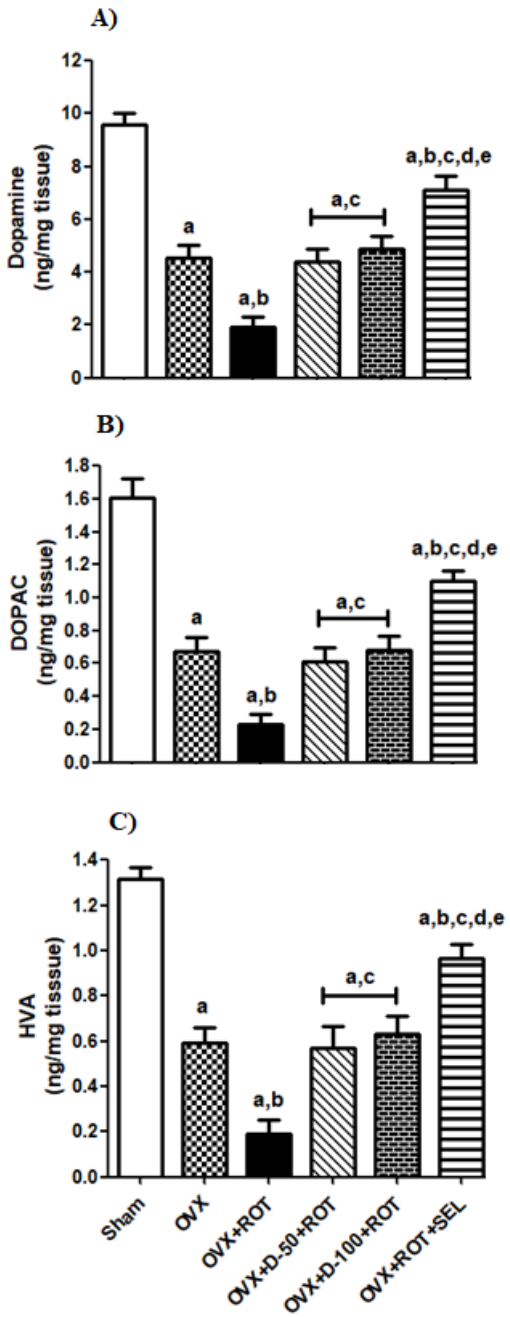

Figure 7: Effect of daidzein (50 and 100 mg/kg) on rotenone-induced variations in the striatal levels of(A) Dopamine (B) DOPAC and (C) HVA. All values are expressed as mean±SEM (N=6). [a]p<0.05 compared to Sham, [b]p<0.05 compared to OVX, [c]p<0.05 compared to OVX+ROT, [d]p<0.05 compared to OVX+D-1+ROT, [e]p<0.05 compared to OVX+D-2+ROT (one-way ANOVA followed by Tukey's –Multiple–Comparison Post-hoc test).

CHAPTER 5

DISCUSSION

Chapter 4: Discussion

This study demonstrates the effects of daidzein on the rotenone-induced PD model. The study also evaluates behavioral and biochemical parameters and discern information about the effects of daidzein on PD. Rotenone injection in the SNpc leads to behavioral abnormalities in rats and ovariectomy exacerbates the motor deficits. Further, daidzein decreases rotenone-induced neurotoxic effects in the nigrostriatal system of rats and protects against rotenone-induced decreased levels of dopamine in the striatum. At the sub-cellular level, daidzein attenuates rotenone-induced apoptosis and increases antioxidant enzyme activity in the SNpc of rats. These findings clearly indicate that daidzein may be considered as an alternate option in the treatment of Parkinson's disease.

The present study also shows that OVX causes a significant change in behavioral and biochemical parameters when compared to sham group. This alteration could be attributed to a decrease in the number of dopamine neurons after OVX, as reported earlier [89,90]. This changed neurotransmission after gonadal hormone depletion may lead to menopausal CNS disorders in susceptible women. In addition, numerous studies have demonstrated the beneficial effects of estrogen in motor disabilities in post-menopausal women [91,92]. Therefore, it can be concluded that estrogen plays a protective role in terms of susceptibility to PD.

The disruption of motor functions is well recognized in the pathogenesis of Parkinson's disease. In this study, rotenone led to significant dysfunction in the motor skills of rats. Also, the neuroprotective effect of estrogen and other phytoestrogens against rotenone has been reported in other studies [93–95]. Daidzein elicited a substantial improvement in the motor behavior of the experimental animals.

The latency time for the narrow beam walk test was used to evaluate motor function and coordination, whilst the number of foot faults was used to assess balance [96]. Here, we observed that daidzein treated group of rats showed a significantly reduced latency period and number of foot slips, compared to the rotenone-treated group. We determined that the motor function of the Parkinson-induced rats was significantly improved. And, this change can be attributed to the neuroprotective role of daidzein. Similar results on other phytoestrogens have been reported earlier [97].

Open field test is designed to evaluate the voluntary movement, anxiety, and exploratory behavior of rats in a confined environment. Parameters including the distance traveled, immobility period, number of rearing, and total lines crossed by hindlimb are indicators of limb activity in rats. All these parameters were increased in the model rats, after the administration of daidzein, indicating that daidzein can significantly improve voluntary movement dysfunction in a rotenone-induced PD rat model. A study exhibiting similar results in open field test has been reported previously [75].

The rotarod test evaluates the motor ability and motor coordination of rats or mice [98,99]. In this study, a significant increase in the retention time is indicative of the locomotor activity of rats. An increase in the retention time of the animal group undergoing daidzein treatment when compared with the OVX + rotenone group might be contributed to the protective effect of daidzein. Thus, the rotarod test, as previously reported, convincingly demonstrated the efficacy of daidzein [100].

Catalepsy bar tests are commonly used to assess the inability to alter an imposed posture caused by muscle rigidity [101]. We determined the latency of rats to remove one of their hind-limbs from the bar. In this experiment, daidzein treated group of animals showed significant improvement in their cataleptic behavior. Therefore, the presence of the protective

effect of daidzein in motor deficits like catalepsy was very well exhibited from this test. The beneficial effect of daidzein on motor disorders like catalepsy can be supported by similar studies [102].

Grip strength test is used to assess muscle strength and body composition in experimental animals. And, grip strength can be defined as a rat's maximum tensile force. The neuromuscular strength of all daidzein-treated animals was remarkably alleviated as the fall-offs and escapes from the apparatus were significantly reduced. In addition, attempts to climb on the string with the fore and hind paws also increased. The effect of daidzein on experimental rats has been previously evaluated on grip strength test [103].

Spontaneous locomotor activity was measured using an actophotometer. In this study, the immobility period of rats was measured as an indication of rat's locomotor activity. Improvement in the locomotor activity of rats was observed as the immobility time period of the animal group exposed to daidzein, was evidently reduced. Here, we successfully determined the neuroprotective effect of estrogen, as this reduced immobility period of rats after daidzein administration can be attributed to its restorative role in PD and other neurodegenerative disorders, as reported earlier [19,75].

The gait of the animals was examined using footprint analysis, by tracking the footprints of the animals. The gait variables like stride length of fore and hind paw as well as base width of fore and hind paw. Improvement in the gait of the animals was observed in daidzein-treated rats. This improvement may be due to daidzein's protective role in motor dysfunction caused due to rotenone-induced PD. This improved walking performance of rats by daidzein can be supported by previous studies [104].

The muscular structures of all rats must work regularly in order for them to successfully carry out these motor activity tests. These tests are more efficient diagnostic approaches in dopamine insufficiency in this scenario. Similarly, biochemical data show that these tests yield an appropriate diagnosis in Parkinson's disease patients.

Past studies have shown rotenone causes dopaminergic neuronal loss in the substantia nigra and decreases striatal dopamine levels, resulting in motor impairments in experimental animals [105]. Dopamine is converted into DOPAC and HVA when catalyzed by catechol-O-methyltransferase and monoamineoxidase, DOPAC and HVA levels in the brain are proportional to dopamine concentrations [106]. The levels of dopamine, DOPAC, and HVA in the striatum were also evaluated. Daidzein was found to increase the expression of dopamine, DOPAC, and HVA. These findings were consistent with the motor improvement of daidzein observed in motor activity tests. Therefore, these results imply that daidzein enhances motor abilities in rotenone-challenged rats, possibly via reducing dopaminergic toxicity.

In this study, rotenone lowered the GPx activity in rat’s SNpc, consistent with prior results [107]. Daidzein exacerbated the rotenone-persuaded decrease in the activity of GPx in the SNpc of the rats. Noteworthy, daidzein’s role in the alleviation of glutathione has been explored earlier [108]. Furthermore, increased striatal GPx activity in response to daidzein implies that this drug delivers neuroprotection against rotenone-induced oxidative stress, possibly through its ability to act as an antioxidant, which is consistent with previous research [109,110].

The pathophysiology of Parkinson's disease entails the death of a huge number of cells (apoptosis). It is well known that both intrinsic and extrinsic routes contribute to the degeneration of dopaminergic neurons. In this context, the caspase-3 activity was determined.

A statistically significant decrease in the caspase-3 activity was observed in daidzein treated group of rats in compaison to the PD group. Similar results were reported earlier [111]. Daidzein's capacity to protect against rotenone-induced nigral apoptosis could potentially explain its protective effect. The antiapoptotic action of daidzein is consistent with a study that reported daidzein's ability to decrease apoptosis and enhance cell survival in a PD cell culture model. It has been documented that daidzein's anti-apoptotic and pro-apoptotic actions on the PD model are related to the repression of pro-apoptotic proteins and stimulation of anti-apoptotic proteins [112].

Finally, the outcomes of this study successfully imply that daidzein may have had significant regulatory and reformative effects on the course and symptoms of PD in an experimental rat model.

CHAPTER 6

SUMMARY AND CONCLUSION

Chapter 6: Summary and Conclusion

Daidzein exerted a neuroprotective effect against rotenone-induced motor deficits. Furthermore, rotenone-induced biochemical aberrations were restored, where daidzein was able to alleviate oxidative stress and neuroinflammation in neuronal cells in the brain. As a result, it seems that daidzein mimics the function of estrogen in the ovariectomized rats and further prevents rotenone-mediated neuronal degeneration. Therefore, the present study recommends the use of daidzein in the treatment of neurodegenerative disorders.

CHAPTER 7

REFERENCES

Chapter 7: References

[1] Burke, R.E.; O'Malley, K. Axon Degeneration in Parkinson's Disease. *Experimental Neurology*, **2013**, *246*, 72–83.

[2] Geibl, F.F.; Henrich, M.T.; Oertel, W.H. Mesencephalic and Extramesencephalic Dopaminergic Systems in Parkinson's Disease. *Journal of Neural Transmission*, **2019**, *126*, 377–396.

[3] Makav, M.; Eroğlu, H.A. Recuperative Effect of Estrogen on Rotenone-Induced Experimental Model of Parkinson's Disease in Rats. *Environmental Science and Pollution Research*, **2021**, 1–10.

[4] Aryal, S.; Skinner, T.; Bridges, B.; Weber, J.T. The Pathology of Parkinson's Disease and Potential Benefit of Dietary Polyphenols. *Molecules*, **2020**, *25*.

[5] Jankovic, J.; Tan, E.K. Parkinson's Disease: Etiopathogenesis and Treatment. *Journal of Neurology, Neurosurgery and Psychiatry*, **2020**, *91*, 795–808.

[6] Vaidya, B.; Dhamija, K.; Guru, P.; Sharma, S.S. Parkinson's Disease in Women: Mechanisms Underlying Sex Differences. *European Journal of Pharmacology*, **2021**, *895*.

[7] R, M.; J, D.; N, H.; K, M.; MX, T.; LJ, C.; Y, S. A Population-Based Investigation of Parkinson's Disease with and without Dementia. Relationship to Age and Gender. *Archives of neurology*, **1992**, *49*, 492–497.

[8] Eusebi, P.; Franchini, D.; de Giorgi, M.; Abraha, I.; Montedori, A.; Casucci, P.; Calabresi, P.; Tambasco, N. Incidence and Prevalence of Parkinson's Disease in the Italian Region of Umbria: A Population-Based Study Using Healthcare Administrative Databases. *Neurological Sciences*, **2019**, *40*, 1709–1712.

[9] Kyuhou, S. ichi. Preventive Effects of Genistein on Motor Dysfunction Following 6-Hydroxydopamine Injection in Ovariectomized Rats. *Neuroscience Letters*, **2008**, *448*, 10–14.

[10] Liu, R.; Baird, D.; Park, Y.; Freedman, N.D.; Huang, X.; Hollenbeck, A.; Blair, A.; Chen, H. Female Reproductive Factors, Menopausal Hormone Use, and Parkinson's Disease. *Movement Disorders*, **2014**, *29*, 889–896.

[11] Nitkowska, M.; Czyżyk, M.; Friedman, A. Reproductive Life Characteristics in Females Affected with Parkinson's Disease and in Healthy Control Subjects – a Comparative Study on Polish Population. *NeurologiaiNeurochirurgiaPolska*, **2014**, *48*, 322–327.

[12] Haaxma, C.A.; Bloem, B.R.; Borm, G.F.; Oyen, W.J.G.; Leenders, K.L.; Eshuis, S.; Booij, J.; Dluzen, D.E.; Horstink, M.W.I.M. Gender Differences in Parkinson's Disease. *Journal of Neurology, Neurosurgery and Psychiatry*, **2007**, *78*, 819–824.

[13] Rossouw, J.E.; Anderson, G.L.; Prentice, R.L.; LaCroix, A.Z.; Kooperberg, C.; Stefanick, M.L.; Jackson, R.D.; Beresford, S.A.A.; Howard, B. v.; Johnson, K.C.; Kotchen, J.M.; Ockene, J. Risks and Benefits of Estrogen plus Progestin in Healthy Postmenopausal Women: Principal Results from the Women's Health Initiative Randomized Controlled Trial. *Journal of the American Medical Association*, **2002**, *288*, 321–333.

[14] Reeves, G.K.; Beral, V.; Green, J.; Gathani, T.; Bull, D. Hormonal Therapy for Menopause and Breast-Cancer Risk by Histological Type: A Cohort Study and Meta-Analysis. *Lancet Oncology*, **2006**, *7*, 910–918.

[15] Bagheri, M.; Joghataei, M.T.; Mohseni, S.; Roghani, M. Genistein Ameliorates Learning and Memory Deficits in Amyloid β(1-40) Rat Model of Alzheimer's Disease. *Neurobiology of Learning and Memory*, **2011**, *95*, 270–276.

[16] Guo, J.; Wang, Q.; Zhang, Y.; Sun, W.; Zhang, S.; Li, Y.; Wang, J.; Bao, Y. Functional Daidzein Enhances the Anticancer Effect of Topotecan and Reverses BCRP-Mediated Drug Resistance in Breast Cancer. *Pharmacological Research*, **2019**, *147*, 104387.

[17] Yang, T.; Feng, C.; Wang, D.; Qu, Y.; Yang, Y.; Wang, Y.; Sun, Z. Neuroprotective and Anti-Inflammatory Effect of Tangeretin Against Cerebral Ischemia-Reperfusion Injury in Rats. *Inflammation*, **2020**, *43*, 2332–2343.

[18] Laddha, A.P.; Murugesan, S.; Kulkarni, Y.A. *In-Vivo* and *in-Silico* Toxicity Studies of Daidzein: An Isoflavone from Soy. *Drug and Chemical Toxicology*, **2020**, 1–9.

[19] Wei, J.; Yang, F.; Gong, C.; Shi, X.; Wang, G. Protective Effect of Daidzein against Streptozotocin-Induced Alzheimer's Disease via Improving Cognitive Dysfunction and Oxidative Stress in Rat Model. *Journal of Biochemical and Molecular Toxicology*, **2019**, *33*.

[20] Morelli, S.; Piscioneri, A.; Guarnieri, G.; Morelli, A.; Drioli, E.; de Bartolo, L. Anti-neuroinflammatory Effect of Daidzein in Human Hypothalamic <scp>GnRH</Scp> Neurons in an in Vitro Membrane-based Model. *BioFactors*, **2021**, *47*, 93–111.

[21] Johnson, S.L.; Park, H.Y.; Vattem, D.A.; Grammas, P.; Ma, H.; Seeram, N.P. Equol, a Blood–Brain Barrier Permeable Gut Microbial Metabolite of Dietary Isoflavone Daidzein, Exhibits Neuroprotective Effects against Neurotoxins Induced Toxicity in Human Neuroblastoma SH-SY5Y Cells and Caenorhabditis Elegans. *Plant Foods for Human Nutrition*, **2020**, *75*, 512–517.

[22] Liskova, A.; Stefanicka, P.; Samec, M.; Smejkal, K.; Zubor, P.; Bielik, T.; Biskupska-Bodova, K.; Kwon, T.K.; Danko, J.; Büsselberg, D.; Adamek, M.; Rodrigo, L.; Kruzliak, P.; Shleikin, A.; Kubatka, P. Dietary Phytochemicals as the Potential Protectors against

Carcinogenesis and Their Role in Cancer Chemoprevention. *Clinical and Experimental Medicine*, **2020**, *20*, 173–190.

[23] JT, G.; R, B.; TB, S. The Rotenone Model of Parkinson's Disease: Genes, Environment and Mitochondria. *Parkinsonism & related disorders*, **2003**, *9 Suppl 2*, 59–64.

[24] Blandini, F.; Armentero, M.-T. Animal Models of Parkinson's Disease. *The FEBS Journal*, **2012**, *279*, 1156–1166.

[25] Carriere, C.H.; Kang, N.H.; Niles, L.P. Neuroprotection by Valproic Acid in an Intrastriatal Rotenone Model of Parkinson's Disease. *Neuroscience*, **2014**, *267*, 114–121.

[26] Liu, L.X.; Chen, W.F.; Xie, J.X.; Wong, M.S. Neuroprotective Effects of Genistein on Dopaminergic Neurons in the Mice Model of Parkinson's Disease. *Neuroscience Research*, **2008**, *60*, 156–161.

[27] Park, A.; Stacy, M. *Non-Motor Symptoms in Parkinson's Disease* In: Proceedings of the Journal of Neurology; **2009**; Vol. 256.

[28] Diamond, S.G.; Markham, ; C H; Hoehn, ; M M; Mcdowell, ; F H; Muenter, M.D. *An Examination of Male-Female Differences in Progression and Mortality of Parkinson's Disease*; **1990**.

[29] Mayeux, R.; Marder, K.; Cote, L.J.; Denaro, J.; Hemenegildo, N.; Mejia, H.; Tang, M.X.; Lantigua, R.; Wilder, D.; Gurland, B.; Hauser, A. The Frequency of Idiopathic Parkinson's Disease by Age, Ethnic Group, and Sex in Northern Manhattan, 1988-1993. *American Journal of Epidemiology*, **1995**, *142*, 820–827.

[30] Lesage, S.; Brice, A. Parkinson's Disease: From Monogenic Forms to Genetic Susceptibility Factors.

[31] Callier, S.; Morissette, M.; Grandbois, M.; Pélaprat, D.; di Paolo, T. Neuroprotective Properties of 17β-Estradiol, Progesterone, and Raloxifene in MPTP C57Bl/6 Mice. *Synapse*, **2001**, *41*, 131–138.

[32] Ramirez, A.D.; Liu, X.; Menniti, F.S. Repeated Estradiol Treatment Prevents MPTP-Induced Dopamine Depletion in Male Mice. *Neuroendocrinology*, **2003**, *77*, 223–231.

[33] Murray, H.E.; Pillai, A. v.; Mcarthur, S.R.; Razvi, N.; Datla, K.P.; Dexter, D.T.; Gillies, G.E. Dose- and Sex-Dependent Effects of the Neurotoxin 6-Hydroxydopamine on the Nigrostriatal Dopaminergic Pathway of Adult Rats: Differential Actions of Estrogen in Males and Females. *Neuroscience*, **2003**, *116*, 213–222.

[34] Warren, M.P. A Comparative Review of the Risks and Benefits of Hormone Replacement Therapy Regimens. *American journal of obstetrics and gynecology*, **2004**, *190*, 1141–1167.

[35] GK, R.; V, B.; J, G.; T, G.; D, B. Hormonal Therapy for Menopause and Breast-Cancer Risk by Histological Type: A Cohort Study and Meta-Analysis. *The Lancet. Oncology*, **2006**, *7*, 910–918.

[36] C, G.; D, P. Phytonutrients as Therapeutic Agents. *Journal of complementary & integrative medicine*, **2014**, *11*, 151–169.

[37] S, G.; MG, M. Neuroprotective Effect of Estradiol and Phytoestrogens on MPP+-Induced Cytotoxicity in Neuronal PC12 Cells. *Journal of neuroscience research*, **2002**, *70*, 90–96.

[38] Rowe, I.J.; Baber, R.J. The Effects of Phytoestrogens on Postmenopausal Health. *Climacteric*, **2021**, *24*, 57–63.

[39] Ramassamy, C. Emerging Role of Polyphenolic Compounds in the Treatment of Neurodegenerative Diseases: A Review of Their Intracellular Targets. *European Journal of Pharmacology*, **2006**, *545*, 51–64.

[40] Singh, A.; Tripathi, P.; Yadawa, A.K.; Singh, S. Promising Polyphenols in Parkinson's Disease Therapeutics. *Neurochemical Research*, **2020**, *45*, 1731–1745.

[41] Jung, U.J.; Kim, S.R. Beneficial Effects of Flavonoids Against Parkinson's Disease. *Journal of Medicinal Food*, **2018**, *21*, 421–432.

[42] Ross, J.A.; Kasum, C.M. Dietary Flavonoids: Bioavailability, Metabolic Effects, and Safety. *Annual Review of Nutrition*, **2002**, *22*, 19–34.

[43] Tanwar, A.K.; Dhiman, N.; Kumar, A.; Jaitak, V. Engagement of Phytoestrogens in Breast Cancer Suppression: Structural Classification and Mechanistic Approach. *European Journal of Medicinal Chemistry*, **2020**, *213*.

[44] F, L.; Y, L.; H, L.; MN, C. Classification of Natural Estrogen-like Isoflavonoids and Diphenolics by QSAR Tools. *Combinatorial chemistry & high throughput screening*, **2015**, *18*, 712–722.

[45] Leis, K.; Kulczyńska, A.; Racinowski, M.; Kaczor, P.; Gołębiewski, J.; Januszko-Giergielewicz, B. Genistein–a Supplement Improving Efficiency of the Human Body: A Review. *Science and Sports*, **2021**.

[46] E, S.; QG, Z.; R, W.; R, V.; D, B. Estrogen Neuroprotection and the Critical Period Hypothesis. *Frontiers in neuroendocrinology*, **2012**, *33*, 85–104.

[47] S, A.; C, B. Neuroprotection by Estrogen in the Brain: The Mitochondrial Compartment as Presumed Therapeutic Target. *Journal of neurochemistry*, **2009**, *110*, 1–11.

[48] S, L.; F, D.; F, F.; F, P. Phytochemicals Targeting Estrogen Receptors: Beneficial Rather Than Adverse Effects? *International journal of molecular sciences*, **2017**, *18*.

[49] Arevalo, M.A.; Azcoitia, I.; Garcia-Segura, L.M. The Neuroprotective Actions of Oestradiol and Oestrogen Receptors. *Nature Reviews Neuroscience*, **2015**, *16*, 17–29.

[50] Sanchez, R.; Nguyen, D.; Rocha, W.; White, J.H.; Mader, S. Diversity in the Mechanisms of Gene Regulation by Estrogen Receptors. *BioEssays*, **2002**, *24*, 244–254.

[51] Almey, A.; Milner, T.A.; Brake, W.G. Estrogen Receptors in the Central Nervous System and Their Implication for Dopamine-Dependent Cognition in Females. *Hormones and Behavior*, **2015**, *74*, 125–138.

[52] A, G.; D, G. Roflumilast Attenuates Cognitive Deficits in Estrogen Insufficient Rats. *Behavioural pharmacology*, **2020**, *31*, 671–687.

[53] J, S.; O, M.; A, C.; E, S.; J, M.; J, K. Estrogen Receptors in Cell Membranes: Regulation and Signaling. *Advances in anatomy, embryology, and cell biology*, **2017**, *227*, 93–105.

[54] FA, R.; AP, de O.; MS, de C.; W, V.; EA, V. Evaluation of Estrogenic Potential of Flavonoids Using a Recombinant Yeast Strain and MCF7/BUS Cell Proliferation Assay. *PloS one*, **2013**, *8*.

[55] D, T.; F, P.; M, G.; V, G.; N, S.; Z, H.; P, B.; C, S. Evidence of ERalpha and ERbeta Selectivity and Partial Estrogen Agonism in Traditional Chinese Medicine. *Reproductive biology and endocrinology : RB&E*, **2014**, *12*, 97.

[56] Thangavel, P.; Puga-Olguín, A.; Rodríguez-Landa, J.F.; Zepeda, R.C. Genistein as Potential Therapeutic Candidate for Menopausal Symptoms and Other Related Diseases. *Molecules*, **2019**, *24*, 1–17.

[57] Kuiper, G.G.J.M.; Lemmen, J.G.; Carlsson, B.; Corton, J.C.; Safe, S.H.; van der Saag, P.T.; van der Burg, B.; Gustafsson, J.Å. Interaction of Estrogenic Chemicals and Phytoestrogens with Estrogen Receptor β. *Endocrinology*, **1998**, *139*, 4252–4263.

[58] Leclercq, G.; Jacquot, Y. Interactions of Isoflavones and Other Plant Derived Estrogens with Estrogen Receptors for Prevention and Treatment of Breast Cancer - Considerations Concerning Related Efficacy and Safety. *Journal of Steroid Biochemistry and Molecular Biology*, **2014**, *139*, 237–244.

[59] Bourque, M.; Dluzen, D.E.; di Paolo, T. Neuroprotective Actions of Sex Steroids in Parkinson's Disease. *Frontiers in Neuroendocrinology*, **2009**, *30*, 142–157.

[60] Morissette, M.; Sweidi, S. al; Callier, S.; di Paolo, T. Estrogen and SERM Neuroprotection in Animal Models of Parkinson's Disease. *Molecular and Cellular Endocrinology*, **2008**, *290*, 60–69.

[61] Wang, S.; Ren, P.; Li, X.; Guan, Y.; Zhang, Y.A. 17β-Estradiol Protects Dopaminergic Neurons in Organotypic Slice of Mesencephalon by MAPK-Mediated Activation of Anti-Apoptosis Gene BCL2. *Journal of Molecular Neuroscience*, **2011**, *45*, 236–245.

[62] M, D.; P, M.; M, M.; LM, G.-S.; T, D.P. Implication of the Phosphatidylinositol-3 Kinase/Protein Kinase B Signaling Pathway in the Neuroprotective Effect of Estradiol in the Striatum of 1-Methyl-4-Phenyl-1,2,3,6-Tetrahydropyridine Mice. *Molecular pharmacology*, **2006**, *69*, 1492–1498.

[63] F, M.; R, H.; L, S.; O, F. Modulation of Neurotrophic Signaling Pathways by Polyphenols. *Drug design, development and therapy*, **2015**, *10*, 23–42.

[64] Xu, S.L.; Bi, C.W.C.; Choi, R.C.Y.; Zhu, K.Y.; Miernisha, A.; Dong, T.T.X.; Tsim, K.W.K. Flavonoids Induce the Synthesis and Secretion of Neurotrophic Factors in Cultured Rat

Astrocytes: A Signaling Response Mediated by Estrogen Receptor. *Evidence-based Complementary and Alternative Medicine*, **2013**, *2013*.

[65] Kim, T.Y.; Leem, E.; Lee, J.M.; Kim, S.R. Control of Reactive Oxygen Species for the Prevention of Parkinson's Disease: The Possible Application of Flavonoids. *Antioxidants*, **2020**, *9*, 1–28.

[66] RZ, L.; XW, D.; T, G.; L, A.-N.; TL, B.; JR, B. Beneficial Effect of Genistein on Diabetes-Induced Brain Damage in the Ob/Ob Mouse Model. *Drug design, development and therapy*, **2020**, *14*, 3325–3336.

[67] SJ, A.; JJ, W.; DK, S.; NU, B.; NK, P. GDNF, NGF and BDNF as Therapeutic Options for Neurodegeneration. *Pharmacology & therapeutics*, **2013**, *138*, 155–175.

[68] A, S.; M, I.; O, L.; C, K.; B, L.; A, H.; H, A.; YF, C.; C, M.; Y, M.; L, K.; C, C. Effect of S-Equol and Soy Isoflavones on Heart and Brain. *Current cardiology reviews*, **2019**, *15*, 114–135.

[69] Kajta, M.; Rzemieniec, J.; Litwa, E.; Lason, W.; Lenartowicz, M.; Krzeptowski, W.; Wojtowicz, A.K. The Key Involvement of Estrogen Receptor β and G-Protein-Coupled Receptor 30 in the Neuroprotective Action of Daidzein. *Neuroscience*, **2013**, *238*, 345–360.

[70] CM, L.; RD, L.; ST, C.; YP, L.; WT, C.; JW, L.; FL, H.; MH, L. Neurocytoprotective Effects of the Bioactive Constituents of Pueraria Thomsonii in 6-Hydroxydopamine (6-OHDA)-Treated Nerve Growth Factor (NGF)-Differentiated PC12 Cells. *Phytochemistry*, **2010**, *71*, 2147–2156.

[71] Chinta, S.J.; Ganesan, A.; Reis-Rodrigues, P.; Lithgow, G.J.; Andersen, J.K. Anti-Inflammatory Role of the Isoflavone Diadzein in Lipopolysaccharide- Stimulated Microglia: Implications for Parkinson's Disease. *Neurotoxicity Research*, **2013**, *23*, 145–153.

[72] FK, M.; FJ, B.; AP, T. Determination of the Estrous Cycle Phases of Rats: Some Helpful Considerations. *Brazilian journal of biology = Revistabrasleira de biologia*, **2002**, *62*, 609–614.

[73] C, A.; T, S.; LD, J. Protective Role of Apigenin on Rotenone Induced Rat Model of Parkinson's Disease: Suppression of Neuroinflammation and Oxidative Stress Mediated Apoptosis. *Chemico-biological interactions*, **2017**, *269*, 67–79.

[74] The Rat Brain in Stereotaxic Coordinates: Hard Cover Edition - George Paxinos, Charles Watson - (Accessed Aug 3, **2021**).

[75] Goel, R.; Chaudhary, R. Effect of Daidzein on Parkinson Disease Induced by Reserpine in Rats. *Brazilian Journal of Pharmaceutical Sciences*, **2020**, *56*, 1–7.

[76] D, S.; MM, M.; FA, H. Cognitive Aspects of Congenital Learned Helplessness and Its Reversal by the Monoamine Oxidase (MAO)-B Inhibitor Deprenyl. *Neurobiology of learning and memory*, **2010**, *93*, 291–301.

[77] Henderson, J.M.; Stanic, D.; Tomas, D.; Patch, J.; Horne, M.K.; Bourke, D.; Finkelstein, D.I. Postural Changes after Lesions of the Substantia Nigra Pars Reticulata in Hemiparkinsonian Monkeys. *Behavioural Brain Research*, **2005**, *160*, 267–276.

[78] Kraeuter, A.K.; Guest, P.C.; Sarnyai, Z. The Open Field Test for Measuring Locomotor Activity and Anxiety-Like Behavior. In: *Methods in Molecular Biology*; Humana Press Inc., **2019**; Vol. 1916, pp. 99–103.

[79] Garabadu, D.; Agrawal, N. Naringin Exhibits Neuroprotection Against Rotenone-Induced Neurotoxicity in Experimental Rodents. *NeuroMolecular Medicine*, **2020**, *22*, 314–330.

[80] Gaba, B.; Khan, T.; Haider, M.F.; Alam, T.; Baboota, S.; Parvez, S.; Ali, J. Vitamin E Loaded Naringenin Nanoemulsion via Intranasal Delivery for the Management of Oxidative Stress in a 6-OHDA Parkinson's Disease Model. **2019**.

[81] Ferro, M.M.; Bellissimo, M.I.; Anselmo-Franci, J.A.; Angellucci, M.E.M.; Canteras, N.S.; da Cunha, C. Comparison of Bilaterally 6-OHDA- and MPTP-Lesioned Rats as Models of the Early Phase of Parkinson's Disease: Histological, Neurochemical, Motor and Memory Alterations. *Journal of Neuroscience Methods*, **2005**, *148*, 78–87.

[82] Shrivastava, P.; Vaibhav, K.; Tabassum, R.; Khan, A.; Ishrat, T.; Khan, M.M.; Ahmad, A.; Islam, F.; Safhi, M.M.; Islam, F. Anti-Apoptotic and Anti-Inflammatory Effect of Piperine on 6-OHDA Induced Parkinson's Rat Model. *Journal of Nutritional Biochemistry*, **2013**, *24*, 680–687.

[83] Sanawar, M.; Saleem, U.; Anwar, F.; Nazir, S.; Akhtar, M.F.; Ahmad, B.; Ismail, T. Investigation of Anti-Parkinson Activity of Dicyclomine. *International Journal of Neuroscience*, **2020**.

[84] Madiha, S.; Tabassum, S.; Batool, Z.; Liaquat, L.; Sadir, S.; Shahzad, S.; Perveen, T.; Haider, S. Assessment of Gait Dynamics in Rotenone-Induced Rat Model of Parkinson's Disease by Footprint Method. *Pakistan journal of pharmaceutical sciences*, **2017**, *30*, 943–948.

[85] C, K.; MB, S.; SN, K. Rapid and Sensitive Method for Measuring Norepinephrine, Dopamine, 5-Hydroxytryptamine and Their Major Metabolites in Rat Brain by High-Performance Liquid Chromatography. Differential Effect of Probenecid, Haloperidol and Yohimbine on the Concentrations of Biogenic Amines and Metabolites in Various Regions of Rat Brain. *Journal of chromatography*, **1987**, *386*, 25–35.

[86] D, G.; A, S.; A, A.; VB, J.; B, S.; G, P.; S, K. Eugenol as an Anti-Stress Agent: Modulation of Hypothalamic-Pituitary-Adrenal Axis and Brain Monoaminergic Systems in a Rat Model of Stress. *Stress (Amsterdam, Netherlands)*, **2011**, *14*, 145–155.

[87] CR, W.; JA, S.; NM, E.; ST, O.; DW, K. Automated Assays for Superoxide Dismutase, Catalase, Glutathione Peroxidase, and Glutathione Reductase Activity. *Analytical biochemistry*, **1990**, *184*, 193–199.

[88] S, C.; C, R.; R, P.-C.; M, L.-T.; G, B. Vitamin E Protects Guinea Pig Liver from Lipid Peroxidation without Depressing Levels of Antioxidants. *The international journal of biochemistry & cell biology*, **1995**, *27*, 1175–1181.

[89] M, M.; T, D.P. Effect of Chronic Estradiol and Progesterone Treatments of Ovariectomized Rats on Brain Dopamine Uptake Sites. *Journal of neurochemistry*, **1993**, *60*, 1876–1883.

[90] C, L.; RH, R.; JD, E.; F, N.; TL, H.; DE, R. Estrogen Is Essential for Maintaining Nigrostriatal Dopamine Neurons in Primates: Implications for Parkinson's Disease and Memory. *The Journal of neuroscience : the official journal of the Society for Neuroscience*, **2000**, *20*, 8604–8609.

[91] A, N.; G, A.; P, P.; G, N.; G, T.; F, C.; L, M.; A, Q.; M, Z. Hormonal Replacement Therapy in Women with Parkinson Disease and Levodopa-Induced Dyskinesia: A Crossover Trial. *Clinical neuropharmacology*, **2007**, *30*, 276–280.

[92] KL, T.; SL, H.; SK, L. Estrogen Improves Motor Disability in Parkinsonian Postmenopausal Women with Motor Fluctuations. *Neurology*, **2000**, *54*, 2292–2298.

[93] M, M.; HA, E. Recuperative Effect of Estrogen on Rotenone-Induced Experimental Model of Parkinson's Disease in Rats. *Environmental science and pollution research international*, **2021**, *28*, 21266–21275.

[94] NA, E.-S.; N, S.; AM, Y.; NM, A.E.-F.; TB, E.-A.; AA, H.; WK, A.; G, E.-S.B.; SA, Z. The Protective Effect of Biochanin A against Rotenone-Induced Neurotoxicity in Mice Involves Enhancing of PI3K/Akt/MTOR Signaling and Beclin-1 Production. *Ecotoxicology and environmental safety*, **2020**, *205*.

[95] XZ, L.; CY, S.; Q, C.; YS, Z.; H, Z.; XP, Z. The Effects and Mechanism of Estrogen on Rats with Parkinson's Disease in Different Age Groups. *American journal of translational research*, **2016**, *8*, 4134–4146.

[96] M, P. Regional Specialization of Motor Functions in the Rat Striatum: Implications for the Treatment of Parkinsonism. *Progress in neuro-psychopharmacology & biological psychiatry*, **1988**, *12*, 217–224.

[97] S, S.; S, J.; P, K. Neuroprotective Potential of Quercetin in Combination with Piperine against 1-Methyl-4-Phenyl-1,2,3,6-Tetrahydropyridine-Induced Neurotoxicity. *Neural regeneration research*, **2017**, *12*, 1137–1144.

[98] Monville, C.; Torres, E.M.; Dunnett, S.B. Comparison of Incremental and Accelerating Protocols of the Rotarod Test for the Assessment of Motor Deficits in the 6-OHDA Model. *Journal of Neuroscience Methods*, **2006**, *158*, 219–223.

[99] Brooks, S.P.; Dunnett, S.B. Tests to Assess Motor Phenotype in Mice: A User's Guide. *Nature Reviews Neuroscience 2009 10:7*, **2009**, *10*, 519–529.

[100] Goel, R.; Chaudhary, R. Effect of Daidzein on Parkinson Disease Induced by Reserpine in Rats. *Brazilian Journal of Pharmaceutical Sciences*, **2020**, *56*, 1–7.

[101] KR, L.; JA, F.; JY, K. An Open Source Automated Bar Test for Measuring Catalepsy in Rats. *eNeuro*, **2020**, *7*, 1–5.

[102] Ko, Y.-H.; Kwon, S.-H.; Kim, S.-K.; Lee, B.-R.; Hur, K.-H.; Kim, Y.-J.; Kim, S.-E.; Lee, S.-Y.; Jang, C.-G. Protective Effects of 6,7,4′-Trihydroxyisoflavone, a Major Metabolite of Daidzein, on 6-Hydroxydopamine-Induced Neuronal Cell Death in SH-SY5Y Human Neuroblastoma Cells. *Archives of Pharmacal Research 2019 42:12*, **2019**, *42*, 1081–1091.

[103] Zhang, H.; Chi, M.; Chen, L.; Sun, X.; Wan, L.; Yang, Q.; Guo, C. Daidzein Alleviates Cisplatin-Induced Muscle Atrophy by Regulating Glut4/AMPK/FoxO Pathway. *Phytotherapy Research*, **2021**, *35*, 4363–4376.

[104] JM, S.; AN, K.; WJ, B.; DG, W.; JL, C. Subcutaneous Daidzein Administration Enhances Recovery of Skilled Ladder Rung Walking Performance Following Stroke in Rats. *Behavioural brain research*, **2013**, *256*, 428–431.

[105] M, I.; Y, K.; M, A.; A, T.; K, T.; T, T. Parkinsonian Rotenone Mouse Model: Reevaluation of Long-Term Administration of Rotenone in C57BL/6 Mice. *Biological & pharmaceutical bulletin*, **2011**, *34*, 92–96.

[106] T, W.; C, L.; B, H.; Z, W.; X, M.; L, Z.; J, H.; F, F. Neuroprotective Effects of Danshensu on Rotenone-Induced Parkinson's Disease Models in Vitro and in Vivo. *BMC complementary medicine and therapies*, **2020**, *20*.

[107] DT, D.; J, S.; S, R.; JG, H.; VM, M.; JM, C.; FR, W.; SE, D.; AJ, L.; AH, S. Indices of Oxidative Stress and Mitochondrial Function in Individuals with Incidental Lewy Body Disease. *Annals of neurology*, **1994**, *35*, 38–44.

[108] W, Y.; Q, C.; J, Z.; H, X.; ZH, H.; X, L.; Q, L. 3'-Daidzein Sulfonate Sodium Improves Mitochondrial Functions after Cerebral Ischemia/Reperfusion Injury. *Neural regeneration research*, **2017**, *12*, 235–241.

[109] K, X.; Y, L.; D, C.; B, Y.; Y, L.; X, M.; Z, H.; J, Y.; J, L.; P, Z.; H, Y.; J, H. Daidzein Supplementation Enhances Embryo Survival by Improving Hormones, Antioxidant Capacity, and Metabolic Profiles of Amniotic Fluid in Sows.*Food & function*, **2020**, *11*, 10588–10600.

[110] S, K.; JV, K. Effect of Daidzein on Cisplatin-Induced Hematotoxicity and Hepatotoxicity in Experimental Rats. *Indian journal of pharmacology*, **2017**, *49*, 49–54.

[111] S, S.; VH, K.; MK, G.; DD, M.; SK, R.; NL, B. The Parkinsonian Neurotoxin Rotenone Activates Calpain and Caspase-3 Leading to Motoneuron Degeneration in Spinal Cord of Lewis Rats. *Neuroscience*, **2007**, *146*, 741–755.

[112] XL, L.; WD, C.; J, L.; XL, G.; CJ, G.; XH, M.; SG, S.; LX, W. Protective Effect of Estrogen on Apoptosis in a Cell Culture Model of Parkinson's Disease. *Clinical and investigative medicine. Medecineclinique et experimentale*, **2008**, *31*.

PUBLICATIONS

PUBLICATIONS

Dietary Phytoestrogens: Neuroprotective Role in Parkinson's Disease. Current Neurovascular Research. 2021; 18. (Article in press); Impact factor- 1.99

CONFERENCES

AND

SEMINARS

CONFERENCES AND SEMINARS

Role of Phytoestrogens in Parkinson's Disease

SOCIETY FOR NEUROCHEMISTRY, INDIA
SNCI – 34TH ANNUAL CONFERENCE
2020

Topic: "Brain Diseases, Injuries and Infections: Emerging Challenges and Treatment Strategies"

Certificate of Participation

This to certify that Ms. Aanchal Verma From GLA University, Mathura, participated in poster presentation on the topic entitled "Role of Phytoestrogens in Parkinson's Disease", 34th SNCI Annual Conference (Virtual) entitled "Brain Diseases, Injuries and Infections: Emerging Challenges and treatment strategies" during the period 11th – 13th December 2020.

Organized by Head Quarters – SNCI, University of Hyderabad

Organizer

Project

On

Statistical Analysis of Average Yield of Principal Crops of India

Submitted for the Partial fulfilment of Requirements

For the Degree

Of

Master in Science

in

Mathematics

By

Neeraj Kushwaha (205040002)
Krishna Singh (205040001)
Radheshyam (205040003)

Under supervision
of
Dr. Amit Kumar Saraswat

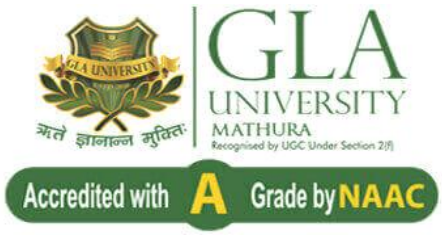

DEPARTMENT OF MATHEMATICS
GLA UNIVERSITY, MATHURA(U.P.), INDIA
JUNE 2021

CANDIDATE'S DECLARATION

We solemnly declare that the project report on "**Statistical Analysis of Average Yield of Principal Crops of India**" in partial fulfilment of the requirements for the award of the Degree of Master of Science is based on our own work carried under the supervision of **Dr. Amit Kumar Saraswat**, Assistant Professor, Department of Mathematics, GLA University, Mathura. We assert the statements made and conclusions drawn are an outcome of our research work. We further certify that

- The work has not been submitted to any other Institution for any other degree/diploma/certificate in this university or any other university of India or abroad.
- We have followed the guidelines provided by the university in writing the report.
- Whenever we have used the materials (data, theoretical analysis and text) from other sources, we have given due credit to them in the text of the report and giving their details in the references.

NeerajKushwaha (205040002)

Krishna Singh (205040001)

Radheshyam (205040003)

This is to certify that the above statements made by the candidates are correct to the best of my knowledge.

Date: 14/06/2021

(**Dr. Amit Kumar Saraswat)**

Supervisor

CERTIFICATE

This is to certify that this thesis report on "**Statistical Analysis of Average Yield of Principal Crops of India**" is the outcome of the work carried by **Neeraj Kushwaha, Krishna Singh** and **Radheshyam** under my supervision. Further, this is mention that to the best of our knowledge, the work reported herein does not form part of any other thesis, report or dissertation on the basis of which a degree or award was conferred on an earlier occasion on this or any other candidate.

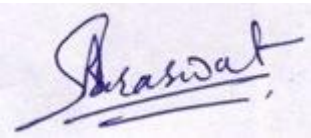

Dr. Amit Kumar Saraswat
(Supervisor)
Assistant Professor,
Department of Mathematics
GLA University, Mathura (U.P.)

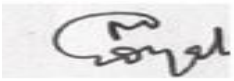

Dr. Manish Goyal
Prof & Head
Department of Mathematics
GLA University, Mathura (U.P.)

Department of Mathematics
GLA University, Mathura (U.P.)

ACKNOWLEDEGEMENT

We would like to thank our thesis supervisor **Dr. Amit Kumar Saraswat** whose constant guidance, insightful suggestions, invaluable support and faith in our abilities led to successful completion of our project work. We really appreciate the probing questions they asked whenever we came with problems, which led us to think thoroughly. Instead of just telling us the right or wrong answer, they helped us identify the gap in our understandings.

We are highly grateful to **Prof. Maish Goyal** (Head), Department of Mathematics, GLA University, Mathura for providing the necessary environment of research in the department, for providing me all specific amenities required during the entire research work.

We wish to pay our sincere thanks to Dr. Sharad Kumar Dixit, Dr. Abhishek Kumar Singh, Dr. Hariom Sharma, Dr. NishaGodani, Dr. Archan Dixit, Dr. Umesh Kumar Sharma, and all other supporting staff of the institute.

Everything we have achieved so far in our life including successful completion of our research work has been possible because of our beloved family and faculty members.

Neeraj Kushwaha
Krishna Singh
Radheshyam

Index

Introduction- As we know India is a leading country in the field agriculture, also the second largest producer country of rice, wheat, sugarcane, groundnut, vegetables, fruit and cotton all over the world. In this project we will study about yield per hectare of some major crops in India.

->Motivation-IN this project we will analyses that whether there is a significance difference or not in the average yield per hectare of some principle crops in India.

->Objective- We will do statistical analysis of yield per hectare of some principal crops in India with the help of ANOVA (Analysis of variance).

Problem statement-

we will analyses the data and set the null hypothesis and alternate hypothesis and check whether the null hypothesis is rejected or accepted.

Data-

Reference URL:

http://mospi.gov.in/

The data refers to All India average yield of Principal Crops (food grains, oil seeds, cotton, jute, banana, black pepper, coconut, turmeric etc.) yearly of 15 years.

We are analyzing only a subset of this data. We have taken data only of four crops (rice, wheat, maize, barley), and arrange the data of these four crops vertically one below the other, and our data set dimension is 56*2.

To see the data, use the link below with(ctrl + click)

https://data.gov.in/resources/all-india-level-average-yield-principal-crops-2001-02-2015-16

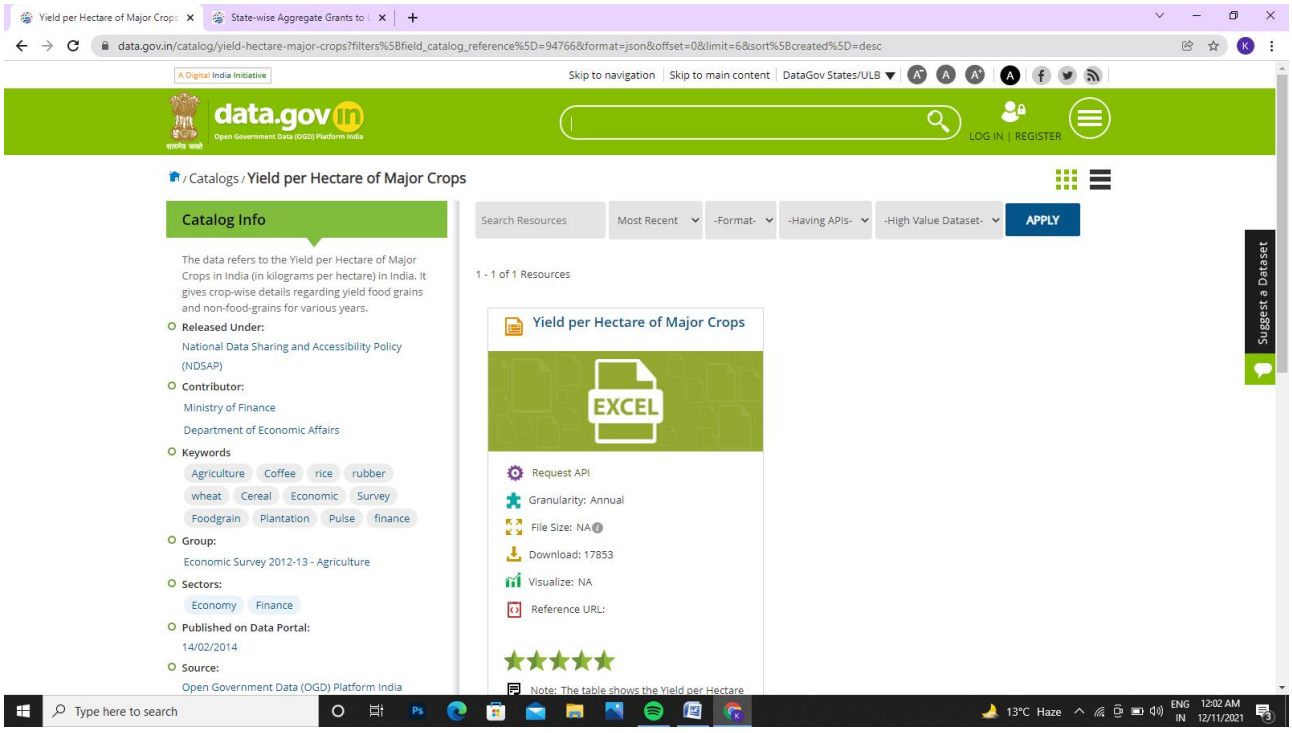

Source of data- data.gov.in

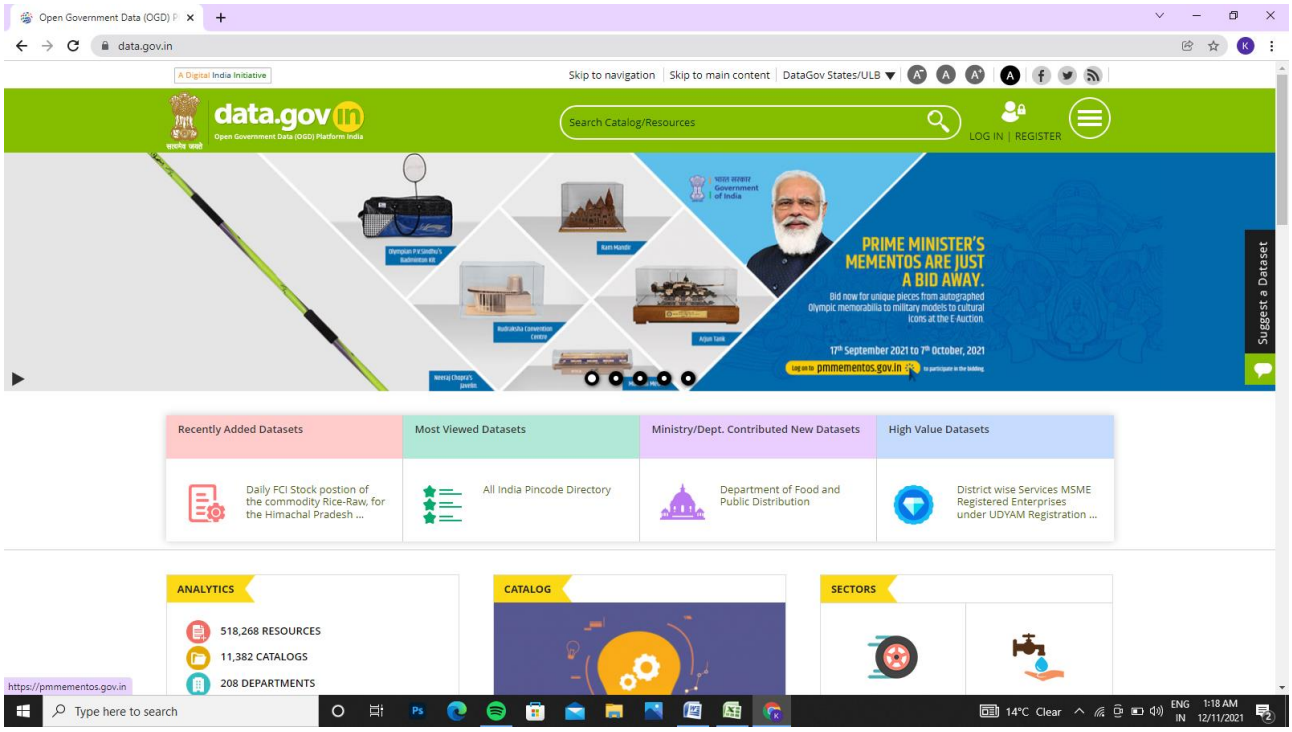

Software Used

R-Programming-

Statistics for relatively advanced users: R **(**3**)** has thousands of packages, designed, maintained, and widely used by statisticians. Statistical graphics: try doing some of our plots in Stata and you won't have much fun. Flexible code: R has a rather liberal syntax, and variables don't need to be declared as they would in (for example) C++, which makes it very easy to code in. This also has disadvantages in terms of how safe the code is. Vectorization: R is designed to make it very easy to write functions which are applied pointwise to every element of a vector. This is extremely useful in statistics. R is powerful: if a command doesn't exist already, you can code it yourself.

Packages used

1. ggplot2 –
   ggplot2 **(5)** is **a system for declaratively creating graphics, based on The Grammar of Graphics**. You provide the data, tell ggplot2 how to map

variables to aesthetics, what graphical primitives to use, and it takes care of the details.

2. gplots-

The package gplots **(**4**)** is a tool for plotting data, including: - calculating and plotting locally smoothed summary function as ('bandplot', 'wapply'), - enhanced versions of standard

plots ('barplot2', 'boxplot2', 'heatmap.2', 'smartlegend'), - manipulating colors ('col2hex',

'colorpanel', 'redgreen', 'greenred', 'bluered', 'redblue', 'rich.colors'), - calculating and plotting two-dimensional data summaries ('ci2d', 'hist2d'), - enhanced regression diagnostic plots ('lmplot2', 'residplot'), - formula-enabled interface to 'stats::lowess' function ('lowess'), - displaying textual data in plots ('textplot', 'sinkplot'), - plotting a matrix where each cell contains a dot whose size reflects the relative magnitude of the elements ('balloonplot'), - plotting "Venn" diagrams ('venn'), - displaying Open-Office style plots ('ooplot'), - plotting multiple data on same region, with separate axes ('overplot'), - plotting means and confidence intervals ('plotCI', 'plotmeans'), - spacing points in an x-y plot so they don't overlap ('space').

Installation of ggplot2

The ggplot2 package can be easily installed using the R function install.packages(). You need to type the following R code in the console:

```
install.packages("ggplot2")
```

The above code will automatically download the ggplot2 package, from the CRAN (Comprehensive R Archive Network) repository, and install it.

Installation of gplots-

```
install.packages("gplots")
```

Methodology

1. Introduction

Analysis of variance (ANOVA) is a statistical procedure concerned with comparing means of several samples. It can be thought of as an extension of the t-test for two independent samples to more than two groups. The purpose is to test for significant differences between class means, and this is done by analysis the variances.

The ANOVA test of the hypothesis is based on a comparison of two independent estimates of the population variance **(**2**).**
When performing an ANOVA procedure, the following assumptions are required:

- The observations are independent of one another.
- The observations in each group come from a normal distribution.

. The population variances in each group are the same (homoscedasticity).
ANOVA is the most commonly quoted advanced research method in the professional business and economic literature. This technique is very useful in revealing important information particularly in interpreting experimental outcomes and in determining the influence of some factors on other processing parameters.

The original ideas of analysis of variance were developed by the English statistician Sir Ronald A. Fisher (1890-1962) in his book “Statistical Methods for Research Workers” **(**1**)**. Much of the early work in this area dealt with agricultural experiments.

2. One-way ANOVA Test Procedure

The simplest case is one-way ANOVA. A one-way analysis of variance is used when the data are divided into groups according to only one factor.

Assume that the data $x_{11}, x_{12}, x_{13}, \dots, x_{1n_1}$ are sample from population 1, $x_{21}, x_{22}, x_{23}, \dots, x_{2n_2}$ are sample from population 2, … , $x_{k1}, x_{k2}, x_{k3}, \dots, x_{kn_k}$ are sample from population *k*. Let x_{ij} denote the data from the i^{th} group (level) and j^{th} observation.

We have values of independent normal random variables $X_{ij},\ i = 1, 2, \dots, k$ and $j = 1, 2, \dots, n_i$ with mean μ_i and constant standard deviation σ, $X_{ij} \sim N(\mu_i, \sigma)$. Alternatively, each $X_{ij} = \mu_i + \varepsilon_{ij}$ where ε_{ij} are normally distributed independent random errors, $\varepsilon_{ij} \sim N(0, \sigma)$. Let $N = n_1 + n_2 + \cdots + n_k$ is the total number of observations (the total sample size across all groups), where n_i is sample size for the i^{th} group.

The parameters of this model are the population means $\mu_1, \mu_2, \dots, \mu_k$ and the common standard deviation σ.

Using many separate two-sample *t*-tests to compare many pairs of means is a bad idea because we don't get a *p*-value or a confidence level for the complete set of comparisons together.

We will be interested in testing the null hypothesis

$$H_0 : \mu_1 = \mu_2 = \cdots = \mu_k \tag{1}$$

against the alternative hypothesis

$$H_1 : \exists\, 1 \le i, l \le k : \mu_i \ne \mu_l \tag{2}$$

(there is at least one pair with unequal means).

Let $\bar{x}_i$ represent the mean sample *i* ($i = 1, 2, \dots, k$):

$$\bar{x}_i = \frac{1}{n_i} \sum_{j=1}^{n_i} x_{ij}, \tag{3}$$

$\bar{x}$ represent the grand mean, the mean of all the data points:

$$\bar{x} = \frac{1}{N} \sum_{i=1}^{k} \sum_{j=1}^{n_i} x_{ij}, \tag{4}$$

s_i^2 represent the sample variance:

$$s_i^2 = \frac{1}{n_i - 1} \sum_{j=1}^{n_i} \left(x_{ij} - \overline{x_i} \right)^2, \tag{5}$$

and $s^2 = MSE$ is an estimate of the variance σ^2 common to all *k* populations,

$$s^2 = \frac{1}{N - k} \sum_{i=1}^{k} \left(n_i - 1 \right) \cdot s_i^2. \tag{6}$$

ANOVA is centered around the idea to compare the variation between groups (levels) and the variation within samples by analyzing their variances.

Define the total sum of squares *SST*, sum of squares for error (or within groups) *SSE*, and the sum of squares for treatments (or between groups) *SSC*:

$$SST = \sum_{i=1}^{k} \sum_{j=1}^{n_i} \left(x_{ij} - \overline{x} \right)^2, \tag{7}$$

$$SSE = \sum_{i=1}^{k} \sum_{j=1}^{n_i} \left(x_{ij} - \overline{x_i} \right)^2 = \sum_{i=1}^{k} \left(n_i - 1 \right) \cdot s_i^2, \tag{8}$$

$$SSC = \sum_{i=1}^{k} \sum_{j=1}^{n_i} \left(\overline{x_i} - \overline{x} \right)^2 = \sum_{i=1}^{k} n_i \cdot \left(\overline{x_i} - \overline{x} \right)^2. \tag{9}$$

Consider the deviation from an observation to the grand mean written in the following way:

$$x_{ij} - \overline{x} = \left(x_{ij} - \overline{x_i} \right) + \left(\overline{x_i} - \overline{x} \right). \tag{10}$$

Notice that the left side is at the heart of *SST*, and the right side has the analogous pieces of *SSE* and *SSC*. It actually works out that:

$$SST = SSE + SSC. \tag{11}$$

The total mean sum of squares *MST*, the mean sums of squares for error *MSE*, and the mean sums of squares for treatment *MSC* are:

(12)

$$MST = \frac{SST}{df(SST)} = \frac{SST}{N-1},$$

$$MSE = \frac{SSE}{df(SSE)} = \frac{SSE}{N-k}, \quad (13)$$

$$MSC = \frac{SSC}{df(SSC)} = \frac{SSC}{k-1}. \quad (14)$$

The one-way ANOVA, assuming the test conditions are satisfied, uses the following test statistic:

$$F = \frac{MSC}{MSE}. \quad (15)$$

Under H_0 this statistic has Fisher's distribution $F(k-1, N-k)$. In case it holds for the test criteria

$$F > F_{1-\alpha, k-1, N-k}, \quad (16)$$

where $F_{1-\alpha, k-1, N-k}$ is $(1-\alpha)$ quantile of F-distribution with $k-1$ and $N-k$ degrees of freedom, then hypothesis

H_0 is rejected on significance level α.

The results of the computations that lead to the F-statistic are presented in an ANOVA table, the form of which is shown in the Table.

Basic one-way ANOVA table

Variance source	Sum of squares *SS*	Degrees of freedom *df*	Mean square *MS*	*F*-statistic	Tail area above *F*
Between	*SSC*	$k-1$	*MSC*	*MSC/MSE*	*p*-value
Within	*SSE*	$N-k$	*MSE*	—	—
Total	*SST*	$N-1$	—	—	—

In statistical software's is used to be in this table column with *p*-value. This *p*-value says the probability of rejection the null hypothesis in case the null hypothesis holds.

In case $p < \alpha$, where α is chosen significance level, is the null hypothesis rejected with probability greater than $(1-\alpha)\cdot 100$% probability.

BOXPLOTS

Boxplots are a measure of how well distributed is the data in a data set. It divides the data set into three quartiles. This graph represents the minimum, maximum, median, first quartile and third quartile in the data set. It is also useful in comparing the distribution of data across data sets by drawing boxplots for each of them.

Boxplots are created in R by using the **boxplot ()** function.

Syntax

The basic syntax to create a boxplot in R is −

boxplot (x, data, notch, varwidth, names, main)

Diagnostic plots

1. Residual vs fitted plot in R

When conducting a residual analysis, a "residuals versus fits plot" is the most frequently created plot. It is **a scatter plot of residuals on the y axis and fitted values (estimated responses) on the x axis**. The plot is used to detect non-linearity, unequal error variances, and outliers.

2. Normal QQ plot

If we run a statistical analysis that assumes our dependent variable is Normally distributed, we can use a Normal Q-Q plot to check that assumption. It's just a visual check, not an air-tight proof, so it is somewhat subjective. But it allows us to see at-a-glance if our assumption is plausible, and if not, how the assumption is violated and what data points contribute to the violation.

Result &Discussion

```
>
> ggplot(yield, aes(Foodgrains,Yield.per.hectare))+geom_boxplot(aes(col=Foodgrains))+labs(title="Boxplot of Yield per hectare of Four different foodgrains")
> model<- aov(Yield.per.hectare~Foodgrains)
> summary(model)
             Df Sum Sq Mean Sq F value   Pr(>F)
Foodgrains    3  419.7  139.90   22.36 1.96e-09 ***
Residuals    52  325.4    6.26
---
Signif. codes:  0 '***' 0.001 '**' 0.01 '*' 0.05 '.' 0.1 ' ' 1
>
```

Variance source	Sum of squaresss	Degree of Freedom df	Mean squares	F-statistic	*Tail area above F*
Food grains	419.7	3	139.90	22.36	1.96e-09
Residuals	325.4	52	6.26		

Summary- As our level of significance ‘a’ is 0.001 and p-value is 1.96e-09, which is less than level of significance a. So null hypothesis is rejected.

Thus the yield per hectare of all four crops is not same in our country.

Boxplot

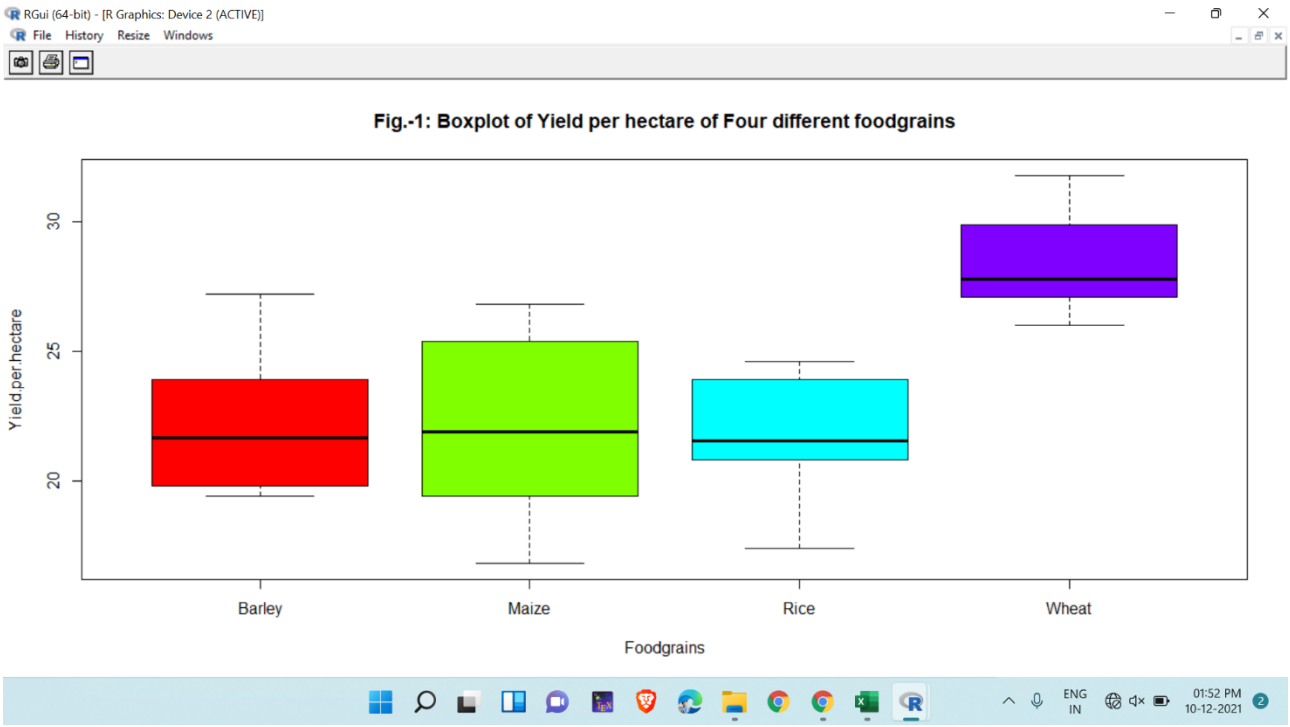

Plot Mean

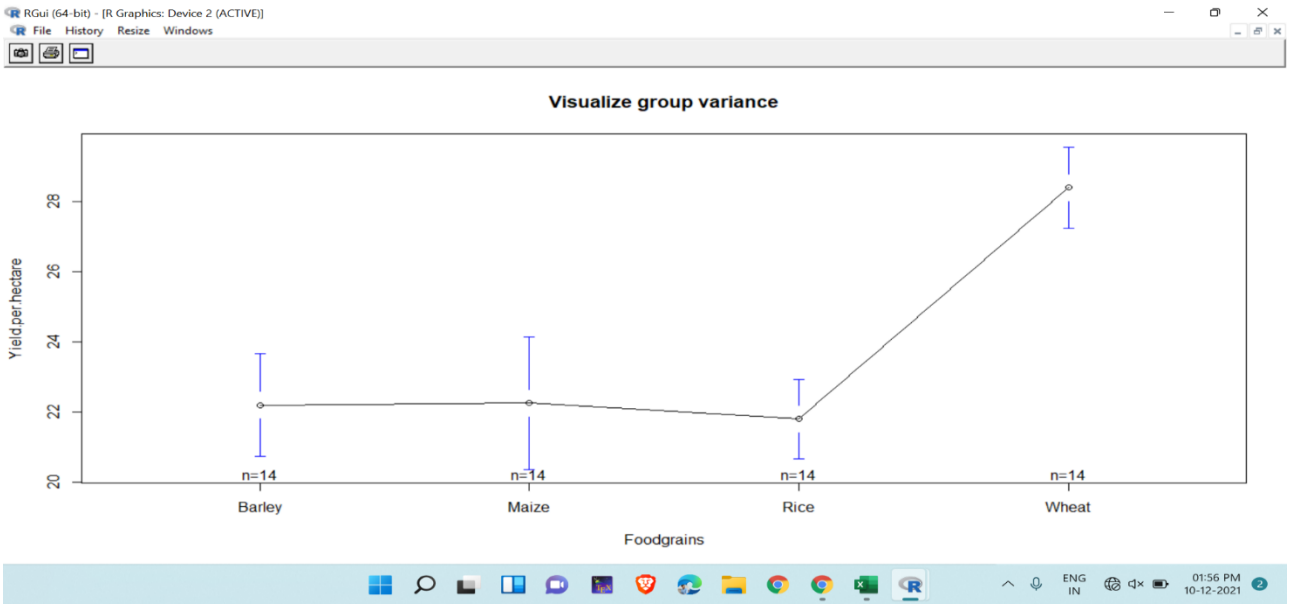

Observation:

there are no outliers in our data

average yield per hectare of barley, maize& rice is approximately same but wheat has much higher value.

Normal Q-Q

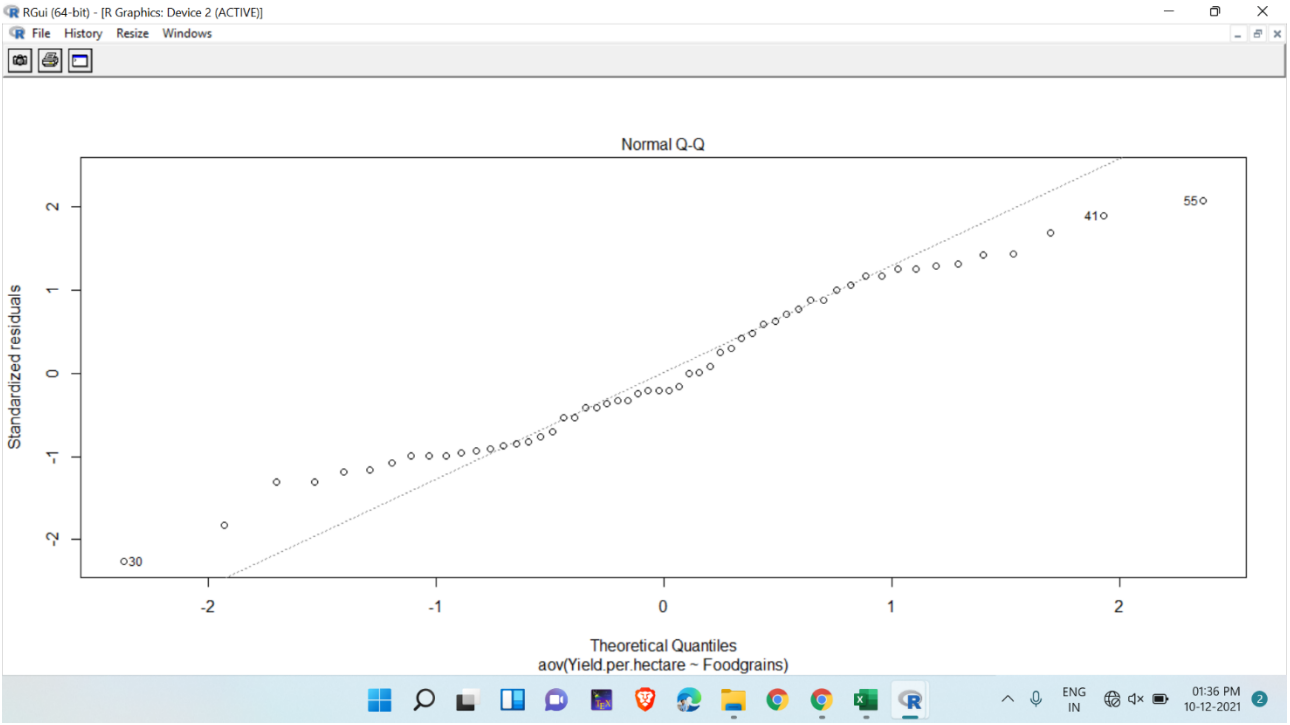

Our data is normally distributed expect for few outliers.

References

1. Fischer, R. A. (1944). Statistical methods for research workers, 1925. *Edinburgh Oliver Boyd*, *518*.
2. Ostertagová, E., & Ostertag, O. (2013). Methodology and application of one-way ANOVA. *American Journal of Mechanical Engineering*, *1*(7), 256-261.
3. Team, R. C. (2019). *R version 3.6. 2: A language and environmental for statistical computing. R Foundation for Statistical Computing, Vienna, Austria*. USBN 3-900051-0700, www. R-project. org. Version 3.0. 1.
4. Warnes, M. G. R., Bolker, B., Bonebakker, L., Gentleman, R., & Huber, W. (2016). Package 'gplots'. *Various R programming tools for plotting data*.
5. Wickham, H. (2011). ggplot2. *Wiley Interdisciplinary Reviews: Computational Statistics*, *3*(2), 180-185.

Appendix:

```
getwd()

setwd("D:/GLA/Project")

library(gplots)

library(ggplot2)

yield<- read.csv("yield.csv",header = TRUE)

attach(yield)

is.factor(Foodgrains)

boxplot(Yield.per.hectare~Foodgrains, main="Fig.-1: Boxplot of Yield per hectare of
Four different foodgrains", col= rainbow(4))

#plot means of yield per hectare agianstfoodgrains with differnt Treatment groups

plotmeans(Yield.per.hectare~Foodgrains,xlab="Foodgrains",

ylab="Yield.per.hectare", main="Visualize group variance")

ggplot(yield,
aes(Foodgrains,Yield.per.hectare))+geom_boxplot(aes(col=Foodgrains))+labs(title="
Boxplot of Yield per hectare of Four different foodgrains")

model<- aov(Yield.per.hectare~Foodgrains)

summary(model)

#Diagnostic plots

plot(model,1)

plot(model,2)  #### Normal QQ plot

#p <- ggplot(yield, aes(x = Foodgrains, y = Yield.per.hectare, fill = Foodgrains))

#p +  geom_boxplot() +

 # ggtitle("Yield data")
```

Project report on
Black hole Solution And its Properties

By

Saurabh Kumar

GLA University, Mathura

A Project submitted to the Department of Physics
In partial fulfilment of requirements
For the degree of

Master of Science

Mentor

Dr. Benoy Kumar Singh

Department of Physics, GLA University, Mathura 281406

June 2021

evaluated
23/06/21

Acknowledgements

I am very much indebted to my thesis supervisor for his generous support, encouragement, guidance and providing me inspiring research atmosphere during the period of my research work. I am also thankful to all the faculty members of Department of Physics and office staff for their kind help and support. Thanks are due to my friends who have always come forward for helping and providing me the moral supports, at various stages of my research work and I have learned many things from them.

Finally, I have no words to express my feelings of gratitude towards my family members, specially my parents, for their unconditional love and support. Without their blessings, inspiration and encouragements this work could have never been accomplished in the present form.

(Saurabh Kumar)

GLA UNIVERSITY
MATHURA
Accredited with A Grade by NAAC
12-B Status from UGC

Certificate

This is to certify that Saurabh Kumar has carried out the **dissertation** work presented in this report entitled "Black hole solution and its properties" under my supervision for the award of **Master of Science in Physics**, from Institute of Applied Science and Humanities, GLA University, Mathura in June 2021.

His conduct during this dissertation work was outstanding.

(Dr. B R K Gupta)
Head
Department of Physics

(Dr. B K Singh)
Supervisor
Department of Physics

Contents

Introduction

In Einstein's theory of general relativity, the Schwarzschild metric (also known as the Schwarzschild vacuum or Schwarzschild solution) is the solution to the Einstein field equations that describes the gravitational field outside a spherical mass, on the assumption that the electric charge of the mass, angular momentum of the mass, and universal cosmological constant are all zero. The solution is a useful approximation for describing slowly rotating astronomical objects such as many stars and planets, including Earth and the Sun. It was found by Karl Schwarzschild in 1916, and around the same time independently by Johannes Droste, who published his much more complete and modern-looking discussion only four months after Schwarzschild.

According to Birkhoff's theorem, the Schwarzschild metric is the most general spherically symmetric vacuum solution of the Einstein field equations. A Schwarzschild black hole or static black hole is a black hole that has neither electric charge nor angular momentum. A Schwarzschild black hole is described by the Schwarzschild metric, and cannot be distinguished from any other Schwarzschild black hole except by its mass.

The Schwarzschild solution is named in honor of Karl Schwarzschild, who found the exact solution in 1915 and published it in January 1916, a little more than a month after the publication of Einstein's theory of general relativity. It was the first exact solution of the Einstein field equations other than the trivial flat space solution. Schwarzschild died shortly after his paper was published, as a result of a disease he developed while serving in the German army during World War I.

Johannes Droste in 1916 independently produced the same solution as Schwarzschild, using a simpler, more direct derivation. In the early years of general relativity there was a lot of confusion about the nature of the singularities found in the Schwarzschild and other solutions of the Einstein field equations. In Schwarzschild's original paper, he put what we now call the event horizon at the origin of his coordinate system. In this paper he also introduced what is now known as the Schwarzschild radial coordinate, as an auxiliary variable. In his equations, Schwarzschild was using a different radial coordinate that was zero at the Schwarzschild radius.

A more complete analysis of the singularity structure was given by David Hilbert in the following year, identifying the singularities both at $r = 0$ and $r = r_s$. Although there was general consensus that the singularity at $r = 0$ was a 'genuine' physical singularity, the nature of the singularity at $r = r_s$ remained unclear.

In 1921 Paul Painlevé and in 1922 Allvar Gullstrand independently produced a metric, a spherically symmetric solution of Einstein's equations, which we now know is coordinate transformation of the

Schwarzschild metric, Gullstrand–Painlevé coordinates, in which there was no singularity at $r = r_s$. They, however, did not recognize that their solutions were just coordinate transforms, and in fact used their solution to argue that Einstein's theory was wrong. In 1924 Arthur Eddington produced the first coordinate transformation (Eddington–Finkelstein coordinates) that showed that the singularity at $r = r_s$ was a coordinate artifact, although he also seems to have been unaware of the significance of this discovery. Later, in 1932, Georges Lemaître gave a different coordinate to the same effect and was the first to recognize that this implied that the singularity at $r = r_s$ was not physical. In 1939 Howard Robertson showed that a free falling observer descending in the Schwarzschild metric would cross the $r = r_s$ singularity in a finite amount of proper time even though this would take an infinite amount of time in terms of coordinate time t.

Black Hole Solutions

"Spherically symmetric" means "having the same symmetries as a sphere Since the object of interest to us is the metric on a differentiable manifold, we are concerned with those metrics that have such symmetries. We know how to characterize symmetries of the metric - they are given by the existence of Killing vectors. Furthermore, we know what the Killing vectors of S2 are, and that there are three of them. Therefore, a spherically symmetric manifold is one that has three Killing vector fields which are just like those on S^2. By "just like" we mean that the commutator of the Killing vectors is the same in either case - in fancier language, that the algebra generated by the vectors is the same. Something that we didn't show, but is true, is that we can choose our three Killing vectors on S^2 to be ($V^{(1)}$, $V^{(2)}$,$V^{(3)}$), such that

$$\begin{aligned} [V(1), V(2)] &= V(3) \\ [V(2), V3)] &= V(1) \\ [V(3), V(1)] &= V(2) \end{aligned} \qquad (1)$$

The commutation relations are exactly those of SO(3), the group of rotations in three dimensions. This is no coincidence, of course, but we won't pursue this here. All we need is that a spherically symmetric manifold is one which possesses three Killing vector fields with the above commutation relations.

Let's consider some examples to bring this down to earth. The simplest example is flat three-dimensional Euclidean space. If we pick an origin, then $\mathbf{R^3}$ is clearly spherically symmetric with respect to rotations around this origin. Under such rotation's points move into each other, but each point stays on an S^2 at a fixed distance from the origin.

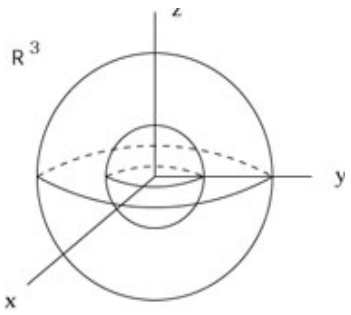

It is these spheres which foliate $\mathbf{R}^3$ .Of course, they don't really foliate all of the space, since the origin itself just stays put under rotations - it doesn't move around on some two-sphere. But it should be clear that almost all of the space is properly foliated, and this will turn out to be enough for us.
In this case the entire manifold can be foliated by two-spheres. This foliated structure suggests that we put coordinates on our manifold in a way which is adapted to the foliation. By this we mean that, if we have an n-dimensional manifold foliated by m-dimensional sub manifolds, we can use a set of m coordinate functions u^1on the sub manifolds and a set of (n- m) coordinate functions v^1 to tell us which sub manifold we are on. the collection of v's and u's coordinatize the entire space. If the sub manifolds are maximally symmetric spaces (as two-spheres are), then there is the following powerful theorem: it is always possible to choose the u-coordinates such that the metric on the entire manifold is of the form

$$ds^2 = g_{\mu V} dx^{\mathcal{V}} = g_{IJ}(v) dv^I \, dv^J + f(v)\gamma_{ij}(u) dv^i \, dv^j \qquad (2)$$

Here γ_{ij}(u) is the metric on the sub manifold. This theorem is saying two things at once: that there are no cross terms $dv^I du^j$,
and that both g_{ij}(v) and f(v) are functions of the v^I alone, independent of the u^i. Proving the theorem is a mess, but you are encouraged to look in chapter 13 of Weinberg. Nevertheless, it is a perfectly sensible result. Roughly speaking, if g_{ij} or f depended on the u^i then the metric would change as we moved in a single sub manifold, which violates the assumption of symmetry. The unwanted cross terms, meanwhile, can be eliminated by making sure that the tangent vectors $\partial \mathrm{I}/_{\partial V}$ are orthogonal to the sub manifolds - in other words, that we line up our sub manifolds in the same way throughout the space.

We are now through with handwaving, and can commence some honest calculation. For the case at hand, our sub manifolds are two-spheres, on which we typically choose coordinates (θ, ϕ) in which the metric takes the form $d\Omega^2 = d\theta^2 + sin^2\theta \; d\phi^2$.Since we are interested in a four-dimensional spacetime, we need two more coordinates, which we can call a and b. The theorem (2) is then telling us that the metric on a spherically symmetric space time can be put in the form

$$ds^2 = g_{aa}(a,b)da^2 + g_{ab}(a,b)(dadb + dbda + g_{bb}(\mathrm{a,b})db^2 + r^2(\mathrm{a,b})d\Omega^2 \qquad (3)$$

Here r(a, b) is some as-yet-undetermined function, to which we have merely given a suggestive label. There is nothing to stop us, however, from changing coordinates from (a, b) to (a, r), by inverting r(a, b). (The one thing that could possibly stop us would be if r were a function of a alone; in this case we

could just as easily switch to (b, r), so we will not consider this situation separately.) The metric is then

$$ds^2 = g_{aa}(a,r)da^2 + g_{ar}(a,r)(dadr + drda + g_{rr}(\text{a,r})dr^2 + r^2(\text{a,r})d\Omega^2 \quad (4)$$

Our next step is to find a function t(a, r) such that, in the (t, r) coordinate system, there are no cross terms $\text{dtdr} + \text{drdt}$ in the metric. Notice that

$$\text{dt} = \frac{\partial t}{\partial a}\text{da} + \frac{\partial t}{\partial r}\text{dr} \quad (5)$$

So,

$$\text{dt}^2 = \left(\frac{\partial t}{\partial a}\right)^2 da^2 + \frac{\partial t}{\partial a}\frac{\partial t}{\partial r}(dadr + drda) + \left(\frac{\partial t}{\partial r}\right)^2 dr^2 \quad (6)$$

We would like to replace the first three terms in the metric (4) by $mdt^2 + ndr^2$, for some functions m and n. This is equivalent to the requirements

$$\text{m}\left(\frac{\partial t}{\partial a}\right)^2 = \text{g}_{\text{aa}} \quad (7)$$

$$\text{n+m}\left(\frac{\partial t}{\partial r}\right)^2 = \text{g}_{\text{rr}} \quad (8)$$

$$\text{m}\,\frac{\partial t}{\partial a}\frac{\partial t}{\partial r} = \text{g}_{\text{ar}} \quad (9)$$

We therefore have three equations for the three unknowns t(a, r), m(a, r), and n(a, r), just enough to determine them precisely (up to initial conditions for t). (Of course, they are "determined “in terms of the unknown functions g_{aa}, g_{ar}, and g_{rr}, so in this sense they are still undetermined.)We can therefore put our metric in the form

$$ds^2 = m(t,r)dt^2 + n(\text{t,r})dr^2 + r^2 d\Omega^2 \quad (10)$$

To this point the only difference between the two coordinates t and r is that we have chosen r to be the one which multiplies the metric for the two-sphere. This choice was motivated by what we know about the metric for flat Minkowski space, which can be written as

$$ds^2 = -dt^2 + dr^2 + r^2 d\Omega^2 \quad (11)$$

We know that the space time under consideration is Lorentzian, so either m or n will have to be negative. Let us choose m, the coefficient of dt^2, to be negative. This is not a choice we are simply

allowed to make, and in fact we will see later that it can go wrong, but we will assume it for now. The assumption is not completely unreasonable, since we know that Minkowski space is itself spherically symmetric, and will therefore be described by (7.12). With this choice we can trade in the functions m and n for new functions and α and β, such that

$$ds^2 = -e^{2\alpha(t,r)}dt^2 + e^{2\beta(t,r)}dr^2 + r^2 d\Omega^2 \qquad (12)$$

This is the best we can do for a general metric in a spherically symmetric spacetime.

Christoffel Symbols

The next step is to actually solve Einstein's equations, which will allow us to determine explicitly the functions α(t,r) and β(t,r). It is unfortunately necessary to compute the Christoffel symbols for (7.13), from which we can get the curvature tensor and thus the Ricci tensor. If we use labels(0, 1, 2, 3) for (t, r,θ, ϕ) in the usual way, the Christoffel symbols are given by

$$\Gamma^0_{00} = \partial_0\alpha \qquad \Gamma^0_{01} = \partial_1\alpha \qquad \Gamma^0_{11} = e^{2(\beta-\alpha)}\partial_0\beta$$

$$\Gamma^1_{00} = e^{2(\alpha-\beta)}\partial_1\alpha \qquad \Gamma^1_{01} = \partial_0\beta \qquad \Gamma^1_{11} = \partial_1\beta$$

$$\Gamma^2_{12} = \frac{1}{r} \qquad \Gamma^1_{22} = -re^{-2(\beta)} \qquad \Gamma^3_{13} = \frac{1}{r}$$

$$\Gamma^1_{33} = -re^{-2(\beta)}sin^2\theta \quad \Gamma^2_{33} = -\sin\theta\cos\theta \qquad \Gamma^3_{33} = \cos\theta/\sin\theta \qquad (13)$$

(Anything not written down explicitly is meant to be zero, or related to what is written by symmetries.) From these we get the following non-vanishing components of the Riemann tensor

$$R^0_{101} = e^{2(\beta-\alpha)}[\partial_0^2\beta + (\partial_0\beta)^2 - \partial_0\alpha\partial_0\beta] + [\partial_1\alpha\partial_1\beta - \partial_1^2\alpha + (\partial_0\alpha)^2]$$

$$R^0_{202} = -re^{-2(\beta)}\partial_1\alpha$$

$$R^0_{303} = -re^{-2(\beta)}sin^2\theta\,\partial_1\alpha$$

$$R^0_{212} = -re^{-2(\alpha)}\partial_0\beta$$

$$R^0_{313} = -re^{-2(\beta)}sin^2\theta\ \partial_1\beta$$

$$R^1_{212} = re^{-2(\beta)}\partial_1\beta$$

$$R^1_{313} = re^{-2(\beta)}sin^2\theta\ \partial_1\beta$$

$$R^2_{323} = (1-e^{-2(\beta)})sin^2\theta \qquad (14)$$

Taking the contraction as usual yields the Ricci tensor:

$$R_{00} = [\partial_0^2\beta + (\partial_0\beta)^2 - \partial_0\alpha\partial_0\beta] + e^{2(\beta-\alpha)}\left[\partial_1^2\alpha + (\partial_1\alpha)^2 - \partial_1\alpha\partial_1\beta + \tfrac{2}{r}\partial_1\alpha\right]$$

$$R_{11} = -\left[\left[\partial_1^2\alpha + (\partial_1\alpha)^2 - \partial_1\alpha\partial_1\beta - \tfrac{2}{r}\partial_1\beta\right] + e^{2(\beta-\alpha)}(\partial_0^2\beta + (\partial_0\beta)^2 - \partial_0\alpha\partial_0\beta)\right]$$

$$R_{01} = -\tfrac{2}{r}\partial_0\beta$$

$$R_{22} = e^{-2\beta}[r(\partial_1\beta - \partial_1\alpha) - 1]+1$$

$$R_{33} = R_{22}\ sin^2\theta \qquad (15)$$

Our job is to set $R_{\mu\nu} = 0$ From $R_{01} = 0$ we get ,

$$\partial_0\beta = 0 \qquad (16)$$

If we consider taking the time derivative of $R_{22} = 0$ and using $\partial_0\beta = 0$, we get

$$\partial_0\partial_1\alpha = 0 \qquad (17)$$

We can therefore write

$$\beta = \beta(r)$$
$$\alpha = f(r) + g(t) \qquad (18)$$

The first term in the metric (11) is therefore - $e^{2f(r)}e^{2g(t)}dt^2$.But we could always simply redefine our time coordinate by replacing $dt \rightarrow e^{-g(t)}dt$; in other words, we are free to choose t such that g(t) = 0, when (t, r) = f (r). We therefore have

$$ds^2 = -e^{2\alpha(r)}dt^2 + e^{\beta(r)}dr^2 + r^2d\Omega^2 \qquad (19)$$

All of the metric components are independent of the coordinate t. We have therefore proven a crucial result: any spherically symmetric vacuum metric possesses a time like Killing vector. This property is so interesting that it gets its own name: a metric which possesses a time like Killing vector is called stationary. There is also a more restrictive property: a metric is called static if it possesses a time like Killing vector which is orthogonal to a family of hyper surfaces. (A hyper surface in an n-dimensional manifold is simply an (n- 1)-dimensional Sub manifold.) The metric (19) is not only stationary, but also static; the Killing vector field ∂_0 Is orthogonal to the surfaces .t= const (since there are no cross terms such as dt dr and so on). Roughly speaking, a static metric is one in which nothing is moving, while a stationary metric allows things to move but only in a symmetric way. For example, the static spherically symmetric metric (19) will describe non-rotating stars or black holes, while rotating systems (which keep rotating in the same way at all times)will be described by stationary metrics. It's hard to remember which word goes with which concept, but the distinction between the two concepts should be understandable. Let's keep going with finding the solution. Since bothR_{00} and R_{11} vanish, we can write

$$0 \;=\; e^{2(\beta-\alpha)}R_{00}+R_{11} = \frac{2}{r}(\partial_1\beta + \partial_1\alpha)\ , \tag{20}$$

which implies $\alpha = -\beta$ + constant. Once again, we can get rid of the constant by scaling our coordinates, so we have

$$\alpha = -\beta \tag{21}$$

Next let us turn to $R_{22} = 0$, which now reads

$$e^{2(\alpha)}(2r\partial_1\alpha + 1) = 1 \tag{22}$$

This is completely equivalent to

$$\partial_1\,(re^{2(\alpha)}) = 1 \tag{23}$$

We can solve this to obtain

$$e^{2(\alpha)} \;=\; 1 + \frac{\mu}{r} \tag{24}$$

where μ is some undetermined constant. With (21) and (24), our metric becomes

$$ds^2 = -\left(1 + \frac{\mu}{r}\right)dt^2 \;+\; \left(1 + \frac{\mu}{r}\right)^{-1} dr^2 + \; r^2 d\Omega^2 \tag{25}$$

We now have no freedom left except for the single constant μ, so this form better solve the remaining equations $R_{00}= 0$ and $R_{11} = 0$; it is straight forward to check that it does, for any value of μ .

The only thing left to do is to interpret the constantt μ in terms of some physical parameter. The most important use of a spherically symmetric vacuum solution is to represent the space timeout side a star or planet or whatnot. In that case we would expect to recover the weak field limit as $r \to \infty$. In this limit, (25) implies

$$g_{00}(r \to \infty) = -\left(1 + \frac{\mu}{r}\right)$$
$$g_{rr}(r \to \infty) = \left(1 - \frac{\mu}{r}\right) \quad (26)$$

The weak field limit, on the other hand, has

$$g_{00} = -(1 + 2\phi)$$
$$g_{rr} = (1 - 2\phi) \quad (27)$$

with the potential $\phi = -GM/r$. Therefore, the metrics do agree in this limit, if we set $\mu = -2GM$.

Our final result is the celebrated Schwarzschild metric,

$$ds^2 = -\left(1 - \frac{2GM}{r}\right)dt^2 + \left(1 - \frac{2GM}{r}\right)^{-1} dr^2 + r^2 d\Omega^2 \quad (28)$$

This is true for any spherically symmetric vacuum solution to Einstein's equations; M functions as a parameter, which we happen to know can be interpreted as the conventional Newtonian mass that we would measure by studying orbits at large distances from the gravitating source. Note that as $M \to 0$ we recover Minkowski space, which is to be expected. Note also that the metric becomes progressively Minkowski an as we go to $r \to \infty$;this property is known as asymptotic flatness.

Singularity

We therefore have a sufficient condition for a point to be considered a singularity. It is not a necessary condition, however, and it is generally harder to show that a given point is non singular; for our purposes we will simply test to see if geodesics are well-behaved at the point in question, and if so then we will consider the point non singular. In the case of the Schwarzschild metric (28), direct calculation reveals that

$$R^{\rho\mu\sigma\nu} R_{\rho\mu\sigma\nu} = \frac{12M^2G^2}{r^6} \quad (29)$$

This is enough to convince us that r= 0 represents an honest singularity. At the other trouble spot, r= 2GM, you could check and see that none of the curvature invariants blows up. We therefore begin to think that it is actually not singular, and we have simply chosen a bad coordinate system. The best thing to do is to transform to more appropriate coordinates if possible. We will soon see that in this case it is in fact possible, and the surface r=2GM is very well-behaved (although interesting) in the Schwarzschild metric

Birkhoff's Theorem

The fact that the Schwarzschild metric is not just a good solution, but is the unique spherically symmetric vacuum solution, is known as Birkhoff's theorem. It is interesting to note that the result is a static metric. We did not say anything about the source except that it be spherically symmetric. Specifically, we did not demand that the source itself be static; it could be a collapsing star, as long as the collapse were symmetric. Therefore a process such as a supernova explosion, which is basically spherical, would be expected to generate very little gravitational radiation (in comparison to the amount of energy released through other channels). This is the same result we would have obtained in electromagnetism, where the electromagnetic fields around a spherical charge distribution do not depend on the radial distribution of the charges.

Before exploring the behavior of test particles in the Schwarzschild geometry, we should say something about singularities. From the form of (7.29), the metric coefficients become infinite at r= 0 and r= 2GM- an apparent sign that something is going wrong. The metric coefficients, of course, are coordinate-dependent quantities, and as such we should not make too much of their values; it is certainly possible to have a "coordinate singularity" which results from a breakdown of a specific coordinate system rather than the underlying manifold. An example occurs at the origin of polar coordinates in the plane, where the metric $ds^2= dr^2+r^2d\theta^2$ becomes degenerate and the component $g^{\theta\theta} = r^{-2}$ of the inverse metric blows up, even though that point of the manifold is no different from any other.

What kind of coordinate-independent signal should we look for as a warning that something about the geometry is out of control? This turns out to be a difficult question to answer, and entire books have been written about the nature of singularities in general relativity. We won't go into this issue in detail, but rather turn to one simple criterion for when something has gone wrong -when the curvature becomes infinite. The curvature is measured by the Riemann tensor, and it is hard to say when a tensor becomes infinite, since its components are coordinate-dependent. But from the curvature we can construct various scalar quantities, and since scalars are coordinate-independent it will be

meaningful to say that they become infinite. This ssimplest such scalar is the Ricci scalar R = $g^{\mu\nu}R_{\mu\nu}$,but we can also construct higher-order scalars such as $R^{\mu\nu}R_{\mu\nu}$, $R^{\rho\mu\sigma\nu}R_{\rho\mu\sigma\nu}$,$R_{\rho\mu\sigma\nu}R^{\rho\lambda\sigma\tau}$, $R^{\mu\nu}_{\tau\lambda}$, and so on. If any of these scalars (not necessarily all of them) go to infinity as we approach some point, we will regard that point as a singularity of the curvature. We should also check that the point is not "infinitely far away"; that is, that it can be reached by travelling a finite distance along a curve.

Having worried a little about singularities, we should point out that the behavior of Schwarzschild at r $\leq$ 2GM is of little day-to-day consequence. The solution we derived is valid only in vacuum, and we expect it to hold outside a spherical body such as a star. However,in the case of the Sun we are dealing with a body which extends to a radius of

$$R_{\odot}=10^{6}GM_{\odot} \tag{30}$$

Thus, r= 2G$M_{\odot}$ is far inside the solar interior, where we do not expect the Schwarzschild metric to imply. In fact, realistic stellar interior solutions are of the form

$$ds^{2} = -\left(1-\frac{2GM}{r}\right)dt^{2} + \left(1-\frac{2GM}{r}\right)^{-1}dr^{2} + r^{2}d\Omega^{2} \tag{31}$$

See Schutz for details. Here m(r) is a function of r which goes to zero faster than r itself, so there are no singularities to deal with at all. Nevertheless, there are objects for which the full Schwarzschild metric is required - black holes - and therefore we will let our imaginations roam far outside the solar system in this section. The first step we will take to understand this metric more fully is to consider the behavior of geodesics. We need the nonzero Christoffel symbols for Schwarzschild

$$\Gamma^{1}_{00}=\frac{GM}{r^{3}}(r-2GM) \qquad \Gamma^{1}_{11}=\frac{-GM}{r(r-2GM)} \qquad \Gamma^{0}_{11}=\frac{GM}{r(r-2GM)}$$
$$\Gamma^{2}_{12}=\frac{1}{r} \qquad \Gamma^{1}_{22}=-(r-2GM) \qquad \Gamma^{3}_{13}=\frac{1}{r}$$

$$\Gamma^{1}_{33}=-(r-2GM)sin^{2}\theta \qquad \Gamma^{2}_{33}=-\sin\theta\cos\theta \qquad \Gamma^{3}_{23}=\cos\theta/\sin\theta \tag{32}$$

The geodesic equation therefore turns into the following four equations, where λ is an affine parameter:

$$\frac{d^{2}t}{d\lambda^{2}}+\frac{2GM}{r(r-2GM)}\frac{dr}{d\lambda}\frac{dt}{d\lambda}=0 \quad , \tag{33}$$

$$\frac{d^2t}{d\lambda^2}+\frac{GM(r-2GM)}{r^3}\left(\frac{dt}{d\lambda}\right)^2 - \frac{GM}{r(r-2GM)}\left(\frac{dr}{d\lambda}\right)^2 - r(r-2GM)\left[\left(\frac{dr}{d\lambda}\right)^2 sin^2\theta \left(\frac{d\phi}{d\lambda}\right)^2\right] = 0 , \quad (34)$$

$$\frac{d^2\theta}{d\lambda^2}+\frac{2}{r}\frac{d\theta}{d\lambda}\frac{dr}{d\lambda} - \sin\theta\cos\theta \left(\frac{d\phi}{d\lambda}\right)^2 = 0 , \quad (35)$$

$$\frac{d^2\phi}{d\lambda^2}+\frac{2}{r}\frac{d\phi}{d\lambda}\frac{dr}{d\lambda} + 2\frac{\cos\theta}{\sin\theta}\frac{d\theta}{d\lambda}\frac{d\phi}{d\lambda} = 0 , \quad (36)$$

There does not seem to be much hope for simply solving this set of coupled equations by inspection. Fortunately our task is greatly simplified by the high degree of symmetry of the Schwarzschild metric. We know that there are four Killing vectors: three for the spherical symmetry, and one for time translations. Each of these will lead to a constant of the motion for a free particle; if K^μ is a Killing vector, we know that

$$K_\mu \frac{dx^\mu}{d\lambda} = \text{constant} \quad (37)$$

In addition, there is another constant of the motion that we always have for geodesics; metric compatibility implies that along the path the quantity

$$\mathcal{E} = -g_{\mu\nu}\frac{dx^\mu}{d\lambda}\frac{dx^\nu}{d\lambda} \quad (38)$$

is constant. Of course, for a massive particle we typically choose λ=τ ,and this relation simply becomes $\mathcal{E} = -g_{\mu\nu}U^\mu U^\nu$ = + 1. For a massless particle we always have = 0. We will also be concerned with space like geodesics (even though they do not correspond to paths of particles), for which we will choose = - 1. Rather than immediately writing out explicit expressions for the four conserved quantities associated with Killing vectors, let's think about what they are telling us. Notice that the symmetries they represent are also present in flat spacetime, where the conserved quantities they lead to are very familiar. Invariance under time translations leads to conservation of energy, while invariance under spatial rotations leads to conservation of the three components of angular momentum. Essentially the same applies to the Schwarzschild metric. We can think of the angular momentum as a three-vector with a magnitude (one component) and direction (two components). Conservation of the direction of angular momentum means that the particle will move in a plane. We can choose this to be the equatorial plane of our coordinate system; if the particle is not in this plane, we can rotate coordinates until it is. Thus, the two Killing vectors which lead to conservation of the direction of angular momentum imply

$$\theta = \frac{\pi}{2} \quad (39)$$

The two remaining Killing vectors correspond to energy and the magnitude of angular momentum. The energy arises from the time like Killing vector K $= \partial_t$ or

$$K_\mu = \left(-\left(\left(1-\frac{2GM}{r}\right)\right), 0,0,0\right). \quad (40)$$

The Killing vector whose conserved quantity is the magnitude of the angular momentum is L = ∂_ϕ or

$$L_\mu = (0,0,0,r^2 sin^2\theta) \quad (41)$$

since (7.40) implies that sin = 1 along the geodesics of interest to us, the two conserved quantities are

$$\left(1-\frac{2GM}{r}\right)\frac{dt}{d\lambda} = \mathrm{E} \quad (42)$$

$$r^2\,\frac{d\phi}{d\lambda} = \mathrm{L} \quad (43)$$

For massless particles these can be thought of as the energy and angular momentum; for massive particles they are the energy and angular momentum per unit mass of the particle. Note that the constancy of (43) is the GR equivalent of Kepler's second law (equal areas are swept out in equal times). Together these conserved quantities provide a convenient way to understand the orbits of particles in the Schwarzschild geometry. Let us expand the expression (7.39) for $\mathcal{E}$ to obtain

$$-\left(1-\frac{2GM}{r}\right)\left(\frac{dt}{d\lambda}\right)^2+\left(1-\frac{2GM}{r}\right)^{-1}\left(\frac{dr}{d\lambda}\right)^2+r^2\left(\frac{d\phi}{d\lambda}\right)^2 = -\epsilon \quad (44)$$

If we multiply this by (1 - 2GM/r) and use our expressions for E and L, we obtain

$$-E^2+\left(\frac{dr}{d\lambda}\right)^2+\left(1-\frac{2GM}{r}\right)\left(\frac{L^2}{r^2}+\epsilon\right) = 0 \quad (45)$$

This is certainly progress, since we have taken a messy system of coupled equations and obtained a single equation for r(λ).It looks even nicer if we rewrite it as

$$\frac{1}{2}\left(\frac{dr}{d\lambda}\right)^2 + \mathrm{V(r)} = \frac{1}{2}E^2 \quad (46)$$

where

$$\mathrm{V(r)} = \frac{\varepsilon}{2} - \varepsilon\frac{GM}{r} + \frac{L^2}{2r^2} - \frac{GML^2}{r^3} \quad (47)$$

In (7.47) we have precisely the equation for a classical particle of unit mass and "energy" $E^2/2$ moving in a one-dimensional potential given by V(r). (The true energy per unit mass is E, but the effective potential for the coordinate r responds to $E^2/2$.)

Of course, our physical situation is quite different from a classical particle moving in one dimension. The trajectories under consideration are orbits around a star or other object:

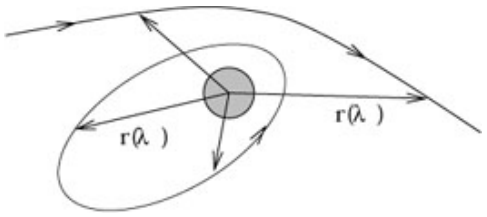

The quantities of interest to us are not only r(λ),but also t(λ) and ϕ(λ). Nevertheless, we can go along way toward understanding all of the orbits by understanding their radial behavior, and it is a great help to reduce this behavior to a problem we know how to solve.

A similar analysis of orbits in Newtonian gravity would have produced a similar result; the general equation (7.47) would have been the same, but the effective potential (47) would not have had the last term. (Note that this equation is not a power series in 1/r, it is exact.) In the potential (47) the first term is just a constant, the second term corresponds exactly to the Newtonian gravitational potential, and the third term is a contribution from angular momentum which takes the same form in Newtonian gravity and general relativity. The last term, the GR contribution, will turn out to make a great deal of difference, especially at small r .

Let us examine the kinds of possible orbits, as illustrated in the figures. There are different curves V(r) for different values of L; for any one of these curves, the behavior of the orbit can be judged by comparing the $E^2/2$ to V(r). The general behavior of the particle will be to move in the potential until it reaches a “turning point" where $V(r) = E^2/2$, where it will begin moving in the other direction. Sometimes there may be no turning point to hit, in which case the particle just keeps going. In other cases the particle may simply move in a circular orbit at radius r_c= const; this can happen if the potential is flat, *dV/dr=0*.Differentiating (7.48), we find that the circular orbits occur when

$$\varepsilon GMr_c^2 - L^2 r_c + 3GML^2\gamma = 0 \qquad (48)$$

where $\gamma = 0$ in Newtonian gravity and $\gamma = 1$ in general relativity. Circular orbits will be stable if they correspond to a minimum of the potential, and unstable if they correspond to a maximum. Bound orbits which are not circular will oscillate around the radius of the stable circular orbit.

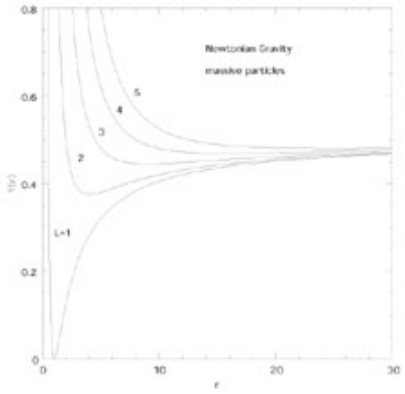

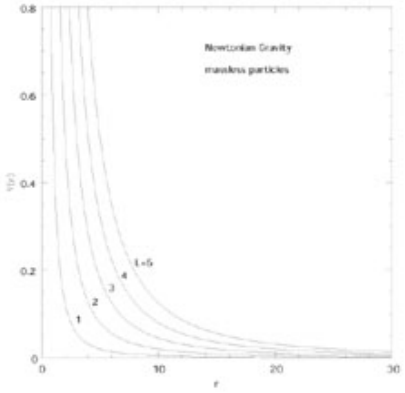

Turning to Newtonian gravity, we find that circular orbits appear at

$$r_c = \frac{L^2}{\epsilon GM} \tag{49}$$

For massless particles $\varepsilon = 0$, and there are no circular orbits;this is consistent with the figure, which illustrates that there are no bound orbits of any sort. Although it is somewhat obscured in this coordinate system, massless particles actually move in a straight line, since the Newtonian gravitational force on a massless particle is zero. (Of course the standing of massless particles in Newtonian theory is somewhat problematic, but we will ignore that for now.) In terms of the effective potential, a

photon with a given energy E will come in from $r = \infty$ and gradually "slowdown" (actually $dr/d\lambda$ will decrease, but the speed of light isn't changing) until it reaches the turning point, when it will start moving away back to $r = \infty$ The lower values of L, for which the photon will come closer before it starts moving away, are simply those trajectories which are initially aimed closer to the gravitating body. For massive particles there will be stable circular orbits at the radius (49), as well as bound orbits which oscillate around this radius. If the energy is greater than the asymptotic value E= 1, the orbits will be unbound, describing a particle that approaches the star and then recedes. We know that the orbits in Newton's theory are conic sections - bound orbits are either circles or ellipses, while unbound ones are either parabolas or hyperbolas - although we won't show that here.

In general relativity the situation is different, but only for r sufficiently small. Since the difference resides in the term - GML^2/r^3 , as $r \to \infty$ the behaviors are identical in the two theories. But as $r \to 0$ the potential goes to ∞ rather than $+\infty$ as in the Newtonian case. At r= 2GM the potential is always zero; inside this radius is the black hole, which we will discuss more thoroughly later. For massless particles there is always a barrier (except for L= 0, for which the potential vanishes identically), but a sufficiently energetic photon will nevertheless go over the barrier and be dragged

inexorably down to the center. (Note that "sufficiently energetic" means "in comparisonn to its angular momentum" - in fact the frequency of the photon is immaterial, only the direction in which it is pointing.) At the top of the barrier there are unstable circular orbits. For $\varepsilon = 0$, $\gamma = 1$, we can easily solve (7.49) to obtain

$$r_c = 3GM \tag{50}$$

This is borne out by the figure, which shows a maximum of V(r) at r= 3GM for every L. This means that a photon can orbit forever in a circle at this radius, but any perturbation will cause it to fly away either to r = 0 or r = ∞

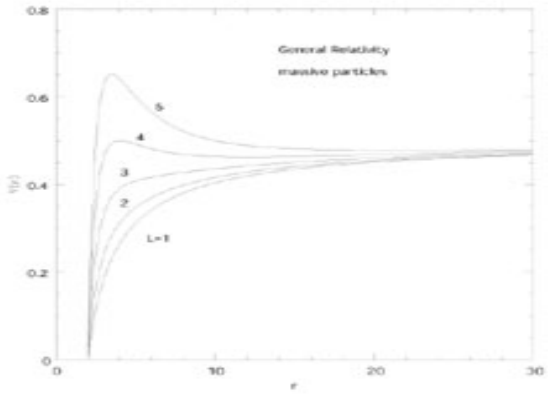

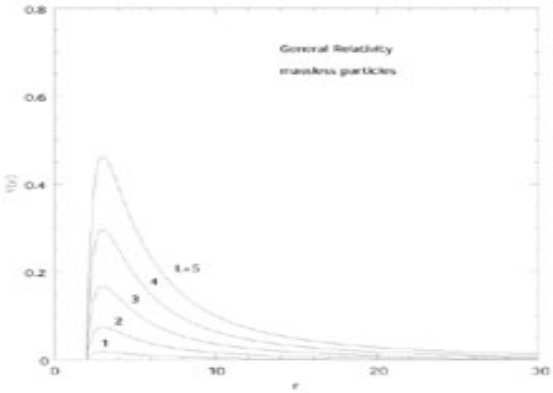

For massive particles there are once again different regimes depending on the angular momentum. The circular orbits are at

$$r_c = \frac{L^2 \pm \sqrt{L^4 - 12(GML)^2}}{2GM} \tag{51}$$

For large L there will be two circular orbits, one stable and one unstable. In the L $\rightarrow \infty$ limit their radii are given by

$$r_c = \frac{L^2 \pm L^2\left(1 - 6G^2M^2/L^2\right)}{2GM} = \left(\frac{L^2}{GM}, 3GM\right), \tag{52}$$

In this limit the stable circular orbit becomes farther and farther away, while the unstable one approaches 3GM, behavior which parallels the massless case. As we decrease L the two circular orbits come closer together; they coincide when the discriminant in(51) vanishes, at

$$L = \sqrt{12}GM \tag{53}$$

for which r_c=6GM (54)

and disappear entirely for smaller L. Thus 6GMis the smallest possible radius of a stable circular orbit in the Schwarzschild metric. There are also unbound orbits, which come in from infinity and turn a round, and bound but non circular ones, which oscillate around the stable circular radius. Note that such orbits, which would describe exact conic sections in Newtonian gravity, will not do so in GR, although we would have to solve the equation for dϕ/dt to demonstrate it. Finally, there are orbits which come in from infinity and continue all the way in to r= 0; this can happen either if the energy is higher than the barrier, or for L <$\sqrt{12}$GM .

We have therefore found that the Schwarzschild solution possesses stable circular orbits for r> 6GM and unstable circular orbits for 3GM< r< 6GM. It's important to remember that these are only the geodesics; there is nothing to stop an accelerating particle from dipping below r = 3GM and emerging, as long as it stays beyondd r = 2GM.

Experimental Verifications

Most experimental tests of general relativity involve the motion of test particles in the solar system, and hence geodesics of the Schwarzschild metric; this is therefore a good place to pause and consider these tests. Einstein suggested three tests: the deflection of light, the precession of perihelia, and gravitational redshift. The deflection of light is observable in the weak-field limit, and therefore is not really a good test of the exact form of the Schwarzschild geometry**.** Using our geodesic equations, we could solve for dϕ/dλ as a power series in the eccentricity e of the orbit, and from that obtain the apsidal frequency ω_a,defined as 2π divided by the time it takes for the ellipse to precess once around. For details you can look in Weinberg; the answer is

$$\omega_a=\frac{3(GM)^{3/2}}{c^2(1-e^2)r^{5/2}} \ , \qquad (55)$$

where we have restored the c to make it easier to compare with observation.(It is a good exercise to derive this yourself to lowest non vanishing order, in which case the $e^2$is missing.) Historically the precession of Mercury was the first test of GR.For Mercury the relevant numbers are

$$\frac{GM_\odot}{C^2} = 1.48\times 10^5\text{cm} \ ,$$

$$\text{a} = 5.55 \times 10^{12}\text{cm} \ , \qquad (56)$$

and of course c= 3.00×10^{10}cm/sec. This gives $\omega_a = 2.35 \times 10^{-14}$sec^{-1}. In other words, the major axis of Mercury's orbit precesses at a rate of 42.9 arcsecs every 100years. The observed value is 5601 arcsecs/100 yrs. However, much of that is due to the precession of equinoxes in our geocentric coordinate system; 5025 arcsecs/100 yrs, to be precise. The gravitational perturbations of the other planets contribute an additional 532 arcsecs/100 yrs, leaving 43 arcsecs/100 yrs to be explained by GR, which it does quite well.

The gravitational redshift, as we have seen, is another effect which is present in the weak field limit, and in fact will be predicted by any theory of gravity which obeys the Principle of Equivalence. However, this only applies to small enough regions of spacetime; over larger distances, the exact amount of redshift will depend on the metric, and thus on the theory under question. It is therefore worth computing the redshift in the Schwarzschild geometry. We consider two observers who are not moving on geodesics, but are stuck at fixed spatial coordinate values (r_1,θ_1, ϕ_1) and (r_2,θ_2, ϕ_2) . According to (7.45), the proper time of observer i will be related to the coordinate time t by

$$\frac{dr_i}{dt} = \left(1 - \frac{2GM}{r_i}\right)^{1/2}. \tag{57}$$

Suppose that the observer O_1emits a light pulse which travels to the observer O_2, such that O_1 measures the time between two successive crests of the light wave to be $\Delta\tau_1$ .Each crest follows the same path to O_2, except that they are separated by a coordinate time

$$\Delta t = \left(1 - \frac{2GM}{r_i}\right)^{-1/2} \Delta\tau_1 \tag{58}$$

This separation in coordinate time does not change along the photon trajectories, but the second observer measures a time between successive crests given by

$$\Delta\tau_2 = \left(1 - \frac{2GM}{r_2}\right)^{1/2} \Delta t$$

$$= \left(\frac{1-\frac{2GM}{r_2}}{1-\frac{2GM}{r_1}}\right)^{1/2} \Delta\tau_1. \tag{59}$$

Since these intervals $\Delta\tau_i$ measure the proper time between two crests of an electromagnetic wave, the observed frequencies will be related by

$$\frac{\omega_2}{\omega_1} = \frac{\Delta\tau_1}{\Delta\tau_2} \left(\frac{1-\frac{2GM}{r_1}}{1-\frac{2GM}{r_2}}\right)^{1/2} \tag{60}$$

This is an exact result for the frequency shift; in the limit r>> 2GM we have

$$\frac{\omega_2}{\omega_1} = 1 - \frac{GM}{r_1} + \frac{GM}{r_2} \qquad (61)$$
$$= 1 - \phi_1 + \phi_2$$

This tells us that the frequency goes down as ϕ increases, which happens as we climb out of a gravitational field; thus, a redshift. You can check that it agrees with our previous calculation based on the equivalence principle.

Since Einstein's proposal of the three classic tests, further tests of GR have been proposed. The most famous is of course the binary pulsar, discussed in the previous section. Another is the gravitational time delay, discovered by (and observed by) Shapiro. This is just the fact that the time elapsed along two different trajectories between two events need not be the same. It has been measured by reflecting radar signals off of Venus and Mars, and once again is consistent with the GR prediction. One effect which has not yet been observed is the Lense- Thirring, or frame-dragging effect. There has been a long-term effort devoted to a proposed satellite, dubbed Gravity Probe B, which would involve extraordinarily precise gyroscopes whose precession could be measured and the contribution from GR sorted out. It has a ways to go before being launched, however, and the survival of such projects is always year-to-year.

We now know something about the behavior of geodesics outside the troublesome radius r= 2GM, which is the regime of interest for the solar system and most other astrophysical situations. We will next turn to the study of objects which are described by the Schwarzschild solution even at radii smaller than 2GM-black holes. (We'll use the term "black hole" for the moment, even though we haven't introduced a precise meaning for such an object.)

One way of understanding a geometry is to explore its causal structure, as defined by the light cones. We therefore consider radial null curves, those for which θ and ϕ are constant and $ds^2 = 0$:

$$ds^2 = 0 = -\left(1 - \frac{2GM}{r}\right)dt^2 + \left(1 - \frac{2GM}{r}\right)^{-1} dr^2 \quad , \qquad (62)$$

from which we see that,

$$\frac{dt}{dr} = \pm \left(1 - \frac{2GM}{r}\right)^{-1} \qquad (63)$$

This of course measures the slope of the light cones on a spacetime diagram of the t-r plane. For large r the slope is ±1,as it would be in flat space, while as we approach r = 2GM we get dt/dr $\rightarrow \pm\infty$, and the light cones "close up":

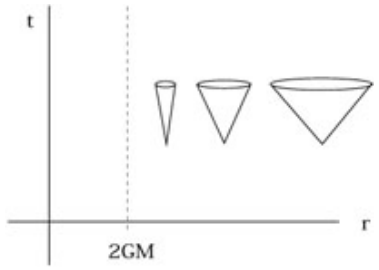

Thus a light ray which approaches r= 2GM never seems to get there, at least in this coordinate system; instead it seems to asymptote to this radius.

As we will see, this is an illusion, and the light ray (or a massive particle) actually has no trouble reaching r= 2GM. But an observer far away would never be able to tell. If we stayed outside while an intrepid observational general relativist dove into the blackhole, sending back signals all the time, we would simply see the signals reach us more and more slowly.

This should be clear from the 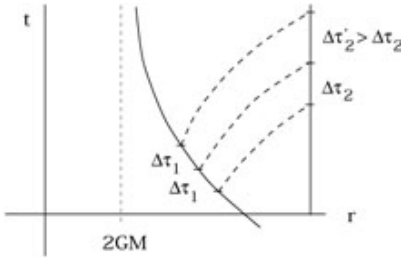

pictures, and is confirmed by our computation of $\Delta\tau_1/\Delta\tau_2$ when we discussed the gravitational redshift (60). As in falling astronauts approach r= 2GM, any fixed interval $\Delta\tau_1$ of their proper time corresponds to a longer and longer interval $\Delta\tau_2$ from our point of view. This continues forever; we would never see the astronaut cross r= 2GM, we would just see them move more and more slowly (and become redder and redder, almost as if they were embarrassed to have done something as stupid as diving into a black hole).

The fact that we never see the in falling astronauts reach r =2GM is a meaningful statement, but the fact that their trajectory in the t-r plane never reaches there is not. It is highly dependent on our coordinate system, and we would like to ask a more coordinate-independent question. The best way to do this is to change coordinates to a system which is better behaved at r= 2GM.There does exist a set of such coordinates, which we now set out to find. There is no way to "derive" a coordinate transformation, of course, we just say what the new coordinates are and plug in the formulas. But we

will develop these coordinates in several steps,in hopes of making the choices seem somewhat motivated.

The problem with our current coordinates is that dt/dr $\to \infty$ along radial null geodesics which approach r= 2GM; progress in the r direction becomes slower and slower with respect to the coordinate time t. We can try to fix this problem by replacing t with a coordinate which "moves more slowly" along null geodesics. First notice that we can explicitly solve the condition (7.64) characterizing radial null curves to obtain

$$t = \pm r^* + \text{constant} \tag{64}$$

where the tortoise coordinate r^* is defined by

$$r^* = r + 2GM \ln\left(\frac{r}{2GM} - 1\right), \tag{65}$$

(The tortoise coordinate is only sensibly related to r when r≥2GM, but beyond there our coordinates aren't very good anyway.) In terms of the tortoise coordinate the Schwarzschild metric becomes

$$ds^2 = \left(1 - \frac{2GM}{r}\right)(-dt^2 + dr^{*2}) + r^2 d\Omega^2 \tag{66}$$

where r is thought of as a function of r*.This represents some progress, since the light cones now don't seem to close up; furthermore, none of the metric coefficients becomes infinite at r = 2GM The price we pay, however, is that the surface of interest at r = 2GM has just been pushed to infinity.

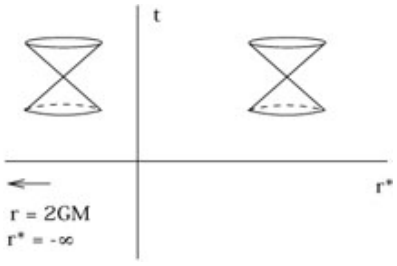

Our next move is to define coordinates which are naturally adapted to the null geodesics. If we let

$$\tilde{u} = t + r^*$$
$$\tilde{v} = t - r^* \tag{67}$$

then in falling radial null geodesics are characterized by $\tilde{u}$ = constant, while the outgoing ones satisfy $\tilde{v}$ = constant.Now consider going back to the original radial coordinate r,but replacing the time like coordinate t with the new coordinate These are known as Eddington-Finkelstein coordinates. In terms of them the metric is

$$ds^2 = -\left(1 - \frac{2GM}{r}\right) d\tilde{u}^2 + d\tilde{u}\,\mathrm{dr} + \mathrm{dr}\; d\tilde{u} + r^2 d\Omega^2. \qquad (68)$$

Here we see our first sign of real progress. Even though the metric coefficient $g_{\tilde{u}\tilde{u}}$ vanishes at r=2GM, there is no real degeneracy; the determinant of the metric is

$$\mathrm{g} = -r^4 sin^2\theta \ , \qquad (69)$$

which is perfectly regular at r = 2GM? Therefore, the metric is invertible, and we see once and for all that r = 2GM is simply a coordinate singularity in our original (t, r, θ, ϕ) system. In the Eddington-Finkelstein coordinates the condition for radial null curves is solved by

$$\frac{d\tilde{u}}{dr} = \begin{cases} 0 & (\ infalling) \\ 2\left(1 - \frac{2GM}{r}\right)^{-1} & (\text{outfalling}) \end{cases} \qquad (70)$$

We can therefore see what has happened: in this coordinate system the light cones remain well-behaved at r= 2GM, and this surface is at a finite coordinate value. There is no problem in tracing the paths of null or time like particles past the surface. On the other hand, something interesting is certainly going on. Although the light cones don't close up, they do tilt over, such that for r < 2GM all future-directed paths are in the direction of decreasing r.

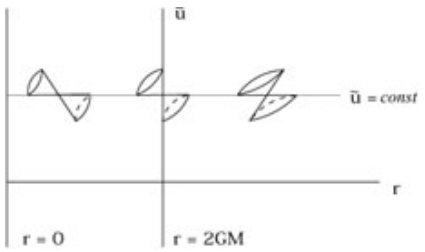

The surface r = 2GM, while being locally perfectly regular, globally functions as a point of no return - once a test particle dips below it, it can never come back. For this reason r = 2GM is known as the event horizon; no event at r $\leq$ 2GM can influence any other event at r> 2GM. Notice that the event horizon is a null surface, not a time like one. Notice also that since nothing can escape the event horizon, it is impossible for us to "see inside" - thus the name black hole.

In fact there are. Notice that in the ($d\tilde{u}$, r) coordinate system we can cross the event horizon on future-directed paths, but not on past-directed ones. This seems unreasonable, since we started with a time-independent solution. But we could have chosen

$$ds^2 = -\left(1 - \frac{2GM}{r}\right) d\tilde{v}^2 + d\tilde{v}\,\mathrm{dr} + \mathrm{dr}\; d\tilde{v} + r^2 d\Omega^2. \qquad (72)$$

Now we can once again pass through the event horizon, but this time only along past-directed curves.

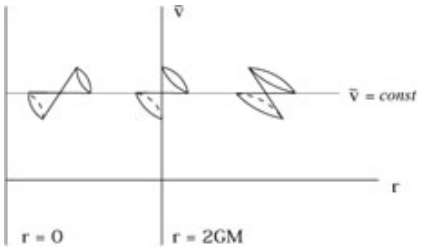

This is perhaps a surprise: we can consistently follow either future-directed or past-directed curves through r= 2GM,but we arrive at different places. It was actually to be expected, since from the definitions (67), if we keep $\tilde{u}$ constant and decrease r we must have t→ ∞ .(The tortoise coordinate r^*goes to - ∞ as r → 2GM .)So we have extended spacetime in two different directions, one to the future and one to the past.

The next step would be to follow space like geodesics to see if we would uncover still more regions. The answer is yes, we would reach yet another piece of the spacetime, but let's shortcut the process by defining coordinates that are good all over. A first guess might be to use both and at once (in place of t and r),which leads to

$$ds^2 = \frac{1}{2}\left(1 - \frac{2GM}{r}\right)^2 (\mathrm{d}\tilde{u}\; d\tilde{v} + d\tilde{v}\,\mathrm{d}\tilde{u}\;) + r^2 d\Omega^2. \qquad (73)$$

with r defined implicitly in terms $\tilde{u}$ of $\tilde{v}$ and by

$$\frac{1}{2}(\tilde{u} - \tilde{v}) = r + 2GM ln\left(\frac{r}{2GM} - 1\right). \qquad (74)$$

We have actually re-introduced the degeneracy with which we started out; in these coordinates r= 2GM is "infinitely far away" (at either $\tilde{u} = -\infty$ or $\tilde{v} = +\infty$.). The thing to do is to change to coordinates which pull these points into finite coordinate values; a good choice is

$$\acute{u} = e^{\tilde{u}/4GM}$$
$$\acute{v} = e^{-\tilde{v}/4GM} \qquad (75)$$

which in terms of our original (t, r) system is

$$\acute{u} \;=\; \left(\frac{r}{2GM}-1\right)^{1/2} e^{(r+t)/4GM}$$

$$\acute{v} \;=\; \left(\frac{r}{2GM}-1\right)^{1/2} e^{(r-t)/4GM} \quad . \tag{76}$$

In the (u',v',θ, ϕ,) system the Schwarzschild metric is

$$ds^{2} = -\frac{16G^{3}M^{3}}{r} e^{-r/2GM} (du' dv' + dv' du') + r^{2} d\Omega^{2}. \tag{77}$$

Finally the non singular nature of r= 2GM becomes completely manifest; in this form none of the metric coefficients behave in any special way at the event horizon.

Both u' and v' are null coordinates, in the sense that their partial derivatives ∂/∂u' and ∂/∂v' are null vectors. There is nothing wrong with this, since the collection of four partial derivative vectors (two null and two space like) in this system serve as a perfectly good basis for the tangent space. Nevertheless, we are somewhat more comfortable working in a system where one coordinate is time like and the rest are space like. We therefore define

$$u = \frac{1}{2} (u' - v')$$

$$= \left(\frac{r}{2GM}-1\right)^{1/2} e^{r/4GM} \cosh\left(\frac{t}{4GM}\right) \tag{78}$$

and

$$u \;=\; \frac{1}{2} (u' + v')$$

$$= \left(\frac{r}{2GM}-1\right)^{1/2} e^{r/4GM} \sinh\left(\frac{t}{4GM}\right) \tag{79}$$

in terms of which the metric becomes

$$ds^{2} = -\frac{32G^{3}M^{3}}{r} e^{-r/2GM} (du^{2} - dv^{2}) + r^{2} d\Omega^{2}. \tag{80}$$

where r is defined implicitly from

$$u^{2} - v^{2} = \left(\frac{r}{2GM}-1\right) e^{r/2GM} \tag{81}$$

The coordinates (v, u,θ,ϕ) are known as Kruskal coordinates, or sometimes Kruskal-Szekeres coordinates. Note that v is the time like coordinate.

Kruskal-Szekeres coordinates

The Kruskal coordinates have a number of miraculous properties. Like the (t, r^*) coordinates, the radial null curves look like they do in flat spacee

$$v = \pm u + \text{constant} \tag{82}$$

Unlike the (t, r^*) coordinates, however, the event horizon r = 2GM is not infinitely far away; in fact it is defined by

$$v = \pm u \tag{83}$$

consistent with it being a null surface. More generally, we can consider the surfaces r = constant. From(81) these satisfy

$$u^2 - v^2 = \text{constant} \tag{84}$$

Thus, they appear as hyperbolae in the u-v plane. Furthermore, the surfaces of constant t are given by

$$\frac{u}{v} = \tanh\left(\frac{t}{4GM}\right) \tag{85}$$

which defines straight lines through the origin with slope tanh(t/4GM). Note that as $t \to \pm\infty$this becomes the same as (7.83); therefore these surfaces are the same as r = 2GM.

Now, our coordinates (v, u) should be allowed to range over every value they can take without hitting the real singularity at r = 2GM; the allowed region is therefore $-\infty \le u \le +\infty$ and $v^2 < u^2 + 1$. We can now draw a spacetime diagram in the v-u plane (with θ and ϕ suppressed), known as a "Kruskal diagram", which represents the entire spacetime corresponding to the Schwarzschild metric.

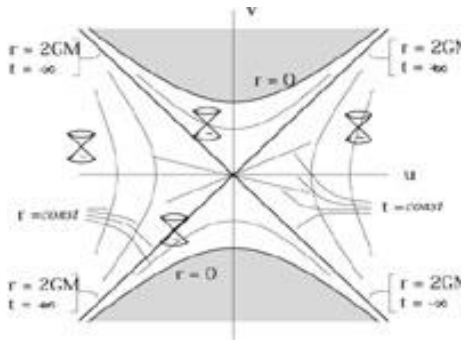

Each point on the diagram is a two-sphere.

Our original coordinates (t, r) were only good for r> 2GM, which is only a part of the manifold portrayed on the Kruskal diagram. It is convenient to divide the diagram into four regions:

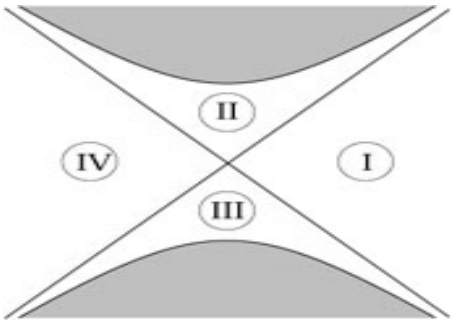

The region in which we started was region I; by following future-directed null rays we reached region II, and by following past-directed null rays we reached region III. If we had explored space like geodesics, we would have been led to region IV.The definitions (78) and (79) which relate (u, v) to(t, r) are really only good in region I; in the other regions it is necessary to introduce appropriate minus signs to prevent the coordinates from becoming imaginary.

Having extended the Schwarzschild geometry as far as it will go, we have described a remarkable spacetime. Region II, of course, is what we think of as the black hole. Once anything travels from region I into II, it can never return. In fact, every future-directed path in region II ends up hitting the singularity at r= 0;once you enter the event horizon, you are utterly doomed. This is worth stressing; not only can you not escape back to region I, you cannot even stop yourself from moving in the direction of decreasing r,since this is simply the time like direction. (This could have been seen in our original coordinate system; for r <2GM, t becomes space like and r becomes time like.) Thus you can no more stop moving toward the singularity than you can stop getting older.Since proper time is maximized along a geodesic, you will live the longest if you don't struggle, but just relax as you approach the singularity. Not that you will have long to relax. (Nor that the voyage will be very relaxing; as you approach the singularity the tidal forces become infinite. As you fall toward the singularity your feet and head will be pulled apart from each other, while your torso is squeezed to infinitesimal thinness.

Regions III and IV might be somewhat unexpected. Region III is simply the time-reverse of region II, a part of spacetime from which things can escape to us, while we can never get there. It can be thought of as a "white hole." There is a singularity in the past, out of which the universe appears to spring. The boundary of region III is sometimes called the past event horizon,while the boundary of region II is called the future event horizon. Region IV, meanwhile, cannot be reached from our region I either forward or backward in time (nor can anybody from over there reach us). It is another asymptotically flat region of spacetime,a mirror image of ours. It can be thought of as being

connected to region I by a "wormhole," a neck-like configuration joining two distinct regions. Consider slicing up the Kruskal diagram into spacelike surfaces of constant v:

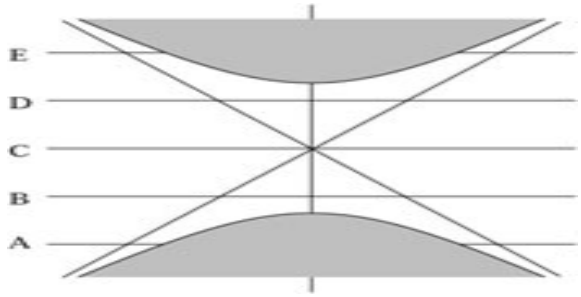

Now we can draw pictures of each slice, restoring one of the angular coordinates for clarity:

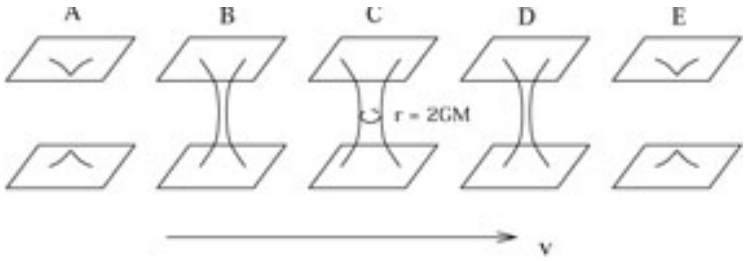

So the Schwarzschild geometry really describes two asymptotically flat regions which reach toward each other, join together via a wormhole for a while, and then disconnect. But the wormhole closes up too quickly for any time-like observer to cross it from one region into the next.

It might seem somewhat implausible, this story about two separate spacetimes reaching toward each other for a while and then letting go. In fact, it is not expected to happen in the real world, since the Schwarzschild metric does not accurately model the entire universe. Remember that it is only valid in vacuum, for example outside a star. If the star has a radius larger than 2GM, we need never worry about any event horizons at all. But we believe that there are stars which collapse under their own gravitational pull, shrinking down to below r= 2GM and further into a singularity, resulting in a black hole. There is no need for a white hole, however, because the past of such a spacetime looks nothing like that of the full Schwarzschild solution. Roughly, a Kruskal-like diagram for stellar collapse would look like the following:

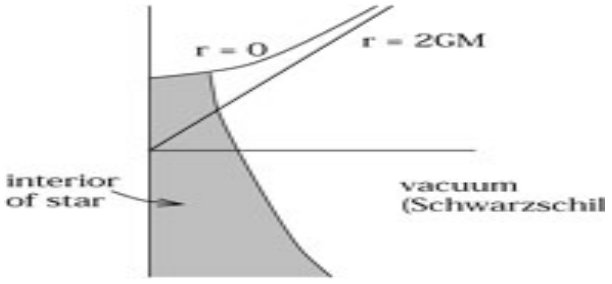

The shaded region is not described by Schwarzschild, so there is no need to fret about white holes and wormholes.

We have seen that the Kruskal coordinate system provides a very useful representation of the Schwarzschild geometry. Before moving onto other types of black holes, we will introduce one more way of thinking about this spacetime, the Penrose (or Carter-Penrose, or conformal) diagram. The idea is to do a conformal transformation which brings the entire manifold onto a compact region such that we can fit the spacetime on a piece of paper.

Let's begin with Minkowski space, to see how the technique works. The metric in polar coordinates is

$$ds^2 = -dt^2 + dr^2 + r^2 d\Omega^2 \tag{86}$$

Nothing unusual will happen to the θ ,ϕ coordinates, but we will want to keep careful track of the ranges of the other two coordinates. In this case of course we have

$$-\infty < t < +\infty$$
$$0 \leq r < +\infty \tag{87}$$

Technically the world line r= 0 represents a coordinate singularity and should be covered by a different patch, but we all know what is going on so we'll just act like r = 0 is well-behaved. Our task is made somewhat easier if we switch to null coordinates:

$$u = \frac{1}{2}(t + r)$$
$$v = \frac{1}{2}(t - r) \ , \tag{88}$$

with corresponding ranges given by

$$-\infty < u < +\infty$$
$$-\infty < v < +\infty \tag{89}$$

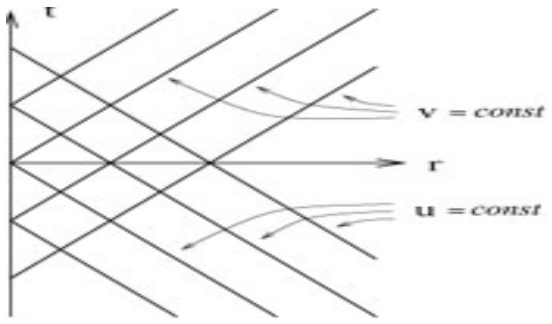

These ranges are as portrayed in the figure, on which each point represents a 2-sphere of radius r= u-v. The metric in these coordinates is given by

$$ds^2 = -2(dudv + dvdu) + (u-v)^2 d\Omega^2 \qquad (90)$$

We now want to change to coordinates in which "infinity" takes on a finite coordinate value. A good choice is

$$U = arctanu$$
$$V = arctanv \qquad (91)$$

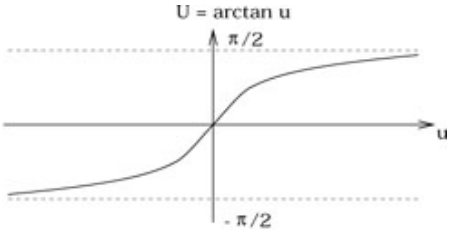

The ranges are now

$$-\frac{\pi}{2} < U < +\frac{\pi}{2}$$

$$-\frac{\pi}{2} < V < +\frac{\pi}{2}$$

$$V \leq U \qquad (92)$$

To get the metric, use

$$dU = \frac{du}{1+u^2}$$

(93)

and $$\cos(arctanu) = \frac{1}{\sqrt{1+u^2}} \qquad (94)$$

and likewise, for v. We are led to

$$dudv + dvdu = \frac{1}{cos^2U\ cos^2V}\ (dUdV + dVdU) \qquad (95)$$

Meanwhile,

$$(u-v)^2 = (tanU - tanV)^2$$

$$= \frac{1}{cos^2U\ cos^2V}\ ((sinUcosV - cosUsinV))^2 \qquad (96)$$

$$= \frac{1}{cos^2U\ cos^2V} sin^2(U - V)$$

Therefore, the Minkowski metric in these coordinates is

$$ds^2 = \frac{1}{cos^2U\ cos^2V}[-2(dUdV + dVdU)\ + sin^2(U - V)d\Omega^2\ ] \qquad (97)$$

This has a certain appeal, since the metric appears as a fairly simple expression multiplied by an overall factor. We can make it even better by transforming back to a timelike coordinate η and a spacelike (radial) coordinate χ, via

$$\eta = U + V$$
$$\chi = U - V \quad , \qquad (98)$$

with ranges

$$-\pi < \eta < +\pi$$
$$0 \leq \chi < \pi \quad , \qquad (99)$$

Now the metric is

$$ds^2 = \omega^{-2}(-d\eta^2 + d\chi^2 + sin^2\chi\, d\Omega^2) \qquad (100)$$

where

$$\omega = cosU\ cosV$$
$$= \frac{1}{2}(\cos\eta + \cos\chi) \qquad (101)$$

The Minkowski metric may therefore be thought of as related by a conformal transformation to the "unphysical" metric

$$d\bar{s}^2 = \omega^2\ ds^2$$
$$= (-d\eta^2 + d\chi^2 + sin^2\chi\, d\Omega^2) \qquad (102)$$

This describes the manifold $\mathbf{R} \times S^3$, where the 3-sphere is maximally symmetric and static. There is curvature in this metric,and it is not a solution to the vacuum Einstein's equations. This shouldn't

bother us, since it is unphysical; the true physical metric, obtained by a conformal transformation, is simply flat spacetime. In fact this metric is that of the "Einstein static universe," a static (but unstable)solution to Einstein's equations with a perfect fluid and a cosmological constant. Of course, the full range of coordinates on $\mathbf{R} \times S^3$ would usually be $-\infty < \eta < +\infty$, $0 \leq \chi \leq \pi$,while Minkowski space is mapped into the subspace defined by (99).The entire $\mathbf{R} \times S^3$ can be drawn as a cylinder, in which each circle is a three - sphere, as shown on the next page.

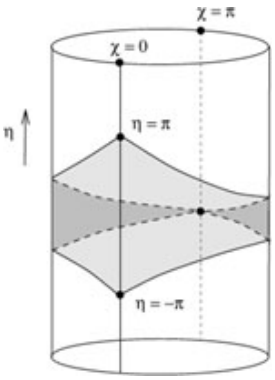

The shaded region represents Minkowski space. Note that each point (η,χ) on this cylinder is half of a two-sphere, where the other half is the point $(\eta,-\chi)$. We can unroll the shaded region to portray Minkowski space as a triangle, as shown in the figure.

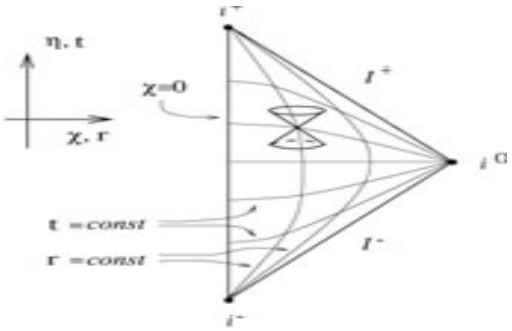

Penrose Diagram

The is the Penrose diagram. Each point represents a two-sphere. In fact Minkowski space is only the interior of the above diagram (including $\chi = 0$); the boundaries are not part of the original spacetime. Together they are referred to as conformal infinity. The structure of the Penrose diagram allows us to subdivide conformal infinity into a few different regions:

$i^+ =$ future timelike infinity $(\eta = \pi, \chi = 0)$

$i^0 =$ spatial infinity $(\eta = 0, \chi = \pi)$

i^- = past timelike infinity ($\eta = -\pi, \chi = 0$

ב$^+$ = future null infinity ($\eta = \pi - \chi, 0 < \chi < \pi$)

ב$^-$ = past null infinity ($\eta = -\pi + \chi, 0 < \chi < \pi$)

(ב$^+$ and ב$^-$are pronounced as "scri-plus" and"scri-minus", respectively.) Note that i^+,i^0, and $i^-$are actually points, since $\chi = 0$ and $\chi = \pi$ are the north and south poles of S^3. Meanwhile +ב$^+$ and ב$^-$ are actually null surfaces, with the topology of $\mathbf{R} \times S^3$.

There are a number of important features of the Penrose diagram for Minkowski spacetime. The points i^+, and i^- can be thought of as the limits of spacelike surfaces whose normals are timelike;conversely, i^0can be thought of as the limit of timelike surfaces whose normals are spacelike. Radial null geodesics are at ±45° in the diagram. All timelike geodesics begin at $i^-$and end at i^+; all null geodesics begin at ב$^-$and end at ב$^+$; all spacelike geodesics both begin and end at i^0. On the other hand, there can be non-geodesic timelike curves that end at null infinity (if they become "asymptotically null").

It is nice to be able to fit all of Minkowski space on a small piece of paper, but we don't really learn much that we didn't already know. Penrose diagrams are more useful when we want to represent slightly more interesting spacetimes, such as those for black holes.The original use of Penrose diagrams was to compare spacetimes to Minkowski space "at infinity" - the rigorous definition of"asymptotically flat" is basically that a spacetime has a conformal infinity just like Minkowski space.We will not pursue these issues in detail, but instead turn directly to analysis of the Penrose diagram for a Schwarzschild black hole.

We will not go through the necessary manipulations in detail, since they parallel the Minkowski case with considerable additional algebraic complexity. We would start with the null version of the Kruskal coordinates, in which the metric takes the form

$$ds^2 = -\frac{16G^3M^3}{r} e^{-r/2GM}(du'\,dv' + dv'\,du') + r^2 d\Omega^2. \qquad (103)$$

where r is defined implicitly via

$$\grave{u}\grave{v} = \left(\frac{r}{2GM} - 1\right)^{1/2} e^{r/4GM} \qquad (104)$$

Then essentially the same transformation as was used in flat spacetime suffices to bring infinity into finite coordinate values:

$$u'' = arctan\left(\frac{u'}{\sqrt{2GM}}\right)$$

$$v'' = arctan\left(\frac{v'}{\sqrt{2GM}}\right), \tag{105}$$

with ranges

$$-\frac{\pi}{2} < u'' < +\frac{\pi}{2}$$

$$-\frac{\pi}{2} < v'' < +\frac{\pi}{2}$$

$$-\pi < u'' + v'' < +\pi$$

The (u", v") part of the metric (that is, at constant angular coordinates) is now conformally related to Minkowski space. In the new coordinates the singularities at r= 0 are straight lines that stretch from time like infinity in one asymptotic region to time like infinity in the other. The Penrose diagram for the maximally extended Schwarzschild solution thus looks like this:

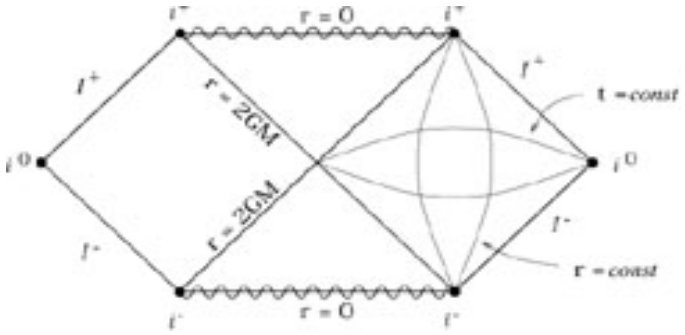

The only real subtlety about this diagram is the necessity to understand that i^+ and i^- are distinct from r = 0 (there are plenty of time like paths that do not hit the singularity). Notice also that the structure of conformal infinity is just like that of Minkowski space, consistent with the claim that Schwarzschild is asymptotically flat. Also, the Penrose diagram for a collapsing star that forms a black hole is what you might expect, as shown on the next page.

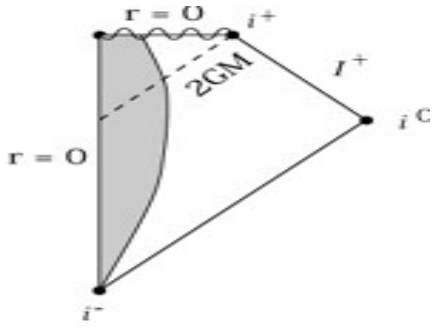

Once again the Penrose diagrams for these spacetimes don't really tell us anything we didn't already know; their usefulness will become evident when we consider more general black holes. In principle there could be a wide variety of types of black holes, depending on the process by which they were formed. Surprisingly, however, this turns out not to be the case; no matter how a blackhole is formed, it settles down (fairly quickly) into a state which is characterized only by the mass, charge, and angular momentum. This property, which must be demonstrated individually for the various types of fields which one might imagine go into the construction of the hole, is often stated as "black holes have no hair." You can demonstrate, for example, that a hole which is formed from an initially in homogeneous collapse "shakes off" any lumpiness by emitting gravitational radiation. This is an example of a "no-hair theorem." If we are interested in the form of the black hole after it has settled down, we thus need only to concern ourselves with charged and rotating holes. In both cases there exist exact solutions for the metric, which we can examine closely.

Black hole evaporation

But first let's take a brief detour to the world of blackhole evaporation. It is strange to think of a black hole "evaporating," but in the real world black holes aren't truly black - they radiate energy as if they were a blackbody of temperature $\mathbf{T= \hbar/8\pi}$ kGM, where M is the mass of the hole and k is Boltzmann's constant. The derivation of this effect, known as Hawking radiation, involves the use of quantum field theory in curved spacetime and is way outside our scope right now. The informal idea is nevertheless understandable.

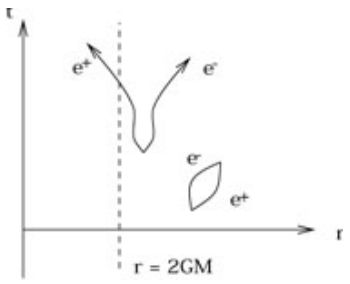

In quantum field theory there are "vacuum fluctuations" - the spontaneous creation and annihilation of particle/antiparticle pairs in empty space. These fluctuations are precisely analogous to the zero-point

fluctuations of a simple harmonic oscillator. Normally such fluctuations are impossible to detect, since they average out to give zero total energy (although nobody knows why; that's the cosmological constant problem). In the presence of an event horizon, though, occasionally one member of a virtual pair will fall into the black hole while its partner escapes to infinity. The particle that reaches infinity will have to have a positive energy, but the total energy is conserved; therefore the blackhole has to lose mass. (If you like you can think of the particle that falls in as having a negative mass.) We see the escaping particles as Hawking radiation. It's not a very big effect, and the temperature goes down as the mass goes up, so for black holes of mass comparable to the sun it is completely negligible. Still, in principle the black hole could lose all of its mass to Hawking radiation, and shrink to nothing in the process. The relevant Penrose diagram might look like this:

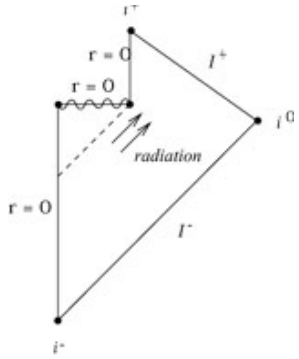

On the other hand, it might not. The problem with this diagram is that "information is lost" - if we draw a spacelike surface to the past of the singularity and evolve it into the future, part of it ends up crashing into the singularity and being destroyed. As a result the radiation itself contains less information than the information that was originally in the spacetime. (This is the worse than a lack of hair on the black hole. It's one thing to think that information has been trapped inside the event horizon, but it is more worrisome to think that it has disappeared entirely.) But such a process violates the conservation of information that is implicit in both general relativity and quantum field theory, the two theories that led to the prediction. This paradox is considered a big deal these days, and there are a number of efforts to understand how the information can somehow be retrieved. A currently popular explanation relies on string theory, and basically says that black holes have a lot of hair, in the form of virtual stringy states living near the event horizon. I hope you will not be disappointed to hear that we won't look at this very closely; but you should know what the problem is and that it is an area of active research these days.

Charged black holes solution

With that out of our system, we now turn to electrically charged black holes. These seem at first like reasonable enough objects, since there is certainly nothing to stop us from throwing some net charge into a previously uncharged black hole. In an astrophysical situation, however, the total amount of charge is expected to be very small, especially when compared with the mass (in terms of the relative gravitational effects). Nevertheless, charged black holes provide a useful testing ground for various thought experiments, so they are worth our consideration.

In this case the full spherical symmetry of the problem is still present; we know therefore that we can write the metric as

$$ds^2 = -e^{2\alpha(r,t)}dt^2 + e^{2\beta(r,t)}dr^2 + r^2 d\Omega^2 \tag{106}$$

Now, however, we are no longer in vacuum, since the hole will have a nonzero electromagnetic field, which in turn acts as a source of energy-momentum. The energy-momentum tensor for electromagnetism is given by

$$T_{\mu\nu} = \frac{1}{4\pi}\left(F_{\mu\rho}F_{\nu}^{\rho} - \frac{1}{4}g_{\mu\nu}F_{\rho\sigma}F^{\rho\sigma}\right), \tag{107}$$

where $F_{\mu\nu}$ is the electromagnetic field strength tensor. Since we have spherical symmetry, the most general field strength tensor will have components

$$F_{tr} = f(r,t) = -F_{rt}$$

$$F_{\theta\phi} = g(r,t)\sin\theta = -F_{\phi\theta}, \tag{108}$$

where f(r,t) and g(r,t) are some functions to be determined by the field equations, and components not written are zero. F_{tr} corresponds to a radial electric field, while $F_{\theta\phi}$ corresponds to a radial magnetic field. (For those of you wondering about the sinθ, recall that the thing which should be independent of θ and ϕ is the radial component of the magnetic field, $B^r = \varepsilon^{o1\mu\nu}F_{\mu\nu}$. For a spherically symmetric metric, $\varepsilon^{\rho\sigma\mu\nu} = \frac{1}{\sqrt{-g}}\tilde{\varepsilon}^{\rho\sigma\mu\nu}$ is proportional to $\sin^{-1}\theta$, so we want a factor of sinθ in $F_{\theta\phi}$.) The field equations in this case are both Einstein's equations and Maxwell's equations:

$$g^{\mu\nu}\nabla_{\mu}F_{\nu\sigma} = 0$$

$$\nabla_{[\mu} F_{\nu\rho]} = 0 \tag{109}$$

The two sets are coupled together, since the electromagnetic field strength tensor enters Einstein's equations through the energy-momentum tensor, while the metric enters explicitly into Maxwell's equations.

The difficulties are not insurmountable, however, and a procedure similar to the one we followed for the vacuum case leads to a solution for the charged case as well. We will not go through the steps explicitly, but merely quote the final answer. The solution is known as the **Reissner-Nordstrøm** metric, and is given by

$$ds^2 = -\Delta dt^2 + \Delta^{-1} dr^2 + r^2 d\Omega^2 , \tag{110}$$

where

$$\Delta = 1 - \frac{2GM}{r} + \frac{G(p^2+q^2)}{r^2} , \tag{111}$$

In this expression, M is once again interpreted as the mass of the hole; q is the total electric charge, and p is the total magnetic charge. Isolated magnetic charges (monopoles)have never been observed in nature, but that doesn't stop us from writing down the metric that they would produce if they did exist. There are good theoretical reasons to think that monopoles exist, but are extremely rare. (Of course, there is also the possibility that a black hole could have magnetic charge even if there aren't any monopoles.) In fact the electric and magnetic charges enter the metric in the same way, so we are not introducing any additional complications by keeping pin our expressions. The electromagnetic fields associated with this solution are given by

$$\begin{aligned} F_{tr} &= \frac{-q}{r^2} \\ F_{\theta\phi} &= -p\sin\theta , \end{aligned} \tag{112}$$

Conservatives are welcome to set p = 0 if they like.

The structure of singularities and event horizons is more complicated in this metric than it was in Schwarzschild, due to the extra term in the function $\Delta(r)$ (which can be thought of as measuring "how much the light cones tip over"). One thing remains the same: at r= 0 there is a true curvature singularity (as could be checked by computing the curvature scalar $R_{\mu\nu\rho\sigma}R^{\mu\nu\rho\sigma}$). Meanwhile, the equivalent of r = 2GM will be the radius where Δ vanishes. This will occur at

$$r_{\pm} = GM \pm \sqrt{G^2M^2 - G(p^2+q^2)} \tag{113}$$

This might constitute two, one, or zero solutions, depending on the relative values of GM^2 and $p^2 + q^2$. We therefore consider each case separately.

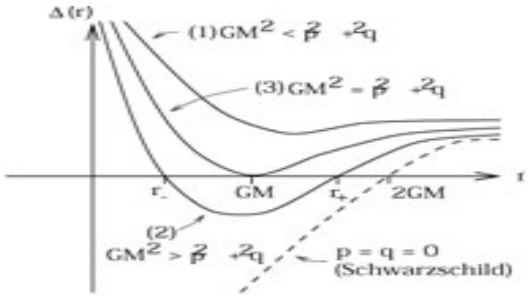

Case One - $GM^2 < p^2 + q^2$

In this case the coefficient Δ is always positive (never zero),and the metric is completely regular in the (t,r,θ,ϕ)coordinates all the way down to r= 0. The coordinate t is always time like, and r is always spacelike. But there still is the singularity at r= 0, which is now a time like line. Since there is no event horizon, there is no obstruction to an observer travelling to the singularity and returning to report on what was observed. This is known as a naked singularity, one which is not shielded by an horizon. A careful analysis of the geodesics reveals, however, that the singularity is "repulsive" - time like geodesics never intersect r= 0, instead they approach and then reverse course and move away. (Null geodesics can reach the singularity, as can non-geodesic time like curves.)

As $r \to \infty$ the solution approaches flat spacetime, and as we have just seen the causal structure is "normal" everywhere. The Penrose diagram will therefore be just like that of Minkowski space, except that now r = 0 is a singularity.

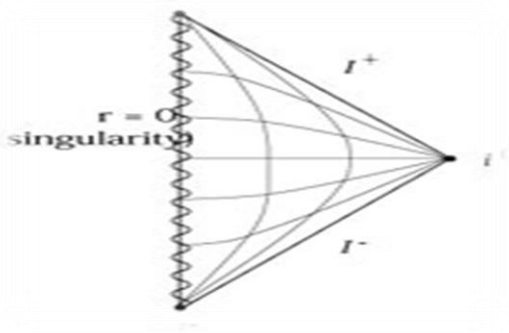

The nakedness of the singularity offends our sense of decency, as well as the cosmic censorship conjecture, which roughly states that the gravitational collapse of physical matter configurations will never produce a naked singularity.(Of course, it's just a conjecture, and it may not be right; there are

some claims from numerical simulations that collapse of spindle-like configurations can lead to naked singularities.)In fact, we should not ever expect to find a black hole with $GM^2 < p^2 + q^2$ as the result of gravitational collapse. Roughly speaking, this condition states that the total energy of the hole is less than the contribution to the energy from the electromagnetic fields alone - that is, the mass of the matter which carried the charge would have had to be negative. This solution is therefore generally considered to be unphysical. Notice also that there are not good Cauchy surfaces (spacelike slices for which every inextensible time like line intersects them) in this spacetime, since time like lines can begin and end at the singularity.

Case Two - $GM^2 > p^2 + q^2$

This is the situation which we expect to apply in real gravitational collapse; the energy in the electromagnetic field is less than the total energy. In this case the metric coefficient $\Delta(r)$ is positive at large rand small r, and negative inside the two vanishing points $r_{\pm} = GM \pm \sqrt{G^2M^2 - G(p^2 + q^2)}$. The metric has coordinate singularities at both r_+ and r_-; in both cases these could be removed by a change of coordinates as we did with Schwarzschild.

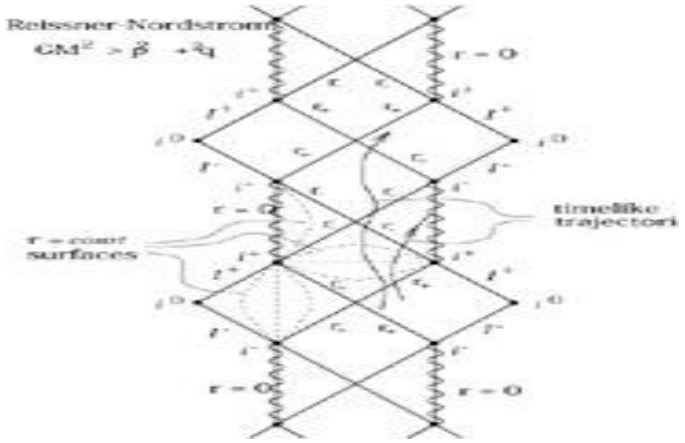

The surfaces defined by $r = r_{\pm}$ are both null, and in fact they are event horizons (in a sense we will make precise in a moment).The singularity at r = 0 is a time like line (not a spacelike surface as in Schwarzschild). If you are an observer falling into the black hole from far away, r_+ is just like 2GM in the Schwarzschild metric; at this radius r switches from being a spacelike coordinate to a time like coordinate, and you necessarily move in the direction of decreasing r. Witnesses outside the black

hole also see the same phenomena that they would outside an uncharged hole -the infalling observer is seen to move more and more slowly, and is increasingly redshifted.

But the inevitable fall from r_+ to ever-decreasing radii only lasts until you reach the null surface r = r-,where r switches back to being a spacelike coordinate and the motion in the direction of decreasing r can be arrested. Therefore you do not have to hit the singularity at r= 0; this is to be expected, since r= 0 is a time like line (and therefore not necessarily in your future). In fact you can choose either to continue on to r= 0, or begin to move in the direction of increasing r back through the null surface at r = r-. Then r will once again be a time like coordinate, but with reversed orientation; you are forced to move in the direction of increasing r. You will eventually be spit out past r = r+ once more, which is like emerging from a white hole into the rest of the universe. From here you can choose to go back into the black hole - this time, a different hole than the one you entered in the first place - and repeat the voyage as many times as you like. This little story corresponds to the accompanying Penrose diagram, which of course can be derived more rigorously by choosing appropriate coordinates and analytically extending the Reissner-Nordstrøm metric as far as it will go.

How much of this is science, as opposed to science fiction? Probably not much. If you think about the world as seen from an observer inside the black hole who is about to cross the event horizon at r-, you will notice that they can look back in time to see the entire history of the external (asymptotically flat)universe, at least as seen from the black hole. But they see this (infinitely long) history in a finite amount of their proper time -thus, any signal that gets to them as they approach r-is infinitely blue shifted. Therefore it is reasonable to believe that any non-spherically symmetric perturbation that comes into a **Reissner-Nordstrøm** black hole will violently disturb the geometry we have described. It's hard to say what the actual geometry will look like, but there is no very good reason to believe that it must contain an infinite number of asymptotically flat regions connecting to each other via various wormholes.

Case Three - $GM^2 = p^2 + q^2$

This case is known as the extreme Reissner-Nordstrøm solution (or simply "extremal black hole"). The mass is exactly balanced in some sense by the charge -you can construct exact solutions consisting of several extremal black holes which remain stationary with respect to each other for all time. On the one hand the extremal hole is an amusing theoretical toy; these solutions are often examined in studies of the information loss paradox, and the role of black holes in quantum gravity. On the other hand it appears very unstable, since adding just a little bit of matter will bring it to Case Two.

References

1) Weinberg, S. (1972). Gravitation and Cosmology: Principles and Applications of the General Theory of Relativity. John Wiley & Sons. Chapter 8. ISBN 0-471-92567-5.

2) Taylor, E. F.; Wheeler, J. A. (2000). Exploring Black Holes: Introduction to General Relativity. Addison-Wesley. ISBN 0-201-38423-X.

3) Heinzle, J. M.; Steinbauer, R. (2002). "Remarks on the distributional Schwarzschild geometry". Journal of Mathematical Physics. 43 (3): 1493–1508.

4) Misner, C. W.; Thorne, K. S.; Wheeler, J. A. (1970). Gravitation. W.H. Freeman. Chapters 31 and 32. ISBN 0-7167-0344-0.

5) Adler, R.; Bazin, M.; Schiffer, M. (1975). Introduction to General Relativity (2nd ed.). McGraw-Hill. Chapter 6. ISBN 0-07-000423-4.

6) Landau, L. D.; Lifshitz, E. M. (1951). The Classical Theory of Fields. Course of Theoretical Physics. 2 (4th Revised English ed.). Pergamon Press. Chapter 12. ISBN 0-08-025072-6.

SEED STORAGE FOR BETTER PLANT STAND

Project

Submitted to the

Faculty of Agricultural Sciences

GLA University, Mathura-281406, India

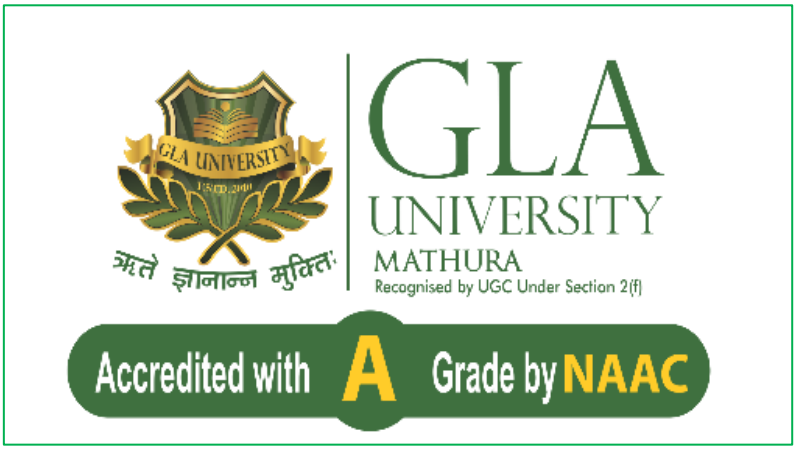

By

Yashveer Singh

B.Sc. (Hons.) Agriculture

CERTIFICATE

This is to certify that Project Report entitled, **"Seed Storage for Better Plant Stand"** which is being submitted by **Yashveer Singh** to the Faculty of Agricultural Sciences of GLA University, is a record of the candidate work carried out by him under my supervision.

Dr. Vineeta Pandey
(Assistant Professor)

ACKNOWLEDGEMENTS

It gives a great pleasure to present the project report undertaken during B.Sc. (Hons.) degree program. I owe special gratitude to (Dr. Vineeta Pandey, Assistant Professor), Faculty of agricultural Sciences, GLA University, Mathura for her constant support and guidance throughout the course of work. Her sincerity and perseverance have been a constant source of inspiration. It is her cognizant efforts that our endeavours' have seen light of the day. I also take the opportunity to acknowledge the contribution of Prof. V.S. Pundhir, Head, Faculty of Agricultural Sciences, GLA University, Mathura for his full support and assistance.

Yashveer Singh

Introduction

Maintenance of seed vigour and viability in terms of germination from harvest until planting is the most important in any seed production programme. Care should be taken at every stage of processing and distribution to maintain the viability and vigour. The harvested seeds of most of the orthodox crop are usually dried and stored for at least one season until the commencement of the next growing season while recalcitrant seeds require high moisture content for safe storage. In the seeds ageing starts at physiological maturity, which is irreversible. Hence seeds become practically worthless if they fail to give adequate plant stands in addition to healthy and vigorous plants. Good storage is therefore a basic requirement in seed production. The Cereals, pulses, oilseeds etc. are very important products for storage. A safe storage place must be provided for the grain produced until it is needed for consumption and multiplication purposes. Since grain production is seasonal, and consumption is continuous, safe storage must maintain grain quality and quantity. This means that grains have to be protected from weather, moulds and other microorganisms, moisture, destructively huge temperatures, insects, rodents, birds, objectionable odours and contamination, and from unauthorized distribution.

OBJECTIVE OF SEED STORAGE

Maintain initial seed quality by providing suitable condition.

PURPOSE OF SEED STORAGE

Seeds have to be stored, of course, because there is usually a period of time between harvest and planting. While the time interval between harvest and planting is the basic reason for storing seed, there are other considerations, especially in the case of extended storage of seed. The purpose of seed storage is to maintain the seed in good physical and physiological condition from the time they are harvested until the time they are planted. It is important to get adequate plant stands in addition to healthy and vigorous plants. Seed suppliers are not always able to market all the seed they produce during the following planting season. In many cases, the unsold seed are “carried over” in storage for marketing during the second planting season after harvest. Problems arise in connection with carryover storage of seed because some kinds,

varieties and lots of seed do not carryover very well. Foundation seed units and others have found this to be an economical, efficient procedure for seeds of varieties for which there is limited demand. Some kinds of seeds are stored for extended periods to improve the percentage and rapidity of germination by providing enough time for a "natural" release from dormancy. Regardless of the specific reasons for storage of seed, the purpose remains the same maintenance of a satisfactory capacity for germination and emergence. The facilities and procedures used in storage, therefore, have to be directed towards the accomplishment of this purpose.

STAGE OF SEED STORAGE

In the broadest sense the storage period for seed begins with attainment of physiological maturity and ends with resumption of active growth of the embryonic axis, i.e., germination.

The entire storage periods can be divided into:

1	**Post maturation/ Pre harvest stage**	Period from physiological maturity to harvest (seed in field).
2	**Bulk seed stage**	Period from harvest to packaging (bulk seed in aeration drying bins, surge bins, etc.).
3	**Packaged seed stage**	Period from packaging to distribution (seed in Packages in warehouse).
4	**Distribution /Marketing stage**	Period during distributing and marketing (packaged seed in transit and / or retailer's storehouse).
5	**On-farm stage**	Period from purchase to planting of seed (seed in on-farm storage).

Seeds are considered to be physiologically and morphologically mature when they reach maximum dry weight. At this stage dehydration of the seed is well underway. Dry-down continues after physiological maturity until moisture content of the seed and fruit decreases to a level which permits effective and efficient harvest and threshing. This stage can be termed as harvest maturity.

There is usually an interval of time between physiological maturity and harvestable maturity, and this interval represents the first segment of the storage period. Any delay in harvesting the seed after they reach harvest maturity prolongs the first segment of the storage period – often to the detriment of seed quality. The second segment of the storage period extends from harvest to the beginning of conditioning. Seed in the combine, grain wagon, and bulk storage or drying bins are in storage and their quality is affected by the same factors that affect the quality of seed during the packaged seed segment of the storage period. The third segment of the storage period begins with the onset of conditioning and ends with packaging. The fourth segment of the storage period is the packaged seed phase which has already been mentioned. The packaged seed segment is followed by storage during distribution and marketing, and finally by storage on the farm before and during planting. The seed quality can be considerably be affected at any of the stages or segments mentioned above unless sound principles involved in seed storage are practiced and the seeds are properly handled.

Orthodox seed

The seeds able to tolerate moisture loss and less seed moisture favours the storage i.e., decreased moisture increased storage period. e.g., Rice, sorghum and most of the cultivated species.

Recalcitrant seed

Just opposite to the orthodox. Seeds not able to tolerate moisture loss. Required high moisture for viability maintenance.

TYPES OF SEED STORAGE

1. Storage at ambient temperature and humidity
2. Dry storage with control of moisture content but not temperature
3. Dry storage with control of both moisture content and temperature
4. Dry storage for long-term gene conservation
5. Moist storage without control of moisture content of temperature
6. Moist cold storage, with control of temperature
7. Cryopreservation

1. Storage at ambient temperature and humidity

Seeds can be stored in piles, single layers, sacks or open containers, under shelter against rain, well ventilated and protected from rodents and store at least for several months.

2. Dry storage with control of moisture content but not temperature

Orthodox seeds will retain viability longer, when dried to low moisture content (4¬8%) and then stored in a sealed container or in a room in which humidity is controlled, than when stored in equilibrium with ambient air humidity. Cool condition is especially favourable.

3. Dry storage with control of both moisture content and temperature

This is recommended for many orthodox species which have periodicity of seeding but which are planted annually in large scale afforestation projects. A combination of 4-8% moisture content and 0 to 5° temperature will maintain viability for 5 years or more.

4. Dry storage for long-term gene conservation

Long-term conservation of gene resources of orthodox agricultural seeds is -18°C temperature and 5±11% moisture content.

5. Moist storage without control of moisture content of temperature

Suitable for storage of recalcitrant seeds, for a few months over winter. Seeds may be stored in heaps on the ground, in shallow pits, in well drained soils or in layers in well ventilated sheds, often covered or mixed with leaves, moist sand, peat or other porous materials. The aim is to maintain moist and cool conditions, with good aeration to avoid overheating which may result from the relatively high rates of respiration associated with moist storage. This may be accomplished by regular turning of the heaps.

6. Moist cold storage, with control of temperature

This method implies controlled low temperature just above freezing or less commonly, just below freezing. Moisture can be controlled within approximate limits by adding moist media e.g., sand, peat or a mixture of both to the seed, in proportions of one part media to 1 part seed by volume, and re-moistening periodically or more accurately by controlling the relative humidity of the store. This method is much applicable to temperate recalcitrant genera.

7. Cryopreservation

It is also called as cryogenic storage. Seeds are placed in liquid nitrogen at -196°C. Seeds are actually placed into the gaseous phase of the liquid nitrogen -150°C for easy handling and safety. Metabolic reactions come to a virtual standstill at the temperature of liquid nitrogen and the cells will remain in an unaltered state until the tissues are removed from the liquid nitrogen and defrosted. Therefore, little detrimental physiological activity takes place at these temperatures, which prolongs the storage life of seeds. It is not practical for commercial seed storage, but is useful to store the valuable germplasm.

HARRINGTON THUMB RULE ON SEED STORAGE

The following thumb rules by Harrington are useful measures for assessing the effect of moisture and temperature on seed storage.

- For every decrease of 1% seed moisture content, the life of the seed doubles. This rule is applicable when moisture content between 5 and 14%.
- For every decrease of 5°C (10°F) in storage temperature the life of the seed doubles. This rule applies between 0°C to 50°C.
- Good seed storage is achieved when the % of relative humidity in storage environment and the storage temperature in degrees Fahrenheit add up to hundred but the contribution from temperature should not exceed 50°F.

NOMOGRAPH

- Roberts (1972) developed formulae to describe the relationship between temperature, seed moisture content and period of viability.
- From these relationships it was possible to construct a seed viability nomograph.
- These nomographs are helpful in predicting the retention of seed viability in defined storage environment for a particular period or to determine combinations of temperature and moisture content which will ensure the retention of a desired level of seed viability for a specific period.

PRINCIPLES OF SEED STORAGE

1. Seed storage conditions should be dry and cool
2. Effective storage pest control
3. Proper sanitation in seed stores
4. Before placing seeds into storage, they should be dried to safe moisture limits.

5. Storing of high-quality seed only i.e., well cleaned treated as well as high germination and vigour.

FACTORS AFFECTING SEED LONGEVITY IN STORAGE

1. Kind (or) variety of seed

2. Initial seed quality

3. Moisture content

4. Relative humidity and temperature during storage

5. Provenance

6. The activity of organisms associated with seeds in storage.

1. Kind or variety of seed

Seed storability is considerably influenced by the kind or variety of seeds. Some seeds are short lived. E.g.: Onion, Soybean and Groundnut. As a general rule starchy seeds can be stored considerably for a longer period compared to proteinaceous or oily seeds because of their hygroscopic nature.

2. Initial seed quality

Seed lots having vigorous undamaged seeds store longer than that of deteriorated. Even seed lots having good germination at the beginning of storage period, may deteriorate at a faster rate depending upon the severity of weathering damage, mechanical injury or otherwise in the field. The low-quality seeds should invariably be rejected. Even at best storage conditions, the initial quality of the seed cannot be improved (except for the dormant seed) but can only be maintained.

3. Moisture content

The most important factor influencing seed viability during storage is the moisture content and the rate of deterioration increases, as the seed moisture content increases. The drier the seed the higher will be the storage life. It is well known that higher moisture content enhances the biological activity in the seeds and causes excessive heating, besides promoting mould and insect activities. The relationship of moisture content of seeds during post-harvest stages furnished below would clearly indicate the role of moisture in the life of seeds in storage.

Role and importance of moisture content in the life of seeds

35-80%	Moisture content of developing seed, seeds not mature enough for harvest
18-40%	Seeds physiologically mature; respiratory rate high; seed susceptible to field deterioration; heating occurs if seed bulked without adequate ventilation; moulds and insects very active; seed susceptible to mechanical damage in harvesting and handling.
13-18%	Seeds store reasonably well for 6 to 18 months in open storage in temperate climates; insects can still be a problem in susceptible seeds; seed susceptible to mechanical damage.
10-13%	Respiratory rate still high; can get heating at highest levels; moulds and insects can be damaging; seed resistant to mechanical damage.
8-10%	Seed sufficiently dry, can be stored for 1 to 3 years open storage in temperate climates; very little insect activity; seed very susceptible to mechanical damage.
4-8%	Safe moisture content for sealed storage.
0-4%	Seeds germinate when they imbibe water to these levels.
33-60%	Extreme desiccation can be damaging to seed; hard seededness develops in some kinds of seed.

The importance of seed moisture content in extending the shelf life of seeds under ideal storage conditions can be well known and understood from the Harrington's thumb rule, that one per cent decrease in seed moisture content nearly doubles the storage potential of the seed.

Use of desiccants

Desiccant like silica gel can maintain the moisture content in equilibrium with the Relative Humidity of 45%. It is kept @ 1kg/10 kg of seeds. When the silica gel turns to pink colour it should be dried at 175^0 in oven and then again placed in the container.

4. Relative humidity and temperature during storage

Seeds are hygroscopic. They attain rather specific and characteristic moisture content when subjected to given level of atmospheric humidity at a particular temperature (equilibrium moisture content). The equilibrium moisture content for a particular kind of seed at a given relative humidity tends to increase as temperature decreases and the deterioration starts. Equilibrium moisture content varies among seed kinds. In general, the equilibrium moisture content of "oily" seed is lower than that of "starchy" seed at the same relative humidity and temperature. This phenomenon can be accounted for by the fact that fats and oils do not mix with water. Thus, in a seed with 50% oil content, the moisture has to be concentrated in half the seed, while in a seed containing 10% oil, the moisture is distributed throughout 90% of the seed. Thus, the maintenance of moisture content of seed during storage is a function of RH and to a lesser extent of temperature. At equilibrium moisture content there is no net gain or loss in seed moisture content when seed is placed in a new environment with RH higher or lower than that of the seed, the seed will gain or lose moisture till it reaches a new equilibrium moisture content at this particular new environment.

Dry, cool conditions during storage

The general prescription for seed storage is a dry and cool environment. At this point, the question naturally arises: How dry and how cool? It is difficult to answer this question unless three factors are known:

(1) kinds of seed to be stored;

(2) desired period of storage and

(3) physiological quality of the seed.

Seed of most grain crops, e.g., corn, wheat, sorghum, barley, rye, oats, rice, will maintain germination for the 8-9 months period from harvest to planting at moisture content of 12-13% and normal warehouse temperature except possibly in Southern coastal areas. For maintenance of vigour as well as germination, moisture content should not exceed 12% (relative humidity below 60%) and temperature in the warehouse should not exceed 65^0 F. In the case of carry-over seed, which means a storage period of 20-21 months, the moisture content of seed of grain crops should be less than 11% and temperature should not exceed 65^0 F. Since the period of carry-over storage encompasses at least one summer period, temperatures and humidity control during the period is most important. Cotton seed stores about as well as seed of grain crops, and the conditions mentioned above are applicable.

Soybeans and peanut seed are poor storers. For one year's storage (actually 8-9 months), moisture content should be 11 to 12% and the warehouse temperature should not exceed 65^0F. Shelled peanuts may have to be stored in a cold room. Carry-over storage should not be attempted unless conditioned storage facilities are available: 65^0F and 50% relative humidity or better. Seed of most forage grass and legume crops will store well for one year at moisture content of 10-11% at normal warehouse temperatures. When "carried-over", moisture content should be about 10% and temperature should not exceed 65%. Vegetable seed vary considerably among kinds in their storage requirements. Generally, however, most kinds will store well for one year at a moisture content of 9-11% and a temperature that does not exceed 65^0F. When a storage period longer than 19-21 months is required, conditioned storage is essential for all kinds of seed. Most kinds of seed will maintain quality for 2-3 years when stored at 60^0F and 50-55% relative humidity or better. For storage longer than 3 years, conditions should be 50^0 F and 50% relative humidity or better.

5. Provenance

The seeds harvested in different climates (or) at different times show differences in viability. Because they would have been subjected to different pre harvest conditions which will have caused different amounts of deterioration by the time, the seeds are harvested.

6. The activity of organisms associated with seeds in storage

The bacteria, fungi, mites, insects, rodents and birds may do harm to seeds in storage.

SANITATION IN STORAGE

Good sanitation should be a continuous practice. It will minimize storage insect infestations. If storage insects are a problem, the judicious use of insecticides and fumigants, combined with sanitation, will alleviate the problem. The best procedure is not to place insect infested lots in storage with other lots unless all the insects have been killed by fumigation or insecticide treatment. In warehouse with concrete floors, seed bags should be stacked on wooden pallets to keep them from contact with the floor as considerable moisture can be transmitted through concrete floors. Seed warehouses should also be adequately ventilated (unless they are conditioned) and protected against rodents.

STORAGE CONDITIONS

Since seed moisture content and ambient relative humidity are in equilibrium during storage, maintenance of a "safe" moisture content requires an average level of relative humidity in the storage environment no higher than that in equilibrium with the "safe" or desired moisture content. This favorable situation can be achieved in only three ways:

(1) location of the storage facility in a region where relative humidity does not rise – on the average – above the critical level;

(2) maintenance of the relative humidity at the desired level by packaging seed in moisture vapor proof containers; or

(3) dehumidification of the storage room atmosphere to the desired level. The desired level of relative humidity for successful storage of seed depends, of course on the kind of seed, the duration of the storage period, and the temperature.

SEED PACKAGING IN RELATION TO SEED STORAGE

In reality the seed package is a small storage container. The kind of container needed is affected by several factors including:

a) The quantity of seed desired in each package

b) The protection desired

c) The cost of the package

d) The value of the seed

e) The storage conditions into which the container is to be placed and

f) The facilities for drying the seeds

Depending upon the cost availability and the period of storage, the packaging materials are to be selected. Normally cereal seeds are being packed in cotton, jute and paper bags. Moisture vapour penetrates in these containers and they offer no protection against high relative humidity. In high humidity locations with inadequate seed storage facilities, consideration should be given to methods of packaging which can protect the seed from moisture vapour. Such moisture vapour proof containers include paper aluminium foil pouches, polyethylene bags of over 700-gauge thickness, sealed tins and gasketed rigid plastic containers. The costs of these are high, for the package of cereal seeds. Polyethylene bags have been regarded as the

most attractive, because of their relatively low cost, compared to other kinds of sealed containers. Rigid plastic containers and sealed tins offer some possibility for hybrid seeds of cotton and vegetables, if the quantity needed is not great.

CLASSIFICATION OF PACKING MATERIALS OR CONTAINERS :-

1. Moisture and vapour pervious containers:

These containers allow entry of water in the form of vapour and liquid. These are suited for short term storage. The seeds in these containers will attain seed equilibrium moisture with the surrounding atmosphere (eg) cloth bags, gunny bags, paper bags etc.


2. Moisture impervious but vapour pervious containers

These allow entry of water in the form of vapour and not in liquid. The seeds in the containers can't be carried over for long period in hot humid conditions e.g., polythene bags of <300-gauge thickness and urea bags.


3. Moisture and vapour proof containers

These containers will not allow entry of moisture in the form of liquid or vapour. These are used for long term storage even in hot humid conditions if the seeds are sealed at optimum m.c. eg., Polythylene bags of >700-gauge thickness, aluminium foil pouches, rigid plastics etc.

Certified seeds of cereals, pulses and oil seeds are normally packed either in gunny bags or cloth bags. However, paper bag, aluminium foil pouches and polyethylene bags are used for packing flower and vegetable seeds.

SEED STORAGE IN RELATION TO SEED DETERIORATION

The Purpose of seed storage has been previously stated, ***viz.***, to preserve or maintain the physiological quality of seed for the period desired through minimization of the rate of deterioration. Since seed storage is basically concerned with "control" of deteriorative processes, some knowledge of these processes is essential for successful seed storage operations.

DETERIORATIVE CHANGES IN SEED AND THEIR CONSEQUENCES

In our consideration of some of the characteristics of deterioration in seed, another might have been added that deterioration is characterized by change. Indeed, in our context, deterioration and change – detrimental change – are almost synonymous. For deterioration is identifiable only in terms of observable or measurable changes in the response reactions of the seed. Conversely, detrimental changes, e.g., loss of germination or vigour, are said to be the result of deterioration.

In the sequence of deteriorative changes postulated in figure 1, it can be readily seen that during deterioration, the "performance potential" of seed becomes progressively impaired (reduced) until they lose their capacity to germinate, at which time "performance potential" is zero. Since loss of the capacity to germinate is the last practically significant consequence of deterioration, the design and evaluation of storage conditions only in terms of "maintenance of germination" is not sufficient. The "lesser consequences" of deterioration must also be considered because collectively they determine the "vigour" level of the seed. And, the vigour of seed determines how well they germinate, emerge, grow, and develop in the farmer's field.

LONGEVITY OF SEED IS A CHARACTERISTIC OF THE SPECIES OR VARIETY

Some kinds of seed are inherently long-lived, others are short-lived, while others have an "intermediate" life span. Differences in storability extend even down to the variety level. It has been known, for example, the certain inbred lines of corn are "poor storers" and that this characteristic is inherited. Inherent differences in seed longevity are facts, the seeds man must accept and contend with as best he can. Among the vegetables, onion seed are notoriously short-lived, radish seed are intermediate in longevity, and watermelon seed are relatively long-lived. Soybean and peanut seed do not store well as compared to seed of wheat, corn, cotton, sorghum and rice. In some cases, seed kinds which have very similar chemical and physical properties differ substantially in longevity. Tall fescue and annual ryegrass seed are similar in structure, chemical composition, and yet, ryegrass seed store better than tall fescue seed.

POSSIBLE SEQUENCE OF CHANGES IN SEED DURING DETERIORATION

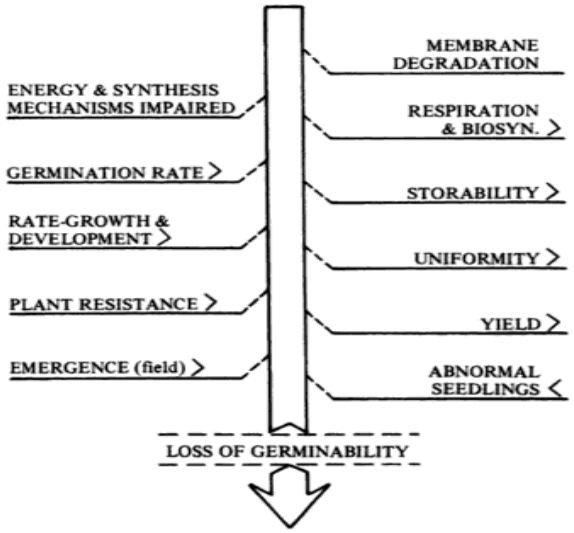

SEED SELECTION FOR EXTENDED STORABILITY

- Store well mature seeds.
- Seeds should be free from mechanical injury
- Seeds should not have met with adverse conditions during maturation
- Seeds should be dried to optimum moisture content.
- Seeds should be treated with fungicides before storage.
- Suitable packaging materials should be used for packing.

STORAGE GODOWNS AND THEIR MAINTENANCE

Seeds undergo deterioration due to aging in storage. This is accelerated by climatic factors and external biotic factors like insects and pathogen. In addition to seed borne pathogen and storage

insects, seeds are damaged by birds and rats for their feed. Clean and hygienic godowns protect the seed from external insects and preserve the seed. Hence care should be taken in construction of godown.

- Seed godown should be in a place where transport facilities are easily available.
- Seed godowns should not be constructed in areas near seashore. Since the high RH of atmospheric air accelerate the deterioration of seed.
- Seed godown should not be constructed in low lying water stagnating areas.
- Seed godown should be constructed in places where atmospheric RH is low, free circulation of air is possible, sunlight is adequate and elevated in nature.
- The ventilators should be at bottom for free air circulation.
- Ground moisture should not reach the floor.
- Should be rat proof with wire mesh.
- Should not be near industries as smoke is injurious.

In maintenance of seed in godown following points are to be considered.

1. Godown should be clean and dry.
2. Seed bags should not be stacked directly on floor. Should be stacked on wooden ballets.
3. The height of the stack should not be more than 6-8 bags.
4. Different seed lot should be kept separately.
5. Godown should be sprayed periodically once in a week or fortnightly with Malathion 50 EC @ 5 lit. sq. m-1 or 0.25% Nuvan @ 1 lit. 100 m^{3-1}.
6. Altering the chemicals at weekly intervals will give better control.
7. Seed lots can be fumigated with Aluminium phophide @ 3 gm/cu.m in air tight condition for 7 days. This can be done as propylatic measure and on minimum infestation by insects.
8. Seed lots should be periodically (once in month) tested for seed quality.
9. Based on seed testing result, seeds can be dried under sun for the removal of moisture. It reduces insect and pathogen infestation.
10. New seed lots should be kept away from old seed lots to avoid secondary infestation of insects.
11. Seeds should be treated with combination of fungicide and insecticide (eg.) Thiram @ 2 g kg-1 + carbaryl @ 200 mg kg-1.
12. Frequent supervision of each and every lot is must.
13. Seed bag should be restacked once in 3 months for free aeration.

14. Instead of gunny bags low-cost interwoven polythene bags should be used to prolong the life of seed.
15. Pesticides, fungicides, fertilizers, rejects should not be stored with seed.
16. Each lot should be labeled accurately and registers for stocks should be maintained.

Project Thesis
On

QUANTITATIVE ANALYSIS OF POTASSIUM DICHROMATE BY TITRIMETRIC METHOD

Submitted for the Partial fulfillment of Requirements
For the Degree
Of
Bachelor in Science
In
Chemistry
By

Roopam Pandey (207010027)
Khushi Verma (207010015)
Anamika Tiwari (207010003)
Shakshi Chaudhary (207010029)
Vidhi Chaudhary (207010033)

Under supervision

Of

Dr. Anupam Srivastava

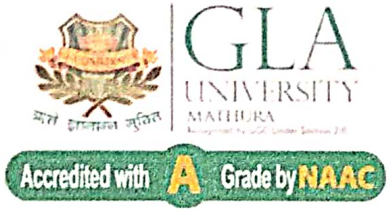

DEPARTMENT OF CHEMISTRY
GLA UNIVERSITY, MATHURA (U.P.), INDIA
JUNE 2021

GLA UNIVERSITY
MATHURA

Accredited with A Grade by NAAC

12-B Status from UGC

CANDIDATE'S DECLARATION

We solemnly declare that the project report on "**QUANTITATIVE ANALYSIS OF POTASSIUM DICHROMATE BY TITRIMETRIC METHOD**" in partial fulfillment of the requirements for the award of the Degree of Bachelor of Sciences based on our own work carried under the supervision of **Dr. Anupam Srivastava**, Assistant Professor, Department of Chemistry, GLA University, Mathura. We assert the statements made and conclusions drawn are an outcome of our research work. We further certify that

- The work has not been submitted to any other Institution for any other degree/diploma/certificate in this university or any other university of India or abroad.
- We have followed the guidelines provided by the university in writing the report.
- Whenever we have used the materials (data, theoretical analysis and text) from other sources, we have given due credit to them in the text of the report and giving their details in the references.

Roopam Pandey
Khushi Verma
Anamika Tiwari
Shakshi Chaudhary
Vidhi Chaudhary

This is to certify that the above statements made by the candidatesare correct to the best of my knowledge.

Date: 24/07/2021

(Dr. Anupam Srivastava)
Supervisor

GLA UNIVERSITY
MATHURA

Accredited with A Grade by NAAC

12-B Status from UGC

CERTIFICATE

This is to certify that this thesis report on "**QUANTITATIVE ANALYSIS OF POTASSIUM DICHROMATE BY TITRIMETRIC METHOD**" is the outcome of the work carried by **Roopam pandey, Khushi verma, Anamika tiwari, Shakshi chaudhary, Vidhi chaudhary** under my supervision. Further, this is mention that to the best of our knowledge, the work reported herein does not form part of any other thesis, report or dissertation on the basis of which a degree or award was conferred on an earlier occasion on this or any other candidate.

Dr. Anupam Srivastava
(Supervisor)
Assistant Professor,
Department of Chemistry
GLA University, Mathura (U.P.)

Countersigned By:

Dr. Anuj Kumar
Project Coordinator

Dr. Deepak K Das
Prof & Head

Dr. Vinod K Vashistha
Program Coordinator

Department of Chemistry
GLA University, Mathura (U.P.)

Department of Chemistry
Dissertation Examined
Date. 24/7/2021
GLA University, Mathura

ACKNOWLEDEGEMENT

We would like to thank our thesis supervisor **Dr. Anupam Srivastava** whose constant guidance, insightful suggestions, invaluable support and faith in our abilities led to successful completion of our project work. We really appreciate the probing questions they asked whenever we came with problems, which led us to think thoroughly. Instead of just telling us the right or wrong answer, they helped us identify the gap in our understandings.

We are highly grateful to **Prof. DK Das** (Head), Department of Chemistry, GLA University, Mathura for providing the necessary environment of research in the department, for providing me all specific amenities required during the entire research work.

We wish to pay our sincere thanks to Dr. Anuj kumar, Dr.Anupam Srivastav, Dr. Abhishek Srivastava, Dr. BasantLal, Dr. Pankaj Kumar Rastogi, Dr. Yogendra Sharma, Mr. Hariom Saraswat, Mr. Rajendra Singh and all other supporting staff of the institute Mr.Chail Bihari Gaur in particular.

Everything we have achieved so far in our life including successful completion of our research work has been possible because of our beloved family and faculty members.

Roopam Pandey

Khushi Verma

Anamika Tiwari

Shakshi Chaudhary

Vidhi Chaudhary

Table of Contents

ABSTRACT

This experiment was conducted in order to analyze, identify and determine the molarity and concentration of potassium dichromate solution. Measuring using laboratory instrument is recommended, to identify the accuracy of the results, such as burette which is used to identify the measurement of the sodium thiosulphate which is prerequisite in reacting with the potassium dichromate completely. These steps are gently pouring in one solution in burette to another until the reactions between two compounds are complete and this called titration.

Titration is a chemist's procedure in laboratory in order to measure and identify the molarity of a solution, and also controlled addition of solution from a laboratory instrument (burette) into a measured volume of a sample solution. Volumetric analysis is specified as equalization the latter solution and any process of analyzing quantity of chemicals in measuring volume sample of standard chemical solutions.

Using this titrimetric method we calculated the strength of potassium dichromate using hypo solution as a standard solution, KI and starch solution as an indicator this principle is employed here to determine the strength of K2Cr2O7 iodometrically. Titration involving with iodine or dealing with iodine liberated in chemical reaction is called iodometric and idimetric titration respectively. This reaction is iodometric because iodine is get from KI.

Chapter 1:Introduction

Analytical chemistry studies and uses instruments and methods used to separate, identify, and quantify matter. Analytical chemistry is the science of obtaining, processing, and communicating information about the composition and structure of matter.

Qualitative and **Quantitative** analysis is analytical techniques in Chemistry that are used for giving details about the components in an unknown sample.

Qualitative analysis in Chemistry gives details of the presence or nonappearance of different chemical components in an unknown sample, while quantitative analysis gives the measure of various chemical components present in a given sample.

Most often, both the techniques are used together, i.e., the use of qualitative analysis followed by quantitative analysis. Qualitative analysis is also called subjective investigation. In the field of Chemistry, it is a part of science that examines the substance piece or chemical composition of a sample.

Quantitative chemical analysis, branch of chemistry that deals with the determination of the amount or percentage of one or more constituents of a sample. A variety of methods is employed for quantitative analyses, which for convenience may be broadly classified as chemical or physical, depending upon which properties are utilized. Chemical methods depend upon such reactions as precipitation, neutralization, oxidation, or, in general, the formation of a new compound. The major types of strictly chemical methods are known as gravimetric analysis and volumetric, or titrimetric, analysis (see volumetric analysis). Physical methods involve the measurement of some physical property such as density, refractive index, absorption or polarization of light, electromotive force, magnetic susceptibility, and numerous others.

Titration -

A quantitative and volumetric technique, to determine the unknown concentration of a solution by the known concentration of a solution in the presence of indicator is called Titration

Titration is a common laboratory method of using quantitative chemical analysis. This method is used to determine the unidentified concentration of a known analyte. The volume measurement is known as volumetric analysis, and it is important in the titration.

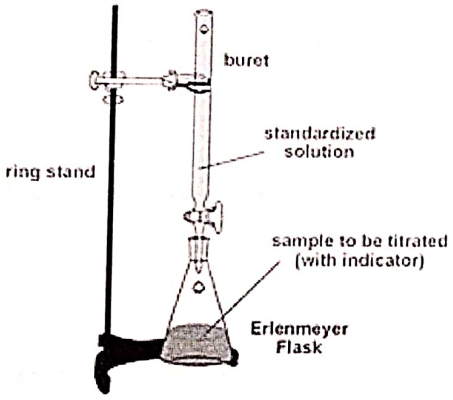

Types of Titration-

There are many types of titration when considering goals and procedures. However, the most common types of titration in quantitative chemical analysis are redox titration and acid-base titration.

Titrations can be classified as:

- Acid-base Titrations
- Redox Titrations.
- Precipitation Titrations.
- Complexometric Titrations.

1. Acid-Base Titration

The strength of an acid can be determined using a standard solution of a base. This process is called acidimetry. In the same way, the strength of a base can be found with the help of a standard solution of an acid, which is known as alkalimetry. Both titrations involve in the neutralization reaction of an alkali.

What is Acid-Base Titration?

It is a quantitative analysis method to determine an acid's or bases' concentration by precisely neutralizing them with a standard solution of either acid or base of known concentration. It is monitored with the help of a pH indicator to know the development of the acid-base reaction.

$HA+BOH \rightarrow BA+H_2O$

Acid + Alkali→Salt + Water

Or $H^+ + A^- + B^+ + OH^- \rightarrow B^+ + A^- + H_2O$

Or $H^+ + OH^- \rightarrow H_2O$

The acid-base titration is based on the reaction that neutralization is between a base or an acidic and analyte. In this type, a reagent is mixed with the sample solution until it reaches the required pH level. This type of titration majorly depends on the track change in pH or a pH meter.

2. Redox Titration

The redox titration is also known as an oxidation-reduction reaction. In this type of titration, the chemical reaction takes place with a transfer of electrons in the reacting ions of aqueous solutions. The titrations are named after the reagent that is used in are as follows;

- Dichromate Titrations

- Iodimetric and Iodometric Titrations
- Permanganate Titrations

In this titration, the potassium permanganate is used as an oxidizing agent. It is maintained with the use of dilute sulphuric acid. Here is the equation.

$2KMnO_4 + 3H_2SO_4 \rightarrow K_2SO_4 + 2MnSO_4 + 3H_2O + 5[O]$

Or $MnO_4^- + 8H^+ + 5e^- \rightarrow Mn^{2+} + 4H_2O$

Further, the solution remains colourless before the endpoint. The potassium permanganate is used to estimate oxalic acid, ferrous salts, hydrogen peroxide, oxalates and more. While the solution of potassium permanganate is always standardized before it is used.

Dichromate Titration

These are titrations in which, potassium dichromate is used as an oxidising agent in acidic medium. The medium is maintained acidic by the use of dilute sulphuric acid. The potential equation is:

$K_2Cr_2O_7 + 4H_2SO_4 \rightarrow K_2SO_4 + Cr_2(SO_4)_3 + 4H_2O + 3[O]$

Or $Cr_2O_7^{2-} + 14H^+ + 6e^- \rightarrow 2\,Cr^{3+} + 7H_2O$

The solution of potassium dichromate can be directly used for titrations. It is mainly used for the estimation of ferrous salts and iodides.

Iodimetric and Iodometric Titration

The reduction of free iodine to iodide ions and oxidation of iodide ions to free occurs in these titrations.

$I_2 + 2e^- \rightarrow 2I^-$..... (reduction)

$2I^- \rightarrow I_2 + 2e^-$ ..... (oxidation)

The solution is used as an indicator. Free iodine is used in the iodometric titration, while in the iodometric titration an oxidation agent is used to react to liberate free iodine.

3. Precipitation Titrations

The titration is based on the insoluble precipitate formation when the two reacting substances are brought into contact are called precipitation titration. For instance, when the solution of silver nitrate is used to a solution of ammonium thiocyanate or sodium chloride, it reacts and forms a white precipitate of silver thiocyanate or silver chloride.

$AgNO3 + NaCl \rightarrow AgCl + NaNO3$

$AgNO3 + NH4CNS \rightarrow AgCNS + NH4NO3$

4. Complexometric Titrations

The complexometric titration is where an undissociated complex is formed at an equivalence point. It is greater than the precipitation titrations, and there will be no error due to co-precipitations.

$Hg2+ + 2SCN- \rightarrow Hg(SCN)2$

$Ag+ + 2CN- \rightarrow [Ag(CN)2]-$

Ethylenediaminetetraacetic acid (EDTA) is an important reagent that forms complexes with metals.

What is the purpose of titration in chemistry?

Titrating a simple solution with a volume of a regular acid solution (of known concentration) needed to neutralize it may be used to determine its concentration. The aim of the titration is to find the equivalence point, which is the point where chemically equivalent quantities of the reactants are combined.

End point

The point in the titration process which is indicated by color change of the indicator is called endpoint.

- It is always indicated by the color change of the reaction mixture.
- It doesn't always give the point where reaction ends.
- It comes either almost with the equivalence point or after the equivalence point.

Equivalence point

The point in the titration process where the chemical reaction in the titration mixture ends is called equivalence point.

- It is the point where the analyte has completely reacted with the titrant.
- It is not always indicated by color change of the reaction mixture
- It gives the point where reaction ends.
- It comes either almost with endpoint or before the endpoint.
- Weak acids can show multiple equivalence points during titration.

What is potassium Dichromate ?

Potassium dichromate is one of the most common causes of chromium dermatitis chromium is highly likely to induce sensitization leading to dermatitis, especially of the hand and fore-arms, which is chronic and difficult to treat.

Potassium dichromate is carcinogenic. The compound is also corrosive and exposure may produce severe eye damage or blindness. Human exposure further encompasses impaired fertility, heritable genetic damage and harm to unborn children.

Potassium dichromate is found naturally as a rare mineral known as lopezite.

Physical Properties of Potassium Dichromate-

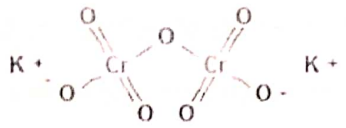

Potassium dichromate has the appearance of red-orange crystals. Normally exist in a solid-state at room temperature.

- It is odorless.
- It is non-combustible and also its nature is highly corrosive.
- The density of Potassium dichromate in the solid state is 2.676 g/cm3.
- It is insoluble in alcohol, acetone.
- Its crystalline structure is triclinic and coordination geometry for the central atom chromium is tetrahedral.

Chemical Properties of Potassium Dichromate and Reactions-

1. Action of Heat-

$K_2Cr_2O_7$ shows decomposition when heated to liberate potassium chromate and evolution of O_2 gas is also observed.

$$4K_2Cr_2O_7 \rightarrow 4K_2CrO_4 + 2Cr_2O_3 + 3\,O_2$$

2. Oxidizing Properties

Potassium dichromate is one of the most powerful oxidizing agents. one mole of $K_2Cr_2O_7$ liberates three moles of oxygen when reacted with dil.H_2SO_4.

The reaction can be depicted as follows:

$$K_2Cr_2O_7 + 4\,H_2SO_4 \rightarrow K_2SO_4 + Cr_2(SO_4)_3 + 4H_2O + 3(O)$$

Potassium dichromate is an oxidizing agent in organic chemistry, and is milder than potassium permanganate. It is used to oxidize alcohols. It converts primary alcohols into aldehydes and, under more forcing conditions, into carboxylic acids.

Importance of Potassium dichromate

- Potassium dichromate ($K_2Cr_2O_7$) is used as a standard solution to determine the percent by weight of iron (as Fe^{2+}) in an unknown solid.
- Potassium dichromate is used to standardize hypo solution because oxidizes the iodide ion in acidic medium to equivalent amount of iodine.
- Potassium dichromate is used for preparing strong cleaning solutions for glassware and for etching materials.

$K_2Cr_2O_7 + 7H_2SO_4 + 6KI \rightarrow 4K_2SO_4 + Cr_2(SO_4)_3 + 7H_2O + 3I_2$

$2Na_2SO_3 + I_2 \rightarrow Na_2S_4O_6 + 2NaI$

$K_2Cr_2O_7 \equiv 3I_2 \equiv 6Na_2S_2O_3$

In this reaction, the strength of potassium dichromate is determined by titration with standardized hypo solution. This is oxidation reduction as well as iodometric titration.

Titration involving with iodine or dealing with iodine liberated in chemical reaction is called iodometric and idimetric titration respectively. This reaction is iodometric because iodine is get from KI.

Here $K_2Cr_2O_7$ is an oxidizing agent while iodine is a reducing agent. In last step of reaction, iodine is oxidizing agent while thiosulphate ion is reducing agent.In the 2nd step of reaction, specific indicator is used that is **Starch** which has significant characteristic on iodine.

When $K_2Cr_2O_7$ reacts with KI in presence of acid (Dil. H_2SO_4 and HCl) ,the dichromate is reduced to green chromic salt and liberates an equivalent amount of iodine which is titrated with a standard hypo solution using starch solution as an indicator. This principle is employed here to determine the strength of $K_2Cr_2O_7$ iodometrically. When the end point is reached the blue colour of iodostarch complex suddenly disappear and the pure green solution due to chromic salt remains.

Chapter 2:Methods& Materials

Experiment no. 1:

Iodometric titration of potassium dichromate using sodium thiosulphate (Hypo-solution)

Objective:

The objective of this experiment is to determine the strength of Potassium dichromate. This reaction is based on oxidation and reduction reaction as well as "iodometric reaction". The main purpose of this experiment is to standardize potassium dichromate with standardized sodium thiosulphate solution.

Apparatus& Chemicals required

BURETTE:- A burette is a graduated glass tube with a tap at one end, for delivering known volumes of a liquid, especially in titrations. It is a long, graduated glass tube, with a stopcock at its lower end and a tapered capillary tube at the stopcock's outlet.

- Borosilicate Glass Burette (25ml)

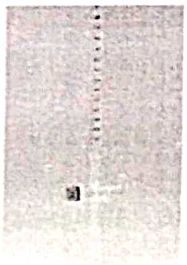

PIPETTE:- A pipette is a laboratory tool commonly used in chemistry, biology and medicine to transport a measured volume of liquid.

- Borosil 25ml pipette

CONICAL FLASK:- Conical flask or a titration flask, is a type of laboratory flask which features a flat bottom,conical body, and a cylindrical neck.

- Borosil 250ml conical flask.

BEAKER:- In laboratory equipment, a beaker is generally a cylindrical container with a flat bottom. Beakers are available in a wide range of sizes, from one milliliter up to several liters.

- Borosil 500ml beaker.

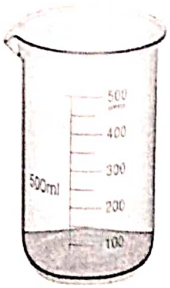

POTASSIUM DICHROMATE:- Potassium dichromate, K2Cr2O7, is a common inorganic chemical reagent, most commonly used as an oxidizing agent in various laboratory and industrial applications.

SULPHURIC ACID:- Sulfuric acid, sulfuric also spelled sulphuric (H2SO4), also called oil of vitriol, or hydrogen sulfate, dense, colourless, oily, corrosive liquid; one of the most commercially important of all chemicals.

Formula: H_2SO_4

IUPAC ID: Sulfuric acid

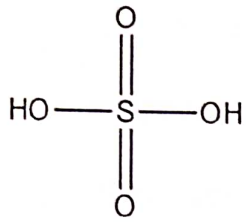

sulphuric acid

POTASSIUM IODIDE:- Potassium iodide is a chemical compound, medication, and dietary supplement. And used in iodometrictitratation for the liberation of iodine.

Formula: KI

Molar mass: 166.0028 g/mol

HYPO SOLUTION:-Hypo solution is basic in nature and it is also known by the name of sodium thio - sulphate or sodium thio – sulfite. It is present in a liquid state and the appearance is yellowish in color. Chemical formula of hypo solution is Na2S2O3.

Chemical reaction:

$K_2Cr_2O_7 + 6KI + 7H_2SO_4 \cdot 4K_2SO_4 + Cr_2(SO_4)_3 + 7H_2O + 3I_2$

$6Na_2SO_3 + 3I_2 \cdot 3Na_2SiO_3 + 6NaI$

Procedure:

- Prepare 10% solution of $K_2Cr_2O_7$ by dissolving 10g of potassium dichromate in 100ml of water.
- Add 10ml of potassium dichromate in a flask and add half test tube of H_2SO_4 in it.
- Add 10-20ml of KI solution in above flask and dilute the mixture of flask with 15-20ml of distilled water.
- Titrate that solution against Na_2SO_3.

- When color of solution changes to yellow, use 1ml of starch as an indicator.
- Appearance of blue color indicate end point. Note the volume of sodium thiosulphate used till end point.
- Repeat the process thrice for better results.

Blank Experiment (procedure): Take 10 ml of distilled water in place of potassium dichromate, and add half test tube of sulphuric acid.

- Add 10-20ml of KI solution in the above flask and dilute the solution mixture of flask with 15-20ml of distilled water.
- Titrate the solution against Na_2SO_3.
- when color of solution changes to transparent, use 1ml of starch as an indicator.
- Appearance of milky color indicate end point. Note the volume of sodium thiosulphate used till end point.
- Repeat the process thrice for better results.
- Take difference of volume of sodium thiosulphate used in procedure of potassium dichromate and blank experiment and use that volume in calculations. Volume of $K_2Cr_2O_7$ used = 10ml

Chapter 3: Observation & Result

Sr no.	Initial volume (ml)	Final volume(ml)	Volume used(ml)
1.	50	28	22
2.	28	05	23
3.	50	28	22

Volume of Na_2SO_3 used for burette according to experimental values = Vs = 22.3ml

Blank Experiment:

Sr no.	Initial volume (ml)	Final volume(ml)	Volume used(ml)
1.	50	37	13
2.	37	23	14
3.	23	11	12

Average volume of Na_2SO_3 used during blank experiment = Vy = 13ml

Calculation

Average volume of Na_2SO_3 used during blank experiment = Vy = 13ml

Volume of Na_2SO_3used = V_2= 22.3 – 13 = 9.9 ml

Volume of $K_2Cr_2O_7$ = V_1 = 10ml

Molarity of $K_2Cr_2O_7$ = M_1 =?

No. of moles of $K_2Cr_2O_7$ = n_1 = 1

Molarity of Na_2SO_3= M_2 = 0.1M

No. of moles of Na_2SO_3= n_2= 6

$K_2Cr_2O_7$ Na_2SO_3

M_1V_1/ n_1 = M_2V_2/n_2

M_1 = (0.1M) (9.9) (1)/(10ml)(6)

M_1 = 0.0165 M

Results:

The strength of given unkown sample of $K_2Cr_2O_7$ solution is = 0.016 M

Chapter 4: Conclusion

In this experiment, redox reaction occur and it is called as iodometric titration because iodine is added in the form of KI. Its main purpose was to determine the strength of potassium dichromate by titrating it against sodium thiosulphate standard solution of 0.1M. two basic procedures are followed in this experiment. 1st one is performed by titration of sodium thiosulphate by using potassium dichromate while in 2nd procedure, i.e blank experiment, sodium thiosulphate has titrated by using distilled water in place of potassium dichromate. The difference in the volume of sodium thiosulphate used in both procedures has used in further calculations. After calculations, the strength of potassium dichromate appears as 0.016M.

Chapter 5: Refrences

[1]D.A.Skoog, D.M.West, F.J.Holler, S.R.Crouch; Fundamentals of Analytical Chemistryí, 8th Ed., Thomson Brooks/Cole, London, (2004).

[2]D.C.Harris; Quantitative Chemical Analysisí, 7th Ed., Freeman, New York, (2007).

[3]F.A.Vogel; Textbook of InorganicAnalysisí, 4 th Ed. 348-351, 370-372, (1978).

[4]C.W.Griffin; Inorganic Quantitative Analysisí, Blackstone company, (1938).

[5]H.C.Anandamurthy, O.G.Palanna; Analytical Chemistry- An Indian Journalí, 7(9), 684-693 (2008). [6] H.C.Anandamurthy, O.G.Palanna; Analytical chemistry - An Indian Journal, 7(9), 694-702 (2008). [7] N.Suma,T.Jeevananda, O.G.Palanna;Asian Journal of Chemistry, Communicated, August (2009).

INSTITUTE OF LEGAL STUDIES AND RESEARCH (ILSR),

GLA UNIVERSITY, MATHURA

COURT DIARY

INTERNSHIP REPORT

DISTRICT COURT MATHURA, UTTAR PRADESH

FROM 2nd August 2021 TO 31st August 2021

UNDER THE GUIDANCE AND SUPERVISION OF Adv. PRABHAT KUMAR NAGINA

Submitted To:

Dr. Soumi Chatterjee

Assistant Professor

Head of Placement and InternshipCommittee

Submitted By:

Aashna

B.A.LLB(Hons)

195110001

TABLE OF CONTENT

CERTIFICATE

Prabhat Kumar Nagina
Advocate
D.G.C. (Civil) Firozabad (U.P.)

Residence
207, Jain Nagar
Firozabad.
Mobile No- 9412721838

Ref. No-

Date- 04.9.2021

INTERNSHIP CERTIFICATE

This is to Certify that Miss Aashna student of B.A. (Hons.)-L.L.B. year VIth Semester bearing Roll No. 195110001, from GLA University, Mathura has Successfully completed her internship in my office from August 02nd , 2021 to August 31st , 2021.

During the course of internship, she attended court proceedings and assisted me in drafting and rescarching on criminal as well as civil matters listed before various courts.

Miss Aashna has good, moral charater and sincerely performed her duties as intern under my guidance. She is very punctual and laborious in nature.

Miss Aashna prossesses sound knowledge of law and she is also good at drafting and legal research.

I wish her all the very best in her future endeavours.

Prabhat Kumar Nagina
D G C (Civil)
Civil Court Firozabad

DECLARATION

This declaration is made regarding the internship report which has been prepared and drafted by **Aashna** under the supervision of **Adv. Prabhat Kumar Nagina,** It contains the work accomplished during the internship which was assigned during the internship. This work was done in respect of the partial fulfillment of the requirement for the award of the degree of LL.B.

This internship report has not been submitted either in whole or in part to any other Law University or affiliated Institute within the territory of India.

Aashna

Roll No- 195110001

Year-3rd

GLA University, Mathura

ACKNOWLEDGEMENT

My warm gratitude towards **(Dr.) Avinash Dadhich** Dean of the **Institute Of Legal Studies And Research GLA University, Mathura.** Our respected teachers encourage us towards internship and how to perform our duty under Internship. I would like to place my warm gratitude towards **Adv. Prabhat Kumar Nagina** under whom I completed my internship, and gained detailed and useful experience for an internship as well as for the profession of advocacy and judiciary in near future. This is to express gratitude towards a person who guided and motivated me throughout my internship period. It gives me immense pleasure to acknowledge my indebtedness and a deep sense of gratitude and respect to my senior without whose constant guidance this internship would have not been possible. I am thankful to him for his valuable teaching and advice were given to me, for helping me in exploring and understanding things better.

Aashna

Year: IIIrd

ILSR, GLA University, Mathura

INTRODUCTION

This report examines the internship program with Advocate, My internship with *Adv. Prabhat Kumar Nagina* Sir. Starting from 02nd August 2021 to 27th August 2022 has immensely been a commendable learning experience for me. The internship where I dealt with people directly to look at problems under the guidance of my senior and other associates with the help of them, I was able to complete mine into their internship with an excellent learning experience. Being a law student, I need to have an in-depth understanding of the practical side of the law. Simply focusing on the theoretical aspects would not hold me in good stead. Therefore, interning under a practicing lawyer is the best way of developing this understanding of the legal system of our country.

I was given case files to read but also to make our notes over those cases, analyze the grounds and question of law. We also prepared briefs for cases such as criminal and civil cases.

All over, my internship was an enriching experience and helped me gain much in terms of understanding the working of our legal system.

DURATION AND TIMINGS OF THE INTERNSHIP

The internship was 31 days long with 5 working days a week. The usual timings were from 11:30 am to 3:00 pm. On some days I left early because of less work and sometimes after 3:00 depending on the amount of work for the particular day.

DAILY INTERNSHIP REPORT

INSTITUTE OF LEGAL STUDIES AND RESEARCH (ILSR), GLA UNIVERSITY, MATHURA

CIVIL COURT FIROZABAD

Timing: 11:00pm- 3:00pm

The first week of the internship was an introductory session with Adv. Himanshu Yadav in that I introduced myself and also talked about the law subjects which I have studied yet in the university. After that, I have a session with his junior advocate, tells us about the procedure of criminal proceedings and he also asked me to read those sections so I can understand the procedure which is done inside the court.

The advocate also tells us about the procedure of criminal proceedings and he also asked me to read those sections so I can understand the procedure which is done inside the court. And I also had a court visit on the same day. The next day my senior appeared for the plaintiff's side and he had arguments with the other party after the arguments finished, he asked for the next date with the judge and the date was fixed for the further arguments. After this, we assigned a case study of a case named Vishnu and Ors. V. the state of U.P. assigned the task of the briefing of that case.

Firstly, you will have to report at his office in defence colony on the day you start with your internship. The person at the reception desk is sweet in nature and she will tell you everything you need to know about this internship. Before starting up the internship session, an introduction with Chander sir is mandatory. After you meet him, you will receive the Court passes from Chander Ji at the basement of his office

And I also had a court visit on the same day. The next day my senior appeared for the plaintiff's side and he had arguments with the other party after the arguments finished, he asked for the next date with the judge and the date was fixed for the further arguments. After this, we assigned a case study of a case named Vishnu and Ors. V. the state of U.P. assigned the task of the briefing of that case.

In this week I was asked to give a brief of the case law which he was given to me and also ask to fill the pro forma as per the given case. After this we had visited the court with our senior for the cross-examination was to be held and he asked us to observe that how to cross-examine. On, the other day I was assigned to observe the counseling the client with the permission of counsel. The client interview and counseling were done by the Ld. Judge, in a matrimonial dispute which is pending before the family court.

However, as per the instructions I observed the interview and counseling of the client. And also meet with the honorable judge Mrs. Sangita Sharma, she tells us about her experience in the judiciary and gives her best wishes for our future.

You have to report 6 days a week, Sunday being a Holiday, though the Associates working under Sir do not get that also. Saturday is a half-day.

From Monday to Friday, you will have to report to the courts at 10.30 am. Then from court to the office (Defence Colony) by 4 pm. In case you are an outsider, connectivity via buses and metro is quite available on these routes. From office, you can leave by 7 pm.

Generally, you are given research work from Sir and his associates. Since it is a big lawyer's office, you will not get to draft petitions or applications. A bit of drafting and some pity things are also given

This week I was assigned the case study sir gave us some orders and judgments to read. And also ask us to write an application for taking a date from the judge in a case, write another application if the client was unable to come on his date. He also gave us a case which was filed by him in the year 2018 Prem Singh v. the State of U.P

In our last weeks, we meet with two judges of the district court justice D k Shukla and justice Mayur Jain who share their experience and tell us the better way of studying for the competitive exams and gave their best wishes for the future. In the end, we have a question-answer session with our senior related to IPC, Constitution of India, the law of torts, contract act, etc.

Good Things

- First of all, you get to learn from the research work you're given. Obviously working under him gives you a chance to visit Delhi High Court and observe great lawyers arguing. The timings are not very strict. You can take a leave whenever needed.

- In addition, Delhi High Court has 3 canteens out of which the Main Canteen is great and very cheap.

- Moreover, a certificate from such a big name will give some help to your CV.

Bad Things

At times, I was also asked to arrange the books in the library but it never used to take much time and I took it positively by having a look around the various journals and books that are available.

You are not given any other work other than research. Suppose you are an interested student who wants to learn to draft, and small works such as filing the petition, searching the cause list, this is certainly not the place for you. This is a very chill internship.

CONCLUSION

This internship helped me in learning the court proceedings which I could learn during the period of internship. Though this much time is not sufficient it was enough to learn the basics. Basics can be learned only in the trial court and I have learned the basics I tried hard to learn them. Every client comes with a new case, new situation, a new problem; I also experience the expression and thoughts of the hon'ble judges. When they are in a good mood, they will tell you how to do things correctly. About advocates, I experience that it is not so easy to work as an advocate; it requires a lot of dedication and hard work. In the office I learned the official work, filing all the documents is very important and if you hold a file, you should know how to use them read them. And I got an idea about most of the sections of IPC, CrPC, and Evidence Act. And I also learned that it is very important to be always reading cases and new enactments, keeping you always sound-minded.

In the end, I would like to thank Advocate Prabhat Kumar Nagina DGC (Civil) at the Civil Court, Firozabad.